AGARD

ADVISORY GROUP FOR AEROSPACE RESEARCH & DEVELOPMENT

7 RUE ANCELLE 92200 NEUILLY SUR SEINE FRANCE

AGARD LECTURE SERIES No. 95

Strap-Down Inertial Systems

NORTH ATLANTIC TREATY ORGANIZATION

REPORT DOCUMENTATION PAGE			
1. Recipient's Reference	2. Originator's Reference AGARD-LS-95	3. Further Reference ISBN 92-835-0214-0	4. Security Classification of Document UNCLASSIFIED

5. Originator: Advisory Group for Aerospace Research and Development
North Atlantic Treaty Organization
7 rue Ancelle, 92200 Neuilly sur Seine, France

6. Title: STRAP-DOWN INERTIAL SYSTEMS

7. Presented: on 6–7 June 1978 in London, UK; 9th June 1978 in Copenhagen, Denmark; 12–13 June in Bolkesjø, Norway; 15–16 June in Cologne, Germany, and 19–20 June 1978 in Rome, Italy.

8. Author(s): Various

9. Date: May 1978

10. Author's Address: Various

11.

13. Keywords/Descriptors

Inertial guidance	Data processing	Strapdown systems
Inertial navigation	Detectors	Navigation

14. Abstract

The state-of-the art in strap-down inertial systems technology has advanced to a state where it seems timely to present it to the NATO Community in the form of a Lecture Series. Until now, this technology has been covered only in many separate papers, and no coherent document covering the whole spectrum of this technology is available.

The Lecture Series will provide an overview of the current technologies being implemented in strap-down navigation, control, and guidance systems. Technology high-lighting the up-to-date techniques employed in the development of inertial sensors, analysis, data-processing and subsystem integration will be discussed, along with predictions of the directions these techniques are likely to take. This will provide the overall background necessary for understanding the principles and mechanisms of real, current-day, strap-down systems and likely future systems using the newest technology.

The material in this publication was assembled to support a Lecture Series under the sponsorship of the Guidance and Control Panel and the Consultant and Exchange Programme of AGARD.

NORTH ATLANTIC TREATY ORGANIZATION

ADVISORY GROUP FOR AEROSPACE RESEARCH AND DEVELOPMENT

(ORGANISATION DU TRAITE DE L'ATLANTIQUE NORD)

AGARD Lecture Series No.95

STRAP-DOWN INERTIAL SYSTEMS

The material in this publication was assembled to support a Lecture Series under the sponsorship of the Guidance and Control Panel and the Consultant and Exchange Programme of AGARD, and was presented on 6–7 June 1978 in London, UK; 9th June 1978 in Copenhagen, Denmark*; 12–13 June 1978 in Bolkesjo, Norway; 15–16 June 1978 in Cologne, Germany, and 19–20 June 1978 in Rome, Italy.

*This being a one-day meeting, the programme was shortened and consisted of the first four Papers only.

THE MISSION OF AGARD

The mission of AGARD is to bring together the leading personalities of the NATO nations in the fields of science and technology relating to aerospace for the following purposes:

- Exchanging of scientific and technical information;
- Continuously stimulating advances in the aerospace sciences relevant to strengthening the common defence posture;
- Improving the co-operation among member nations in aerospace research and development;
- Providing scientific and technical advice and assistance to the North Atlantic Military Committee in the field of aerospace research and development;
- Rendering scientific and technical assistance, as requested, to other NATO bodies and to member nations in connection with research and development problems in the aerospace field;
- Providing assistance to member nations for the purpose of increasing their scientific and technical potential;
- Recommending effective ways for the member nations to use their research and development capabilities for the common benefit of the NATO community.

The highest authority within AGARD is the National Delegates Board consisting of officially appointed senior representatives from each member nation. The mission of AGARD is carried out through the Panels which are composed of experts appointed by the National Delegates, the Consultant and Exchange Program and the Aerospace Applications Studies Program. The results of AGARD work are reported to the member nations and the NATO Authorities through the AGARD series of publications of which this is one.

Participation in AGARD activities is by invitation only and is normally limited to citizens of the NATO nations.

Published May 1978

ISBN 92-835-0214-0

Printed by Technical Editing and Reproduction Ltd
Harford House, 7–9 Charlotte St, London, W1P 1HD

ERRATA SHEET (↑ CORRECTION TERM)

Page

3-9 Eq. 16: $C_{31} = 2(AC + BD)$ ↑

3-10 Eq. 23: $\dot{\alpha} = \tan^{-1}\left(\frac{AD + BC}{BD - AC}\right)$ ↑

3-10 Eq. between 23 and 24: $C_{11} = D$ ↑

3-12 Eq. 25: $\phi = A^2wt/2$ ↑

5-3 Eq. 1: $\dot{\theta}_g$ ←

5-4 Eq. 4, 5, 6: All terms that involve a single angular rate or linear velocity need dots over them, i.e., $\dot{u}$, $\dot{v}$, $\dot{w}$, $\dot{r}$, $\dot{q}$, etc.

6-32 Fig. 30: Velocity Resolution and Accumulation is at 40 Hz ↑ not 10 Hz

6-34 ~ 17th line: ΔV_e ↑ and ΔV_n ↑

8-39 Table 3, first row terms: Previous values of the covariance matrix should be written as $P_{K-1/K-1}$, etc. ↑

8-39 Table 3, last column, last row: $H_{1K})P_{3K/K-1}$ ↑

ii

PREFACE

This Lecture Series No.95, on Strapdown Inertial Systems is sponsored by the Guidance and Control Panel of AGARD and organized by the Consultant and Exchange Programme.

The first four lectures are intended to provide a detailed tutorial to strapdown inertial sensors, algorithms, and systems. The second four lectures emphasize actual system applications using all of the different types of inertial sensors presently available. In that regard, the reader is fortunate in having, in one document, the description of the application of these different sensors to various state-of-the-art applications.

Most of the papers were technically reviewed and have been edited for consistency in format and in nomenclature so that the reader will find a common approach in each presentation. The opinions expressed are, of course, those of the individual lecturers.

George T.SCHMIDT
Lecture Series Director

LIST OF SPEAKERS

Lecture Series Director: Dr G.T.Schmidt
Program Manager
Advanced Systems Department
Charles Stark Draper Laboratory
555 Technology Square, MS No.16
Cambridge, Mass., 02139
USA

Mr P Savage
Staff Engineer
Honeywell, Avionics Division
MS #MN17-2326
2600 Ridgeway Parkway
Minneapolis, Minnesota 55413
USA

Mr A.VanBronkhorst, Manager Systems Development
4141 Eastern Avenue, S.E.
Lear-Siegler Instrument Division
Grand Rapids, Michigan 49508
USA

Dr E. Levinson
Research Department Head
MS 1A15
Sperry Gyroscope
Great Neck, New York
USA

Mr J.R.Catford
Consultant (Advanced Systems)
Gyro Division
Marconi-Elliott Avionics
Rochester, Kent
UK

Dr W.Kubbat
Head, Guidance and Control A/C Division
Messerschmidt-Bolkow-Blohm
Postfach 80 11 60
8 Munich 80
Germany

Mr G.Cattan and Mr J.-L.Michelin
Société de Fabrication
d'Instruments de Mesure (S.F.I.M.)
13 Avenue Ramolfo Garnier, Massy
France

CONTENTS

STRAPDOWN INERTIAL SYSTEMS—THEORY AND APPLICATIONS
INTRODUCTION AND OVERVIEW

by
George T. Schmidt
Advanced Systems Department
The Charles Stark Draper Laboratory, Inc.
Cambridge, MA, U.S.A. 02139

1-1

SUMMARY

Comparisons between conventional gimbal inertial systems and strapdown inertial systems are presented in terms of implementation requirements and performance differences. A generalized approach to inertial-system analysis that can determine the performance of different inertial mechanizations is described.

1. INTRODUCTION

This AGARD Lecture Series is intended to provide both the basic theory of strapdown inertial systems and an overview of the current technologies being implemented. Technology highlighting the up-to-date techniques employed in the development of strapdown inertial sensors, analyses, algorithms, and subsystems integration are presented, along with predictions of the directions these techniques are likely to take.

The intent of this particular lecture is to provide some overall background and introductory material to the detailed lectures, as well as a generalized analysis technique. Then, the following three lectures emphasize in a tutorial manner inertial components, algorithms, and strapdown system design; the remaining four describe applications of these techniques to system implementations.

Previous AGARD publications and other reference material provide the necessary framework for understanding the techniques of inertial navigation.[1-5] These publications have concentrated on gimbal inertial navigation systems, by far, the most common type of inertial system in military, space, and commercial use. All of these references describe the algorithms for navigation in great detail.

In inertial-platform gimbal mechanizations, the gyroscopes mounted on a stable element measure angular rates, and gimbal-drive systems can use the angular-rate information to null the angular motion sensed by the gyroscopes. In this manner, the gyroscopes and accelerometers on the stable element are inertially stabilized from the vehicle motion, and the stable member physically represents an inertial reference frame. By double integration of the specific-force indications from the accelerometers, with a correction for gravity, position determination is possible. Figure 1 illustrates this approach.

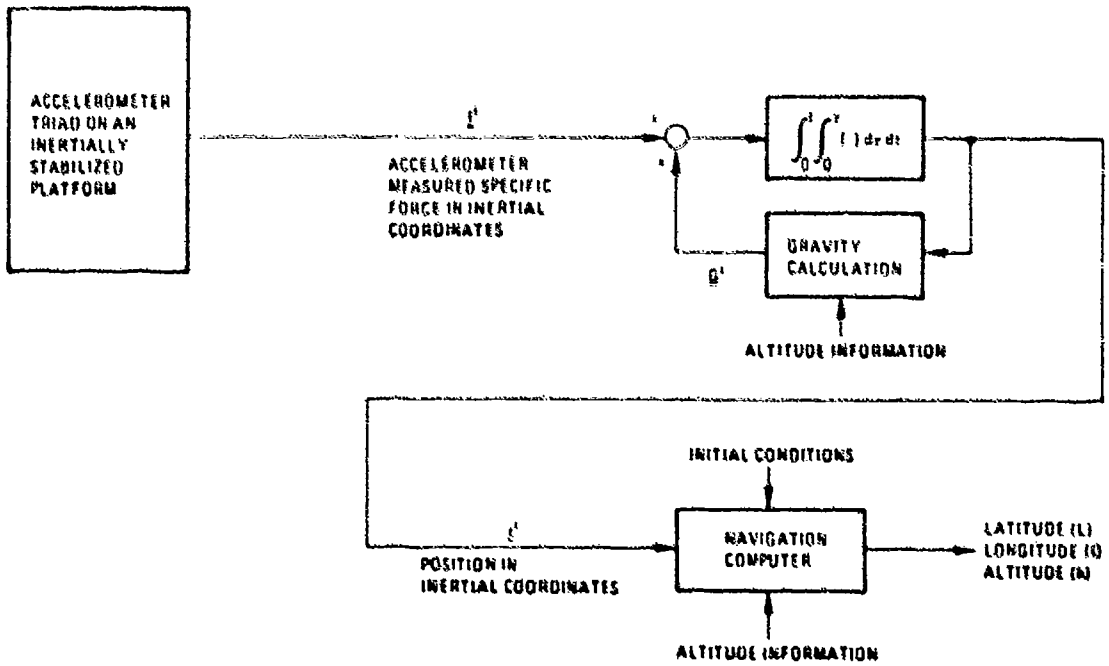

Figure 1. Platform space-stable inertial mechanization.

Gimbal systems provide a good dynamic environment for inertial instruments, particularly in severe angular oscillatory cases, such as a spinning reentry vehicle, since the gimbals isolate the gyros from the environment. In fact, the state-of-the-art is such that navigation performance of gimbal systems can approach almost error-free instrument operation to the point where uncertainties in the knowledge of the gravity field become the dominant sources of navigational error.

In strapdown inertial systems, the sensors are mounted directly (or perhaps with vibration isolators) on the vehicle. Inertial-sensor outputs now represent specific force and angular rate with respect to inertial space coordinitized in vehicle body axes. Therefore, to maintain an inertial reference frame, a

computer-generated transformation-matrix algorithm between body and inertial frames must be used to process the gyro outputs as the vehicle moves and its orientation changes. Then, the accelerometer information must be transformed from the body frame to the inertial reference frame. Figure 2 illustrates this mechanization.

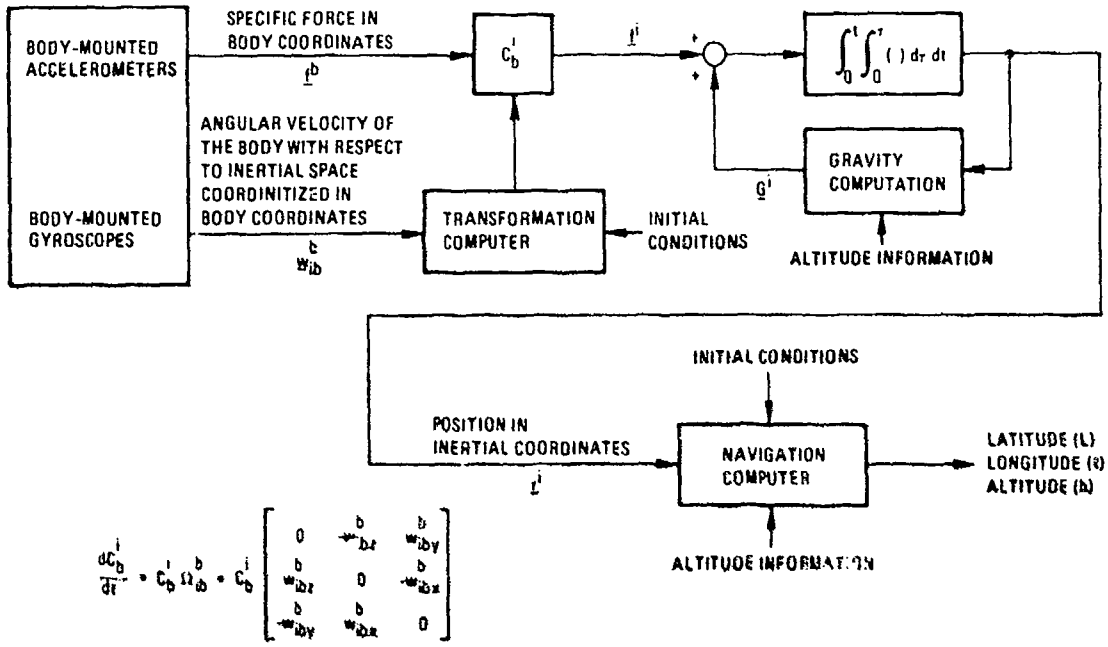

Figure 2. Strapdown system computing in inertial coordinates.

In addition to the added computations, the inertial sensors require a large dynamic range. They are now subjected to the entire vehicle dynamic environment and, in general, will not perform as well had they been isolated from it. Much of the work, in fact, on laser gyros (to be discussed in following papers) stems from their reputed insensitivity to dynamically induced errors, although single-degree-of-freedom gyros, tuned-rotor two-degree-of-freedom gyros, and electrostatic gyros have had strapdown applications.

Strapdown systems are of interest for all but the most demanding performance missions since elimination of the gimbals could possibly result in smaller system size, easier maintenance, less cost, and perhaps improved reliability. If aided-inertial systems such as Global Positioning System (GPS)-inertial are considered, performance differences between gimbal and strapdown systems are even less. The increased computational requirements of strapdown systems appear less important with each advance in computer technology. Furthermore, the instruments' outputs are in body coordinates, which is desirable for autopilot functions. Consequently, much interest and ongoing activity exists in strapdown sensor and system development, and this lecture series has been motivated by these developments.

2. NAVIGATION MECHANIZATIONS

As was illustrated in Figure 2, the mechanization concept for a strapdown system computing in an inertial reference frame requires the use of the gyro outputs in the computation of a transformation matrix between body and inertial coordinates.

Figure 3 illustrates the case when the geographic-north-pointing local-level navigation frame is the instrumented stable-member frame for a gimbal system; Figure 4 shows the case where the local-level navigation frame is the computational reference frame for a strapdown system. The local-level frame is the most

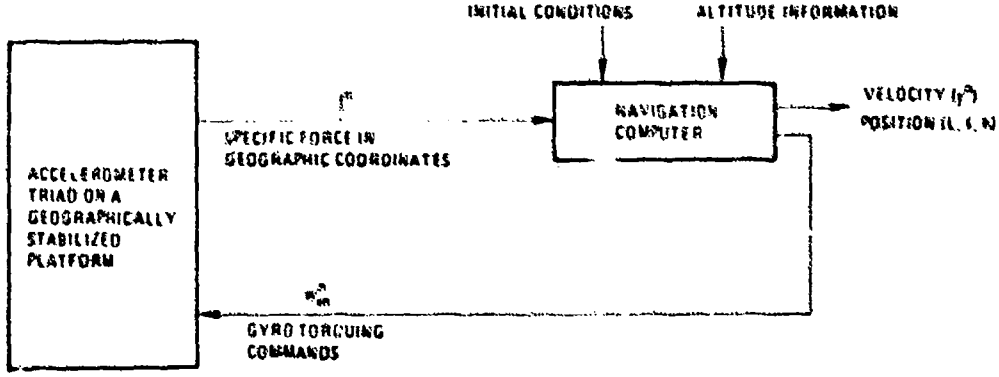

Figure 3. Platform geographic local-vertical mechanization.

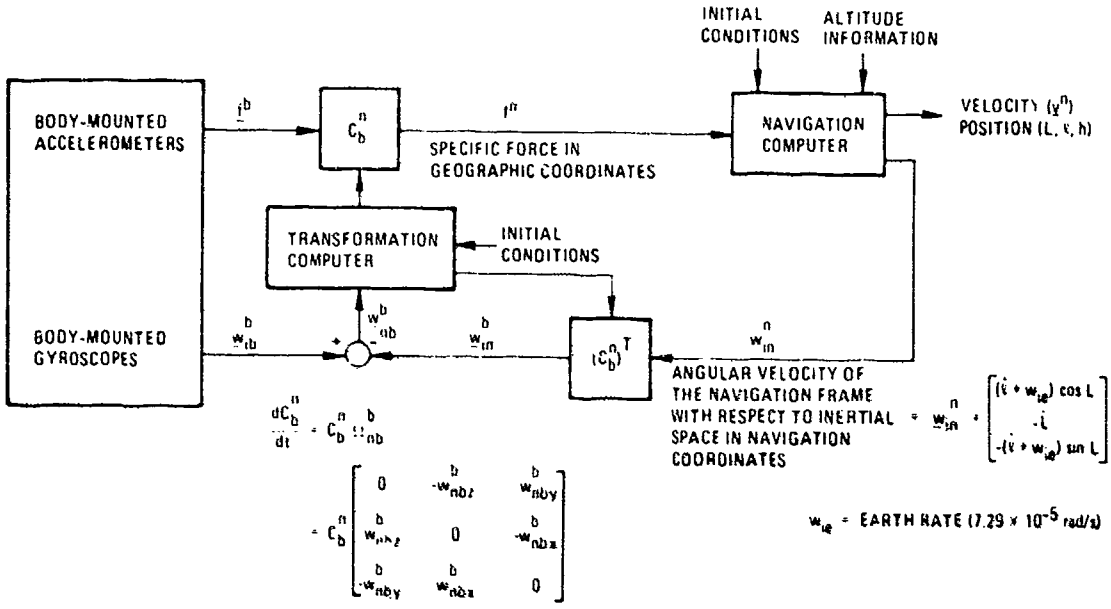

Figure 4. Strapdown system computing in geographic local-vertical coordinates.

common for gimbal systems; for strapdown systems, since the gyros measure body angular rate with respect to inertial space, the inertial frame seems more appropriate. However, since navigation information in geographic coordinates is almost always a desired output, Figure 4 is a typical mechanization.

The local-vertical frame is usually a so-called "wander azimuth" reference frame in which no attempt is made in a gimbal system to point one of the stable-member axes north as illustrated in Figure 5. This mechanization eliminates navigation errors due to errors in torquing the azimuth gyro. Two of the axes are maintained level but free to rotate in azimuth about the third axis, which is maintained along the local vertical. The same reference frame can be implemented as the computational frame for a strapdown system, as illustrated in Figure 6, where again the additional computations in the strapdown system are related to transformation of specific force via a transformation matrix between body and local-level coordinates. A reason for using this reference frame would be if the strapdown hardware were to replace a gimbal system in an operational system employing a wander-azimuth mechanization with minimum software changes.(6)

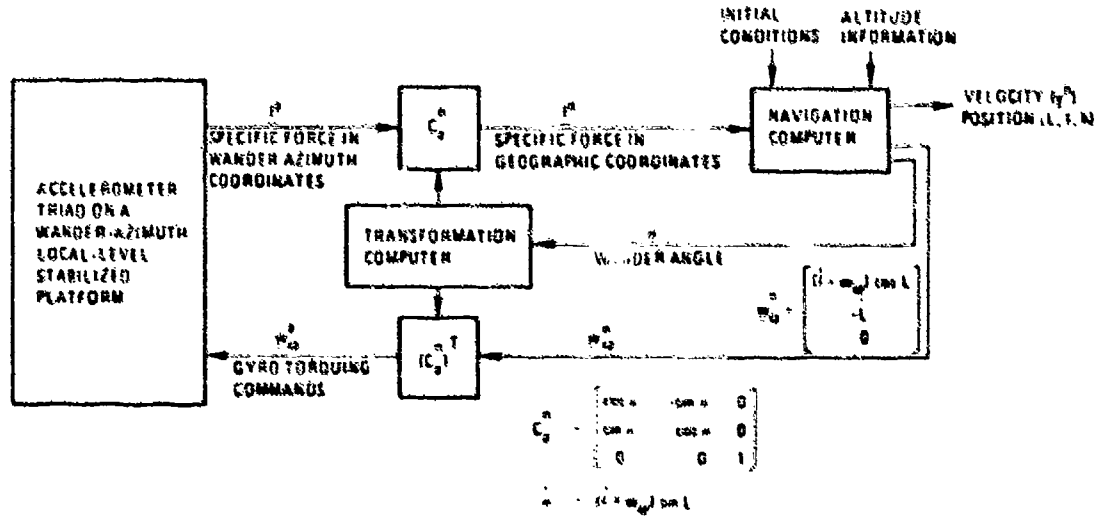

Figure 5. Platform wander-azimuth mechanization.

3. NAVIGATION ERRORS

There are significant differences in the navigation performance between the two system types because of calibration limitations, sensor inaccuracies, computational errors, and sensor-error-propagation effects. An overview of these differences will be discussed in this section; later lectures will discuss them in detail.

Calibration limitations on strapdown systems arise because the inertial sensors, which are rigidly attached to the vehicle, cannot be arbitrarily oriented at different angles to the earth's gravity and angular-velocity vectors. Conversely, a gimbal system is mechanized so that the stable-member inertial-component outputs at different orientations can be compared with the known input components of gravity or

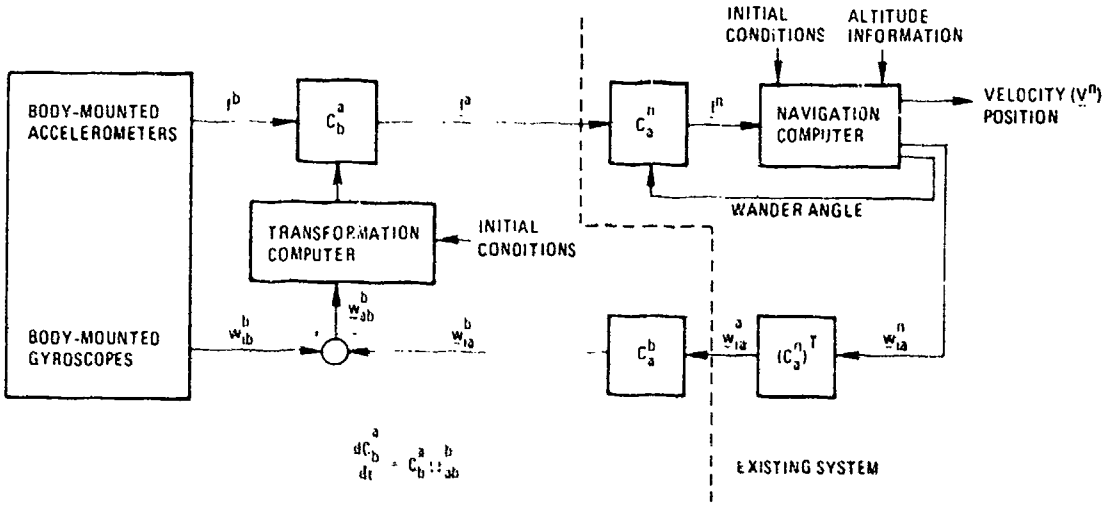

Figure 6. Strapdown wander-azimuth mechanization.

earth rate, and the sensor errors calibrated in a series of test positions that expose the error sources. Since only a few of the strapdown sensor errors (compared to a gimbal system) can be calibrated, the system designer must depend on the stability of the instruments between system removals from the vehicle for calibration. The errors that cannot be calibrated in a strapdown system propagate into navigation errors when the system begins to navigate.

Sensor inaccuracies that arise from motion of the vehicle are even more difficult to calibrate in a strapdown system. The dynamic response characteristics of the inertial sensor under consideration for use in the navigator must be well understood, and the limitations on navigation performance evaluated early in the system design. For example, in single-degree-of-freedom gyros, a gyro drift, called anisoinertia-induced drift, will be present whenever the gyro experiences vibration rates concurrently about its spin and input axes. To eliminate such an error source requires complicated compensation, so that the system designer must understand the interplay between vehicle environment, sensor design, and resulting navigation system performance when picking a particular type of gyroscope for a strapdown system.

Another major source of strapdown system error is in gyro-torquing scale-factor error, particularly asymmetrical scale-factor errors in a vibratory environment. In a gimbal system, gyro scale-factor errors usually have a small effect on navigation system performance, since the torquing angular rates are small and nearly equivalent to the angular velocity of the vehicle over the earth's surface. In a strapdown system, the gyros must also be torqued for the attitude rate of the vehicle, and consequently scale-factor-induced navigation errors can be quite large. Gyro input-axes misalignments in strapdown systems are also important for similar reasons.

A major error source in strapdown single-degree-of-freedom gyros is output-axis-rotation error. In this case, the strapdown gyro has a drift error proportional to the angular acceleration along its output axis. This error source usually dictates how the gyros are mounted in the vehicle, the output axes of two of the gyros are, for example, usually placed along the yaw axis in an aircraft application.

Computational-induced errors in strapdown systems refer to those navigation errors introduced by the incorrect transformation of the body-measured specific forces to the computational frame. The algorithm used to generate the transformation matrix, the speed at which the transformations occur, the computer word length used, and the inertial-sensor quantization all play a part in contributing to computational errors. Since this type of error also depends on the vehicle dynamic environment, most designers evaluate it by computer simulation.[7]

Sensor-induced navigation-error-propagation effects are also different in a strapdown system. For example, in a gimbal system during self-alignment, the accelerometer outputs are used to level the stable member, and the misleveling of the stable member is due primarily to accelerometer bias. When the system starts to navigate, no significant position or velocity errors occur due to this error source, since the platform-tilt-error contribution is exactly canceled by the accelerometer-bias-error contribution. In a strapdown system, where self-alignment occurs by initializing the transformation matrix using the accelerometers for level information, the same type of tilt error occurs. However, when the system starts to navigate and the vehicle heading changes, the orientation of the inertial sensors changes with respect to the alignment (or navigation) axes, and the net result is to introduce a step of acceleration error, equal to the value of the accelerometer bias if the heading changes by 90°. Subsequently, then, velocity and position errors arise from accelerometer bias.

This effect in strapdown navigation systems that have external position or velocity aiding has led to attempts to calibrate accelerometer bias in flight, since it produces an observable error in a strapdown system.

As an illustration of this effect, a simulation was conducted in which a strapdown navigator on an air-launched missile was aligned and calibrated using external velocity information provided by another inertial system on the aircraft. Figure 7 shows the maneuvers made in a horizontal plane by the aircraft during the alignment and calibration sequence.

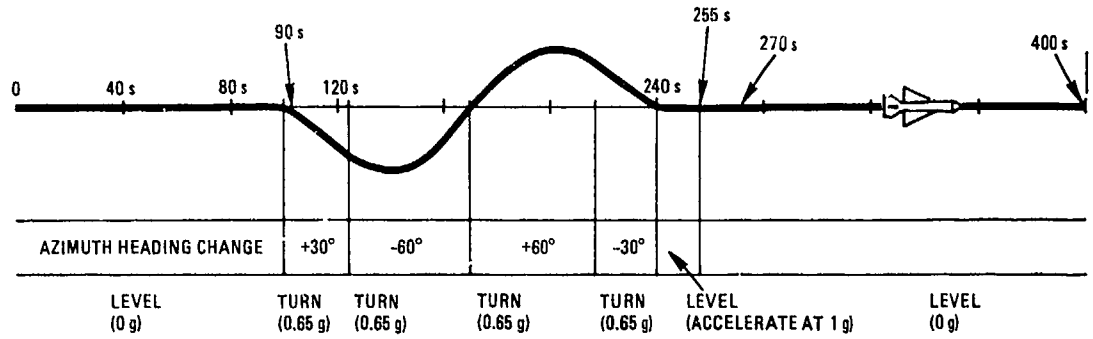

ALL AIRCRAFT TURNS ARE COORDINATED
MAXIMUM AIRCRAFT ROLL RATE = 34°/s
MAXIMUM AIRCRAFT BANK ANGLE = 34°
LAUNCH VELOCITY = MACH 1.4

Figure 7. Calibration and alignment maneuver (viewed from above).

Figure 8 gives the initial estimation uncertainties and those determined for two later times in the strapdown-system transformation matrix between body and local-vertical coordinates, and the estimation uncertainties in the strapdown gyro and accelerometer biases. An optimal filter was used for the estimation approach.[8-10] Note that the maneuvers allow alignment and calibration; after 270 seconds, when the aircraft is flying straight and level, the azimuth uncertainty begins to increase.

ERROR TERM	UNITS	rms UNCERTAINTY		
		INITIAL	AT 270 s	AT 400 s
Misalignment – North	mrad	17	0.114	0.097
Misalignment – East	mrad	17	0.114	0.096
Misalignment – Azimuth	mrad	17	0.150	0.464
Gyro Bias – Roll Axis	°/h	0.5	0.127	0.078
Gyro Bias – Pitch Axis	°/h	0.5	0.150	0.075
Gyro Bias – Yaw Axis	°/h	0.5	0.460	0.460
Accelerometer Bias – Roll	μg	100	86	82.5
Accelerometer Bias – Pitch	μg	100	91.6	88.7
Accelerometer Bias – Yaw	μg	100	65	62

Figure 8. Calibration and alignment results.

Perhaps the best means of studying navigation-error-propagation effects between different inertial-system implementations is to use a generalized covariance-analysis computer-simulation program. The analysis on which such a program was developed is given in the Appendix. The technique was based on a generalized error-analysis approach to inertial systems as derived in References 1 and 11, but in which an error was made in the difference between strapdown and gimbal systems. The approach can analyze inertial and local-vertical gimbal mechanizations, as well as strapdown systems, and has been found to be extremely useful in conducting preliminary system-design performance tradeoffs.

Detailed computer-based evaluation of performance, including algorithm errors, in a strapdown system design requires the use of a whole-number type of simulator rather than a statistical or covariance approach. Effects, such as nonlinear sensor errors and quantization errors may be quantitatively evaluated.[12] Such computer programs are used widely in the inertial-system manufacturing industry.

4. CONCLUDING REMARKS

Navigation-system implementations using strapdown systems for aircraft and ship applications will be described in the following lectures. Although not described in this Lecture Series, strapdown sensors have also had a long history of application in space vehicles and satellites. For example, the backup guidance system for the Lunar Excursion Module, in which the astronauts landed on the moon, was a strapdown system. Also, it is highly probable that strapdown systems employing extra strapdown inertial sensors for fault redundancy will be applied to aircraft in the very near future, and one of the lectures covers that topic.[13-15]

This Lecture Series should provide the basic theory of strapdown sensors and systems design, and the directions current technologies are likely to take in future strapdown implementations. The computational aspects will be treated in detail, because fortunately for strapdown implementations, the increases in processor speed together with decreasing computational costs are making the additional required computations quite easy to implement.

REFERENCES

1. Britting, K.R., Inertial Navigation Systems Analysis, Wiley-Interscience, New York, 1971.

2. Broxmeyer, C., Inertial Navigation Systems, McGraw-Hill, New York, 1962.

3. Leondes, C.T., (editor), Guidance and Control of Aerospace Vehicles, McGraw-Hill, New York, 1963.

4. Inertial Navigation - Systems and Components, AGARD Conference Proceedings, No. 43, May 1968. (AD692540)

5. Inertial Navigation - Components and Systems, AGARD Conference Proceedings, No. 116, February 1973. (AD758127)

6. Sciegienny, J., et al., Inertial Navigation System Standardized Software Development, Vol. II, Charles Stark Draper Laboratory Report R-977, Cambridge, MA, June 1976.

7. McKern, R.A., A Study of Transformation Algorithms for Use in a Digital Computer, Charles Stark Draper Laboratory Report T-493, Cambridge, MA, June 1968.

8. Leondes, C.T., (editor), Theory and Applications of Kalman Filtering, Agardograph 139, February 1970. (AD704306)

9. Schmidt, G.T., (editor), Practical Aspects of Kalman Filtering Implementation, AGARD Lecture Series No. 82, May 1976. (ADA024377)

10. Faurre, P., Navigation Inertielle Optimale et Filtrage Statistique, Dunod, Paris, 1971.

11. Britting, K., et al., North Atlantic Aided Inertial Navigation System Simulation, Vol. 1 and 2, Aerospace Systems, Inc., Burlington, MA, July 1973. (AD770072, AD770073).

12. Caffery, W., et al., Inertial Navigation Strapdown Simulator, Charles Stark Draper Laboratory Report R-969 Cambridge, MA, February 1977.

13. Gilmore, J.P., et al., SIRU - A New Inertial System Concept, Charles Stark Draper Laboratory Report E-2407, Cambridge, MA, March 1969.

14. Daly, K., et al., Development of Capability for Multifunction Integrated Reference Assembly Evaluation, Charles Stark Draper Laboratory Report R-1042, Cambridge, MA, July 1977. Also R-1135, January 1978.

15. Harrington, E., et al., "MIRA: The Multifunction Inertial Reference", NAECON Proceedings, Dayton, Ohio May 1977.

ACKNOWLEDGMENT

The author wishes to acknowledge the dedicated assitance provided by the NATO-AGARD staff, in particular Mr. R. Willaume and Mr. B. Héliot, in arranging and organizing this Lecture Series, and to the individual authors for their able participation.

APPENDIX

GENERALIZED COVARIANCE ERROR ANALYSIS

This appendix describes the equations necessary to conduct a covariance error analysis of various inertial-system configurations—space stable, local level, strapdown, and others—using one general-purpose computer program. Such a program has been implemented by the author and Mr. R. Setterlund at the Charles Stark Draper Laboratory and used in preliminary design tradeoffs of aided and unaided inertial systems.

The development of the required linearized navigation error equations for any inertial system is given in References 1 and 11, which are correct except for a term involving gyro misalignments. (In Eq. (8-112) of Reference 1, the minus sign and the transpose should be used for all systems.) The equations are formulated such that the error state vector for all inertial-system mechanizations is composed of the system's attitude, velocity, and position errors, where the attitude error is defined as the orthogonal transformation error between computed navigation axes (north, east, and down) and true navigation axes. The resulting state-space equation, valid for any inertial-system mechanization is of the form required for covariance analysis

$$\dot{\underline{x}} = F\underline{x} + G\underline{q} \tag{A-1}$$

where $\underline{x}$ is the nine-dimensional error state vector

$$\underline{x} = \begin{bmatrix} \delta\theta_N \\ \delta\theta_E \\ \delta\theta_D \\ \delta\dot{L} \\ \delta\dot{\ell} \\ \delta\dot{h} \\ \delta L \\ \delta\ell \\ \delta h \end{bmatrix}$$

- $\delta\theta_N$ attitude error around the north axis
- $\delta\theta_E$ attitude error around the east axis
- $\delta\theta_D$ attitude error around the vertical axis
- $\delta\dot{L}$ latitude rate error
- $\delta\dot{\ell}$ longitude rate error
- $\delta\dot{h}$ altitude rate error
- δL latitude error
- $\delta\ell$ longitude error
- δh altitude error

and $G\underline{q}$ is a nine-dimensional vector of forcing errors to be described later.

For systems that employ barometric damping in a second-order loop (as shown in Figure A-1) the F matrix is given by Eq. (A-2).

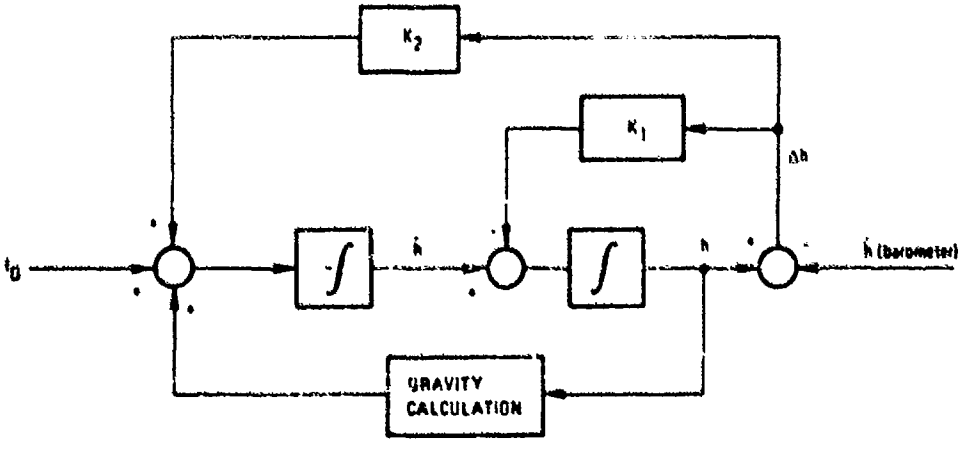

WHERE

f_D = SPECIFIC FORCE IN THE "DOWN" DIRECTION
h = ALTITUDE
K_1, K_2 = ALTIMETER LOOP GAINS

Figure A-1. Barometric damping loop.

$$\frac{d}{dt}\begin{bmatrix}\delta\theta_N\\ \delta\theta_E\\ \delta\theta_D\\ \delta\dot{L}\\ \delta\dot{\ell}\\ \delta\dot{h}\\ \delta L\\ \delta\ell\\ \delta h\end{bmatrix} = \underbrace{\begin{bmatrix} 0 & F_{12} & F_{13} & 0 & F_{15} & 0 & F_{17} & 0 & 0\\ F_{21} & 0 & F_{23} & F_{24} & 0 & 0 & 0 & 0 & 0\\ F_{31} & F_{32} & 0 & 0 & F_{35} & 0 & F_{37} & 0 & 0\\ 0 & F_{42} & F_{43} & F_{44} & F_{45} & F_{46} & F_{47} & 0 & F_{49}\\ F_{51} & 0 & F_{53} & F_{54} & F_{55} & F_{56} & F_{57} & 0 & F_{59}\\ F_{61} & F_{62} & 0 & F_{64} & F_{65} & 0 & F_{67} & 0 & F_{69}\\ 0 & 0 & 0 & 1 & 0 & 0 & 0 & 0 & 0\\ 0 & 0 & 0 & 0 & 1 & 0 & 0 & 0 & 0\\ 0 & 0 & 0 & 0 & 0 & 1 & 0 & 0 & -K_1 \end{bmatrix}}_{F}\begin{bmatrix}\delta\theta_N\\ \delta\theta_E\\ \delta\theta_D\\ \delta\dot{L}\\ \delta\dot{\ell}\\ \delta\dot{h}\\ \delta L\\ \delta\ell\\ \delta h\end{bmatrix} \qquad (A\text{-}2)$$

where

$F_{12} = -\dot{\lambda}\sin(L)$

$F_{13} = \dot{L}$

$F_{15} = \cos(L)$

$F_{17} = -\dot{\lambda}\sin(L)$

$F_{21} = \dot{\lambda}\sin(\,.\,)$

$F_{23} = \dot{\lambda}\cos(L)$

$F_{24} = -1$

$F_{31} = -\dot{L}$

$F_{32} = -\dot{\lambda}\cos(L)$

$F_{35} = -\sin(L)$

$F_{37} = -\dot{\lambda}\cos(L)$

$F_{42} = -f_D/R$

$F_{43} = f_E/R$

$F_{44} = -2\dot{h}/R$

$F_{45} = -\dot{\lambda}\sin(2L)$

$F_{46} = -2\dot{L}/R$

$F_{47} = -\dot{\ell}(\dot{\ell} + 2w_{ie})\cos(2L)$

$F_{49} = -[\ddot{L} + \dot{L}(\dot{\ell} + 2w_{ie})\sin(2L)/2]/R$

$F_{51} = f_D/(R\cos(L))$

$F_{53} = -f_N/(R\cos(L))$

$F_{54} = 2\dot{\lambda}\tan(L)$

$F_{55} = -2[(\dot{h}/R) - \dot{L}\tan(L)]$

$F_{56} = -2\dot{\lambda}/R$

$F_{57} = [\ddot{\ell} + (2/R)\dot{\ell}\dot{h}]\tan(L) + 2\dot{\lambda}\dot{L}$

$F_{59} = -[\ddot{\ell} - 2\dot{L}\dot{\lambda}\tan(L)]/R$

$F_{61} = f_E$

$F_{62} = -f_N$

$F_{64} = 2R\dot{L}$

$F_{65} = 2R\dot{\lambda}\cos^2(L)$

$F_{67} = -R\dot{\ell}(\dot{\ell} + 2w_{ie})\sin(2L)$

$F_{69} = \dot{L}^2 + \dot{\ell}(\dot{\ell} + 2w_{ie})\cos^2(L) + 2w_s^2 - K_2$

and where

f_N, f_E, f_D = north, east, down, components of specific force

L, ℓ, h = latitude, longitude, altitude

$\dot{\lambda}$ = celestial longitude rate ($= \dot{\ell} + w_{ie}$)

w_{ie} = earth rate (7.2921×10^{-5} rad/s)

R = radius from earth center to platform (function of L and h)

K_1, K_2 = altimeter loop gains

$w_s = \sqrt{g/R}$ = Schuler frequency

g = gravity (function of L and h)

All of the quantities in F, such as L, $\dot{L}$, etc., are functions of the vehicle's trajectory, and must be provided by the simulation program.

The matrix G is a 9×10 matrix

$$G = \left[\begin{array}{c|c|c|c} C_g^n & 0 & 0 & \begin{matrix}0\\0\\0\end{matrix} \\ \hline 0 & DC_a^n & D & \begin{matrix}0\\0\\K_2\end{matrix} \\ \hline 0 & 0 & 0 & \begin{matrix}0\\0\\K_2\end{matrix} \end{array}\right] \qquad \text{(A-3)}$$

where

C_g^n = direction-cosine transformation from nominal gyro axes to geographic navigation axes. This is a function of platform mechanization.

C_a^n = direction-cosine transformation from nominal accelerometer axes to geographic navigation axes. This is a function of platform mechanization.

D = transformation matrix relating linear velocity errors to latitude and longitude rate errors.

$$D = \begin{bmatrix} \frac{1}{R} & 0 & 0 \\ 0 & \frac{1}{R\cos(L)} & 0 \\ 0 & 0 & -1 \end{bmatrix} \qquad \text{(A-4)}$$

The 10×1 vector $\underline{q}$ is

$$\underline{q} = \begin{bmatrix} \delta\underline{w}_{ip}^p \\ \delta\underline{f}_{ip}^p \\ \Delta\underline{G}^n \\ \delta h \end{bmatrix} \qquad \text{(A-5)}$$

where

$\delta\underline{w}_{ip}^p$ = angular velocity error of the platform with respect to inertial space in platform coordinates, due to gyro-related errors (bias, scale factor, nonorthogonality, etc.)

$\delta\underline{f}_{ip}^p$ = specific-force measurement error due to accelerometer-related errors (bias, scale factor, nonorthogonality, etc.)

$\Delta\underline{G}^n$ = deviation of gravitational field from that associated with the reference ellipsoid, expressed in the geographic navigation frame

δh = altimeter bias

The differences between various inertial mechanizations are reflected in the matrices C_g^n and C_a^n, and in the vector $\underline{q}$. For example, the transformation matrices for several systems will be written for the case

$$C_g^n = C_a^n \tag{A-6}$$

and assuming the inertial system mechanized is initially aligned to the geographic axes.

(1) Space-Stable Inertial Mechanization

$$C_g^n = \begin{bmatrix} -\sin(L)\cos(\lambda) & -\sin(L)\sin(\lambda) & \cos(L) \\ -\sin(\lambda) & \cos(\lambda) & 0 \\ -\cos(L)\cos(\lambda) & -\cos(L)\sin(\lambda) & -\sin(L) \end{bmatrix} \tag{A-7}$$

(2) Local-Vertical Geographic

$$C_g^n = I \tag{A-8}$$

(3) Wander-Azimuth Local Level

$$C_g^n = \begin{bmatrix} \cos\alpha & -\sin\alpha & 0 \\ \sin\alpha & \cos\alpha & 0 \\ 0 & 0 & 1 \end{bmatrix} \tag{A-9}$$

(4) Strapdown

C_g^n = function of strapdown system orientation with respect to the vehicle, and vehicle attitude (pitch, roll, heading)

Reference (1) also lists several other inertial-system mechanizations.

The specific terms used in the forcing vector $\underline{q}$ depend upon the error sources of the inertial instruments. In the improbable event that $\underline{q}$ can be modeled as white noise, then the covariance-analysis approach can be applied directly to Eq. (A-1).

Usually $\underline{q}$ will be made up of bias errors, orthogonality errors, acceleration-sensitive terms, and so on, which will then require further matrix partitioning and augmentation of the error state vector before a covariance analysis can be applied. This effort is quite laborious, but when completely programmed will provide an extremely flexible analysis tool.

STRAPDOWN SENSORS

By

2-1

Paul G. Savage
Staff Engineer, Navigation Systems
Honeywell Inc., Avionics Division
2600 Ridgway Parkway NE
Minneapolis, Minnesota 55413

SUMMARY

Gyros and accelerometers currently available for strapdown-digital-system application are described and compared. Instruments discussed are the single-degree-of-freedom floated rate-integrating gyro, the tuned-rotor gyro, the electrostatic gyro, the laser gyro, and the pendulous accelerometer. For each sensor, the theory of operation and mechanization approach is described, an analytical error model is developed, performance characteristics are analyzed (relative to the other sensors), advantages and limitations are discussed, and application areas identified. A section is included describing torque-loop electronic design approaches that have been utilized with the torque-rebalance strapdown sensors (the floated gyro, tuned-rotor gyro, and the pendulous accelerometer).

1. INTRODUCTION

The state of the art in strapdown inertial navigation technology has achieved a level of maturity in recent years that makes it a serious contender for general avionics usage in the near future. Computer limitations, which handicapped strapdown compared to gimbaled technology in the past, are now virtually nonexistent due to the advent of the low-cost, high-speed minicomputer. Recent advances in gyro technology, particularly the laser gyro, (1, 2) have virtually eliminated the dynamic-range problems that previously limited the accuracy potential of strapdown systems. The capabilities of today's strapdown technology have been demonstrated to be in the classical 1-nmi/h gimbaled performance category, (3, 4, 5, 6) with production system costs projected to be one half that of gimbaled systems with comparable accuracy (7, 8, 9). The traditional strapdown versus gimbaled tradeoffs used by strapdown proponents for the past decade to tout the advantages of strapdown technology must now be given more serious evaluation. Due to the assortment of strapdown sensor types available today, the tradeoff analyses must extend to the sensor level such that overall system capabilities can be assessed for the particular strapdown mechanizations available.

This paper describes the operating characteristics, performance capabilities, and limitations of the inertial sensors (gyros and accelerometers) that are available for strapdown application. The primary focus is on the available gyro technology, since this has traditionally been the determining factor for strapdown (and gimbaled) system performance. Accelerometers are also addressed because, more-so than in gimbaled applications, strapdown accelerometers can have a significant impact on overall system performance, particularly the effect of accelerometer bias and alignment error on system velocity accuracy (10, 11). Strapdown gyro technology has now advanced to the point where the accelerometer has become a major portion of the system error budget. As the gyro technology further evolves, the accelerometer may well become the limiting error source for strapdown systems unless new accelerometer designs are developed specifically for strapdown application. Work in this regard has been initiated, although not yet at the level of funding dedication being afforded to the strapdown gyro.

Gyros analyzed in this paper are the floated rate-integrating gyro, tuned-rotor gyro, electrostatic gyro, and the laser gyro. The discussion on accelerometers is limited to the pendulous torque-to-balance type because this instrument, originally designed for gimbaled applications, continues to be the mainstream acceleration-sensing device being utilized for strapdown applications. A separate section is included on torque-loop electronics mechanization approaches for torque-to-balance instruments. Three of the sensors discussed require such electronics as an integral part of their operation (and performance) in strapdown applications.

For each of the sensors, a functional description is provided defining the basic hardware configuration of the device and its principle of operation. An analytical description is presented which defines the input/output characteristics of each unit, identifying its error sources and dynamic characteristics. Finally, a performance assessment is provided that categorizes the sensor accuracy capabilities, limitations, and associated application areas.

2. SENSOR PERFORMANCE REQUIREMENTS

Table 1 defines the accuracy capabilities typically required from strapdown sensors in two application areas: the 1-nmi/h accuracy long-term (1 to 10 hours) terrestrial strapdown inertial navigation system (INS), and the strapdown Attitude and Heading Reference System (AHRS). The performance figures in Table 1 for the two systems represent the upper and lower ends of the performance requirements spectrum for strapdown sensors in general. The INS application is the most demanding and has only recently been achievable; the AHRS area is representative of a broader class of strapdown applications, some of which have been in production for the past few years (e. g., tactical missile midcourse guidance).

With regard to rate-gyro bandwidth requirements in Table 1, the indicated levels are needed in the high-performance area in severe vibration dynamic environments to assure that adequate data is provided to the system computer defining the angular vibrations of the sensor assembly. Failure to account for correlated out-of-phase angular vibrations in two axes (i. e., coning) produces an error in the system computer due to the inability to account for actual attitude movement developed about the third axis from

kinematic rectification (or noncommutativity). (13, 60) For the AHRS-type applications, bandwidth is generally determined by strapdown rate signal output requirements for other vehicle functions (e. g., stabilization).

Table 1. Typical Strapdown Sensor Performance Requirements

Performance Parameter	Performance Requirements	
	Inertial Navigator	AHRS
Gyro Rate Range (deg/sec)	100-400	100-400
Gyro Bias Uncertainty (deg/hr)	0.01	1.0-10.0
Gyro Random Noise (deg/$\sqrt{hr}$)*	0.003	0.2
Rate-Gyro Scale-Factor Uncertainty (ppm)	5-50	100-1000
Rate-Gyro Scale-Factor Low Rate Assymetry (ppm)	1	100
Rate-Gyro Bandwidth (Hz)	30-300	30-80
Rate-Gyro Output-Pulse Quantization ($\widehat{sec}$)	2-10	10-100
Attitude Gyro Readout Uncertainty ($\widehat{sec}$)	10	200
Accelerometer Bias Uncertainty (μg)	50	1000
Accelerometer Scale-Factor Uncertainty (ppm)	200	1000
Sensor Alignment Uncertainty ($\widehat{sec}$)	5	200
Sensor Warm-Up Time (min)	1-5	0.5-1.0
Sensor Minimum Calibration Interval (yr)	0.5	2

*Note: This error source is a characteristic principally of laser gyros (see Section 7.2). It should be noted that the other gyros also have random noise output errors, but generally with a narrower-bandwidth and lower-amplitude power-spectral-density compared to the laser gyro.

The calibration interval requirement in Table 1 is an important performance consideration for strapdown systems in high-accuracy applications due to the need to remove the sensor assembly from the user vehicle when calibration is necessary (for turntable testing to excite the measurable sensor errors and to separate g-sensitive errors and earth-rate input effects)*. In essence, a strapdown sensor assembly calibration requirement imposes the same burden on the user as any other maintenance action; hence, it is generally considered a part of the equipment Mean-Time-Between-Removals (MTBR) reliability figure. For gimbaled systems, the gimbal assembly can be utilized to perform the test turntable function, and the system can be calibrated aboard the user vehicle through a special built-in-test mode.

3. SINGLE-DEGREE-OF-FREEDOM FLOATED RATE-INTEGRATING GYRO

The floated rate-integrating gyro (16, 17, 18, 19, 20, 12) pictured schematically in Figure 1 is the gyro with the longest production history and is the original high-accuracy gimbaled-platform gyro. The device consists of a cylindrical hermetically sealed momentum-wheel/spinmotor assembly (float) contained in a cylindrical hermetically sealed case. The float is interfaced to the case by a precision suspension assembly that is laterally rigid (normal to the cylinder axis) but allows "frictionless" angular movement of the float relative to the case about the cylinder axis. The cavity between the case and float is filled with a fluid that serves the dual purpose of suspending the float at neutral buoyancy, and providing viscous damping to resist relative float-case angular motion about the suspension axis.

A ball-bearing or gas-bearing synchronous-hysteresis spinmotor is utilized in the float to maintain constant rotor spinspeed, hence constant float angular momentum. A signal-generator/pickoff provides an electrical output signal from the gyro proportional to the angular displacement of the float relative to the case. An electrical torque generator provides the capability for applying known torques to the float about the suspension axis proportional to an applied electrical input current. Delicate flex leads are used to transmit electrical signals and power between the case and float.

Under applied angular rates about the input axis, the gyro float develops a precessional rate about the output axis (rotation rate of the angle sensed by the signal-generator/pickoff, see Figure 1). The pickoff-angle rate generates a viscous torque on the float about the output axis (due to the damping fluid) which sums with the electrically applied torque-generator torque to precess the float about the input axis

*It should be noted that a composite-bias calibration procedure has been demonstrated on single-degree-of-freedom floated rate-integrating gyros (14, 15) that can be accomplished statically and therefore, in the user vehicle. Conceptually, the method is to measure the gyro output with the spinmotor operating at two different speeds (e. g., forward and reverse). A comparison between the two readings allows the gyro-bias to be separated from earth-rate input. This calibration technique is limited by its inability to separate g-insensitive from g-sensitive error terms, the inability to measure gyro scale factor errors, and the problem of predicting user vehicle movement during the period when the gyro spinmotor speed is being changed such that performance can be compared in equivalent reference frames.

at the gyro input rate. The pickoff-angle rate thereby becomes proportional to the difference between the input rate and the torque-generator precessional rate; hence the pickoff angle becomes proportional to the integral of the difference between the input and torque-generator rates.

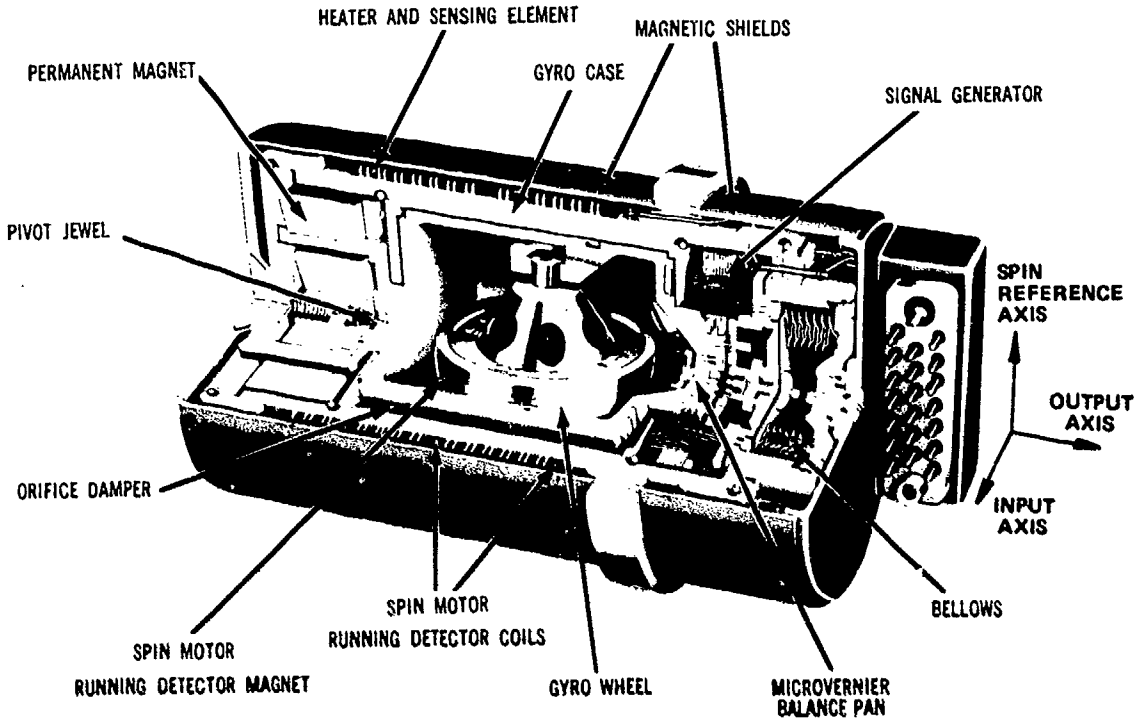

Figure 1. Honeywell GG87 single-degree-of-freedom floated-rate-integrating gyro.

To operate the gyro in a strapdown mode, the pickoff angle is electrically servoed to null by the torque generator which is driven by the signal-generator/pickoff output (through suitable compensation and amplifier electronics). The time integral of the difference between the input and torque-generator precessional rates is thereby maintained at zero, and the integral of the torque-generator rate becomes proportional to the integral of the input rate. Thus, the integral of the torque-generator electrical current provides a measure of the integral of input rate for a rate-gyro strapdown inertial navigation system.

3.1 General Design Considerations

The suspension assembly for the floated gyro is typically of the pivot-and-jewel type. Some units additionally employ a magnetic suspension around the pivots to eliminate friction under benign flight conditions, and to compensate for off-nominal flotation.

The signal-generator/pickoff is either of the moving-coil or variable-reluctance type. For the moving-coil pickoff, a small receiver coil is mounted to the float and an a-c excitation coil is attached to the case. Movement of the float relative to the case modifies the flux linkage sensed by the receiver coil; hence, a d-c voltage-output is generated from the receiver coil proportional to float-case angular displacement. For the variable-reluctance pickoff, the excitation and receiver coils are mounted to the case, and a soft-iron assembly is attached to the float in the flux return path between the excitation and receiver coils. Movement of the float relative to the case varies the orientation of the soft iron in the excitation field, thereby modifying the return flux to the receiver coil. The receiver-coil voltage thereby becomes proportional to float-case angular displacement. The tradeoff between the two pickoff approaches is the addition of two flex leads (and associated error-torque uncertainties on the float) for the moving-coil pickoff versus increased error-torque magnetic sensitivity (to internally generated fields) for the variable-reluctance pickoff.

The floated gyro torque-generator is either of the permanent-magnet or electromagnetic (microsyn) type. For the permanent-magnet torquer, a coil cup is attached to the float (or case) and a permanent magnet is mounted to the case (or float). Applied electrical current to the torquer coil generates magnetic flux which interacts with the permanent-magnet field, thereby producing a torque on the float. The tradeoff between a case-versus float-mounted magnet is the addition of two flex leads (for the case-mounted magnet) versus increased float size and increased error-torque magnetic sensitivity to internally generated fields (for the float-mounted magnet). For the electro-magnetic torquer, a soft iron assembly is mounted to the float, and an electromagnetic coil is attached to the case. Applied current to the coil generates a magnetic field that interacts with the iron to produce the desired torque on the float. The advantage of the electromagnetic torquer is the elimination of the permanent magnet and associated scale-factor variations due to aging (field strength decay), and the ability to implement the torque generator without flex leads. Disadvantages are increased torquer scale-factor nonlinearities and thermal sensitivities, and increased float magnetic-error-torque susceptability to internally generated fields.

2.4

3.2 Analytical Description and Error Model

Consider the float assembly for the single-degree-of-freedom floated rate-integrating gyro, and define a coordinate frame for it with z along the rotor spin axis, y along the float suspension axis, and x to complete the orthogonal triad (as shown in Figure 2). The torque-momentum transfer equation for the float assembly about the float (y) axis is

$$\tau_y = J_y\dot{\omega}_y + (J_x - J_z)\,\omega_z\omega_x - \omega_x J_r\omega_r \qquad (1)$$

where

τ_y = net torque on the float assembly about the y axis

$\omega_x, \omega_y, \omega_z$ = inertial angular rates of rotation of the float assembly about the x, y, and z axes

ω_r = angular rate of the rotor relative to the float (about z)

J_x, J_y, J_z = moments of inertia of the float assembly (including the rotor) about the x, y, and z axes

J_r = moment of inertia of the rotor about the spinmotor axis

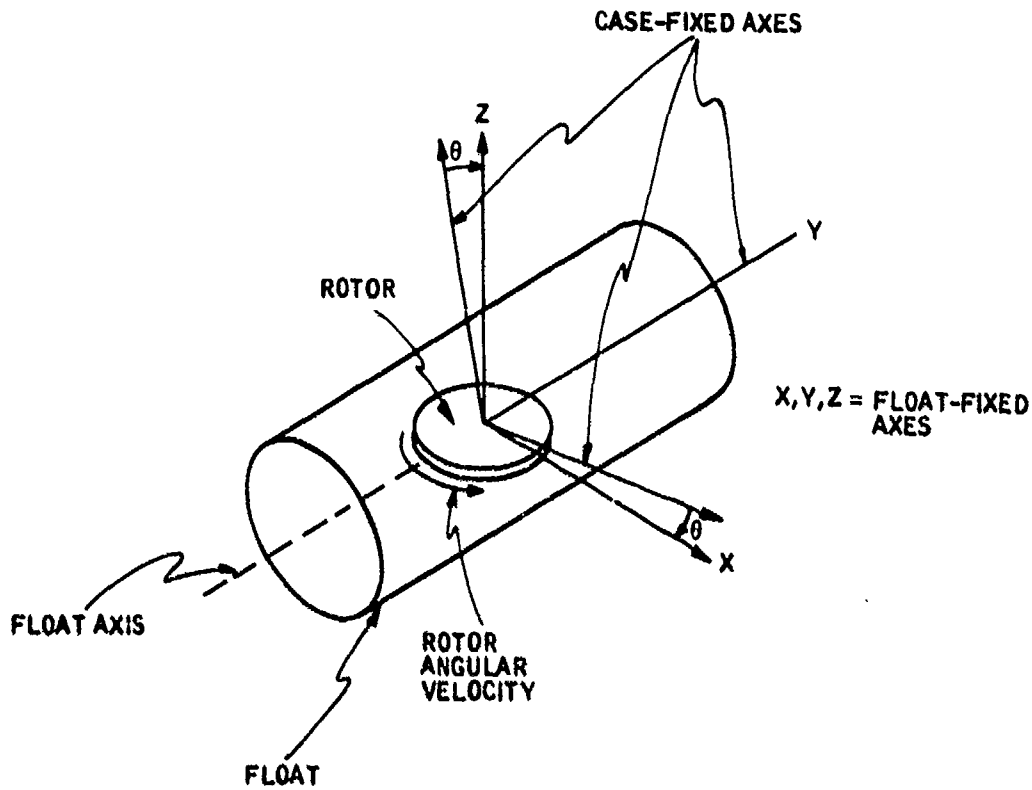

Figure 2. Gyro gimbal and case axes.

The corresponding momentum-transfer equation for the rotor about the spin axis is

$$J_r(\dot{\omega}_z - \dot{\omega}_r) = \tau_r = f(\delta\omega_r) \qquad (2)$$

with

$$\delta\omega_r = \omega_r - \omega_o \qquad (3)$$

where

ωr_o = nominal spinmotor rotor speed

$\delta\omega_r$ = variation in the rotor speed from nominal

τ_r = rotor spinmotor torque designed to maintain nominal rotor speed (i.e., hold $\delta\omega_r$ at null)

$f(\delta\omega_r)$ = functional operator indicating that the spinmotor torque is a function of the deviation of the rotor speed from nominal

The torque on the float assembly (τ_y in Eq. (1)) is composed of three terms: viscous flotation-fluid torques due to rotation rates of the float about the float axis relative to the gyro case; torques intentionally applied to the float assembly through the electromagnetic torque-generator; and unwanted torques due to imperfections in the gyro from its idealized theoretical configuration

$$\tau_y = -C\dot{\theta} + \tau_T + \tau_e \tag{4}$$

where

C = viscous torque coefficient

θ = angle of the gyro relative to the gyro case (that would be sensed by the gyro signal-generator/pickoff)

τ_T = applied torque-generator torque

τ_e = unwanted error-torque

The torque-generator torque in Eq. (4) is defined in terms of the input axis (x) precessional rate it is intended to generate (a torquer-input command-rate) with an associated torquer scale-factor error (the error in realizing the torquer command-rate)

$$H_o = J_r \omega r_o$$
$$\tau_T = -\frac{H_o}{(1+\epsilon)}\omega_T \tag{5}$$

where

H_o = nominal gyro angular momentum

ω_T = intended torque-generator-induced precessional rate

ϵ = torque-generator (and associated electronics) scale-factor error

The unwanted error-torque in Eq. (4) is equated to a bias rate which is defined as the torque-generator-input command-rate needed to nullify the effect of the error torque on the float

$$\tau_e = \frac{H_o}{(1+\epsilon)}\omega_B \tag{6}$$

where

ω_B = gyro bias rate

The float angular rates in Eq. (1) can be related to angular rates along nominal gyro axes*. The float is misaligned from the gyro case by the pickoff angle (θ) and the gyro case may be misaligned from the nominal gyro axes (due to imperfections in the gyro mounting surfaces and the gyro-system mounting), hence

$$\omega_x = \omega_{IA} + \gamma_{SRA}\omega_{OA} - (\gamma_{OA} + \theta)\omega_{SRA}$$
$$\omega_y = \omega_{OA} + \gamma_{IA}\omega_{SRA} - \gamma_{SRA}\omega_{IA} + \dot{\theta} \tag{7}$$
$$\omega_z = \omega_{SRA} + (\gamma_{OA} + \theta)\omega_{IA} - \gamma_{IA}\omega_{OA}$$

where

IA, OA, SRA = nominal gyro axes (IA = input axis, OA = output axis, SRA = spin-reference axis, Figure 1)

$\omega_{IA}, \omega_{OA}, \omega_{SRA}$ = angular rates of the gyro about the nominal gyro axes

$\gamma_{IA}, \gamma_{OA}, \gamma_{SRA}$ = misalignments of the gyro case axes relative to nominal gyro axes

*Nominal gyro axes are defined as the gyro axis orientation assumed in the strapdown system computer.

Eq. (3) through (7) are now substituted into Eq. (1) to obtain the input/output equation for the single-degree-of-freedom floated rate-integrating gyro. After neglecting higher-order effects and rearranging, the result is

$$\omega_T = (1+\epsilon)\Big[\omega_{IA} + \gamma_{SRA}\omega_{OA} - (\gamma_{OA} + \theta)\,\omega_{SRA} + \frac{(J_z - J_x)}{H_o}\,\omega_{SRA}\,\omega_{IA} + \frac{J_r}{H_o}\,\omega_{IA}\,\delta\omega_r\Big] + \omega_B - \frac{1}{H_o}\left[J_y(\dot{\omega}_{OA} + \ddot{\theta}) + C\dot{\theta}\right] \tag{8}$$

The associated equation for the $\delta\omega_r$ spinmotor rate variation is similarly obtained from Eq. (2) and (3)

$$\dot{\delta\omega}_r = \dot{\omega}_s - \frac{1}{J_r}\,f(\delta\omega_r) \tag{9}$$

Equation (8) shows that the command rate (ω_T) input to the gyro torque generator is proportional to the gyro input rate (ω_{IA}), plus dynamic and cross-coupling effects, the principal one being the $C\theta$ term. The integral of Eq. (8) can be rearranged to show that the pickoff angle (θ) is principally proportional to the integral of the difference between the torque-generator command rate and the gyro input rate.

The floated rate-integrating gyro can be utilized in two basic modes of operation: open loop and closed loop. For open-loop operation, the gyro pickoff angle (θ) is used to measure single-axis attitude variations from nominal of a platform to which the device is mounted. The nominal attitude is the integral of the command-rate (ω_T). For such applications, the platform attitude about the gyro input-axis is controlled (e. g., by servomotors in the case of a gimbaled inertial navigation platform) to maintain the gyro pickoff angle at null. The platform can then be made to rotate at a specified rate about the input-axis by torquing the gyro with ω_T equal to the desired rotation rate. The platform controller will drive the platform to maintain θ at null, thereby driving ω_{IA}, the platform rate, to equal ω_T in the integral sense.

The closed-loop mode of operation is utilized in strapdown applications where the gyro is used to sense input rate. In the closed-loop mode, the gyro is electrically caged by generating a command rate into the torque-generator to maintain the pickoff angle θ at null. Figure 3 is a block diagram of Eq. (8) and (9) illustrating this concept. From the block diagram it should be apparent that for proper dynamic characteristics designed into the gyro torque-generator electronics, the pickoff angle can be maintained near null with the resulting torque-generator command-rate (ω_T) becoming proportional to the input rate (ω_{IA}) in the integral sense (plus additional error terms). The bandwidth (or dynamic response time) of the instrument (output ω_T compared to input ω_{IA}) is determined by the gain and form of the command-electronics mechanization. Several approaches are possible as described in Section 4.

The input-error terms in Figure 3 that corrupt the accuracy of the gyro in measuring ω_I are the mechanical misalignment errors (γ_{OA} and γ_{SRA}), the float-to-case misalignment angle error (θ), output-axis angular acceleration ($\dot{\omega}_{OA}$), anisoinertia effects ($J_z - J_x$), spinmotor loop dynamics ($f(\delta\omega_r)$), torque-generator/electronics scale-factor error (ϵ), and gyro bias errors (ω_B). The float-to-case misalignment error is caused by signal-generator/pickoff angle bias (pickoff null different from θ null), and dynamic effects in the torque loop. (12) The anisoinertia, spinmotor dynamic, and angular acceleration effects, as well as the bandwidth limitations of the device (which impacts the pickoff misalignment error), are design limitations intrinsic to the basic gyro concept. The remaining errors (mechanical misalignment, pickoff-angle detector bias, scale-factor error, and bias error) are caused by imperfections in the gyro that deviate from the theoretically perfect design.

A typical model of the scale-factor error for the floated gyro in the strapdown closed-loop mode of operation is given by

$$\epsilon = \epsilon_o + \epsilon_1 \frac{\omega_{IA}}{|\omega_I|} + \epsilon_2\,\omega_{IA} + \epsilon_3\,\omega_{IA}^2 \tag{10}$$

where

- ϵ_o = basic "fixed" scale-factor error
- ϵ_1 = scale factor asymmetry error (positive scale factor different from negative scale factor)
- ϵ_2, ϵ_3 = linearity-error effects that modify the scale-factor error under high rates

The scale-factor-linearity errors are functions of the torque-loop mechanization approach utilized, and, for a permanent-magnet torque-generator, the tightness of the torquing loop (ability to minimize pickoff angle movement which could produce variations in the electromagnetic interface between the gyro-torquer-coil and torquer-magnets). The presence of the ϵ_1 coefficient depends on the torque-loop electronics implementation utilized (see Section 4.). If the term exists, it can be particularly troublesome due to its ability to rectify low rate oscillatory inputs (such as vehicle limit-cycling). The ϵ_o coefficient is dependent on the torque-generator temperature (due principally to torquer magnetic-field-strength thermal sensitivity), and to scale-factor error in the torque-loop electronics.

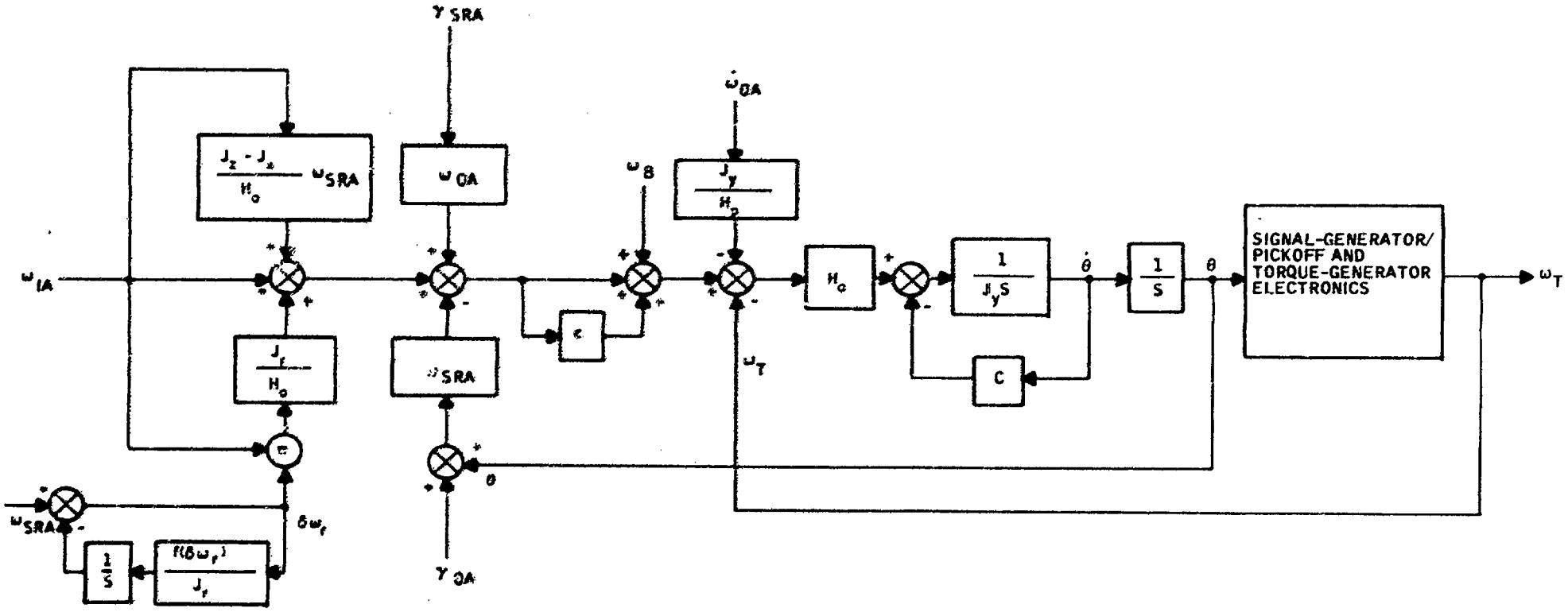

NOTE: ⊙ = MULTIPLICATION

Figure 3. Single-degree-of-freedom floated-rate-integrating gyro analytical response diagram.

The ω_B bias error includes several effects associated with manufacturing tolerances and electromechanical instabilities. A typical error model for the bias is illustrated by Eq. (11)

$$\omega_B = B_0 + B_1 a_{IA} + B_2 a_{SRA} + B_3 a_{IA} a_{SRA} + n \qquad (11)$$

where

a_{IA}, a_{SRA} = accelerations of the gyro along the input (IA) and spin-reference (SRA) axes

B_0 = g-insensitive bias error

B_1 = g-sensitive bias coefficient created from gyro float mass unbalance (relative to the gimbal pivots) along the spinmotor axis. (A principal error source in this regard is movement of the rotor along the spin axis due to spinmotor bearing compliance.)

B_2 = g-sensitive bias coefficient created from float mass-unbalance along the input axis

B_3 = anisoelastic bias error coefficient created by unequal compliance of the gyro float assembly along the input and spin axes

n = zero-mean random bias term representable as a stochastic noise process

For the floated rate-integrating gyro, the B_0 term is typically caused by residual flex-lead torques, residual thermal gradients across the gyro that produce flotation-fluid flow around the float assembly, magnetic torques on the float assembly caused by eddy current fields from the gyro case (generated from stray spinmotor fields entering the case), pivot torques due to off-nominal flotation in gyros without magnetic suspensions (caused by fluid temperature variations and float manufacturing tolerances), pivot stiction due to pivot reaction torque under gyro rotations about the output axis (the torque needed to precess the float about the input axis), and torque-loop/pulse-electronics bias errors (for binary torque-loops, or analog torque-loops with follow-up analog-to-digital conversion; see Section 4).

Random noise is created by zero mean instabilities in the gyro that have short correlation times (i.e., minutes or less). Examples are variations in the g-insensitive bias due to variations in pivot friction, and variations in the g-sensitive bias due to random movements of the rotor along the spin axis.

In general, the B and c coefficients in Eq. (10) and (11) have predictable and unpredictable components. The predictable components can be measured a priori and used in the inverse sense to correct (compensate) the gyro-output data (typically in the system computer where the gyro data is input). The B, c coefficients can be modeled in the computer as simple constants, or in the more sophisticated applications, can include predictable temperature variations as functions of sensor temperature measurements. The degree to which the measured coefficients characterize the actual gyro errors is, in general, a function of time, temperature/vibration exposure, input profile, and number of device turn-ons. The time period for which the measured coefficients accurately characterize the gyro constitutes the long-term stability of the gyro and its associated calibration interval (to remeasure and correct the error coefficients).

The dynamic errors in Figure 3 can also be compensated in the same manner as the bias and scale-factor errors within the bandwidth limitations of the uncompensated sensor-output signals (the signals utilized in the system computer sensor-compensation models). With regard to bandwidth limitations of dynamic compensation, the anisoinertia, spinmotor dynamic, and pickoff angle dynamic cross-coupling effects can be particularly troublesome because of their ability to rectify high-frequency inputs about the spin and input axes (12) (a similar problem exists for the anisoelastic bias error). The pickoff-angle cross-coupling rectification error is caused by the torque-loop bandwidth limitation through the dynamic servo error (θ) generated under high-frequency input-axis angular-rate, and the resulting cross-coupling of spin-axis rate into the gyro output (see Figure 3). Compensation for spinmotor effects can have additional inaccuracies because of the difficulty in accurately modeling the motor-speed control-loop dynamics.

3.3 Performance and Application Areas

Simplified low-cost versions of the floated gyro have been successfully utilized in tactical missile and spacecraft booster guidance applications where the AIRS sensor figures from Table 1 are representative of gyro performance requirements. Examples are the midcourse systems employed on the Harpoon and Standard Missile-2 tactical missiles, the booster inertial guidance systems on the Agena and Delta launch vehicles, the backup guidance system utilized in the Apollo Lunar Module, and the guidance and navigation system utilized in the Prime Reentry Vehicle (the first nondevelopmental strapdown guidance system application). To the author's knowledge, floated-gyro performance consistant with Table 1 1-nmi/hr strapdown navigator requirements has yet to be demonstrated in a statistically valid system flight test. Results of flight tests conducted in 1965 at Holloman Air Force Base on a Honeywell system using high-quality floated gyros yielded 2- to 4-nmi/hr CEP unaided performance. (21) These results are not necessarily representative of what is attainable with today's technology; however, sceptics believe that 1-nmi/hr accuracies for floated rate-integrating gyro strapdown systems are not quite achievable with reasonably priced instruments.* Particulars regarding the capability of the floated gyro in meeting the Table 1 sensor requirements are discussed in the following paragraphs.

---

*Some floated gyro enthusiasts believe that the more sophisticated strapdown floated gyro configurations can meet 1-nmi/hr navigation system requirements. Floated gyro manufacturers, however, are not promoting the use of these instruments today for 1-nmi/hr strapdown applications because of their higher cost and/or performance deficiencies (in the case of the lower cost units) compared to the other available strapdown gyro types.

The bias error for the floated rate-integrating gyro (both g-sensitive and g-insensitive effects) has long-term trending characteristics that require calibration to achieve high-accuracy performance compatible with Table 1 INS requirements. Thermal effects on the bias error are significant, and difficult to accurately model for compensation (e.g., pickoff null movement and associated flex-lead error-torque variations; spinmotor axial shifts due to motor-bearing preload variations; and off-nominal fluid temperature, hence off-nominal flotation, a problem for non-magnetic float suspensions). As a result, thermal controls are generally required to achieve high accuracy*, and a warmup time penalty is incurred. Care must be taken in using the device to assure that input vibration levels and vector direction (linear and angular) do not rectify the dynamically sensitive bias terms (anisoelasticity, anisoinertia, spinmotor dynamics, pickoff angle dynamic response error) beyond application performance limits. An unfortunate aspect of the latter consideration is that vibration profiles at the sensor or even system level are difficult to obtain during the development cycle (particularly regarding angular vibrations and linear-vibration vector direction). Computer compensation can be employed to reduce dynamic errors for low-frequency inputs (within the bandwidth of the sensor torque loop).

Increasing angular momentum [to reduce bias error, see Eq. (6)] also creates additional error torques on the float due to stiffer pivots to handle the increased-momentum reaction-torque loading under output axis rotations; a larger float assembly (for the larger spinmotor and larger torque generator to precess the increased angular momentum) with an associated increase in mass unbalance, float-case electromagnetic-interraction error torques, and float-suspension error torques; heavier flex leads for the larger spinmotor; and (for a permanent-magnet torque-generator with float-mounted coil) heavier flex leads for the larger torquer-coil assembly. The net result is that increased momentum has only a limited capability in reducing floated-gyro bias error, and some form of regular calibration is probably needed to achieve the long-term stability needed to meet Table 1 INS requirements. A concept such as the dual-speed spinmotor technique (see Section 2) appears necessary for conveniently calibrating these gyros frequently if the requirements in Table 1 are to be met. The inability for this calibration technique to separate g-sensitive from g-insensitive errors, however, probably restricts the floated gyro to strapdown applications in fairly benign flight environments if unaided 1-nmi/hr performance is to be achieved. For lower-performance applications (such as the AHRS in Table 1), performance requirements are readily achievable.

Due to torque-generator thermal sensitivities and, in the case of the permanent-magnet torquer, aging effects in the torquer magnet, scale factor accuracies in torque-rebalance instruments (such as the floated gyro) are generally limited to 50 ppm. Compared to Table 1 requirements, the 50-ppm limitation places a serious handicap on torque-rebalance gyros for high performance applications. Relative to the 1-ppm low-rate asymmetry requirement for rate gyros, Honeywell's experience with a GG1009H floated gyro has shown that this performance level is achievable with careful design practice.

Due to its torque-rebalance nature, the floated gyro has a limited-bandwidth input-rate-sensing capability. As a result, sensor-assembly coning-rate vibration frequencies near or above the bandwidth of this sensor will result in attitude drift errors unless the vibration levels are naturally small or intentionally attenuated (through shock mounts). Honeywell's experience with a strapdown GG1009H navigation-grade floated rate-integrating gyro has shown that 80-Hz bandwidths are easily achieved, including a factor of 7 rise in torque-loop stiffness at low (0-5 Hz) frequencies (i.e. lag-lead compensation). For most applications, this bandwidth level is sufficient to meet system needs. Care must be taken in severe vibration applications, however, to assure that unanticipated coning effects will not constitute a major error source.

Alignment stabilities of 5 seconds of arc (the Table 1 requirement) may be achievable with the floated gyro, but not without careful design work. Mechanical instabilities of the gyro-system mount, gimbal pivot, and spinmotor axis, torque-loop servo errors; and pickoff detector null shifts, all contribute to the alignment error. The overall alignment error must remain within allowable limits for several months, over thermal, vibration, angular rate, and linear acceleration environments so that frequent calibration is not required. Thermal modeling may be needed to compensate for pickoff null movement.

The random noise from the floated gyro is generally well within the Table 1 requirements; hence, it does not constitute a major error source. The required rate capability is designed into the unit (through specification of the angular momentum and torque-generator design) and, as such, can be selected to meet the Table 1 requirements. Higher rate requirements impact gyro accuracy through a larger torque-generator requirement and associated bias error effects (e.g., mass unbalance).

Due to the need for thermal controls in high-accuracy applications, a warmup time delay of 5 to 10 minutes is needed to allow the floated gyro to come up to temperature and stabilize. To this must be added an additional 5 minutes for calibration (e.g., using spinmotor reversal). An overall warmup time of 15 minutes results which generally is not compatible with high-performance system requirements. For the lower-performance applications, gyro accuracy is acceptable without heaters (or the output accuracy is acceptable during gyro warmup); hence, the "warmup" time limit is the time for spinmotor run-up, which is typically achievable in 30 seconds.

---

*Another reason for temperature controls in high-performance floated gyros is to maintain nominal damping characteristics in the damping fluid [i.e., the C-coefficient in Eq. (8)] to retain nominal dynamic response performance in the torque-rebalance loop. Typical flotation fluids vary their damping characteristics significantly with temperature and lose their fluid characteristics at low temperatures. Mechanical devices (e.g., orifice dampers) can be utilized in the gyro float-case cavity that provide passive control of damping, and achieve high damping levels with thinner fluids. Unfortunately, these devices also add residual error torques and, therefore, are typically utilized in only the lower-performance application areas.

Quantization levels achievable with the floated gyro depend on the torque-loop/pulse-electronics implementation utilized (see Section 4) which can be selected to meet Table 1 requirements.

4. TORQUE LOOP MECHANIZATION APPROACHES FOR TORQUE-REBALANCE INSTRUMENTS

The implementation of the torque loop for torque-to-balance instruments (such as the floated rate-integrating gyro) can be performed using either of two basic approaches: digital torque rebalance, or analog torque rebalance with follow-up analog-to-digital conversion. Both concepts are illustrated in Figure 4.

4.1 Digital-Torque Rebalance

For the digital-rebalance concept, precision time-amplitude current pulses are generated and gated into the sensor torquer to maintain the pickoff angle at null. Dynamic analog compensation is utilized in the torque loop (if necessary) to provide sufficient wide-bandwidth stable performance (pickoff angle maintained at null under expected dynamic input-rate conditions).

Each current pulse input to the torque generator has the same time-amplitude content; hence, the integral per pulse of the current into the torquer is fixed. This corresponds to an equivalent integral quantum of input data to the sensor (input rate in the case of a gyro) that caused the pulse to be generated (through the forward pickoff/current-command loop). Hence, the occurrence of a rebalance pulse provides a digital indication (to the system computer) that (for a gyro) the device has been rotated through a known fixed quantum of angle about its input axis. For an accelerometer, the pulse occurrence represents a fixed incremental velocity change. Implementation approaches for the pulse command logic vary, depending on sensor-application requirements. In general, two methods are possible: pulse-on-demand and binary torquing.

For the pulse-on-demand concept, a pulse is only input to the torquer when it is needed to drive the analog input to the pulse-command logic toward null. Otherwise, the torquer current is maintained at

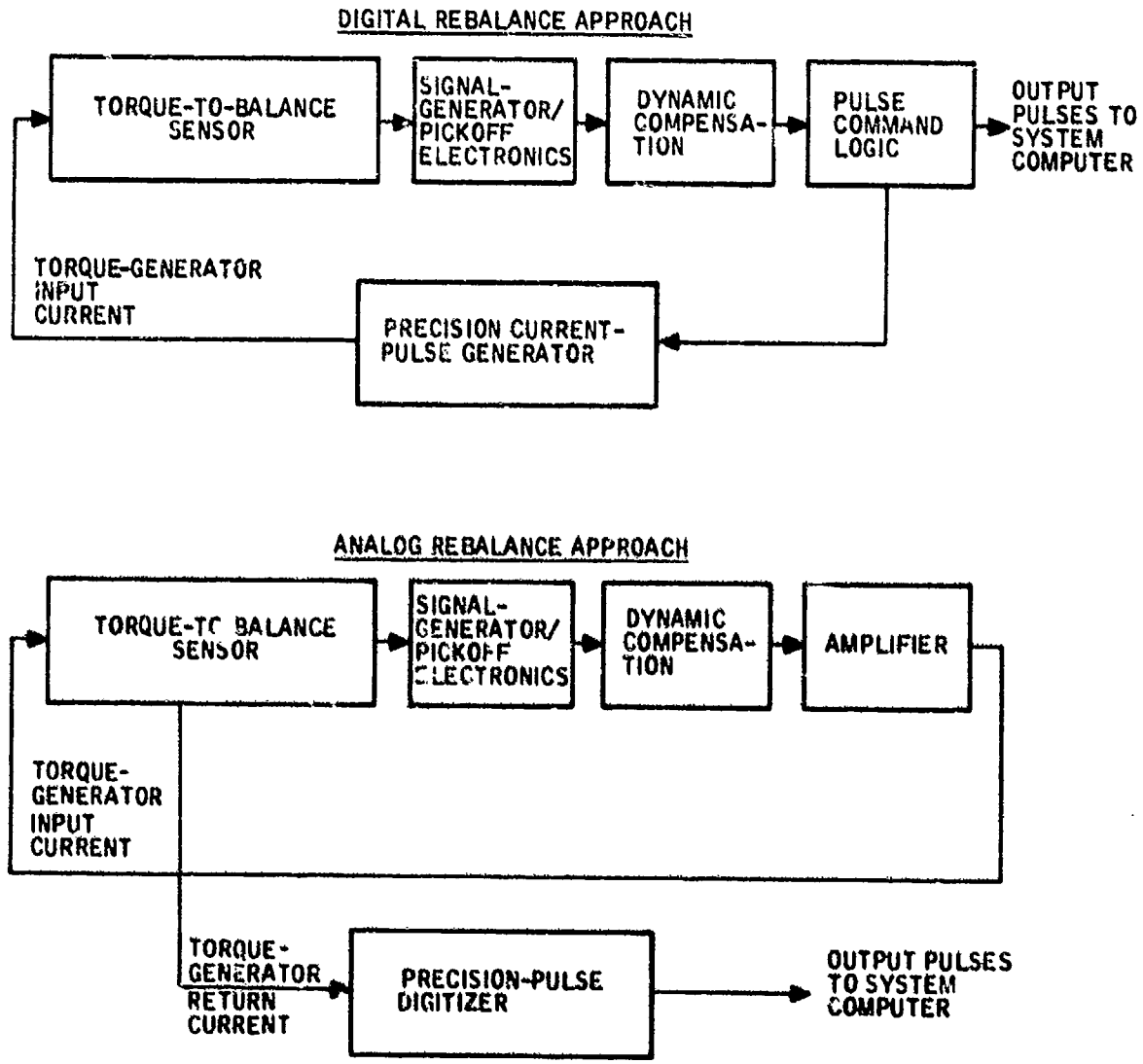

Figure 4. Torque-rebalance-loop concepts.

zero. Figure 5 illustrates two commonly used methods for implementing the pulse-on-demand logic. For the approach at the top of Figure 5, a pulse is issued when the analog-input-signal magnitude exceeds a specified threshold. After the threshold is exceeded, pulses are generated at a constant rate into the sensor torquer with a phase sense (plus or minus) to drive the input signal (through the sensor response) below the threshold limit. The pulse size is set so that for the pulse-frequency capability of the current-pulse generator, sufficient current is generated through the torquer to maintain sensor pickoff null capture under maximum sensor-input conditions. For each pulse transmitted to the torquer, a pulse is output to the system computer to indicate that an incremental change in the sensor input has occurred and has been rebalanced electrically.

2-11

For the approach in the lower half of Figure 5, pulses are generated into the torquer at a rate (frequency) proportional to the analog-signal input level. The pulse size for this approach is also set to hold the pickoff at null under maximum input conditions for which the voltage-to-pulse-frequency converter generates its maximum output pulse frequency.

In general, the tradeoff between the two pulse-on-demand logic approaches in Figure 5 hinges on the effective bandwidth in the overall sensor torque loop versus the torque-loop accuracy under zero and dynamic input conditions (off-null pickoff angle, which leads to cross-coupling errors (see Figure 3), and pulse limit-cycling, which indicates erroneous attitude oscillations to the system computer).

For the binary pulse-command logic approach, constant-amplitude pulses are applied to the sensor torque-generator at a constant rate. The percentage of positive (compared to negative) pulses is controlled to balance the sensor input. Figure 6 illustrates two common binary-torquing configurations: fixed-pulse-width torquing, and pulse-width-modulated torquing.

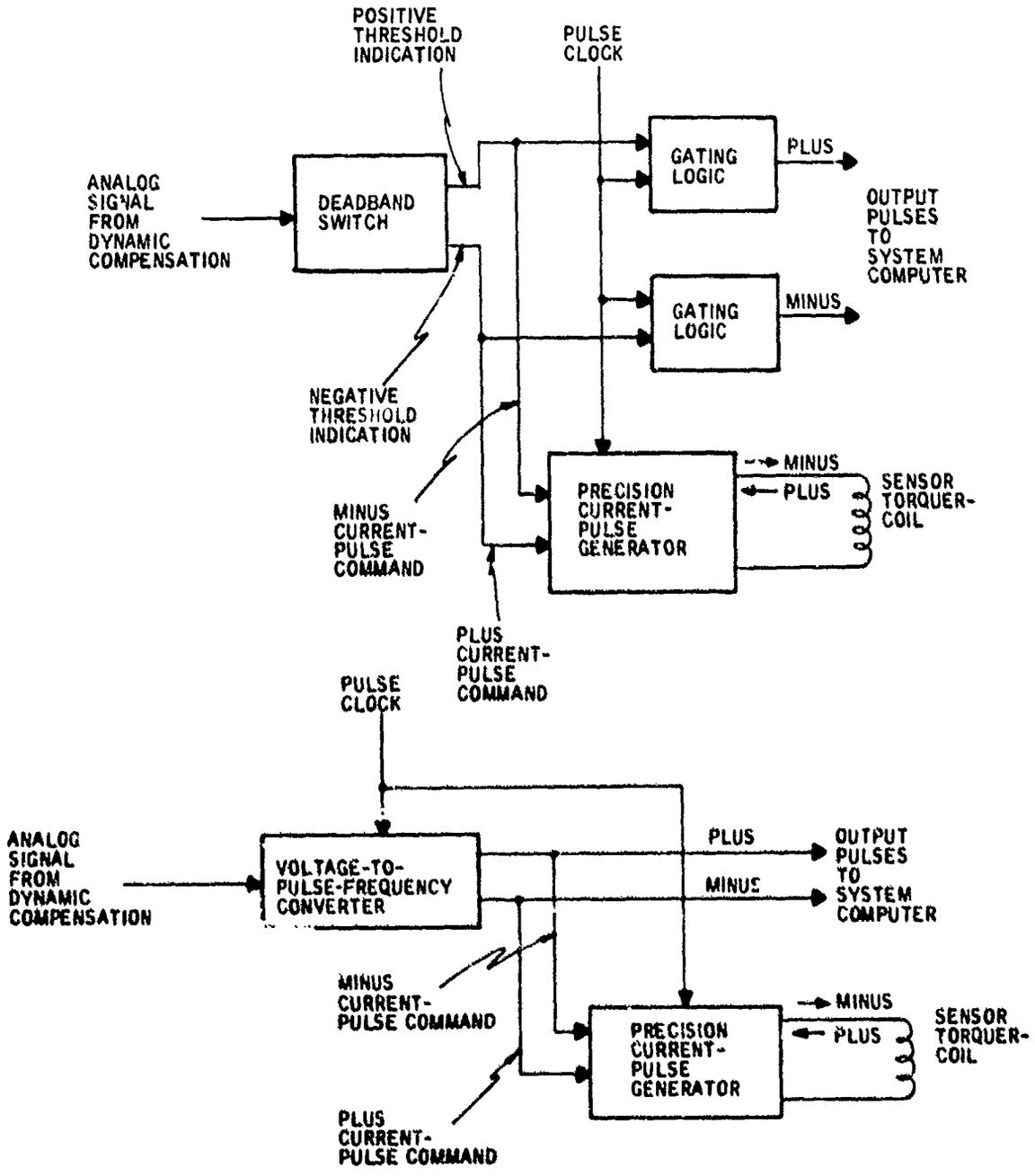

Figure 5. Pulse-on-demand torquer-current command-logic concepts.

2-12

For the binary fixed-pulse-width concept, constant-amplitude constant-width pulses are continuously gated into the torque generator in the positive or negative sense, depending on the phasing of the input signal to the command logic (see Figures 4 and 6). With no input to the sensor, the pulse logic establishes a torque-loop limit-cycle condition in which half the pulses delivered to the torque generator are positive and half are negative (i.e., no net torque is delivered on the average). When an input is applied to the sensor, a larger percentage of pulses is generated with phasing that balances the sensor input. The average difference between the positive and the negative pulses delivered per unit time becomes proportional to the sensor input, and the average pulse-count (positive minus negative) becomes proportional to the integral of the sensor input. The pulse size is established so that for the torque-loop pulse-frequency utilized, sufficient current is generated under maximum sensor input conditions to balance the sensor input.

For the binary pulse-width-modulated torque loop approach (59) (Figure 6), a constant-frequency, constant-amplitude variable-width square-wave is generated by the torque-command electronics, with the difference between the plus and minus wave widths proportional to the input to the command logic (see Figure 4). The variable-width square wave is edge-synchronized with a high-frequency clock, and then used to gate a precision constant current into the sensor torque-generator: positive for the positive cycle of the square-wave, negative for the negative cycle. Thus, the average current into the torquer becomes proportional to the difference between the square-wave positive and negative wave-widths, and

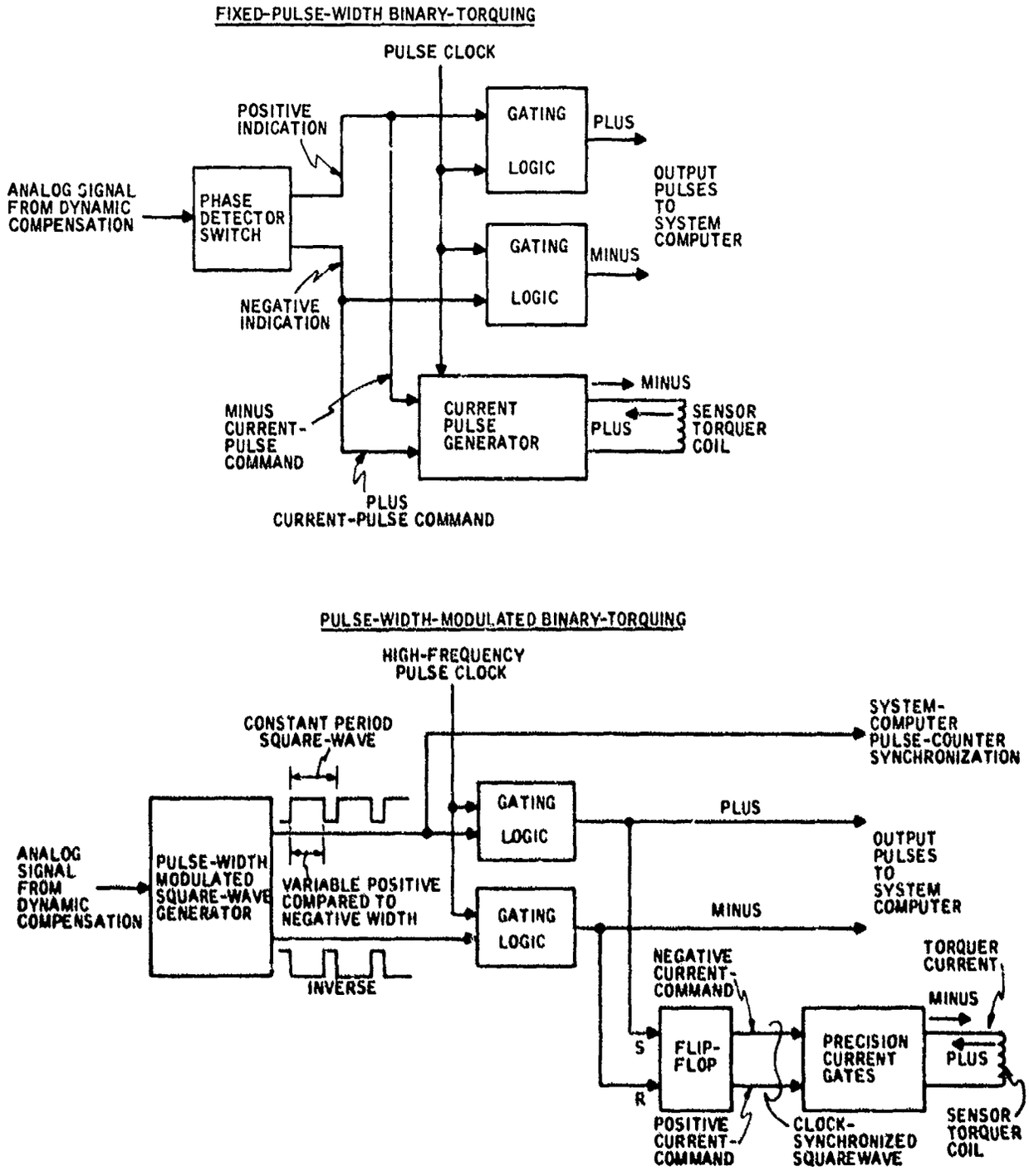

Figure 6. Binary torquer-current command-logic concepts.

thereby proportional to the command-logic input signal. During the time that positive current is being commanded, the high-frequency pulse clock is gated as the gyro pulse output along the positive output line, and conversely for negative current. Since the torquing current square wave is edge synchronized with the high-frequency clock, the total time period for a current pulse (positive or negative) into the torquer is proportional to an integral number of high-frequency pulse counts. As a result, each high-frequency pulse represents a quantum of known integrated torquer current-time (the high-frequency clock period times the torquer current). By counting the positive minus the negative high-frequency pulses in the system computer over each square wave cycle (a count synchronizer is needed; see Figure 6), a fine resolution measure of integrated sensor input is obtained.

An advantage of the binary pulse-width-modulated concept compared to the pulse-on-demand or binary fixed-pulse-width approaches is that finer pulse size (resolution) is achievable with the former. The pulse size for each concept is determined by the maximum torquing rate divided by the maximum pulse frequency (at maximum rate). For the binary pulse-width-modulated concept, the maximum output-pulse frequency is established by the pulse clock, and is independent of the torquing pulse frequency (established by the square-wave period; see Figure 6). For example, for a 400-degree-per-second maximum rate requirement and a 1-MHz pulse clock (not untypical), the pulse size is 400×10^{-6} degrees or 1.5 sec of arc. For the pulse-on demand or binary fixed-pulse-width concepts, the output and torquer pulse-frequencies are equivalent since both are generated from the same source (the pulse clock in Figures 5 and 6). As a result, the output-pulse frequency must be limited to the maximum frequency for which torquer-current pulses can be accurately generated (a function of electronic delays, inductive torquer-coil transients, and the current levels needed for the particular torque-generator design). For strapdown gyros, 5 KHz is a typical maximum torque-rebalance pulse-frequency. For strapdown accelerometers, higher pulse-torquing frequencies are attainable due to the lower current levels involved (e.g., 20 KHz). Hence, the pulse resolution for the pulse-on-demand or binary fixed-pulse-width schemes is generally one to two orders of magnitude coarser than for the binary pulse-width-modulated approach for the same maximum torquing-rate capability. Finer resolution can be achieved with the pulse-on-demand or binary fixed-pulse-width approaches by switching to a lower current level under low sensor input conditions, a design complication that still does not provide fine resolution at high sensor inputs if required. Alternatively, the residual analog signal on the sensor output can be sampled and brought into the system computer through an analog-to-digital converter as a correction to the sensor pulse count accumulated in the computer. The accuracy of this technique is limited by the error (principally scale factor) of the sensor signal-generator/pickoff, generally a poor-quality signal for high-accuracy attitude measurement.

Another advantage for the binary torquing schemes is that total current load into the sensor torque generator is maintained at a constant value (sum of absolute positive and negative current), hence, the thermal effect on the sensor torquer is constant. Since torquer scale-factor accuracy is a function of torquer temperature, operation at a constant thermal load condition tends to minimize torquer scale-factor variations due to thermal gradient loading. For the pulse-on-demand implementation, since average current delivered to the torquer is proportional to input rate, torquer heating becomes proportional to input rate, and thermal transient scale factor variations can be introduced as a function of sensor input. Torquer scale-factor temperature-error effects can be compensated to some extent by installing a thermal detector in the sensor torque generator and using the output signal to correct for device scale-factor variations (either electronically in the actual sensor, or through software in the system computer). The technique can be utilized in unheated sensor applications to improve performance (for both pulse-on-demand and binary torque loops). It also partially compensates for the added thermal transient error that occurs for the pulse-on-demand scheme under dynamic input conditions.

The principal disadvantage of the binary rebalance scheme is the need to operate continuously at maximum positive and negative current loads into the torquer, even at zero sensor-input conditions. As a result, the torque-loop scale-factor symmetry (plus compared to minus current/torque transfer) must be extremely accurate to avoid generating a net large bias error. For example, for a gyro torque loop designed to handle a 400-deg/sec input rate, a 1-ppm asymmetry results in an equivalent bias error of $400 \times 10^{-6} \times 3600$ or 1.4-deg/hr under zero input-rate conditions.

The advantage of digital rebalance schemes in general (either pulse-on-demand or binary) compared to the analog rebalance approach discussed in Section 4.2 is that the torquer current-pulse waveforms have two fixed shapes (positive or negative pulse or square-wave), independent of the average torquing rate. As a result, torquer-linearity error effects [the c_2, c_3 terms in Eq. (10)] are largely absent. Care must still be taken, however, for the pulse-on-demand implementation to assure that the c_1 asymmetry error is small (a function of the positive and negative torquer-current electronics design match) so that normal low-level oscillatory sensor inputs will not rectify into a bias error. For the binary torque-loop schemes, the c_1 symmetry is not an error source (torque-loop asymmetry generates the bias-error effect described in the previous paragraph).

4.2 Analog Torque-Rebalance with Follow-Up Analog-to-Digital Conversion

The alternate to digital rebalance is capture of the sensor element with an analog torque loop (Figure 4). The analog current into the torque generator becomes a continuous measure (in the integral sense) of sensor input. To develop the incremental pulse signals required by the computer, a digitizer circuit is utilized. The digitizer circuit integrates the analog input signal from the torquer, and incrementally rebalances the integrator with fixed current-time (or voltage-time depending on implementation) increments to maintain the integrator output at null. For each rebalance pulse issued to the integrator, an output pulse is issued to the system computer indicating that a known increment of integrated torquer current has been accrued; hence, the integral of the sensor input has also incremented by a known value. The digitizer circuit is typically implemented in much the same manner as the pulse-on-demand digital torque-loop scheme at the top of Figure 5, with the digitizer electronic integrator operating as the sensor does in Figure 5.

An advantage of the analog-torquing loop approach is that wider bandwidth performance is easily achieved and tighter sensor nulls can generally be held compared with the digital-rebalance schemes where continuous off-null oscillatory operation is produced through the pulse-torquing (i. e., the sensor pickoff-angle is nulled within a pulse). In addition, the design of the digital-rebalance portion of the digitizer can be simplified by operating at lower maximum current levels (through scaling of the integrator input), a technique that is prohibitive with digital rebalance where the torquer current to sustain sensor-element capture must be maintained by the digital pulses. Another advantage for analog torquing is that the design of the sensor torque-loop electronics is simplified and essentially uncoupled from the more sophisticated digital-pulse circuitry. As a result, the design of the digitizer can be accomplished independently from the sensor and a common digitizer design configuration may be compatible with several different sensors (e. g., the gyros and accelerometers in a system, or different manufacturer designs for one class of sensor in multiple-source procurements).

Disadvantages of the analog-rebalance concept are the added error (particularly bias) associated with the digitizer, and the sensor scale-factor errors associated with high-rate linearity and torquer heating as a function of input magnitude. Regarding the bias-error effect, the state of the art in analog circuitry has progressed to the point where low bias accuracies (relative to sensor bias) can be achieved with careful design practice. Regarding the scale-factor-error effects, dynamic compensation can be utilized to virtually eliminate the scale-factor-linearity error. Thermal transient error can be eliminated to a degree by thermal measurement and modeling, the adequacy depending on the dynamic-rate environment and accuracy requirements for the particular application. Since mechanization approaches for the digitizer parallel those for the pulse-on-demand digital-rebalance concept, tradeoffs associated with resolution capabilities also apply. It should be noted that the rescaling technique utilized with pulse-on-demand torquing (similarly applicable to the digitizer to increase resolution under low input conditions) also reduces the effective digitizer bias error under low rate conditions (due to rescaling of the digitizer input-signal relative to the sensor rebalance current and digitizer-integrator input-offset current or voltage). In the case of a digitizer based on current input (utilized to reduce integrator bias), a current-input rescaling may be required under high input conditions due to limitations in low-drift electronic integrator amplifiers to absorb the total torquer current from the sensor.

5. TUNED-ROTOR GYRO

The tuned-rotor gyro (22, 23, 24, 25, 26) is the most advanced gyro in large-scale production today for aircraft 1-nmi/hr gimbaled platforms. Due to its simplicity (compared to the floated rate-integrating gyro), the tuned-roto gyro is theoretically lower in cost and more reliable. A drawing of a representative tuned-rotor gyro is presented in Figure 7. Figure 8 is a schematic illustration of the gyro rotor assembly.

The gyro consists of a momentum wheel (rotor) connected by a flexible gimbal to a case-fixed synchronous-hysteresis ball-bearing spinmotor drive shaft. The gimbal is attached to the motor and rotor through members that are torsionally flexible but laterally rigid. A two-axis variable-reluctance signal-generator/pickoff is included that measures the angular deviation of the rotor (in two axes) relative to the case (to which the motor is attached). Also included is a two-axis permanent-magnet torque generator that allows the rotor to be torqued relative to the case on current command. The torquer magnets are attached to the rotor, and the torquer coils are attached to the gyro case.

As for all angular-momentum-based rate-sensing devices, the key design feature of the gyro is the means by which it can contain the reference momentum (the spinning rotor), without introducing torques (drift rates) in the process. For the tuned-rotor gyro, the method is linked to the dynamic effect of the flexible gimbal attachment between the rotor and the motor. Geometrical reasoning reveals that when the rotor is spinning at an angle that deviates from the motor-shaft direction, the gimbal is driven into a cyclic oscillation in and out of the rotor plane at twice the rotor frequency. Dynamic analysis shows that the reaction torque on the rotor to sustain this motion has a systematic component along the angular-deviation vector that is proportional to the angular displacement, but that acts as a spring with a negative spring constant. The flexible pivots between the rotor and gimbal, on the other hand, provide a similar spring torque to the rotor, but of opposite sign. Hence, to free the rotor from systematic torques associated with the angular displacement, it is only necessary to set the gimbal pivot springs such that their effect cancels the inverse spring effect of the gimbal. The result (tuning) is a rotor suspension that is insensitive to angular movement of the case.

Use of the tuned-rotor gyro in a strapdown mode parallels the technique used for the floated rate-integrating gyro. Exceptions are that damping must be provided electrically in the caging loop, as there is no fluid, and that the gyro must be caged in two axes simultaneously. The latter effect couples the two caging loops together due to the gyroscopic cross-axis reaction of the rotor to applied torques.

5.1 Analytical Description and Error Model

Consider the rotor assembly for the tuned-rotor gyro and define four coordinate frames for it as shown in Figure 9: one attached to the rotor (R), one attached to the gimbal (G), one attached to the gyro case (C), and pickoff axes (P) defined with X and Y axes in the plane of the rotor, but displaced from the case axes by small-angle Euler rotations θ_x and θ_y. These are the pickoff angles for the gyro. The Y-axis of the gimbal frame is along the inner torsional flexure that connects the gimbal to the spinmotor shaft. The gimbal-frame X-axis is displaced angularly about the Z-axis from the gyro-case axes by the motor-shaft angle ϕ. The gimbal X-Y plane is displaced from the case X-Y plane by the flexure angle β. The X-axis of the rotor is aligned with the outer flexure axis that connects the rotor to the gimbal. The rotor axes are displaced from the gimbal frame by the flexure angle α.

From the geometry in Figure 9, the kinematic constraint relations for the pickoff and flexure angles can be written as

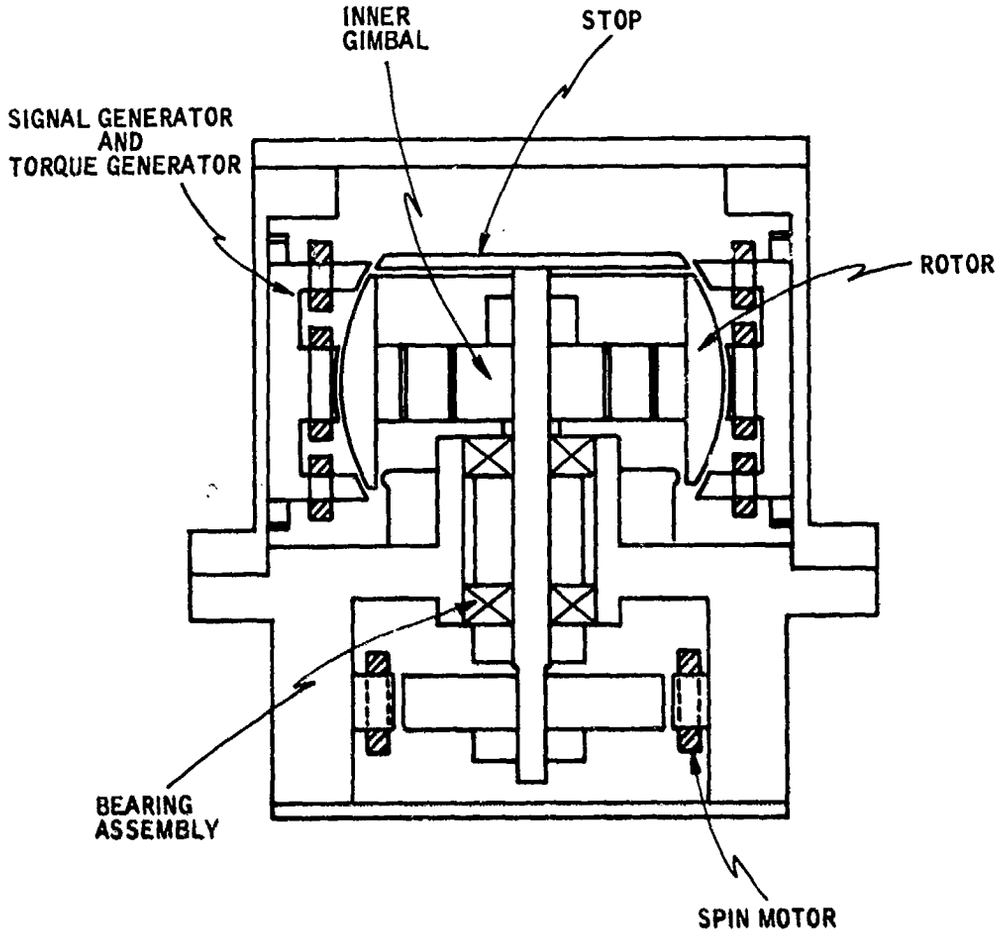

Figure 7. Typical tuned-rotor gyro configuration.

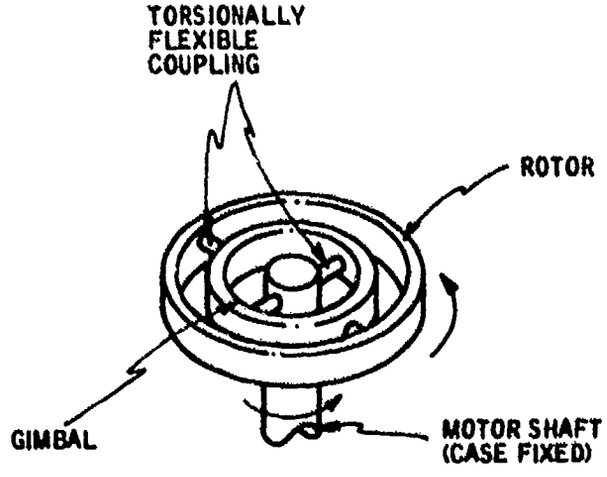

Figure 8. Tuned-rotor-gyro rotor assembly.

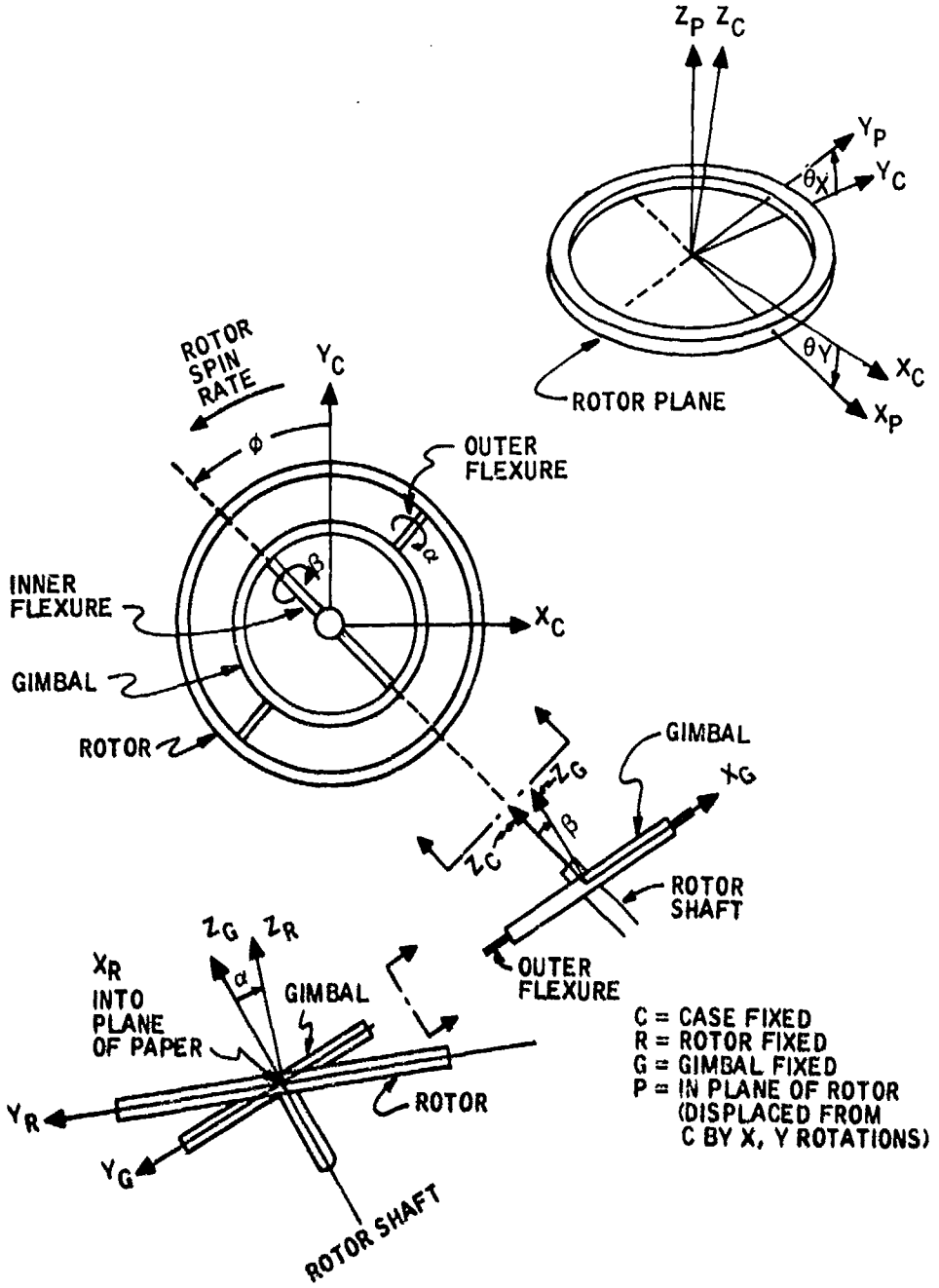

Figure 9. Tuned-rotor-gyro coordinate-frame geometry.

$$\alpha = \theta_x \cos\phi + \theta_y \sin\phi$$
$$\beta = \theta_y \cos\phi - \theta_x \sin\phi \qquad (12a)$$

and their inverse

$$\theta_x = \alpha \cos\phi - \beta \sin\phi$$
$$\theta_y = \beta \cos\phi + \alpha \sin\phi \qquad (12b)$$

The torque equation for the gimbal and rotor about the gimbal Y-axis is

$$\tau^G_{G_y} = \tau^G_{G\alpha_y} - C_\beta\dot{\beta} - K_\beta\beta + \tau^G_{Ge_y}$$

or

$$\tau^G_{G\alpha_y} = \tau^G_{G_y} + C_\beta\dot{\beta} + K_\beta\beta - \tau^G_{Ge_y} \qquad (13)$$

where

$\tau^G_{G_y}$ = total torque on the gimbal about the gimbal (superscript) Y-axis

K_β = torsional spring constant for the β flexure

C_β = torsional damping torque associated with β flexure movement (e.g., caused by interaction of the gimbal with the surrounding gas)

$\tau^G_{G\alpha_y}$ = Y-axis reaction torque on the gimbal at the α flexure junction

$\tau^G_{Ge_y}$ = spurious (unwanted) error producing torques on the gimbal about the gimbal Y-axis

Torques on the rotor can be similarly written along gimbal X, Y, and Z axes

$$\begin{aligned}
\tau^G_{R_x} &= \tau^G_{RT_x} - C_\alpha\dot{\alpha} - K_\alpha\alpha + \tau^G_{Re_x} \\
\tau^G_{R_y} &= \tau^G_{RT_y} + \tau^G_{R\alpha_y} + \tau^G_{Re_y} = \tau^G_{RT_y} + \tau^G_{Re_y} - \tau^G_{G\alpha_y} \\
\tau^G_{R_z} &= \tau^G_{RT_z} + \tau^G_{R\alpha_z} + \tau^G_{Re_z}
\end{aligned} \tag{14}$$

where

$\tau^G_{R_i}$ = total torque on the rotor about the gimbal i-axis (i = X, Y, or Z)

K_α = torsional spring constant for the α flexure

C_α = damping torque associated with α flexure movement

$\tau_{R\alpha_i}$ = reaction torque on the rotor at the α flexure junction about the gimbal i-axis (i = Y or Z)

$\tau^G_{Re_i}$ = error torque on the rotor about the gimbal i-axis (i = X, Y, or Z)

$\tau^G_{RT_i}$ = electrically applied torque-generator torque on the rotor about the gimbal i-axis (i = X, Y, or Z) intentionally applied through the gyro torquer

The Y-axis component of Eq. (14) relates the Y-axis torque on the rotor at the α flexure ($\tau^G_{R\alpha_y}$) to the negative of the equivalent reaction torque on the gimbal ($\tau^G_{G\alpha_y}$) given by Eq. (13).

Equations (14) with (13) can now be transformed to their equivalent form in pickoff coordinates

$$\underline{\tau}^P_R = C^P_G \left(\underline{\tau}^G_{RT} + \underline{\tau}^G_{Re} + \begin{bmatrix} -C_\alpha\dot{\alpha} - K_\alpha\alpha \\ -\left(\tau^G_{G_y} + K_\beta\beta + C_\beta\dot{\beta}\right) + \tau^G_{Ge_y} \\ \tau^G_{R\alpha_z} \end{bmatrix} \right) \tag{15}$$

where

C^P_G = direction cosine matrix relating gimbal and pickoff coordinate axes

$\underline{\tau}^G_{RT}$, $\underline{\tau}^G_{Re}$ = vectors with Eq. (14) gimbal-frame components $\tau^G_{RT_x}$, $\tau^G_{RT_y}$, etc.

$\underline{\tau}^P_R$ = net rotor torque in pickoff axes

Using small-angle theory (for α, β), the C^P_G matrix can be shown to be

$$C^P_G = \begin{bmatrix} \cos\phi & -\sin\phi & -\alpha\sin\phi \\ \sin\phi & \cos\phi & \alpha\cos\phi \\ 0 & -\alpha & 1 \end{bmatrix}$$

Substituting in Eq. (15) and expanding

2-18

$$\tau^P_{R_x} = \tau^P_{RT_x} + (\tau^P_{Re_x} - \tau^G_{Ge_y} \sin\phi) - (C_\alpha\dot{\alpha} + K_\alpha\alpha)\cos\phi$$
$$+ (\tau^G_{G_y} + C_\beta\dot{\beta} + K_\beta\beta)\sin\phi - \tau^G_{R\alpha_z}\,\alpha\sin\phi$$
$$\tau^P_{R_y} = \tau^P_{RT_y} + (\tau^P_{Re_y} + \tau^G_{Ge_y}\cos\phi) - (C_\alpha\dot{\alpha} + K_\alpha\alpha)\sin\phi \qquad (16)$$
$$- (\tau^G_{G_y} + C_\beta\dot{\beta} + K_\beta\beta)\cos\phi + \tau^G_{R\alpha_z}\,\alpha\cos\phi$$
$$\tau^P_{R_z} = (\tau^P_{Re_z} - \alpha\,\tau^G_{Ge_y}) + \tau^G_{R\alpha_z} + \alpha\,(\tau^G_{G_y} + K_\beta\beta + C_\beta\dot{\beta})$$

where

$$\tau^P_{R_i},\ \tau^P_{RT_i},\ \tau^P_{Re_i} = \text{components of } \underline{\tau}^P_R,\ \underline{\tau}^P_{RT},\ \underline{\tau}^P_{Re}$$

Note that the Z component of $\underline{\tau}^P_{RT}$ is absent in Eq. (16). This is because the gyro torquer is designed to apply torque to only the rotor in the rotor plane.

The Z expression in Eq. (16) can be used to solve for $\tau^G_{R\alpha_z}$ for substitution in the X, Y equations. After dropping α-squared terms as second order, the result is

$$\tau^P_{R_x} = \tau^P_{RT_x} - \tau^P_{R_z}\,\alpha\sin\phi - (C_\alpha\dot{\alpha} + K_\alpha\alpha)\cos\phi$$
$$+ (\tau^G_{G_y} + C_\beta\dot{\beta} + K_\beta\beta)\sin\phi + \tau_{e_x}$$
$$\tau^P_{R_y} = \tau^P_{RT_y} + \tau^P_{R_z}\,\alpha\cos\phi - (C_\alpha\dot{\alpha} + K_\alpha\alpha)\sin\phi \qquad (17)$$
$$- (\tau^G_{G_y} + C_\beta\dot{\beta} + K_\beta\beta)\cos\phi + \tau_{e_y}$$

In Eq. (17), the τ_{e_x} and τ_{e_y} terms are the composite of all the error effects in the X, Y torque equations.

The momentum transfer equations relating the torques in Eq. (17) to rotational movement of the rotor assembly are now developed to obtain the input/output equations for the tuned-rotor gyro.

The angular rate of the gimbal in gimbal axes is given by

$$\underline{\omega}^G_G = C^G_C\,(\underline{\omega}^C_C + \underline{\omega}^C_r) + \dot{\beta}^G \qquad (18)$$

where

$\underline{\omega}^G_G$ = gimbal inertial angular rate vector in gimbal axes

$\underline{\omega}^C_C$ = gyro case angular rate vector in case axes

$\underline{\omega}^C_r$ = spin-motor rate vector in case axes

$\dot{\beta}^G$ = rate of change of the β angle-vector ($\underline{\beta}^G$) in gimbal axes

C^G_C = direction-cosine matrix relating case and gimbal axes

The C^G_C matrix is given from Figure 9 by

$$C^G_C = \begin{bmatrix} \cos\phi & \sin\phi & -\beta \\ -\sin\phi & \cos\phi & 0 \\ \beta\cos\phi & \beta\sin\phi & 1 \end{bmatrix} \qquad (19)$$

The momentum-transfer equation for the gimbal in gimbal axes is given by

$$\underline{\tau}^G_G = I^G_G\,\dot{\underline{\omega}}^G_G + \underline{\omega}^G_G \times (I^G_G\,\underline{\omega}^G_G) \qquad (20)$$

where

I_G^G = inertia tensor for the gimbal in gimbal axes

With Figure 9, the components of the elements in Eq. (18) and (20) can be defined as

$$\underline{\omega}_C^C = \begin{pmatrix} \omega_\mu \\ \omega_\nu \\ \omega_\xi \end{pmatrix}$$

$$\underline{\omega}_r^C = \begin{pmatrix} 0 \\ 0 \\ \omega_r \end{pmatrix} \qquad (21)$$

$$\underline{\dot{\beta}}^G = \begin{pmatrix} 0 \\ \dot{\beta} \\ 0 \end{pmatrix}$$

$$I_G^G = \begin{bmatrix} I_G & 0 & 0 \\ 0 & I_G & 0 \\ 0 & 0 & J_G \end{bmatrix}$$

where

ω_μ, ω_ν, ω_ξ = X, Y, Z components of case rate $\underline{\omega}_C$ in case axes

ω_r = spinmotor rate

I_G, J_G = gimbal moments of inertia about the X, Y axes, and about the Z polar axis

Substituting Eq. (18), (19), and (21) into Eq. (20), noting that $\dot{\phi} = \omega_r$, and neglecting β-squared effects as second-order yields the expression for the gimbal Y-axis torque for Eq. (17)

$$\tau_{G_y}^G = I_G \left[\ddot{\beta} + (\dot{\omega}_\nu - \omega_r \omega_\mu) \cos\phi - (\dot{\omega}_\mu + \omega_r \omega_\nu) \sin\phi \right] + (I_G - J_G) \left[-\beta \omega_r^2 + \omega_r (\omega_\mu \cos\phi + \omega_\nu \sin\phi - 2\beta\omega_\xi) + \omega_\xi (\omega_\mu \cos\phi + \omega_\nu \sin\phi) \right] \qquad (22)$$

The $\dot{\alpha}$, $\dot{\beta}$, $\ddot{\beta}$ expressions for Eq. (17) and (22) are obtained by differentiating Eq. (11)

$$\begin{aligned} \dot{\alpha} &= \dot{\theta}_x \cos\phi + \dot{\theta}_y \sin\phi + \omega_r \beta \\ \dot{\beta} &= \dot{\theta}_y \cos\phi - \dot{\theta}_x \sin\phi - \omega_r \alpha \\ \ddot{\beta} &= \ddot{\theta}_y \cos\phi - \ddot{\theta}_x \sin\phi - \alpha\dot{\omega}_r - 2\omega_r (\dot{\theta}_y \sin\phi + \dot{\theta}_x \cos\phi) - \omega_r^2 \beta \end{aligned} \qquad (23)$$

To develop an expression for the rotor torque-momentum-transfer equation (for $\tau_{R_x}^P$ and $\tau_{R_y}^P$ in Eq. (17)), the net rotor angular rate in the P frame is first defined as the sum of its consecutive (Euler) angular-rate-vector components

$$\underline{\omega}_R^P = C_C^P (\underline{\omega}_C^C + \underline{\omega}_r^C) + C_G^P (\dot{\alpha}^G + \dot{\beta}^G) \qquad (24)$$

where

$\underline{\omega}_R^P$ = total rotor inertial angular rate in P coordinates

$\dot{\underline{\alpha}}^G$ = rate of change of the α torsion flexure angle-vector in gimbal-frame coordinates

C_C^P, C_G^P = direction-cosine matrices relating P, C, and G

The pickoff angle θ is the angle between case and pickoff axes, hence, the first term in Eq. (24) assuming small angles is

$$C_C^P(\underline{\omega}_C^C + \underline{\omega}_r^C) = \underline{\omega}_C^C + \underline{\omega}_r^C - \underline{\theta}^C \times (\underline{\omega}_C^C + \underline{\omega}_r^C) \tag{25}$$

2.20

If the α,β effects in C_G^P are neglected as second order, C_G^P in Eq. (24) can be approximated by the cosine matrix for Z-axis ϕ angle rotation generated by ω_r (see Figure 9). Recognizing that $\underline{\theta}$ is the vector sum of $\underline{\alpha}$ and $\underline{\beta}$, the second term in Eq. (24) can be written as

$$C_G^P(\dot{\underline{\beta}}^G + \dot{\underline{\alpha}}^G) = C_G^P \dot{\underline{\theta}}^G \approx \dot{\underline{\theta}}^C + \underline{\theta}^C \times \underline{\omega}_r^C \tag{26}$$

where

$\dot{\underline{\theta}}^C$ = rate of change of the pickoff angle $\underline{\theta}$ as measured in case (or pickoff) coordinates

Substituting Eq. (25) and (26) into Eq. (24) defines the rotor rate in terms of known matrix quantities

$$\underline{\omega}_R^P = \underline{\omega}_C^C + \underline{\omega}_r^C - \underline{\theta}_C^C \times \underline{\omega}_C^C \tag{27}$$

An expression for the P frame rotation rate as measured in the P frame is obtained similarly

$$\underline{\omega}_P^P = C_C^P \underline{\omega}_C^C + \dot{\underline{\theta}}^C = \underline{\omega}_C^C + \dot{\underline{\theta}}^C - \underline{\theta}^C \times \underline{\omega}_C^C \tag{28}$$

The momentum transfer equation for the rotor can be written in P coordinates as

$$\underline{\tau}_R^P = I_R^P \dot{\underline{\omega}}_R^P + \underline{\omega}_P^P \times (I_R^P \underline{\omega}_R^P) \tag{29}$$

where

$\underline{\tau}_R^P$ = net torque on the rotor assembly in P coordinates

I_R^P = inertia tensor for the rotor in P coordinates

Particular vector and matrix elements in Eq. (27) through (29) are defined as

$$\underline{\theta}^C = \begin{pmatrix} \theta_x \\ \theta_y \\ 0 \end{pmatrix}$$

$$\dot{\underline{\theta}}^C = \begin{pmatrix} \dot{\theta}_x \\ \dot{\theta}_y \\ 0 \end{pmatrix}$$

$$I_R^P = \begin{bmatrix} I_R & 0 & 0 \\ 0 & I_R & 0 \\ 0 & 0 & J_R \end{bmatrix}$$

With Eq. (21) for the remaining vector definitions, Eq. (29) can be expanded to obtain the desired scalar expressions for the torque-momentum-transfer equations along P frame axes

$$\begin{aligned}
\tau_{R_x}^P &= I_R(\dot{\omega}_\mu + \ddot{\theta}_x - \theta_y\omega_\xi - \theta_y\dot{\omega}_\xi) + J_R\omega_r(\omega_\upsilon + \dot{\theta}_y + \theta_x\omega_\xi) + (J_R - I_R)\omega_\xi(\omega_\upsilon + \dot{\theta}_y) \\
\tau_{R_y}^P &= I_R(\dot{\omega}_\upsilon + \ddot{\theta}_y + \dot{\theta}_x\omega_\xi + \theta_x\dot{\omega}_\xi) - J_R\omega_r(\omega_\mu + \dot{\theta}_x - \theta_y\omega_\xi) - (J_R - I_R)\omega_\xi(\omega_\mu + \dot{\theta}_x) \\
\tau_{R_z}^P &= J_R(\dot{\omega}_r + \dot{\omega}_\xi)
\end{aligned} \tag{30}$$

Equations (17), (22), and (30), with Eq. (12a) and (23) in combination define the dynamic response relations for the tuned-rotor gyro. Before combining, additional nomenclature is introduced to simplify the form of the final result and to account for gyro-case misalignments.

The α and β torsion-flexure spring constants are defined to be equal to a nominal value K_o plus small error variations

$$\begin{aligned}
K_\alpha &= K_o + \Delta K_\alpha \\
K_\beta &= K_o + \Delta K_\beta
\end{aligned} \tag{31}$$

The following definitions are introduced for the inertia terms

$$J = J_R + \tfrac{1}{2} J_G$$
$$I = I_R + \tfrac{1}{2} I_G \qquad (32)$$
$$L_G = I_G - \tfrac{1}{2} J_G$$

The spinmotor rate is defined as a nominal value (ω_{r_o}) plus a variation ($\delta\omega_r$) due to motor dynamics; and a nominal gyro angular momentum (H_o) is defined

$$\omega_r = \omega_{r_o} + \delta\omega_r$$
$$H_o = J\omega_{r_o} \qquad (33)$$

The torque-generator torque is defined in terms of a gyroscopic precessional command rate with a scale-factor and cross-coupling error; and the error torque is equated to a bias rate defined as the torque-generator command-rate needed to nullify the effect of the error torque on the rotor

$$\tau_{RT_x} = \frac{H_o}{(1+\epsilon_y)}\omega_{T_y} + \beta_{y_x}\omega_{T_x}$$
$$\tau_{RT_y} = -\frac{H_o}{(1+\epsilon_x)}\omega_{T_x} + \beta_{x_y}\omega_{T_y}$$
$$\tau_{e_x} = -\frac{H_o}{(1+\epsilon_y)}\omega_{\beta_y} \qquad (34)$$
$$\tau_{e_y} = \frac{H_o}{(1+\epsilon_x)}\omega_{\beta_x}$$

where

ω_{T_x}, ω_{T_y} = X- and Y-axis torquer command rates

β_{y_x}, β_{x_y} = torquer cross-coupling errors (Y command rate into X-axis, and X command rate into Y-axis)

ϵ_x, ϵ_y = X- and Y-axis torquer scale-factor errors

ω_{B_x}, ω_{B_y} = gyro X- and Y-axis bias rates

The gyro case axes may be misaligned from nominal gyro axes by small misalignment angles γ_x, γ_y, and γ_z

$$\omega_u = \omega_x + \gamma_z\omega_y - \gamma_y\omega_z$$
$$\omega_v = \omega_y + \gamma_x\omega_z - \gamma_z\omega_x \qquad (35)$$
$$\omega_w = \omega_z + \gamma_y\omega_x - \gamma_x\omega_y$$

Finally, the following trigonometric identities are noted

$$\sin^2\phi = \tfrac{1}{2} - \tfrac{1}{2}\cos 2\phi$$
$$\cos^2\phi = \tfrac{1}{2} + \tfrac{1}{2}\cos 2\phi \qquad (36)$$
$$\sin\phi\cos\phi = \tfrac{1}{2}\sin 2\phi$$

With Eq. (31) through (36), Eq. (11), (17), (22), (23), and (30) can now be combined to yield the input/output equations for the tuned-rotor gyro. Upon combination, rearrangement, introducing the fact that the gimbal inertia is significantly less than the rotor inertia, neglecting higher-order effects, and assuming that angular vibration inputs at exactly twice spin-frequency have negligible likelihood, yields the results in Eq. (37a) and (37b).

2-22

$$\omega_{T_x} = (1+\epsilon_x)\left[(\omega_x+\dot\theta_x)+\gamma_z\omega_y-(\gamma_y+\theta_y)\omega_z+\beta_{x_y}\omega_{T_y}-\frac{I}{H_o}(\dot\omega_y+\ddot\theta_y)+\frac{(J-I)}{H_o}\omega_z(\omega_x+\dot\theta_x)\right.$$

$$\left.+\frac{J}{H_o}(\omega_x+\dot\theta_x)\delta\omega_r\right]+\omega_{B_x}-\frac{1}{H_o}\left[(K_o-L_G\omega_{r_o}^2)-2L_G\omega_{r_o}\delta\omega_r+\frac{1}{2}(\Delta K_\alpha+\Delta K_\beta)\right]\theta_y \qquad (37a)$$

$$+\frac{1}{2J}(C_\alpha+C_\beta)\theta_x$$

$$\omega_{T_y} = (1+\epsilon_y)\left[(\omega_y+\dot\theta_y)-\gamma_z\omega_x+(\gamma_x+\theta_x)\omega_z-\beta_{y_x}\omega_{T_x}+\frac{I}{H_o}(\dot\omega_x+\ddot\theta_x)+\frac{(J-I)}{H_o}\omega_z(\omega_y+\dot\theta_y)\right. \qquad (37b)$$

$$\left.+\frac{J}{H_o}(\omega_y+\dot\theta_y)\delta\omega_r\right]+\omega_{B_y}+\frac{1}{H_o}\left[(K_o-L_G\omega_{r_o}^2)-2L_G\omega_{r_o}\delta\omega_r+\frac{1}{2}(\Delta K_\alpha-\Delta K_\beta)\right]\theta_x$$

$$+\frac{1}{2J}(C_\alpha+C_\beta)\theta_y$$

The $\delta\omega_r$ term in Eq. (37a)and (37b) is a function of the spinmotor dynamics, and can be described analytically by considering the rotor-gimbal assembly as the inertial load to the spinmotor. Neglecting gimbal-angle and misalignment effects as second order, and assuming that the rotor inertia is much larger than the gimbal inertia, provides the result given by Eq. (38)

$$J(\omega_z+\delta\omega_r) = \tau_r = f(\delta\omega_r) \qquad (38)$$

where

τ_r = spinmotor torque designed to maintain the rotor at nominal speed ω_{r_o}

$f(\delta\omega_r)$ = functional operator indicating that the spinmotor torque is a function of the deviation of the rotor speed from nominal

Equations (37a) and (37b) show that the X and Y torquer command rates to the gyro (ω_{T_x}, ω_{T_y}) are proportional to the X- and Y-axis gyro input rates (ω_x, ω_y) plus dynamic and cross-coupling effects, the principal one being the pickoff-angle (θ_x, θ_y) nominal spring dynamic effect $[(K_o - L_G\omega_{r_o}^2)\theta]$. Due to the magnitude of K_o and $L_G\omega_{r_o}^2$, this term could generate a significant rate error in the gyro for off-null pickoff operation (which is generally the case due to the inability to operate the gyro ideally with the pickoff angle held precisely at zero). To eliminate this as an error source, the nominal torsional-flexure spring constant K_o is designed to cancel the dynamic term $L_G\omega_{r_o}^2$

$$K_o = L_G\omega_{r_o}^2 \qquad (39)$$

Setting the gimbal spring rates as specified by Eq. (39), the condition known as tuning, cancels the spring dynamic effect, and makes the rotor appear to be free of the gimbal case under off-null pickoff-angle conditions. Hence, the rotor is effectively uncoupled from the gyro case without the use of special pivots or flotation fluid as with the single-degree-of-freedom floated rate-integrating gyro. Note that the rotor-case freedom effect can be seen directly from Eq. (37a) and (37b) if the error terms and command rates are equated to zero. Under these conditions the equations collapse to the simplified form

$$\dot\theta_x = -\omega_x$$

$$\dot\theta_y = -\omega_y \qquad (40)$$

Hence, the pickoff angle becomes equal to the negative of the integral of the gyro-case motion, or equivalently, the gyro rotor is fixed inertially with the pickoff angle providing a direct measure of the gyro-case angular motion (i. e., the gyro acts as an ideal two-degree-of-freedom attitude sensor).

In strapdown applications the pickoff angle is maintained near null through closed-loop torquing, with the torquer command signals thereby becoming measures of input rate (in the integral sense). Such a scheme is illustrated by the analytical block diagram in Figure 10 which is a schematic representation of Eq. (37a), (37b), and (38) with Eq. (39).

If Eq. (37a), (38), and Figure 10 for the tuned-rotor gyro are compared with Eq. (8), (9), and Figure 3 for the single-degree-of-freedom floated rate-integrating gyro, it will be apparent that the two gyros contain similar dynamic error terms (γ_y, γ_x, θ_y misalignment coupling, ω_y and $\dot\theta_y$ angular acceleration effects, $\omega_z\omega_x$ anisoinertia, and $\omega_x\delta\omega_r$ motor dynamics). In addition, the tuned-rotor gyro contains the cross-coupling rate term ($\dot\theta_x$), torquer cross-coupling effects (β_{x_y}), gimbal damping effects ($C_\alpha + C_\beta$), and the residual spring torque terms due to off-nominal tuning(the $(\Delta K_\alpha + \Delta K_\beta)$ effect with nominal gyro spin speed and the effect of $\delta\omega_r$ spin-speed error with nominal spring constants)). It should also be apparent that the torque loops for the tuned rotor are dynamically more complex (due to two-axis cross-coupling) and undamped (the $C\dot\theta$ term for the floated gyro is not present in the tuned rotor). Hence, additional compensation electronics are required in the Figure 10 command electronics to achieve wide-bandwidth stable performance. In other respects, mechanization approaches for the torque loops are as described previously for torque-to-balance instruments in general.

The scale-factor-error model for the tuned-rotor gyro operating in the strapdown mode is given by Eq. (41) and is entirely equivalent to that for the floated rate-integrating gyro [Eq. (10)].

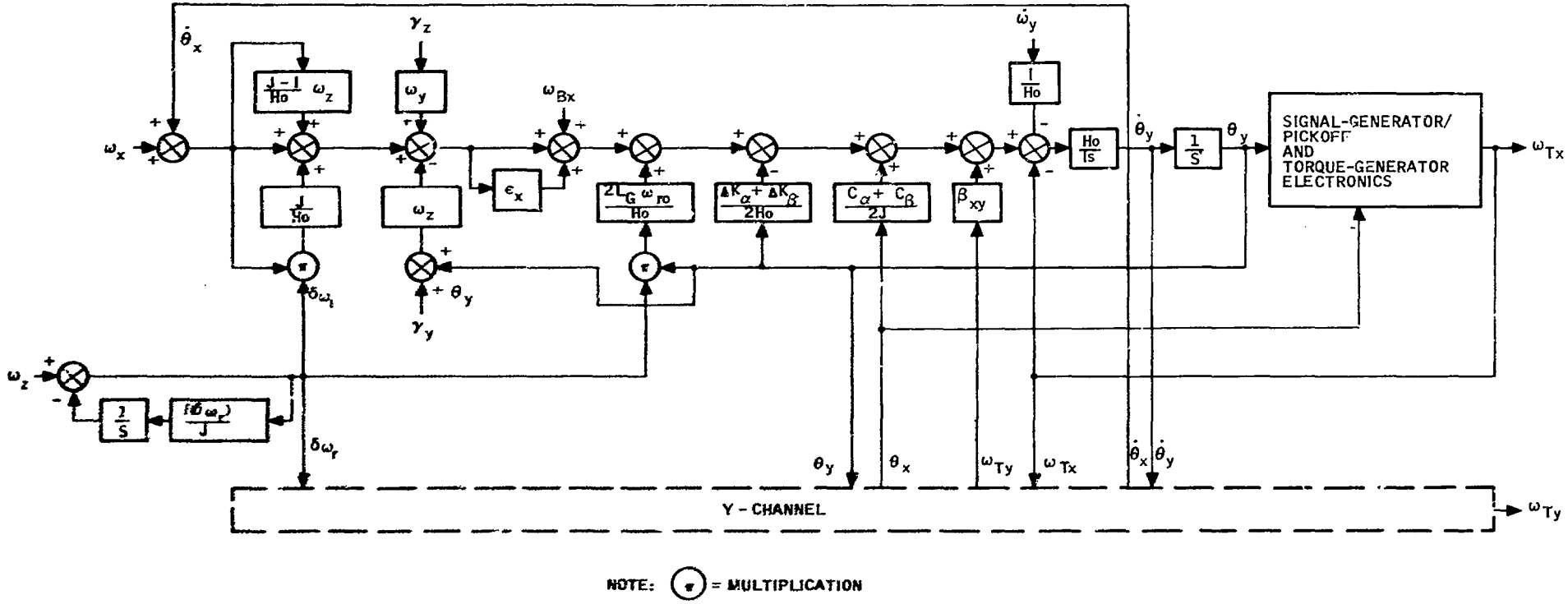

Figure 10. Tuned-rotor-gyro analytical response diagram.

2.24

$$\epsilon_x = \epsilon_{0_x} + \epsilon_{1_x} \frac{\omega_x}{|\omega_x|} + \epsilon_{2_x} \omega_x + \epsilon_{3_x} \omega_x^2$$

$$\epsilon_y = \epsilon_{0_y} + \epsilon_{1_y} \frac{\omega_y}{|\omega_y|} + \epsilon_{2_y} \omega_y + \epsilon_{3_y} \omega_y^2 \qquad (41)$$

The bias errors for the tuned-rotor gyro (ω_{B_x} and ω_{B_y}) can modeled (25, 26) as

$$\omega_{B_x} = B_{0_x} + B_1 a_x + B_2 a_y + B_3 a_x a_z + n_x$$

$$\omega_{B_y} = B_{0_y} + B_1 a_y - B_2 a_x + B_3 a_y a_z + n_y \qquad (42)$$

where

a_x, a_y, a_z = accelerations of the gyro along the x, y, and z nominal gyro axes.

Note that the acceleration-sensitive bias coefficients in Eq. (42) are identical between axes (because they are caused by rotor-assembly effects which are common to X, Y channel outputs). A comparison between Eq. (42) and Eq. (11) (for the floated gyro) shows that the bias-error equations are of the same form. Sources of B_0 bias error for the tuned-rotor gyro are stray internally generated magnetic fields that interact with the rotor-mounted torquer magnet, and torque-loop/pulse-electronics bias errors (for binary torque loops or analog torque loops with follow-up analog-to-digital conversion, see Section 4). The effects of off-nominal tuning and gimbal damping in Eq. (37a) and (37b) are usually included as part of the B_0 bias error (in conjunction with pickoff-angle offsets caused, for example, by spinmotor-shaft misalignments or signal-generator/pickoff bias). Additional, but unlikely B_0 bias errors for the tuned-rotor gyro are caused by acceleration inputs at spin frequency along the spin axis rectifying radial mass-unbalance effects in the rotor assembly (relative to the center of torsional support for the rotor assembly), acceleration inputs at twice spin frequency normal to the spin axis rectifying gimbal mass-unbalance along the spin axis, and rectification of twice spin-speed angular-rate inputs to the gyro due to alternating inertial/spring reaction loads of the rotor-gimbal assembly relative to the motor shaft. (25, 26) The latter effect is predictable by the expressions used to develop Eq. (37a) and (37b) (neglected in the final Eq. (37a) and (37b) forms presented).

The B_1 g-sensitive coefficient is caused by mass-unbalance of the rotor assembly along the spin axis, and the B_2 coefficient, by geometrical imperfections in the torsional elements. (25, 27) The B_3 coefficient is the anisoelastic effect for the gyro caused by unequal compliance of the rotor assembly along the X, Y, Z directions. The n noise terms are stochastic errors that have relatively short correlation times (caused, for example, by spinmotor-shaft orientation changes due to ball bearing preload variations and resulting error torques created by off-nominal tuning).

As with the floated gyro, several errors in the tuned-rotor gyro are inherent in the basic instrument design (bandwidth limitation, anisoinertia, and angular acceleration sensitivity). The remaining errors are caused by imperfections in the gyro manufacture, many of which are predictable over long time intervals. System-level software compensation can be utilized to remove the predictable error effects within the bandwidth limitations of the uncompensated sensor-output signals (the signals utilized to compensate the dynamic-error effects).

5.2 Performance and Application Areas

The strapdown version of the tuned-rotor gyro has been developed for applications requiring performance in, or close to, the 1-nmi/hr category (refer to Table 1). Applications receiving the greatest attention have been for transport aircraft as a navigation system that also (and in some cases, primarily) provides high-quality outputs for flight-control-system use (Schuler-tuned attitude, inertially derived heading, body rates and accelerations, horizontal and vertical velocity) (8, 28). Enthusiasts for the strapdown tuned-rotor technology envision its ultimate utilization in higher-performance military aircraft (29). The lower-performance application areas (such as for tactical missile midcourse guidance) have not been pursued by tuned-rotor technologists, probably because of difficulties in competing with the lower-cost floated-gyro technologies that currently dominate this area. Some consideration is being given to the utilization of tuned-rotor inertial strapdown systems for spacecraft booster guidance, a small specialized area from a production standpoint, and one that has traditionally utilized high-quality floated rate-integrating gyros for implementation.

Specific performance capabilities of the tuned-rotor gyro parallel those for the floated gyro, with some notable exceptions. The tuned-rotor gyro was developed to eliminate some of the problems (in cost and performance) associated with older floated rate-integrating gyro technology. Proponents of the tuned-rotor technology point to its advantages compared to the floated gyro: fewer parts, two axes per gyro, elimination of the need for the fluid suspension and associated error mechanisms, elimination of flex-lead-error torques, elimination of spinmotor axial mass unbalance as an error source and associated simplifications in spinmotor bearing design, and more predictable instrument warmup characteristics. These advantages are partially offset by the addition of errors caused by imperfect rotor tuning, windage torques and drift errors associated with dynamic viscous coupling of the off-null gimbal motion with the surrounding gas; and rotor heating and motor bearing lubricant containment problems if a near vacuum is held around the rotor to eliminate the latter gas-dynamic effects.

For the tuned-rotor gyro, bias instabilities can be overcome largely through increased angular momentum [see Eq. (34)], with additional complexity in the torque loops due to the higher current levels needed for angular momentum caging. Based on the 1-nmi/hr system-level performance obtained in transport aircraft using strapdown tuned-rotor gyros with large angular momentum wheels, (4, 5) it can

be assumed that the bias performance levels of Table 1 are achievable in benign flight environments using temperature modeling for compensation (without thermal controls). In dynamic flight environments, g-sensitive bias effects will degrade performance to some extent. Potential rectification errors that contribute to bias in the floated gyro are also present in the tuned rotor. As such, the potential for large bias error also exists for the tuned rotor in high linear- and angular-vibration environments (due to anisoinertia, spinmotor dynamics, anisoelasticity, pickoff-angle dynamic error, and bandwidth limitations for compensation).

Rate capability, bandwidth, and scale-factor accuracy for the strapdown tuned-rotor gyro (a torque-to-balance instrument) directly parallel that for the strapdown floated gyro with similar limitations (high vibration and angular rates). Bandwidths of 75 Hz and scale-factor accuracies of 50 ppm (with thermal modeling for compensation) have been achieved for tuned-rotor gyros at Boeing (30), and Litton (31) claims that bandwidths in excess of 85 percent of spin speed are achievable using new caging techniques. For typical tuned-rotor spin rates, this translates into a bandwidth in the 50- to 150-Hz area.

Alignment errors for tuned-rotor gyros are caused by pickoff null shift, torquer input-axis misalignment, dynamic torque-rebalance servo error, and gyro-system-mount misalignment. Due to the absence of the gimbal pivot and spinmotor-axis misalignment errors associated with the floated gyro, 5-seconds-of-arc alignment accuracy should be more easily achievable with the tuned-rotor gyro. As with the floated gyro, random noise is not a major error source for the tuned-rotor gyro.

For systems using tuned-rotor gyros with large angular momentum wheels, calibration intervals of greater than 6-months have been experienced for 1-nmi/hr benign environment system applications. (4, 5) Note, that if needed, the dual-speed spinmotor calibration technique developed for the floated gyro (see Section 2) can also be used with the tuned rotor, if necessary, to reduce the frequency of removals for system recalibration. Warmup times in the 2- to 5-minute category (for spinmotor runup and thermal stabilization) have been demonstrated by high-accuracy tuned-rotor gyros with thermal modeling for error compensation. (4, 5)

6. ELECTROSTATIC GYRO

Of the three angular-momentum devices considered in this paper, the electrostatic gyro comes closest to achieving the theoretically ideal suspension system. In the electrostatic gyro, a spherical rotor is suspended in a vacuum by an electrostatic field generated by case-fixed electrodes; hence, there is no physical contact with the rotor assembly. Pickoffs on the case sense the orientation of the case relative to the rotor. Figure 11 illustrates the implementation concept.

Some mechanizations of the electrostatic-gyro pickoff (17) have used optical detectors that sense scribe marks etched on the rotor. For such an approach, the rotor is a hollow shell, 1 to 2 inches in diameter (see Figure 11). Alternatively, a small solid rotor (typically 1 centimeter in diameter) can be used with a radially offset mass. (32) The resulting modulation in the suspension field (due to the mass unbalance) is used to determine the relative case/rotor orientation. Each of these approaches is being considered for gimbaled application. (32, 33, 34) However, only the small solid rotor approach is being considered today for strapdown application. (9, 34)

The electrostatic gyro can be used only as an attitude gyro (there is no torque-to-balance concept for the instrument); hence, in strapdown applications where large angular motion is common, the accuracy of the pickoff (which must sense the total attitude) is a key performance parameter. In this respect, the gyro differs from the floated and tuned-rotor instruments that are operated in strapdown applications with the pickoff-angle held near null.

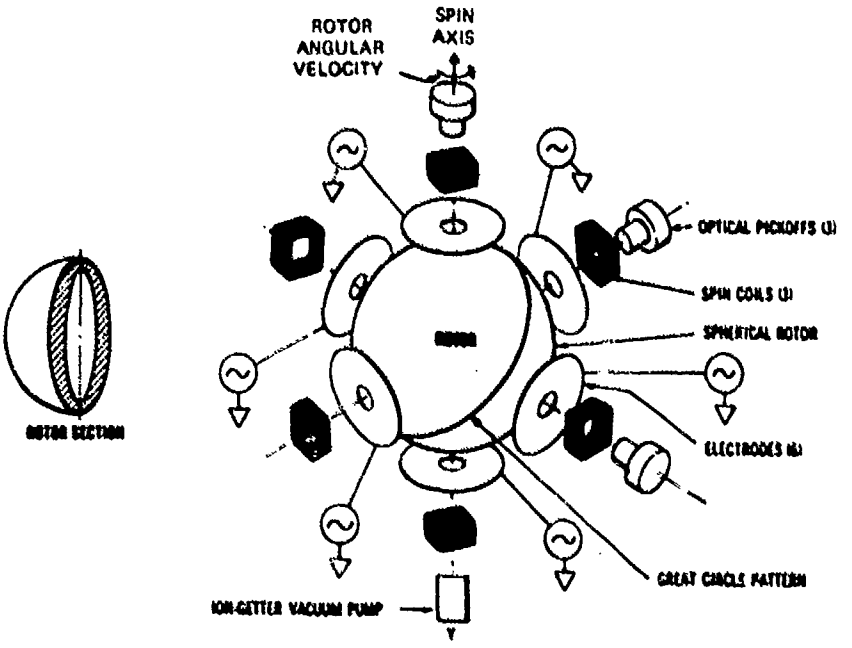

Figure 11. Electrostatic-gyro configuration.

2-26

One of the principal advantages of the electrostatic gyro compared to the other spinning-mass instruments is the elimination of mechanical friction producing mechanisms (i.e., spinmotor bearings) and associated reliability problems. A disadvantage for the electrostatic gyro from a reliability standpoint is the potential damage to the rotor and case that can result during a momentary loss in gyro-rotor suspension voltage while the rotor is spinning.

6.1 Analytical Description and Error Model

In one respect, the analytical model for the electrostatic gyro is much simplified compared to the torque-to-balance strapdown gyros (tuned-rotor and floated rate-integrating gyros) due to the lack of dynamic-error terms implicit in the design of the latter instruments. If the electrostatic gyro could be manufactured perfectly with ideal materials, it would have no error effects, and its output would be a true indication of the orientation of the gyro case relative to an inertially fixed rotor spin-axis (i.e., an ideal two-degree-of-freedom attitude gyro). However, due to imperfections that must exist in any real device, errors are present in the instrument that can be divided into two categories: bias errors, and (for strapdown applications) attitude readout errors. In very general terms, these errors can be represented as

$$
\begin{aligned}
\omega_{B_x} &= f_x(a_x, a_y, a_z, u_x, u_y, u_z) \\
\omega_{B_y} &= f_y(a_x, a_y, a_z, u_x, u_y, u_z) \\
\omega_{B_z} &= f_z(a_x, a_y, a_z, u_x, u_y, u_z) \\
\delta u_x &= g_x(u_x, u_y, u_z) + \gamma_z u_x - \gamma_x u_z \\
\delta u_y &= g_y(u_x, u_y, u_z) + \gamma_x u_y - \gamma_y u_x \\
\delta u_z &= g_z(u_x, u_y, u_z) + \gamma_y u_z - \gamma_z u_y
\end{aligned}
\qquad (43)
$$

where

$\omega_{B_x}, \omega_{B_y}, \omega_{B_z}$ = components of gyro bias rate (in case axes); the bias vector represents the precessional rate of the rotor, and is normal to the rotor spin-axis

a_x, a_y, a_z = three-axis acceleration components of the gyro case (in case axes)

u_x, u_y, u_z = cosines of the angles between the rotor spin-axis and gyro-case axes (i.e., the attitude information sensed by the read-out detectors)

$f_x(\,), f_y(\,), f_z(\,)$ = functional operators indicating a functional dependence of the bias numerical values on the bracketed quantities

$\delta u_x, \delta u_y, \delta u_z$ = net attitude readout errors

$g_x(\,), g_y(\,), g_z(\,)$ = functional operators associated with the gyro readout mechanism indicating a functional dependence of the numerical values on the bracketed quantities

$\gamma_x, \gamma_y, \gamma_z$ = misalignments of gyro-case axes from nominal gyro axes

Due principally to the full spherical attitude operating mode of the strapdown electrostatic gyro, the bias and attitude readout error effects are complex functions of case-rotor orientation and accelerations in three dimensions. The bias attitude sensitivity is caused by the different orientation of the gyro suspension coils relative to the rotor and associated variations in the electrostatic suspension field (from nominal) in the rotor cavity that produces a net moment on the spinning rotor. Acceleration-induced bias-sensitivity effects are caused by the center of electrostatic suspension force on the rotor not coinciding with the rotor center of mass, also a function of the orientation of the case relative to the rotor. Attitude readout errors are caused by electronic instabilities and attitude nonlinearities in the pickoff over the full spherical readout range.

The f( ) and g( ) elements in Eq. (43) are typically expressed as a set of compensation models that analytically characterize the error phenomena as a function of sensed acceleration (a_x, a_y, a_z), rotor-axis cosines (u_x, u_y, u_z), and gyro parameters (e.g., rotor case-envelope, and suspension-servo characteristics). (9) The gyro parameters in the models are the measurable quantities that characterize each gyro for calibration purposes (i.e., calibration coefficients). The stability of the coefficients from turn-on to turn-on, over temperature, vibration, and acceleration, as well as the complexity (number of terms) in the error model utilized, ultimately determines the performance capabilities of the gyro (and the complexity and frequency of calibration).

6.2 Performance and Application Areas

2-27

The principal focus for strapdown electrostatic gyro application has been in the 1-nmi/hr navigation system area where its proponents point to the cost and reliability advantages it affords compared to equivalent gimbaled INS technologies. However, because the electrostatic gyro is inherently an attitude-sensing instrument, its utility in other strapdown application areas (28, 29, 35) is limited (compared to the other strapdown gyros) due to its inability to also provide a rate-signal output. Deriving rate analytically in the electrostatic-gyro system computer (a nontrivial function of the calculated rate of change of the computed attitude data) provides a noisy signal (due to differentiated attitude pickoff noise) that must be filtered for reasonable low-noise rate-output performance. The resulting dynamic lag can introduce stability problems (in flight-control systems, for example) where the rate signal is utilized.

For a specified case orientation relative to the rotor (as in gimbaled applications), and with accurate thermal controls, electrostatic-gyro errors can be remarkably predictable and compensatible. However, for strapdown applications where the case can be at arbitrary orientations relative to the rotor, compensation is difficult. Due to the nonprecise mechanical nature and large size (relative to the rotor) of the suspension coils, it is difficult to manufacture a gyro that has a fixed center of suspension in the rotor cavity for all orientations of the rotor, case, and specific-force vector (hence, the problem of complex three-dimensional modeling for bias calibration coefficients. (6, 9). The calibration problem is further complicated by thermal expansion movement of the mechanical assemblies, and associated variations in the error coefficients. To compensate for this effect, thermal modeling has been used, but with limited success. Thermal control for the electrostatic gyro appears to be the only accurate method for direct bias-error control in strapdown applications.

To overcome some of these difficulties, Autonetics, the principal proponent of the electrostatic gyro for strapdown inertial navigation, has developed a turntable assembly for their MICRON strapdown electrostatic-gyro system, on which the inertial sensors are mounted. The turntable is rotated at a known rate relative to the system chassis, typically about the user vehicle yaw axis. The result is an averaging of the case-correlated bias-error effects such that the overall navigation error is improved. The effect of case rotation is expected to eliminate the need for the frequent calibrations that have accompanied the performance instabilities experienced in the past with the strapdown electrostatic gyro.

Reaction times for the electrostatic gyro have been a significant problem area in the past due to the sensitivity of gyro performance to temperature effects, and the difficulty in spinning up the gyros and thermally stabilizing the system (with temperature controls) in a reasonable time period. (6) Recent improvements in gyro design (for reduced thermal gradients) and the introduction of the turntable for error averaging are expected to allow reasonable reaction times (less than 10 minutes at the system level) for new strapdown electrostatic-gyro systems.

An important advantage for the electrostatic gyro in maneuvering applications is that direct attitude readout is provided and is, therefore, not subject to the unbounded computational attitude-error-buildup effects associated with rate-sensing strapdown gyros where attitude is calculated in the system computer (through a rate-integration process that also integrates the effects of rate-gyro scale factor error, misalignment cross-coupling, pulse-output quantization uncertainty, and finite bandwidth*). As a result, the alignment (and pickoff) accuracy requirements for the electrostatic gyro are somewhat relaxed compared to the other strapdown gyros because the associated attitude error over short maneuver times (relative to the Schuler period) is bounded (i. e., equals the bias on the gyro attitude-output signal).

For the strapdown solid-rotor electrostatic gyro, wide-angle readout accuracies of 18 seconds of arc have been achieved in the past (9, 34). This performance is somewhat marginal in high velocity-accuracy applications. However, it is reasonable to assume that improvements will be made such that the 10-second-of-arc goal in Table 1 is achieved in future production units. The alignment accuracy for the instrument is determined by the stability of the gyro-system mount, which should be well within Table 1 requirements.

The bandwidth and rate-gyro scale-factor accuracy requirements in Table 1 are not applicable to the electrostatic gyro. Random noise for the instrument is not a significant error source.

7. RING LASER GYRO

Unlike the gyros that utilize rotating mass for angular-measurement reference, the laser-gyro operating principal is based on the relativistic properties of light. The device has no moving parts; hence, it has the potential for extremely high reliability. References 36 and 37 describe this unique instrument, its mechanization approach, and performance characteristics.

Figure 12 depicts the basic operating elements in a laser gyro: a closed optical cavity containing two beams of correlated (single-frequency) light. The beams travel continuously between the reflecting surface of the cavity in a closed optical-path; one beam travels in the clockwise direction, the other in the counterclockwise direction, each occupying the same physical space in the cavity. The light beams are generated from the lasing action of a helium-neon gas discharge within the optical cavity. The reflecting surfaces are dielectric mirrors designed to selectively reflect the frequency associated with the particular helium-neon transition being used.

---

*The extent to which these error-effects accumulate in the rate-gyro strapdown-system computer is determined by the user vehicle angular-rate (and vibration) profile.

2-20

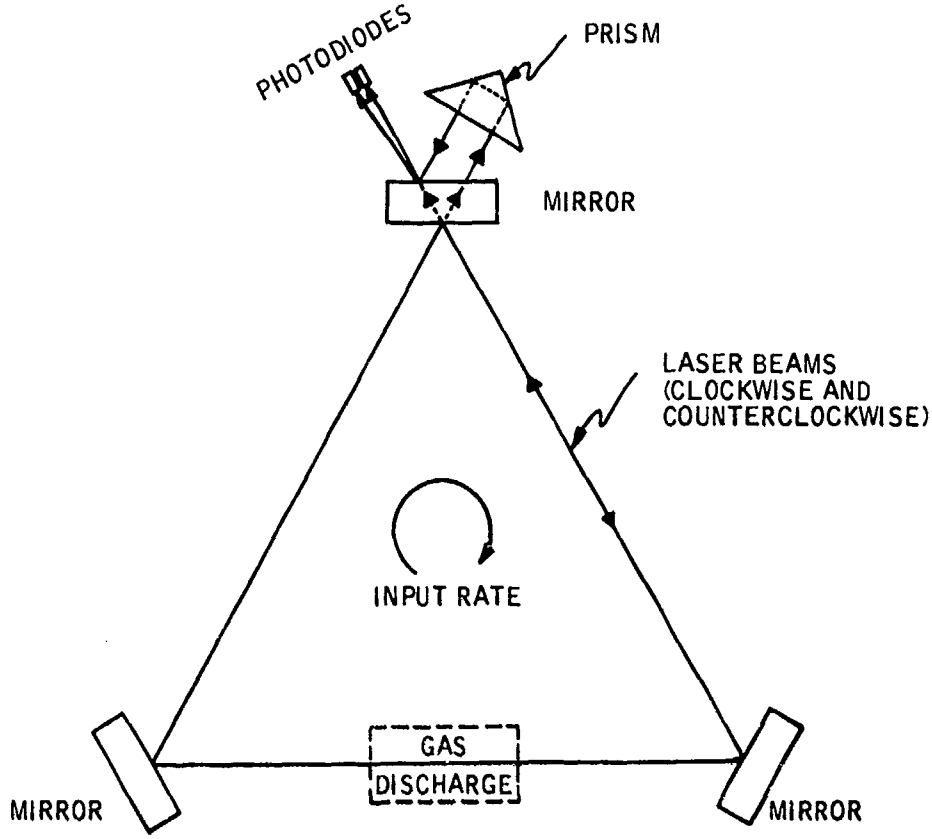

Figure 13. Laser-gyro operating elements.

To understand the operation of the laser gyro, consider the effect of cavity rotation on an observer rotating with the cavity. Relative to the observer, it takes longer for a wave of light to traverse the distance around the optical path in the direction of rotation than in the direction opposite to the rotation. Due to the constancy of the speed of light, this effect is interpreted by the observer as a lengthening of the net optical path length in the direction of rotation, and a shortening of the path length in the opposite direction. Because a fixed integral number of light waves must exist around the path at any instant of time (the beams are continuous, closing on themselves), the path-length shift must also be accompanied by a frequency shift in the opposite sense. The frequency difference between the two beams thereby becomes a measure of rotation rate.

The frequency difference is measured in the laser gyro by allowing a small percentage of the laser radiation to escape through one of the mirrors (Figure 12). A prism is typically used to reflect one of the beams such that it crosses the other in almost the same direction at a small angle (wedge angle). Due to the finite width of the beams, the effect of the wedge angle is to generate an optical fringe pattern in the readout zone. When the frequencies between the two laser beams are equal (under zero rate conditions), the fringes are stationary relative to the observer. When the frequencies of the two beams are different (under rotational rates), the fringe pattern moves relative to the observer at a rate and direction proportional to the frequency difference (i.e., proportional to the angular rate). More importantly, the passage of each fringe indicates that the integrated frequency difference (integrated input rate) has changed by a specified increment. Hence, each fringe passage is a direct indication of an incremental integrated rate movement, the exact form of the output needed for a rate-gyro strapdown navigation system.

Digital integrated-rate-increment pulses are generated from the laser gyro from the outputs of two photodiodes mounted in the fringe area and spaced 90 degrees apart (in fringe space). As the fringes pass by the diodes, sinusoidal output signals are generated, with each cycle of a sine wave corresponding to the movement of one fringe over the diodes. By observing which diode output is leading the other (by 90 degrees), the direction of rotation is determined. Simple digital-pulse triggering and direction logic operating on the photodiode outputs convert the sinusoidal signals to digital pulses for computer input.

The pulse size (quantization) for the laser gyro depends on the wavelength of the laser beam and the path length between the mirrors. For a typical triangular-optical-path laser gyro with 0.63 micron wavelength and pathlength between mirrors (each leg of the triangle) of 4.2 inches, the pulse size is 2 seconds of arc.*

*This pulse sizing assumes pulse triggering at the positive-going zero-crossing of one of the photodiode outputs. A factor of four finer pulse size is attainable if required by triggering output pulses at the positive- and negative-going zero crossings from both photodiode output signals. The penalty is a proportional decrease in maximum rate capability (or increased readout electronics complexity for increased bandwidth to maintain the same rate capability).

7.1 General Design Considerations

7.1.1 Construction -- The accuracy of the laser gyro depends on the manner in which the laser beams are affected by the influences of the lasing cavity. A key requirement in this regard is that the average of the path lengths around the lasing triangle for the clockwise and counterclockwise beams be constant and equal to the value for peak average lasing power. The peak-laser-power condition corresponds to the laser frequency being centered at the peak of the helium-neon gas-discharge Doppler gain curve. (38) Many of the error parameters in the laser gyro are stationary for small variations in gyro operation about the center of the Doppler gain curve. (37)

To achieve a high degree of path-length stability, the laser-gyro optical cavity is typically constructed of ceramic-vitreous (Cervit) material, which has an extremely low coefficient of thermal expansion. Figure 13 illustrates a typical laser-gyro mechanization concept. A Cervit structure is used to contain the helium-neon gas, with the lasing mirrors and electrodes forming the seals. High voltage (typically 1500 volts) applied across the electrodes (one cathode and two anodes) ionizes the helium-neon gas mixture, thereby providing the required laser pumping action. High-quality optical seals must be used in the Figure 13 configuration to avoid introducing contaminants into the helium-neon mixture, thereby degrading performance and ultimately limiting lifetime. Alternatively, a gain tube that contains the helium-gas can be inserted in the cavity, with optical windows (Brewster windows) provided for laser beam entry and exit (39). The advantage of the gain-tube approach is that the beam-cavity seal requirement (particularly for the mirrors) can be relaxed, since the helium-neon is no longer in contact with the mirror seals. The disadvantage is the addition of seals for the gain tube (Brewster window seals), and the introduction of acceleration and thermally sensitive gyro bias uncertainties due to differential phase shifts and energy losses (between the two laser beams) generated from birefringent (40) and anisotropic optical effects in the Brewster window optics.

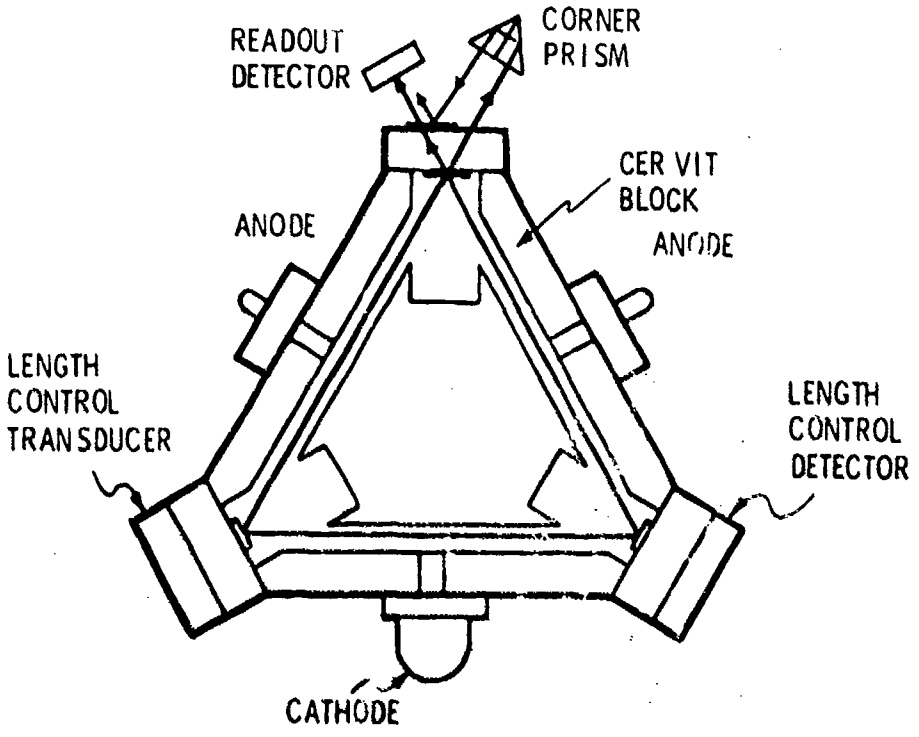

Figure 13. Laser-gyro block assembly.

Figure 14 illustrates the interface between a typical laser gyro block assembly and the gyro electronics. A piezoelectric transducer mounted on one of the mirror substrates is typically used to control the path length of the cavity (Figures 13 and 14). The control signal for the transducer is proportional to the deviation from the peak of the average power in the laser beams; hence, the control loop is designed to maintain a path length that produces peak average lasing power. The average beam power is measured by a photodiode mounted on one of the mirrors that senses a small percentage of the radiation from both the clockwise and counterclockwise beams.

Flow phenomena in the laser gyro (e.g., Langmuir flow) can cause bias shifts due to differential changes in the index of refraction of light along the forward and reverse beam-paths. (37, 41) To reduce the possibility of net circular-flow phenomena in the gyro, circuitry is typically provided to maintain a constant balance between the net current flows in each of the two ionization paths (see Figure 14).

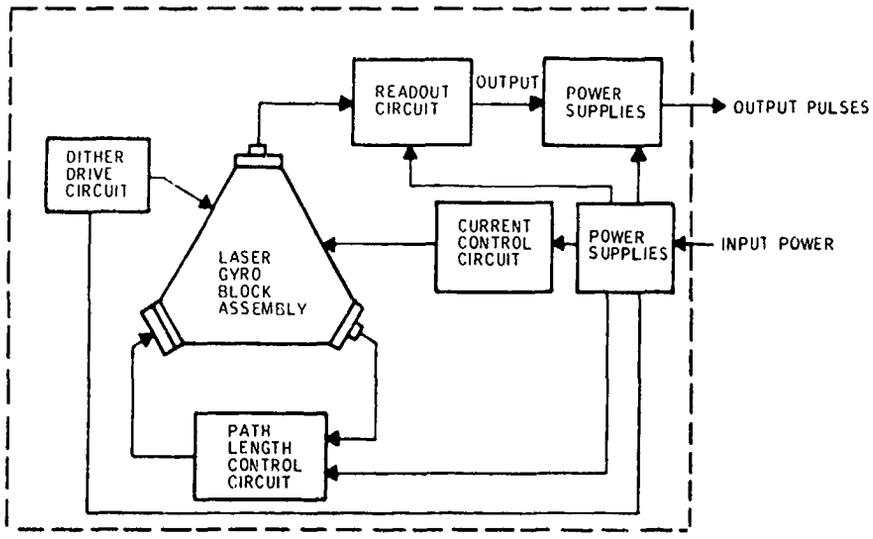

Figure 14. Laser-gyro electronic elements.

7.1.2 Packaging -- Figure 15 illustrates a typical laser gyro packaging concept. The electronics to control the laser and to provide readout pulses are mounted with the laser block in a single box. The high-voltage supply is included for gyro operations (regulated low-level voltages are gyro inputs). The box is hermetically sealed to avoid problems associated with high-voltage arcing at high altitudes.

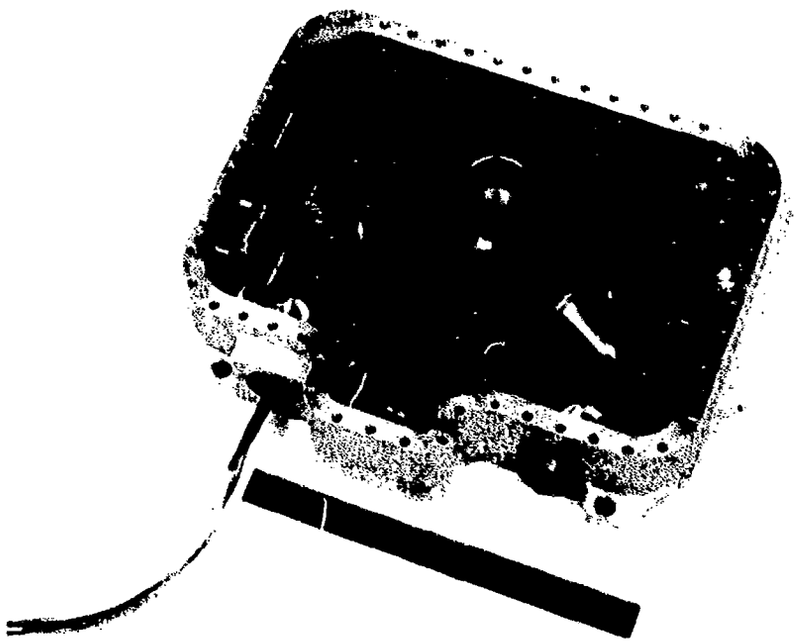

Figure 15. Honeywell GG1300 laser gyro.

Alternative packaging approaches incorporate three laser cavities in a single block of Cervit (e.g., Figure 16 or References 42 and 43). The advantage of the latter integrated concept is precise alignment-stability between gyro axes, and small size due to the ability to interweave the laser triangles. Disadvantages are the inability to replace a single gyro for maintenance actions, and difficulties in implementing mechanical dither for lock-in compensation.

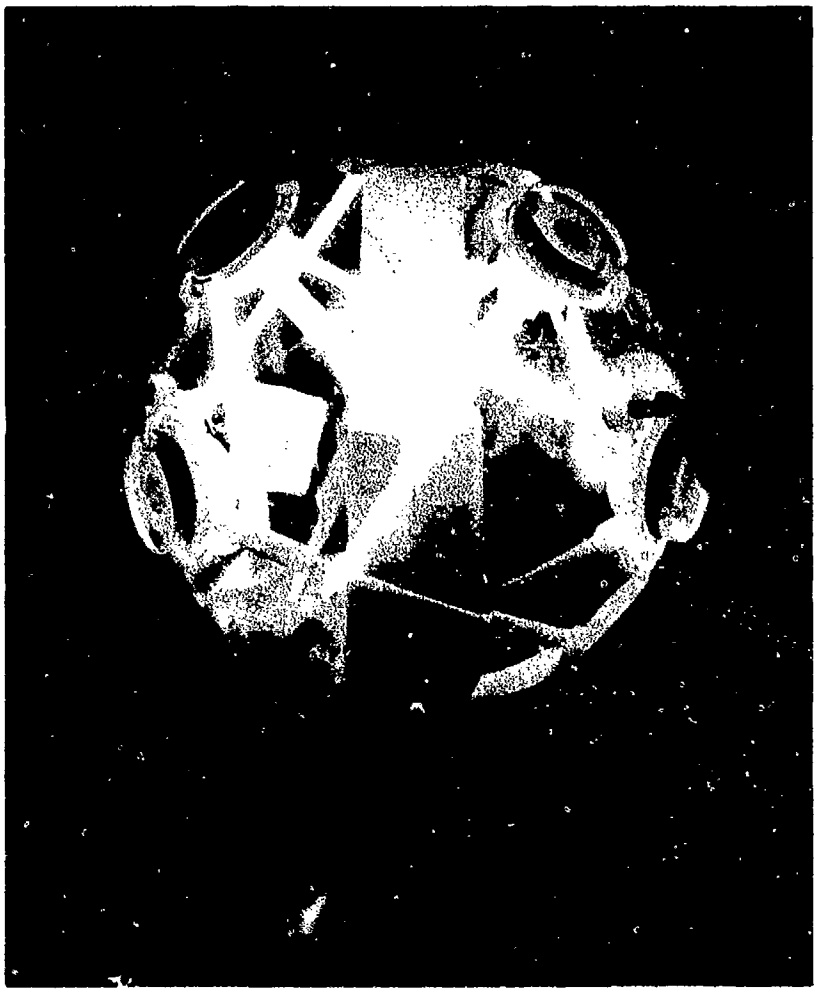

Figure 16. Honeywell GG1330 laser triad rate gyro.

7.1.3 Lock-in -- The phenomenon of lock-in has historically been a most prominent error source in the laser gyro and the most difficult to handle. The means for compensating lock-in has been the principal factor determining the configuration and performance of laser gyros from different manufacturers.

The phenomenon of laser-gyro lock-in arises because of imperfections in the lasing cavity, principally the mirrors, that produce backscattering from one laser beam into the other. (44) The resulting coupling action tends to pull the frequencies of the two beams together at low rates producing a scale-factor error. For rates below a threshold known as the lock-in rate, the two beams lock together at the same frequency producing no output (i.e., a dead-zone). Figure 17 illustrates the effect of lock-in on the output of the laser gyro as a function of steady input rate*.

The magnitude of the lock-in effect depends primarily on the quality of the mirrors. In general, lock-in rates on the order of 0.01 to 0.1 degree-per-second are the lowest levels achievable with today's laser gyro technology (with 0.63-micron laser wavelength). Compared with 0.01-degree-per-hour navigation requirements, this is a serious error source that must be overcome.

A straight-forward and effective approach for overcoming lock-in is mechanically dithering the laser block at high frequency through a stiff dither flexure suspension built into the gyro assembly. The spoked wheel-like structure in Figure 15 is a rotary spring. One spring on each side of the laser block suspends it from the center post. Piezoelectric transducers on one of the springs provide the dither-motor drive mechanism (Figure 14) to vibrate the lasing block at its resonant frequency about the input axis through a small angle but at high rates. The dither rate amplitude and acceleration are designed so that the dwell time in the lock-in zone is short such that lock-in will never develop. The result is a gyro that has continuous resolution over the complete rate range. The residual effect of lock-in is a negligible scale factor nonlinearity due to the averaging of the gyro input rate across the lock-in region (37), and a small random error in the gyro output (random rate noise) that is introduced each time the block passes through lock-in (at twice the dither frequency).

---

*Figure 17 illustrates the effect of lock-in under steady-state conditions (i.e., under relatively constant input rates). Lock-in is actually a nonlinear dynamic characteristic whose response is dependent on both the amplitude and frequency content of the gyro input rate. (37)

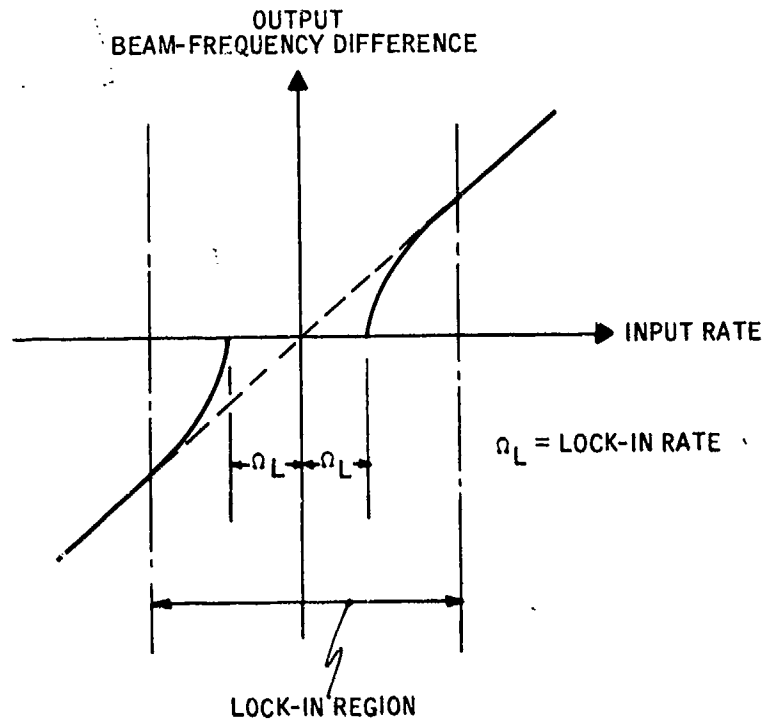

Figure 17. Laser gyro lock-in.

By mounting the readout reflector prism on the gyro case and the readout photodiodes on the block (Figure 13), a simple mechanism can be provided to remove the dither signal from the gyro output. If the gyro center of rotation is selected properly, the translation of the dither beam across the prism causes a fringe motion at the detector that identically cancels the dither rate sensed by the block. The result is an output signal that accurately measures the rotation of the gyro case, free from the dither oscillation. Alternatively, the readout-prism can be mounted with the readout-diodes directly on the gyro block, with a digital filter used to eliminate the unwanted dither motion from the gyro output. The penalty is the bandwidth limitation associated with the digital filter dynamic response.

7.1.4 Other Methods for Lock-in Compensation -- The original alternative to mechanical dither was the use of a Faraday cell within the laser cavity (37). A Faraday cell contains a magnetically active optical material whose index-of-refraction to circularly-polarized light can be altered by an applied magnetic field. Since laser gyros operate with plane-polarized laser beams, quarter wave plates must be included in the Faraday-cell to circularly polarize the light entering, and plane-polarize the light leaving the cell. By applying a magnetic field across the Faraday cell, a differential index-of-refraction shift is created between the clockwise and counterclockwise laser beams, producing a differential change in the optical path length between the two beams. A frequency difference or bias is thereby generated between the two beams with amplitude and phase determined by the amplitude and phase of the applied magnetic field. Typical Faraday-cell mechanizations have incorporated ac-coupled square-wave magnetic control-fields to washout bias errors associated with control-electronics offsets. The resulting bias, having known magnitude and phase is then easily removed from the gyro pulse-output circuitry by digital subtraction.

An alternate to the Faraday-cell approach is the magnetic-mirror concept (based on the transverse Kerr effect) in which a magnetically sensitive inner coating (e.g., iron) is applied to one of the laser mirrors. (39, 45) By applying a magnetic field to the mirror transverse to the laser beam, a differential phase shift is introduced between the reflected clockwise and counterclockwise beams which appears as a differential path-length change around the cavity. The result is a bias imposed on the gyro output that is controllable by the applied magnetic field. Bias uncertainties can be compensated through use of an alternating biasing technique (such as the square-wave approach utilized with the Faraday cell). Additionally, the magnetic mirror can be operated in a saturated bias state to eliminate bias error susceptibility to stray magnetic fields, a problem with the Faraday cell which has generally required magnetic shielding around the gyro to minimize magnetically induced error effects.

An advantage for the Faraday-cell or magnetic-mirror concepts is the ability to develop lock-in bias compensation electrically without a mechanical dither flexure requirement for each gyro. As a result, high packaging densities are achievable through multi-gyro integration (e.g., Figure 16). Another advantage arises because of the ability to generate a square-wave dithered bias that has a low frequency and a rapid traversal rate through lock-in (i.e., short dwell time in the lock-in zone for each traversal, and few traversals per unit of time). Thus, lower random noise is generated from this potential error source (as contrasted with mechanically dithered units where, due to the inertial/spring physical characteristics of the gyro block/dither assembly, high traversal rates through lock-in to reduce random error each dither cycle tend to be accompanied by high dither frequencies, hence many random errors per unit time -- see subsection 7.1.3).

The principal difficulty with the Faraday-cell has been the introduction of thermally and acceleration-sensitive bias errors into the gyro through unpredictable birefringent and anisotropic effects in the Faraday cell. The latter error can be decreased by reducing the length of the Faraday cell (and its associated biasing capability). Reduction of bias capability, however, generates scale-factor nonlinearities due to the inability to keep the average rate into the gyro well outside of the lock-in region.

Little has been published on the error mechanisms associated with magnetic mirrors. Reference 45 indicates that magnetic mirrors designed for a large lock-in biasing capability also introduce large losses into the lasing cavity due to their accompanying low reflectivity. The loss effect is diluted as bias amplitude capability is reduced. Since higher gain and an accompanying degradation in gyro performance stability (see subsection 7.1.5) are required to overcome added cavity losses, this suggests that a tradeoff exists in the design of magnetic mirrors between increased gyro scale-factor nonlinearities (for low-bias-amplitude mirrors, hence less effective lock-in compensation) versus decreased gyro stability (for high-bias-amplitude mirrors). It also suggests that magnetic-mirror technology may be difficult to apply in 0.63-micron lasers (a higher accuracy gyro configuration compared to the 1.15-micron wavelength units but with lower available gain to overcome cavity losses; see subsection 7.1.5). Except for experimental models, laser gyros incorporating magnetic mirrors to date have only utilized the 1.15-micron transition, and have been implemented with lower amplitude lock-in biasing capabilities compared with mechanically dithered instruments. (39,46)

Another approach for overcoming lock-in has been the multioscillator or differential laser gyro (DILAG) concept. (45,47,48,49) This method also incorporates a Faraday bias cell, but in a manner that tends to cancel the effects of bias shift generated by the intrusion of the cell into the laser cavity. A polarizing crystal is used within the cavity to create two pairs of counter-rotating beams, each pair oppositely polarized from the other. Hence, two laser gyros are created in the same cavity, each being separable through use of a polaroid filter on the output. The effect of the opposite polarization between the two laser sets is to make each respond in the opposite sense to the applied Faraday bias. Hence, one gyro output becomes biased in the opposite direction from the other. Summing the two signals doubles the sensed rate signal and theoretically cancels the Faraday bias from the output, including the deleterious effects of bias uncertainties. As a result, high amplitudes of Faraday bias can be used, providing adequate capability for compensating lock-in. In addition, the need to use alternating bias is eliminated due to the cancellation of bias offset uncertainties at the gyro output.

The accuracy of the DILAG approach hinges on the degree to which error effects in the gyro pairs are equal and opposite. Little has been published in this regard in the open literature. One possible source of noncancelling bias error in the DILAG is anisotropic and birefringent effects in the polarizing crystal. Reference 50 suggests that the effect of off-nominal cavity tuning (i.e., operation off the center of the Doppler gain curve) can have a significant contribution to noncancelling bias errors in the DILAG. Because of the polarizing crystal and Faraday cell in the laser cavity, higher losses are present in the DILAG which must be compensated by higher gain. Decreased accuracy can thereby result (see subsection 7.1.5).

7.1.5 Laser Gyro Operating Wavelength -- Laser gyros have been designed for operation with 0.63-micron (visible red) or 1.15-micron (infrared) laser wavelengths. In general, the tradeoff between the two wavelength configurations has been higher accuracy but a more sophisticated design and manufacturing technology for the visible lasers, versus lower performance but simpler design and manufacturing methods for the infrared units.

From a performance standpoint, laser gyro lock-in, bias and scale-factor errors are generally lower for the 0.63-micron instruments. Lock-in is proportional to the operating wavelength squared (44), hence, other factors being equal, is a factor-of-four smaller for the 0.63-micron gyro. Laser gyro readout detectors (typically silicon) have a higher amplitude response to the 0.63-micron compared to the 1.15-micron wavelength, hence higher gains are generally required in 1.15-micron lasers for adequate output signal strength. Since laser gyro scale-factor error increases with laser gain (37,44,51) decreased scale-factor accuracy results. Langmuir flow also increases with increasing gyro gain (41), thus lower gyro bias stability is generally characteristic of 1.15-micron laser-gyro configurations.

Laser gain increases with increasing wavelength (38), hence higher gains are typically achievable with 1.15-micron units and cavity losses are more easily overcome (or conversely, cavity loss design and manufacturing requirements can be relaxed). For the 0.63-micron laser gyro, cavity design and manufacturing processes must be carefully controlled to assure that losses are stable and less than the available gain. From a mirror technology standpoint, the 1.15-micron laser dielectric mirror is typically simpler to design and manufacture, due to the lower sensitivity of its transmissibility characteristic with material parameter variations. The 0.63-micron mirror technology on the other hand can have significant transmissibility variations with parameter changes. Consequently 0.63-micron mirror materials must be more stable to maintain constant gain/loss characteristics in the laser cavity for repeatable gyro performance.

7.1.6 Size Versus Performance -- General scaling laws for laser gyros vary, depending upon gyro configuration and analytical error theory assumptions. Honeywell's experience with mechanically dithered units has been that lock-in and bias uncertainty vary inversely between the square and cube of the gyro path length, and scale-factor uncertainty varies inversely as the path length. (37,51) Thus, laser gyro performance is heavily influenced by gyro size with the larger units being the most accurate.

7.2 Analytical Description and Error Model

Because the laser gyro is based on optical rather than inertial mass principles, the device has no acceleration-sensitive bias errors that corrupt its accuracy. Theoretically (without instrument imperfections), the laser gyro is an ideal single-degree-of-freedom incremental rate-integrating sensor.

The analytical model for the laser gyro parallels that for the single-degree-of-freedom floated gyro (see Eq. (8), (10), and (11)) with errors associated with mass properties removed

$$\omega_{OUTPUT} = (1 + \epsilon)(\omega_x + \gamma_z \omega_y - \gamma_y \omega_z) + \omega_B$$

$$\epsilon = \epsilon_o + f(|\omega_x|) + g(\omega_x) \qquad (44)$$

$$\omega_B = B_o + n_1 + n_2$$

where

ω_{OUTPUT} = gyro-output signal

ω_x = gyro-input rate

ϵ = gyro scale-factor error

ω_B = gyro bias error

γ_y, γ_z = misalignments of the gyro lasing plane relative to the nominal gyro input axis

ω_y, ω_z = angular rotation rates of the gyro case normal to the input axis

ϵ_o = "fixed" scale-factor error

$f(|\omega_x|)$ = symmetrical (relative to positive and negative input rates) linearity error

$g(\omega_x)$ = generalized linearity error (containing symmetrical and asymmetrical components)

B_o = "fixed" bias error

n_1 = random bias error with unbounded integral value

n_2 = random bias error with bounded integral value

It should be noted that the analytical model defined by Eq. (44) represents the net effective input/output relation for the laser gyro with control loops and lock-in compensation implemented. Analytical models for the "open-loop" gyro are available in the literature that define the dynamic characteristics of the lock-in effect (37, 44). In general, however, these models are valuable principally for gyro design; they are not useful for system-error-analysis purposes.

The "fixed" scale-factor-error coefficient (ϵ_o) in Eq. (44) is caused principally by gain/loss variations in the laser cavity, laser path-length deviations from nominal due to manufacturing tolerances and, depending on design adequacy, residual thermal effects (anomalies in the path-length control loops in compensating residual thermal expansion of the Cervit laser cavity). The symmetrical scale-factor-error term ($f(|\omega_x|)$) is the residual effect of lock-in for laser gyros employing mechanical dither for compensation. (67) The $g(\omega_x)$ term is the residual effect of lock-in for gyros incorporating nonmechanical lock-in compensation. In general, the magnitude of the scale-factor linearity error for a given input rate is proportional to the degree to which the biased gyro input is removed from the lock-in region (on the average) divided by input rate being sensed (i. e., the linearity error is measured as a fraction of input rate). The width of the lock-in region is proportional to lock-in rate, thus, low scale-factor linearity error is achieved with a high ratio of applied bias to lock-in rate.

The B_o fixed-bias term in the laser gyro is caused by circulating flow phenomena in the lasing cavity that cause differential optical path-length variations between the clockwise and counterclockwise laser beams (37, 41), forward-scattering effects caused by laser cavity interference with the laser (e. g., beam interractions with imperfect mirror surfaces) that produce differential phase shifts between the laser beams, and residual errors introduced by the lock-in compensation device. The latter effect is peculiar to laser gyros using nonmechanical lock-in compensation techniques.

The n_1 error is a white- or colored white-noise effect generated within the lasing cavity. A classical cause, in the case of mechanically-dithered laser gyros, is a random-angle error introduced each time the gyro input rate is cycled through the lock-in zone (twice each dither cycle). For laser gyros utilizing nonmechanical lock-in compensation, the n_1 random noise term is present, but its source is not as well understood. In general, n_1 is caused by random instabilities in the bias-producing mechanisms in the lasing cavity. The n_1 error is typically measured in terms of the root-mean-square value of its integral over a specified time period (that is long compared to the n_1 noise-process correlation-time). As with classical zero-mean random-noise processes, the average magnitude of the square of the integral of n_1 builds linearly with time; hence, the root-mean-square value builds as the square-root of time. The performance figure for n_1 is typically expressed in degrees-per-square-root-of-hour (deg/$\sqrt{\text{hr}}$, see Table 1).

The n_2 bounded-noise term (on an integral basis) is caused by scale-factor errors in the mechanism used to eliminate lock-in compensation bias from the output of laser gyros employing alternating bias. For mechanically dithered gyros with an off-block readout-prism mount for passive-mechanical bias removal (see subsection 7. 1. 3), n_2 is caused by an off-nominal center-of-dither rotation. For

mechanically dithered gyros with block-mounted readout prism, n_2 is caused by anomalies or design limitations in the dynamic filter used for dither rate attenuation. For either mechanical dither compensation figuration, the n_2 effect is measured in terms of the root-mean-square value of its integral (i.e., seconds-of-arc), and is usually considered as a part of the gyro-output-pulse quantization uncertainty for error analysis purposes. For laser gyros employing alternating electro-optical bias for lock-in compensation, n_2 is caused by scale factor uncertainties in the applied electro-optical bias, hence, errors introduced in digitally subtracting an equivalent bias rate from the gyro pulse-output. For error analysis purposes, the effect can be modeled as a saw-tooth waveform with amplitude expressed in seconds of arc and period equal to the alternating bias period.

In general, the B_o, ϵ_o, γ_y, γ_z terms in Eq. (44) are measurable and predictable to a large extent for purposes of compensation. The stability of the measured error effects (over time and temperature) is heavily influenced by the gyro-mechanization approach utilized, particularly with regard to lock-in compensation. The remaining errors in Eq. (44) are generally unpredictable (in a practical sense) and controllable only through gyro design and manufacturing practices established to satisfy application requirements.

7.3 Performance and Application Areas

Because of its high rate capability that is independent of bias accuracy, performance insensitivity to acceleration, rugged construction, and inherently high reliability (due to the absence of moving parts), proposed utilization areas for the laser gyro have spanned the spectrum from benign to rugged environmental applications with low- to high-accuracy performance requirements. The versatility of the instrument is one of its principal attributes due to the potential for large-volume production with associated reductions in cost and increases in reliability that accompany large-scale production programs.

Performance figures compatible with 1-nmi/hr inertial navigator requirements (see Table 1) have been demonstrated with mechanically dithered triangular laser gyros with 0.63-micron wavelength and 5.7-inch size (each triangle leg) by gyro laboratory testing and system flight testing. (3, 7, 10, 52, 53) These performance capabilities have been achieved without thermal controls, through thermal and vibration exposures, from turn-on to turn-on, and over several years without calibration. The warm-up time for these instruments (as for all laser gyros) is negligible; full gyro operation is attained at the instant of turn-on including full performance capabilities compatible with Table 1 high accuracy requirements for the newer technology configurations. (10) Limited data under high-g sled tests have confirmed the predicted g-insensitivity of the device (54).

Performance capabilities of laser gyros utilizing nonmechanical bias for lock-in compensation have been more compatible with the lower accuracy (e.g., AHRS) applications (see Table 1). Laser gyros designed with magnetic-mirror technology using the 1.15-micron transition for AHRS-accuracy applications have readily achieved performance levels in the Table 1 AHRS category. (39, 42, 43, 46, 55) Laser gyros designed around the DILAG concept have utilized the 0.63-micron transition and have had performance goals compatible with the 1-nmi/hr INS requirements in Table 1. The limited test data available on the DILAG, however, suggest that further development is needed before the concept can be seriously considered for 1-nmi/hr applications (56). The additional complexity in implementing the concept (i.e., four mirrors, polarizing crystal, dual-gyro electronics and readout) (47) would appear to make the DILAG unattractive for the lower accuracy AHRS-class applications where its demonstrated performance level is acceptable.

Random noise for the laser gyro is one of its important error sources in 1-nmi/hr inertial navigation applications that must be overcome to achieve fast reaction times. High random noise extends the time for system-heading determination to filter the earth-rate signal from the gyro noise in establishing initial heading. (10) The 0.003-deg/$\sqrt{\text{hr}}$ figure in Table 1 is consistent with fast reaction times desired in advanced aircraft. Random noise for mechanically dithered laser gyros is principally a function of mirror quality and manufacturer experience. The technology level at Honeywell with a 0.63-micron wavelength transition is routinely achieving random-noise coefficients in the 0.002- to 0.008-deg/$\sqrt{\text{hr}}$ range. With the benefits of learning as laser gyro technology phases into production, 0.003-deg/$\sqrt{\text{hr}}$ should become standard performance.

Rate capabilities for laser gyros are inherently high, limited only by the noise/bandwidth characteristics of the readout electronics. Requirements in Table 1 are easily achieved with today's technology. The scale-factor accuracy of the 0.63-micron gyro is exceptionally high (10), meeting the Table-1 higher accuracy 5-ppm performance figure. The high rate and scale-factor accuracy capabilities of the laser gyro are principal reasons that the device is well suited for high-accuracy use in high-dynamic rate environments, an application area where torque-to-balance gyros have limited utility (due to scale-factor-accuracy limitations).

Sensor alignment accuracy for the laser gyro is determined by the structural stability of the mechanical interface between the lasing plane and the sensor mount. Notably absent is the misalignment caused by torque-loop servodynamic error (present with the torque-to-balance instruments) and the effect of pickoff null movement (present with all rotating mass gyros). Alignment accuracy capabilities of 5 seconds-of-arc (commensurate with Table 1 INS requirements) are readily achievable with mechanically dithered laser gyros. In the case of the nonmechanically-dithered gyro, utilization of the integrated multiple-gyro packaging design (e.g., Figure 16) provides exceptional alignment stability between gyro input axes for applications requiring high alignment accuracy in severe dynamic environments. (57, 58)

The deficiency of today's mechanically dithered laser gyro is its size. The GG1300 (Figure 15), the largest laser gyro produced by Honeywell, and which has demonstrated the highest performance levels thus far achieved with laser-gyro technology, has a 5.7-inch path length (each side of the lasing triangle) and is 115 cubic inches in volume. The newer-technology GG1342 laser gyro currently in development at Honeywell for 1-nmi/hr INS applications, has a 4.2-inch path length, and outside

dimensions of 6.8 by 5.8 by 2.1 inches (or 84 cubic inches in volume). Comparable figures for the alternate high-accuracy strapdown momentum-wheel gyros are generally half the volume of the GG1342 (including electronics). For lower accuracy applications where nonmechanically dithered performance is adequate, the laser-gyro size disadvantage can be eliminated through integrated multiple-gyro packaging.

8. PENDULOUS ACCELEROMETER

Accelerometers utilized to date in strapdown attitude reference and navigation applications have almost exclusively been of the pendulous torque-to-balance design. (18) A typical pendulous accelerometer is shown in Figure 18. The unit consists of a hinged pendulum assembly, a moving-coil signal-generator/pickoff that senses angular movement of the pendulum from a nominally null position, and a permanent-magnet torque-generator that enables the pendulum to be torqued by electrical input. The torquer magnet is fixed to the accelerometer case, and the coil assembly is mounted to the pendulum. Delicate flex leads provide electrical access to the coil across the pendulum/case hinge junction. Electronics are included for pickoff readout and for generating current to the torquer.

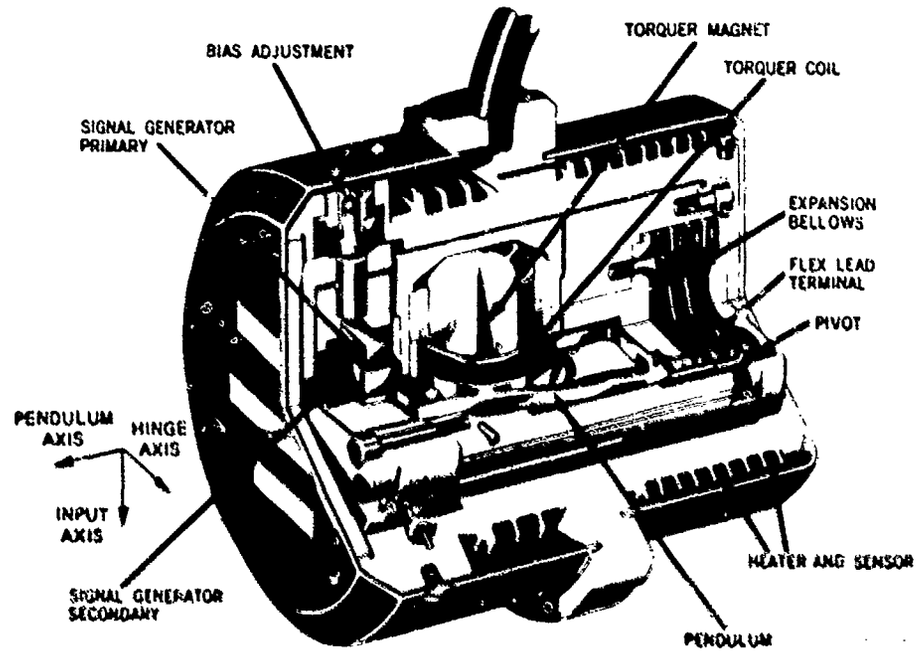

Figure 18. Honeywell GG177 fluid-damped pendulous accelerometer.

The device is operated in the caged mode by applying electrical current to the torquer at the proper magnitude and phasing to maintain the pickoff at null. Under these conditions, the electrically generated torque on the pendulum balances the dynamic torque generated by input acceleration normal to the pendulum plane. Hence, the electrical current through the torquer becomes proportional to the input acceleration, and is the output signal for the device.

8.1 General Design Considerations

Mechanization approaches for the pendulous accelerometer vary between manufacturers, but generally fall into two categories: fluid filled and dry units. Fluid-filled devices utilize a viscous fluid in the cavity between the pendulum and case for damping and partial flotation. The dry units use dry air, nitrogen, or electromagnetic damping.

Utilization of the fluid-filled approach generally simplifies the pendulum design due to the natural damping of pendulum resonances afforded by the fluid, the ability to achieve a given pendulosity with a larger pendulum assembly (due to the partial fluid flotation) with associated reductions in manufacturing tolerances, and the ease in achieving good damping in the torque-to-balance loop. The disadvantage of the fluid-filled concept is the addition of the fluid with its unique design and manufacturing problems (bellows assembly for fluid expansion, seals for the case and portions of the pendulum assembly, and filling the unit without introducing bubbles that deteriorate performance). The advantage of the dry accelerometer design is the elimination of the problems associated with the fluid. The disadvantage is a more exacting pendulum design (for a given level of performance) to achieve damping without fluid, and to enable device manufacture with generally tighter dimensional tolerances due to the direct transfer of pendulum manufacturing errors to device performance (i.e., without the attenuating effect of partial flotation afforded in the fluid-filled device).

The hinge element for the pendulous accelerometer is a flexible member that is stiff normal to the hinge line to maintain mechanical stability of the hinge axis relative to the case under dynamic loading, but flexible about the hinge line to minimize unpredictable spring restraint torques that cannot be distinguished from acceleration inputs. Materials selected for the hinge are chosen for low mechanical hysteresis to minimize unpredictable spring-torque errors. To minimize hysteresis effects, the hinge dimensions are selected to assure that hinge stresses under dynamic inputs and pendulum movement are well below the yield-stress for the hinge material.

Beryllium-copper has been a commonly used pendulum-hinge material due to its high ratio of yield-stress to Young's modulus (i.e., the ability to provide large flexures without exceeding material yield-stress). A popular low-cost design approach for dry accelerometers has utilized fused quartz for both the hinge and pendulum by etching the complete assembly from a single-piece quartz substrate (see Figure 19). Performance capabilities of the quartz-flexure hinge design have been limited, however, due to the relatively large flexure thickness (hence, spring effect) needed to avoid hinge-fracture under shock and dynamic loads, and the associated bias error that develops due to pickoff null movement (principally a function of temperature).

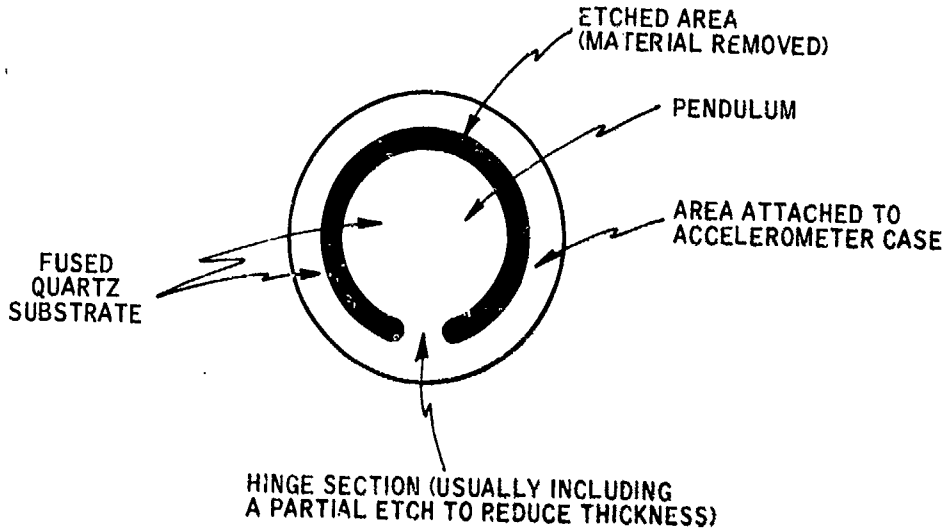

Figure 19. Quartz-flexure pendulum/hinge concept.

8.2 Analytical Description and Error Model

Consider the pendulum assembly for the pendulous accelerometer and define a coordinate frame for it with X normal to the plane of the pendulum, Y along the hinge axis, and Z along the pendulum axis (see Figure 20). A point B is defined on the hinge axis in the plane of symmetry of the pendulum, and length ℓ_{CG} is defined from B to the pendulum center of mass. Case-fixed coordinate axes are also defined to be nominally parallel to the pendulum axes except for small angular displacement θ of the pendulum relative to the case about the hinge axis (i.e., the angle sensed by the accelerometer pickoff). A reference point A is defined as fixed to case axes and lying on a line from point B through the pendulum center of mass when $\theta = 0$. An equation can now be derived for the accelerometer output in terms of the acceleration of the reference point A.

First group the forces on the pendulum into four categories

$$\underline{F}_P = \underline{F}_H + \underline{F}_D + \underline{F}_T + \underline{F}_e \qquad (45)$$

where

$\underline{F}_P$ = net force on the pendulum

$\underline{F}_H$ = reaction force at the hinge

$\underline{F}_D$ = damping force (proportional to $\dot{\theta}$) provided by a damping mechanism designed into the instrument (e.g., electromagnetic)

$\underline{F}_T$ = force provided by the torque-generator

$\underline{F}_e$ = residual error forces created by instrument imperfections

The associated net moment applied to the pendulum about an axis parallel to the hinge axis (y) and through the pendulum center-of-mass is

$$M_{y_P} = [-(\underline{\ell}_{CG} \times \underline{F}_H) + \underline{M}_s + \underline{M}_D^* + \underline{M}_T^* + \underline{M}_e^*] \cdot \underline{u}_y \qquad (46)$$

where

M_{y_P} = Net y-axis moment on the pendulum about the center-of-mass

$\underline{M}_s$ = Spring torque about the hinge axis associated with the pendulum suspension mechanism

$\underline{M}^*_D, \underline{M}^*_T, \underline{M}^*_e$ = moments about the center of mass associated with $\underline{F}_D, \underline{F}_T$, and $\underline{F}_e$

$\underline{\ell}_{CG}$ = distance vector with magnitude ℓ_{CG} from point B to the pendulum center-of-mass

$\underline{u}_y$ = unit vector parallel to the hinge axis (y)

The form of the moment term associated with $\underline{F}_H$ in Eq. (46) is the simple cross-product relation indicated about the hinge axis because $\underline{\ell}_{CG}$ intersects the hinge line. Consequently, only the components of $\underline{F}_H$ along the hinge line and normal to the pendulum can have a moment about the center-of-mass and along $\underline{u}_y$. Since the moment arm for each of these $\underline{F}_H$ components is the same ($\underline{\ell}_{CG}$), the composite force vector $\underline{F}_H$ can be used in total without regard to the individual moment arms for the separate $\underline{F}_H$ hinge force components.

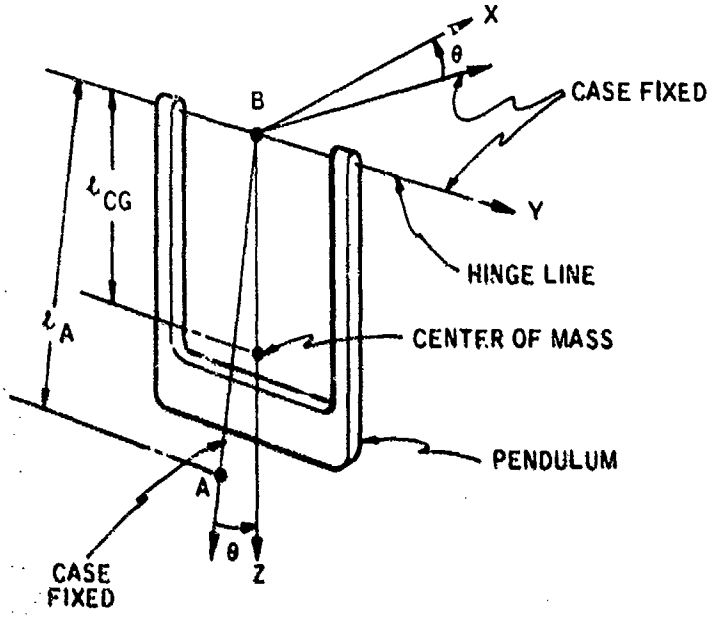

Figure 20. Pendulous-accelerometer coordinate frame definition.

With Eq. (45) for $\underline{F}_H$, Eq. (46) becomes

$$M_{y_P} = [-(\underline{\ell}_{CG} \times \underline{F}_P) + \underline{M}_s + (\underline{M}^*_D + \underline{\ell}_{CG} \times \underline{F}_D) + (\underline{M}^*_T + \underline{\ell}_{CG} \times \underline{F}_T) + (\underline{M}^*_e + \underline{\ell}_{CG} \times \underline{F}_e)] \cdot \underline{u}_y = [-(\underline{\ell}_{CG} \times \underline{F}_P) + \underline{M}_s + \underline{M}_D + \underline{M}_T + \underline{M}_e] \cdot \underline{u}_y \quad (47)$$

where

$\underline{M}_D, \underline{M}_T, \underline{M}_e$ = composite error moment terms in brackets [ ] in Eq. (47)

M_{y_P} = net y-axis moment on the pendulum about the center-of-mass

The vector components in Eq. (47) are defined in pendulum axes as

$$\underline{F}_P = \begin{pmatrix} F_{x_P} \\ - \\ - \end{pmatrix}$$

$$\underline{\ell}_{CG} = \begin{pmatrix} 0 \\ 0 \\ \ell_{CG} \end{pmatrix}$$

$$\underline{M}_s = \begin{pmatrix} - \\ M_s \\ - \end{pmatrix}$$

$$\underline{M}_D = \begin{pmatrix} - \\ M_D \\ - \end{pmatrix}$$

$$\underline{M}_T = \begin{pmatrix} - \\ M_T \\ - \end{pmatrix}$$

$$\underline{M}_e = \begin{pmatrix} - \\ M_e \\ - \end{pmatrix}$$

with

$$M_s = -K\theta$$

$$M_D = -C\dot{\theta}$$

where

K = pendulum spring-torque spring-constant

C = pendulum angular motion ($\dot{\theta}$) damping coefficient

M_T = pendulum torque provided by the torque-generator

M_e = net error torque on the pendulum about the hinge axis

Substitution in Eq. (47) provides the equivalent scalar form for the net y-axis moment on the pendulum about the center-of-mass

$$M_{y_p} = -F_{x_p} \ell_{CG} - C\dot{\theta} - K\theta + M_T + M_e \tag{48}$$

The x-force and y-moment momentum-transfer relations for the pendulum are now introduced for the M_{y_p} and F_{x_p} terms in Eq. (48)

$$F_{x_p} = m\, a_{x_{CG}}$$

$$M_{y_p} = J_y(\dot{\omega}_y + \ddot{\theta}) + (J_x - J_z)\omega_x \omega_z \tag{49}$$

where

m = pendulum mass

J_x, J_y, J_z = pendulum moments of inertia about the pendulum center-of-mass along axes parallel to the pendulum x, y, and z axes

$a_{x_{CG}}$ = acceleration of the pendulum center-of-mass parallel to the pendulum x-axis

$\omega_x, \omega_y, \omega_z$ = inertial angular rate components of accelerometer case parallel to pendulum x, y, and z axes

2.40

The $a_{x_{CG}}$ term in Eq. (49) can be related to the x-axis acceleration of reference point A (see Figure 20). First define $\underline{\omega}$ as the angular velocity of the pendulum relative to inertial (nonrotating) space, $\underline{\omega}_C$ as the inertial rotation rate of the accelerometer case, and $\underline{\omega}_P$ as the rotation rate of the pendulum relative to the case (due to rotation about the hinge axis). The acceleration of the pendulum center of mass can be equated to the acceleration of point B on the hinge axis (see Figure 20) plus centripetal and angular acceleration effects

$$\underline{a}_{CG} = \underline{a}_B + \dot{\underline{\omega}} \times \underline{\ell}_{CG} + \underline{\omega} \times (\underline{\omega} \times \underline{\ell}_{CG}) \tag{50}$$

with

$$\underline{\omega} = \underline{\omega}_C + \underline{\omega}_P \tag{51}$$

and where

$\underline{a}_{CG}$ = acceleration of the pendulum center of mass

$\underline{a}_B$ = acceleration of point B on the accelerometer hinge axis

A similar expression can be written for the acceleration of point A on the accelerometer case

$$\underline{a}_A = \underline{a}_B + \dot{\underline{\omega}}_C \times \underline{\ell}_A + \underline{\omega}_C \times (\underline{\omega}_C \times \underline{\ell}_A) \tag{52}$$

where

$\underline{a}_A$ = acceleration of the case-fixed accelerometer reference point A

$\underline{\ell}_A$ = distance vector with magnitude ℓ_A from point B to point A

An equation for $\underline{a}_{CG}$ in terms of $\underline{a}_A$ is obtained by combining Eq. (50) to (52)

$$\underline{a}_{CG} = \underline{a}_A - \dot{\underline{\omega}}_C \times \underline{\ell}_A - \underline{\omega}_C \times (\underline{\omega}_C \times \underline{\ell}_A) + (\dot{\underline{\omega}}_C + \dot{\underline{\omega}}_P) \times \underline{\ell}_{CG} + (\underline{\omega}_C + \underline{\omega}_P) \times [(\underline{\omega}_C + \underline{\omega}_P) \times \underline{\ell}_{CG}] \tag{53}$$

The x-axis component of Eq. (53) in pendulum axes is the desired relationship between $a_{x_{CG}}$ in Eq. (49) and a_{x_A} (the x-axis acceleration of the reference point A on the accelerometer case). The vector quantities in Eq. (53) are defined in terms of their X, Y, and Z components in pendulum axes as

$$\underline{\omega}_C = \begin{pmatrix} \omega_x \\ \omega_y \\ \omega_z \end{pmatrix}$$

$$\underline{\omega}_P \begin{pmatrix} 0 \\ \dot{\theta} \\ 0 \end{pmatrix}$$

$$\underline{\ell}_{CG} \begin{pmatrix} 0 \\ 0 \\ \ell_{CG} \end{pmatrix}$$

$$\underline{\ell}_A \begin{pmatrix} -0\ell_A \\ 0 \\ \ell_A \end{pmatrix}$$

Substituting in Eq. (53), neglecting $\theta\,\omega$ compared to ω terms, and evaluating for the x-axis components yields the desired relationship between $a_{x_{CG}}$ and a_{x_A}

$$a_{x_{CG}} = a_{x_A} - (\ell_A - \ell_{CG})\,\omega_y - (\ell_A - \ell_{CG})\,\omega_x\,\omega_z + \ell_{CG}\,\ddot{\theta} \tag{54}$$

Equations (48), (49), and (54) in combination define the dynamic response relation for the pendulous accelerometer. Before combining, revised nomenclature and the effect of accelerometer misalignments are introduced.

The pendulosity (Q) of the accelerometer is defined as the product of the pendulum mass with the distance from the hinge axis to the pendulum center-of-mass

$$Q = m \ell_{CG} \tag{55}$$

The torque-generator torque is defined in terms of an equivalent command-acceleration with a scale-factor error; and the error torque is equated to an acceleration bias defined as the torque-generator command-acceleration needed to nullify the effect of the error torque on the pendulum

$$\begin{aligned} M_T &= \frac{Q}{(1+\epsilon)} a_T \\ M_e &= -\frac{Q}{(1+\epsilon)} a_B \end{aligned} \tag{56}$$

where

a_T = torque-generator command-acceleration

a_B = accelerometer bias

The case angular rate components in pendulum axes (ω_x, ω_y, ω_z) can be related to acceleration components along nominal accelerometer axes. The pendulum is misaligned from the accelerometer case by the pickoff angle (θ) and the accelerometer case may be misaligned from the nominal accelerometer axes, hence

$$\begin{aligned} a_{x_A} &= a_I + \gamma_P a_H - (\gamma_H + \theta) \omega_P \\ \omega_x &= \omega_I + \gamma_P \omega_H - (\gamma_H + \theta) \omega_P \\ \omega_y &= \omega_H + \gamma_I \omega_P - \gamma_P \omega_I \\ \omega_z &= \omega_P + (\gamma_H + \theta) \omega_I - \gamma_I \omega_H \end{aligned} \tag{57}$$

where

I, H, P = nominal accelerometer axes (I = input; H = hinge; P = pendulum; see Figure 18)

With Eq. (55) to (57), Eq. (48), (49), and (54) can be combined to yield the input/output equation for the pendulous accelerometer. Upon combination, rearrangement, and neglecting higher order terms, the result is

$$\begin{aligned} a_T = (1+\epsilon) \Big[& a_I + \gamma_P a_H - (\gamma_H + \theta) a_P - (\ell_A - \ell_{CG} - \frac{J_y}{Q}) \dot{\omega}_H \\ & - (\frac{J_z - J_x}{Q} + \ell_A - \ell_{CG}) \omega_I \omega_P \Big] + a_B + \frac{1}{Q} (J_H \ddot{\theta} + C \dot{\theta} + K \theta) \end{aligned} \tag{58}$$

where

J_H = moment of inertia of the pendulum about the hinge axis (i.e., $J_H = J_y + m \ell_{CG}^2$)

Since ℓ_A (the distance to the acceleration measurement reference point) was arbitrarily defined, it can be selected to simplify the error model. A convenient selection nulls the $\dot{\omega}_H$ effect in Eq. (56)

$$\ell_A = \ell_{CG} + \frac{J_y}{Q} \tag{59}$$

It should be recognized that this selection corresponds to the center of percussion for the pendulum assembly. With Eq. (59), Eq. (58) becomes the final dynamic model form given below:

$$\begin{aligned} a_T = (1+\epsilon) \Big[& a_I + \gamma_P a_H - (\gamma_H + \theta) a_P \\ & - \frac{(J_z + J_y - J_x)}{Q} \omega_I \omega_P \Big] + a_B + \frac{1}{Q} (J_H \ddot{\theta} + C \dot{\theta} + K \theta) \end{aligned} \tag{60}$$

Equation (60) with (59) defines the input/output characteristic for the pendulous accelerometer. In operational usage, the accelerometer is operated in closed-loop fashion such that the command-acceleration (a_T) torquer input is used to maintain the pickoff angle at null. Eq. (59) and (60) are illustrated with this concept in block diagram form in Figure 21. Figure 21 shows that the accelerometer output a_T is proportional to the input a_I (plus error terms) with a bandwidth characteristic determined by the form of the torque-loop mechanization. Implementations commonly utilized for the accelerometer torque-loop electronics are the digital-rebalance pulse-on-demand concept, and the analog-rebalance followup-digitizer approach (see Section 4.).

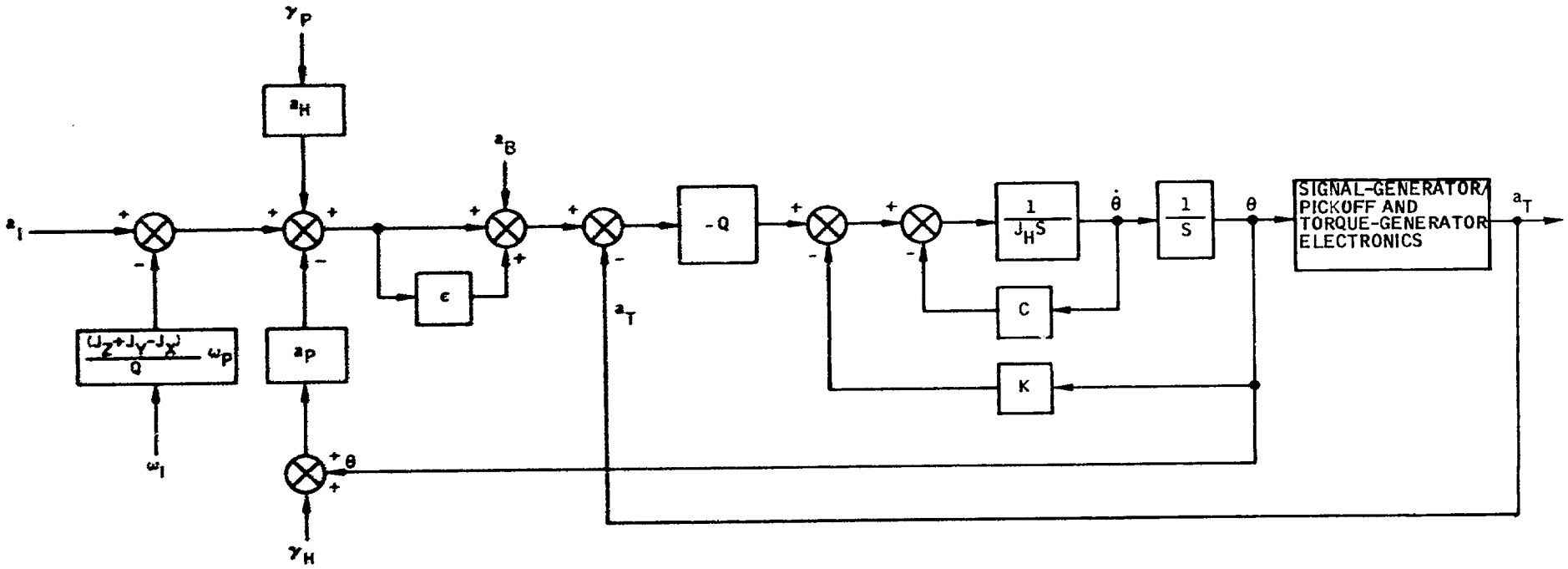

Figure 21. Pendulous-accelerometer analytical response diagram.

Error-input terms in Figure 21 for the pendulous accelerometer include the accelerometer mechanical misalignment errors (γ_H and γ_P), spring-restraint (K) bias and misalignment error due to off-null pickoff angle θ (caused by pickoff-detector null bias and torque-loop dynamic effects), anisoinertia angular-input error ($J_z + J_y - J_x$), torquer scale-factor error (ϵ), and bias error a_B. Of these, the anisoinertia, spring restraint, and pickoff misalignment effects (due to torque-loop bandwidth limitations) are intrinsic to the basic instrument design; the remaining errors are caused by imperfections in the instrument manufacture compared to the ideal design configuration.

A key error source in the pendulous accelerometer is the K θ spring effect in Figure 21. If a significant spring constant K is generated as a result of the pendulum suspension design, care must be taken to assure that the null (under zero input) is stable. Otherwise, large error-torque variations will be generated that cannot be compensated. Variations in θ are caused by pickoff-detector null movement (mechanical movement and electrical bias shifts) and the resulting closed-loop torquing of the pendulum to an offset θ angle position.

The accelerometer-bias term is composed of several contributing factors; a typical error model is given by

$$a_B = C_0 + C_1 + C_2 a_I a_P + n \qquad (61)$$

where

C_0 = g-insensitive bias error

C_1 = bias error generated by vibration inputs (linear and angular) that is unmodelable for purposes of compensation

C_2 = anisoelastic error coefficient caused by unequal compliance (relative to the pivots) in the accelerometer pendulum assembly under g-loading along the pendulum and input axes

n = stochastic random-bias error caused by randomly varying instabilities in the accelerometer assembly

A typical cause for the C_0 g-insensitive bias error is pickoff offset (e.g., caused by pickoff electrical null shift) in conjunction with residual spring torques in the pivots about the hinge line (caused by flex-leads for example). The equivalent error associated with the pivot spring and hysteresis effects in Figure 21 is usually included as part of the C_0 coefficient. The C_1 term has been included to account for the fluid dynamic or gas dynamic effects that are present in accelerometers utilizing fluid or gas (between the pendulum and case) for damping. The inertial and viscous properties of the fluid (or gas) as it interacts with the pendulum have been neglected in the development of Eq. (60) (and Figure 21).

The scale-factor error for the pendulous accelerometer includes linearity error effects and is typically modeled as

$$\epsilon = \epsilon_0 + \epsilon_1 \frac{a_I}{|a_I|} + \epsilon_2 a_I + \epsilon_3 a_I^2 \qquad (62)$$

The terms in Eq. (62) directly parallel those for the floated-gyro scale-factor-error model (Eq. (10)) discussed previously.

Compensation for the pendulous accelerometer is designed to remove the predictable error terms from the output by measuring their values and using them in the system computer for sensor-output correction. The stability of the measured coefficients over time, temperature, vibration, input profile, and from turn-on to turn-on ultimately determines the device accuracy (and required calibration interval).

8.3 Performance and Application Areas

Both fluid-filled and dry versions of the pendulous accelerometer have been utilized in strapdown applications where performance in the Table 1 1-nmi/hr INS category has been required. One of the original strapdown applications for the device was in the velocity cut-off switch for several spacecraft launch vehicles (e.g., a dry unit was utilized on the original Agena upper-stage booster, and a fluid-filled unit was incorporated in the original Delta upper-stage vehicle). Fluid-filled versions are now in use on the advanced Agena and Delta inertial guidance systems. Fluid-filled units have recently demonstrated adequate performance in 1-nmi/hr long-term terrestrial cruise strapdown INS developmental flight tests (3, 4, 5) in moderate vibration environments without heaters utilizing temperature to compensate for thermally sensitive errors (principally scale-factor error and pickoff null instability). An advanced development model strapdown laser-gyro INS has recently been designed for general 1-nmi/hr application utilizing a fluid-filled accelerometer and has initiated developmental testing. (7)

Lower performance strapdown systems (e.g., tactical missile systems) in recent years have almost exclusively utilized the dry quartz-flexure design due to its low-cost benefits. Performance capabilities of the device in these applications have generally been compatible with Table 1 (AHRS) requirements without using heaters for temperature control. Use of the dry design in the higher performance areas has been limited, and has generally required heaters to stabilize performance; e.g., ATIGS. (7, 54) Temperature measurements can be used to compensate for predictable performance variations. However, for the dry quartz-flexure unit, the bias temperature-variations (e.g., pickoff null movement and flex-lead error-torques) have been too large to be accurately calibratable by

temperature measurements alone, hence temperature control has been required to achieve high accuracy (with an accompanying reaction time penalty for warmup, and a cost penalty for temperature controls).

In severe vibrations (possibly amplified by sensor-assembly mounting-structure resonances) rectification of the anisoinertia, and particularly the pickoff-angle cross-coupling error, can produce bias deviations in the pendulous accelerometer (see Figure 21). The latter effect (also known as vibropendulous error), is produced by torque-loop dynamic error under high-frequency acceleration inputs (I), and the resulting cross-coupling of P-axis acceleration into the sensor output (i.e., a g-squared error effect). For I- and P-axis acceleration components at the same frequency, a rectification is possible, depending on the relative phasing of the acceleration components. Worst-case vibropendulous error occurs for acceleration vibration-vector inputs normal to the hinge line, and 45 degrees from the input axis. The magnitude of the vibropendulous effect depends on the bandwidth of the accelerometer loop relative to the vibration frequencies encountered. Bandwidths in the 100- to 300-Hz region are representative of fluid-filled accelerometers, which is generally wide enough to maintain the vibropendulous effect at a tolerable level for most applications (10 $\mu g/g^2$ for typical military vibration profiles including the input-vibration frequency-attenuation effect typically afforded by the strapdown sensor assembly mount). For the dry accelerometer configuration, vibropendulous effects have generally not been as much of a concern because loop bandwidths have been typically wider (e.g. - 800 Hz).

With regard to bandwidth effects, it should be noted that a disadvantage for the pendulous accelerometer in some applications is the need for wide bandwidth to reduce vibropendulous error. This limits the ability of the accelerometer pendulum to filter out high-amplitude vibration inputs that may be present on the input signal. As a result, current levels for the torque loop and associated digitizing electronics (see Section 4.) may be higher and more difficult to handle accurately.

9. CONCLUDING REMARKS

Several sensors are available today that generally meet strapdown system performance requirements, each with advantages and limitations, depending on the area of application. The ultimate selection of a sensor to meet particular requirements can be made only through a careful tradeoff evaluation that assesses reliability, maintainability, cost, size, weight, and power factors, as well as performance. One of the principal tradeoffs in the selection of a strapdown gyro are the potential advantages projected for the newer-technology instruments not yet in production (i.e., the electrostatic and laser gyros) versus the known capabilities and limitations of established production-gyro technology (i.e., the floated rate-integrating and tuned-rotor gyros). For the strapdown accelerometer, tradeoff selection alternatives will remain limited until new innovations are developed specifically for strapdown application that overcome the limitations in existing pendulous accelerometers originally designed for gimbaled application.

10. ACKNOWLEDGMENTS

I would like to express my appreciation to J. Killpatrick, F. Aronowitz, T. J. Podgorski, W. N. Johnson, and V. H. Aske for their valuable comments during the preparation of this paper.

REFERENCES

1. Klass, Philip J., "Laser Gyro Reemerges as INS Contender," Aviation Week and Space Technology, 13 January 1975.

2. Klass, Philip J., "Laser Gyros Find Increased Applications," Aviation Week & Space Technology, 25 July 1977.

3. Developmental Test of the Honeywell Laser Inertial Navigation System (LINS), Final Report, Central Inertial Guidance Test Facility, 6585th Test Group, Holloman Air Force Base, Report ADTC-TR-75-74, November 1975.

4. Strapdown 727 Flight Test Summary Results, Boeing Report B-8182-5-48A, October 1975.

5. Strapdown 747 Flight Test Summary Results, Boeing Report B-8182-6-3A, January 1976.

6. Development Flight Testing of the N-57A Inertial Navigation System, , Central Inertial Guidance Test Facility, 6585th Test Group, Holloman Air Force Base, Report ADTC-TR-75-86, November 1975.

7. Bachman, K. L. and Carson, E. W., "Advanced Development Program for the Ring Laser Gyro Navigator," ION National Aerospace Meeting, Warminster, PA, 28 April 1976.

8. Investigation of Application of Two-Degree-of-Freedom Dry Tuned-Gimbal Gyroscopes to Strapdown Navigation Systems, Final Report, NASA Report CR-132419, April 1974.

9. Duncan, Robert R., "MICRON - A Strapdown Inertial Navigator Using Miniature Electrostatic Gyros," SAE Aerospace Control and Guidance Systems Committee, Paradise Valley, Arizona, 15-17 May 1974.

10. Savage, Paul G., "Laser Gyros in Strapdown Inertial Navigation Systems," IEEE 1976 Position Location and Navigation Symposium, San Diego, California, 1-3 November 1976.

11. Peterson, Roland, "Advantages of Gimbaled Inertial Navigation Systems," NAECON, Dayton, Ohio, 18-20 May 1976.

12. Dynamic Errors in Strapdown Inertial Navigation Systems, NASA Report CR-1962, December 1971.

13. Bortz, J. E., "A New Mathematical Formulation for Strapdown Inertial Navigation," IEEE Transactions on Aerospace and Electronic Systems, Volume AES-7, No. 1, January 1971.

14. Roantree, James P., "Advancements in Strapdown Navigation," NAECON, Dayton, Ohio, 1974.

15. Eberlein, A. J., "Inertial Navigation Interim Report," Honeywell Internal Interoffice Correspondence, 3 May 1972.

16. Pitman, George R. Jr., ed., Inertial Guidance, John Wiley and Sons, New York, 1962.

17. Leondes, Cornelius T., ed., Guidance and Control of Aerospace Vehicles, McGraw-Hill, 1963.

18. Macomber, George R. and Fernandes, Manuel, Inertial Guidance Engineering, Prentice-Hall, Englewood Cliffs, New Jersey, 1962.

19. Britting, Kenneth R., Inertial Navigation System Analysis, John Wiley and Sons, New York, 1971.

20. Wrigley, W., Hollister, W. M., and Denhard, W. G., "Gyroscopic Theory, Design, and Instrumentation," M. I. T. Press, 1969.

21. Flight Test of the Sign III Kalman Inertial Doppler System, Final Report, Central Inertial Guidance Test Facility, 6585th Test Group, Holloman Air Force Base, Report AFSWC-TR-71-94, April 1967.

22. Howe, Edwin W., "A Free Rotor Gyro," Symposium on Unconventional Inertial Sensors, Farmingdale, New York, 1963.

23. Savet, Paul H., "New Trends in Non-floated Precision Gyroscopes," Grumman Research Department Memorandum RM-247J, October 1964.

24. Craig, Robert J. G., "Theory of Operation of Elastically Supported Tuned Gyroscope," IEEE Transactions on Aerospace and Electronic Systems, Vol. AES-8, No. 3, May 1972.

25. Craig, Robert J. G., "Theory of Errors of a Multigimbal, Elastically Supported, Tuned Gyroscope," IEEE Transactions on Aerospace and Electronic Systems, Vol. AES-8, No. 3, May 1972.

26. Craig, Robert J. G., "Dynamically Tuned Gyros in Strapdown Systems," AGARD Conference Proceedings No. 116 on Inertial Navigation Components and Systems, AD-758 127, Paris, France, February 1973.

27. Kornbluth, B., "Derivation of And Test Techniques Used to Investigate Support Mechanism Problems Associated with the Litton Vibrator Gyro," Proc. ION/NASA Meeting on Problems in Inertial Guidance, 21-22 January 1970.

28. Shaw, Jack C., "Benefits of Strapdown Over Gimbal Systems for Aircraft Application," NAECON, Dayton, Ohio, 18-20 May 1976.

29. Harrington, Jr., Captain Edwin V., Bell, Jackie W., and Raroha, Major George H., "MIRA: A New Approach to Integrated Reference Systems," NAECON, Dayton, Ohio, 18-20 May 1976.

30. "Development Test Results of Boeing ISADS System," Informal Discussions with Jack C. Shaw (Boeing) regarding design experience during the development of the Boeing Integrated Strapdown Air Data System, a strapdown navigation system utilizing Teledyne tuned rotor gyros with Boeing-designed gyro electronics (Flight Test Results Reported in References 4 and 5).

31. Craig, Robert J. G., and Russel, James G., "Cost Considerations in a Strapdown Navigation System Using Dry-Tuned Instruments," INTERCON 1975, New York City, New York, 8-10 April 1975.

32. Moore, J. P., "Trident Electrostatically Suspended Gyro Monitor (ESGM)," SAE Aerospace Control and Guidance Systems Committee, Phoenix, Arizona, 17 May 1974.

33. Bold, N. T., Engebretson, H. J., and Moore, J. P., "Universal Marine System Gyro-ESG," ION Conference, Long Island, New York, 23-24 October 1973.

34. Warzynski, Captain Robert R. and Ringo, Ronald L., "The Evolution of ESG Technology," Agard Symposium, June 1971.

35. Eberlein, A. J., and Savage, P. G., Strapdown Cost Trend Study and Forecast, NASA Report CR-137585.

36. Killpatrick, Joseph, "The Laser Gyro," IEEE Spectrum, October 1967.

37. Aronowitz, Frederick, "The Laser Gyro," Laser Applications, Vol. 1, Academic Press, New York, 1971.

38. Garrett, C. G. B., "Gas Lasers," McGraw-Hill, 1967.

39. Morrison, Robert F., Laser Gyro Reaction Time Investigation Program, AFAL Report AFAL-TR-74-169, September 1974.

40. Jenkins, F.A., and White, H.E., Fundamentals of Optics, McGraw-Hill, 1950.

41. Podgorski, Ted J., and Aronowitz, Fred, "Langmuir Flow Effects in the Laser Gyro," IEEE Journal of Quantum Electronics, Vol. QE-4, No. 1, January 1968.

42. Morrison, R.F., Levinson, Dr. E., and Bryant Jr., B.L., "The SLIC-7 Laser Gyro, Inertial Guidance System," NAECON, Dayton, Ohio, 1977.

43. Morrison, R., Levinson, Dr. E., and McAdory, R., "The SLIC-15 Laser Gyro IMU for Mid-course Missile Guidance," ION National Aerospace Symposium, Warminster, Pennsylvania, 27-28 April 1976.

44. Aronowitz, Frederick, and Collins, R.J., "Mode Coupling Due to Back Scattering in a HeNe Traveling Wave Ring Laser," Applied Physics Letters, Vol. 9, No. 1, 1 July 1966.

45. Dewar, Dr. D., "The Laser Gyroscope," Royal Aeronautical Society, London, 12 January 1977.

46. Feldman, Julius, Gootkind, David, and Helfant, Stephan, Sperry ASLG 15 Laser-Gyro Performance and Error Model, Final Report, Charles Stark Draper Laboratory Report R-989, July 1976.

47. Roantree, James P., Burns, John E., and McAdory, Robert W., "Differential Laser Gyro Technology," NAECON, Dayton, Ohio, 1975.

48. Bresman, J., Cook, H., and Lysobey, D., "Differential Laser Gyro Development," ION National Aerospace Meeting, Warminster, Pennsylvania, 28 April 1976.

49. Mathews, J.B., "The Laser Gyro and its Impact on Guidance and Navigation Applications," 9th Annual Electro-Optics/Laser Conference, Anaheim, California, 25-27 October 1977.

50. Grant, D., Hambenne, J., Hutchings, T., Sanders, V., Scully, M., "A Multioscillator (Four-Mode) Ring Laser Gyro Report," NAECON, Dayton, Ohio, 1977.

51. Aronowitz, F., and Lim, W.L., "Positive Scale Factor Correction in the Laser Gyro," IEEE Journal of Quantum Electronics, Vol. QE-13, No. 5, May 1977.

52. Savage, Paul G., and Ignagni, Mario B., "Honeywell Laser Inertial Navigation System (LINS) Test Results," Ninth Joint Services Data Exchange Group for Inertial Systems, St. Petersburg, Florida, 18-19 November 1975.

53. Feldman, J., and Helfant, S., "A Laser Gyro Evaluation Plan and Test Results," NAECON, Dayton, Ohio, 1977.

54. Rocket Sled and Centrifuge Testing of the Advanced Tactical Inertial System (ATICS), Central Inertial Test Facility, 6585th Test Group, Holloman Air Force Base, Report ADTC-TR-77-7, January 1977.

55. Pasik, Donald J., Gneses, Morris I., and Taylor, George R., "A Ring Laser Gyro Strapdown Inertial Navigation System: Performance Analysis and Test Results," AIAA Guidance and Control Conference, Boston, Massachusetts, 20-22 August 1975.

56. Stowell, W.K., McAdory, R.W., and Roantree, J.P., "Differential Laser Gyro," IEEE Southeast Conference, Clemson, South Carolina, 5-7 April 1976.

57. Laser Triad Rate Gyro, McDonnell Douglas Report G3236, August 1972.

58. "ABMDA UPSTAGE Experiment," Presentation to Congress by U.S. Department of Defense Directorate of Development, Research, and Engineering, Advanced Research Projects Agency, October 1972.

59. Scoville, A.E., and Yamron, J., "The Mechanization of a Strapdown Inertial System Based on Time-Modulated Torquing," AIAA/JACC Guidance and Control Conference, Seattle, Washington, 15-17 August 1966.

60. A Study of Critical Computational Problems Associated with Strapdown Inertial Navigation Systems, NASA Report CR-968, April 1968.

STRAPDOWN SYSTEM ALGORITHMS

Alan VanBronkhorst
Lear Siegler, Inc., Instrument Division
4141 Eastern Avenue, S. E.
Grand Rapids, Michigan 49508

3-1

SUMMARY

Strapdown system algorithms are the mathematical definition of processes which convert the measured outputs of inertial sensors that are fixed to a vehicle body axis into quantities which can be used to control the vehicle. The outputs of body-fixed inertial sensors are angular rates and linear velocities along orthogonal axes. The measured angular rates are converted into changes in attitude of the vehicle with respect to its initial orientation. The resulting attitude transformation matrix is used to convert the measured velocities from body axes to reference coordinates.

The algorithms which define the direct initial operations on the measured outputs of the sensors are critical and specific for strapdown systems. Operational algorithms for initializing the system and for converting the velocities in reference coordinates into navigation, guidance and control parameters are essentially equivalent to similar algorithms for gimballed inertial systems.

Strapdown system algorithms are always a compromise between accuracy and cost of implementation in airborne digital computers. High iteration rates, sophisticated integration techniques and long word lengths in general improve performance but increase costs. The algorithms are optimized by simulation and/or emulation using a general purpose laboratory digital computer.

This paper describes the essential algorithms in terms of the analytic equations and the procedures for optimizing the critical algorithms.

1. INTRODUCTION

Algorithms for strapdown inertial systems are the specific operations or mathematical processes by which a digital computer transforms measured outputs of the body-fixed sensors into useful parameters for control of the carrying vehicle. The required control parameters (such as vehicle attitude, velocity, and position) in a reference coordinate system, as well as their characteristics (such as resolution, accuracy, and dynamic range) are established by the intended application of the system. Detailed algorithms at the machine level are a function of the instruction set of the computer and the programmer or microprocessor designer. This paper describes only the highest order algorithms: the analytic equations.

The algorithms for a strapdown system are set by the system functional requirements. The only absolutely requisite function for all strapdown systems is the generation of a direction-cosine transformation matrix that relates the attitude of the carrying-vehicle frame axes to an arbitrarily specified reference coordinate system with a known relation to inertial space. The critical processing requirement for any strapdown system is the algorithm that generates this transformation matrix by operation on angle increments measured by the gyroscopes.

2. STRAPDOWN-SYSTEM PROCESSING REQUIREMENTS

The total processing requirements for a strapdown system vary widely, depending on the intended application of the system. Applications range from a simple unslaved uncompensated attitude reference device to a precision autonomous inertial navigation system.

Figure 1 is a logic flow chart showing the computer functions for a typical autonomous strapdown inertial navigation system for a cruise-vehicle application. Although this flow chart shows a main-line high-repetition-rate solution for generating the attitude transformation matrix, and a lower repetition-rate subroutine for generating navigation guidance and control functions, this partitioning scheme is not mandatory. For some applications, a single fixed-iteration program is more effective.

Deviations from the sequence may also be expected in operational systems. Some of the control functions (e.g., attitude) might be calculated before the navigation equations, and the computer self-test processes might be accomplished on a regular basis in flight.

3. SPECIFIC ALGORITHMS

The major algorithms for detailed discussion are start-up, initialization, generation of the transformation algorithm, navigation, and control.

3.1 Start-up and self-test

The operational readiness of almost all state-of-the-art strapdown systems is determined immediately after prime power is applied at turn-on by built-in stimuli-

response go/no-go tests. The complexity of these built-in tests (BIT) and associated built-in test equipment (BITE) is usually determined by the system mechanical configuration and maintainability requirements for fault isolation.

As a general rule, the built-in tests must isolate a very high percentage of system faults to a single functional module such as the gyroscopes, accelerometers, control electronics, and processors. The procedures are straightforward for most systems.

Because sensors are almost always closed-loop servo systems, a conventional test technique is to insert sequential step-function biases in two polarities, using BITE and testing the output-response amplitude as a function of time. For spinning-wheel gyroscopes, it is also necessary to test back emf of the gyro wheels to know that they are synchronized. Sensor tests often include temperature monitoring. Electronics are checked by application of a known input and verification of the expected output.

The processor is checked by a sample problem using inputs stored in memory to represent sensor measurements. The outputs are compared to the known solutions, which are also stored in memory. These outputs are selected to maximize the hardware and software used to arrive at the solutions. These go/no-go sample-problem computer checks are often periodically solved in flight.

Figure 2 is a block diagram of the go/no-go test sequence for an operational strapdown inertial system for missile guidance application.

3.2 Initialization

Any strapdown inertial system, as a dead-reckoning device, must know the initial conditions of the velocity and position vector it must measure. The initial velocity vector direction is established by the process of alignment. Vector magnitude is defined with respect to initial-position and velocity coordinates inserted in the computer from an external source. The initialization process often includes self-calibration of the sensors. These processes are shown in the functional flow diagram of Figure 3.

3.2.1 Alignment

Alignment is the process of initially locating the sensitive axes of the accelerometers with respect to the reference or navigation coordinate system axes.

Alignment may be either autonomous (without recourse to other equipment), or slaved (by matching the strapdown-system outputs to some external system), or any combination of the two techniques. Because practical navigation is most often referenced to an earth-oriented coordinate system, autonomous alignment is feasible by measuring the direction

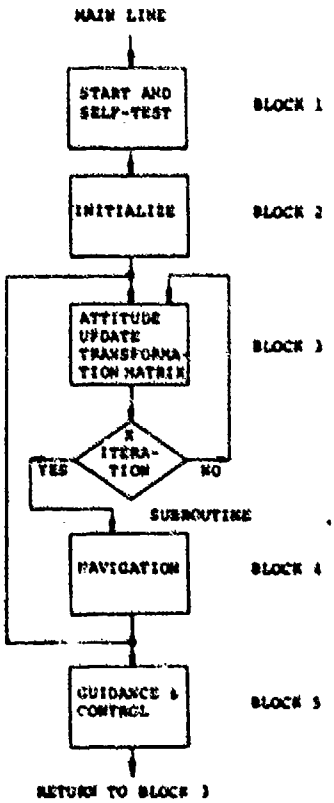

Figure 1. Functional flow diagram, strapdown algorithms.

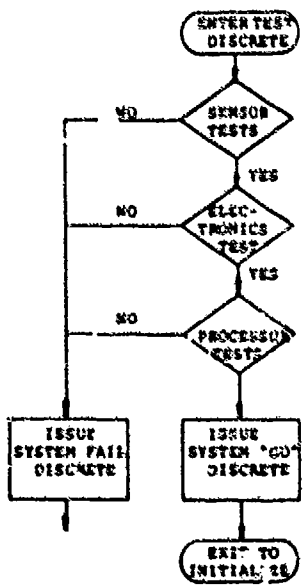

Figure 2. Functional flow diagram, start-up and self-check algorithms.

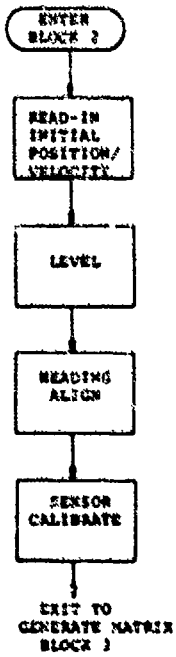

Figure 3. Functional flow diagram, initialization algorithms.

of earth-rate and gravity vectors with the strapdown-system sensors. Autonomous alignment consists of the two-step process of self-leveling and gyrocompassing.

Accelerometers measure both earth-gravity and case accelerations without distinction. In a vehicle that is not accelerating with respect to the earth, self-leveling is accomplished by initial computation of the direction cosine transformation matrix to force the transformed velocity vector (from earth gravity acting on the accelerometers) to have zero components in the horizontal reference coordinate directions.

The analytic relation between the strapdown-system measurements and earth-fixed forcing vectors (gravity and rotation rate) are given by

$$\vec{g} = \begin{bmatrix} 0 \\ 0 \\ g \end{bmatrix}^{*} = \left[C\right]_{B}^{N} \begin{bmatrix} a_x \\ a_y \\ a_z \end{bmatrix} \tag{1a}$$

and

$$\vec{\Omega} = \begin{bmatrix} \Omega_N \\ \Omega_E \\ \Omega_V \end{bmatrix} = \begin{bmatrix} \Omega \cos\lambda_0 \\ 0 \\ \Omega \sin\lambda_0 \end{bmatrix} = \left[C\right]_{B}^{N} \begin{bmatrix} p \\ q \\ r \end{bmatrix} \tag{1b}$$

In these equations

$\vec{g}$ = earth gravity vector
= 32.16 ft/sec^2

$\vec{\Omega}$ = earth rotation vector
= 15.04 °/h

λ_0 = initial latitude of the system

a_x, a_y, a_z = outputs of the system accelerometers

p, q, r = outputs of the system rate gyroscopes

$\left[C\right]_{B}^{N}$ = transformation matrix relating body axes to earth-referenced navigation coordinates

All nine elements of the 3 times 3 direction-cosine transformation matrix can be uniquely specified by three independent parameters: pitch, roll, and azimuth. Since azimuth is a rotation about the vertical axis, defined by the direction of g, the earth-gravity vector, Eq. (1a) may be solved for pitch and roll.

Gyrocompassing is a closed-loop process of locating true North by computing heading as an element of the transformation matrix that has been initially leveled. In strapdown systems, gyrocompassing is exactly analogous to the same process in gimballed systems. [1,2] The analytic gimbals are torqued until the East component of the gyro angular-rate measurement in the horizontal plane is nulled. Equation (1b) is solved by using the solution of Eq. (1a).

The closed-loop gyrocompassing process provides a convenient technique by which gyro bias drifts can be measured and compensated. The p, q, r outputs of the gyroscopes are a combination of response to the earth-rate forcing function input, and their own internally generated error drift rates. Obviously, gyrocompassing can measure a total drift rate about the vertical axis by recursive solutions of ψ until the easterly rate is zero. Also, since the initial latitude of the strapdown system is known, the true magnitude of North component of earth rate is calculable and may be compared to the measured magnitude of North component of earth rate to determine a correction draft rate.

In gimballed inertial systems, this calibration process during gyrocompass alignment is often expanded by rotating the inner frame through 90 degrees so that the gyros which initially measured rate about the East horizontal axis are now along North, allowing estimate of bias drift. This technique not only improves inflight performance by reducing the gyro bias drifts, but also improves the initial heading error estimate. This results because the North direction is now obtained by [illegible] the East horizontal earth rates using gyroscopes whose bias drift has been calibrated and compensated. Strapdown systems, however, have the gyros fixed to the vehicle frame, and cannot incorporate this sophistication without rotating the carrying vehicle through 90 degrees in heading, a procedure that is operationally cumbersome.

* Centrifugal-force corrections resulting from earth rate must be included if the navigation coordinates are earth-centered rather than local-level.

3.4

Although self-leveling, alignment and calibration are defined as sequential processes they are most often implemented simultaneously by Kalman filtering.[3]

The most common form of alignment is by slaving the strapdown system to an external reference: an optical sighting system or a reference navigation system including master inertial or electronic systems such as Omega, loran, Global Positioning System (GPS), or local-precision Distance Measuring Equipment (DME) position network.

The peculiar strapdown characteristics of having the sensitive axes of the accelerometers in a known and fixed relation to the vehicle body, though somewhat detrimental to gyrocompassing, is helpful for case-alignment methods. For applications such as surface-to-surface missile, for example, an external optical system or other instrumentation of the launcher may be used for azimuth alignment of the missile frame and therefore the inertial system. An equivalent technique for alignment of a gimballed inertial system introduces errors inherent in electrical or mechanical caging of the gimbals, or in providing look-through windows in the missile skin for theodolite observation of a prism on the inner gimbal.

Mechanical-alignment techniques, however, have very limited application as compared to the process of aligning the strapdown inertial system to an external reference navigation system. Because alignment is determining the orientation of the sensitive axes of the strapdown accelerometers with the coordinate axes established by the reference navigation system, the general alignment technique is velocity matching. When the velocity outputs of the strapdown inertial system and reference system are "identical", for a common forcing function generated by the vehicle maneuvers, the relationship between the two systems is given by

$$\begin{bmatrix} V_N \\ V_E \\ V_V \end{bmatrix}_{REF} = \left[C\right]_B^N \begin{bmatrix} v_x \\ v_y \\ v_z \end{bmatrix}_{SD} \qquad (2)$$

where

V_N, V_E, V_V = output velocities in North, East, and vertical of the reference system

v_x, v_y, v_z = measured output velocities of the strapdown inertial system

$\left[C\right]_B^N$ = transformation direction-cosine matrix relating the strapdown-measurement and earth-referenced (navigation) coordinate axes

Since the measured velocity outputs of the strapdown inertial system are time integrals of the accelerometer outputs, the forcing-function vehicle maneuver must supply accelerations along the axes that must be aligned.

If the strapdown inertial system and reference system had no errors in measuring the magnitude of the velocity vector, then a single deterministic solution of Eq. (2) would solve their differences in measuring the direction of the velocity vector and determine alignment. For real-world solutions, however, only best estimates of misalignment can be achieved using digital filtering techniques and accounting for measurement errors by a combination of deterministic and statistical mathematical modeling.

This type of alignment, performed periodically in flight, is the basis for state-of-the-art integrated strapdown inertial radio navigation systems.[4-7] These systems combine the high-frequency response characteristics of the strapdown inertial system with the long-term stability and accuracy of the radio system for better performance than can be achieved by either system alone.

Figure 4 is a block diagram of a simple digital alignment filter that is currently operational as part of the U.S. Navy Air Combat Maneuvering Range for integration of a low-performance strapdown inertial system with precision DME measurements of vehicle position and velocity.

3.2.2 Sensor calibration

During the alignment process, maximum performance of any strapdown inertial system requires some calibration of the sensors. This calibration counters the unpredictable turn-on-to-turn-on or day-to-day shifts in sensor performance that result from time, temperature changes, or electromagnetic environment changes of the sensor.

As previously described, the self-leveling and gyrocompassing modes of alignment offer possibilities for a limited calibration of the total bias drift of the vertical and northerly gyros. The limitation in calibration capabilities results because the forcing functions of earth-rate and gravity vectors are fixed in magnitude and direction with respect to sensor sensitive axes; this limits the observability of sensor errors.

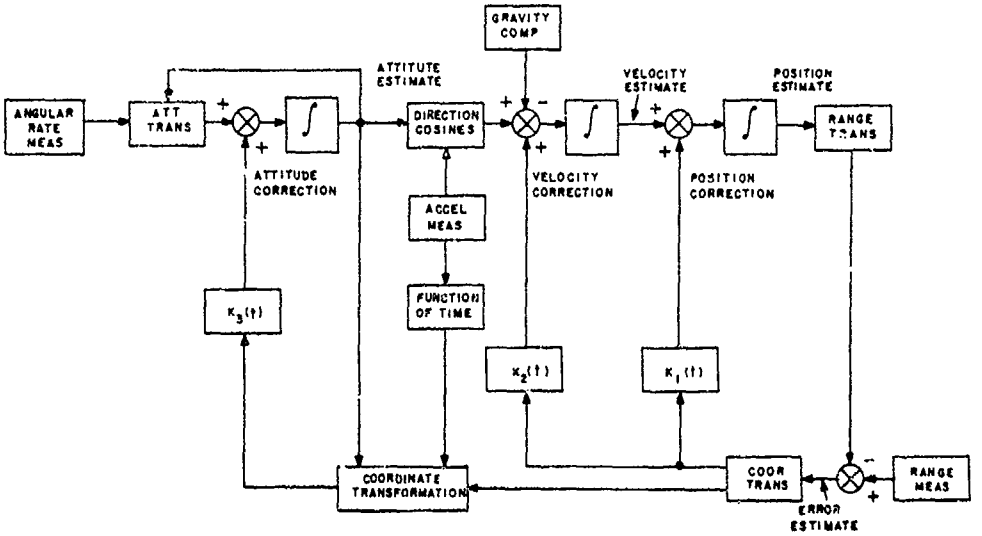

Figure 4. Least squares integration filter.

In principle, velocity-matching techniques allow complete separation and calibration of any sensor error that can be measured in the laboratory and then related to a mathematical model of the sensor. In practice, this type of dynamic-error compensation is limited to only a few major errors of each sensor. Limitations come from practical considerations of the speed and accuracy of avionics systems digital processors used to perform the calculations of an n-state-vector as well as the ability to precisely model the system.

Other limitations are in the inherent characteristics and performance accuracy of the reference system, operational restrictions on time allowed for sensor calibration, and flexibility of the input acceleration forcing functions.

3.2.3 Initialization

Because the strapdown inertial system is a dead-reckoning device, it must know the origin of the position vector it is measuring, the intended terminal of that vector for the guidance function, and the initial velocity vector. The initial conditions of system position and velocity, and target coordinates must be entered into the strapdown system by communication with some external input device: a digital keyset, or fire-control computer.

3.3 Calculating the transformation matrix

The distinguishing algorithm of strapdown inertial systems, as opposed to gimballed inertial systems, is the calculation of the direction-cosine transformation matrix. The transformation matrix is a 3 times 3 orthogonal normal matrix that relates the orientation of the accelerometer measurement axes, which are fixed with respect to the vehicle frame, to the selected navigation coordinate system. This mathematical relationship, as previously defined in Eq. (2), is

$$\left[V\right]_N = \left[C\right]_B^N \left[V\right]_B \tag{3}$$

where

$\left[V\right]_B$ = measured velocity vector in body axes

$\left[C\right]_B^N$ = transformation matrix

$\left[V\right]_N$ = velocity vector transformed into navigation or reference coordinates

The total functional flow diagram of the process of generating the transformation matrix is shown in Figure 5.

Calculation of the direction-cosine matrix begins with read-in, scaling, and compensation of the rate-gyro outputs.

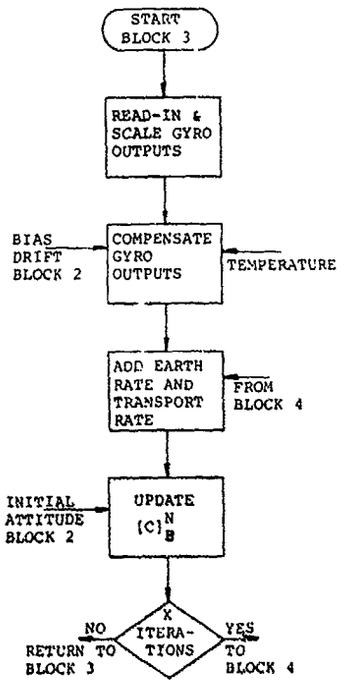

Figure 5. Functional flow diagram matrix updating algorithm.

The outputs of the rate gyros (p, q, r) are continuously quantized in time-integral increments ($p\Delta t$, $q\Delta t$, $r\Delta t$) of angle, and stored in accumulators. The contents of the accumulators are entered into the computer at the start of each computational cycle. The computer must convert the sum of the angular increments into a binary word equivalent for further processing.

Before operating on the inputs, the computer may provide compensations for sensor errors. For example, these compensations might include:

(1) Bias drift, particularly as a function of sensor temperature.

(2) Nonlinearity of the gyro as a function of applied angular rate and linear acceleration.

(3) Compensation for mechanical skewness in adjustment of the gyro sensitive-axis orthogonality.

(4) Compensation for cross coupling errors such as angular acceleration sensitivity of conventional rate gyroscopes. An angular acceleration about the output axis of a gyroscope causes an error rate about the input axis which is proportional to the ratio of inertia-to-angular momentum of the gyro wheel. Because the gyroscopes are orthogonal, input axes along i,j,k are parallel to output axes along j,k,i. Therefore

$$\omega_{(p,q,r)} = k(J/H)\dot{\alpha}_{(q,r,p)}$$

In addition, for usable system navigation outputs, earth rate and transport rate (the equivalent angular rate which results from motion over the spherical earth surface) are converted to body-axis rates and added to the gyro outputs so that the final transformation matrix converts from body axis to a navigation coordinate system referenced to the earth, rather than an inertial coordinate system referenced to the "fixed start" (see Section 3.4).

3.3.1 Development of analytical equations

A gimbal set that isolates an inner frame stabilized in an earth-referenced navigation coordinate system against the case motions of the carrying vehicle is a physical representation of the strapdown-system transformation matrix. If resolvers are mounted on each axis of a three-gimbal platform, a vector generated electrically by the outputs of an orthogonal triad of accelerometers on the inner frame can be converted into an equivalent acceleration in body coordinates by successive resolution of the measured outputs through three sequential resolvers

$$[X]_B = [\phi]\,[\theta]\,[\psi]\,[X]_N \qquad (4)$$

where ψ is a rotation about the vertical, or azimuth axis, of the inner frame

$$[\psi] = \begin{bmatrix} c\psi & s\psi & 0 \\ -s\psi & c\psi & 0 \\ 0 & 0 & 1 \end{bmatrix}$$

θ is the vehicle pitch attitude or elevation angle of the second gimbal with respect to the local level of the inner frame

$$[\theta] = \begin{bmatrix} c\theta & 0 & -s\theta \\ 0 & 1 & 0 \\ s\theta & 0 & c\theta \end{bmatrix}$$

and ϕ is the vehicle roll attitude as measured by the relative displacement of the outer gimbal with respect to the middle gimbal

$$[\phi] = \begin{bmatrix} 1 & 0 & 0 \\ 0 & c\phi & s\phi \\ 0 & -s\phi & c\phi \end{bmatrix}$$

In these equations, c represents the cosine and s the sine of the designated angles. Then

$$[X]_B = \begin{bmatrix} c\theta c\psi & c\theta s\psi & -s\theta \\ -s\psi c\phi + s\theta c\psi s\phi & c\phi c\psi + s\phi s\theta s\psi & s\phi c\theta \\ s\psi s\phi + s\theta c\psi c\phi & -s\phi c\psi + c\phi s\theta s\psi & c\phi c\theta \end{bmatrix} [X]_N \qquad (5)$$

$$= [C]_N^B [X]_N$$

This transformation matrix is both orthogonal and normal since it is the product of three orthogonal normal matrices. Then

$$[C]_N^B [C]_N^{B^T} = [C]_N^B [C]_N^{B^{-1}} = [1] \qquad (6)$$

where [1] is a 3 times 3 identity matrix.

The inverse or transposed matrix, $[C]_B^N$, which converts vectors in body axes to equivalent vectors in navigation coordinates, is the matrix which must be generated in the strapdown system as a function of the corrected and compensated outputs of the rate gyroscopes. The normality characteristic of this matrix assures that the absolute magnitude of any vector remains unchanged by operation of the transformation matrix.

Finally, [C] is unique. For any given spatial relation between the two sets of coordinate axes, there is only one transformation matrix, which will be shown to have many parametrical representations.

Several techniques have been investigated and implemented for updating the transformation matrix. Limitations on computational speed of airborne digital computers led early investigators [8,9] to concentrate on direct integration of the direction-cosine-matrix differential equations.

The classical Coriolis equation for differentiation of a vector, $\vec{X}$, rotating at rate, ω, is

$$\frac{d}{dt} [\vec{X}]_N = \frac{d}{dt} [\vec{X}]_B + [\vec{\omega}]_B \times [\vec{X}]_B \qquad (7)$$

where the last term is a vector cross product. But

$$[\vec{X}]_B = [C]_N^B [\vec{X}]_N \qquad (8)$$

By substitution and assuming that $[X]_N$ is constant over the time interval, then

$$\frac{d}{dt} [C]_N^B [\vec{I}] = - [\vec{\omega}]_B \times [C]_N^B [\vec{I}] \qquad (9)$$

where

$[\vec{I}]$ = a unit vector

$[\vec{\omega}]_B$ = a skew-symmetric matrix for the rate of rotation of the vehicle body axes with respect to navigation coordinates

$$[\vec{\omega}]_B = \begin{bmatrix} 0 & -\omega_z & \omega_y \\ \omega_z & 0 & -\omega_x \\ -\omega_z & \omega_x & 0 \end{bmatrix} \qquad (10a)$$

or

$$[\vec{\omega}]_B = \begin{bmatrix} 0 & -r' & q' \\ r' & 0 & -p' \\ -q' & p' & 0 \end{bmatrix} \qquad (10b)$$

Expanded, Eq. (9) becomes a series of nine linear differential equations of the form

3-8

$$\dot{C}_{11} = r'C_{12} - q'C_{13}$$

$$\vdots$$

$$\dot{C}_{33} = q'C_{31} - p'C_{32}$$

where

$p' = p \pm p_c$ the roll angular rate of the vehicle with respect to inertial space output from the roll body axis gyroscope plus the computed correction roll rate of the navigation local-level coordinates with respect to inertial coordinates (Section 3.4)

$q' = q \pm q_c$ measured plus computed pitch angular rates

$r' = r \pm r_c$ measured plus computed yaw angular rates

These equations are ideally suited for solution by the high-speed Digital Differential Analyzer (DDA) type of digital computers, and therefore could be solved at adequate updating rates by the existing state-of-the-art hardware. However, because the matrix was generated by nine independent computations of matrix elements that are functions of only three mathematically independent parameters, the total matrix solution accumulates errors that made it drift from the desired characteristics of orthogonality and normality.

Sophisticated algorithms which cyclically changed the order of solution of these equations to orthonormalize the matrix are of limited benefit. The degree of departure of the computed matrix from the ideal orthonormality is straightforward to determine Eq. (6). The principal difficulty in applying a correction is that the many degrees of freedom do not allow the orthonormality constraints to uniquely define a solution.

An updating technique that circumvents this problem solves directly for ϕ, θ, ψ in terms of the quantities p', q', r', and uses the updated angle quantities to generate the updated transformation matrix.

Again, a gimbal set provides a physical means for representing the relations. Since ϕ, θ, ψ are gimbal angles, $\dot{\phi}$, $\dot{\theta}$, $\dot{\psi}$ (gimbal rates) can be related to p', q', r' (equivalent body rates. Then

$$\begin{bmatrix} p' \\ q' \\ r' \end{bmatrix} = \begin{bmatrix} \dot{\phi} \\ 0 \\ 0 \end{bmatrix} + [\phi] \begin{bmatrix} 0 \\ \dot{\theta} \\ 0 \end{bmatrix} + [\phi]\,[\theta] \begin{bmatrix} 0 \\ 0 \\ \dot{\psi} \end{bmatrix} \tag{11}$$

For convenience, Eq. (11) can be written in matrix notation as

$$\begin{bmatrix} \dot{\phi} \\ \dot{\theta} \\ \dot{\psi} \end{bmatrix} = \begin{bmatrix} 1 & s\phi t\theta & c\phi t\theta \\ 0 & c\phi & -s\phi \\ 0 & s\phi/c\theta & c\phi/c\theta \end{bmatrix} \begin{bmatrix} p' \\ q' \\ r' \end{bmatrix} \tag{12}$$

where t represents the tangent of the designated angles.

Although this updating technique always generates an orthonormal transformation matrix, it has the disadvantage of incorporating a mathematical singularity that is identical to the problem of gimbal lock in three gimbal platforms. Also, the solution involves transcendental functions, which, for most digital computers, require polynomial expansion approximations with attendant complex processing. However, in the early 1960s, when processing speeds of airborne digital computers were marginal for strapdown systems, this algorithm was studied [9,10] and proposed for strapdown missile guidance systems that incorporated either DDA mechanized computers, or preferably, whole-number computers specifically developed for solution of loran and Omega navigation problems.

Current four-parameter techniques for updating the transformation matrix combine the best features of both the three- and nine-parameter methods. These techniques are computational algorithms that are not attitude limited, and always provide an orthonormal matrix.

Consider a vector rotation through three Euler angles α, β, γ

$$[X]_E = [\alpha]_Z \cdot [\beta]_Y [\gamma]_Z [X]_N \tag{13}$$

where

γ = rotation about the local vertical, or Z axis

β = rotation about the Y axis

α = rotation about the Z axis displaced through β

Since α, β, γ are single-axis rotation matrices, the expanded transformation matrix is

$$[C]_N^B = \begin{bmatrix} c\alpha c\beta c\gamma - s\beta s\gamma & c\alpha c\beta s\gamma + s\alpha c\beta & -c\alpha s\beta \\ s\alpha c\beta c\gamma - c\beta s\gamma & -s\alpha c\beta s\gamma + c\alpha c\beta & s\alpha s\beta \\ s\beta c\gamma & s\beta s\gamma & c\beta \end{bmatrix} \quad (14)$$

Since the transformation matrices are unique, this matrix is term-by-term identical to the matrix developed using gimbal angle parameters [Eq. (5)].

Define four Euler parameters in terms of the Euler angles

$$\begin{aligned} A &= \sin \beta/2 \sin \left(\frac{\alpha - \gamma}{2}\right) \\ B &= \sin \beta/2 \cos \left(\frac{\alpha - \gamma}{2}\right) \\ C &= \cos \beta/2 \sin \left(\frac{\alpha + \gamma}{2}\right) \\ D &= \cos \beta/2 \cos \left(\frac{\alpha + \gamma}{2}\right) \end{aligned} \quad (15)$$

where

$$A^2 + B^2 + C^2 + D^2 = 1$$

By algebraic manipulation, the transcendental functions of α, β, and γ (and hence the transformation matrix) may be expressed in terms of Eq. (15).

$$[C]_N^B = \begin{bmatrix} A^2 + D^2 - B^2 - C^2 & 2(AB + CD) & 2(AC - BD) \\ 2(AB - CD) & -A^2 + B^2 - C^2 + D^2 & 2(BC + AD) \\ 2(AB + BD) & 2(BC - AD) & -A^2 - B^2 + C^2 + D^2 \end{bmatrix} \quad (16)$$

A quaternion (Q) is defined as a combination of a scalar (q_0) and a vector with orthogonal components of q_i

$$\begin{aligned} Q &= q_0 + \vec{q} \\ &= q_0 + q_1\vec{i} + q_2\vec{j} + q_3\vec{k} \end{aligned} \quad (17)$$

the quaternion conjugate

$$Q^* = q_0 - \vec{q}$$

and

$$\begin{aligned} QQ^* &= Q^*Q \\ &= q_0^2 + \sum_1^3 q_i^2 \end{aligned}$$

To show that the Euler parameters as defined satisfy the characteristics of quaternions, consider the direction cosine of the transformation matrix

$$\begin{aligned} C_{11} + C_{22} &= 2(D^2 - C^2) \\ C_{11} + C_{33} &= 2(D^2 - B^2) \\ C_{22} + C_{33} &= 2(D^2 - A^2) \end{aligned} \quad (18)$$

Also, since

$$A^2 + B^2 + C^2 + D^2 = 1$$

solving

$$\begin{aligned} A^2 &= \tfrac{1}{4} + \tfrac{1}{4}\left(C_{11}^2 + C_{22}^2 + C_{33}^2\right) \\ B^2 &= \tfrac{1}{4} + \tfrac{1}{4}\left(C_{11}^2 - C_{22}^2 - C_{33}^2\right) \\ C^2 &= \tfrac{1}{4} + \tfrac{1}{4}\left(-C_{11}^2 + C_{22}^2 - C_{33}^2\right) \\ D^2 &= \tfrac{1}{4} + \tfrac{1}{4}\left(-C_{11}^2 - C_{22}^2 + C_{33}^2\right) \end{aligned} \tag{19}$$

These parameters then are of the form

$$QQ^* = q_0^2 + \sum_1^3 q_i^2 \tag{20}$$

where

q_i = direction cosines of the transformation matrix

The Euler parameter or quaternion matrix [Eq. (16)] is updated by an algorithm that generates the new parameters in terms of body-axis rates and then calculates the new transformation matrix.

In terms of the original rotation Euler angles

$$\begin{bmatrix} p' \\ q' \\ r' \end{bmatrix} = \begin{bmatrix} 0 \\ 0 \\ \dot{\alpha} \end{bmatrix} + [\alpha]_Z \begin{bmatrix} 0 \\ \dot{\beta} \\ 0 \end{bmatrix} + [\alpha]_Z\,[\beta]_Y \begin{bmatrix} 0 \\ 0 \\ \dot{\gamma} \end{bmatrix} \tag{21}$$

The solution, using identities of the four-parameter transformation matrix, is

$$\begin{bmatrix} p' \\ q' \\ r' \end{bmatrix} = \begin{bmatrix} 0 & (AD + BC)/E & -2(BD - AC) \\ 0 & (BD - AC)/E & 2(AD + BC) \\ 1 & 0 & -A^2 - B^2 + C^2 + D^2 \end{bmatrix} \begin{bmatrix} \dot{\alpha} \\ \dot{\beta} \\ \dot{\gamma} \end{bmatrix} \tag{22}$$

where

$$E = \left[(A^2 + B^2)(C^2 + D^2)\right]^{1/2}$$

The angle rates ($\dot{\alpha}$, $\dot{\beta}$, $\dot{\gamma}$) are expressed in terms of the quaternion by differentiating the arc tangents of the angles, as developed from Eq. (15).

$$\begin{bmatrix} \dot{\alpha} \\ \dot{\beta} \\ \dot{\gamma} \end{bmatrix} = \frac{d}{dt} \begin{bmatrix} \tan^{-1} \dfrac{AD + BC}{BC - AC} \\ \tan^{-1} \dfrac{2E}{2(C^2 + D^2) - 1} \\ \tan^{-1} \dfrac{BC - AD}{BD + AC} \end{bmatrix} \tag{23}$$

Substituting these angle rates into Eq. (22), and rearranging

$$\begin{bmatrix} \dot{A} \\ \dot{B} \\ \dot{C} \\ \dot{D} \end{bmatrix} = \frac{1}{2} \begin{bmatrix} C & -C & B \\ C & D & -A \\ -B & A & D \\ -A & -B & -C \end{bmatrix} \begin{bmatrix} p' \\ q' \\ r' \end{bmatrix}$$

$$= \frac{1}{2} \begin{bmatrix} 2 - \epsilon_k & r' & -q' & p' \\ -r' & 2 - \epsilon_k & p' & q' \\ q' & -p' & 2 - \epsilon_k & r' \\ -p' & -q' & -r' & 2 - \epsilon_k \end{bmatrix} \begin{bmatrix} A \\ B \\ C \\ D \end{bmatrix} \tag{24}$$

These equations are solved for updating A, B, C, D, and the new parameters are used for updating the matrix of Eq. (16). This matrix is always orthogonal and maintained normal by the factor

$$\epsilon_k = k_1(A^2 + B^2 + C^2 + D^2 - 1)$$

3.3.2 Problems in numerical solution

The major error sources that are inherent in the digital processing for numerical solution of the algorithms for updating the transformation matrix are

(1) commutation
(2) integration
(3) round-off
(4) quantization

Commutation errors result primarily from fixed-sequence numerical processing techniques incorporated in most strapdown-system mechanizations.

Numerical processing commutation errors result because, for each solution update of the transformation matrix, the processor operates sequentially on the input increments of the rate sensors in a fixed order that may not correspond to the actual time-ordered sequence in which the angles were accumulated by the vehicle. Since vehicle attitude is dependent on the time order of angular changes about its axes, this commutation error, particularly for cyclical or repetitive inputs, can cause rectification drift errors of the transformation matrix. The commutation error can be minimized by decreasing the angle increment size involved in each computation update. However, this requires increased computer speed.

Consider a rate sensor whose sensitive axis is mounted along the major body axis (roll axis) of a missile (see Figure 6). Under classical coning motion of the vehicle in flight, the sensor input axis will have an average input rate.

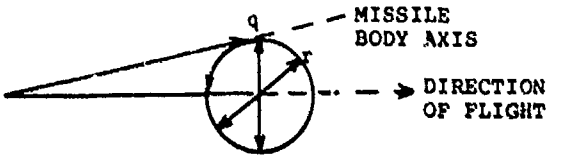

Figure 6. Classical coning-motion input rates.

Assume that the vehicle-body coning-motion rates, measured by the rate sensors, are

$$p = 0$$

$$q = A\omega \cos \omega t$$

$$r = A\omega \sin \omega t$$

Then, by Eq. (12)

$$\dot{\phi} = qs\phi t\theta + rt\theta$$

$$\dot{\theta} = qc\phi - rs\phi$$

$$\dot{\psi} = (qs\phi/c\theta) + (rc\phi/c\theta)$$

Let

$$\phi_0 = \theta_0 = \psi_0 = 0$$

Then, by substituting small angle approximations

$$\dot{\phi} = r \tan \theta = r\theta$$

$$= A\omega \cos \omega t \cdot \theta$$

$$\dot{\theta} = q$$

$$= A\omega \cos \omega t$$

Then

$$\theta = -A \sin \omega t$$

and

$$\phi = \int A^2 \sin^2 \omega t$$

$$= \frac{A^2 \omega}{2} \text{ (average)} \tag{25}$$

so that cyclical input motions can cause rectification drifts through commutation errors. This error is equivalent to gyro drifts in its effect on system performance.

Integration errors result from numerical approximation integration of differential equations that have no true analytical solutions.

The general forms of the differential equations for updating the direction cosines [refer to Eq. (9)] or the quaternions [refer to Eq. (24)] are

$$[\dot{C}]_B^N = [C]_B^N [\omega] \tag{26a}$$

and

$$\dot{\rho} = \rho \omega/2 \tag{26b}$$

These equations are of the form

$$dx/x = a$$

and the analytic solution is given by

$$\log x = \int_{t_0}^{t} a \, dt$$

$$= \Delta a$$

Hence

$$x = e^{\Delta a} \tag{27}$$

Because $\dot{a}$ is a measured rate vector, the analytic integration is correct only for those time intervals, $t_0 \rightarrow t$, when its vector direction in space is constant. This restriction is so severe that this true (or analytic) solution is very seldom correct for an operational strapdown system.

Further, in an operational system, the solution must be evaluated by a truncated series

$$e^{\Delta a} = 1 + \Delta a + \frac{\Delta a^2}{2!} + \frac{\Delta a^3}{3!} + \ldots + \frac{\Delta a^n}{(n-1)!} + \ldots \tag{28}$$

For quaternions [from Eq. (24)] Δa is

$$\Delta a = \frac{1}{2} \begin{bmatrix} 0 & \Delta R & -\Delta Q & \Delta P \\ -\Delta R & 0 & \Delta P & \Delta Q \\ \Delta Q & -\Delta P & 0 & \Delta R \\ -\Delta P & -\Delta Q & -\Delta P & 0 \end{bmatrix}$$

where

$$\Delta P = \int_{t_n}^{t_{n+1}} p \, dt$$

$$\Delta Q = \int_{t_n}^{t_{n+1}} q \, dt$$

$$\Delta R = \int_{t_n}^{t_{n+1}} r \, dt$$

By substitution in Eq. (28), the updating integration algorithm through the first three terms becomes

$$\begin{bmatrix} A \\ B \\ C \\ D \end{bmatrix} = \left\{ [I] + [\Delta\alpha] - \frac{1}{4}[\theta_0^2][I] - \frac{1}{6}[\theta_0^2][I][\Delta\alpha] + \ldots. \right\} \begin{bmatrix} A \\ B \\ C \\ D \end{bmatrix}_{t_0} \quad (29)$$

where

$$[I] = \text{unity matrix}$$

$$\theta_0^2 = \Delta P^2 + \Delta Q^2 + \Delta R^2$$

The facts that a truncated series must be evaluated for the integration, and that the conditions of constant input rate necessary for the analytic solution to be correct are hardly ever valid for an operational system, demonstrate that integration algorithms are always approximations.

The performance of the numerical integration algorithms is obviously improved by either increasing the order (i.e., increasing the number of terms of the series that are evaluated), or decreasing the integration time increment. These solutions require increasing computer workloads, but decrease errors by effectively providing improved estimates of the true input rates during the updating cycle. Increasing the sophistication of the integration algorithm, however, quickly reaches a point of diminishing returns. The higher order terms are too little and get lost in the computer round-off processes.

For many applications, a predictor-corrector trapezoidal integration technique is an acceptable trade between processing complexity and performance. This technique is equivalent to the analytic solution [Eq. (29)] through second-order terms of the series expansion. For example, the general form of Eq. (24) can be written

$$\dot{X} = X \cdot U$$

where X corresponds to the quaternions and U to the incremental angles accumulated over each update period

$$U = \int_{t_n}^{t_{n+1}} u(t)dt$$

A predicted X is

$$X^P_{t_{n+1}} = X_{t_n} + U \cdot X_{t_n}$$

The corrected value is

$$X^C_{t_{n+1}} = X_{t_n} + U \cdot X^P_{t_{n+1}}$$

and the average

$$X_{t_{n+1}} = \frac{1}{2}\left[X^P_{t_{n+1}} + X^C_{t_{n+1}}\right]$$

is a simple second-order integration technique which may be compared to the second-order Runge-Kutta rate extraction algorithm (Section 3.5).

Round-off errors result because the finite word length of the computer limits or truncates the resolution of all internal data. The process of rounding off all internal computations to the value of the least-significant bit causes error buildup in a "random walk" process. Most state-of-the-art airborne processors use 16-bit word lengths. Except for special applications, this resolution is not adequate for computation of the matrix parameters, so that "double-precision" operations are required. This may require either increased computer hardware or increased computer workload if the double-precision capability is software.

Quantization comes from the process of converting the analog outputs of the sensors into discrete increments of angle and velocity, which can be input as a series of pulses into the digital computer. This quantization process causes the input to the computer to always lag the outputs of the sensors. The average value of this quantization (or sensor storage error) is one-half the quantization angle ($\Delta\theta$) or quantization velocity (Δv). Since this information is not lost but retrieved on the next update cycle, quantization appears as a specific type of noise on the data that must be modeled for best performance of the strapdown system when applied to an integrated system using a digital-filter state-vector estimator.[12] Decreasing the quantization level requires increased data-storage registers at the computer input.

In summary, major strapdown-system errors in implementing the algorithms occur in the critical computation process of updating the transformation matrix. These errors are shown in Table 1.

3-14

Table 1. Strapdown-system errors in implementation of algorithms.

Error Type	Source and Effect	System Trades
Commutation	Possible rectification drift, under cyclical inputs, due to inaccurate generation of the profile	Increased update rates
Integration	Discrete approximate solution of a continuous process, and equations which have no analytic solution	Sophisticated algorithm; increased update rate
Round-off	Finite resolution of data causes "random-walk" error buildup in multiple computations	Double-precision for critical operation
Quantization	Analog-to-digital conversion of sensor-measured outputs	Increased storage hardware; mathematical modeling

The general effect of the solution update rate of the transformation matrix on errors from the various sources is shown in Figure 7. The actual amplitude of the errors is very dependent on the input rates. The total error in computation is some combination of the individual errors. If the matrix is orthogonal and maintained normal, the errors all contribute to matrix drift rate which is equivalent to gyro drift rate.

Although the quantization error is shown independent of update rate, an increase in update rate may allow decreasing the quantization level without increasing input storage hardware.

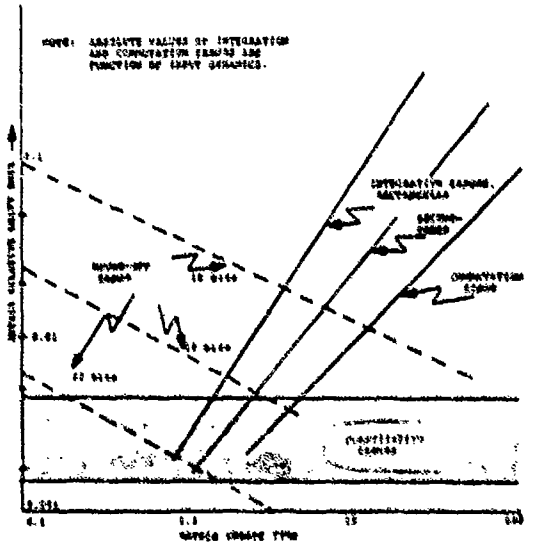

Figure 7. Relative error effects.

3.3.3 Simulation techniques for optimizing the solution

Obviously a cost-effective system is based on providing only the performance required for a particular application. This system cost/performance optimization is most readily determined by computer simulation.

Figure 8 shows a general block diagram for simulation of a strapdown system for cost-optimization studies. A good general-purpose simulator will have the following capabilities:

(1) Variable inputs, including both functions for which there is an analytic solution for determining ultimate performance of the system under stress inputs such as coning motion, and general flight-profile trajectories typical of the mission. [13]

(2) Analytic- and reference-solution generator. Since the simulation does not have to be real-time or programmable in an airborne digital computer, the reference solution must be the best possible, providing matrix update in shortest time periods, and using double-precision arithmetic, and fourth-order Runge-Kutta integration.

(3) Variable mathematical models of the system sensors.

(4) Variable integration techniques, update rates, quantization levels, and bit-by-bit simulation of the system computer.

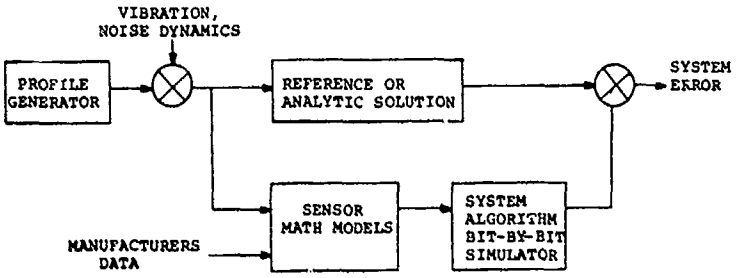

Figure 8. Simulation facility functional block diagram.

3.4 Navigation algorithms

Although the transformation-matrix updating algorithm is critical for any strapdown system, the final purpose of any system is for guidance and/or control of the carrying vehicle.

The general navigation equation, as derived by differentiation of its position vector, describes the motion of a point mass over the surface of the earth.

$$\frac{d}{dt}\vec{v} = \vec{a} - 2(\vec{\Omega} + \vec{\rho})\times\vec{v} - \vec{\Omega}\times\vec{\Omega}\times\vec{r} \qquad (30)$$

where

a, v = acceleration and velocity of the vehicle relative to the earth in the defined navigation coordinate system

$\vec{\Omega}$ = earth rotation vector

$\vec{\rho}$ = angular rate of the navigation coordinate relative to the earth which results from vehicle motion

$\vec{r}$ = the position vector of the vehicle with respect to earth center

Then

$2(\vec{\Omega} + \vec{\rho})\times\vec{v}$ = the Coriolis correction which converts from inertial to navigation coordinates

$\vec{\Omega}\times\vec{\Omega}\times\vec{r}$ = centrifugal-force acceleration

Because the accelerometers cannot distinguish between thrust acceleration and mass attraction gravity, the accelerometer outputs are

$$a_m = a - g(r)$$

where

$g(r)$ = combination of earth gravity and centrifugal force at the vehicle location

Then, Eq. (30) becomes

$$\frac{d}{dt}(\vec{v}) = \vec{a}_m + g(\vec{r}) - 2(\vec{\Omega} + \vec{\rho})\times\vec{v} \qquad (31)$$

Specific details of this navigation algorithm depend on the specific navigation coordinate frame of the vehicle. In general, long-range cruise vehicles (such as manned aircraft) use local-level north-referenced coordinates, and short-range vehicles (such as tactical missiles) use tangent-plane north-referenced navigation coordinates.

A tangent-plane coordinate system is level, or tangent to the earth, at some fixed point, usually the vehicle launch point.

In either coordinate system, as shown in Figure 9, the navigation algorithms are initiated by read-in and proper scaling conversion of the accelerometer outputs, accumulated during the past computation cycle, into suitable digital words for entry into the computer.

The incremental velocities as entered are transformed by the transformation matrix from the body-axis (or measurement) coordinate system to the navigation coordinate

$$[\Delta v]_N = [C]_B^N [\Delta v]_B \tag{32}$$

where

$[C]_B^N$ = the transformation matrix from body axis to the navigation coordinate axes

$$[\Delta v]_B = \int_{t_i}^{t_{i+1}} [a_m + g(r)]\, dt \tag{33}$$

= accumulated velocity-pulses output by the accelerometers over the previous update period

The current position and velocity vector of the system are obtained by straightforward summation of the transformed velocity increments corrected for Coriolis [Eq. (31)]. To compute position in latitude and longitude coordinates

$$\lambda = \lambda_0 - \sum_{t_0}^{t} \left[V_N \Delta t/(r+h)\right]$$

$$\ell = \ell_0 - \sum_{t_0}^{t} \left[V_E \Delta t/((r+h)\cos\lambda)\right]$$

where

λ_0, ℓ_0 = initial latitude and longitude of the carrying vehicle

$V_N \Delta t$, $V_E \Delta t$ = North and East accumulated position vector

h = vehicle altitude

r = earth radius which may be a fixed value or the calculated radius of the theoretical approximation of the earth ellipsoid (World Geodetic System, 72)

For a local-level coordinate system, as shown in Figure 10, the vertical, or down direction, is always along the direction of local gravity so that the gravity correction to the accelerometer outputs is computed as a function of vehicle altitude (h) only. Then g(r) of Eq. (33) is

$$g(r) = g_0 \left(\frac{r}{r+h}\right)^2 \tag{34}$$

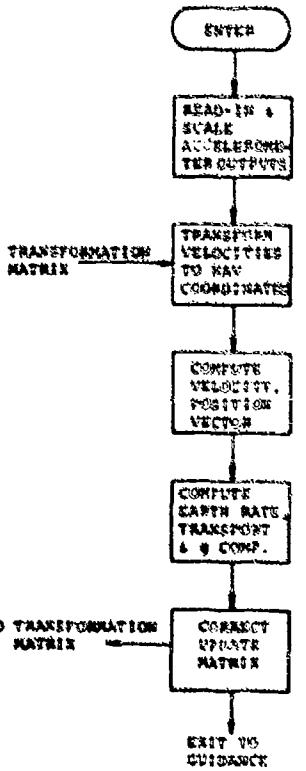

Figure 9. Functional flow diagram, navigation algorithms

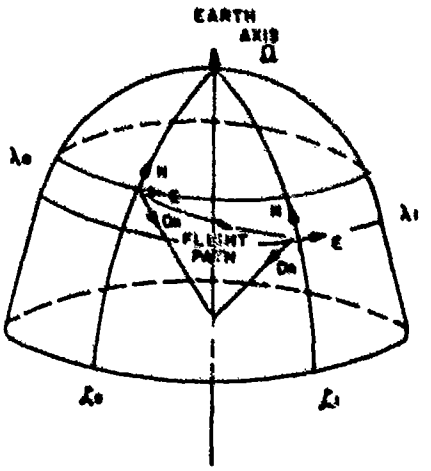

Figure 10. Local-level coordinate system geometry

The navigation coordinate system rotates, as a function of earth rate, in inertial space. The components of earth rate along the North, East, down directions of the navigation coordinate system are

$$[\Omega]_N = |\Omega| \begin{bmatrix} \cos\lambda \\ 0 \\ \sin\lambda \end{bmatrix} \tag{35}$$

where

λ = latitude of the vehicle position

Ω = earth's sidereal rate

The motion, or change of position of the navigation coordinate system, also involves an equivalent rotation rate of the coordinate system with respect to inertial space

$$[\rho]_N = \left|\frac{1}{r+h}\right| \begin{bmatrix} V_E \\ -V_N \\ -V_E \tan\lambda \end{bmatrix} \tag{36}$$

Since these coordinate-system rates are in navigation coordinates, they must be converted through the inverse transformation matrix and applied as corrections to the rate-gyro outputs. This will force the updating of the transformation matrix to convert from body-axis to navigation coordinate system rather than body-axis to inertial coordinate system. Then

$$[\omega_N]_B = [C]_N^B \left([\Omega]_N + [\rho]_N\right) \tag{37}$$
$$= [C]_N^B [\omega_N]_N$$

These correction rates of navigation coordinates with respect to inertial space [Eq. (10)] may be implemented using the parameters directly, rather than the inverse of the transformation matrix.

$$\frac{d}{dt}\begin{bmatrix} A \\ B \\ C \\ D \end{bmatrix} = \frac{1}{2}\begin{bmatrix} D & -C & B \\ C & D & -A \\ -B & A & D \\ -A & -B & -C \end{bmatrix}\begin{bmatrix} p \\ q \\ r \end{bmatrix} - \frac{1}{2}\begin{bmatrix} D & -C & B \\ C & D & -A \\ -B & A & D \\ -A & -B & -C \end{bmatrix}[C]_N^B [\omega_N]_N$$

$$+ \frac{1}{2}\begin{bmatrix} D & -C & B \\ C & D & -A \\ -B & A & D \\ -A & -B & -C \end{bmatrix}\begin{bmatrix} p \\ q \\ r \end{bmatrix} - \frac{1}{2}\begin{bmatrix} D & C & -B \\ -C & D & A \\ B & -A & D \\ -A & -B & -C \end{bmatrix}[\omega_N]_N \tag{38}$$

The total body-axis to navigation coordinate transformation matrix, $[C]_B^N$, is then computed from these updated parameters. The form is identical to Eq. (16).

A tangent-plane navigation coordinate system is commonly used for navigation of short-range vehicles such as tactical missiles. The tangent-plane navigation system is initially aligned to North and local-vertical, and maintained in that initial attitude during flight. The velocity equation for navigation is, then

$$\frac{d}{dt}(\vec{v}^t) = \vec{a}_m^t + \vec{g}^t(r) - 2\vec{\Omega}_0 \times \vec{v}^t \tag{39}$$

where $g^t(r)$ must be computed in body coordinates by transformation through the tangent plane to body-axis matrix to correct the gravity reading of each accelerometer. In flight, the direction of gravity changes in t coordinates. Then

$$[g^t(r)]_B = [C]_t^t \frac{g_0 r^2}{(r+h)^2} \tag{40}$$

and Ω_0 is the earth rate at launch point. Then, as before

3-10

$$[\omega_t]_B = [C]_t^B [\omega_t]_t = [C]_t^B |\Omega| \begin{bmatrix} \cos \lambda_0 \\ 0 \\ \sin \lambda_0 \end{bmatrix} \tag{41}$$

$$= [C]_t^B \begin{bmatrix} k_1 \\ 0 \\ k_2 \end{bmatrix}$$

since earth rate and initial latitude are constants.

Then the parameters to update the body-axis to tangent-plane transformation matrix are computed by

$$\frac{d}{dt}\begin{bmatrix} A \\ B \\ C \\ D \end{bmatrix} = \frac{1}{2}\begin{bmatrix} D & -C & B \\ C & D & -A \\ -B & A & D \\ -A & -B & -C \end{bmatrix}\begin{bmatrix} p \\ q \\ r \end{bmatrix} - \frac{1}{2}\begin{bmatrix} D & -B \\ -C & A \\ B & D \\ -A & C \end{bmatrix}\begin{bmatrix} k_1 \\ k_2 \end{bmatrix} \tag{42}$$

and $[C]_B^t$ is computed from the updated parameters as shown in Eq. (16), and velocities transformed as in Eq. (32).

The preceding discussions have assumed that the navigation coordinate systems, either local-level or tangent-plane, are North oriented. In most operating systems, however, the actual navigation may be oriented with respect to coordinates other than North-East. For example, tangent-plane navigation is most often oriented with respect to track and cross track, where the track direction is the direction, with respect to North, of the vehicle-velocity vector at launch. In local-level navigation, the coordinate system may not be "torqued" to North, but held in inertial space at its initial attitude, which may be North-pointing at the launch location. This is a "wander-azimuth" system, initially required by gimballed systems when the gyro/gimbal combination could not be torqued at rates necessary for adequate navigation accuracy in the polar regions. Although strapdown systems mitigate this problem, since they are capable of much higher "torquing" rates than gimbal systems, the azimuth-wander mechanization may still be required for some applications.

In any case, the algorithm modifications are straightforward. The local-level coordinate rotation rate is modified by the wander-azimuth angle

$$[\omega_N]_{\omega A} = [\psi]_N^{\omega A}\left\{[\Omega]_N + [\rho]_N\right\} \tag{43}$$

where

$$\psi = \lambda_0 - \lambda$$

= a function of present position of the vehicle

The conversion for tangent-plane navigation is also similar. Equation (40) is modified by $[\psi_0]_{T/CT}$ where ψ_0 is the fixed heading at launch between track direction and North.

Although the algorithms presented are for autonomous navigation, the current trend in operating systems is the application of strapdown systems integrated with other navigation systems. These systems combine the good high-frequency short-term characteristics of inertial systems with the good long-term characteristics of radio navigation systems such as Omega, loran, GPS, and DME.

Normally, the integration is accomplished by a digital filter, which generates a best estimate of the vehicle position, velocity, and attitude, and quite often estimates corrections to the sensor outputs in body-axis coordinates.[13]

3.5 Guidance and control

The ultimate purpose of navigation is for guidance of a controlled vehicle. Navigation determines the present position and velocity vector of the vehicle. Guidance generates commands to the vehicle to modify the velocity and position vectors to conform to desired trajectory. The vehicle, as a plant, is stabilized by the control functions (see Figure 11).

The strapdown system, then, closes the stabilization command inner loop of the flight control system of the vehicle (Figure 12) and may, either automatically or through driving displays for pilot follow-up, close the guidance command outer loop.

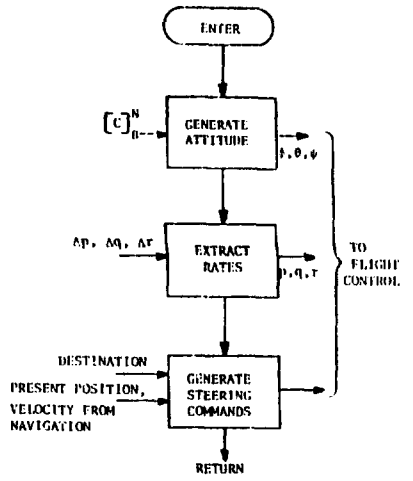

Figure 11. Functional flow diagram, guidance and control algorithms

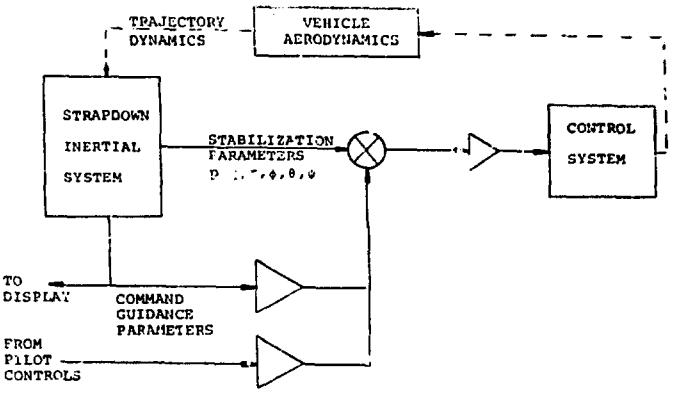

Figure 12. Systems operations block diagram

Most strapdown inertial systems will supply outputs of vehicle attitude to the control system. They also are inherently capable of supplying body-axis rates necessary for vehicle stabilization. This capability makes strapdown systems extremely attractive for application to low-cost vehicles, such as missiles, where size and weight are especially critical. New manned vehicles, however, are also good candidates for central inertial systems that provide both navigation and control functions.

Because the transformation matrices that relate body coordinates to a given navigation coordinate system are unique, the $[C]_N^B$ of Eq. (5) and (16) are term-for-term identical.

$$\phi = \tan^{-1}\frac{C_{23}}{C_{33}} = \tan^{-1}\frac{s\phi c\theta}{c\phi c\theta} = \tan^{-1}\frac{2(BC + AD)}{-A^2 - B^2 + C^2 + D^2}$$

Similarly

$$\theta = \tan^{-1}\frac{2(BD - AC)}{[(A^2 - B^2 - C^2 + D^2)^2 + 4(AB + CD)^2]^{\frac{1}{2}}}$$

$$= \tan^{-1}\frac{2(BD - AC)}{1 - 4(BD - AC)^2} \qquad (44)$$

and

$$\psi = \tan^{-1}\frac{2(AB + CD)}{A^2 - B^2 - C^2 + D^2}$$

In some strapdown inertial systems using conventional spinning-wheel angular rate sensors, the sensor closure-loop electronics may be analog so that body-axis rates may be obtained directly by analog-to-digital conversion, using conventional successive approximation converters.

For most new strapdown systems, however, the output of the rate sensors is a series of pulses. Each pulse represents a fixed angular increment of attitude change of the vehicle about its body axis. For some of these systems special algorithms are required to extract body-axis rates from the pulse series output. As has been previously discussed, these algorithms may be incorporated as part of the higher order integration algorithms for generating the transformation matrix.

The gyro samples into the computer at each update interval are

$$\sum_{\Delta t}\begin{bmatrix}\Delta P\\ \Delta Q\\ \Delta R\end{bmatrix} = \sum_{\Delta t}\left\{\int_{t_k}\begin{bmatrix}p(t)\\ q(t)\\ r(t)\end{bmatrix}dt\right\} \qquad (45)$$

where

$p(t), q(t), r(t)$ = actual angular rates of the vehicle

$\Delta P, \Delta Q, \Delta R$ = the angular increment pulses stored in the input registers over the computer cycle time, Δt

t_k = a variable time increment in which each pulse is generated by the analog-to-frequency converter or pulse torquer

3.20

For some applications, control rates may be obtained by simply computing

$$p = \frac{\Delta\theta}{\Delta t} = \frac{\Delta P_{i+1} - \Delta P_i}{\Delta t} \tag{46}$$

This simple solution, however, generally provides poor resolution.

The general technique for rate extraction is to curve-fit a second or higher order function to successive values of the gyro samples, and then take the derivative of the function at the required times. This technique, illustrated in Figure 13, for a second-order curve fit, is implemented for Runge-Kutta integration. However, the bandwidth, resolution, and accuracy requirements for control system rates are normally much less than for the transformation matrix updating process.

The curve is fit at each sampling point where the processor inputs the data accumulated from the gyros during the previous update cycle time. The time at which the curve is differentiated, however, depends for best results on particular application of the signal. Differentiating at the sampling point (a forced-fit point of the curve) is most noisy (will have most errors), but will also have least time lag, and hence will allow maximum control-loop gains.

If quantization angles are small, the generated second-order curve will have fine resolution, but will also allow more noise into the rate signal. Decreasing the update time decreases the time-lag problem and improves stability, but increases the differentiation noise in the rate signal.

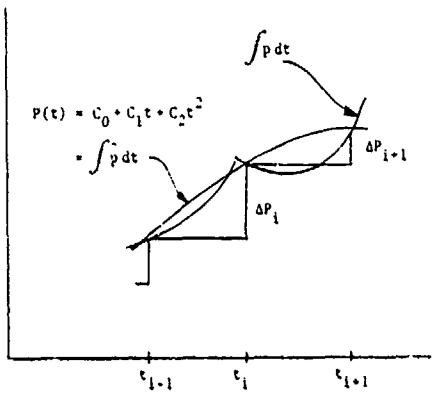

Figure 13. Second-order fit rate extraction.

The equations for extracting rate with minimum time lag at the sample point, t_{i+1}, where k is the update time increment, are developed below.

$$P(t) = C_0 + C_1 t + C_2 t^2 \tag{47}$$

$$\begin{aligned} \Delta P_i &= P(t_i) - P(t_i - h) \\ &= C_0 + C_1 t_i + C_2 t_i^2 - C_0 - C_1(t_i - h) - C_2(t_i - h)^2 \\ &= C_1 h + 2C_2 t_i h - C_2 h^2 \end{aligned} \tag{48}$$

$$\begin{aligned} \Delta P_{i+1} &= P(t_i + h) - P(t_i) \\ &= C_0 + C_1(t_i + h) + C_2(t_i + h)^2 - C_0 - C_1 t_i - C_2 t_i^2 \\ &= C_1 h + 2C_2 t_i h + C_2 h^2 \end{aligned} \tag{49}$$

Also

$$\hat{p}(t) = \frac{d}{dt} P(t) = C_1 + 2C_2 t \tag{50}$$

$$\hat{p}(t_{i+1}) = \hat{p}(t_i + h) = C_1 + 2C_2(t_i + h) \tag{51}$$

From Eq. (48) and (49) we have

$$C_1 + 2C_2 t_i = \frac{1}{2h}(\Delta P_{i+1} + \Delta P_i) \tag{52}$$

and

$$2C_2 h = \frac{1}{h}(\Delta P_{i+1} - \Delta P_i) \tag{53}$$

Then

$$\hat{p}(t_{i+1}) = \frac{3\Delta P_{i+1} - \Delta P_i}{2h} \tag{54}$$

Guidance algorithms generate destination steering commands to the stabilized vehicle. The inputs to these algorithms, in addition to the destination, are navigation-system outputs of present position and velocity. The desired destination may be a simple final point or a sequential series of points that define a space-time trajectory.

The commands for a manned vehicle are normally attitude changes displayed on cross pointers of an Attitude Director Indicator, or acceleration commands to the autopilot generated as simple functions of the

$$N_c = f(\varepsilon_{CT}, \varepsilon_T)$$

track and cross-track position errors.

The commands for a missile are generally acceleration commands to implement a specific form of proportional navigation

$$\alpha_c = K\dot{\theta}$$

where

$\dot{\theta}$ = rate of angular change in inertial space of the line-of-sight vector from missile to destination

A specific form of this general algorithm, which is easier to implement with the form of strapdown inertial systems outputs, is the cross-product guidance law

$$[\vec{a}]_\varepsilon = [\vec{V}] \times [\vec{R}_{TG}]$$

where

$\vec{R}_{TG}$ = range-to-go to the target

$\vec{V}$ = missile velocity vector

When operating in the tangent-plane coordinate system, the range may be a single target location or a sequence of precomputed spatial coordinates designed to shape the trajectory. Since a target fixed on earth coordinates is rotating with respect to the missile tangent-plane navigation coordinates, the final target location is offset as a function of time in such a way as to minimize error sensitivity to time-of-flight variations of the vehicle. The target coordinates are corrected at a fixed rate, which in the fire-control solution, will be correct at the end of nominal time of flight of the missile. The target-coordinate initial offset, then, is the difference between the target offset resulting from the fixed rate over the total time of flight, and the precomputed target offset at nominal time of flight from the fire-control solution. At the end of nominal time of flight, then, the target offset is correct, and target offset rate is correct, which results in minimum errors

4. CONCLUSION

The critical algorithm for any strapdown system is the transformation-matrix-updating technique. The options available to the software designer are not only the basic algorithms of this paper, but also variations on each technique. For example, a Cayley-Klein four-parameter representation of the transformation algorithm may be implemented.[14] In addition, the critical process of every matrix-updating algorithm is the integration technique. Again, the designer has realistic options that range from simple rectangular, a second-order predictor-corrector, first- or second-order Taylor series, to second- or even fourth-order Runge-Kutta algorithms. The software designer also has limited options in selection of update rate and quantization levels of the measurement inputs.

To achieve required performance with modest processing requirements, Lear Siegler is currently investigating a small angle approximation, three-axis transformation using DDA equivalent processing methods as a vernier update technique. This vernier solves the matrix update problem with high-speed rectangular integration. This high-speed tracking provides excellent integration of the variable rates. The resulting angular increments are then used to update the normal four-parameter mechanization of the transformation matrix on the standard computer update times.

Since the user will almost certainly require some degree of cost optimization of a system for his application, the designer needs a flexible computer simulator as a design tool for system-algorithm definition.

The total algorithm definition for any strapdown system, however, may be constrained by hardware limitations (computer speed, memory, input/output, power), and functional and operational requirements of the total system in its application.

REFERENCES

[1] Pitman, G. R., Inertial Guidance, John Wiley & Sons, New York, 1962.

[2] Lipton, A. H., Alignment of Inertial Systems on a Moving Base, NASA TN D-4110, September 1967.

[3] Kortum, W., "Design and Analysis of Low-Order Filters Applied to the Alignment of Inertial Platforms", AGARD lecture series No. 82 on Practical Aspects of Kalman Filtering Implementation, March 1976.

[4] Wierenga, R. D., "4-D Navigation Using Integrated Strapdown Inertial/Differential Loran", NAECON, June 1975.

[5] Sutherland, A. A., and C. D. Bayne, Aided Inertial Guidance for Air-to-Surface Missiles: In-Flight Alignment, The Analytical Sciences Corporation, Reading, Massachusetts.

[6] Wierenga, R. D. Systems Integration Using the Method of Least Squares, Lear Siegler, Inc., Grand Rapids, Michigan, Report GTD-008-0571.

[7] Wierenga, R. D., "A Precision Weapon System Using Integrated Strapdown Inertial/DME Navigation", NATO AGARD Guidance and Control Panel, 16th Symposium on Precision Weapon Delivery Systems, Eglin Air Force Base, Florida, June 1973.

[8] Ball, W. F., Strapped Down Inertial Guidance: The Coordinate Transformation Updating Problem, U. S. Naval Ordnance Test Station, China Lake, California, NOTS TP4267, April 1967.

[9] Harasty, G. A., Evaluation and Error Analysis of the DDA Transformation Matrix Computer for Strapdown Inertial Systems, IBM Report 64-550-018, June 1964.

[10] Otten, D. D., Body Fixed, Three-Axis Reference System Study, TRW Report No. 4499-6007-R000, May 1966.

[11] VanBronkhorst, A., "Euler Angle Strapped Down Computer", NATO AGARD Symposium on Inertial Navigation: Components, Braunschweig, Germany 1968.

[12] Bird, M., "Elimination of Kalman Filter Divergence Due to Quantization Errors", Second Symposium on Nonlinear Estimation Theory and its Application, University of California, Los Angeles, California, 1975.

[13] Schmidt, G. T., et al, "Practical Aspects of Kalman Filtering Implementation", AGARD Lecture Series 82, May 1976.

[14] Koenke, E. J., and D. R. Downing, "Evaluating Strapdown Algorithms: A Unified Approach", Fourth Inertial Guidance Test Symposium.

STRAPDOWN SYSTEM SYNTHESIS

Alan VanBronkhorst
Lear Siegler, Inc., Instrument Division
4141 Eastern Avenue, S. E.
Grand Rapids, Michigan 49508

4-1

SUMMARY

Strapdown system synthesis is the process of developing a cost/performance optimized assembly for application in a particular weapon system. The procedure is a two-way process of definition and demonstration.

Definition begins with the weapon system requirements and generates the specifications, in a top-down process, of the system, subassemblies, and elements. Demonstration begins with the physical elements and their defined specifications and, in a step-by-step bottom-up integration process, completes the synthesis of the system.

Effective strapdown system synthesis for a particular application requires an extensive engineering data base on state-of-the-art components such as gyroscopes, accelerometers, and microprocessors, and facilities and capabilities for computer simulation of sophisticated digital and electromechanical equipment.

The exact procedure for strapdown system synthesis is arbitrary, governed both by the critical requirements of each application and skill and experience of the development engineer. This paper, then, is only a litany of the major factors and tasks which characterize the process of strapdown system synthesis.

1. INTRODUCTION

Strapdown system synthesis is the application of engineering tools and techniques to integrate a combination of elements that, in the intended application, will operate together to provide the required system functions. The most likely criteria for excellence in system synthesis is to achieve the requisite functions at minimum costs. The costs that must be considered are not only the primary life-cycle costs associated with the total system logistics, but may include, as well, secondary cost factors that affect the application of the strapdown system in the vehicle. For example, these secondary costs may include weight, packaging flexibility, energy, and interface to auxiliary equipment.

The major tasks of strapdown system synthesis and their discussion sequence in this document are shown in Figure 1.

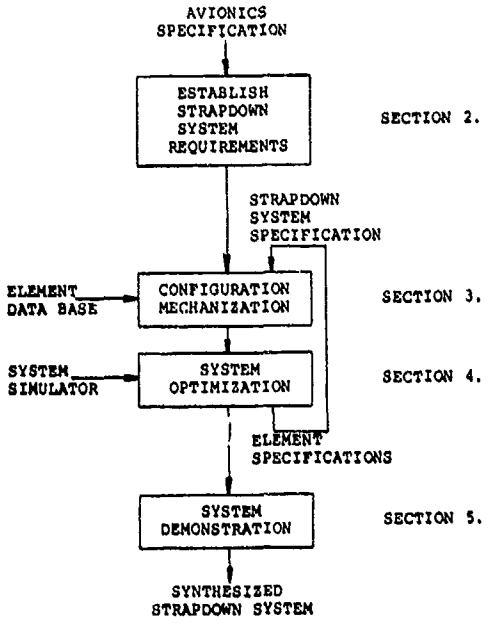

Figure 1. System Synthesis tasks.

Although this paper is written primarily as a "how-to" document, there are as many useful ways of synthesizing a strapdown system as there are strapdown system designers. This is because the total process of system synthesis is iterative in nature and because experienced designers, from hard-earned knowledge of significant parameters, can cut corners with respect to cookbook procedures. Also, many designers operate under real-world constraints of demonstrating that one particular mechanization (for example, a straightforward modification or adaptation of a component or system produced by their company) is optimum for the application. In these cases, synthesis procedures are not all that important.

The parameters that affect the cost and performance of a system, and which are discussed in this paper, are independent of the precise procedures by which the compromises are obtained for a cost-effective system.

2. SYSTEM REQUIREMENTS DEFINITION

Synthesis of a cost/performance optimized strapdown system must begin with defining the detailed specification of the system to achieve the total requirements of the integrated avionics suite of the vehicle. These specific strapdown system requirements are generated by synthesis of a total vehicle specified as a major element of a weapon system.

4.2

Weapon system synthesis begins with missions and operations requirements analysis, which ultimately defines the functions and operations of the vehicle and its total avionics complement. These avionics functions are then partitioned to various discrete subsystems for mechanization. System synthesis, then, results in top-down generation of a specification tree (Figure 2). The guidance/control system specification that ultimately results is the input to the task of strapdown system synthesis.

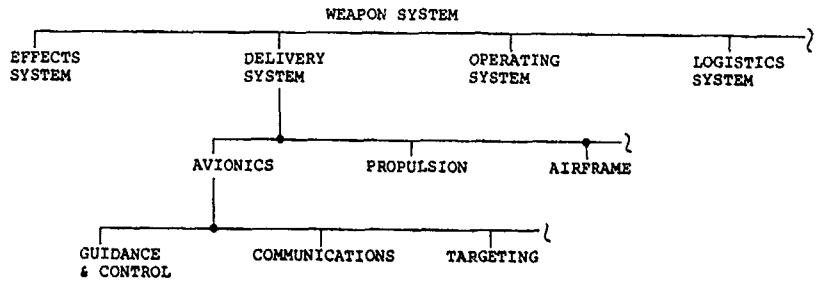

Figure 2. Illustrative specification tree.

This specification will define both function and operations, performance, operating environment, physical characteristics, reliability and maintainability, and interfaces to the vehicle and avionics suite.

Table 1 is a summary chart of the requirements for typical strapdown inertial systems for aircraft and missile applications.

Table 1. Summary of requirements for typical strapdown inertial systems.

	Cruise Vehicle	Short-Range Missile
INPUTS		
. Angular Rates, p, q, r	. ±5, ±2, ±2 rad/s	. ±6, ±3, ±3 rad/s
. Linear Accelerations, A_x, A_y, A_z	. ±10 g all axes	. ±10 g all axes
. Prime Power	. 115 Vrms, 400 Hz, 200 W	. +28 Vdc, 150 W
. Test Discretes	. System Go, LRU Fault Isolate	. System Go
. Initialization Constants (Digital Data Words)	. Position, Velocity, Destination, Magnetic Variation Corrections, Sensor Compensations	. Position, Velocity, Target Coordinates Sensor Compensations
. Flight Data (Digital Data Words)	. Baro Altitude, Flux-valve Position, Velocity, Position Corrections	. Position, Velocity, Attitude Corrections
. Temperature Control	. External and Internal	. Internal Only
OUTPUTS		
. Attitude, ψ, θ, φ	. 118 Vrms, 400 Hz, Synchro	. Digital Data
. Inertial Vectors	. Position, Velocity	. Position Velocity
. Guidance Commands	. (Not required)	. Pitch, Yaw Axis
. Body Rates, p, q, r	. (Not required)	. Digital or Analog
. Body Accelerations, $\ddot{x}$, $\ddot{y}$, $\ddot{z}$	. (Not required	. Digital or Analog
. Discretes	. System Go, LRU No-Go	. System Go
PERFORMANCE		
. Position	. 1 to 5 nmi/h (CEP)	. 1 to 10 mils CEP
. Velocity	. 3 to 10 ft/s (1σ)	. (Not required)
. Attitude	. ∿0.1°	. (Not required)
. Coordinate System	. Local Level	. Tangent Plane
. Reaction Time	. 10 min	. 10 s
PHYSICAL PARAMETERS		
. Size and Weight	. 3/4 ATR, 30 lb	. 500 $in.^3$, 15 lb
. Reliability	. 2000 h MTBF	. 0.999 Mission Success Probability
. Maintainability	. 0.5 h MTTR	. --
. Environmental Capability	. Standard Military Specifications	. 10 yr

The functions specified for the strapdown system may include flight reference (attitude) and control (body-axis angular rates and linear accelerations), vehicle navigation and guidance, and synergistic integration with other avionics subsystems.

The strapdown system generates most of these specified functions by digital processing of the basic measurement output of body-fixed sensors. This processing may be mechanized in a central avionics system computer, or in a computer that is specific for the strapdown system, or partially in both computers.

The critical strapdown system computational process is updating of the transformation matrix. This process requires a fixed-program moderate-computational-speed computer with a small memory. Some of the functions, however, such as navigation and guidance, which require small amounts of processing time and read/write memories, might be located in the central computer to take advantage of available spare locations in its programmable memory (Figure 3).

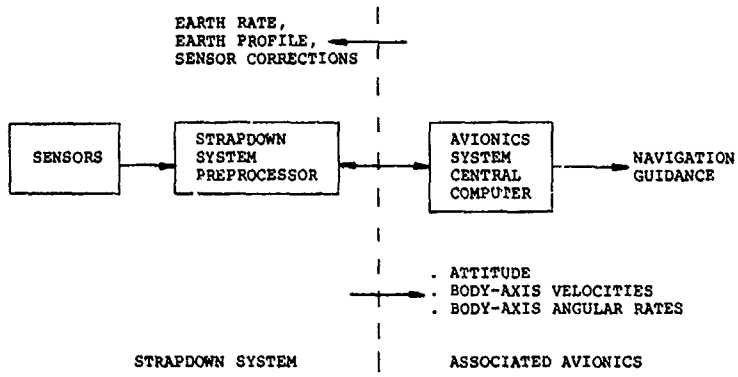

Figure 3. Typical strapdown system software partitioning.

This trade is real and quantifiable in terms of both primary and secondary costs because nonvolatile programmable memory is expensive, and is available only in large increments relative to the strapdown system requirements. The disadvantage of this software partitioning scheme is that the reliability of the navigation function of the strapdown system is reduced since it now requires two processors operating in series. In the event the central computer fails, however, the attitude output of the strapdown system can be preserved for vehicle flight reference by reverting to a first-order erected Attitude Heading Reference System operational mode.

The processing capability of the system, independently of the software partitioning mechanization, must be adequate in speed and memory size to provide integration capability with other avionics equipment. For example, a digital communications link or a targeting subsystem might be used for aiding initialization or updating the system. Outputs of a body-fixed homing or targeting system might be converted to navigation coordinates as part of the total avionics function.

3. SYSTEM CONFIGURATION

The initial system configuration is obtained by selection of alternate operations and hardware/software mechanizations that, by preliminary analysis, will achieve the specification.

3.1 System Operations

Operational variations include initialization techniques and coordinate systems.

Coordinate systems are most often explicitly defined in the specification. However, some cost/performance trades may be available with respect to the sophistication of the navigation processing in the specified coordinates. For example, the system may operate in North/East or Track/Cross-Track coordinates, wander or true azimuth angle, fixed or variable earth radius.

Strapdown system initialization consists of alignment, calibration of sensors, and definition of the system-position and velocity-vector starting conditions.

Two general methods are available for establishing the alignment or orientation of the sensitive axes of the accelerometer with the desired navigation coordinate system.[1] These methods are

(1) Autonomous direct alignment using self-leveling and gyrocompassing.

(2) Transfer alignment, which determines the system orientation relative to some intermediate system whose orientation with respect to the navigation coordinates is independently established.

These methods are often combined using transfer alignment in heading and self-leveling to the vertical.

Although transfer alignment has an intermediate system interposed between the strapdown measurement axes and the navigation coordinates, this technique is usually more operationally attractive than gyrocompassing. This results because the alignment is achieved using acceleration magnitude measurements and therefore is faster, more reliable over all operating conditions, and may provide sensor calibration as well as alignment.

The choice of alignment technique, then, is most often dictated by the availability of suitable transfer-alignment systems. These systems may be either another inertial navigation system or a radio navigation system (omega, loran, distance measuring equipment (DME)) onboard the vehicle.

The strapdown system engineer must determine only the characteristics of the accelerometers that are necessary to obtain the required accuracy of correlation of their outputs with the outputs of the transfer system when they are driven by a common, operationally feasible, input. The accelerometer characteristics that affect that alignment

are sensitivity and frequency response. The operational limits to the driving-function input may result from reaction-time requirements or actual dynamic limits of the vehicle or transfer system.

The final process of initialization is to define the starting point of the position and velocity vectors that the system will measure. For vehicles that are stationary with respect to the earth during the initialization process, the system designer must specify only the accuracy of measuring the initial position of the vehicle. For moving vehicles, the transfer-alignment process that is normally implemented measures the best possible estimate of vehicle position and velocity for initializing the strapdown system.

3.2 System Mechanization

Candidate systems are mechanized by suitable combination of state-of-the-art sensors (gyroscopes and accelerometers) and digital computers. The input to this task is a detailed catalog of available units listing their relevant parameters. In addition, the system designer should have a knowledge of the developmental state-of-the-art of the relevant parameters of units that could be available within the reasonable development schedule and cost.

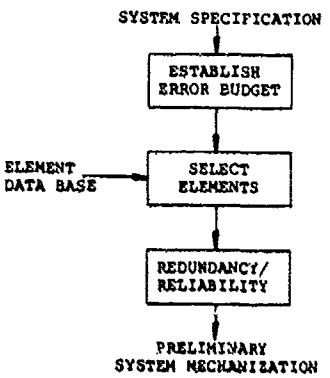

Figure 4. Task flow chart configuration mechanization.

The principal tasks in establishing a preliminary or initial system mechanization are shown in Figure 4.

Navigation system errors accumulate in both absolute magnitude and direction of the vehicle position vector. The principal contributors to direction errors are initial alignment, gyroscope measuring errors, and computer processing of the gyroscope outputs. The error in the initial velocity-vector magnitude and accelerometer measurement errors account for vector magnitude errors.

In general, system errors should be budgeted such that vector directional errors dominate. This is because gyroscope performance is more expensive than accelerometer performance.

A block diagram of a typical strapdown system (Figure 5) defines the elements that must be mechanized. These elements consist of angular-rate and linear-acceleration sensors along orthogonal axes; a means of converting the continuous dynamic measurements into discrete quantities for subsequent processing in the digital computer; and a power conditioner.

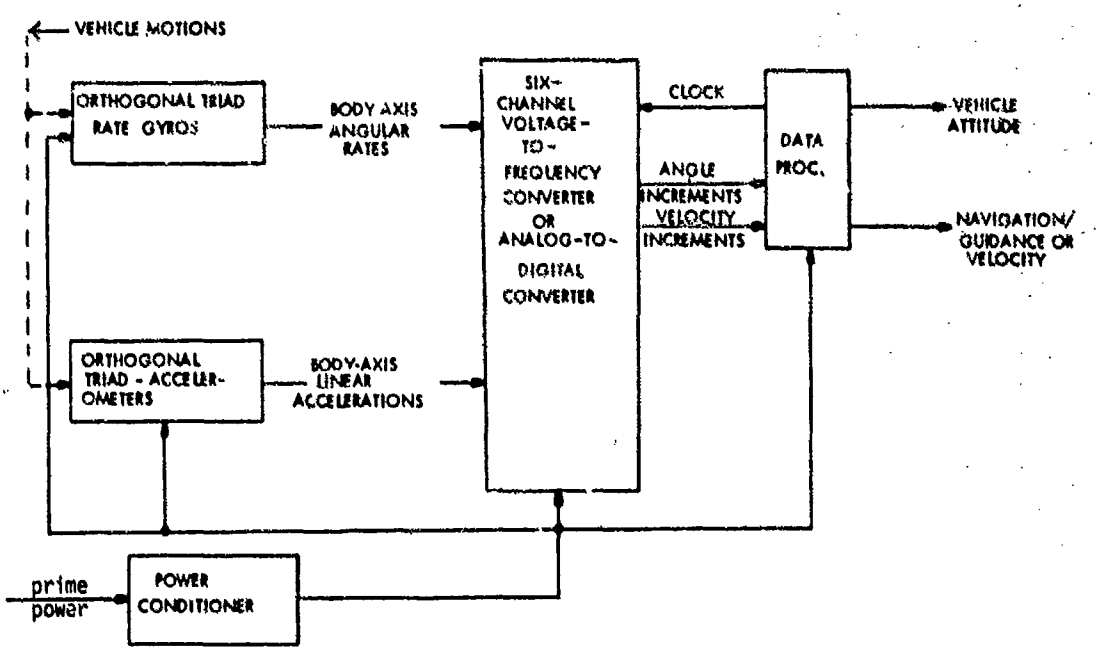

Figure 5. Strapdown system block diagram

Possible mechanization variations are shown in Table 2.

Sensor types and performance ranges have been previously discussed. Selection of sensors in a preliminary mechanization to achieve cost and performance goals of the system requires both cost and error sensitivity analyses.

Table 2. Mechanization elements.

Gyroscopes	drift uncertainty
Ring-laser	1.0 to 0.01 °/h
Flexure, two-axis	1.0 to 0.01 °/h
Floated, single degree of freedom	10 to 0.01 °/h
Accelerometers	bias uncertainty
Pendulous, single-axis	10^{-3} to 10^{-5} g
Converters	
Computers	
Power Conditioner	

Preliminary approximate performance estimates can be obtained by simple paper and pencil analysis. Tables 3 and 4 show typical error equations and sensitivities for cruise vehicles and rocket-powered missiles. The inputs to the tables are piecewise linearized trajectories of the vehicle.

Analysis of quoted manufacturer's cost data for strapdown sensors, [2,3,4] in the recent U.S. Air Force-sponsored Low Cost Inertial Guidance System Study, indicates that the cost/performance ratio of these units will plot within a rather narrow band defined by parallel lines on a log-log coordinate graph (Figure 6). Also, this study established 1.8 as an approximate multiplying factor to apply to total sensor costs to obtain system costs.

Obviously, in establishing a preliminary mechanization, the choice of elements may be restricted by other factors of the specification such as operating environment, size and weight restrictions, reaction time, and input power limitations.

Many of the sensors of Table 2 are directly mechanized with digital phased-lock loops or delta modulation capture-loop electronics so that the output is directly quantized in form suitable for accumulation in storage registers at the computer input.

Some sensors, however, are operated in an analog mode with followup quantizers. Two basic types of quantizer are available: an analog-voltage-to-pulse-frequency converter, and conventional analog-voltage-to-digital-word converter.

The voltage-to-frequency converter operates as a reset or rebalance analog integrator principle. When the integrator output achieves a reference voltage level, it is reset, and a pulse or quanta of sensor output measurement

Table 3. Cruise vehicle, local-level coordinates.

Source	Position Error Magnitude	Notes
1. Level Gyro Drift	$\dot{\epsilon}R(t - (1/\omega_0)\sin\omega_0 t)$	$\dot{\epsilon}$ = $\dot{\phi}$ or $\dot{\theta}$ = pitch and roll angular rates
2. Azimuth Gyro Drift	$0.7\left(\dot{\epsilon}v\left[\frac{t^2}{2} - \frac{(1-\cos\omega_0 t)}{\omega_0^2}\right]\right)$	R = earth radius = 2×10^7 ft ω_0 = Schuler period = $g/R = 1.2\times10^{-3}$ rad/s $\dot{\psi}$ = azimuth angular rate v = vehicle velocity t = time of flight
3. Accelerometer Bias Shift	$\frac{K_B}{\omega_0^2}(1-\cos\omega_0 t)$	K_B = accelerometer turn-on bias plus bias shift after initial alignment. Turn-on bias is correlated with misleveling error as a function of change in heading of the vehicle.
4. Accelerometer Scale Factor	$K_S v\left(t - \frac{1}{\omega_0}\sin\omega_0 t\right)$	K_S = accelerometer scale factor For $\Delta\psi = 0$, turn-on bias error is cancelled by initial leveling error.
5. Matrix Transformation	See 1 and 2 above	Essentially equivalent to gyro drift
6. Initialization Mislevel	$\frac{\Delta\psi K_B}{\omega_0^2}\left[\frac{t^2}{2} - \frac{1-\cos\omega_0 t}{\omega_0^2}\right]$	$\Delta\psi$ = change in heading See note on accelerometer turn-on bias.
Heading	$\epsilon\psi vt$	$\epsilon\psi$ = initial heading alignment error
Velocity	$\epsilon v_i/\omega_0 \sin\omega_0 t$	ϵv_i = initial velocity error

4-6

$$\Delta\theta = \int_{t_k}^{t_{k+1}} \omega \, dt \quad \text{or} \quad \Delta v = \int_{t_k}^{t_{k+1}} a \, dt$$

is applied as a bit of input into accumulators at the computer. The pulse-rate output, or pulse-repetition frequency, is proportional to the voltage-amplitude output of the sensor.

Table 4. Short-range vehicle, tangent-plane coordinates.

Source	Magnitude	Notes
1. Gyro Drift	$\sum_n (\frac{1}{2}[c\alpha]t_n^2 + [c\alpha]t_n T)$	$[c\alpha] = \begin{bmatrix} c\alpha_x \\ c\alpha_y \\ c\alpha_z \end{bmatrix} = \begin{bmatrix} 0 & c\psi & -c\theta \\ -c\psi & 0 & c\phi \\ c\theta & -c\phi & 0 \end{bmatrix} \begin{bmatrix} a_x \\ a_y \\ a_z \end{bmatrix}$ where $c\phi, c\theta, c\psi$ = drift angles accumulated by total angular drift rate of gyro over time t_n; a_x, a_y, a_z = average accelerations of vehicle over time t_n; $T = \sum_n t_n$
2. Accelerometer Bias	$k_B t_f^2/2$	t_f = total time of flight; k_B = turn-on bias plus bias shift at launch
3. Accelerometer Scale Factor	$\sum_n k_S[a]t_n^2/2$	
4. Matrix Transformation	See 1 above	Equivalent to gyro drift
5. Initialization		
Mislevel	$c\alpha \cdot g \cdot t_f^2/2$	$c\alpha$ = initial mislevel angle. This error is correlated with accelerometer bias error as a function of heading change of the vehicle. Initially mislevel error cancels accelerometer bias error.
Heading	$c\phi \cdot R$	R = total vehicle range in x-y plane
Velocity	$[cv] \cdot t_f$	$[cv] = \begin{bmatrix} cv_x \\ cv_y \\ cv_z \end{bmatrix}$

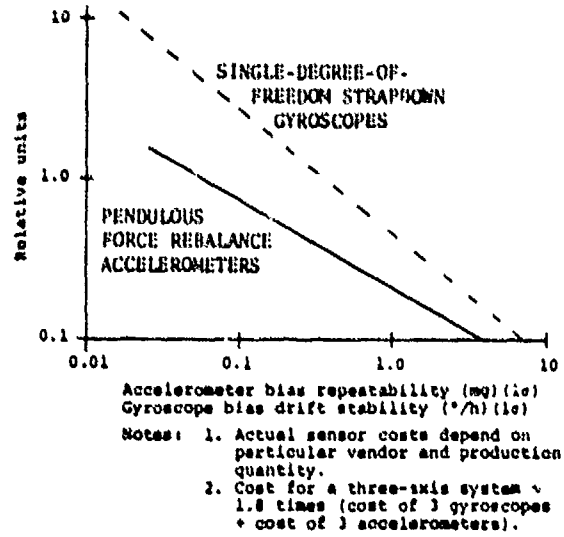

Figure 6. Plot of cost/performance ratio for strapdown sensors.

For some special applications, a conventional successive approximation analog-to-digital converter may be applied. This type of converter requires less hardware to implement since a single converter may be time-multiplexed to process all the sensor inputs. The basic limitation, however, is that it is less accurate than the voltage-to-frequency converter, since it implements a first-order rectangular integration rather than linear integration of the sensor outputs; it is also limited in practical applications to a dynamic range of 2^{12}.

4.1

This range may be extended by increasing the resolution using the technique of injecting a known dithering voltage at the input, and performing a statistical averaging of the output. This will provide adequate dynamic range for processing accelerometer outputs for some systems, but is still far short of the dynamic range of outputs of the gyroscopes, which may be as high as 2^{24}.

In the selection of computer hardware (Figure 7) the system designer has greater freedom of choice than in any other element. The problem for the designer is that the development of new integrated circuits and associated microprocessors is so fast that any design is literally obsolete between system concept and first production.

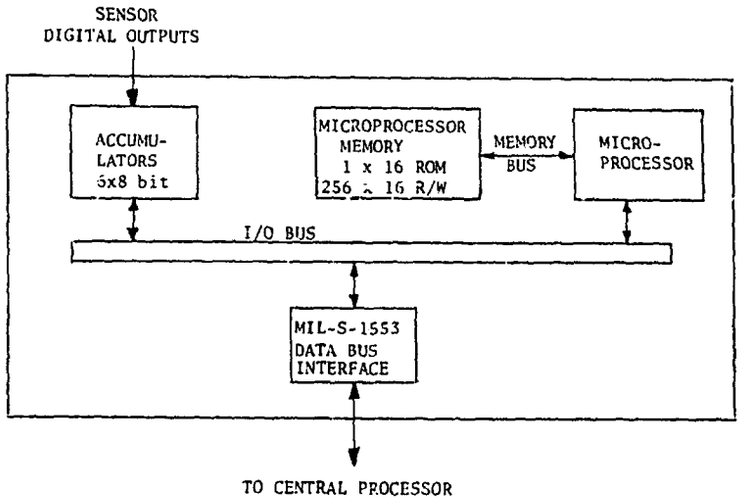

Figure 7. Strapdown processor block diagram.

Figure 8 illustrates the recent changes in computer logic circuitry size with advancing technology.[5] In general, the decreasing size of the newer technology is accompanied by decreasing cost and complexity of the manufacturing process.

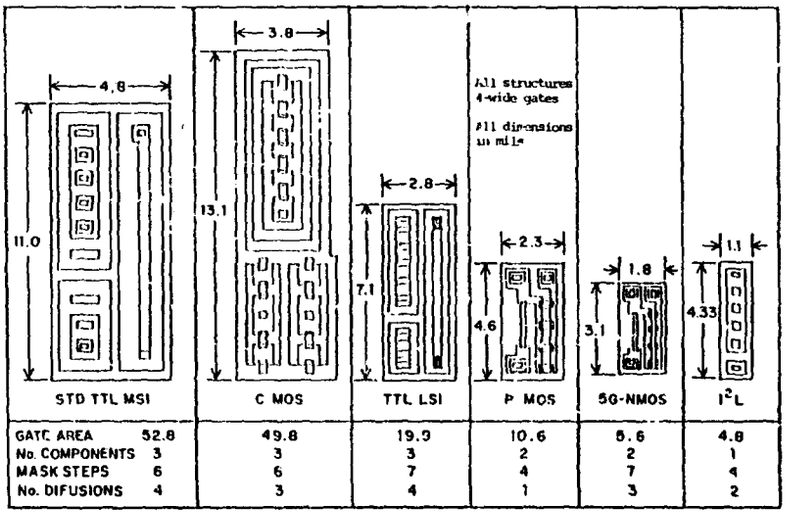

	STD TTL MSI	C MOS	TTL LSI	P MOS	SG-NMOS	I^2L
GATE AREA	52.8	49.8	19.9	10.6	5.6	4.8
No. COMPONENTS	3	3	3	2	2	1
MASK STEPS	6	6	7	4	7	4
No. DIFUSIONS	4	3	4	1	3	2

Figure 8. Comparison of logic circuits showing change of size with advancing technology.

* Reprinted by permission, Texas Instruments Corp., Dallas, Texas.

Also, as circuit density increases, the associated single-chip functional capability and operational speed increases.[6,7] Complete 16-bit single-chip microprocessors are already available, and by the early 1980s single-chip 16-bit microcomputers, including both computational unit and memory adequate for strapdown systems, should be available. The anticipated progress of integrated circuit technology is illustrated in Figure 9.

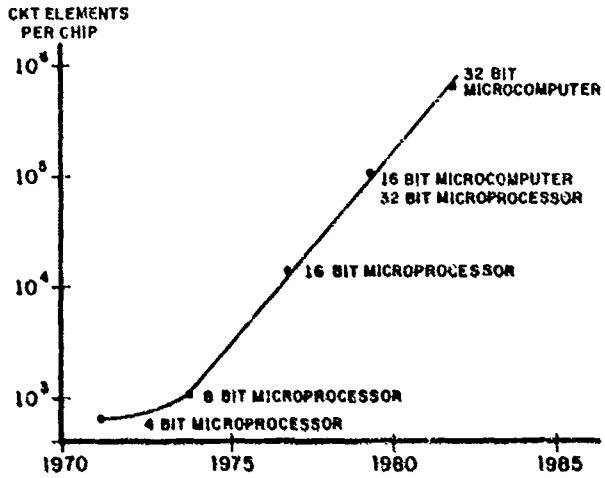

Figure 9. Projected advances in processor technology.

Other advances projected for avionics computers through Large Scale Integration are increased functional modularity and increased reliability by fault-tolerant architecture.[8]

In addition to determining the type of sensors and computer to be used, the system design must also determine the degree of redundancy in these units in order to achieve the required level of system reliability for certain applications. This degree of redundancy may vary from a minimum "fail-safe" configuration, which incorporates only a single redundant-sensor channel in a four-channel skewed orientation, to a full "fail-operational, fail-operational, fail-safe" quadruply redundant system often specified for flight safety equipment. Redundant mechanizations are also applicable to space vehicles which require long operating life. An advantage often cited for strapdown systems with respect to gimbal systems is that the full fail-op/fail-op/fail-safe system configuration requires only six independent sensor channels.

Figures 10 and 11 are functional block diagrams of these redundant system configurations. Obviously, any configuration between these two extremes may be implemented to achieve the specified system reliability.

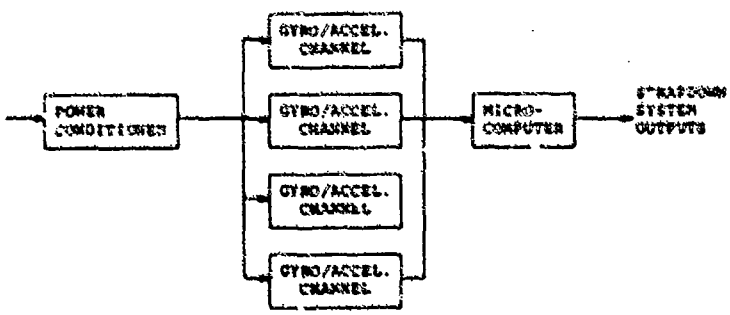

Figure 10. Minimum fail-safe strapdown system configuration.

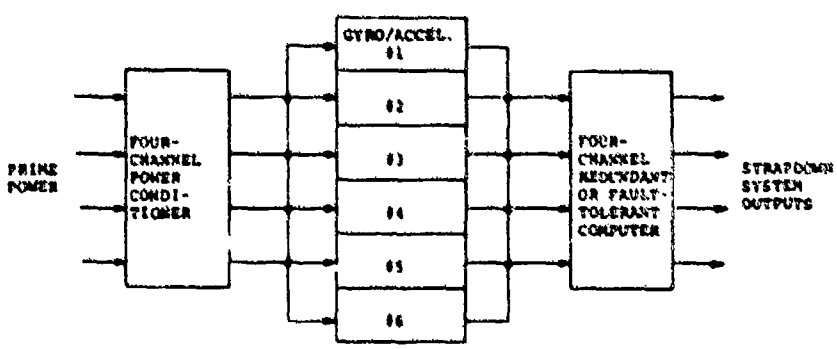

If the sensors are mounted so that no three sensitive (input) axes are coplanar, the strapdown solution is valid in either configuration with only the outputs of any three of the sensor channels. Redundant systems, however, are normally operated in an active redundancy mode: all equipment is operating during the entire flight. This mode of operation improves system performance since the strapdown solution may be obtained by averaging certain sensor errors by combining their outputs into a single solution. In addition, active redundancy operation prevents any system "down time" in the event of a single sensor failure, while a standby sensor is brought into operational status.

The minimum four-channel system provides fail-safe sensor operation in that it can detect that a failure of one of the sensor channels has occurred without external aids. A minimum of five channels, however, is required to isolate a single failure. The minimum fail-safe configuration, then, is useful primarily in an augmented or integrated navigation system where the external navigation sensor can be used to isolate any failed strapdown system channel failure.

The inability of a four-channel system to fault isolate results, because a failed channel signal will appear in three of the four solutions. The contribution of this failed channel sensor to any of these three solutions is variable. Then a failed channel will only result in four different solutions to the input vector and voting, to determine the one invalid solution, is impossible.

With 5 channels, however, 10 system solutions using the output of any 4 of the channels is feasible. But a failed channel can contribute to only six of these solutions. All of these solutions will again be different for a fixed input. The remaining four solutions, which are identical within the normal error limits of the sensors, will all be solutions using sensor outputs that do not include the failed channel. This permits isolation of the failed channel.

The six-channel redundant system can isolate two channel failures and detect a third, thereby providing fail-op/fail-op/fail-safe redundancy level.

Many algorithms have been investigated and reported in the literature [9,10,11] on fault isolation of a redundant-channel strapdown system.

The error sources of the sensors are statistical in nature: representative of a population of sensors whose errors are randomly distributed and uncorrelated between sensors. If, then, the transformation matrix is obtained by processing of redundant-sensor information, the accuracy of the final solution is upgraded by statistical averaging. The amount of this upgrading depends on the level of redundancy and the relative orientation of the sensors.

The optimum performance configuration of the system depends on the error characteristics of the sensors, and the degree of redundancy of the sensor channels,[12] the relative orientation of the sensors, and the orientation of the sensors to the linear and angular acceleration vectors of the vehicle.

For cruise vehicles, where dynamic inputs are likely to be small, the optimum orientation of the sensors is with equal space angles between the sensitive axes of the sensors. The sensitive axes of the four-channel sensors, then, are normal to the planes formed by the sides of an equilateral tetrad, and the sensors of the six-channel configuration are normal to the planes formed by the sides of a regular hexad.

Recent studies, however, show that there is little, if any, performance difference between a symmetrically skewed hexad [13] configuration and a dual orthogonal triad configuration if the two orthogonal triads are related to each other by rotation of one triad by 60 degrees around a 1,1,1 axis of rotation of the other triad. This 2 times 3 configuration has a distinct physical packaging advantage since the orthogonal triad is the normal packaging configuration of strapdown inertial systems.

For trade-study parameters, the degree of performance improvement may be represented by

$$\sigma_a = \sqrt{3/N}\ \sigma_c$$

where

σ_a = error per axis

σ_c = error per channel

N = number of sensor channels

Then

$\sigma_a = \sqrt{3/4} = 0.87\ \sigma_c$ for fail-safe configuration

$\sigma_a = \sqrt{3/6} = 0.707\ \sigma_c$ for fail-op/fail-op/fail-safe configuration

4. COST/PERFORMANCE OPTIMIZATION

The cost/performance ratio of the preliminary system mechanization is optimized using the principal tool of system simulation. The subtasks of optimization are shown in Figure 12. The inputs to the optimization task are the preliminary system configuration and specific cost and performance data on the selected elements of the configuration.

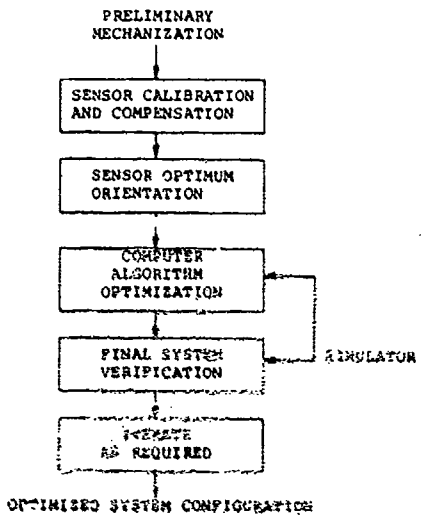

Figure 12. Cost/performance optimization tasks.

Sensor calibration and compensation, as a viable option for systems optimization, is limited both by the ability to measure the sensor errors and by the stability of those errors as a function of time and operation in a stressful environment.

The errors of strapdown sensors are not readily measured because when the sensors are mounted in a vehicle there are no easy means for applying a precisely known input rate or acceleration vector.

Some sensor errors, such as misalignment of the sensitive axes from orthogonality, scale-factor nonlinearities, and angular acceleration sensitivity (which have good long-term stability) are calibrated before the system is installed. These errors may be compensated either by specific circuitry in the sensors or special software in the processor.

Sensor errors that are temperature dependent, such as scale factor, may be corrected by either temperature control of the system or by thermal modeling and compensation by software as a function of measured temperature. Temperature control is most accurate but requires more energy and limits system reaction time to achieve thermal stability.

Errors (such as bias, randomness, and threshold) that change day-to-day or start-to-start or as a result of thermal cycles or variable vibration environment are most difficult to measure. A transfer-alignment technique using Kalman filtering to correlate the sensor outputs may be implemented with enough sophistication to separate all measurable error terms. The cost is processor time and memory, and adequate driving-function input. Because these costs are significant, the system synthesizer must carefully model the system and determine error-sensitivity coefficients for the operational flight program to limit measurement and compensation to only the significant sensor errors. For example, an air-to-air surface missile system, which is normally launched along the target line-of-sight, may compensate for pitch gyro bias but not azimuth or roll gyro biases although all are easily measurable.

Sensor orientation of sensitive axes with respect to the principal measurement vectors may be optimized for best performance for initial alignment and/or flight operations.[14]

In self-leveling and gyrocompassing operations, the sensors are operating as null seekers, and in transfer alignment, the sensors must accurately measure an absolute vector magnitude. For major instrument errors of misalignment, bias and scale-factor,[15] Table 5 shows the relationship of measurement errors as a function of the orientation of the instruments with respect to the measured vector direction.

Table 5. Errors as function of sensitive-axis orientation.

Vector Direction	Magnitude Error	Null Detecting Error
Along any instrument sensitive axis	Max	Min
Center of triad	Min	Max

For example, in self-leveling

$$\sigma^2 = 2\left[\sigma_{SA}^2 + (\sigma_b/g)^2\right] \text{ for two accelerometers}$$

and

$$\sigma^2 = (3/2)\sigma_{SA}^2 + 2(\sigma_b/g)^2 + \sigma_{SF}^2\left(1 - \sum_1^3 \cos^4\phi\right)$$

where

σ = error in indicating the vertical

σ_{SA} = misalignment angle

σ_b = bias error

and

σ_{SF} = scale-factor error

4.11

Sensor input axes also have optimum orientations with respect to the vehicle dynamics for in-flight operation. For example, with simultaneous application of accelerations perpendicular to both input and pivot axes of a pendulous accelerometer, the displacement of the pendulum from null results in a cross-axis error. This error is minimized if the pivot axes of the accelerometers are mounted along the major thrust axis of the vehicle as shown in Table 6. In this table X is the direction of the longitudinal, or thrust axis of the vehicle, Y and Z are normal to X with Z the nominally vertical axis.

Table 6. Optimum accelerometer orientation example.

Input Axis	Pivot Axis
X	Z
Y	X
Z	X

As a second example, vehicle roll rates are generally much higher than pitch and yaw rates. Orienting a gyro cluster so that vehicle roll/pitch rates are measured by two gyros whose outputs are resolved by the computer to generate body-axis roll/pitch rates will reduce the dynamic range requirements of the two gyros with consequent reduction in measurement linearity errors.

If the vehicle modes and directions of vibrations in flight are known, the orientation of sensor axes may be optimized to reduce nonlinear rectification errors. For example, with single degree-of-freedom gyroscopes, anisoelastic drift results from accelerations applied simultaneously along the input axis (IA) and spin axis (SA). For this reason it may be desirable to orient the gyroscopes so that either its input axis or spin axis lies along the vehicle body axis which has minimal accelerations in flight. For a missile launched along the line-of-sight to the target this body axis may be Y. This assumes the following coordinates:

X is along the longitudinal or thrust axis.

Y and Z are normal to X with Z nominally vertical.

Then, an optimum gyro orientation to reduce anisoelastic drift from vibration or steady-state accelerations is shown in Table 7.

Table 7. Optimum gyroscope orientation example.

Input Axis (IA)	Spin Axis (SA)	Output Axis (OA)
X	Y	Z
Y	Z	X
Z	Y	X

Complete system simulation is the tool for optimization of the computer algorithms and final verification of the optimized system configuration. The simulation capability is shown in Figure 13 in block diagram form.

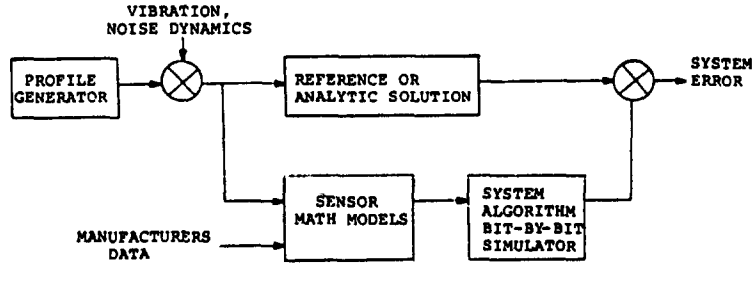

Figure 13. Simulation facility functional block diagram.

4-12

A general criteria for an optimum strapdown algorithm is to establish update rates, sensor quantization levels, integration techniques just sufficient to achieve a computational error rate that is small (< 10%) with respect to the total system error budget. The simulator input for this optimization task is often simple coning motion. Coning motion has an analytic solution so that reference solution errors do not affect the observed algorithm performance; coning motions are a severe exercise of the principal strapdown algorithm.[16,17,18]

The final definition task is verification by simulation of the optimized system. This simulation can be either a digital computer solution of the error equations or a complete representation of the system including the computer algorithms, and mathematical models of the sensors in their optimum mounting configuration.

The input to this simulation should be a dynamic nonlinear trajectory segment or flight profile that is representative of the vehicle in its assigned mission. The profile generator is a six-degree-of-freedom simulation of the vehicle under thrust acceleration and programmed maneuvers.

The advantage of simulating only the error equations is in reduced computer time and costs. An advantage of the complete system simulation, as will be shown, is that the simulator may later be used in the final demonstration process of system synthesis to verify the physical system.

The selected sensors should be modeled with error coefficients specified by the manufacturer to provide some assurance that the simulated system is in fact physically realizable. However, some caution is advised:

(1) Many more error sources of sensors can be analytically modeled [18] and even demonstrated by careful test procedures on the instruments than should, for economic reasons, be included in the simulation. At most, two or three error sources of each sensor dominate the system performance.

(2) Values of coefficients that are quoted as one sigma or rms imply that the coefficient values of the population of sensors has a standard distribution. In fact, the pressure to achieve production schedules almost always results in a coefficient magnitude distribution that is skewed toward the maximum allowable acceptance testing limits.

(3) The degree of risk involved in assuming that some error coefficients may be calibrated or measured and compensated is almost directly proportional to the magnitude of the affected coefficient. Before simulating compensated errors it is necessary to know the day-to-day turn-on-to-turn-on temperature and acceleration shock stability of the error coefficient. These values are not always specified, or even known, by the manufacturer.

(4) For application of a strapdown system that requires input to a Kalman filter (for example, for transfer alignment or for operation in a hybrid radio/inertial system), an important performance characteristic is the correlation time of the randomness. Again, the risk in accepting manufacturer's data for correlation time or power-spectral-density values of the randomness is related to the magnitude of the randomness coefficient. The difficulty of testing combined with the variation in the population of sensors makes meaningful data on this parameter a function of instrument quality.

Obviously, in synthesis of a strapdown system, some of the tasks discussed above may be omitted or modified. Other tasks may have to be iterated for a final configuration, depending on the degree of optimization desired.

5. SYSTEM DEMONSTRATION

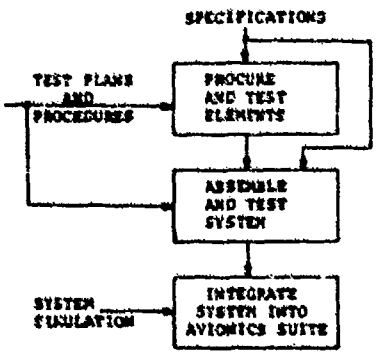

Figure 14. System demonstration tasks.

Strapdown system synthesis involves both generating of specifications from top level down, and assembly and testing from the bottom level up.

The top-down specification tasks described above begin with weapon system requirements, and culminate in detailed specifications and test plans and procedures for the optimized system and its major elements. System demonstration is the step-by-step inverse process (Figure 14) of converting these specifications into operational hardware and software.

The specified major elements may be procured through engineering development or by direct purchase of existing units.

The final phase of system synthesis, then, is testing of the elements, assembly of the demonstrated elements into a strapdown system, testing of the system, and finally, integration and demonstration of the system with the total avionics suite of the vehicle.

Integration of the physical system into the total avionics is aided by the complete system simulation. The veracity of the simulation is first tested by comparing it to the operating hardware performance for a particular dynamic input that can be generated and measured in the laboratory. Specific examples are constant angular rates using a centrifuge, or complex coning motion using scorsby or servo-driven tables. The verified strapdown system simulation, interchangeably with the physical system, may then be incorporated in a total avionics suite simulation to check for adverse effects of interactions under dynamic operating conditions. This is a cost-effective technique for systems integration prior to actually installing the physical system in the carrying vehicle.

REFERENCES

[1] Ryan, T. J., Alignment and Calibration of a Strapdown Inertial Measuring Unit, MIT Measurement Systems Laboratory, Report RE-67.

[2] Perlmutter, L. D., et al., "Strapdown Inertial Sensor Requirements for Tactical Guidance", NAECON, 1977.

[3] Mueller, C. E., R. K. Phelps and R. Scheidenhelm, "Tactical Guidance Requirements for Strapdown Inertial", NAECON, 1977.

[4] Eberlein, A. J., and P. G. Savage, Strapdown Cost Trend Study and Forecast, NTIS Document N75-17378, 1975.

[5] Horton, R. L., J. Englade and G. McGee, "I^2L Takes Bipolar Integration a Significant Step Forward", Electronics, 6 February 1975.

[6] Altman, L. and C. L. Cohen, "The Gathering Wave of Japanese Technology", Electronics, 9 June 1977.

[7] Moher, A. J., "Impact of Microcomputers on Avionics", Navigation, Vol. 24, No. 2, 1977.

[8] Turn, R., "Aerospace Computers in the 1980s", NAECON, 1975.

[9] Wilcox, J. C., "Competitive Evaluation of Failure Detection Algorithms for Strapdown Redundant Inertial Instruments", Journal of Spacecraft and Rockets, Vol. II, No. 7, July 1974.

[10] Potter, J. E. and J. C. Deckert, "Minimax Failure Detection and Identification in Redundant Gyro and Accelerometer Systems", Journal of Spacecraft and Rockets, Vol. 10, No. 4, April 1973.

[11] McKern, R. A., "Redundancy Management of Inertial Systems", AIAA Guidance and Control Conference, 1973.

[12] Pejsa, A. J., "Optimum Skewed Redundant Inertial Navigators", AIAA Journal, Vol. 12, No. 7, July 1974.

[13] Weinstein, W. D., "Optimum Skew Angle Between Redundant Inertial Sensors", Proceedings of the ION Meeting on Space Shuttle, February 1971.

[14] Giardina, C. R., "Optimal Gyro Mounting Configurations for a Strapdown System", NAECON, 1974.

[15] Lipton, A. H., Alignment of Inertial Systems on a Moving Base, NASA TN D-4110, September 1967.

[16] McKern, R. A., A Study of Transformation Algorithms for Use in a Digital Computer, MIT M.S. Thesis, T-493, January 1968.

[17] Marcus, F. J., Computational Comparison of Strapdown Systems Attitude Algorithm, MIT M.S. Thesis, 1971.

[18] Caffery, et al., Inertial Navigation Strapdown Simulator, Draper Laboratories, MIT Report R-969, February 1977.

[19] Crawford, B. C., "Dynamic Single-Axis Testing of Single-Degree-of-Freedom Strapdown Sensors", TASC, Reading, Massachusetts, Fifth Inertial Guidance Test Symposium, Holloman Air Force Base.

APPLICATION OF STRAPDOWN INERTIAL SYSTEMS

WITH PARTICULAR REFERENCE TO UNDERWATER VEHICLES

5-1

J R CATFORD B.Sc.,C.Eng. MRAeS
Marconi-Elliott Avionic Systems Limited
Rochester, Kent. UK

1. INTRODUCTION

1.1 Background To The Lecture

This lecture concerns a fairly simple application of strapdown inertial techniques. The mathematical background that is presented is straightforward (which may well be a welcome relief after the remarkably clear but nonetheless esoteric algebra of yesterday). The objective of this lecture however is to examine a simple, yet interesting application of strapdown that is about to go into production after the manufacture of thirty or so prototype and engineering development models.

A simple approach to strapdown attitude sensing is possible in underwater weapons because the dynamics of the vehicle allow simplifying approximations to be made to the coordinate transformations.

The theory of the strapdown attitude sensing mechanisation is explained, and the experience gained from early trials is illustrated.

The current, digital mechanisation of the attitude sensing function is described and the results of the continuing trials programme are reviewed.

A brief examination is made of the way in which the techniques developed for the underwater weapon environment can be extended for other relatively low accuracy strapdown inertial mechanisations.

1.2 The Benefits of Strapdown for Underwater Weapon Applications

The first figure summarises the benefits of the strapdown approach.

The background to these will be investigated a little further in a later section. Suffice it to say that in 1964 the Admiralty Underwater Weapons Establishment (A.U.W.E.) of the Ministry of Defence (Navy), MOD(N), were about to initiate work on a new generation of weapons and they were conscious that vehicle attitude measurement and control system was an area in which a major improvement was required. They held initial discussions with industry to explore the possibility of a strapdown approach which, at that time, was novel. The discussions with my Company established an agreement that the strapdown approach should be the correct one.

Hence in the summer of 1964 A.U.W.E. let a contract for the Initial Systems Studies of a Torpedo Control System. These studies compared a gimballed platform, two degree of freedom gyro, and strapdown approaches and within a few months had established that the strapdown technique showed the most promise.

2. THE CONTROL PROBLEM FOR AN AIR LAUNCHED TORPEDO

The air launched torpedo represents a very severe control problem. Figure 2 illustrates a possible air drop, pullout, search and terminal homing trajectory. Each of these phases places constraints on the vehicle motion sensing and control system which will be reviewed.

Whilst the weapon aboard the carrier, which can be helicopter, conventional aircraft, guided weapon or surface craft, data on the target is loaded into non-volatile store. This data would include direction of target, if known, and would specify tactical parameters such as search depth, water depth etc. It is, in general, to include data about the mother vehicle attitude and motion as this necessitates an interface between the mother vehicle flight systems and the weapon, and as a variety of mother vehicles are involved, this results in a proliferation of differing standards of interface unit. Because of this it is desirable to release the weapon with sensors and control systems inert. A possible alternative is to energise the align weapon sensors while on the mother vehicle but this necessitates a power supply to cover the airdrop phase as well as a sensing and computation capable of dealing with the severe manoeuvres encountered during parachute deployment and water impact.

In particular an all angle attitude system is required to cover the air drop phase because the weapon may undergo multiple rolls in addition to large pitch excursions.

Water entry involves severe shocks and high transient angular rates. A few seconds after water entry the battery output begins to rise, current is available for control functions and the propulsion system starts accelerating. The vehicles control functions must start up in a very short time, in this phase, or the vehicle will commence violent manoeuvres during which it would be impossible to align the control system.

The control system aligned and the vehicle under control, descent to a preset search depth may be initiated, followed by a search manoeuvre which allows the sonar to survey a selected volume of sea. If no target is detected, a run out on a predetermined heading may be initiated, followed by a search at the same, or a different, depth. When a target is detected, a terminal homing based on a lead angle computing procedure and terminal manoeuvre to ensure a hit against a vulnerable region of the target, are initiated.

The manoeuvres illustrated are typical, weaving manoeuvres and spiral dives may also be specified.

5.2

A prime constraint is that the homing array which provides a basically horizontal fan of sonar energy, must be kept horizontal if reflections from the surface, the bottom, or isothermal layers are not to confuse the system.

Weapon roll excursions must therefore be restricted to about $\pm 2^{\circ}$ during search phases which implies a roll attitude sensing accuracy of the order of $\pm\frac{1}{2}^{\circ}$.

Against this background we can examine the attributes of strapdown recorded in the slide.

The benefit of ruggedness is self evident, the problems of alignment on the carrier and carrying that alignment through the air drop phase have already been mentioned.

Continuous updating wherein the accelerometers used to align the system are heavily filtered and used in a long time constant gravity update mode is a significant advantage as this approach facilitates the use of relatively small (and therefore rugged) moderate performance rate gyros.

Rapid run up has already been identified as a necessary attribute.

The fact that the strapdown approach enables a topple free mechanisation, or at least provides a capability to recover from and align after a topple, is of course a significant advantage when the strapdown approach is compared with a two degree of freedom gyro or platform solution.

3. THE REQUIREMENTS FOR ATTITUDE SENSING FOR AN UNDERWATER WEAPON

As originally set out the design requirements for the system were,

(a) Roll Angle ϕ to be measured over the range $\pm 90^{\circ}$ to an accuracy better than 1 degree

(b) Pitch Angle θ to be measured over the range $\pm 85^{\circ}$ to an accuracy better than 1° when $-45^{\circ} \leq \theta \leq 45^{\circ}$

(c) Azimuth Angle ψ continuous rotation to an accuracy of better than 5°

(d) Roll rate $\dot{\phi}$ to be measured over the range $\pm 100^{\circ}$/second with an accuracy of 5%

(e) Azimuth rate $\dot{\psi}$ to be measured to an accuracy of 5%

(f) Body Angular rates q and r to be measured (q pitch r yaw)

(g) $\int_{T}^{T+t} q\,dt$ and $\int_{T}^{T+t} r\,dt$ to be measured where T and t are variable

(h) Depth Z_o to be measured over an accuracy of $\pm$ 0.5% of full range

(j) The system to provide power outputs to drive electro-hydraulic control surface actuators according to the following approximate control laws

Search Phase

$$\begin{cases} \text{Roll Control Surface Demand} = a_1 \phi + a_2 \dot{\phi} \\ \text{Pitch Control Surface Demand} = b_1 (Z_o - Z_D) + b_2 \theta \\ \text{Yaw Control Surface Demand} = c_1 (\psi - \psi_D) + c_2 \dot{\psi} \end{cases}$$

Homing Phase

$$\begin{cases} \text{Roll Control Surface Demand} = a_1 \phi + a_2 \dot{\phi} \\ \text{Pitch Control Surface Demand} = b_3 \int_{T}^{T+t} q\,dt + b_4 q \\ \text{Yaw Control Surface Demand} = c_3 \int_{T}^{T+t} r\,dt + c_4 r \end{cases}$$

(k) Size weight and cost to be minimal, consistent with the above

The most important parameters are noted in Fig.3 which also summarises the environmental requirements. It should be noted that many of these parameters have subsequently changed. However the requirements today are very similar overall and no parameter has changed so significantly to alter the basis for the system.

Reviewing these parameters it is clear that roll and pitch range and accuracy are critical particularly when coupled with the alignment problems briefly reviewed in 1.2.

Before describing the mechanisation of the chosen system in more detail it is necessary to very briefly discuss some of the alternates that were discussed at the time.

The competing sensor and computational approaches are summarised in Fig.4.

As this lecture is only incidentally historic, only a brief review of the pros and cons of each is necessary.

Both the Two Degree of Freedom gyros and platform solutions necessitate the generation of the required body rate data by differentiation of gimbal angle outputs with consequent noise problems. The available Two Degree of Freedom gyros had adequate drift performance or activation time but not both. Available platforms had slow erection time and inadequate shock performance. These considerations apply today in that the rate gyro/accelerometer solution is the cost effective one.

The computing story has of course changed. Whereas the 1967 decision was marginally in favour of analogue, electronic computing with a digital mechanisation a close second and mechanical analogue a poor third, the digital approach is now obviously superior in many cases and in fact the project implementation of the ASU was redesigned to incorporate a digital computing mechanisation in 1971.

4. SYSTEMS MECHANISATION OF THE ATTITUDE SENSING UNIT (ASU)

A block diagram of the ASU is shown in Fig.5.

In essence the three rate gyro outputs p, q & r are resolved into Euler axes and integrated to provide Euler angles ϕg and θg. These Euler Angles are updated by filtered, resolved, accelerometer outputs monitoring the gravity vector.

A fluxgate system consisting of three orthogonal fluxgates and magnetic compensation circuitry provides the azimuth reference.

The nature of torpedo dynamics allow a number of valid approximations to the acceleration equations that enable a good estimate of gravity vector direction with a filter time constant of ten seconds or so.

The Euler Rate Unit is a mechanisation of the following Euler Transformation,

$$\begin{bmatrix} \dot{\phi}_g \\ \theta_g \\ \dot{\psi}_g \end{bmatrix} = \begin{bmatrix} 1 & \tan\theta_m \sin\phi_m & \tan\theta_m \cos\phi_m \\ 0 & \cos\phi_m & -\sin\phi_m \\ 0 & \sec\theta_m \sin\phi_m & \sec\theta_m \cos\phi_m \end{bmatrix} \begin{bmatrix} p_m \\ q_m \\ r_m \end{bmatrix} \qquad -1$$

The suffix g indicates gyro derived information and the suffix m, measured data.

The updating unit mechanises a set of equations such as,

$$\phi_m = \frac{s\dot{\phi}_g + (k_1 s + k_1 k_2)\phi_a}{s^2 + k_1 s + k_1 k_2} \qquad -2$$

$$\theta_m = \frac{s\theta_g + (k_3 s + k_3 k_4)\theta_a}{s^2 + k_3 s + k_3 k_4} \qquad -3$$

This particular form of updating or mixing is termed second order and it is important to have a physical understanding of it. This may be obtained from a brief look at a block diagram implementation of the equations shown in Fig.6.

$$\phi_m = \frac{\dot{\phi}_g}{s} + \frac{k_1}{s}(\phi_a - \phi_m) + \frac{k_1 k_2}{s^2}(\phi_a - \phi_m)$$

Collecting terms multiply through by s^2

$$\phi_m = \frac{s\dot{\phi}_g + k_1 s\phi_a + k_1 k_2 \phi_a}{s^2 + k_1 s + k_1 k_2} \qquad -2$$

In effect the integrator (k_2) stores the null offset error in $\dot{\phi}_g$.

$\frac{}{(s)}$

54

4.1 Gravity Angle Unit

If α_x α_y and α_z are the outputs of accelerometers mounted along the x,y and z axis respectively then the accelerometer outputs are,

$$\alpha_x = u + qw - vr + a_x(-q^2 - r^2) + a_y(-r + pq) + a_z(q + pr) + g \sin\theta \quad -4$$

$$\alpha_y = v - pw + ur + a_x(r + qp) + a_y(-p^2 - r^2) + a_z(-p + qr) - g \sin\phi \cos\theta \quad -5$$

$$\alpha_z = w + pv - qu + a_x(-q + rp) + a_y(p + rq) + a_z(-p^2 - q^2) - g \cos\theta \cos\phi \quad -6$$

the gravity terms g sin θ and -g sin φ cos θ are the terms required, all the others, in this instance, are contamination. The α_z equation is not utilised in many applications.

The fourth, fifth and six terms, all depending on sensor displacement from the CG, and all determinate if p, q and r and their first differentials are available.

The first three terms require knowledge of vehicle velocity. This could be obtained inertially or hydrodynamically. In either case the cost of an ASU would rise considerably.

v and w remain at or near zero except during major manoeuvres, hence much of the effect of these terms may be removed by low pass filtering. In addition u may be satisfactorily approximated by a law using propulsor rpm as the only variable.

To summarise -

(a) Resolved and integrated gyro outputs provide the 'short term' inertial reference. 'Short term' could be less than ten seconds (for straightforward spring restrained rate gyros) to a 100 seconds or so for rugged high torquer capability rate integrating gyros. In fact the azimuth output may be left unmixed to represent the free drift output of the yaw gyro plus contamination due to errors in the measurement of the vertical, though this is only realistic for a vehicle that runs "straight and level" for a considerable portion of the mission.

(b) The filtered output from accelerometers provide the long term vehicle reference. The filtering may be augmented by compensation for various non-gravity acceleration. The need for and success of these compensations will depend on the quality of the gyroscopes fitted and the characteristics of the dynamics of the vehicle.

4.2 Fluxgate Elements and Azimuth Angle Unit

So far we have made no detailed reference to the azimuth system. The fluxgate system comprises three orthogonal gates mounted along axes parallel to the principal axes of the vehicle.

The fluxgates are a standard type consisting of primary and secondary coils wound on a pair of soft iron cores. The primary is excited by an audio sinusoidal frequency current of sufficient amplitude to drive the cores into saturation at the current peaks. The secondary, wound differentially about the two cores picks up the second harmonic content caused by the change in inductance at saturation. This output is approximately proportional to field strength for applied static fields less than the saturation field for the cores. To improve the linearity of output the fluxgates are utilised in a feedback mode. The secondary output is demodulated and fed back to the primary so that the net field in the cores is zero and the d.c. current in the primary a measure of the impressed field.

Of course such devices measure any low frequency field, not just the component of earth magnetic field along the axis of a particular gate.

The fluxgate outputs are therefore compensated for the 'hard' iron and soft iron effects caused by the torpedo.

If the free geomagnetic field along the torpedo axes ($f_x f_y f_z$) and the fluxgates measure the actual field at their location ($g_x g_y g_z$) then,

$$\begin{pmatrix} g_x \\ g_y \\ g_z \end{pmatrix} = (S) \begin{pmatrix} f_x \\ f_y \\ f_z \end{pmatrix} + \begin{bmatrix} h \end{bmatrix} \quad -7$$

Where (S) is a matrix of coefficients varying with field distortion (the soft iron effects) h is a superimposed magnetic field fixed relative to the torpedo axes.

The earth field may be represented by Horizontal and Vertical components H and Z so that,

$$\begin{pmatrix} f_x \\ f_y \\ f_z \end{pmatrix} = \begin{pmatrix} \cos\theta & 0 & -\sin\theta \\ \sin\theta \sin\phi & \cos\phi & \cos\theta \sin\phi \\ \sin\theta \cos\phi & -\sin\phi & \cos\theta \cos\phi \end{pmatrix} \begin{pmatrix} H\cos\psi \\ -H\sin\psi \\ Z \end{pmatrix} \quad -8$$

Let the matrix of equation 8 be A, then,

$$[g] = (S)\ (A)\ \begin{pmatrix} H\cos\psi \\ \\ -H\sin\psi \\ \\ Z \end{pmatrix} + [h]$$

$$(A)\ \begin{pmatrix} H\cos\psi \\ \\ -H\sin\psi \end{pmatrix} = [S]^{-1}[(g)-(h)] \qquad -9$$

so that if the soft iron characteristics (S) and the hard iron characteristics (h) are stored in the ASU before the mission, the LHS of equation can be determined.

The RHS of equation appears fairly complex. In fact, if it can be assumed that roll angle is controlled to zero, which is normally the case for torpedoes as was explained in the introduction, a straight forward computation for azimuth demand is available.

If the desired magnetic heading is ψ_d and $\phi = 0$ then,

$$\begin{pmatrix} f_x \\ \\ f_y \\ \\ f_z \end{pmatrix} = (A) \begin{pmatrix} H\cos\psi \\ \\ -H\sin\psi \end{pmatrix} = \begin{pmatrix} \cos\theta & 0 & -\sin\theta \\ \\ 0 & 1 & 0 \\ \\ \sin\theta & 0 & \cos\theta \end{pmatrix} \begin{pmatrix} H\cos\psi \\ \\ -H\sin\psi \\ \\ Z \end{pmatrix}$$

and $H\sin(\psi - \psi_d) = H\sin\psi\cos\psi_d - H\cos\psi\sin\psi_d$

So that $\sin(\psi - \psi_d) = \frac{-1}{H}\left[(f_x\cos\theta + f_z\sin\theta)\sin\psi_d + f_y\cos\psi_d\right]$ -10

5. REVIEW OF ATTITUDE SENSING UNIT HARDWARE

The ASU hardware has been through three major phases,

(a) A prototype analogue system that was subjected to extensive ground trials and elementary underwater trials.

(b) A project orientated analogue system that was converted mid-programme into,

(c) A largely digitally mechanised system that has undergone some tens of underwater trials.

It is not appropriate to belabour the original analogue mechanisation of the ASU, nonetheless it may be pertinent to remind the audience that elegant analogue computing solutions to some problems are available and can still compete with digital approaches.

An appropriate example is the mechanisation of sine and cosine generation.

Two mechanisations were developed, a Limited Angle Sine Cosine Generator and an Integrating Sine Cosine Generator, Fig.7 and Fig.8 respectively.

The limited angle unit used in the pitch channel of the analogue ASU is configured around the precision waveform generator producing sin wt and cos wt waveforms at 2K Hz.

These waveforms are required for gyro and fluxgate drive in addition to the LA SG function.

A pitch angle input appropriately scaled is pulse width modulated and chops the sin and cosine waveforms. The smoothed output from the gates is sin and cos

for instance, $\int_{-\theta}^{\theta} A\cos wt\,dt = \frac{2A}{w}\sin w\theta$

and the average of this output after low pass filtering is $\frac{A}{2}\sin\theta$

The integrating sine cosine generator is rather more elegant.

Ignoring for a moment the dashed single paths, the loop generating z sin and z cos is almost self explanatory.

The single paths in red form an amplitude control.

The error term,

$$= k\left[a^2 - z^2(\sin^2\phi + \cos^2\phi)\right]$$

5.6

is used to modulate feedback around the integrators to maintain the scaling factor z equal to the desired value a.

The circuitry associated with these two block diagrams was developed to the requisite accuracy using late 1960s generation linear integrated circuits.

With currently available component technology, these circuits can be more accurate, cheaper and significantly smaller. In small vehicles attitude controls systems using these techniques may well remain competitive with digital mechanisations for some time in the future.

5.1 Digital Implementation of Attitude Functions

The attitude sensing unit was redesigned in a digital implementation, not because of inherent weakness in the analogue approach or because of any major cost or size benefit from digitisation. The provision of pre-programming and logic units associated with mission profiles etc., within the project vehicle has resulted in the incorporation of a special purpose, general purpose organised minicomputer. Investigations showed that this machine could be modified to include the attitude sensing functions for a fairly small penalty.

Initial examinations of the digitisation of the attitude control functions were carried out in the context of a 12 bit data, 12 bit address serial machine with an add time of 7μS and resulted in the following estimates.

	Time for 1 iteration
Inner loop functions 100 samples/sec	5.9ms
Mode Control etc. 10 samples/sec	1.7ms

Core Storage 650 words Programme

250 words Data

The attitude functions hence absorbed approximately 61% of the available cycle time. Subsequent refinement of programme structure and consolidation of the attitude functions with other computer functions reduced the overhead due to the attitude functions very considerably, so that the store locations required were reduced to 410 whilst the occupancy was down to 15% or so in a faster 5 ms add time machine.

The simulation of the digitally mechanised attitude functions revealed few problems even though the original Euler transformation approach was used which is not very efficient in a digital implementation. Subsequently changes in vehicle dynamics did highlight some problems in the roll loop, and further shaping of control laws was required.

As an insurance against quantization and aliasing problems, a four parameter Euler implementation was also simulated and shown to save storage and reduce occupancy. It was not proceeded with further as no practical problems were found with the conventional Euler Approach.

5.2 Sensors

There are two basic determinates for the accuracy of the attitude sensing function whether the computing is digital or analogue. They are the accuracy of the sensors, and the adequacy of accelerometer compensation and the impact of these is inter-related.

In this section we will restrict ourselves to sensor accuracy.

As has been explained, the original implementation of the strapdown attitude sensing unit was for an air launched weapon, and a fluxgate 'compass' was employed in the azimuth axis.

While the accuracy requirements for the rate gyros were not severe, the environmental requirements were.

A rugged, fluid damped, spring restrained rate gyro of the following performance was appropriate:

Full scale rate	± 80°/sec
Null over the temp range	± 0.25% FS
Hysteresis	0.1% FS
Scale Factor	± ½% FS (otr)

In fact simulation indicated that some relaxation in these parameters was possible but dependent on likely vehicle trajectories.

The accelerometer performance is, in some ways, more critical as long term attitude accuracy is directly related to accelerometer errors.

If we consider the ∝y accelerometer, which was scaled to ± 3g because of the considerable centripetal accelerations experienced, then ±¼° error is equivalent to an error of ± 0.15% FS and this error should not be exceeded at the normal search turn rates of the vehicle approaching 1.0g.

Of course the gyro and accelerometer parameters quoted are exceeded by many orders in strapdown navigation systems. Nonetheless the achievement of say the 10°/hr gyro drift rate and 50μg accelerometer performance which could be required for the most accurate implementations of the ASU remains difficult when the reaction time and environment are considered.

5-1

5.3 Initial Trials of the A.S.U.

The initial trials of the ASU were performed in a van. A 'brass board' ASU was tested against an Elliott E3 inertial platform in a van. These trials proved that:

(a) The ASU functioned correctly and was accurate to within $\pm i^{\circ}$ of the accuracy estimated from a mathematical model.

(b) Some fairly hair-raising manoeuvres can be carried out in a van.

Subsequently an ASU was run in an underwater test vehicle in the English Channel mainly to evaluate the performance of the fluxgates in an electrically propelled vehicle. Again the trials were successful although the bang-bang limit cycle operation of the roll control system in this test vehicle produced some unexpected effects. These effects were subsequently established as being due to the approximations in the ASU computing.

The digital implementation of the ASU has now completed thirty or so trial runs which have explored most of its "flight envelope". No problems directly associated with the ASU function have been discovered, although electrical noise levels in the test vehicles have been higher than expected and work is proceeding to reduce these.

6. FURTHER DEVELOPMENT OF THE STRAPDOWN ATTITUDE SENSOR

A development of the ASU is currently undergoing development model trials.

The major new systems requirement for this development was an azimuth performance in the 2°/h class free drift with no updating available after launch from the mother vehicle.

The vertical performance accuracy was fairly trivial by comparison so that the azimuth performance was the driving requirement.

It was obvious that a digital mechanisation was appropriate from the start, and that the performance of the azimuth gyro was critical.

The approach taken to the sensor problem was to use a rate integrating gyroscope, such as the Northrop GI-G6 and provide temperature control before launch to obtain near optimum drift performance. Currently testing of both ball bearing and gas bearing wheel gyros in the azimuth axis is proceeding.

6.1 System Design

There are three areas in which significant improvement has been made in systems design aspects.

(a) Improved manipulation of attitude and mixing algorithms

(b) Statistical sensor filtering

(c) Improved sensors

It is appropriate to review (a) and (b) in a little detail.

The Euler symmetrical parameter approach was chosen and applied in the way set out below. The System Block Diagram is at Fig.9.

6.2 Attitude Algorithm

The attitude of the torpedo with respect of Earth co-ordinates may be represented in several ways, the Euler Symmetrical (or Cayley-Klein parameters) is the method chosen for this application.

The principle of Symmetrical Parameters is that one single rotation about a suitable position axis will result in coincidence of a moving axes set xo yo zo with axes x y z whose orientation it is desired to specify.

Let $e_0 = \cos \mu/2$

$e_1 = \alpha \sin \mu/2$

$e_2 = \beta \sin \mu/2$

$e_3 = \gamma \sin \mu/2$

Then (e_0, e_1, e_2, e_3) can be used to specify the attitude (x, y, z) with respect to (ox, yo, zo).

The rate matrix form is as follows:

30

$$\frac{d}{dt}\begin{vmatrix} e_0 \\ e_1 \\ e_2 \\ e_3 \end{vmatrix} = \frac{1}{2}\begin{vmatrix} -e_1 & -e_2 & -e_3 \\ e_0 & -e_3 & e_2 \\ e_3 & e_0 & -e_1 \\ -e_2 & e_1 & e_0 \end{vmatrix}\begin{vmatrix} p \\ q \\ r \end{vmatrix} \qquad -11$$

Because four parameters are being used to describe orientation when only three are necessary, a constraint equation exists of the form:

$$e_0^2 + e_1^2 + e_2^2 + e_3^2 = 1 \qquad -12$$

6.3 Deriving Symmetrical Parameters

Suppose a vector is x^e in Earth's co-ordinates (North, East, Down) and x^v in vehicle co-ordinates (yaw, pitch, roll).

Then $x^e = A_{ev}x^v$ or $x^v = A_{ve}x^e$ where A_{ev} is the earth-to-vehicle transformation matrix.

$$A_{ev}^{-1} = A_{evt} = A_{ve} = A_{vet}^{-1} \quad \text{(where } M_t \text{ is the transpose of M)}. \qquad -13$$

In particular if unit vectors pointing North, East, Down are respectively U_N, U_E and U_D then :

$$U_N^e = \begin{bmatrix} 1 \\ 0 \\ 0 \end{bmatrix} \quad U_E^e = \begin{bmatrix} 0 \\ 1 \\ 0 \end{bmatrix} \quad U_D^e = \begin{bmatrix} 0 \\ 0 \\ 1 \end{bmatrix} \qquad -14$$

$$A_{ve} = A_{ve}U = A_{ve}\begin{bmatrix} 1 & 0 & 0 \\ 0 & 1 & 0 \\ 0 & 0 & 1 \end{bmatrix}$$

$$= A_{ve}\begin{bmatrix} U_N^e & U_E^e & U_D^e \end{bmatrix} \qquad -15$$

$$= \begin{bmatrix} U_N^v & U_E^v & U_D^v \end{bmatrix} \qquad -16$$

If the vehicle has angular velocity $W = [p, q, r]$ measured in body axes, then U_N^v has an angular velocity $-W$ with respect to the torpedo, so that

$$\dot{U}_N = -W \times U_N^v$$

$$= -\begin{bmatrix} 0 & -r & q \\ r & 0 & -p \\ -q & p & 0 \end{bmatrix} U_N^v \qquad -17$$

(Where $\times$ denotes the cross product and $\dot{x} = \frac{dx}{dt}$)

Similarly $U_E = WXU_E^V$ and $U_D = WXU_D^V$ so that

$$\frac{d}{dt}\begin{bmatrix} U_N^V & U_E^V & U_D^V \end{bmatrix} = -\begin{bmatrix} 0 & -r & q \\ r & 0 & -p \\ -q & p & 0 \end{bmatrix}\begin{bmatrix} U_N^V & U_E^V & U_D^V \end{bmatrix}$$

$$\frac{d}{dt} A = -\begin{bmatrix} 0 & -r & q \\ r & 0 & -p \\ -q & p & 0 \end{bmatrix} A \qquad -18$$

which may be written - W X A

Therefore $\frac{dA}{dt} + W \times A = 0$ -19

Values of p q and r are available to allow solution of the above equation given initial values of A.

It can be shown that equation 11 may be re-arranged into the following form:

$$\frac{dq}{dt} = \Omega q \qquad -20$$

where $\Omega = \frac{1}{2}\begin{bmatrix} 0 & -p & -q & -r \\ p & 0 & r & -q \\ q & -r & 0 & p \\ r & q & -p & 0 \end{bmatrix}$ -21

If w, and thus Ω may be considered constant between times t - T and t where T is small then an approximate solution to the differential equation is:

$$q(t) = q(t-T) + \Omega T q(t-T) \qquad -22$$
$$= (U + \Omega T)\, q(t-T)$$

A better approximation is:

$$q(t) = \exp(\Omega T)\, q(t-T)$$

$$\exp(\Omega T) = U + \Omega T + \frac{\Omega^2 T^2}{2!} + \frac{\Omega^3 T^3}{3!} \ldots\ldots \text{ etc}$$

now $\Omega^2 = \frac{1}{4}\begin{bmatrix} -p^2 & -q^2 & -r^2 & 0 & 0 & 0 \\ 0 & -p^2 & -q^2 & -r^2 & 0 & 0 \\ 0 & 0 & -p^2 & -q^2 & -r^2 & 0 \\ 0 & 0 & 0 & -p^2 & -q^2 & -r^2 \end{bmatrix}$

$$= -\left(\frac{p^2 + q^2 + r^2}{4}\right) U$$

$$= -\frac{|w|^2}{4} U$$

$$= -\frac{1}{4} w_t^2 U$$

5-10

$$\text{so exp } (\Omega T) = U + T\Omega - \frac{T^2}{2!}\left[\frac{|W|}{2}\right]^2 U - \frac{T^3}{3!}\left[\frac{|W|}{2}\right]^2 + \frac{T^4}{4!}\left[\frac{|W|}{2}\right]^4 U \ldots$$

$$= \left[1 - \frac{1}{2!}\left[\frac{|W|T}{2}\right]^2 + \frac{1}{4!}\left[\frac{|W|T}{2}\right]^4 - \ldots\ldots\right]U$$

$$+ \Omega\left[T - \frac{T}{3!}\frac{|W|T^2}{2} + \frac{T}{5!}\frac{U\,|W|T^4}{2} - \ldots\ldots\right]$$

$$= \cos\frac{|W|T\,U}{2} + \frac{2}{|W|}\sin\frac{|W|\,T\,\Omega}{2} \qquad -23$$

and thus:

$$e(t) = \cos\frac{|W|T}{2}\,e(t-T) + \frac{2}{W}\sin\frac{|W|\,T\,\Omega}{2}\,e(t-T)$$

$$= \begin{bmatrix} e_0 \\ e_1 \\ e_2 \\ e_3 \end{bmatrix}_{t-T} \cos\frac{|W|\,T}{2} + \begin{bmatrix} -pe_1 & -qe_2 & -re_3 \\ pe_0 & +re_2 & -qe_3 \\ qe_0 & -re_1 & +pe_3 \\ re_0 & +qe_1 & -pe_2 \end{bmatrix}_{t-T} \frac{\sin\frac{|W|\,T}{2}}{|W|} \qquad -24$$

It is worth noting that equation 24 will yield equation 21 if only the first term of equation 23 is used. Equation 24 will be implemented within the ASU to maintain the required heading accuracy. More powerful solutions/approximations such as a fourth order Rung have been considered but the accuracy gained in the Algorithm translation by the slower iteration response T is not considered worth while in this particular application.

6.4 Long Term Monitoring

Mixing a filtered accelerometer information to offset drifts and non-linearities in rate gyroscopes was again chosen as the long term monitoring mechanisation using the approach outlined below and illustrated in Fig.10.

$$x_e(t) = D^{-1}\left[\dot{x}_s(t) + G\left[x_1(t) - x_e(t)\right]\right]$$

$$\text{Where } D = \frac{d}{dt},\ D^{-1} = \int_0^t (\,)dt,\ G = \tau^{-1}$$

τ is the mixing time constant.

$x_1(t)$ is the estimate of x (t) from the long term (monitoring) sensor (accelerometer) $x_e(t)$ is the "best" estimate of x(t), $x_s(t)$ is the estimate of x (t) from the short term sensor (rate gyro)

$$x_e(t) = \frac{D^{-1}\,\dot{x}_s(t) + GD^{-1}\,x_1(t)}{1 + GD^{-1}}$$

$$= \frac{G^{-1}D}{1+G^{-1}D}\,x_s(t) + \frac{1}{1+G^{-1}D}\,x_1(t)$$

$$= \frac{D}{1+\tau D}\,x_s(t) + \frac{1}{1+\tau D}\,x_1(t) \qquad -25$$

The mixing time constant τ should be greater than any acceleration transients, control loop or external disturbances but obviously not so long as to make drift errors significant. The dominant factor is wave motion near the surface and a time constant of about 30 seconds will be appropriate.

The operator - functions $\frac{\tau D}{1 + \tau D}$ and $\frac{1}{1 + \tau D}$ are known as "Wash out" and "Lag" respectively.

5-11

If both x_s and x_1 are perfect (ie = x) then the system estimate

$$x_e t = \frac{\tau D}{1 + \tau D} x_s(t) + \frac{1}{1 + \tau D} x_1(t) = x(t)$$

6.5 Constraint Equation

When equation 18 is used to integrate equation 22 computational errors will tend to accumulate, due to such limitations as word length, so that

$$e_0^2 + e_1^2 + e_2^2 + e_3^2 = |e| \neq 1$$

This error is corrected by dividing e by $|e|$ at a sub-multiple of the iteration frequency fs.

$$e_n = e/|e| = e \Big/ \sqrt{e_0^2 + e_1^2 + e_2^2 + e_3^2}$$

$$= e \Big/ \sqrt{(1 - (1 - \sum_{i=0}^{1=3} e_i^2))}$$

$$= \left[1 + K (1 - \sum e_i^2)\right] e \qquad -26$$

Where K is selected on the basis of trials and is approximately $\frac{1}{2}$.

The overall mechanisation of the software system is shown in Fig.9. It should be noted that an independent measure of vehicle forward velocity U is again required in the accelerometer correction equations.

The object of this section was to provide an overview of the mechanisation of a modern application of strapdown to the attitude control of a vehicle and to show that the mechanisation can be relatively simple in certain restricted cases.

The 'bottom up' gravity monitored approach to strapdown vehicle attitude control is a valuable approach to system mechanisation and in a limited number of cases a simpler alternative to a full Schuler Tuned Inertial System.

7. AIRCRAFT STRAPDOWN SYSTEMS

Over the last four or five years a considerable amount of effort has been expended in the UK on the development of strapdown techniques for aircraft attitude sensing and navigation.

One programme has continued during this period at Marconi-Elliott, its beginnings based on the torpedo attitude sensor work described earlier and the Company's 20 years of experience with platform IN systems.

This programme has now divided into two development activities, one directed at the development of a gyro suitable for Strapdown Navigation and the other the flight trials of a strapdown attitude reference using conventional pulsed torqued floated gyros.

These flight trials are aimed at verification of the algorithms that have been developed by Marconi-Elliott and to this end the algorithms are being modified during the trials so that comparative performance may be evaluated.

It is only possible to provide a very brief description of the systems approach taken in this trials equipment, so that the experimental results shown later can be placed in context.

The gyros selected are in the 0.2°/hr random drift class and the design aim performance of the attitude and heading reference system is,

1 σ level accuracy 10 mins.

1 σ free heading drift 2°/hr.

7.1 Schuler Tuning

An air data velocity source is used to minimise gyro drift effects. The velocity mixing filter is third order, though it approximates to a second order system with a time content roughly an order smaller than the Schuler period.

7.2 Attitude Update Algorithm

The Four Parameter Euler approach is used with an update algorithm of the fourth order Rung type.

viz. $\bar{e}_{n+1} = \bar{e}_n + \frac{1}{6} (\bar{m}_1 + 2\bar{m}_2 + 2\bar{m}_3 + \bar{m}4)$

where $\bar{m}_1 = \frac{1}{2} \Omega_1 \bar{e}_n t$

$\bar{m}_2 = \frac{1}{2} \Omega_2 (\bar{e}_n + \bar{m}_1/2) t$

$\bar{m}_3 = \frac{1}{2} \Omega_2 (\bar{e}_n + \bar{m}_{2/2}) t$

$\bar{m}_4 = \frac{1}{2} \Omega_3 (\bar{e}_n + \bar{m}_3) t$

$\bar{e}_n$ is the 'e' vector at time n

$\bar{e}_1$ is the 'e' vector at time n + 1

Ω, Ω_2 are the rate matrix Ω at successive iteration intervals.

7.3 Conclusion

An objective of this paper was to show that there is a range of practical applications of strapdown in which cost and performance vary over two orders of magnitude or more. The emphasis in the paper has been on the lower end of this range where it has been shown that for certain classes of vehicle strapdown attitude sensing was the cost effective approach a decade ago.

This cost advantage has increased over the years.

Though many strapdown systems are mechanised using digital computing experience from a decade ago, coupled with recent advances in linear integrated circuits, it shows that for the simpler vehicles, attitude sensing using analogue computing may well be economic and bear serious consideration. The majority of angular rate and acceleration sensors that are available and suitable for small vehicle applications have an analogue output, most actuation systems demand an analogue input. Though this situation is changing and is continuing to change, analogue sensors may hold sway for many applications for some time to come.

Finally I would like to thank colleagues within Marconi-Elliott Avionics and at the Admiralty Underwater Weapon Establishment, Portland Dorset, also Marconi Space and Defence Systems, Stanmore Middlesex for their valued contributions to this paper.

- RUGGEDNESS
- PRACTICALITY OF SYSTEM ALIGNMENT AFTER LAUNCH
- CONTINUOUS UPDATING POSSIBLE
- RAPID RUN UP
- TOPPLE FREE OR SELF RIGHTING AFTER TOPPLE (DEPENDS ON COMPUTING IMPLEMENTATION)
- GOOD ACCURACY : COST RATIO

Fig.1 Benefits of Strapdown for Underwater Weapons Applications when Compared with Gimballed Approach

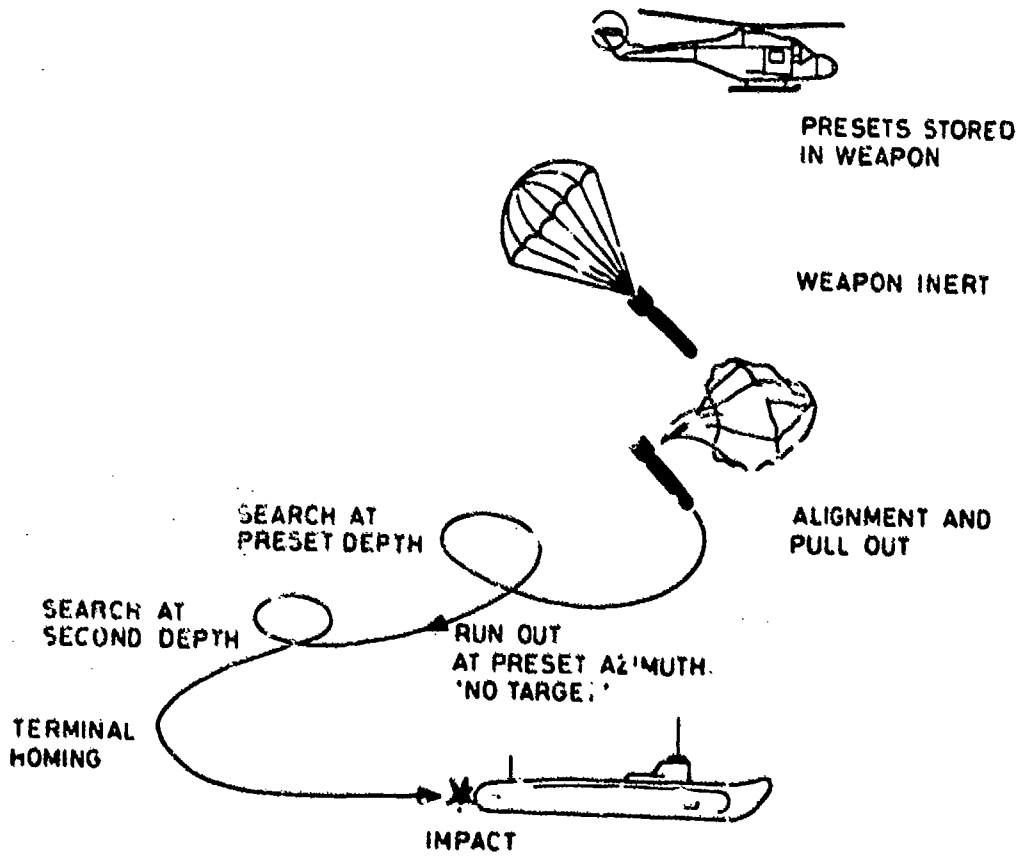

Fig.2 Possible Weapon Trajectory

5·14

PARAMETER	RANGE	ACCURACY
ϕ	±90°	±1°
θ	+85°	±1° ($-45° \leq \theta \leq 45°$)
ψ	360°	±5°
$\dot{\phi}$	±100°/SEC	±5%
$\dot{\psi}$		±5%

ENVIRONMENTAL REQUIREMENTS:

OPERATIONAL TEMPERATURE RANGE -20°C TO +43°C

SHOCK ± 100g SINUSOIDAL 20mSEC HALF PERIOD

Fig.3 Summary of Requirements for an Attitude Sensor

- SENSING
  - a) TWO 2 DEGREE OF FREEDOM GYROS
  - b) MINIATURE PLATFORM
  - c) RATE GYROS + ACCELEROMETERS
- COMPUTING
  - a) ANALOGUE ELECTRONIC
  - b) ANALOGUE ELECTRO-MECHANICAL
  - c) DIGITAL

Fig.4 Alternate Approaches to the Underwater Weapon Attitude Sensor Requirements

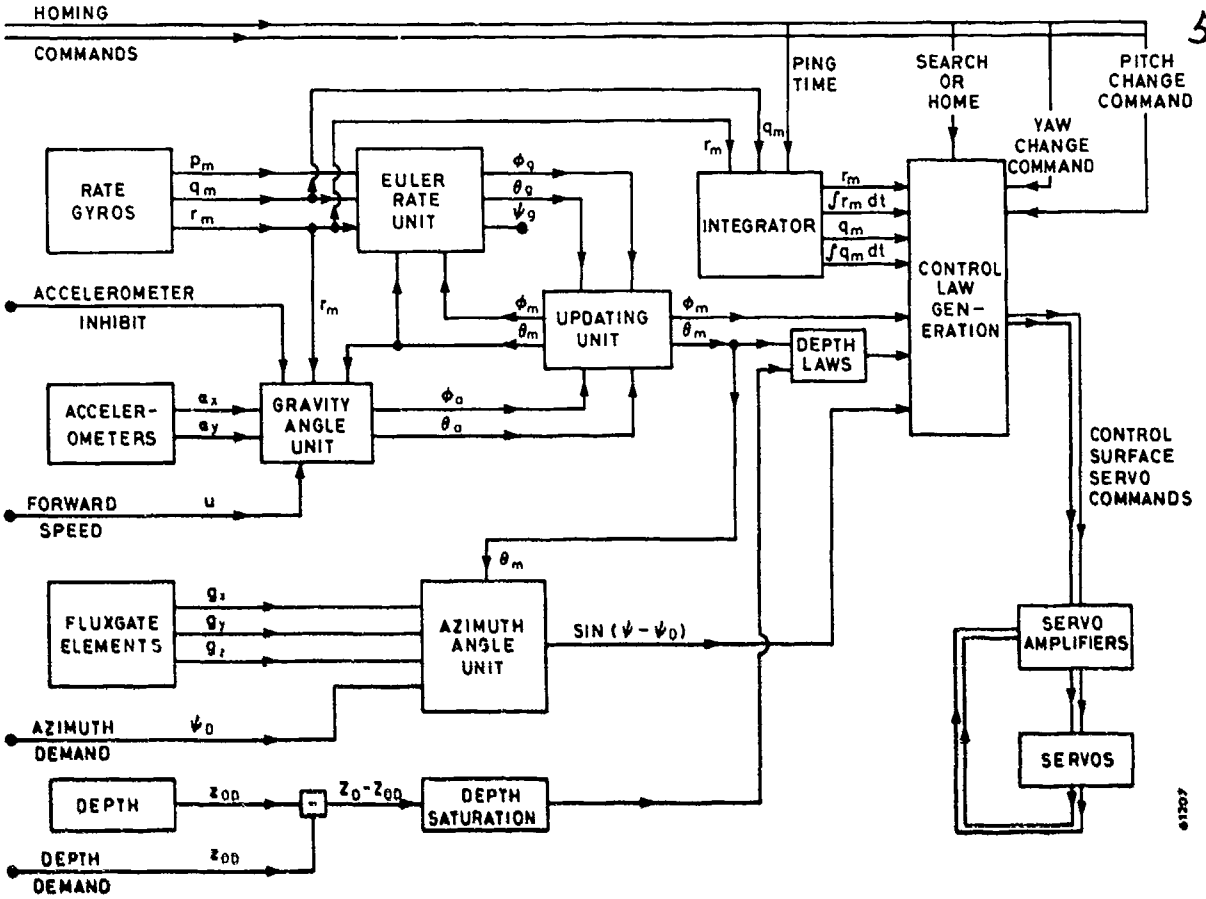

Fig.5 Block Diagram of Attitude Sensor

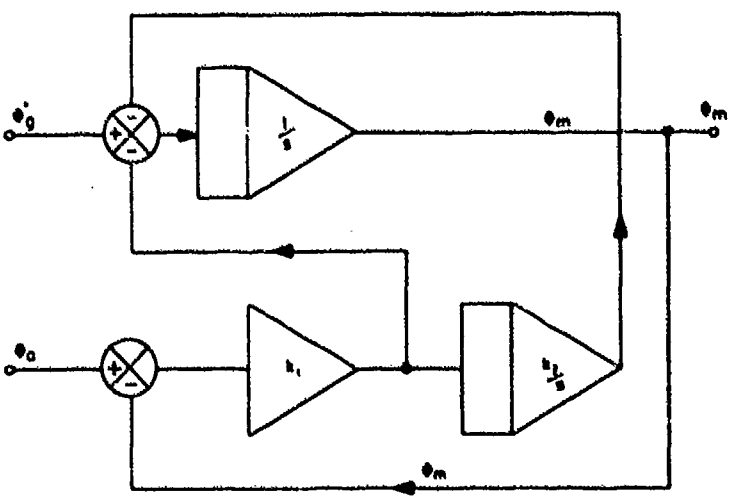

$$\phi_m = \frac{s\phi_g + k_1 s\phi_a + k_1 k_2 \phi_a}{s^2 + k_1 s + k_1 k_2}$$

5-14

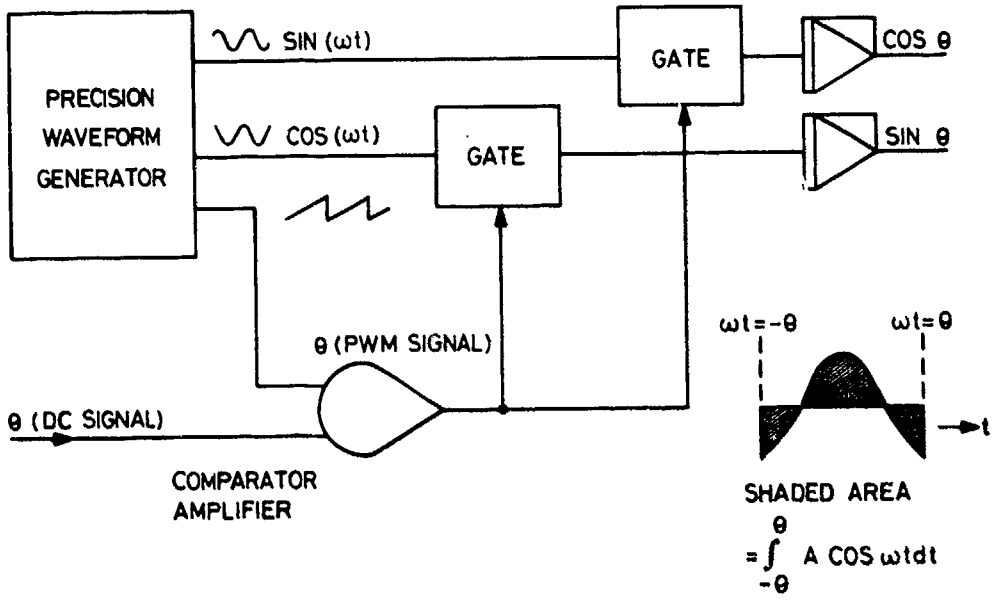

Fig.7 Limited Angle Sin Cos Generator

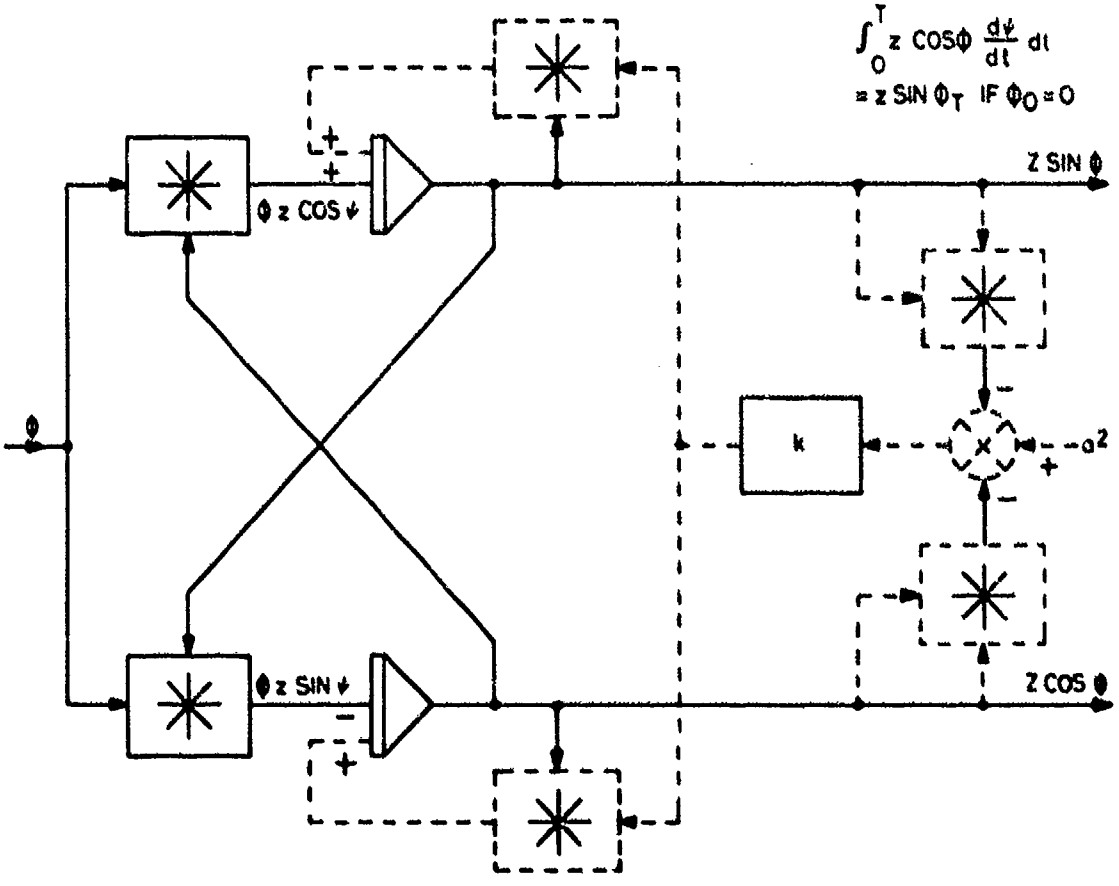

Fig.8 Integrating Sin Cos Generator

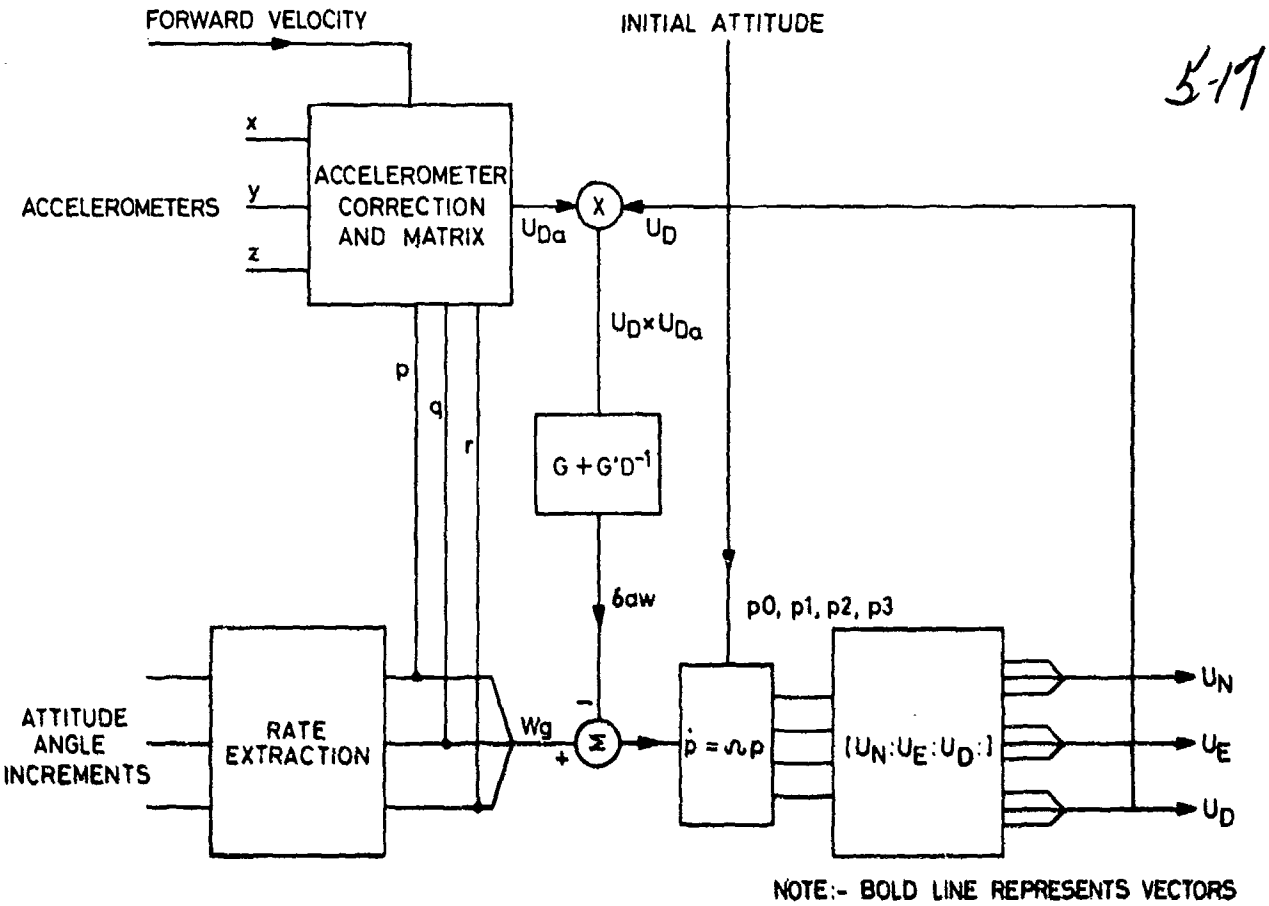

Fig.9 System Block Diagram

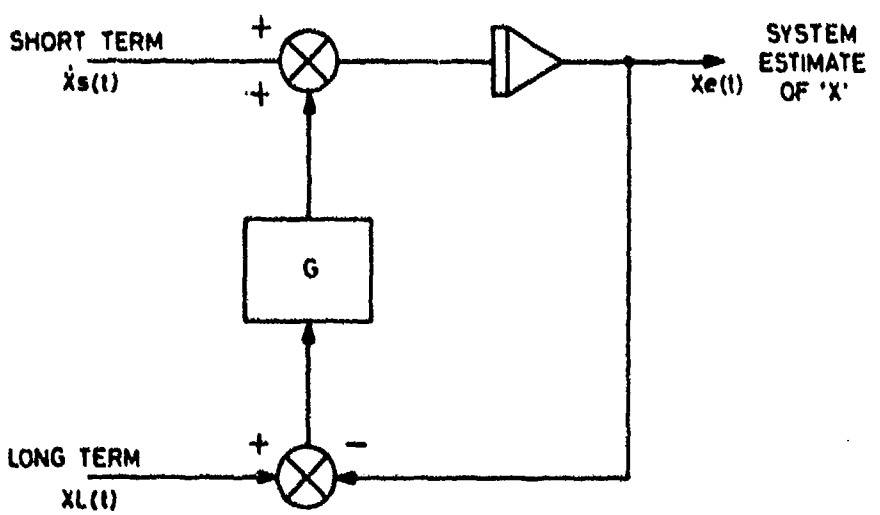

LASER-GYRO STRAPDOWN INERTIAL SYSTEM APPLICATIONS

6-1

DR. EMANUEL LEVINSON
SPERRY GYROSCOPE DIV., SPERRY RAND CORP.
GREAT NECK, L.I., N.Y. 11020

SUMMARY

Laser-gyro strapdown inertial systems are now available that can satisfy a broad range of aerospace and marine applications. This paper describes three widely different applications:

1. Tactical Air-To-Surface Missile Midcourse Guidance
2. Shipboard Fire Control Attitude Reference
3. Aircraft Inertial Navigator

Mission requirements, system configuration, alignment techniques, and existing hardware and software are delineated for each application. Error analysis, simulation, and test data are presented which clearly demonstrate the capability of the laser-gyro strapdown system to meet the specific application requirements.

1. INTRODUCTION

Laser gyro strapdown inertial systems are beginning to be used in a broad range of aerospace and marine applications. This paper focuses on three of these applications:

(1) Tactical Air-To-Surface Missile Midcourse Guidance

(2) Shipboard Fire Control Attitude Reference

(3) Aircraft Inertial Navigator

These particular applications were selected because of their advanced state of development, their wide disparity in component performance requirements, and their encompassing general interest. The tactical Air-To-Surface Missile midcourse guidance system has been successfully flight-tested at Holloman Air Force Base. Engineering development models have been designed and fabricated for the Shipboard Fire Control System (U.S. Navy MK 16 Stable Element) attitude reference, which is likely to be the first operational use of a laser gyro system. A prototype aircraft inertial navigator has also been successfully flight tested at Holloman. This self-align 1 nm/h navigator requires an order-of-magnitude better laser gyro performance compared to the other applications.

The following topics are covered for each application:

(1) Typical Mission Profile

(2) Mission Requirements

(3) System Functional Block Diagram

(4) System Operating Modes - Alignment Technique

(5) Specific System Synthesis - Hardware Description and Strapdown Software Description

(6) System Performance Analysis and Error Propagation Relationships - Inertial Component Error Models

(7) Test and/or Simulation Results

There are certain common elements associated with each application. These are treated primarily in the first application in which they arise. Subsequent applications refer back to the earlier discussions.

Noteworthy concepts and contributions and critical parameter areas for each application are pointed out.

6.2

2. TACTICAL AIR-TO-SURFACE MISSILE MIDCOURSE GUIDANCE APPLICATION

Ring-laser-gyro strapdown systems are now available in small-size low-cost configurations with performance capabilities suitable for many air-to-surface missile midcourse guidance applications. This fact has been conclusively demonstrated at Holloman Air Force Base by successful flight tests of a tactical missile guidance system developed by U. S. Air Force/Lockheed Missiles and Space Co. using a Sperry SLIC-15 Inertial Measurement Unit[1].

This section describes a typical tactical Air-to-Surface Missile mission application and the key features of the laser-gyro strapdown system that can satisfy mission requirements. Selected Holloman flight test results are presented.

2.1 Typical Mission Profile and Requirements

A typical air-launched tactical missile mission is sketched in Figure 1. The strapdown inertial system must provide suitable "basket" navigation accuracy during missile flight so that the terminal or midcourse fix sensor can capture the target or the scene within the reference-map dimensions. Initial velocity and initial position data are provided by the mother-aircraft master navigation system prior to launch. The availability of this aircraft reference data and the time duration of captive flight enables the missile inertial system to be leveled, aligned, and calibrated en route to the target area utilizing the aircraft reference data. This greatly minimizes the inertial component performance requirements of the missile inertial system.

The missile inertial system also provides pointing and stabilizing data to the fix sensor and body rates, body accelerations, and attitude data for flight control purposes. The missile inertial system could also provide missile altitude information. In applications where this is not accurate enough, a separate altimeter sensor is utilized in conjunction with the inertial system.

For accuracy analysis purposes, a typical guided glide bomb trajectory after launch is depicted in Figure 2. In this case, terminal fixing begins 10 minutes after launch, followed by a terminal maneuver to the target.

Lockheed specifications for the U. S. Air Force Radiometric Area Correlation Guidance flight test program were 3000 feet rms per axis after 10 minutes of inertial flight, following a 15 minute align/calibrate period prior to launch. This was taken to require much tighter position errors at shorter times of flight following launch, for use of a midcourse position fix, and for position build-up between fixes.

Accuracy analyses of typical tactical Air-to-Surface Missile missions have been performed which result in the approximate set of inertial system requirements shown in Table 1. Many missions can be satisfied with lesser requirements. One point worth noting from Table 1 is that azimuth bias drift is nowhere near as important an error contributor as horizontal axis bias drifts. Additional information on tactical missile inertial system requirements can be obtained from References 2 and 3.

TABLE 1

INERTIAL SYSTEM ACCURACY REQUIREMENTS

TO SATISFY MOST TACTICAL AIR-TO-SURFACE MISSILE MISSIONS (1σ)

Laser-Gyros		
Residual bias drift (after in-air align/calibrate)		
Horizontal Axes	0.1	$^{o}/h$
Vertical Axis	1.0	$^{o}/h$
Random White Noise Drift	0.03	$^{o}/\sqrt{h}$
Random Markovian Drift (1 HR correlation Time)	0.1	$^{o}/h$
Scale-Factor Stability	200	**PPM**
Scale-Factor Asymmetry	10	**PPM**
Accelerometers		
Bias Stability	150	μg
Scale-Factor Stability	500	**PPM**
Initial Tilt per Axis	0.4	**MIN**
Initial Azimuth	10	**MIN**
Initial Velocity per Axis	1.5	**ft/s**
Initial Position per Axis	200	**ft**

2.2 System Functional Block Diagram

Figure 3 is a functional block diagram of a strapdown missile guidance system. The strapdown laser gyros and accelerometers with associated electronics provide body angular and velocity increments to a digital microcomputer. The computer performs the functions indicated to yield velocity and position information for navigation and guidance. 6-3

2.3 System Operating Modes - Alignment Techniques

As shown in Figure 1, a typical air-launched tactical missile inertial system will have three basic operating modes:

(1) Ground coarse align and checkout

(2) Married flight fine align

(3) Missile flight navigation

The IMU itself has only one operating mode. The differences in the inertial system modes all take place in the computer via the software program.

2.3.1 Ground Coarse Align and Checkout Mode

Depending on the time available on the ground before takeoff, a coarse leveling, alignment, and gyro bias calibration is performed and a rough checkout of the IMU is accomplished. One approach, used in the Sperry Gyroscope Division laboratory, is as follows. A simple Kalman filter approach, used in the Holloman flight-test program, is described later under in-air align.

The Euler Parameters are first initialized approximately from operator-inserted values of aircraft heading, pitch, and roll angles. They are then updated from integration of gyro-measured body angular increments and corrected (leveled and aligned) by means of the velocity difference and azimuth difference feedback loops shown in Figure 4.

Any tendency of the velocity and azimuth differences to keep building up is assumed to be caused by gyro drifts. The angular correction information is summed over a 3-minute time period, and a least squares filtering (smoothing) is performed to yield a best estimate of the gyro bias drifts over that period. These bias corrections are then inserted as a calibration of the gyro drifts. If more time is available on the ground the bias calibrations will be repeated every 3 minutes until takeoff.

The best available true heading from the aircraft is utilized as the heading reference during this mode. This could be a magnetic flux valve or the aircraft IMU (which is presumably performing its own self-alignment at this time). Including flexure and boresighting errors, the magnetic heading reference should be accurate to better than 2 degrees and the aircraft IMU reference accuracy might approach 30 minutes of arc. Sperry has performed a computer analysis of a ground-align mode similar to this, assuming a 2-degree heading reference with 15-minute of arc white-noise disturbances and SLIC 15 RLG/Q-Flex accelerometer performance. (A Kalman filter was employed in place of the least-squares filter.) The results are depicted in Figure 5. It is observed that after about 3 minutes of time, the inertial system:

(1) Is leveled to about 0.5 minute of arc per axis (strongly balanced against horizontal accelerometer biases)

(2) Is aligned in azimuth to the accuracy of the azimuth reference

(3) Has its equivalent North-axis drift calibrated to about 0.15 degree per hour (determined by white noise random drift smoothing capability in 3 minutes)

(4) Has its equivalent East-axis drift calibrated in balance against the heading offset, according to

$$\epsilon_d = \Omega_E \cos\lambda \quad \delta H$$

The improperly resolved coordinate frame rate (earth rate) is balanced against a bias drift to keep the leveling loops happy. This is about 0.3 degree per hour at 45 degrees Latitude for $\delta H = 2$ degrees

(5) Has its equivalent azimuth drift slowly being calibrated (determined by the white-noise heading-variation smoothing capability in the time available).

The equivalent vertical acceleration bias can also be calibrated on the ground, utilizing the knowledge that vertical velocity equals zero.

6-4

The IMU will also be checked out automatically during this ground period. Malfunction indications can be provided if any of the following exceed a predetermined test tolerance:

(1) Deviation of pitch and roll angle from nominal values

(2) Measured value of one g acceleration

(3) Amplitude of error signals in leveling loops

(4) Amplitude of gyro bias corrections

(5) Various built-in-test equipment (BITE) measurements

(6) Component temperatures

2.3.2 Married Flight Fine Align Mode

When the aircraft is ready for takeoff, the inertial system shifts to an in-air alignment mode. For a least-squares filter approach, this is similar in many respects to the ground-alignment mode (see Figure 4). A sub-optimal Kalman filter approach is described at the end of this subsection.

During married flight, the master navigator in the aircraft is used to provide velocity, position, and heading references in place of the known zero velocities and other information used on the ground. The velocity differences and azimuth difference are utilized in much the same way as in ground align to maintain the inertial system leveled, aligned, and calibrated. Lever-arm corrections are applied to the reference velocities to account for translation velocity differences due to distances between the master navigator and the missile inertial system.

This simple alignment arrangement will work out fairly well for obtaining accurate leveling and accurate calibration of the equivalent North and East gyro bias drifts (East drift again being balanced against heading offset), assuming that there are long enough stretches (several 0.5-minute periods) of approximately straight and level flight. Highly maneuvering situations will be sensed and the alignment loops will be opened up during those times.

Because of flexures and boresight variations between the master navigator in the aircraft and the missile IMU, the azimuth alignment obtained by azimuth matching will probably be no better than 30 minutes of arc, and the calibration of the azimuth gyro drift will probably be no better than 0.5 degree per hour.

Another possible heading alignment technique is an inflight gyrocompassing of the missile IMU. However, the gyro drift performance of a low-cost IMU, even if 0.05 degree per hour, would contribute 17 minutes of arc heading error in such a gyrocompassing operation. Furthermore, any boresight errors between the velocity reference and the IMU come into play if one tries to avoid problems in westerly flight where longitude rate approaches earth rate. These boresight errors are precisely what we are trying to avoid by resorting to an alternative alignment technique.

There is only one known method for achieving an accurate heading alignment without adding additional equipment in the missile. This is to perform a velocity change match, requiring a small aircraft maneuver. An accuracy analysis of this technique shows that heading alignment approaching the accuracy of the reference heading of the aircraft system can be achieved.

The aircraft flies a slightly offset course so that it can make a turn of 20 to 30 degrees shortly before launch (or fly an "S" manuever). During the turn, the feedback from the aircraft IMU is cut off. Following the turn, the feedback is resumed and the new velocity differences are used to compute an azimuth correction. A heading error (δH) causes a velocity error perpendicular to the ΔV change occurring during the maneuver. This measured velocity difference is utilized to correct the δH. As previously stated, the δH offset was correlated with East gyro drift, so that East gyro drift is also corrected as a result of the manuevers. Then, the missile vertical errors are again quickly damped out using the velocity and position feedback prior to launch.

A second aircraft manuever could be performed if it were desired to get a better calibration of azimuth gyro drift in the air. However, error analysis of typical tactical missile missions indicate that much larger azimuth gyro drift error can be tolerated (1 degree per hour or more) than North or East-axis drifts.

Various automatic checkout and BITE indications can be performed during the married portion of the flight to enable a GO or NO-GO decision to be made at launch.

At the conclusion of the in-air alignment and maneuver mode prior to launch, the missile IMU should be leveled to better than 0.5 minute of arc per axis, and North and East gyro bias drifts should be calibrated to about 0.1 degree per hour. Depending on the accuracy of the master navigator, azimuth align to about 6 minutes of arc, azimuth drift to about 0.5 degree per hour, initial position to a few hundred feet per axis, and initial velocity to about 1.5 feet per second per axis are attainable.

If a rapid takeoff is necessary, the inertial system can start in the air in the fine-alignment mode. The ability to align, starting in the air, provides a quick-reaction capability. Of course, to use it, the master aircraft IMU must have a very quick reaction capability itself.

An alternate in-air (and ground) alignment/calibration approach makes use of a sub-optimal Kalman filter in place of the least-squares-filter approach just described. Lockheed personnel devised a simple six-state (three misalignment angles about North, East, and vertical and three gyro drifts about the X, Y, and Z body axes) Kalman filter that was utilized and proven out in the Holloman flight tests. Figure 6 is a block diagram of the Kalman Filter utilization. The flow within the Kalman filter is conventional. Estimates of the six states are calculated once every 5 seconds, using the horizontal velocity differences between the master and slave navigation systems as measurements. During alignment, the system is closed-loop; that is, the misalignment angles and the gyro drifts estimated by the filter, as well as the current master navigator position and velocity, are entered as corrections into the missile-system software.

As shown in the derivation and equations of this Kalman filter in Appendix A, the use of only six states and various other simplifying assumptions leads to a set of very simple relationships and a minimal computer burden. The fact that several important states (e.g., accelerometer biases) are not modeled could lead to disturbances during the aircraft maneuvers needed for azimuth alignment. However, this worry did not prove to be serious under the flight-test conditions used.

2.3.3 Navigation Mode

The missile IMU may enter the navigation mode immediately at launch or a little earlier. In the navigation mode, the inertial system operates exactly as in the alignment mode except that there is no feedback for external position and velocity references. The only exception is when fix data is available. At this time, there is a correction to inertial position and to velocity, based on memory of the time of the last correction. This allows greater accuracy after a midcourse fix and makes it easier to fly a narrowing basket near the very end of flight.

2.4 System Synthesis - Hardware Description

The strapdown inertial system for the U.S. Air Force flight test program consisted of the Sperry SLIC-15 laser gyro IMU and the Delco Magic 362 computer, integrated together by the Lockheed Missiles and Space Company. These elements are briefly described in the following sections.

2.4.1 SLIC-15 IMU Description

Figure 7 is a photograph of the SLIC-15 IMU, as configured for the Air Force RACO flight test program. The IMU consists of two assemblies; a sensor assembly containing the strapdown laser gyros and accelerometers, and an electronics assembly containing laser gyro control and signal-processing circuits, accelerometer signal processing circuits, computer interface, and power-supply regulators. The electronics assembly packaging for the flight test program is a brassboard configuration. A major size and weight reduction can be accomplished by a combination of hybridization and the shifting of some hardware functions into software.

Sensor Assembly. The sensor assembly contains three laser gyros and three accelerometers in a unique integrated design wherein the three laser gyros are machined into a single block of CER-VIT (low-expansion ceramic vitreous material) so that their optical paths are interleaved. The basic gyro features a modular design approach in which the gyro elements (mirrors and discharge tube) are separable assemblies. This approach has been adopted because of the lower costs associated with increased production yield and service repairability.

The gyro triad consists of three identical 15-inch-perimeter units mounted on a common block, such that the three sensitive axes are mutually orthogonal. This structural approach significantly reduces laser gyro size and makes a more rugged assembly. The laser-gyro-triad volume is reduced to less than half of what it would be if single-axis gyros, of the same perimeter size, were used.

Additional advantages realized from this design are:

(1) Reduced cost - Many single-axis assembly parts are eliminated and assembly operations performed once suffice for three gyros.

(2) Sensitive axis alignment and stability - A single rigid structure, precisely machined, orients the sensitive axes and guarantees alignment stability, an important strapdown consideration.

(3) Efficient inertial sensor packaging - Accelerometers can be accommodated on the same rigid structure with no increase in volume. A single enclosure effectively houses six sensors; three gyros and three accelerometers.

(4) Accelerometer sensitive-axis alignment and stability - Sharing the same block as the gyros assures sensitive axis alignment and stability.

The accelerometers selected for use in the IMU are the force rebalanced Q-Flex Sundstrand accelerometers. These units were selected because of their proven performance and low cost.

Figure 8 is a photograph of the sensor assembly with cover removed. The unit is 7-1/2 inches in diameter by 8-1/2 inches long, and weighs approximately 20 pounds. Factory calibration determines a sensitive-axis-alignment matrix, relative to the reference surfaces, for computer software inputs.

There are no inertial component heaters utilized in the SLIC-15 IMU. Passive thermal compensation circuitry is included to compensate for certain gyro and accelerometer effects.

Tables 2 and 3 list the current performance characteristics of the SLIC-15 laser gyro and the Q-Flex accelerometer, based on extensive testing of many units.

Electronics Assembly. The IMU electronics assembly is functionally divided into three major areas:

(1) Signal Conditioner

(2) Laser Gyro Control

(3) Power Supply

A simplified block diagram is shown in Figure 9.

The signal conditioner operates on laser gyro and accelerometer output signals to condition these signals for multiplexing into the digital computer. The laser gyro signal conditioning consists of pulse-forming, bias and scale factor compensations to translate gyro output signals into scaled body angle increments. The accelerometer conditioning consists of a pulse converter to digitize the accelerometer analog outputs. The accelerometer outputs are digital representations of body axis incremental velocities.

TABLE 2

SLIC-15 LASER GYRO CHARACTERISTICS (1σ)

g Insensitive Drift (Turn-on Repeatability)	1.0 $^{o}/h$
White-Noise Random Drift	0.03 $^{o}/\sqrt{h}$
Markovian Random Drift (> 1 HR correlation time)	0.1 $^{o}/h$
g Sensitive Drift	NIL
Anisoelastic Drift	NIL
Scale-Factor Nominal Value	3.3 $\overline{sec}$/pulse
Scale-Factor Stability	0.01 %
Scale-Factor Linearity	0.01 %
Sensitive-Axis Alignment Stability	6 $\overline{sec}$

TABLE 3

Q-FLEX ACCELEROMETER CHARACTERISTICS

Range	±10g
Scale-Factor	1.0 volt/g
Scale-Factor Stability	100 PPM (1σ)
Temperature Compensation Variation	100 PPM (1σ)
Linearity Stability	0.003% (1σ) of input
Absolute Bias	1.5 mg
Bias Stability (1 yr)	150 μg (1σ)
(Bias Temp. Coefficient. Can Be Temperature Compensated)	5 $\mu g/^{o}F$ (1σ)
Alignment Stability	±0.1 mrad max.
Vibration Rectification (Random Vibration 20-2000 Hz)	±5 $\mu g/g^2$ max.

The signal conditioner also contains a customized interface to accommodate gyro and accelerometer data transfer into the system's general-purpose computer. Upon address by the computer, the gyro and accelerometer angle and velocity increments are multiplexed in 12-bit parallel form into the computer. 6-1

The laser-gyro control contains the circuitry necessary for satisfactory operation of the three laser gyros. Each laser gyro requires the following three closed-loop control servos:

(1) Optical bias current regulation

(2) Cavity path length control

(3) Gas discharge tube current regulation

The power supply contains regulated dc-to-dc converters for all of the primary IMU power requirements. It operates from an unregulated 28-Vdc supply. Included in the power-supply module is an elapsed-time meter to record total IMU operating hours.

Built into the electronics assembly is circuitry to continuously monitor specific key operating parameters. Reasonability checks are continuously made; in the event of an indicated failure, an output discrete is generated to alert the digital computer of the existence of a possible failure. This BITE also generates a fault isolation indication that enables the failed module to be immediately identified by lighting a light-emitting diode. Plug-in replaceability assures rapid maintenance to restore the IMU to operational status.

The present electronics assembly consists of five plug-in circuit modules and a removable power supply. The physical characteristics of this brassboard configuration are as follows:

Size: 8 x 9 x 7 in

Weight: 18 lb

Power: 85 W

Design studies using the latest hybridized printed-circuit-board techniques indicate that the electronics and power supply could be packaged in a unit of about 150 cubic inches in size and weighing less than 9 pounds. In addition many of the gyro conditioning functions can be performed in software instead of hardware, leading to further size and weight reductions.

Reliability and Life. The SLIC-15 IMU is predicted to have an exceptionally high reliability because of its mechanical simplicity and complete absence of moving parts. Gimbal drives and conventional wheel gyros with their inherent mechanical complexity are not employed. The accelerometer used is an extremely simple quartz flex type.

Based on U.S. Government standard MIL-HDBK-217B, the IMU is predicted to have a mean time before-failure of about 7000 hours in a ground environment. Applying stress levels for aircraft and missile environments, the probability of mission success for a typical air launched missile profile (20 minutes on the ground, 2 hours in captive flight, 10 minutes in free flight) is a very high 0.9978.

Operational experience with SLIC-15 units, to date, has thus far supported the excellent reliability expected.

The confidence in these reliability predictions is further enhanced via the experience with the exceptionally long-life laser tube employed in this design. This gas discharge tube has a seven year history of operation without a failure. About 50 laser gyros have been built and tested in this period with one still operating after 60,000 hours.

2.4.2 Digital Navigation Computer

The digital computer used in the flight test program was a standard production model Magic 362 built by Delco Electronics and used in the Carousel series of inertial navigation systems. It was selected for this test program because of its proven capability and adequate performance capacity. There have been significant advances in the computing state-of-the-art over the last few years, and any production tactical missile strapdown guidance system would utilize the most modern microcomputer available.

2.5 System Synthesis - Strapdown Software Description

An optimal set of strapdown algorithms has been synthesized for use with the SLIC-15 IMU. The algorithms employed convert body-axes angular and velocity increments into earth-reference-frame velocity increments and Euler angles. Essentially, these algorithms represent the added computational

The basic objectives in "designing" a set of strapdown algorithms are to ensure that any computational errors introduced are within allowable bounds and to minimize the time and memory burden on the computer employed. The Sperry strapdown configuration and algorithms satisfy these basic objectives.

The strapdown computational flow is shown in Figure 10. For the U.S. Air Force flight-test program and the Delco Magic 362 computer, a basic computational rate of 25 per second, with front-end operations at 100 per second and 50 per second, was utilized. For more modern higher-speed computers such as the Sperry SP-2000, the algorithms are performed at twice these rates.

At the 25 per second rate, the computational errors are an equivalent drift rate of under 0.05 degree per hour and an equivalent acceleration of less than 50 μg for severe angular rate and coning inputs. The algorithms require only about 1500 words and 20 percent of the time capacity of the Delco Magic 362.

The following are some of the key features incorporated into the strapdown computation:

(1) Four-parameter (quaternion) attitude representation

(2) Simplified third-order Taylor series attitude integration including noncommutativity terms

(3) First-order extrapolation of coordinate frame rate transformation

(4) Orthonormalization of attitude matrix

(5) Coriolis rotational corrections to body velocity increments

(6) High speed incremental direction cosine integration to yield higher rate attitude data

(7) Double-precision or unbiased round-off where appropriate

(8) High-speed body rate and acceleration outputs for flight control

An independent assessment of these algorithms was made by the Charles Stark Draper Laboratory where it was shown that coning motion errors were equivalent to standard third-order quaternions being performed at twice the computing speed.

There are several "unconventional" techniques employed in this set of algorithms that are worth noting. Credit for development of most of these techniques is due to Dr. Bernard Schwartz of Sperry Gyroscope Division.

It may be observed from the computational flow diagram that there is no "rate extraction" module. This is accomplished by using a 2:1 speed ratio between the gyro inputs and the quaternion integration, and by expressing the quaternion integration in terms of the "half" angular increments directly (instead of using angular rates).

The technique of performing Coriolis body rotational corrections on the body velocity increments is also unique. These corrections are required to compensate for the fact that the body may be rotating during the integration interval when the velocity increments were being accumulated. The need for these corrections and a derivation of the rotation correction terms to the third order are presented in Appendix B.

For those applications requiring accurate attitude information at a faster output rate than 25 times per second (e.g. for fix sensor pointing without smearing), a special fine/coarse incremental direction cosine integration technique is performed as observed in Figure 10. Thus, to yield 100 per second attitude data, gyro inputs are taken in at this rate, rotated (without certain corrections), and integrated in a simple single-precision first-order direction cosine update routine at a 100-per-second rate. Every fourth period (25 per second), the incremental integration routine is reinitialized from the very accurate higher-order attitude integration normally taking place. Accurate direction-cosine data is then available at a 100-per-second rate. This incremental parallel path approach adds only about 115 words and 5 percent of time to the basic strapdown computing burden. This was found to be much more efficient and flexible than high-order extrapolation schemes or a direct increase in the basic attitude update speed.

This set of strapdown algorithms has not only been successfully programmed by Lockheed on the Delco Magic 362 computer, but also by Sperry on an Interdata 70 computer and on an SP-1000 computer (at twice the speed).

The digital computer software also contains conventional navigation routines, which will not be detailed here, and the align/calibration Kalman filter which was described in Section 2.3.

2.6 System Performance Analysis

An error analysis of the SLIC-15 laser gyro strapdown inertial system was performed for a typical guided glide-bomb mission. The error propagation relationships and the resultant positional errors are presented in Table 4. The mission trajectory depicted in Figure 2 was employed for the error analysis.

TABLE 4

ERROR ANALYSIS FOR ASSUMED GLIDE BOMB MISSION

Error Source	Downrange Position Error	Crossrange Position Error	Error Source Magnitude	At t = 10 min. Downrange Position Error (ft)	Crossrange Position Error (ft)
Gyros					
X Bias (B_x)	$(1/24)g(\Omega\dot{\Omega}(\sin\lambda)B_x t^4$	$(1/6)gB_x t^3$	0.1°/h	8	562
X Random Drift (N_x) (White)		$(1/\sqrt{20})gN_x t^{5/2}$	$0.03°/\sqrt{h}$		554
Y Bias (B_y)	$(1/6)gB_y t^3$	$(1/24)g(\Omega\dot{\Omega}(\sin\lambda)B_y t^4$	0.06°/h	337	5
Y Random Drift (N_y) (White)	$(1/\sqrt{20})gN_y t^{5/2}$		$0.03°/\sqrt{h}$	554	
		$[(1/24)g(\Omega\dot{\Omega}(\cos\lambda)B_z t^4$			
Z Bias (B_z)		$+B_z\int_0^t[\int_0^t t\,\frac{dV_{GE}}{dt}dt]\,dt$	1.12°/h		17
Accelerometers					
X Bias Unbalance (e_{AxB})	$(1/2)\,e_{AxB}t^2$		56 μg	325	
X Scale Factor (δ_{Ax})	$\delta_{Ax}\int_0^t[\int_0^t(\frac{dV_{GE}}{dt})dt]dt$		0.05%	46	
X Quantization (ΔV_x)	$\Delta V_x t/\sqrt{3}$		2^{-4} ft/sec	22	
Y Bias Unbalance (e_{AyB})		$(1/2)e_{AyB}t^2$	58 μg		325
Y Scale Factor (δA_y)			0.05%		
Y Quantization (ΔV_y)		$\Delta V_y t/\sqrt{3}$	2^{-4} ft/sec		22
Initial Conditions					
X TILT (θ_{xo})	$(1/6)g(\Omega\dot{\Omega}(\sin\lambda)\theta_{xo}t^3$	$(1/2)g\theta_{xo}t^2$	0.31 min	16	522
Y Tilt (θ_{yo})	$(1/2)g\theta_{yo}t^2$	$(1/6)g(\Omega\dot{\Omega}(\sin\lambda)\theta_{yo}t^3$	0.31 min	522	10
Azimuth (θ_{zo})		$\theta_{zo}\left[\int_0^t[\int_0^t\frac{dV_{GE}}{dt}dt]\,dt\right.$ $\left.+1/6g(\Omega\dot{\Omega}(\cos\lambda)t^3\right]$	10 min		20
N Velocity (e_{VGNo})		$e_{VGNo}t$	1.5 ft/sec		900
E Velocity (e_{VGEo})	$e_{VGEo}t$		1.5 ft/sec	900	
N Position (e_{pNo})		e_{pNo}	200 ft		200
E Position (e_{pEo})	e_{pEo}		200 ft	200	
Computer					
Roundoff, Quantization, Truncation, Etc.			Error Less than that due to 0.035°/h drift, 35 μg unbalance	197 283	197 283
			RSS Total	1316	1301
			Radial RSS	1915	
			CEP	1801	

6-10

For simplicity of analysis, the glide bomb flight was assumed to be due East at a latitude of 45 degrees. The velocity was approximated to be linearly decreasing with time according to

$$(V_{GE} = 820 - 0.5t)$$

An average V_{GE} of 670 feet per second was employed for certain error coefficients.

Initial position was assumed to be obtained from the mother-ship navigation system.

Initial velocity and initial vertical alignment and "horizontal" gyro bias calibration were assumed to be performed by means of a velocity matching to the mother-ship navigation system during a leveling mode. Initial azimuth was assumed to be obtained by a velocity-change matching to the mother-ship navigation system during a special turn-alignment mode.

A simplified error flow diagram for this mission is depicted in Figure 11. For the 10-minute flight time, errors propagate approximately in an "open-loop" fashion, even though the inertial system is Schuler-tuned. This is because the 84-minute period Schuler loop and the several hour-period earth loop have not had time to cause feedback effects on error propagation to come into play. Substitution of $t < 10$ minutes in the more exact Schuler-loop propagation relationships will confirm this fact.

The major error sources are:

(1) Various gyro errors that either measure body motions incorrectly or cause drift rate (giving a body motion indication when none exists). These error sources will produce attitude errors that build up with time. These errors in turn cause the accelerations being measured to be transformed improperly from body axes to earth coordinates. This means that vertical acceleration (1g) components will appear in the horizontal acceleration outputs, and an East acceleration output will appear on the North acceleration output (cross-coupling effects) and vice versa. This is directly analogous to a gimballed system where the accelerometer platform is tilted off of a true vertical and misaligned in azimuth from a desired direction. In this case, a "phantom" platform exists in the strapdown computer. The incorrect earth-referenced velocity increments are then integrated into incorrect velocities and position.

(2) Various accelerometer measurement errors that are integrated into velocity and position errors.

(3) Initial condition errors:

  (a) Initial position primarily yields a direct position error.

  (b) Initial velocity primarily integrates into position errors.

  (c) Initial attitude matrix errors (analogous to initial vertical tilts and initial azimuth misalignment) in addition to direct attitude errors cause an improper transformation of accelerations into earth coordinates (cross-coupling of 1g into East and North, cross-coupling of East acceleration into North and vice versa). These incorrect earth referenced velocity increments then integrate into velocity and position errors. A secondary effect of an incorrect attitude matrix is to incorrectly transform the coordinate-frame rates into body axes. This is analogous to improper "torquing" in a gimbal system.

(4) Computing errors. Each of the computing blocks shown in Figure 11 can contribute to attitude or position errors, or both, because of inexact computations. The computations are inexact because of truncation errors (use of inexact or limited-order algorithms), round-off errors (finite word-length), senescence errors (computing time lag), sampling time effects (computing cycle time is not zero), and quantization errors (increments are not infinitesimal).

(5) Mounting and boresight errors. Any structural misalignments between the inertial-sensor assembly and the vehicle reference axes will contribute to output attitude errors. They will not cause any navigational errors.

In a 10-minute free-flight navigation, a position CEP of less than 1600 feet results.

Figure 12 depicts the positional error build-up with time for the SLIC-15 system, without and with a positional update.

If a fix is made near the middle of the missile flight, it can be shown that:

6-11

(1) Corrections can be made to the position errors existing at the time of the fix to the accuracy limits of the position fix.

(2) Corrections can be made to the "average" velocity error that existed from the time of launch to the time of the fix, to the limits of the position fix error divided by the time to the fix.

(3) Corrections to gyro bias drift or other individual error sources are not fruitful for the error magnitudes utilized.

As can be observed from Table 4, the requirements on azimuth gyro drift are much less stringent than on residual horizontal axes drift. This is fortunate, since azimuth gyro drift is much more difficult to calibrate during in-air alignment. The very small error contribution due to initial azimuth listed in Table 4 is somewhat misleading. It results from a subtraction of dependent errors for a due East flight at 45 degrees latitude. For example, the net error due to 10 minutes-of-arc initial azimuth for a similar due West flight at 45 degrees latitude is 330 feet crossrange. Initial azimuth error propagation is also more significant for those powered tactical missiles that have a large acceleration after launch.

It is also noted that gyro scale-factor errors and misalignment errors are not listed in Table 4. This is because of their negligible effect for the nonmaneuvering missile profile employed in the error analysis. Fairly tight specifications for these error sources should be maintained to achieve good in-air alignment-maneuver results, to minimize the effects of coning motions and vehicle perturbation, and to minimize the effects of any maneuver angular changes that might occur on other missile missions.

Thus, for a circular coning motion of half-cone angle α and radian frequency ω, the rectified coning drift due to a scale factor error δ_{SF} can be shown to be

$$E\omega_D = \delta_{SF} \frac{\alpha^2 \omega}{2}$$

For a 2-degree 1-HZ coning motion, a δ_{SF} of 0.01 percent yields a drift rate of 0.08 degree per hour.

Scale-factor symmetry is especially important if vehicle perturbations are taking place. One of the major advantages of laser gyro sensors is that they have inherent scale-factor symmetry. If there is an oscillation of angle α with radian frequency ω, the rectified drift rate due to scale-factor difference, $ksf_+ - ksf_-$ can be shown to be

$$E\omega_D = (k_{SF+} - k_{SF-}) \frac{a\omega}{\pi}$$

For a 2-degree 1-HZ perturbation, an 0.001 percent scale difference results in a drift rate of 0.144 degree per hour.

2.7 Test Data

Table 5 is a summary of typical test data on the SLIC-15 IMU units at Sperry prior to or during acceptance testing and at Holloman Air Force Base. These data indicate performance well within acceptance test specification and close to that predicted.

One of the most severe tests of a strapdown system is navigation under a coning motion (simultaneous sinusoidal motion in two axes, 90 degrees out of phase with each other). This type of input exercises gyro scale-factor and linearity (including polarity symmetry) errors, accelerometer size-effect error, and computational noncommutativity errors, as well as most of the other error sources. The test results shown in Table 5 confirm good strapdown performance of both the inertial sensors and the software algorithms.

The purpose of the Holloman flight tests was to prove out the simplified Kalman filter in-air align technique, as well as to verify missile system navigation performance. Various in-air maneuver patterns (four S-turns, three S-turns, two S-turns with different periods of straight and level flight after the last maneuver) and alignment times were tried out. Post launch heading changes and altitude descents were also tried out. The rms performance was well within specification in all cases. A 10-minute in-air alignment time with two S-turns was found to be more than adequate.

The 10 August 1976 flight test runs utilized a 3-minute straight and level period following the last S-turn maneuver prior to launch. This enables maneuver induced effects due to any unmodeled filter states to settle out before launch and yields optimum system performance. Best estimates of resident leveling, alignment, and calibration errors achieved by the SLIC-15 system using the in-air alignment Kalman-filter technique for the six runs of 10 August 1976 were:

6.12

$\epsilon\Delta\theta_E = 0.74$ min rms $\quad \epsilon\omega_{dx} = 0.14\ ^\circ/h$

$\epsilon\Delta\theta_N = 0.61$ min rms $\quad \epsilon\omega_{dy} = 0.30\ ^\circ/h$

$\epsilon\Delta\theta_K = 5.88$ min rms $\quad \epsilon\omega_{dz} = 0.67\ ^\circ/h$

TABLE 5

SLIC 15 IMU TEST RESULTS

NAV. ERRORS AT END OF 10 MINUTES

(FOLLOWING 15 MIN. WARMUP & 15 MIN. ALIGN/CAL.)

EXCLUDING INITIAL POSITION AND INITIAL VELOCITY ERRORS

	North Distance (Ft)	East Distance (Ft)	
Acceptance Test Spec (RMS)	3000	3000	For guided glide bomb application
Accuracy Analysis Prediction (RMS)	1100	1100	Based on predicted gyro performance
Static RMS of 4 Runs	1374	1394	S/N 004 - 12/17/75 30 minutes off between runs
Scorsby Coning Motion RMS of 5 Runs	1699	2372	S/N 003 - 10/1/75 $\pm 2.1^\circ$, 1 Hz
Random Vibration RMS of 5 Runs	1388	1095	S/N 003 - 10/1/75 2g RMS 20-2000 Hz
Elev. Temp. RMS of 7 Runs	2344	2175	S/N 003 - 10/23-24/75 During $+50^\circ$F Temp. Rise
FLT Test RMS of 6 Runs	1469	958	S/N 004 8/10/76 In C141 at Holloman AFB
*FLT Test RMS of 47 Runs	2547	1818	S/N 004 June 1977 in C141 at Holloman AFB

*Includes some runs with 10-minute Align/Calibrate, and some runs with 30 degree heading change after "launch".

Certain straightforward improvements could yield improved performance to that demonstrated in Table 5, without requiring any changes to the basic inertial components. For the flight-test program, a velocity-increment resolution of 2^{-4} ft/s/pulse was employed in the accelerometer digitizing electronics. Designs are now available that can give 2^{-6} ft/s/pulse and better over the same acceleration range. For a 5-second sample time, the 2^{-4} ft/s/pulse resolution yields rms equivalent tilts of 0.78 minutes-of-arc. Sperry had intended to use an effective sampling time of about 20 seconds for the leveling mode (this was employed in the Sperry factory) to reduce this error. Improving the velocity-increment resolution by four times to 2^{-6} ft/s/pulse, which is readily achievable, should make for a significant improvement in leveling alignment and overall system performance.

The SLIC-15 flight-test units contained certain limited inertial-component temperature compensations in hardware. Later-designed Sperry systems have more sophisticated compensations performed in the computer software that will maintain better inertial-component performance with either internally generated or externally generated temperature variations.

The advances in computing speeds and reductions in computing memory costs now enable a more exact alignment Kalman filter to be synthesized. The addition of certain states, such as accelerometer biases, should yield improvements in maneuver alignment, with possible reduced alignment time.

2.8 SLIC-7 Laser Gyro Inertial Guidance System

Many tactical missile missions have shorter flight times or more frequent position updates than those discussed here. It is also highly desirable to have a smaller size system for many of these missiles. Sperry is presently developing a miniature SLIC-7 Laser Gyro Strapdown Inertial Guidance System that is suitable for those applications [4].

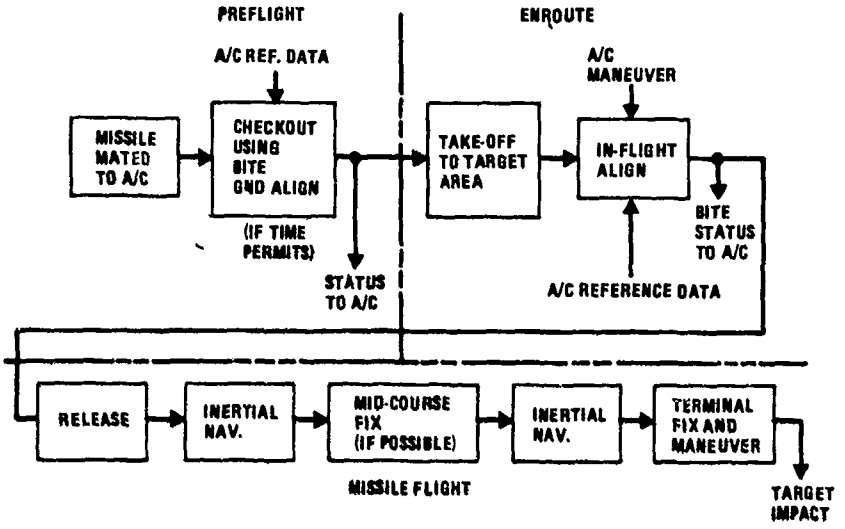

Figure 1. Typical Mission Sequence

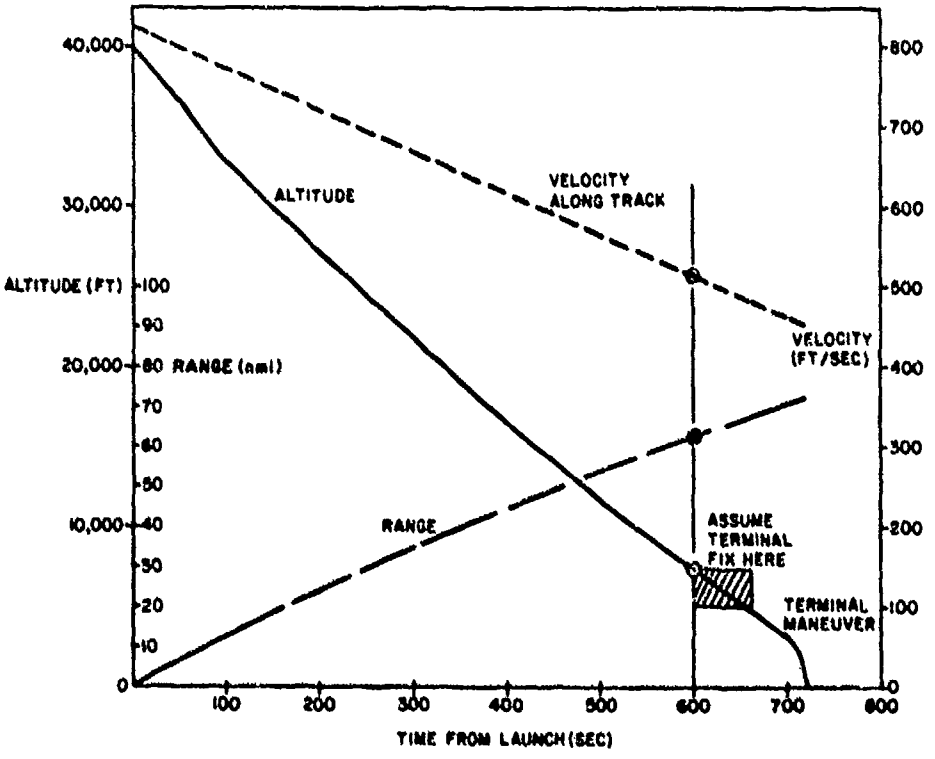

Figure 2. Typical Mission Profile for Error Analysis

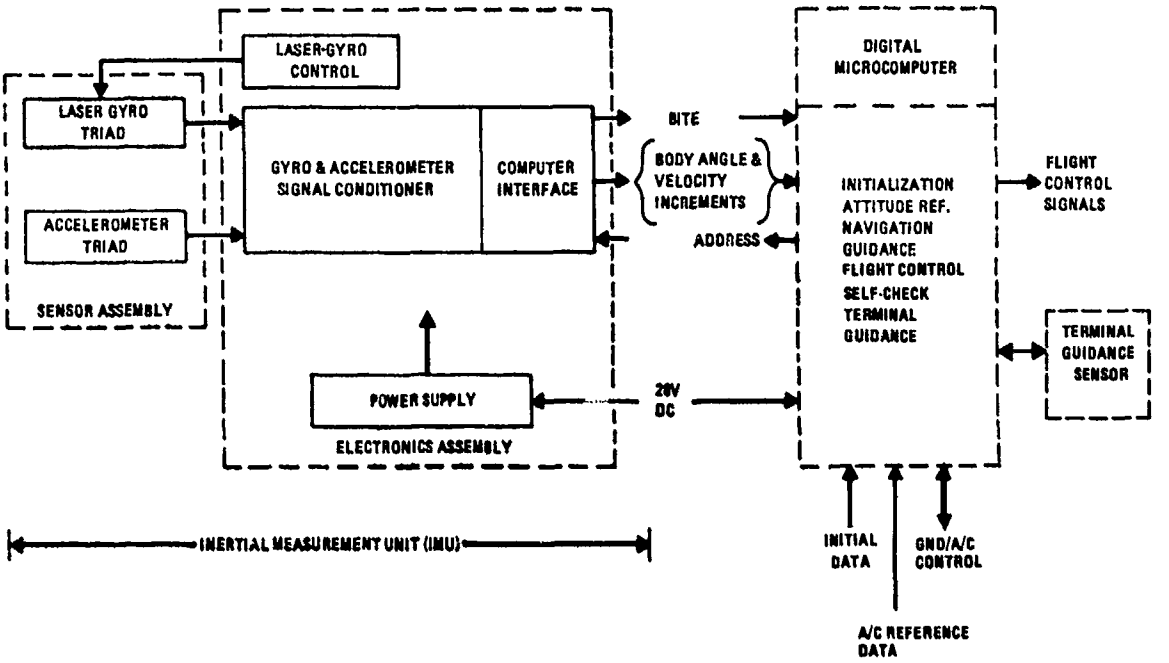

Figure 3. Laser Gyro Strapdown System
Functional Block Diagram

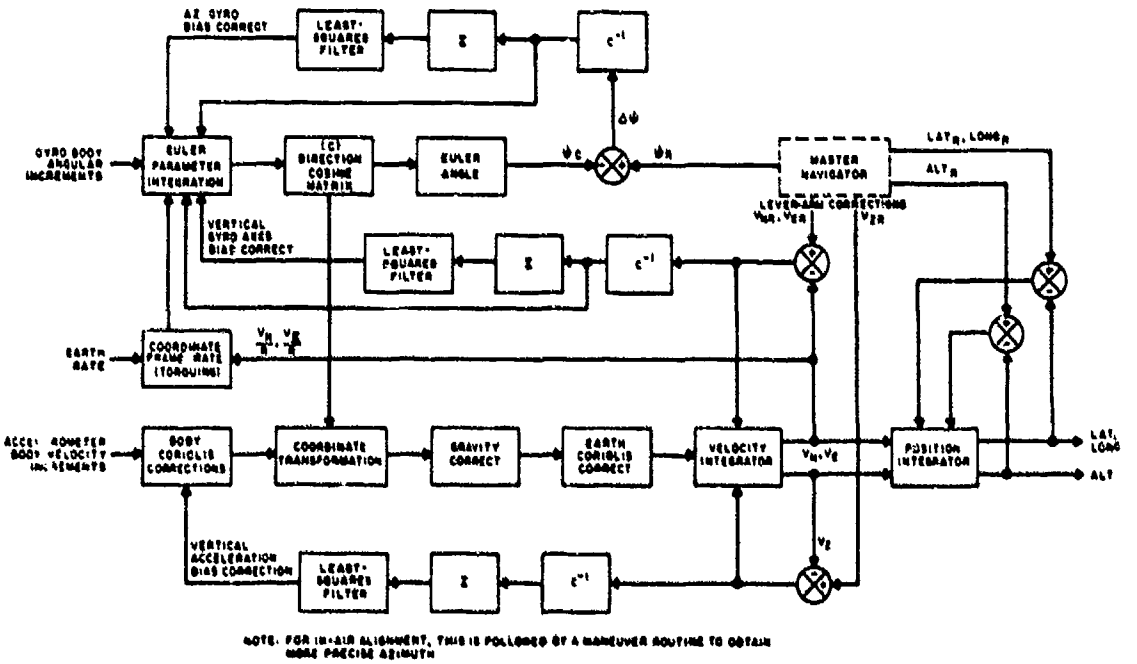

NOTE: FOR IN-AIR ALIGNMENT, THIS IS FOLLOWED BY A MANEUVER ROUTINE TO OBTAIN MORE PRECISE AZIMUTH

Figure 4. Leveling, Alignment, and Calibration

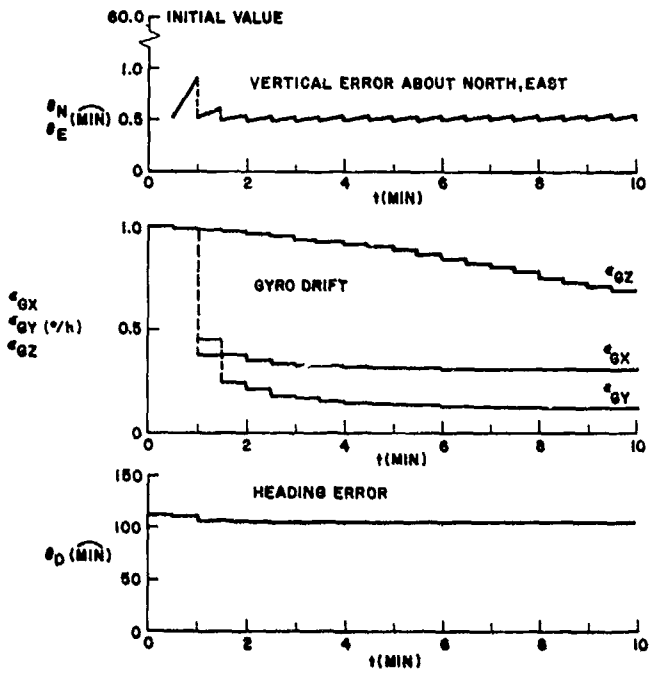

Figure 5. Ground Align Mode Analysis Results, Magnetic Flux Valve Reference

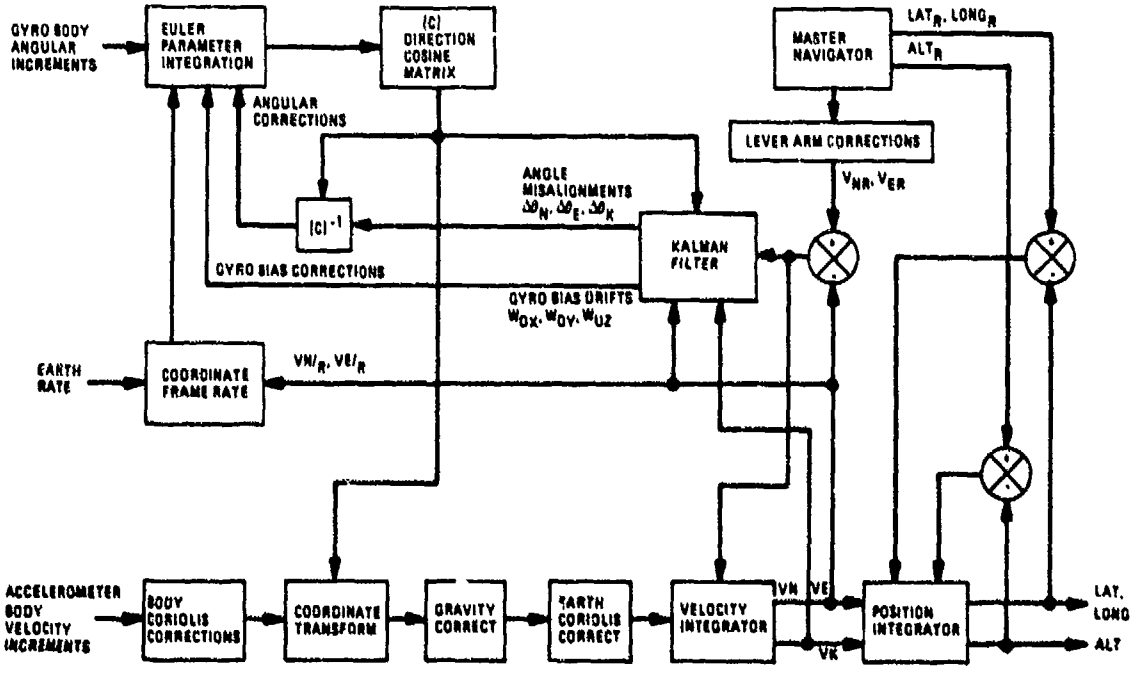

Figure 6. Simplified Kalman Filter Align/Calibrate

6-16

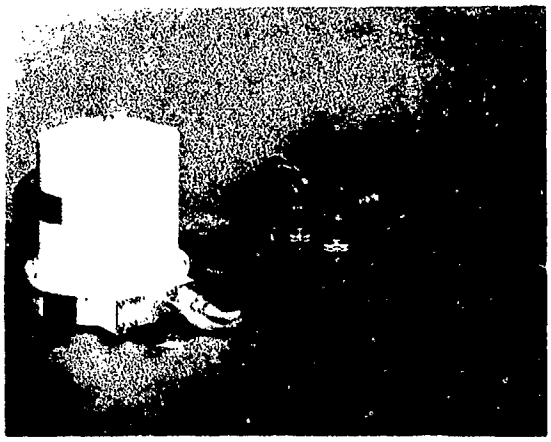

Figure 7. SLIC-15 IMU

Figure 8. SLIC-15 Sensor Assembly

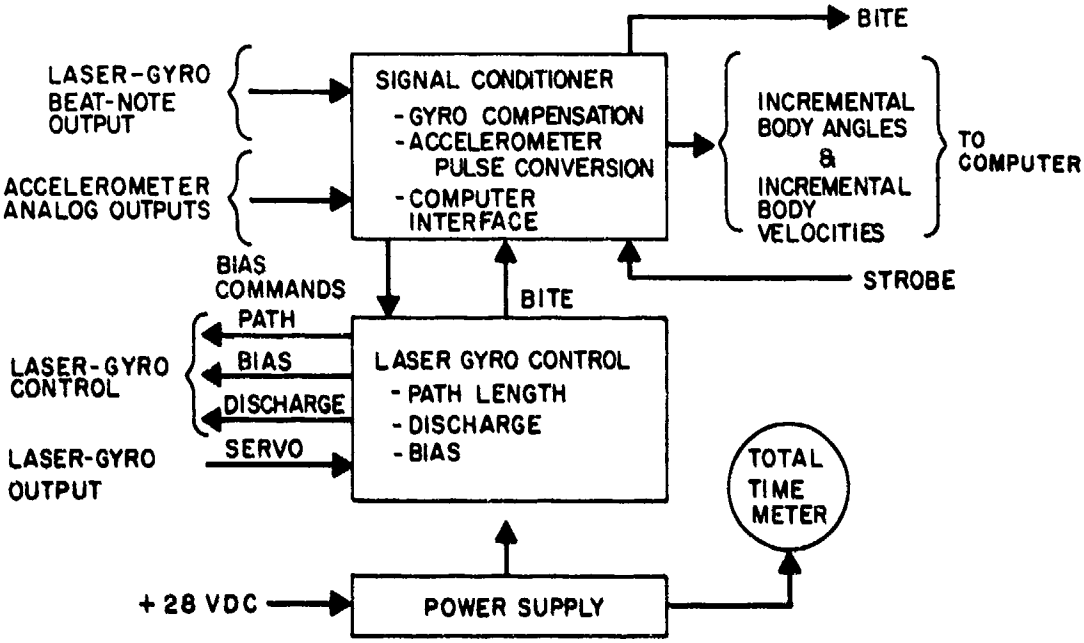

Figure 9. Electronics Assembly Block Diagram

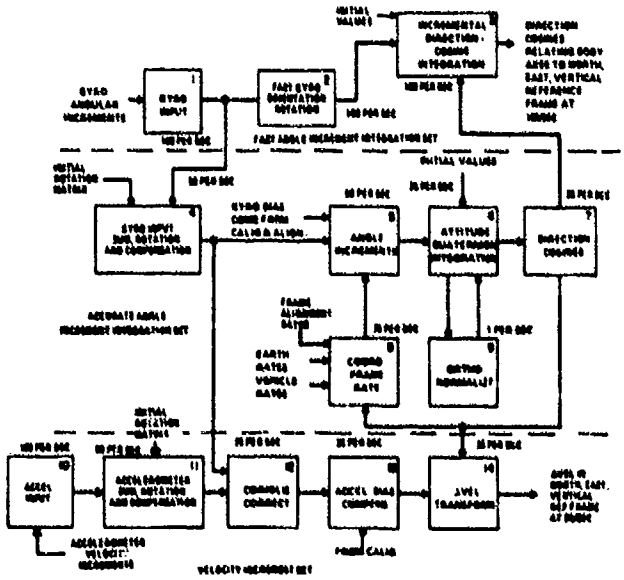

Figure 10. Strapdown Computational Flow Diagram

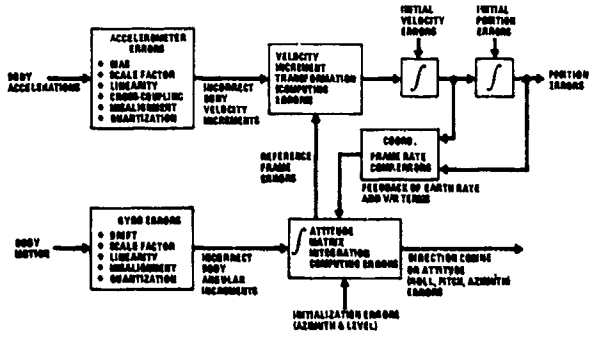

Figure 11. Simplified Error Flow Diagram For Strapdown Inertial System

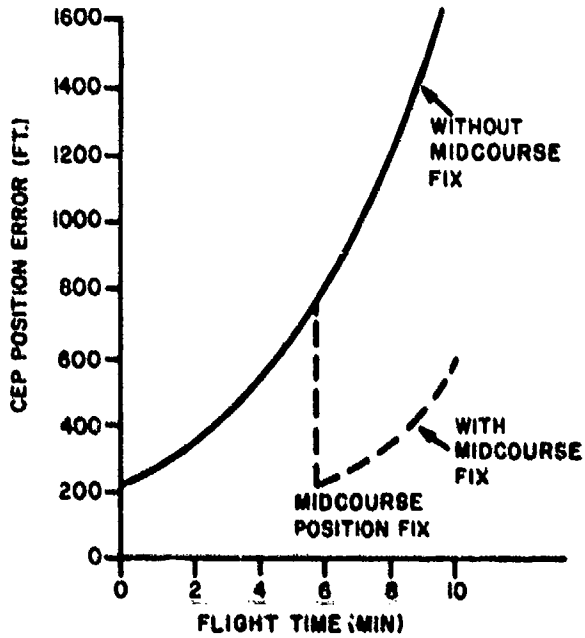

Figure 12. CEP Position Error Without and With a Mid-Course Fix

6-18

3. SHIPBOARD FIRE-CONTROL ATTITUDE-REFERENCE APPLICATION

A large number of U.S. Navy shipboard gun fire-control systems presently contain an attitude reference unit known as the MK 16 Stable Element to provide stabilization data (either ship pitch and roll or level and cross-level) to the gun-laying computer. The present Stable Element utilizes conventional gyros, gimbals, and various electromechanical components. Sperry has developed under U.S. Navy sponsorship an all solid-state strapdown laser-gyro MK 16 replacement that is much more reliable, much more maintainable, more accurate, and much more flexible than current Stable Element units. If sea trials of the engineering development models are successful, the laser-gyro unit will be retrofitted into the fleet. This could represent the first large production application of laser gyro systems.

This section describes the laser-gyro MK 16 MOD 11 Stable Element[5], delineates its key features (such as a 14-state Kalman filter), and presents performance analysis and test results vis a vis mission requirements.

3.1 MK 16 Stable Element Mission and Requirements

The MK 16 Stable Element receives ship longitudinal velocity from the ship log, ship heading from the ship compass, and train from the gun director. Utilizing its own inertial references, the Stable Element must then provide continuous ship pitch and roll (or level and cross-level) stabilization data. Accuracy requirements are 1.5 minutes-of-arc per axis rms at sea, in the face of ship turning maneuvers, and within 15 minutes of turn-on. It is also desired that the Stable Element compute its own earth rates (self-determination of latitude), with at most a rough initial latitude input. Information is to be provided in synchro format and on a digital display. Self-test and fault localization to a replaceable assembly are required maintenance features.

The Stable Element is continually operating in a closed-loop leveling, alignment, calibration mode similar to that described in Section 2.3. Accuracy analyses of these loops employing sub-optimal Kalman-filter mixing of the reference and inertial information indicate that the performance capabilities of the Sperry 15-inch-perimeter laser gyro (Table 2) and the Sundstrand Q-Flex accelerometer (Table 3) are satisfactory (and are the necessary order of magnitude) to meet the mission requirements.

3.2 MK 16 MOD 11 Stable Element Functional Block Diagram

Figure 13 depicts the equipment elements and the functional block diagram of the laser-gyro MK 16 MOD 11 Stable Element. Ship speed, ship heading, and director train are received by the digital microprocessor (DMP) through solid-state synchro-to-digital converters. The DMP also receives body angular increments from the strapdown laser gyros and body velocity increments from the strapdown accelerometers (via pulse-rate converters). Temperature-sensor and various coefficient data on the inertial components are also digitized and sent to the DMP for compensation purposes.

The microprocessor performs the basic functions shown in Figure 14. The body angular increments are appropriately integrated to obtain the attitude of the ship at all times (direction cosine matrix) with respect to an earth reference frame. The Euler angles (pitch, roll, and heading) are extracted from the direction cosines. With proper use of the train angle, level and cross-level are obtained in place of pitch and roll, if desired.

The direction cosines are also employed to transform the body axis velocity increments into earth reference frame velocity increments. These are integrated to provide velocity (for comparison to reference velocity and for coordinate-frame-rate "torquing") and latitude (for the earth-rate portion of the coordinate frame rate).

The attitude information is leveled, aligned, and maintained accurate by performing optimal Kalman-filter gain multiplications on the differences between reference velocity and inertial velocity, and between reference heading and inertial heading. Kalman-filter corrections are obtained and applied to correct inertial attitude, gyro biases, accelerometer biases, velocity, and latitude data in a feedback closed-loop manner that will yield minimal variance errors in the various states.

The DMP supplies output level and cross-level (or pitch and roll) data to solid-state digital-to-synchro converters. The DMP also provides and receives data to and from a control and display panel. It also performs various self-test and performance monitoring/localization functions. Digital output data to another computer can also be provided, if desired.

3.3 Specific System Synthesis - Hardware Description

The strapdown laser gyro Stable Element is depicted in Figures 15 and 16. As shown in Figure 15, the system consists of six major functional units contained in a single enclosure. These units are as follows:

(1) Sensor Assembly. Contains three laser gyros and three accelerometers (on a common mounting block) which measure all of the ship angular and linear motions.

(2) Sensor Electronics. Contains electronic circuits to control the laser gyros, process the gyro and accelerometer signals, and transmit the data to the DMP.

(3) Digital Microprocessor (DMP). Performs all data processing and handles the data inputs from the input converters and the control panel, and the output data to the output converters and control panel.

(4) Input and Output Converters. Convert input synchro signals to digital data and output digital data to synchro and dc analog outputs.

(5) Control Panel. Provides the means for the operator to control the equipment and to observe equipment status and data.

(6) Power Supply. Supplies all dc power required for proper operation of the equipment.

Thermal environmental control is completely passive (except for some electronics precision-reference ovens). There are no fans or blowers, and there are no inertial-component heaters.

To meet the U.S. Navy desire for low-cost sparing and ease of maintenance, and because of the relaxed size and weight constraints of marine equipment, the laser gyros employed in the Stable Element are housed in separate individual packages, rather than interleaved on a common structure as was the case for the SLIC-15. Figure 17 is a photograph of one of the Stable Element laser gyros. The basic design features of this gyro are similar to those employed in the SLIC-15 unit.

Each laser-gyro unit has been designed to be interchangeable and readily replaceable without any realignments or adjustments as is also the case with each Q-Flex accelerometer unit. Each sensor contains an integral calibration programmable-read-only-memory (PROM) that provides data and coefficients for processor software compensation. PROM calibration data for each sensor includes bias, scale-factor, misalignment and temperature coefficient information.

Each laser gyro interfaces with a gyro electronics card (one per axis) that performs the functions shown in Figure 18, and uses hybrid circuits that have been proven out on many previous Sperry laser-gyro applications. Each accelerometer interfaces with an acceleration digitizer card (one per axis) that converts the accelerometer output dc voltage into a 12-bit parallel binary data word, representing the velocity change sensed during the preceding 0.01-second interrupt period. The digitizer employs proven precision voltage-to-frequency converter circuits, whose output pulse train is accumulated in an up/down counter. A compensation electronics card contains a multiplexed analog/digital converter that converts inertial sensor analog temperature data into 12-bit parallel binary data words. Each of these sensor electronics cards contains BITE circuitry that detects various malfunction situations. Activation of the failure detector energize an LED on the card, and produces a logical "low" at the BITE output terminal.

A timer card, a computer interface card, and an installation PROM (to insert certain data peculiar to a given ship; e.g. lever-arm distances) complete the complement of ten 5.7 x 6.5 inch sensor electronics cards.

The DMP is the Sperry SP-1000 computer, a printed circuit card version of the hybridized SP-2000, which is described in Reference 4. The SP-1000 microprogrammable architecture is designed to emulate a major subset of the instruction repertoire of the U.S. Navy standard AN/UYK-20 computer.

As such, the development, testing, and operational programming has been greatly simplified through the use of the substantial and proven software support areas currently available for this military standard machine.

The SP-1000 architecture features microprogram control, 16 general-purpose registers, parallel 16-bit word organization, an extensive instruction repertoire, and a versatile addressing structure. The computer process unit design uses large-scale-integrated microprocessor devices which provide the ALU, 16 accumulators, shifters, and input/output bus. As indicated in Figure 19, microinstructions stored in main memory are executed by microprogrammed routines stored in the microcontrol memory (CROM). Execution of a macro-instruction requires one to several micro-instructions. An instruction is read from main memory, and its 8-bit operation code and format field serve as an address to an emulation ROM and CROM sequencer, which provides the appropriate entry into the CROM. The remaining 8 bits of the instruction designate registers used in the operation, and these are gated to the microprocessor. Each micro-instruction is 40 bits wide. The primary microfield, in turn, generates a nanoinstruction to the microprocessor elements. The remaining microinstruction bits provide controls to the logic. Each microinstruction contains fields designating data sources and destination registers, and also controls address generation. The sequence logic provides sequential addresses until the last microinstruction is executed, and then accepts the next entry from the emulation ROM. An asynchronous memory interface, incorporated within the SP-1000, provides compatibility with memories of diverse type and speed.

For the Stable Element application, a 12K x 16 bipolar ROM (on two cards) and a 4K x 16 N-MOS RAM scratchpad memory (on two cards) are utilized.

The SP-1000 processor is basically a 16-bit computer structured to enable it to handle either 16- or 32-bit data words. Two sequential words in memory or two continuous registers are used, as required, to contain 32-bit operands. Using this capability provides for an extensive instruction set with implicit program design flexibility. 32-bit precision, at hardware speed, is an important advantage.

The internal cycle time of a CPU microinstruction is 360 nanoseconds.

Typical cycle times for Register-to-Register instructions resident in bipolar memory include:

ADD	0.36 μsec
ADD DOUBLE	0.72 μsec
MPY	3.52 μsec
MPY DOUBLE	12.60 μsec
DIVIDE	11.52 μsec
SHIFT	1.44 + 0.36N μsec

The SP-1000 CPU (including input/output) is comprised of twelve 5.7 x 6.5 inch printed wiring board modules. These 12 cards plus the 4 memory cards constitute the DMP.

The control and display panel shown in Figure 16 consists of a 6-digit plus sign LED display, a keyboard, and various controls for mode and display selection.

The predicted MTBF for this "no moving parts" strapdown system, including all input and output converters is 3520 hours. The predicted mean-time-to-repair (MTTR) aboard ship is about 20 minutes. Key maintainability features of the MK 16 MOD 11 Stable Element design include:

(1) Functional Modularity. A single cabinet with all parts readily accessible with maximum use of plug-in modules.

(2) Interchangeability. All modules are completely interchangeable without alignments or adjustments.

(3) Built In Test. Performance Monitoring/Fault Localization (PM/FL) circuits and software provide rapid identification of problem and isolation to a given replaceable subassembly. Minimizes specialized external test equipment and maintenance training.

(4) Minimum Preventive Maintenance. No "wearout" parts, no filters, fans or lubrication points. Daily system operational test (DSOT) only.

3.4 Specific System Synthesis - Software

As shown in the strapdown computation function flow diagram of Figure 20, the basic strapdown algorithms employed by the MK 16 Mod 11 Stable Element are identical to those described in Section 2.5 for the tactical missile guidance system. In this case, because of the increased speed capability of the SP-1000 computer, the basic strapdown computational modules are performed at a 50 per second rate instead of 25 per second.

Also, in this case, because of the use of direction train information on the direction cosines, a fairly simple extrapolation is performed to yield pitch and roll (or level and cross-level) output data at 500 per second rates, instead of using the high-speed incremental direction-cosine-integration parallel-path technique.

For the MK 16 MOD 11 Stable Element, several of the inertial-component corrections and compensations that were performed in hardware on the SLIC-15 IMU are now included in the "front-end" of the strapdown software. This minimizes hardware complexity and cost, and enables more sophisticated and more flexible inertial-component compensations.

One of the more significant new contributions synthesized for the Stable Element program was the incorporation of a 14-state leveling, alignment, and calibration filter that is continually in operation as part of the normal mode of the Stable Element (See Figure 14.) The Kalman-filter function provides optimal damping for the otherwise Schuler-tuned vertical loops. This function

(1) Compares inertial velocities and heading with reference velocity (corrected for lever-arm effects) and reference heading data.

(2) Operates on these "measurements" to generate corrections to the modeled system states. Corrections are made to velocities, tilts, heading, latitude, gyro biases, and accelerometer biases.

6-21

The basic iteration interval is 2.56 seconds. Most of the "internal" operations of the Kalman filter (optimal gains computation and covariance matrix extrapolation and update) are performed in double-word floating point to obviate scaling difficulties. Certain reasonable tests on various parameters are also included in the Kalman-filter program.

Additional details of this Kalman-filter, the development of which is primarily due to Carlo P. San Giovanni, Jr., of Sperry Gyroscope, are presented in Appendix C. Many of the computations involved are greatly simplified by appropriate matrix partitioning and the preponderance of zeros in the transition matrix and the measurement matrix.

3.5 System Performance Analysis

Simulations of at-sea maneuver situations were performed, using the Sperry CAESAR generalized-error-analysis program. Carlo P. San Giovanni, Jr., set up the simulation and generated the analysis runs. Gyro and accelerometer error models based on Tables 2 and 3 were utilized and reference error models (1.5 knots rms, 10-minute correlation time plus 0.3 knots bias and 0.4-knot white noise for reference velocities; 13.7-minutes-of-arc rms, 30 minute correlation time plus 6-minute-of-arc bias and 6-minute-of-arc white noise for reference heading) based on U.S. Navy specification and prior experience were incorporated. The simulation program employs a strapdown mechanization and a Kalman filter (22 states rather than 14) analogous to the Stable Element design. The performance analysis results, shown in Figures 21 through 26, are well within U.S. Navy requirements.

Figure 21 depicts a typical pitch/roll error response, in the face of high turning-rate maneuvers, for a case where latitude was initially inserted to within 5 minutes of arc. Pitch/roll performance to better than 0.9 minutes-of-arc rms is observed.

The covariance analysis results indicate that the occurrence of 180° turns does not significantly affect pitch/roll accuracy performance. In particular, the time period immediately following the turn is marked by a temporary improvement in pitch/ roll accuracy. Subsequently, the error increases slightly and then settles essentially to the original rms value. The temporary improvement in accuracy is attributable to a temporary calibration of log velocity error associated with the use of the Kalman-filter mixing configuration and the occurrence of the 180° turn. Such calibration is anticipated when conditions are such that the duration of the turn is less than the 10-minute correlation time of the log error. As indicated by subsequent pitch/roll error behavior, the relatively high-frequency nature of the log error in this case leads to a relatively rapid loss of any such calibration. It is noted that processing of velocity differences during periods immediately before and after 90 and 180° ship turns is a standard technique for calibrating ship log bias on certain Navy ships with inertial navigation equipment.

When the ship maneuvers, additional information is available to the Kalman-filter, which permits automatic calibration of strapdown accelerometer biases. Operation of the leveling loop causes ΔV to go to zero. Therefore, a bias of a horizontal accelerometer is balanced out by a corresponding tilt error. When the ship turns, the tilt errors remain the same in earth coordinates, but the accelerometer turns with the vessel. For a 90° turn, the accelerometer is put into a position where its bias is uncorrelated with tilt. For a 180° turn, it is negatively correlated. Therefore, during turns, there is a large amount of information available to calibrate the accelerometers. The bias error is estimated automatically during the turn and the accuracy is improved as long as the Stable Element continues to operate. Repeated turns continue to improve the accelerometers, although the improvement increment gets smaller with time.

Performance is less than the specification value of 1.5 minutes-of-arc rms in about 12 minutes after turn-on, and is usable in a much shorter time (less than 2 minute-of-arc rms in about 7 minutes after turn-on).

Various other maneuver pattern runs were performed (slower turns, 360° turn, 45° turns) with comparable results.

Figures 22 and 23 indicate the self-determination-of-latitude capability of the system. Starting with an initial latitude error of 12 degrees, performance is degraded only during the first turn, and even then, the resultant errors are barely outside tolerable limits.

These same results are applicable for even larger initial latitude errors because, as shown in Figure 23, the Kalman-filter mechanization provides a latitude-correction capability. Prior to any turn maneuvers, the operation of the heading reference and velocity reference matching loops are such as to balance out earth-rate errors (due to latitude errors) against gyro bias drift. Latitude is rapidly corrected (see Figure 23 prior to the first turn maneuver) to the level (225 minutes-of-arc) where this balance occurs. During the first 180° turn, the gyro bias drifts for the strapdown system remain along the ship coordinate axes, whereas earth rates remain along north and vertical earth coordinate axes. The gyro bias drifts and the earth-rate (latitude) errors thus become uncorrelated, and the Kalman filter can compute a much better estimate of both the gyro biases and the earth rates (latitude). This is

clearly shown in Figure 23 where the latitude accuracy is improved to 11 arc-minutes after the first turn. Because of this improvement in latitude (and earth rates) accuracy, the vertical errors during subsequent turn maneuvers are reduced to normal levels (see Figure 22).

Additional simulations were conducted for operating latitudes of 0 and 70°N, again starting with a very large initial latitude error of 12 degrees.

Results are shown in Figures 24 and 25. In particular, Figure 24 provides a plot of rms roll error versus time after turn-on at operating latitudes of 0, 45, and 70°N. The behavior of the rms latitude error is shown for these same operating latitudes in Figure 25.

Figure 24 shows the initial settling transient for pitch/roll errors to be quite similar for the assumed range of operating latitudes; this also applies to accuracy performance subsequent to the first (180°) turn. The peak (rms) roll error introduced as a result of the first 180° turn is slightly greater at $\lambda = 70°$N (2.5 minutes-of-arc) than at $\lambda = 45°$N (2.2 minutes-of-arc). The transient errors introduced by the first 180° turn at $\lambda = 0°$ are quite small, and generally resemble the performance of the baseline model (i.e., small initial latitude errors). As previously discussed (for an operating latitude of 45°N), the transient that occurs during the first turn is primarily associated with errors in horizontal earth rate (due to the latitude errors). The error in horizontal earth rate can generally be expressed as $(\Omega \sin \lambda \Delta\lambda)$; at an operating latitude of 0°, the error in horizontal earth rate is then theoretically zero. For the magnitude of latitude errors under consideration, this indicates that as shown in Figure 24, the "first-turn" transients can be expected to be substantically less at $\lambda = 0°$ than at $\lambda = 45°$ and 70°. It is noted that the error in vertical earth rate is $(\Omega \cos \lambda \Delta\lambda)$; at $\lambda = 0°$, the error in latitude is primarily observable through the heading measurements and the Z axis gyro bias drift.

At $\lambda = 45$ and 70°, the "first-turn" disturbances in pitch/roll error lead to the estimation of latitude error and, therefore, to minimal perturbations during subsequent maneuvers. Figure 25 shows that latitude is estimated to approximately 11 nmi at $\lambda = 45°$ and 8.5 nmi at $\lambda = 70°$. Since disturbances due to latitude errors are of minor magnitude at $\lambda = 0°$, then the occurrence of turns is not expected to assist the estimation of latitude error for this operating condition; latitude error at $\lambda = 0°$ will, however, be estimated to a level compatible with the error in estimating Z-gyro bias.

Thus, satisfactory performance is attined at all operating latitudes, without the need of any latitude update by the operator. A rough initial latitude insertion is desirable to minimize output attitude errors during the first turn following system turn-on.

The analysis simulations described to this point utilized a "real-world" system involving a 22-state Kalman filter. The Stable Element design uses a 14 state reduced Kalman filter to minimize the onboard computer burden. Sperry has performed sensitivity analyses, using its SEAP program, to compare the performance of the 14-state sub-optimal filter with that of the 22-state simulation. The results show nearly identical performance as depicted in Figure 26, for example.

Figure 26 provides a plot of X gyro bias estimation error for the 22/14 sensitivity analysis and the 22/22 optimal analysis. Performance with the reduced state filter is observed to be quite similar to the performance with the optimal 22 state filter.

This last plot, incidentally, confirms the discussion statement about the "balance" of earth-rate (latitude) errors with gyro bias drift, and also shows that X gyro bias drift will be calibrated to about 0.1 degrees per hour under this set of maneuver and initial latitude conditions.

The simulation analysis results do not include converter-transmission errors and computer errors; because of not incorporating gyro and accelerometer scale-factor errors and misalignment instabilities, certain dynamic errors are also not included. Hardware and software design choices were made that make all of these additional error sources essentially negligible compared to those used in the simulation. Velocity-increment resolution is 2^{-7} ft/s/pulse. Specifications for the digital-synchro converters require a resolution of 14 bits and an accuracy of 5 minute-of-arc maximum (at 36 speed) over all environments. This yields rms errors of 0.14 minute-of-arc when referred to single speed. Software algorithms, sampling speeds, and use of double precision (where necessary) have been selected to contribute negligible accuracy impact. Inertial-component misalignment, mounting, and boresight instabilities are held to an overall rms of less than 0.2 minute-of-arc about the tilt axes.

Dynamic errors due to scale-factor errors and nonlinearities will be fairly small in this application because of the closed loops involved, the sinusoidal nature of ship's pitch and roll motions, and the relatively mild shipboard acceleration environment. For example, for a maximum roll motion of 30 degrees, the rms roll error due to an 0.01 percent gyro scale-factor error is

$$\frac{(30)\ (60)\ 10^{-4}}{\sqrt{2}} = 0.13 \text{ min.}$$

3.6 Stable Element Test Data

Several overall system tests have been performed that verify the Stable Element capabilities discussed in the previous subsection. Some typical results are described in the following paragraph.

As part of the Factory Acceptance Test, the Stable Element is mounted on a Scorsby table and ship's pitch and roll motions are simulated:

Pitch	5 degrees,	6 second period
Roll	15 degrees,	9 second period

Stable Element pitch and roll readouts are compared to those of the Scorsby table and errors are recorded. The results for the first two MK 16 MOD 11 Stable Element Engineering Development Models are depicted in Table 6. Performance is observed to be well within specification values.

The first Laser Gyro Stable Element successfully completed its first sea-trail (Feb. 13-16) aboard the U.S.S. Sellers. It performed markedly better than the existing Stable Element, with "horizon" tests under various maneuver conditions generally indicating about one minute-of-arc accuracy.

TABLE 6

MK 16 MOD 11 STABLE ELEMENT PERFORMANCE RESULTS UNDER SCORSBY MOTION

	Unit 1	Unit 2	U.S. Navy Specification
Response Time (minutes)	9	10	15
Pitch Error ($\widehat{\text{min}}$ rms)	0.80	0.68	1
Roll Error ($\widehat{\text{min}}$ rms)	0.70	0.62	1

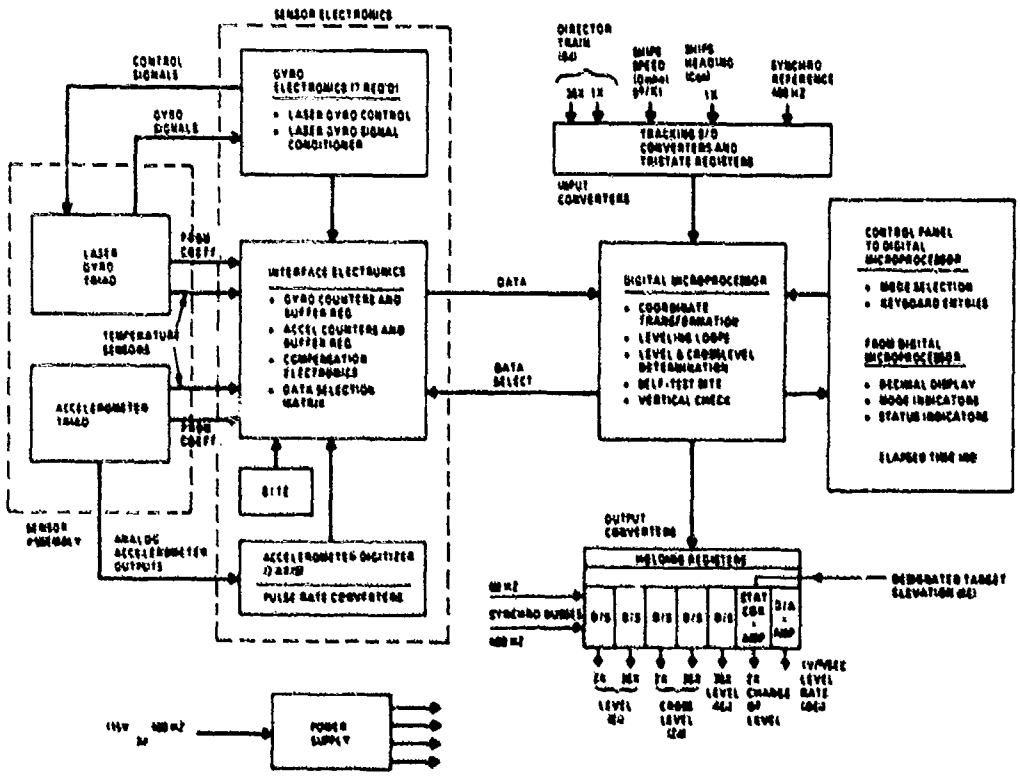

Figure 13. Stable Element Functional Block Diagram

6-24

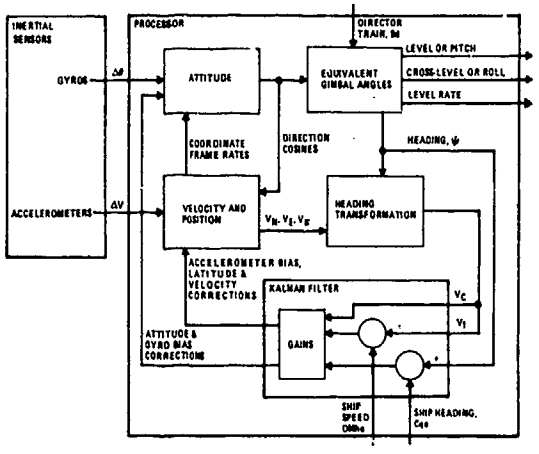

Figure 14. Stable Element Basic Processor Functions

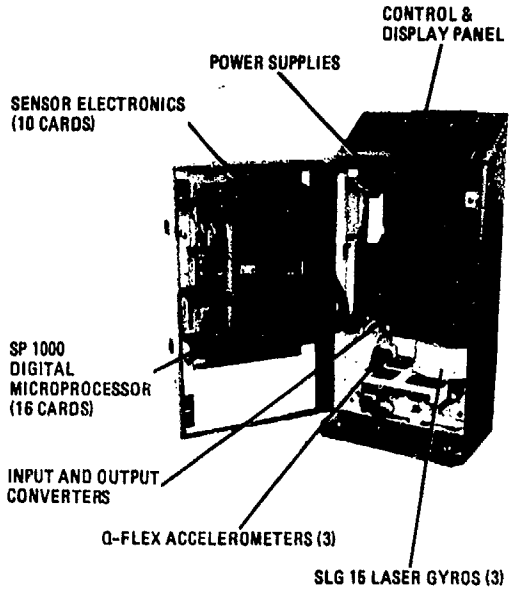

Figure 15. MK-16 MOD-11 Stable Element

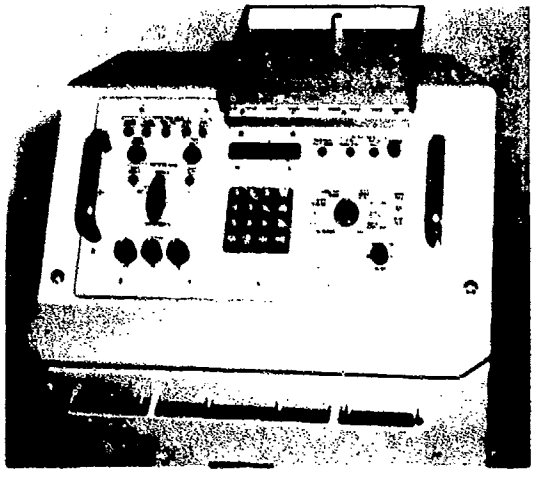

Figure 16. Stable Element Control and Display Panel

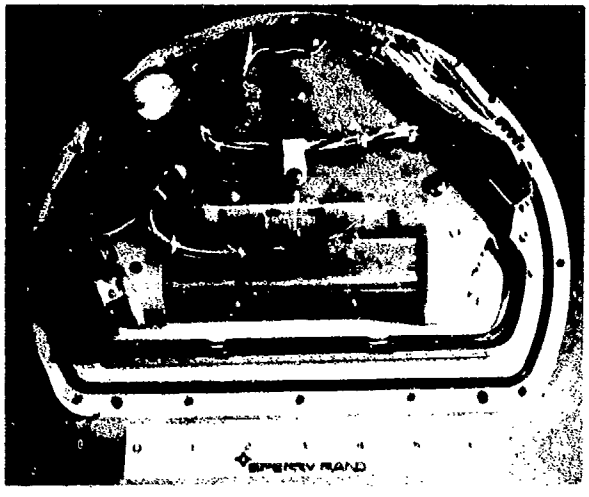

Figure 17. Stable Element Laser Gyro

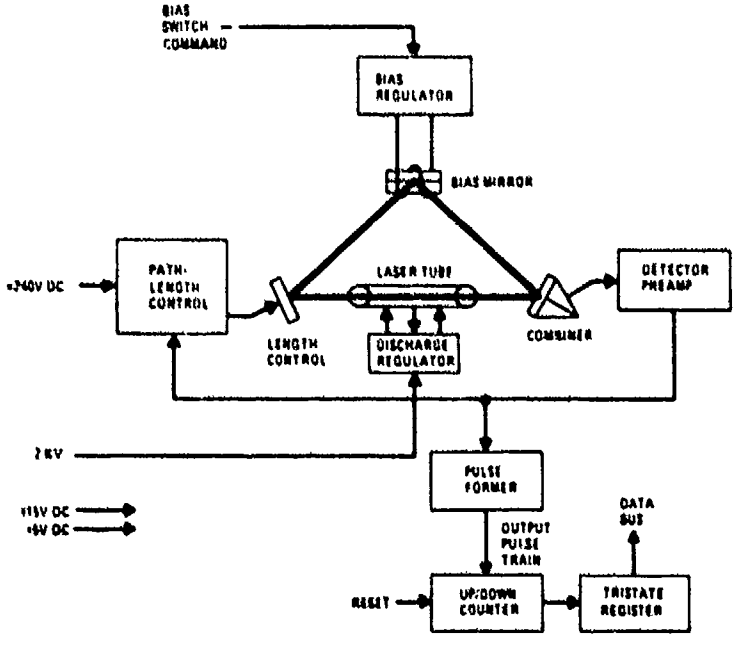

Figure 18. Laser Gyro Electronics Schematic Diagram

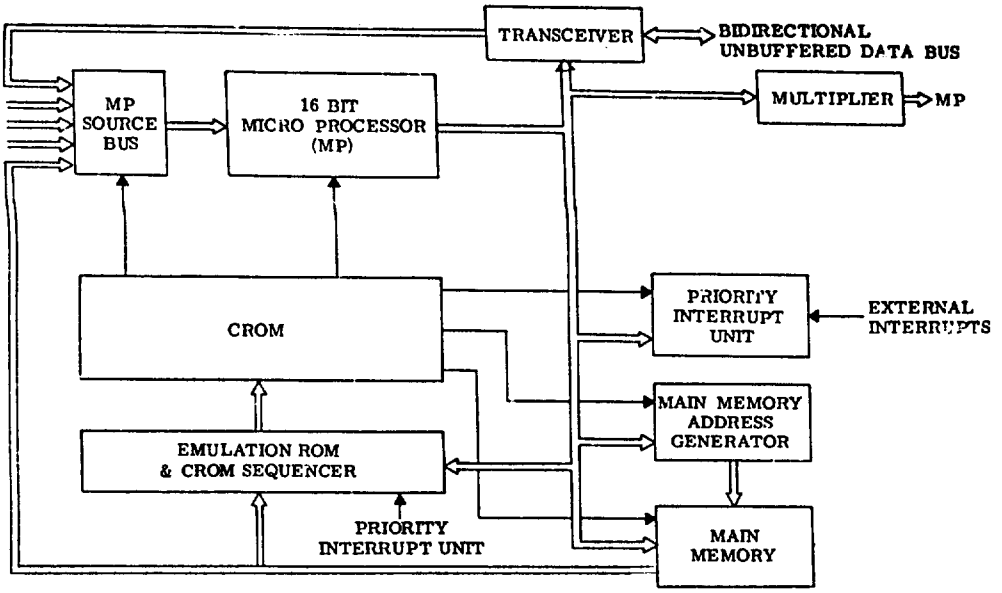

Figure 19. DMP Data and Control

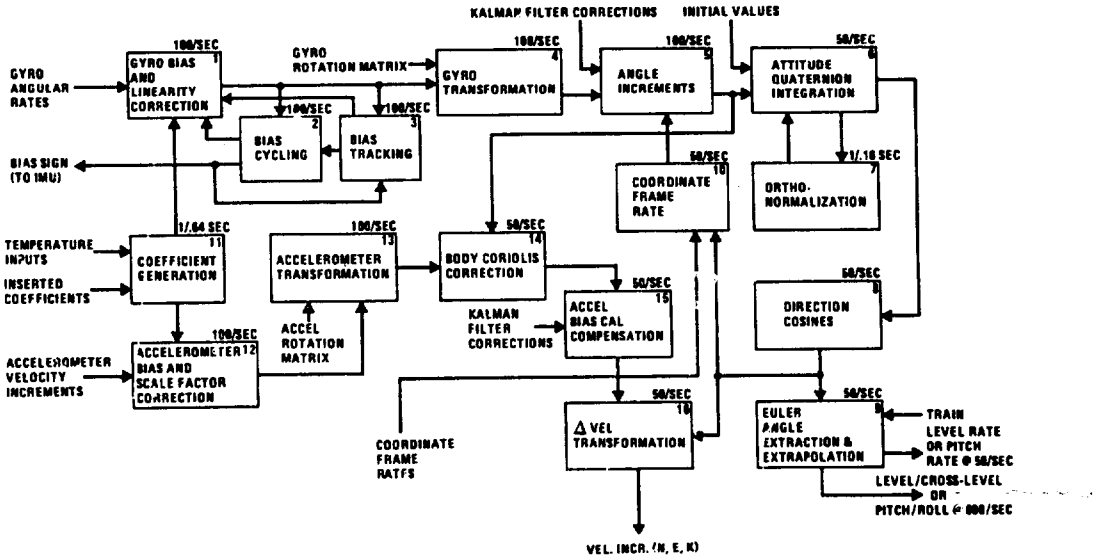

Figure 20. Strapdown Computation Function Flow Diagram

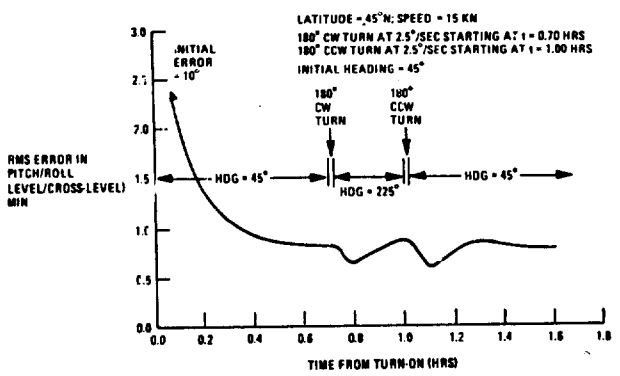

Figure 21. RMS Pitch/Roll Error for Laser

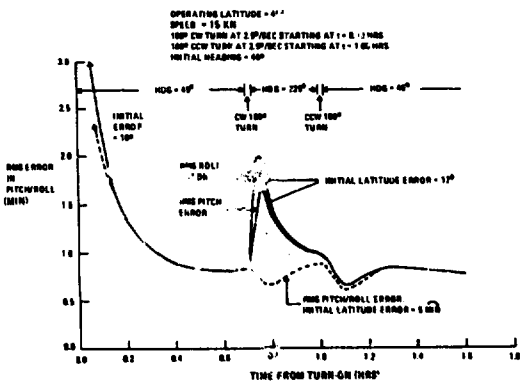

Figure 22. At-Sea Performance-Effects of

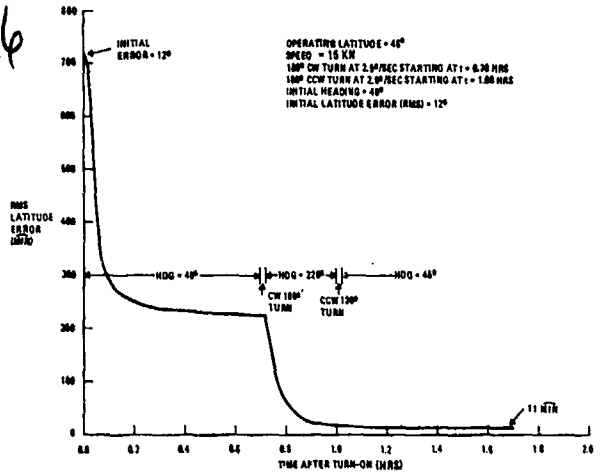

Figure 23. RMS Latitude Error At-Sea Performance

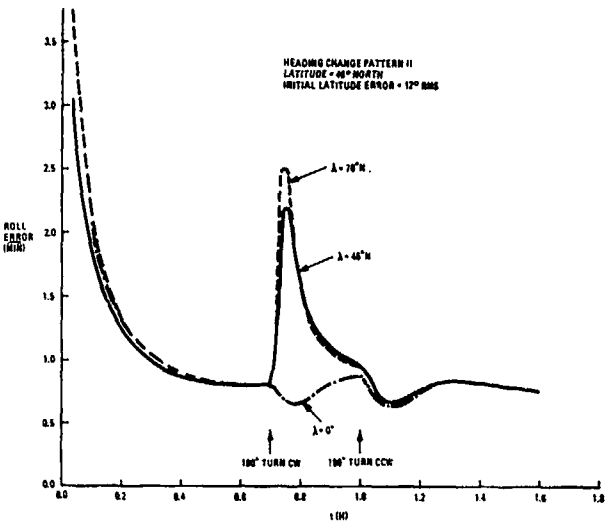

Figure 24. Effect of Operating Latitude on Roll Error

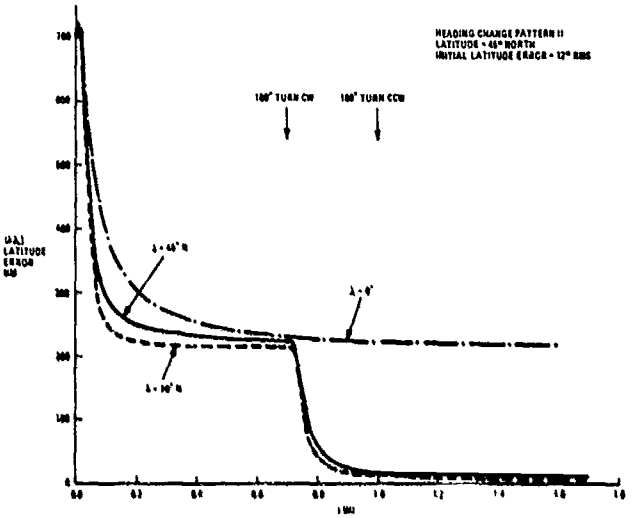

Figure 25. Effect of Operating Latitude on Latitude Error

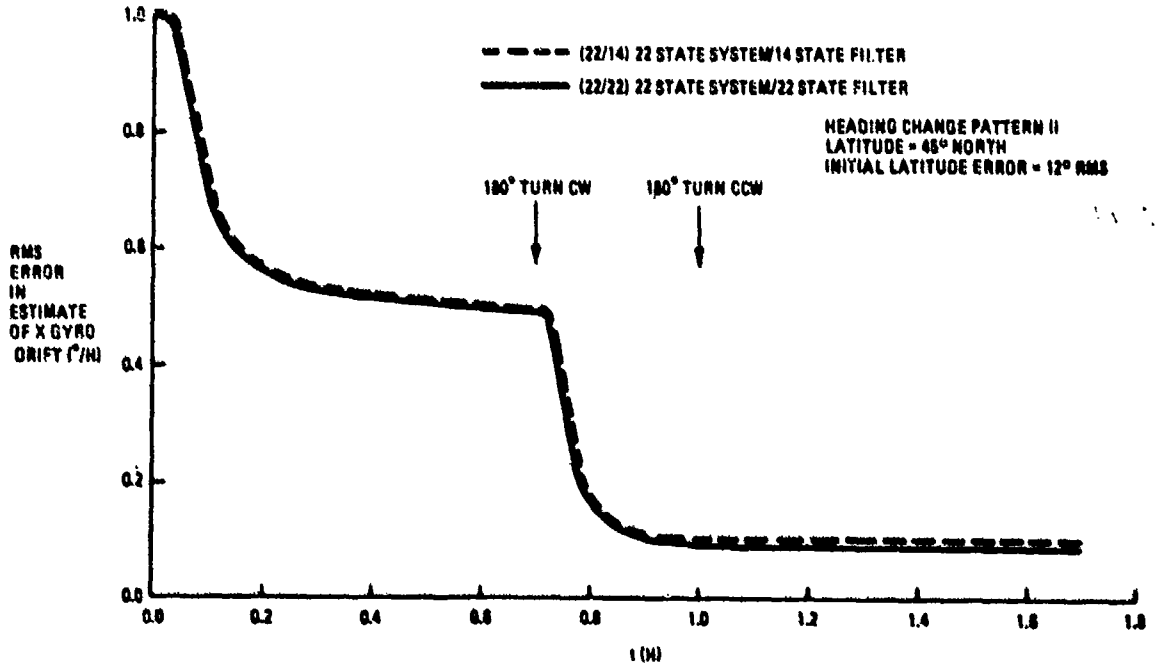

Figure 26. Error in Estimate of "X" Gyro Bias Drift 22/14 Sensitivity Analyses

4. AIRCRAFT INERTIAL NAVIGATOR APPLICATION

Laser gyro strapdown inertial systems are now available that can achieve better than 1 nmi/h pure inertial performance capability, following a self-align gyrocompassing mode. This is the quality standard that is considered suitable for many military aircraft applications. This laser-gyro capability has been conclusively demonstrated by successful flight tests conducted in a C-141 aircraft at Holloman Air Force Base, New Mexico, and at U.S. Air Force bases in Alaska, using a Honeywell LINS system.

This section describes some of the very stringent requirements demanded of a self-aligning 1 nmi/h strapdown laser-gyro navigator, briefly discusses the Honeywell LINS system, and presents the flight-test results achieved.

4.1 Typical Aircraft Mission and Requirements

Aircraft mission profiles differ greatly, of course, between the relatively maneuver-free commercial and military transports on one end of the spectrum and highly maneuverable fighter aircraft on the other end. Generally there is a pretakeoff period for alignment on the ground (or on an aircraft carrier), which should be as short as possible. This is followed by a taxi, a takeoff climb to cruise altitude, a turn to cruise heading, and some cruise flight time to a destination. Various terminal maneuvers may occur at the destination, depending on the nature of the aircraft mission. Some missions will end (land) at the destination; others will turn back to home base.

The strapdown inertial system must level and align itself on the ground and then provide suitable navigation to the destination. Attitude and body rates and accelerations are supplied by the system for flight-control purposes, and velocities are desired in some applications for weapon-delivery requirements.

The following representative mission characteristics will be assumed for analysis simplicity (propagation relationships can be obtained in closed form) to obtain a feeling for the inertial component accuracies required:

(1) 600-knot due East flight at 45° Latitude of about 2 hours duration, following a 20-minute self-alignment on the ground.

(2) Ground alignment is assumed to take place with the aircraft pointing due North (taxiing or turning to East at takeoff)

The latter situation is conservative and helps to justify the assumptions of independence between initial heading offset and East gyro drift, and independence between initial tilts and horizontal accelerometer biases during flight.

The system is leveled and aligned on the ground in a gyrocompassing configuration such as that shown in Figure 27. Many variations of this configuration, including Kalman filtering, may be employed, but this serves to point out the basic action that is taking place. The leveling operation is identical to that described in Section 2.3. A tilt $\delta\theta$ couples a gravity component ($g\,\delta\theta$) into horizontal acceleration, which integrates into a horizontal velocity, which should be zero; any horizontal velocity that is measured is fed back appropriately to correct the tilt and level the system. Any tendency of the horizontal velocity to keep building up is assumed to be caused by angular drifts. The basic gyrocompassing action is the assumption that the East-axis drift (estimated from summed East-axis tilt corrections) is due to an azimuth misalignment $\Delta\theta_K$, which couples the North component of earth rate into the East axis; i.e.

$$\text{East-axis drift} = \Omega_E \cos\lambda \quad \Delta\theta_K$$

Thus, the measured East-axis drift is used to correct azimuth offset instead of gyro bias according to

$$\Delta\theta_K = \frac{\dot{\Delta\theta}_E}{\Omega_E \cos\lambda}$$

Any part of the East-axis drift that is a true gyro bias drift will cause an over compensation of the azimuth offset and yield a resultant heading error

$$\delta\psi = \frac{B_{DE}}{\Omega_E \cos\lambda}$$

It can be shown that gyro white noise random drift, over a smoothing time T, yields a residual bias drift equal to $A_N/\sqrt{T}$. The dominant heading error at the end of a gyrocompassing alignment of time T for a laser gyro strapdown system is thus given by

$$\delta\psi = \frac{B_{DTO} \oplus A_N/\sqrt{T}}{\Omega_E \cos\lambda}$$

where

B_{DTO} = turn-on uncompensated bias drift of the equivalent East-axis gyro

A_N = white noise amplitude random drift of that gyro

In the "steady-state", the alignment loop yields a balance where the residual East axis drift is zeroed out. This balance is such that

$$\delta\psi \quad \Omega_E \cos\lambda - (B_{DTO} \oplus A_N/\sqrt{T}) = 0$$

For the case considered here, with ground align taking place with the aircraft pointing North, there is a residual bias drift on the Y-gyro axis ($B_{DTO} \oplus A_N/\sqrt{T}$), which is balanced against a heading error (incorrect set of direction cosines). Now, when the aircraft turns 90 degrees, the Y gyro (in a strapdown system) becomes a South axis instead of an East axis; the balance no longer exists and both the heading error and the Y-axis drift propagate into navigation errors.

Also, during the self-align mode, a horizontal accelerometer bias error integrates into velocity error, which is interpreted as caused by a tilt. In the steady state, a balance occurs

$$\delta\theta_E = -\frac{A_{BN}}{g}$$

$$\delta\theta_N = \frac{A_{BE}}{g}$$

In a conventional gimballed system, these platform tilts keep balancing out the accelerometer bias errors at all headings, so that navigation errors do not propagate as long as the bias error does not change. However, in a strapdown system, the tilt and the bias error become unbalanced if the vehicle changes heading and both the tilt and the bias error propagate into navigation errors.

In this specific example, when the aircraft turns 90 degrees after the alignment, the originally North (X-axis) axis accelerometer is now East, and the originally East (Y-axis) axis accelerometer is now South.

Depending on the accuracy of the turn-on to turn-on gyro drift repeatability and the accuracy of the white noise random drift, there may be little, if any, gyro drift bias calibration that can take place during the ground alignment. This is especially true for the Z (vertical) gyro axis, where the drift estimation is observed to involve a double "integration". It can be shown that the Z-bias drift estimate in the face of white-noise random drift is given by

$$\hat{B}_{DZ} = \frac{2\sqrt{3}\,A_N}{\Omega_E \cos\lambda \quad T^{3/2}}$$

If this term is greater than the turn-on drift repeatability value, then it does not pay to attempt to calibrate the Z-axis drift. This is generally the case for the Z-axis.

The corresponding estimate for the North-axis drift estimate in the face of white noise is

$$\hat{B}_{DN} = A_N/\sqrt{T}$$

The decision to calibrate the North-axis drift depends on whether this term is less than or greater than the turn-on bias drift repeatability. For the requisite values needed for a 1 nmi/h navigator, these terms are approximately the same order of magnitude, with the required turn-on bias drift being somewhat smaller.

Utilizing the propagation relationships shown in Appendix D for this aircraft mission, the inertial system requirements that are necessary to achieve a 1 nmi/h capability after a 20-minute self-alignment on the ground are listed in Table 7. The position error CEP versus time for an inertial system of this calibre is plotted in Figure 28. It is observed from Table 7 that the laser-gyro requirements

are more than an order of magnitude more stringent for this application than for any of the others discussed in this paper. Gyro scale-factor precision and allowable asymmetry were established to yield negligible rectified drifts (0.002°/h) in the face of 3-degree 0.1-Hz coning motions and perturbations (see Section 2.6 for rectified drift relationships).

6-29

TABLE 7

INERTIAL COMPONENT ACCURACY REQUIREMENTS

TO SATISFY 1 NM/HR SELF-ALIGN CAPABILITY

Gyros	
Turn-On to Turn-On Repeatability	
Horizontal Axes	0.004 °/h
Vertical Axis	0.01 °/h
Random White-Noise Drift	0.004 $^{\circ}/\sqrt{h}$
Scale-Factor Repeatability, Stability	10 ppm
Scale-Factor Asymmetry	1 ppm
Misalignment Repeatability, Stability	6 $\widehat{\text{sec.}}$
Accelerometers	
Bias Repeatability, Stability	100 μg
Scale-Factor Repeatability, Stability	500 ppm
Misalignment Repeatability, Stability	0.5 mrad

For the normal aircraft application, it is preferable to mount the accelerometers along the principal body axes (not skewed), so that the "horizontal" accelerometers do not see a large component of gravity. For the case where the accelerometer axes are skewed to the principal body axes, each accelerometer measures a large component of g, and accelerometer scale-factor error causes an equivalent horizontal bias error. This will impose a scale-factor requirement that is much tighter than that needed to measure the velocity change during takeoff.

If the aircraft were to make many 360-degree turns or loops or roll-overs in the same direction, the laser gyro scale-factor errors would have to be tightened up further. However, it is unlikely that such a maneuver pattern would take place, even in fighter aircraft.

4.2 Specific System Synthesis

The Honeywell developmental laser-gyro system that was flight tested as an aircraft inertial navigator is designated LINS-0 and is described in Reference 6. A brief description of this system, excerpted from the reference, is provided in this subsection. This development system contained several growth flexibility features, including provisions for a fourth skewed laser gyro and additional computer processing to enable redundant operations. Honeywell has been developing various other LINS packaging configurations that are more compact than the LINS-0 system.

Figure 29 defines the black-box assemblies that comprise the LINS-0 configuration. The hardware consists of an inertial sensor assembly (ISA), a strapdown navigation computer (SNC), separate alterable memory units for the computer, a control/display unit (CDU), a computer control unit (CCU), and a non-interruptable power supply that enables system operation through aircraft power switchover transients from standby to primary power.

The ISA contains three orthogonal (principal body axes) GG1300 single-axis laser gyros (with space for a fourth gyro skewed relative to the other three), and three Systron Donner 4841 accelerometers.

Because the gyros and accelerometers are thermally insensitive, the ISA is operated without a heater. Due to the low power dissipation in the ISA (50 W), ducted air cooling is not required below 130°F ambient.

Extensive laboratory tests of the GG1300 laser gyro and the 4841 accelerometer demonstrate the requisite performance characteristics for a self-aligning 1 nmi/h aircraft navigator as listed in Table 7.

4.30

The Honeywell HDC-301 metal-oxide-semiconductor large-scale integrated circuit (MOS LSIC) processor is used in the SNC to perform the arithmetic functions. The HDC-301 is a military-qualified 16-bit parallel digital general-purpose processor with double-precision capability and basic instruction times of 3.8 microseconds for add and 16 microseconds for multiply. It is packaged on a single 6-inch square multilayer plug-in card.

The SNC also includes an ISA interface, a CCU interface for rapid computer program changes, and a CDU interface for pilot-system communications. For the Holloman flight tests, an interface was included for a barometric altimeter input and a flight recorder output. The SNC contains provisions for a second HDC-301 processor and additional input/output card slots.

The LINS software block diagram is depicted in Figure 30. The attitude update incorporates a fifth-order direction cosine algorithm updated at 40 Hz to 32-bit precision in conjunction with a 160-Hz coning compensation algorithm to provide the combined equivalent of 160-Hz total attitude update rate.

The position/velocity update is based on azimuth wander geodetic vertical navigation coordinates for an all-earth capability with an ellipsoidal earth model. Altitude stabilization is accomplished with a third-order blending filter using barometric-altitude input data. Compensation is included for angular rotation during acceleration transformation, accelerometer assembly size effect, and accelerometer misalignment, scale factor, and bias error.

4.3 LINS-0 Flight Test Results

The following discussion of LINS-0 flight test results is excerpted from Reference 6.

4.3.1 Holloman Test Conditions

The LINS engineering hardware was delivered to Holloman Air Force Base on 14 April 1975. Final system calibrations were completed on 16 April 1975. From 16 April 1975 until completion of the Holloman test program on 14 July 1975, no system calibrations were performed. Over 268 operating hours were accumulated on the system during the test period (including 82 aircraft navigation operating hours and 65 aircraft navigation flight hours) with no system failures.

All system tests were performed without temperature controls. For the C-141 flights, approximately 40°F temperature variations were experienced during the tests (high aircraft internal temperature at system turn-on on the ground followed by cool-down to 70°F or lower after the engines were started and aircraft airconditioning systems began operating).

All system test runs were initiated from a cold condition (preceded by at least 3 hours of system off time). All system runs entered the navigate mode after 20 minutes from turn-on (10 minutes for warmup and 10 minutes for alignment). An exception was the eighth flight-test run where an extended warmup period (50 minutes) was needed for memory-loading procedures.

All system alignments were performed inertially with no a priori knowledge of coarse heading. No external optical alignment devices were used in alignment sequence, and the only external input to the system during the test program was barometric altitude provided in the C-141 for altitude channel stabilization.

4.3.2 Holloman Flight Tests

Flight testing of the LINS system was conducted at Holloman Air Force Base in a C-141 aircraft during the period from 14 May to 27 June 1975. A total of 13 flight tests were carried out at three Air Force facilities: Holloman Air Force Base (Alamagordo, New Mexico); Elmendorf Air Force Base (Anchorage, Alaska); and Eielson Air Force Base (Fairbanks, Alaska). Table 8 gives a general description of the 13 flight-test profiles.

Navigational errors for the LINS system were established on each flight by periodic comparisons (typically about once every 5 minutes) of the navigator's indicated position and the known position of a checkpoint being traversed. This provided a set of "quick-look" results, which was subsequently refined using a photograph of each checkpoint as it was traversed. The photograph is necessary because the checkpoints are not traversed exactly. The adjusted checkpoint position errors also provide the data base for deriving LINS velocity-error histories for each flight by using a Holloman data-smoothing program.

The thirteenth flight test did not yield valid position reference data for comparison due to a procedural problem on the C-141.

TABLE 8. LINS FLIGHT TEST PROFILES

Flight Test	Location	Align Orientation	Flight Path	Flight Time (Hrs)	Nav Time (Hrs)
1	Holloman (N. M.)	N	N-S	2.83	4.17
2	Holloman (N. M.)	N	W-E	6.13	7.67
3	Holloman (N. M.)	N	N-S	2.97	4.17
4	Holloman (N. M.)	N	W-E	6.05	8.00
5	Holloman (N. M.) to Elmendorf (ALAS.)	N	N/W	9.17	10.37
6	Elmendorf (ALAS.)	E	N-S	3.00	4.25
7	Elmendorf (ALAS.)	E	N-S	3.18	4.67
8	Elmendorf (ALAS.)	N	W-E-W-E	7.13	8.00
9	Eielson (ALAS.)	N	W-E	2.93	4.33
10	Eielson (ALAS.)	N	W-E	2.85	3.92
11	Eielson (ALAS.)	N	N-S-N-S	6.98	8.33
12	Eielson (ALAS.) to Holloman (N. M.)	N	S/E	10.23	11.50
13	Holloman (N. M.)	N	Circling	1.35	3.00
	Summary Data	Total Hours		64.80	82.38

4.3.3 Flight Test Results

The radial position error ensemble for the first 12 flights are depicted in Figure 31. Several of these missions involved an alignment at one heading and flight at a heading 90 degrees apart, with various turn maneuvers during flight. The results clearly demonstrate a 1 nm/h navigation performance capability.

4.4 Aided Aircraft Navigation Systems

With the availability of low-cost radio navigation aids (such as Omega, Loran, Tacan, etc.), many aircraft applications do not require a precision 1 nm/h pure inertial navigation capability. These "continuous" position-fix devices can be employed to update, damp, and calibrate the inertial system, thus enabling much looser inertial-component accuracies and possibly overall lower-cost equipment. This will especially be true when the Global Positioning System navigational satellite system becomes operational.

One example of an aided strapdown laser-gyro system is described in Reference 7. This is where a simple Differential-Omega receiver is incorporated in the aircraft and optimally mixed with the strapdown inertial system. The simulation analysis results presented in Reference 7 indicate that the performance capabilities of the SLIC-15 IMU (Tables 2 and 3) are satisfactory to meet typical mission requirements.

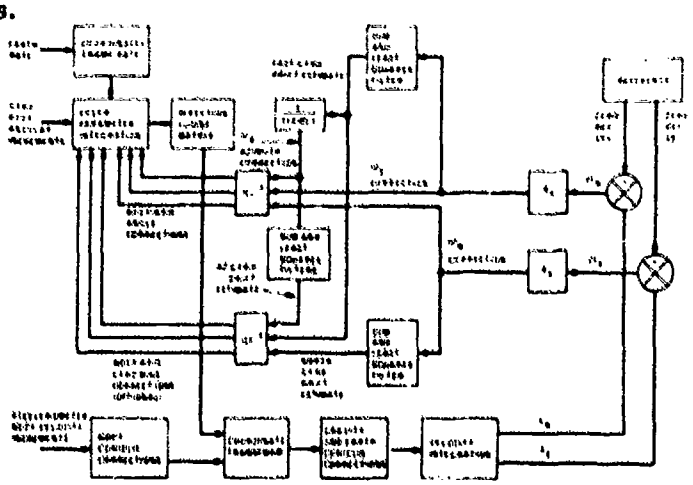

Figure 27. Leveling, Gyrocompassing Ground-Align Configuration.

6-32

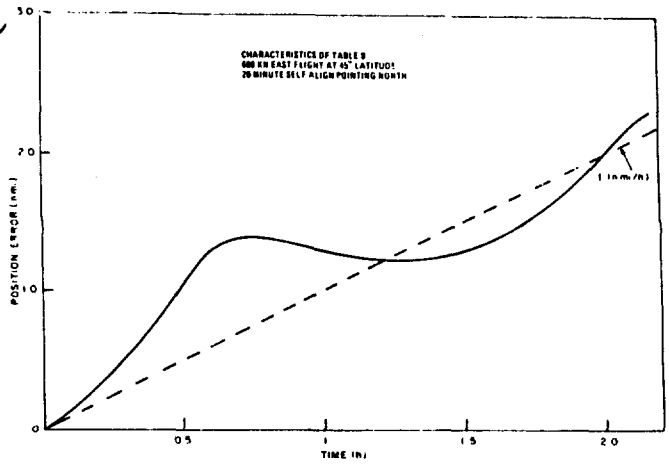

Figure 28. CEP Position Error for Laser Gyro Strapdown Navigation

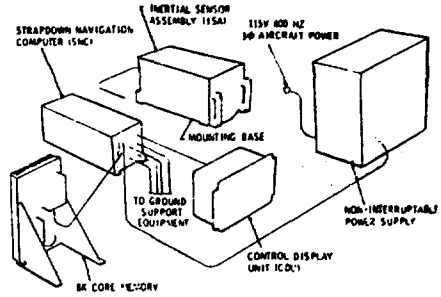

Figure 29. LINS-O Engineering Hardware

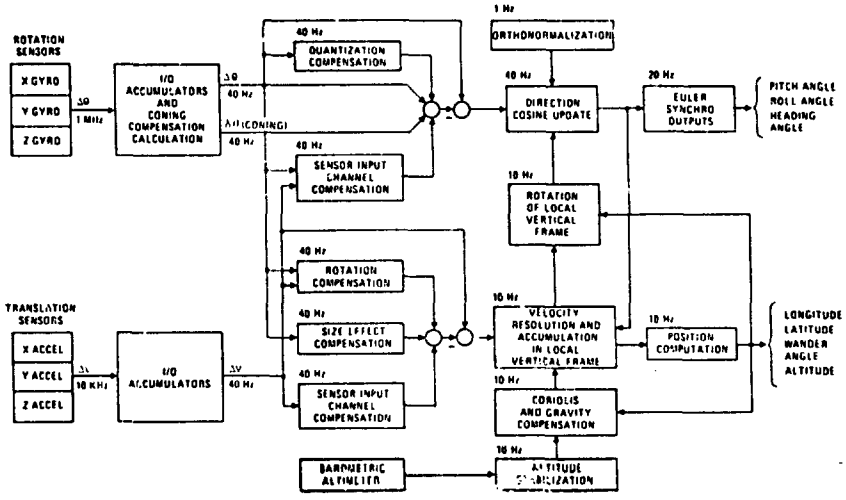

Figure 30. LINS Software Flow Diagram

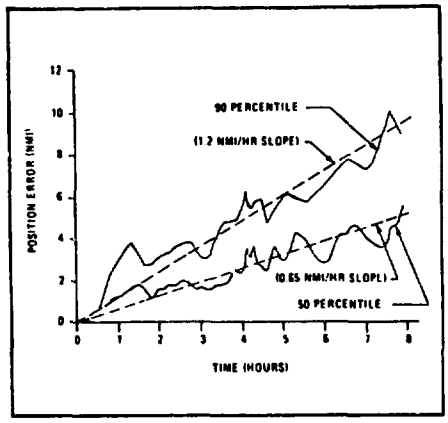

Figure 31. Fifty and Ninety Percentile Flight Test Radial Position Errors as a Function of Navigation Time

5. CONCLUSIONS

It is clear from the test results and other material presented in this paper that laser-gyro strapdown systems are now available that can satisfy each of the applications discussed as well as a broad spectrum of additional applications with performance requirements within the range that has been covered here. Furthermore, a selection of laser-gyro systems, having different size, performance, and cost factors, are available for tradeoff to yield the most cost-effective system for any given application.

Technology improvements are continuously being made in both laser gyros and microprocessors that will widen the scope of applications even further.

REFERENCES

1. Morrison, R., Dr. E. Levinson, and R. McAdory, "The SLIC-15 Laser Gyro IMU For Midcourse Missile Guidance" Institute of Navigation National Aerospace Symposium, Warminster, Pennsylvania 27-28 April 1976, Proceedings pp. 59-68.

2. Perlmutter, L., J. Kraemer, and N. Roessler, "Strapdown Inertial Sensor Requirements For Tactical Guidance" NAECON 1977, 17-19 May 1977, Proceedings pp. 424-432.

3. Mueller, C., R. Phelps, and R. Scheidenhelm, "Tactical Guidance Requirements For Strapdown Inertial" NAECON 1977, 17-19 May 1977, Proceedings pp. 433-440.

4. Morrison, R., Dr. E. Levinson, and B. Bryant, Jr. "The SLIC-7 Laser Gyro Inertial Guidance System" NAECON 1977, 17-19 May 1977, Proceedings pp. 1045-1061.

5. Thomson, K., Dr. B. Schwartz, C. San Giovanni, and E. Young, "The Laser Gyro MK 16 Mod 11 Shipboard Stable Element", accepted for publication in NAECON 1978 Proceedings, May 1978.

6. Savage, P., and M. Ignagni, "Honeywell Laser Inertial Navigation System (LINS) Test Results", Ninth Data Exchange for Inertial Systems, 18-19 November 1975, Proceedings pp. 37-48.

7. San Giovanni, C., "Performance of a Differential Omega-Laser Gyro Strapdown Aircraft Navigator", accepted for presentation at NAECON 1978, May 1978.

ACKNOWLEDGMENT

The laser-gyro systems described in this paper are the result of contributions made by many individuals at Sperry Gyroscope, Honeywell, and Lockheed and by personnel at: the U.S. Air Force Avionics Laboratory, Wright Patterson Air Force Base; the U.S. Air Force Armament Development and Test Center, Eglin Air Force Base; the Central Inertial Guidance Test Facility, Holloman Air Force Base; the Naval Weapons Center, China Lake; the Naval Ordnance Station, Louisville; the U.S. Army Missile Command; and NASA, Marshall. Acknowledgment and appreciation is hereby given to all those people.

The author wishes to particularly note the contributions made by Dr. Bernard Schwartz and Carlo P. San Giovanni, Jr., of Sperry Gyroscope, who were instrumental in the generation of many of the algorithms, analyses, and simulations presented herein.

APPENDIX A

SIMPLIFIED SIX-STATE ALIGN/CALIBRATE KALMAN FILTER

The six dominant states that are modelled in the suboptimal Kalman Filter are:

$X_1 = \Delta\theta_E$; misalignment (tilt) about the nominally East axis

$X_2 = \Delta\theta_N$; misalignment (tilt) about the nominally North axis

$X_3 = \Delta\theta_K$; azimuth misalignment about the nominally vertical-down axis

$X_4 = \omega_{DX}$; gyro bias drift about the body X-axis

$X_5 = \omega_{DY}$; gyro bias drift about the body Y-axis

$X_6 = \omega_{DZ}$; gyro bias drift about the body Z-axis

One further simplifying assumption is that the velocity difference occurring over a 5-second sample period is predominantly caused by incorrect transformation of accelerations, caused by the direction-cosine matrix equivalent misalignments. It can readily be shown that

$$\begin{bmatrix} 0 & -V_k & V_n \\ V_k & 0 & -V_e \end{bmatrix} \begin{bmatrix} \Delta\theta_E \\ \Delta\theta_N \\ \Delta\theta_K \end{bmatrix} = \begin{bmatrix} \Delta V_e \\ \Delta V_n \end{bmatrix} \tag{A-1}$$

where

V_n, V_e, V_k = velocity changes in five seconds along N, E, K axes.

This is identical to a tilt on a gimballed platform causing a horizontal accelerometer to measure a component of gravity and an azimuth misalignment cross-coupling horizontal acceleration.

Since V_e and V_n are the measurements being made by the Kalman Filter, placing Equation (A-1) into the conventional measurement form

$$Z(n) = H(n)\, X(n) + \gamma(n)$$

Then the measurement matrix of this Kalman Filter is observed to be

$$[H] = \begin{bmatrix} 0 & -V_k & V_n & 0 & 0 & 0 \\ V_k & 0 & -V_e & 0 & 0 & 0 \end{bmatrix} \tag{A-2}$$

A second simplifying assumption is that the misalignments are increased predominantly due to constant gyro bias drifts (except for white noise), and that the gyro bias drift states are constant (except for white noise). Thus

$$\Delta\theta_E\,(n+1) = \Delta\theta_E\,(n) + \int_n^{n+1} \omega_{DE}\, dt \tag{A-3}$$

$$\Delta\theta_N\,(n+1) = \Delta\theta_N\,(n) + \int_n^{n+1} \omega_{DN}\, dt \tag{A-4}$$

$$\Delta\theta_K\,(n+1) = \Delta\theta_K\,(n) + \int_n^{n+1} \omega_{DK}\, dt \tag{A-5}$$

Now gyro bias drifts along N, E, K axes are related to gyro bias drifts along body X, Y, Z axes through the direction cosine matrix according to

$$\begin{bmatrix} \omega_{DN} \\ \omega_{DE} \\ \omega_{DK} \end{bmatrix} = \begin{bmatrix} C_{11} & C_{12} & C_{13} \\ C_{21} & C_{22} & C_{23} \\ C_{31} & C_{32} & C_{33} \end{bmatrix}_B^E \begin{bmatrix} \omega_{DX} \\ \omega_{DY} \\ \omega_{DZ} \end{bmatrix} \tag{A-6}$$

and

$$\int \omega_{DE}\, dt = \omega_{DX} \int C_{21}\, dt + \omega_{DY} \int C_{22}\, dt + \omega_{DZ} \int C_{23}\, dt \qquad \text{(A-7)}$$

$$\int \omega_{DN}\, dt = \omega_{DX} \int C_{11}\, dt + \omega_{DY} \int C_{12}\, dt + \omega_{DZ} \int C_{13}\, dt \qquad \text{(A-8)}$$

$$\int \omega_{DK}\, dt = \omega_{DX} \int C_{31}\, dt + \omega_{DY} \int C_{32}\, dt + \omega_{DZ} \int C_{33}\, dt \qquad \text{(A-9)}$$

calling the

$$\int C_{ij}\, dt = \ell_{ij}$$

substituting in equations (A-3) through (A-5), and noting that

$$\omega_{Di}\,(n+1) = \omega_{Di}\,(n) \;\; ; \;\; i = X, Y, Z$$

the following transition matrix for this Kalman Filter is obtained

$$\left[\Phi\right] = \begin{bmatrix} 1 & 0 & 0 & \ell_{21} & \ell_{22} & \ell_{23} \\ 0 & 1 & 0 & \ell_{11} & \ell_{12} & \ell_{13} \\ 0 & 0 & 1 & \ell_{31} & \ell_{32} & \ell_{33} \\ 0 & 0 & 0 & 1 & 0 & 0 \\ 0 & 0 & 0 & 0 & 1 & 0 \\ 0 & 0 & 0 & 0 & 0 & 1 \end{bmatrix} \qquad \text{(A-10)}$$

Only the integrals of the direction-cosine coefficients over the 5-second sample period are required for the transition matrix.

The conventional Kalman Filter extrapolation, gain computation, and updates are then performed to yield the misalignment and gyro drift corrections. These matrix equations are greatly simplified because of the zero partitions of both the Measurement Matrix and the Transition Matrix.

6-36

APPENDIX B

BODY CORIOLIS CORRECTION DISCUSSION AND DERIVATION

B.1 CORIOLIS BODY ROTATIONAL CORRECTION DISCUSSION

Because of the pulse-rate conversion of the accelerometer measurements into digital pulses, and the sampling nature of the computer input, one does not obtain instantaneous acceleration measurements, but rather discrete velocity increments (each of which is the integral of acceleration over some time period).

If the body simultaneously rotates during this integration interval, then certain rotational correction terms must be subtracted from the velocity increments to arrive at a set of velocity increments along body axes which, when transformed by the direction cosine attitude matrix, will yield proper velocity increments with respect to an earth reference frame. (It should be noted that the techniques employed here eventually result in the identical velocity increments that would be obtained from a set of three accelerometers mounted on a stabilized earth reference platform. That is, the normal earth-frame Coriolis corrections must still be applied in the navigation software module.)

The need for these body rotational corrections can be readily illustrated by the following simple example.

Assume a body on the earth that is rotating at a constant rate ω_y about the body y-axis (which is horizontal to the right, body is pitching upward), but not translating. In the sketch below, $\hat{x}$ is initially forward and pointing North along $\hat{n}$, and $\hat{z}$ is initially down along the earth vertical axis, $\hat{k}$. A very short time later, the picture is as shown in Figure B1.

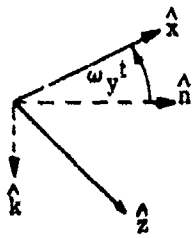

Figure B1. Example Definition of Axes

The specific force is -g in the $\hat{k}$ direction

The specific force measured by the $\hat{x}$ accelerometer is g sin $\omega_y t$, and that measured by the $\hat{z}$ accelerometer is -g cos $\omega_y t$. The $\hat{y}$ accelerometer reads 0.

Over a period ΔT, the x-axis velocity increment from the x-axis accelerometer is

$$\Delta V_1 = \int_0^{\Delta T} g \sin \omega_y t \, dt = \frac{g}{\omega_y} \left[1 - \cos \omega_y \Delta T \right]$$

Similarly, the z-axis velocity increment is:

$$\Delta V_3 = \int_0^{\Delta T} -g \cos \omega_y t \, dt = \frac{g}{\omega_y} \left\{ - \left[\sin \omega_y \Delta T \right] \right\}$$

Now it is observed from Figure B1 that the direction-cosine matrix relating the body axes to the earth reference axes is given by

$$\left[C \right]_B^E = \begin{bmatrix} \cos \omega_y t & 0 & \sin \omega_y t \\ 0 & 1 & 0 \\ - \sin \omega_y t & 0 & \cos \omega_y t \end{bmatrix}$$

The value of the C matrix at $t = \Delta T$ is

$$\left[C \right] = \begin{bmatrix} \cos \omega_y \Delta T & 0 & \sin \omega_y \Delta T \\ 0 & 1 & 0 \\ - \sin \omega_y \Delta T & 0 & \cos \omega_y \Delta T \end{bmatrix}$$

If one were to transform the uncorrected velocity increments by this C matrix, the following velocity increments along North, East, and vertical would result:

$$\Delta V_n = \frac{g}{\omega_y}\left\{ \cos \omega_y \Delta T \left[1 - \cos \omega_y \Delta T\right] + \sin \omega_y \Delta T \left[-\sin \omega_y \Delta T\right]\right\}$$

or

$$\Delta V_n = \frac{g}{\omega_y}\left\{ \cos \omega_y \Delta T - 1\right\}$$

$$\Delta V_e = 0$$

$$\Delta V_k = \frac{g}{\omega_y}\left\{ -\sin \omega_y \Delta T \left[1 - \cos \omega_y \Delta T\right] + \cos \omega_y \Delta T \left[- \sin \omega_y \Delta T\right]\right\}$$

or

$$\Delta V_k = -\frac{g}{\omega_y} \sin \omega_y \Delta T$$

The exact values for the earth-referenced velocity increments should be

$$\Delta V_n = 0, \Delta V_e = 0, \Delta V_k = -g\Delta T$$

Expanding

$$\cos \omega_y \Delta T \cong 1 - \frac{(\omega_y \Delta T)^2}{2} + \ldots$$

and

$$\sin \omega_y \Delta T \cong \omega_y \Delta T - \frac{\omega_y^3 \Delta T^3}{6} + \ldots$$

it is observed that the error in ΔV_n is approximately

$$g\omega_y \frac{\Delta T^2}{2}$$

and the error in ΔV_k is approximately

$$g\omega_y^2 \frac{\Delta T^3}{6}$$

The equivalent acceleration errors are:

$$\delta a_n = \frac{1}{2} g\omega_y \Delta T$$

$$\delta a_k = \frac{1}{6} g\omega_y^2 \Delta T^2$$

If ω_y = 1 rad/sec and ΔT = 1/25 second,

$$\delta a_n = 0.02\ g$$

$$\delta a_k = 270\ \mu g$$

It is obvious that rotational corrections are required. Furthermore, since fairly higher acceleration levels may be encountered, correctional terms up to and including the third order are necessary. The rotation correction terms to the third order are derived in Section B2 and are summarized in Figure B2.

The previous simple example will now again be employed, using these correction terms. This will confirm that the overall approach presented here is a proper one. (Other simple examples, such as a centrifuge case, or a body on a rotating earth, have been tried out and the correction terms have been shown to be proper for those cases also.)

Over the first half-period, the x-axis velocity increment from the x-axis accelerometer is

$$\delta V_{11} = \int_0^{\Delta T/2} g \sin \omega_y t\, dt = \frac{g}{\omega_y}\left[1 - \cos \frac{\omega_y \Delta T}{2}\right]$$

$$\cong \frac{1}{8} g\, \omega_y \Delta T^2 + \text{fourth-order terms and higher}$$

$$\Delta V_{xc} = \Delta V_1 - \frac{1}{2}(\delta\theta_y \Delta V_z - \delta\theta_z \Delta V_y) + \frac{1}{6}\delta\theta_y(\delta\theta_x \Delta V_y - \delta\theta_y \Delta V_x - \Delta a_z)$$
$$- \frac{1}{6}\delta\theta_z(\delta\theta_z \Delta V_x - \delta\theta_x \Delta V_z - \Delta a_y) - \frac{1}{3}(\Delta\omega_y \Delta V_z - \Delta\omega_z \Delta V_y)$$

$$\Delta V_{yc} = \Delta V_2 - \frac{1}{2}(\delta\theta_z \Delta V_x - \delta\theta_x \Delta V_z) + \frac{1}{6}\delta\theta_z(\delta\theta_y \Delta V_z - \delta\theta_z \Delta V_y - \Delta a_x)$$
$$- \frac{1}{6}\delta\theta_x(\delta\theta_x \Delta V_y - \delta\theta_y \Delta V_x - \Delta a_z) - \frac{1}{3}(\Delta\omega_z \Delta V_x - \Delta\omega_x \Delta V_z)$$

$$\Delta V_{zc} = \Delta V_3 - \frac{1}{2}(\delta\theta_x \Delta V_y - \delta\theta_y \Delta V_x) + \frac{1}{6}\delta\theta_x(\delta\theta_z \Delta V_x - \delta\theta_x \Delta V_z - \Delta a_y)$$
$$- \frac{1}{6}\delta\theta_y(\delta\theta_y \Delta V_z - \delta\theta_z \Delta V_z - \Delta a_x) - \frac{1}{3}(\Delta\omega_x \Delta V_y - \Delta\omega_y \Delta V_x)$$

$$\Delta V_i = (\delta V_{i1} + \delta V_{i2});\ \delta\theta_j = (3\,\delta\theta_{i1} - \delta\theta_{i2});\ \Delta V_j = (3\,\delta V_{i1} - \delta V_{i2})$$
$$\Delta\omega_j = 4(\delta\theta_{i2} - \delta\theta_{i1});\ \Delta a_j = 4(\delta V_{i2} - \delta V_{i1})$$
$$j = x, y, z \text{ for } i = 1, 2, 3$$

Figure B2. Coriolis Rotational Correction

Over the second half-period

$$\delta V_{12} = \int_{\Delta T/2}^{\Delta T} g \sin \omega_y t\, dt = \frac{g}{\omega_y}\left[\cos\left(\frac{\omega_y \Delta T}{2}\right) - \cos(\omega_y \Delta T)\right]$$
$$\simeq \frac{3}{8} g\, \omega_y \Delta T^2 + \ldots.$$

Similarly

$$\delta V_{31} = \int_{0}^{\Delta T/2} -g \cos \omega_y t\, dt = \frac{g}{\omega_y}\left[-\sin \omega_y \frac{\Delta T}{2}\right]$$
$$\simeq -g\frac{\Delta T}{2} + \frac{1}{48} g\, \omega_y{}^2 \Delta T^3 + \ldots.$$

and

$$\delta V_{32} = \int_{\Delta T/2}^{\Delta T} -g \cos \omega_y t\, dt = \frac{g}{\omega_y}\left[\sin\left(\omega_y \frac{\Delta T}{2}\right) - \sin(\omega_y \Delta T)\right]$$
$$\simeq -g\frac{\Delta T}{2} + \frac{7}{48} g\, \omega_y{}^2 \Delta T^3 + \ldots.$$

also $\bar{\omega} = \omega_y \hat{y}$. Over the first half-period.

$$\delta\theta_{21} = \omega_y \frac{\Delta T}{2}$$

and over the second half period

$$\delta\theta_{22} = \omega_y \frac{\Delta T}{2}$$

also $\delta\theta_1$, $\delta\theta_3$, and δV_2 are all equal to zero. Substituting these δ relations into Figure B2

$$\delta\theta_y = \omega_y \Delta T$$
$$\delta\theta_x = \delta\theta_z = 0$$
$$\Delta V_x = 0$$
$$\Delta V_z = -g\Delta T - \frac{1}{12} g\, \omega_y{}^2 \Delta T^3$$
$$\Delta V_y = 0$$

$$\Delta V_1 = \frac{1}{2} g\,\omega_y \Delta T^2 \qquad \Delta\omega_x = \Delta\omega_y = \Delta\omega_z = 0$$

$$\Delta V_3 = -g\,\Delta T + \frac{1}{6} g\,\omega_y{}^2\,\Delta T^3 \qquad \Delta a_x = g\omega_y \Delta T^2$$

$$\Delta V_2 = \Delta a_y = 0 \qquad \Delta a_z = \frac{1}{2} g\omega_y{}^2\,\Delta T^3$$

Substituting into Figure B2 relationships, the corrected velocity increments after applying the Coriolis rotational corrections to ΔV_1, ΔV_2, and ΔV_3, are

$$\Delta V_{xc} = g\,\omega_y \Delta T^2 + \text{fourth-order terms and higher}$$

$$\Delta V_{yc} = 0$$

$$\Delta V_{zc} = -g\Delta T + \frac{1}{2} g\,\omega_y{}^2\,\Delta T^3 + \text{higher order terms}$$

Transforming by the C matrix

$$\Delta V_n = g\,\omega_y \Delta T^2 \cos(\omega_y \Delta T) - \left(g\,\Delta T + \frac{1}{3} g\,\omega_y{}^2\,\Delta T^3\right) \sin(\omega_y \Delta T)$$

which for small ΔT, yields

$$\Delta V_n = 0 + \text{fourth-order and higher terms}$$

$$\Delta V_e = 0$$

$$\Delta V_k = -g\,\omega_y \Delta T^2 \sin(\omega_y \Delta T) - (g\,\Delta T - \frac{1}{2} g\,\omega_y{}^2\,\Delta T^3) \cos(\omega_y \Delta T)$$

or

$$\Delta V_k = -g\Delta T + \text{fourth order and higher terms}$$

Thus, the proper velocity increments along the earth-referenced axes are obtained. It should be noted that the $[C]$ matrix employed at the end of the same ΔT sampling interval (within the same computing cycle) is the proper value of $[C]$ to employ. There is no need for any extrapolations on $[C]$ for the transformation of the velocity increments.

B.2 CORIOLIS ROTATIONAL CORRECTION COMPUTATION DERIVATION

If E is the reference or earth frame, then at any time

$$\left[A_E\right] = \left[C\right]\left[A_B\right]$$

where the brackets refer to matrix multiplication, A_E is the inertial acceleration in the E frame, and A_B is the inertial acceleration in the body frame. Then, the velocity change $\left[\Delta V_E\right]$ in the integration time ΔT is

$$\left[\Delta V_E\right] = \int_0^{\Delta T} \left[C\right]\left[A_B\right] dt$$

In order to compute $\left[\Delta V_E\right]$ in terms of the final time t_f, $\left[C\right]$ is expanded in a power series about time $t_f = \Delta T$.

$$\left[C\right] = \left[C\right]_f + \left[\dot{C}\right]_f (t - t_f) + \left[\ddot{C}\right]_f \frac{(t - t_f)^2}{2!} + \cdots$$

Similarly

$$\left[A\right] = \left[A\right]_f + \left[\dot{A}\right]_f (t - t_f) + \left[\ddot{A}\right]_f \frac{(t - t_f)^2}{2!} + \cdots$$

Then, if $q = t - t_f$

$$\left[\Delta V_E\right] = \int_{-\Delta T}^{0} \left[C\right]\left[A\right] dq$$

$$[\Delta V_E] = [C]_f [A]_f \Delta T - ([C]_f [\dot{A}]_f + [\dot{C}]_f [A]_f)\frac{\Delta T^2}{2} + \left(\frac{[C]_f [\ddot{A}]_f}{6} + \frac{[\dot{C}]_f [\dot{A}]_f}{3} + \frac{[\ddot{C}]_f [A]_f}{6}\right)\Delta T^3 + \ldots.$$

$$[\Delta V_E] = C_f\left\{ [A]_f \Delta T - [\dot{A}]_f \frac{\Delta T^2}{2} + [\ddot{A}]_f \frac{\Delta T^3}{6} + \ldots.\right\} - [\dot{C}]_f [A]_f \frac{\Delta T^2}{2} + \left(\frac{[\dot{C}]_f [\dot{A}]_f}{3} + \frac{[\ddot{C}]_f [A]_f}{6}\right)\Delta T^3 + \ldots.$$

The accelerometer output is

$$[\Delta V] = [A]_f \Delta T - [\dot{A}]_f \frac{\Delta T^2}{2} + [\ddot{A}]_f \frac{\Delta T^3}{6} + \ldots.$$

To evaluate the remaining terms

$$[\dot{C}] = -[C][\omega]$$

$$[\ddot{C}] = -[\dot{C}][\omega] - [C][\dot{\omega}] = [C]([\omega]^2 - [\dot{\omega}])$$

Then

$$[\Delta V_E] = [C]_f \left\{ [\Delta V] + [\omega]_f [A]_f \frac{\Delta T^2}{2} + \left([\omega]_f \frac{[\dot{A}]_f}{3} + \frac{([\omega]_f^2 - [\dot{\omega}]_f)[A]_f}{6}\right)\Delta T^3 + \ldots.\right\}$$

Using initial values for $[A]$ and $[\omega]$

$$[A]_f = [A]_o + [\dot{A}]_o \Delta T + [\ddot{A}]_o \frac{\Delta T^2}{2}$$

$$[\dot{A}]_f = [\dot{A}]_o + [\ddot{A}]_o \Delta T$$

$$[\omega]_f = [\omega]_o + [\dot{\omega}]_o \Delta T$$

$$[\dot{\omega}]_f = [\dot{\omega}]_o$$

assuming no higher derivatives. Making these substitutions

$$[\Delta V_E] = [C]_f \left\{ [\Delta V] + [\omega]_o [A]_o \frac{\Delta T^2}{2} + \left(\frac{[\omega]_o [\dot{A}]_o}{6} + \frac{[\dot{\omega}]_o [A]_o}{3} + \frac{[\omega]_o^2 [A_o]}{6}\right)\Delta T^3 \right\}$$

In the strapdown program, $[C]_f$ and $[A]$ and its derivatives at t = 0 are computed. Also

$$[\omega] = \begin{bmatrix} 0 & \omega_3 & -\omega_2 \\ -\omega_3 & 0 & \omega_1 \\ \omega_2 & -\omega_1 & 0 \end{bmatrix}$$

$$[\omega]^2 = \begin{bmatrix} -\omega_2^2 - \omega_3^2 & \omega_1 \omega_2 & \omega_1 \omega_3 \\ \omega_1 \omega_2 & -\omega_1^2 - \omega_3^2 & \omega_2 \omega_3 \\ \omega_1 \omega_3 & \omega_2 \omega_3 & -\omega_1^2 - \omega_2^2 \end{bmatrix}$$

The strapdown program also has ω_{1-0}, ω_{2-0}, ω_{3-0} and $\dot{\omega}_{1-0}$, $\dot{\omega}_{2-0}$, $\dot{\omega}_{3-0}$.

If $\left[\Delta V_E\right] = \left[C\right]_f \left[\Delta V_B\right]$, then

$$\left[\Delta V_B\right]_1 = \Delta V_1 + (\omega_{3-0}\, a_{2-0} - \omega_{2-0}\, a_{3-0})\frac{\Delta T^2}{2}$$

$$+\left\{\frac{(\omega_{3-0}\, \dot{a}_{2-0} - \omega_{2-0}\, \dot{a}_{3-0})}{6} + \frac{(\dot{\omega}_{3-0}\, a_{2-0} - \dot{\omega}_{2-0}\, a_{3-0})}{3}\right.$$

$$\left. - \frac{(\omega_{2-0}^2 + \omega_{3-0}^2)\, a_{1-0}}{6} + \frac{\omega_{1-0}\, \omega_{2-0}\, a_{2-0}}{6} + \frac{\omega_{1-0}\, \omega_{3-0}\, a_{3-0}}{6}\right\}\Delta T^3$$

Letting

$$\omega_{i-o}\, \Delta T = \delta\theta_j$$

$$\dot{\omega}_{i-o}\, \Delta T = \Delta\omega_j$$

$$a_{i-o}\, \Delta T = \Delta V_j$$

$$\dot{a}_{i-o}\, \Delta T = \Delta a_j$$

with

$$j = x, y, z \quad \text{for} \quad i = 1, 2, 3$$

and combining some terms

$$\Delta V_{B1} = \Delta V_1 - \frac{1}{2}(\delta\theta_y\, \Delta V_z - \delta\theta_z\, \Delta V_y)$$

$$- \frac{1}{6}(\delta\theta_y \Delta a_z - \delta\theta_z \Delta a_y) - \frac{1}{3}(\Delta\omega_y\, \Delta V_z - \Delta\omega_z\, \Delta V_y)$$

$$+ \frac{1}{6}\delta\theta_y\, (\delta\theta_x\, \Delta V_y - \delta\theta_y\, \Delta V_x)$$

$$- \frac{1}{6}\delta\theta_z\, (\delta\theta_z\, \Delta V_x - \delta\theta_x\, \Delta V_z)$$

with similar relations for the other components.

Here, as derived in Section B3

$$\Delta V_i = \delta V_{i1} + \delta V_{i2}, \text{ for } i = 1, 2, 3$$

Also

$$\Delta V_j = 3\delta V_{i1} - \delta V_{i2}$$

$$\Delta\omega_j = 4\,(\delta\theta_{i2} - \delta\theta_{i1})$$

$$\Delta a_j = 4\,(\delta V_{i2} - \delta V_{i1})$$

$$\Delta\theta_j = 3\delta\theta_{i1} - \delta\theta_{i2}$$

with $j = x, y, z$ for $i = 1, 2, 3$

B.3 ω AND $\dot{\omega}$ IN TERMS OF ANGULAR INCREMENTS a AND $\dot{a}$ IN TERMS OF VELOCITY INCREMENTS

Given an angular increment $\delta\theta_{k1}$ that occurred over time $\Delta T/2$ and an angular increment $\delta\theta_{k2}$ that occurred over the time interval from $\Delta T/2$ to ΔT, it is desired to determine the best estimate for the angular rate ω_{kn} and angular acceleration $\dot{\omega}_{kn}$ at the beginning of the interval.

Since it is allowable to assume that ω_k is constant over the interval,

let $$\dot{\omega}_k = c. \qquad \text{(B-1)}$$

Then $$\omega_k = ct + d \qquad \text{(B-2)}$$

and $$\theta_k = \frac{1}{2}ct^2 + dt + e \qquad \text{(B-3)}$$

Now at $t = 0$ (beginning of interval), $\theta_k = 0$ (therefore $e = 0$)

$$\omega_k = \omega_{kn} = d,$$

$$\dot{\omega}_k = \dot{\omega}_{kn} = c$$

at $t = \Delta T/2$

$$\theta = \delta\theta_{k1} = \frac{1}{2} c \frac{\Delta T^2}{4} + d\frac{\Delta T}{2} \tag{B-4}$$

at $t = \Delta T$

$$\theta = \delta\theta_{k1} + \delta\theta_{k2} = \frac{1}{2} c \Delta T^2 + d\Delta T \tag{B-5}$$

Equations (B-4) and (B-5) are solved to yield

$$d = \omega_{kn} = \frac{3\delta\theta_{k1} - \delta\theta_{k2}}{\Delta T} \tag{B-6}$$

and

$$c = \dot{\omega}_{kn} = \frac{4\left(\delta\theta_{k2} - \delta\theta_{k1}\right)}{\Delta T^2} \tag{B-7}$$

Similar relations can be derived for a_n and $\dot{a}_n$ in terms of velocity half-increments

$$a_{kn} = \frac{3\delta V_{k1} - \delta V_{k2}}{\Delta T} \tag{B-8}$$

and

$$\dot{a}_{kn} = \frac{4(\delta V_{k2} - \delta V_{k1})}{\Delta T^2} \tag{B-9}$$

APPENDIX C

SOME DETAILS OF THE STABLE ELEMENT KALMAN FILTER

The suboptimal Stable Element Kalman Filter models the following 14 states:

State 1: $X_1 = \delta V_N$ = North inertial velocity error

State 2: $X_2 = \delta V_E$ = East Inertial velocity error

State 3: $X_3 = \delta\theta_N$ = Tilt about the North axis

State 4: $X_4 = \delta\theta_E$ = Tilt about the East axis

State 5: $X_5 = \delta\theta_K$ = Inertial heading error

State 6: $X_6 = \delta\lambda$ = Latitude error

State 7: $X_7 = \epsilon_{Gx}$ = Body X-axis gyro drift

State 8: $X_8 = \epsilon_{Gy}$ = Body Y-axis gyro drift

State 9: $X_9 = \epsilon_{Gz}$ = Body Z-axis gyro drift

State 10: $X_{10} = \epsilon_{Ax}$ = Body X-axis accelerometer bias

State 11: $X_{11} = \epsilon_{Ay}$ = Body Y-axis accelerometer bias

State 12: $X_{12} = \epsilon\psi_R$ = Heading reference error

State 13: $X_{13} = \epsilon V_{LR}$ = Longitudinal velocity reference (log) error

State 14: $X_{14} = \epsilon V_{TR}$ = Transverse velocity reference error

Corrections are applied to all but the last three states.

The basic measurements $Z = H X + \gamma$ are a heading difference $\Delta\psi$, a longitudinal velocity difference ΔV_L, and a transverse velocity difference ΔV_T.

The heading difference is essentially the difference between the heading reference error (State 12) and the inertial heading error (State 5). The longitudinal velocity difference is essentially the difference between the longitudinal velocity reference error (State 13) and the longitudinal velocity error component of the inertial velocity error. This is the body X component or $C_{11}\,\delta V_N + C_{21}\,\delta V_E$, where δV_N is State 1, δV_E is State 2 and C_{11}, C_{21} are direction cosines relating body to earth coordinate frames. The transverse velocity difference is essentially the difference between the transverse velocity reference error (State 14) and the transverse velocity error component (body Y-axis component) of the inertial velocity error ($C_{12}\,\delta V_N + C_{22}\,\delta V_E$). Inertial heading error (State 5) multiplied by the longitudinal inertial velocity also contributes to a transverse velocity difference. The measurement matrix for this Kalman Filter is thus given by the following

$$\begin{bmatrix} \Delta\psi \\ \Delta V_L \\ \Delta V_T \end{bmatrix} = \begin{bmatrix} H \end{bmatrix} \begin{bmatrix} X \end{bmatrix} + \begin{bmatrix} \gamma \end{bmatrix}$$

where

$$\begin{bmatrix} H \end{bmatrix} = \begin{bmatrix} 0 & 0 & 0 & 0 & -1 & 0 & 0 & 0 & 0 & 0 & 0 & 1 & 0 & 0 \\ -C_{11} & -C_{21} & 0 & 0 & 0 & 0 & 0 & 0 & 0 & 0 & 0 & 0 & 1 & 0 \\ -C_{12} & -C_{22} & 0 & 0 & -V_{LI} & 0 & 0 & 0 & 0 & 0 & 0 & 0 & 0 & 1 \end{bmatrix} \quad \text{(C-1)}$$

The effects of the tilts in causing improper transformation of velocity increments and creating δV_N and δV_E are taken into account in the transition matrix in this filter, since both the velocity states and the tilt states are modeled.

Because of the short iteration time, the assumption is made that the transition matrix Φ for

$$X(n+1) = \Phi(n)\,X(n) + U(n)$$

can be approximated by

$$\Phi = I + A\,(t_{n+1} - t_n)$$

As was derived in Appendix A, the misalignments are assumed to increase predominantly due to gyro bias drifts (See equations A-3 to A-10). Therefore, here also

$$\phi(3,7) = \ell_{11} \qquad \phi(3,8) = \ell_{12} \qquad \phi(3,9) = \ell_{13}$$
$$\phi(4,7) = \ell_{21} \qquad \phi(4,8) = \ell_{22} \qquad \phi(4,9) = \ell_{23}$$
$$\phi(5,7) = \ell_{31} \qquad \phi(5,8) = \ell_{32} \qquad \phi(5,9) = \ell_{33}$$

In an analogous fashion, due to body axis accelerometer biases

$$\delta V_N(n+1) = \delta V_N(n) + \int_{t_n}^{t_{n+1}} a_{BN}\, dt \tag{C-2}$$

$$\delta V_E(n+1) = \delta V_E(n) + \int_{t_n}^{t_{n+1}} a_{BE}\, dt \tag{C-3}$$

now

$$\begin{bmatrix} a_{BN} \\ a_{BE} \end{bmatrix} \simeq \begin{bmatrix} C_{11} & C_{12} \\ C_{21} & C_{22} \end{bmatrix} \begin{bmatrix} a_{Bx} \\ a_{By} \end{bmatrix} \tag{C-4}$$

Therefore,

$$\int_{t_n}^{t_{n+1}} a_{BN}\, dt = a_{Bx} \int_{t_n}^{t_{n+1}} C_{11}\, dt + a_{By} \int_{t_n}^{t_{n+1}} C_{12}\, dt$$
$$= \ell_{11}\, a_{Bx} + \ell_{12}\, a_{By} \tag{C-5}$$

and

$$\int_{t_n}^{t_{n+1}} a_{BE}\, dt = \ell_{21}\, a_{Bx} + \ell_{22}\, a_{By} \tag{C-6}$$

Therefore, substituting in (C-2) and (C-3)

$$\phi(1,10) = \ell_{11} = \phi(3,7)$$
$$\phi(1,11) = \ell_{12} = \phi(3,8)$$
$$\phi(2,10) = \ell_{21} = \phi(4,7)$$
$$\phi(2,11) = \ell_{22} = \phi(4,8)$$

Due to the tilts $\delta\theta_N$, $\delta\theta_E$, gravitational acceleration will be coupled into the horizontal axes causing δV_N and δV_E errors according to

$$\delta V_N = g\Delta t\, \delta\theta_E \tag{C-7}$$

$$\delta V_E = -g\Delta t\, \delta\theta_N \tag{C-8}$$

Thus

$$\phi(1,4) = -\phi(2,3) = g\Delta t$$

The tilts are also increased by improper coordinate-frame rates ("torquing rates") which act like gyro bias drifts.

The nominal torquing rates for a north referenced coordinate frame are

$$\omega_N = \Omega_E \cos\lambda + V_E/R \tag{C-9}$$

$$\omega_E = -V_N/R \tag{C-10}$$

$$\omega_K = -V_E/R \tan\lambda - \Omega_E \sin\lambda \tag{C-11}$$

Thus, due to improper V/R torquing

$$\delta\theta_N = \delta V_E/R\Delta t \tag{C-12}$$

$$\delta\theta_E = -\delta V_N/R\Delta t \tag{C-13}$$

$$\delta\theta_K = -\delta V_E/R \tan\lambda\Delta t \tag{C-14}$$

and therefore

$$\phi(3,2) = -\phi(4,1) = \Delta t/R$$

and

$$\phi(5,2) = -\tan\lambda\Delta t/R$$

Due to incorrect latitude

$$\delta\theta_N = -(\Omega_E \sin\lambda)\Delta t\,\delta\lambda \tag{C-15}$$

and

$$\delta\theta_K = -(V_E/R \sec^2\lambda + \Omega_E \cos\lambda)\Delta t\,\delta\lambda \tag{C-16}$$

so that

$$\phi(3,6) = -\Omega_E \sin\lambda\Delta t$$

and

$$\phi(5,6) = -(V_E/R \sec^2\lambda + \Omega_E \cos\lambda)\Delta t$$

Because of the misalignments, the torquing rates are coupled into the wrong axes, creating new cross-coupled misalignments.

Thus

$$\delta\theta_N = \omega_K\Delta t\,\delta\theta_E - \omega_E\Delta t\,\delta\theta_K \tag{C-17}$$

$$\delta\theta_E = -\omega_K\Delta t\,\delta\theta_N + \omega_N\Delta t\,\delta\theta_K \tag{C-18}$$

$$\delta\theta_K = -\omega_N\Delta t\,\delta\theta_E + \omega_E\Delta t\,\delta\theta_N \tag{C-19}$$

so that

$$\phi(3,4) = \omega_K\Delta t$$

$$\phi(3,5) = -\omega_E\Delta t$$

$$\phi(4,3) = -\omega_K\Delta t = -\phi(3,4)$$

$$\phi(4,5) = \omega_N\Delta t$$

$\phi(5,3)$ and $\phi(5,4)$ are neglected as being of secondary consequence.

The dominant earth coriolis acceleration corrections on the North and East axes are

$$a_{CN} = -(2V_E\Omega_E \sin\lambda + V_E^2/R \tan\lambda) \tag{C-20}$$

and

$$a_{CE} = 2V_N\Omega_E \sin\lambda + \frac{V_N V_E}{R} \tan\lambda \tag{C-21}$$

Thus, due to incorrect velocities, incorrect Coriolis corrections result

$$\delta V_N = -(2\Omega_E \sin\lambda + 2V_E/R \tan\lambda)\Delta t\,\delta V_E = 2\omega_K\Delta t\,\delta V_E \tag{C-22}$$

$$\delta V_E = (2\Omega_E \sin\lambda + V_E/R \tan\lambda)\Delta t\,\delta V_N \tag{C-23}$$

Therefore

$$\phi(1,2) = 2\omega_K\Delta t = 2\phi(3,4)$$

and

$$\phi(2,1) = -\omega_K\Delta t + \Omega_E \sin\lambda\Delta t = -\left[\phi(3,4) + \phi(3,6)\right]$$

$\phi(1,6)$ and $\phi(2,6)$ (effect of $\delta\lambda$ on δV_N and δV_E due to incorrect Coriolis corrections) are neglected here. So is the self-effect of δV_E in Equation (C-21).

$$\text{Latitude } (n+1) = \text{Latitude } (n) + \int_{t_n}^{t_{n+1}} V_N/R\,dt$$

$$\text{or} \qquad \lambda(n+1) \cong \lambda(n) + V_N/R\Delta t \tag{C-24}$$

Therefore, due to incorrect North velocity

$$\delta\lambda = \delta V_N \Delta t/R \qquad \text{(C-25)}$$

and thus

$$\phi(6,1) = \Delta t/R = -\phi(4,1)$$

Since plant noise is considered white for all states except the reference-error states (States 12, 13, 14), all $\phi(i,i)$; i = 1 to 11 are equal to 1.

For the reference error states (States 12, 13, 14) plant noise is Markovian ($\dot{X} = -1/\tau X + \eta$). Therefore

$$\phi(12, 12) = 1 - 1/\tau_{12}\Delta t$$

$$\phi(13, 13) = 1 - 1/\tau_{13}\Delta t$$

$$\phi(14, 14) = 1 - 1/\tau_{14}\Delta t$$

All other Φ matrix coefficients are treated as negligible or are zero. Thus only 41 out of 196 coefficients have some value. Eleven of these equal 1. The remaining 155 coefficients are zero including all ϕ ij , i = 7 to 14 , j = 1 to 14 and not equal to i.

This fact, coupled with the large zero portions of the $[H]$ matrix (see Equation C-1) enables significant simplications in the computation of the conventional Kalman Filter relationships.

The Q matrix (white plant noise) consists of 14 diagonal elements, with Q (6, 6) (Latitude error state) set to zero. Q (3, 3), Q (4, 4), and Q (5, 5) represent the white noise random drift characteristic of laser gyros. Q (12, 12), Q (13, 13), Q (14, 14) have the appropriate form: $(2\sigma^2/\tau\Delta t)$ where σ is the rms amplitude of the Markovian reference error noise and τ is the correlation time.

The R matrix (measurement noise) consists of three diagonal elements. R (1, 1) for Heading, R (2, 2) for longitudinal velocity, and R (3, 3) for transverse velocity. The R values are employed to represent the white-noise reference errors, whereas the Q (12, 12), Q (13, 13), and Q (14, 14) values represent the Markovian random reference errors.

APPENDIX D
POSITION ERROR PROPAGATION RELATIONSHIPS FOR LASER GYRO AIRCRAFT INERTIAL NAVIGATOR

The following approximate error propagation relationships can be shown to occur for the dominant error sources in a laser-gyro strapdown inertial system for the particular flight situation:

(1) 600 knots due East at 45 degrees Latitude for about 2 hours duration.

(2) Following a 20 minute self-align on the ground while pointing North.

X, Y, and Z are principal body axes; longitudinal, lateral to the right, and normal down.

Due to X-Gyro Drift

$$\delta\lambda = B_{XR}\left(t - \frac{1}{w_s}\sin w_s t\right) \oplus A_{NX}\sqrt{\left(\frac{3t}{2} - \frac{2}{w_s}\sin w_s t + \frac{1}{4w_s}\sin 2w_s t\right)} \qquad \text{(D-1)}$$

$$\delta f \cos\lambda = B_{XR}\sin\lambda\,\frac{\left[1 - \cos(\Omega_E + \dot{f})t\right]}{(\Omega_E + \dot{f})} \qquad \text{(D-2)}$$

Where

f = Longitude,

λ = Latitude,

w_s = Schuler Frequency (4.5 rad/hr)

$\oplus$ = is rss addition

B_{XR} = residual X axis bias drift at start of flight (assumed to equal turn-on drift in this case)

A_{NX} = white noise X axis random drift

Due to Y Gyro Drift

$$\delta\lambda = B_{YR}\sin\lambda\,\frac{\left[1 - \cos(\Omega_E + \dot{f})t\right]}{(\Omega_E + \dot{f})} \qquad \text{(D-3)}$$

$$\delta f \cos\lambda = B_{YR}\left(t - \frac{1}{w_s}\sin w_s t\right) \oplus A_{NY}\sqrt{\left(\frac{3t}{2} - \frac{2}{w_s}\sin w_s t + \frac{1}{4w_s}\sin 2w_s t\right)} \qquad \text{(D-4)}$$

$B_{YR} = B_{DTO} \oplus A_N/\sqrt{T}$, the residual Y-axis bias drift as a result of the gyrocompassing self-alignment of duration T.

Due to Z-Gyro Drift

$$\delta\lambda = B_{ZR}\cos\lambda\,\frac{\left[1 - \cos(\Omega_E + \dot{f})t\right]}{(\Omega_E + \dot{f})} \qquad \text{(D-5)}$$

$$\delta f \cos\lambda = B_{ZR}\sin\lambda\cos\lambda\left[t - \frac{\sin(\Omega_E + \dot{f})t}{(\Omega_E + \dot{f})}\right] \qquad \text{(D-6)}$$

B_{ZR} is residual Z axis bias drift at start of flight (assumed to equal turn-on drift in this case. It is assumed that white-noise-drift effects in the Z-axis are negligible compared to the residual bias drift effects.

Due to Initial Azimuth Error

$$\delta\lambda = \delta\psi_o\cos\lambda\left[\sin(\Omega_E + \dot{f})t - \frac{\Omega_E}{w_s}\sin w_s t\right] \qquad \text{(D-7)}$$

$$\delta f \cos\lambda = \delta\psi_o\sin\lambda\cos\lambda\left[1 - \cos(\Omega_E + \dot{f})t\right] \qquad \text{(D-8)}$$

where

$\delta\psi_o$ is the rss sum of $\delta\psi_{01} \oplus \delta\psi_{02}$

$\delta\psi_{01} = \dfrac{B_{DTOY} \oplus A_{NY}/\sqrt{T}}{\Omega_E \cos\lambda}$ the azimuth error resulting from the gyrocompassing self-alignment

6.48

$\delta\psi_{02} = \delta_{SF} \times 90^{0}$ the additional azimuth error caused by gyro scale-factor inaccuracy in measuring the 90 degree turn to East.

Due to Y-Axis Accelerometer Bias (ABY)

$$\delta\lambda = \frac{ABY}{g}\left(1 - \cos\left[w_s t\right]\right) \tag{D-9}$$

$$\delta\ell\cos\lambda = \frac{ABY}{g}\cos(w_s t)\sin\left[(\Omega_E + \dot{\ell})\sin\lambda t\right] \tag{D-10}$$

Due to X-Axis Accelerometer Bias (ABX)

$$\delta\lambda = \frac{ABX}{g}\cos(w_s t)\sin\left[(\Omega_E + \dot{\ell})\sin\lambda t\right] \tag{D-11}$$

$$\delta\ell\cos\lambda = \frac{ABX}{g}\left(1 - \cos\left[w_s t\right]\right) \tag{D-12}$$

Due to Initial Tilt about North

$$\delta\lambda = \theta_{NO}\left\{\sin\lambda\sin(\Omega_E + \dot{\ell})t - \cos(w_s t)\sin\left[(\Omega_E + \dot{\ell})\sin\lambda t\right]\right\} \tag{D-13}$$

$$\delta\ell\cos\lambda = \theta_{NO}\left\{\cos(\Omega_E + \dot{\ell})t - \cos w_s t + \cos^2\lambda\left[1 - \cos(\Omega_E + \dot{\ell})t\right]\right\} \tag{D-14}$$

where

θ_{NO} is the rss sum of $\theta_{N01} \oplus \theta_{N02}$

$\theta_{N01} = \frac{ABY}{g}$ the initial tilt resulting from the self-alignment

$\theta_{N02} = \delta_{MAG} \times 90^{0}$ the additional tilt error caused by gyro misalignment cross-coupling the 90 degree azimuth motion into a motion about a horizontal axis

Due to Initial Tilt about East

$$\delta\lambda = \theta_{EO}\left[\cos(\Omega_E + \dot{\ell})t - \cos w_s t\right] \tag{D-15}$$

$$\delta\ell\cos\lambda = \theta_{EO}\left\{\sin\lambda\sin(\Omega_E + \dot{\ell})t - \cos w_s t\sin\left[(\Omega_E + \dot{\ell})\sin\lambda t\right]\right\} \tag{D-16}$$

where θ_{EO} is defined similarly to θ_{NO} for orthogonal axes.

Due to Initial East Velocity Error

$$\delta\lambda_{NM} = \delta V_{EO}\frac{\sin w_s t}{w_s}\sin\left[(\Omega_E + \dot{\ell})\sin\lambda t\right] \tag{D-17}$$

$$\delta\ell\cos\lambda_{NM} = \delta V_{EO}\frac{\sin w_s t}{w_s} \tag{D-18}$$

where δV_{EO} is the initial East velocity error, caused in this case by the X-axis accelerometer scale-factor error in measuring the 600-knot change in East velocity at takeoff

$$\delta V_{EO} = \delta_{SFAX} \times 600 \text{ knots.}$$

Due to Initial North Velocity Error

(Other than effect of initial azimuth error, which has been included in equation (D-7))

$$\delta\lambda_{NM} = \delta V_{NO}\frac{\sin w_s t}{w_s} \tag{D-19}$$

$$\delta\ell\cos\lambda_{NM} = \delta V_{NO}\frac{\sin w_s t}{w_s}\sin\left[(\Omega_E + \dot{\ell})\sin\lambda t\right] \tag{D-20}$$

where δV_{NO} is the initial North velocity error, other than that due to initial azimuth error, caused in this case by the Y-axis accelerometer misalignment, cross-coupling the 600-knot change at take-off into the North axis

$$\delta V_{NO} = \delta_{MAAY} \times 600 \text{ knots}$$

APPLICATION OF STRAPDOWN INERTIAL NAVIGATION TO HIGH PERFORMANCE FIGHTER AIRCRAFT

by
Dr. Wolfgang J. Kubbat
MESSERSCHMITT-BÖLKOW-BLOHM GMBH
Aircraft Division
8000 München 80, Postfach

7-1

SUMMARY

The paper describes an experimental strapdown inertial navigation system which is part of an integrated guidance and control system. Based upon technical requirements and a general comparison between a gimballed solution vs a strapdown solution a description of the major elements of the RIICS (Redundant Inertial Information and Computation System) is given.

The redundancy management problem is addressed as well as software timing and memory occupation. The paper concludes with some aspects of advanced configurations such as sensor skewing and data bus application.

1. TECHNICAL REQUIREMENTS

Inertially based information is needed in an aircraft at many different locations for many different purposes:

Aircraft Stabilization (SAS, CSAS)	Sensor stabilization
Autopilot	Weapon delivery
Radar reference	Terrain following
Sight system stabilization	Pilot reference/information
Navigation	Ride quality control/Gust alleviation

The conventional approach to obtaining inertial reference information uses individual sensors for each task or piece of equipment. The result is that in many aircraft duplication of sensor signals (of different or even equal qualities) is found. Interfaces between existing and newly installed equipment are rare; when used, they become expensive and complicated. On the other hand, we are confronted with steadily increasing requirements for aircraft in service and under design.

In spite of additional financial constraints, the arising technical demand is to do more with less equipment. In addition, with regard to the many modifications of aircraft in service that we experienced, a second very important requirement must be observed: make simple modification with only local impact. Last but not least, the flight-safety requirements related to obtaining inertial reference information demand the observation of flight-safety rules, i.e., reliability, redundancy, and vulnerability.

Strapdown inertial technology conforms to all of these rules. It provides more information with less hardware. A comparison of the strapdown and the conventional gimballed platforms is given by Figures 1, 2, and 3.

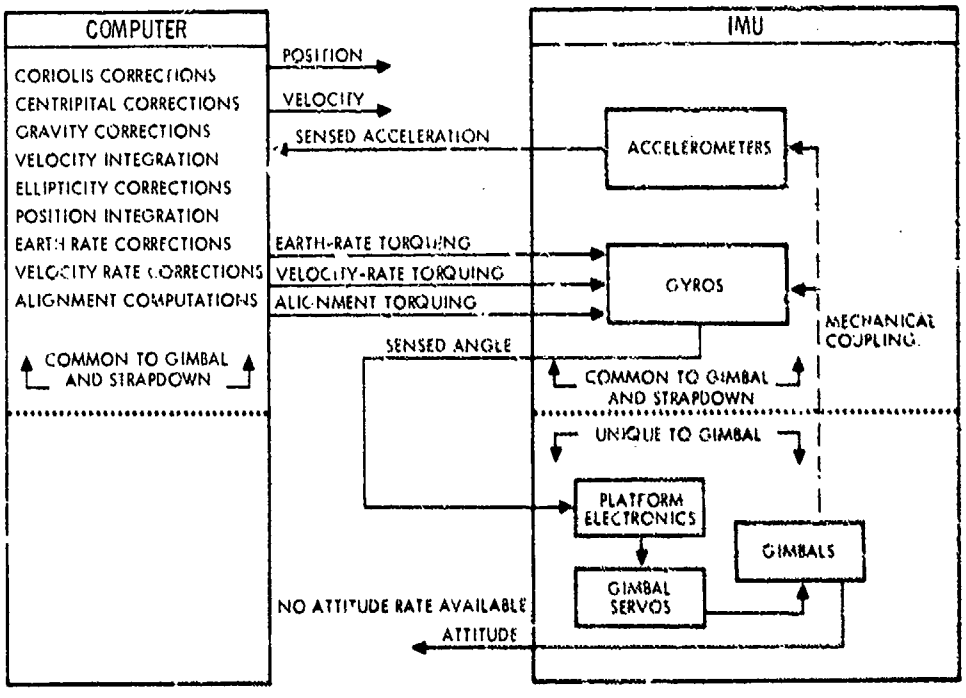

Figure 1. Computer-IMU interface; gimballed system.

1.2

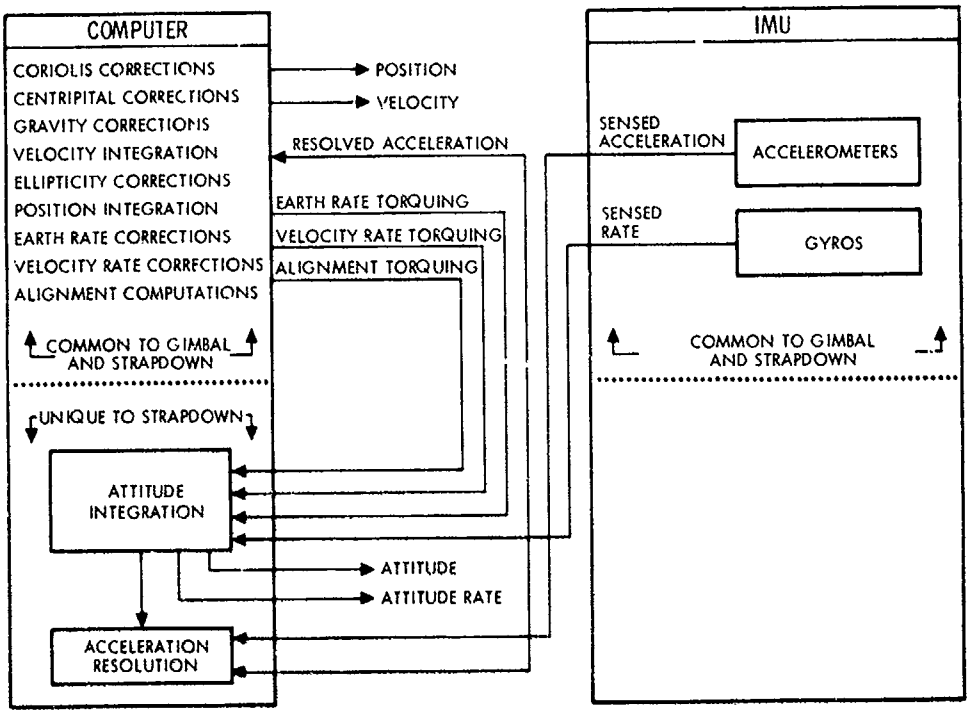

Figure 2. Computer-IMU interface: strapdown system

ITEM	GIMBAL SYSTEM	STRAPDOWN SYSTEM
RELATIVE RELIABILITY	LOWER, MORE TOTAL PARTS	HIGHER, FEWER TOTAL PARTS
RELATIVE COST OF OWNERSHIP	HIGHER, LOWER RELAIBILITY, ACCESSIBILITY OF COMPONENTS MORE DIFFICULT RESULTS IN HIGHER MAINTAINABILITY COSTS.	LOWER, HIGHER RELIABILITY, GREATER ACCESSIBILITY OF COMPONENTS EASES MAINTAINABILITY PROBLEM.
DIRECT THREE-AXIS BODY RATES	NOT AVAILABLE	AVAILABLE
VEHICLE ATTITUDE OUTPUTS	AVAILABLE ONLY AS SYNCHRO OUTPUTS, CONTAMINATED WITH USUAL SYNCHRO ERRORS.	DIRECTLY AND CONTINUOUSLY AVAILABLE
IMU/COMPUTER INTERFACE	TWO WAY COMMUNICATION, INCREMENTAL OUTPUTS MUST BE ACCEPTED.	ONLY ONE WAY COMMUNICATION REQUIRED, WHOLE WORD OUTPUTS DIRECTLY AVAILABLE.
GIMBAL FREEDOM	SPECIAL PROVISIONS TO AVOID "FLIPPING"	NO SPECIAL PROVISIONS, AS NO SINGULARITIES ARE ENCOUNTERED.
HIGH ACCELERATION AND VIBRATIONAL INPUT CAPABILITY	INFERIOR, BECAUSE COMPLIANCE OF FOUR GIMBALS RESULTS IN LOWER STIFFNESS AND MANY MORE UNDESIRABLE RESONANT FREQUENCIES.	SUPERIOR, BECAUSE ONLY HIGHLY RIGID INSTRUMENT MOUNT IS REQUIRED.
EFFECTS OF GYRO ANISOELASTIC ERRORS DURING FLIGHT.	SIGNIFICANT SENSITIVITY BECAUSE OF VARYING ACCELERATION VECTOR RELATIVE TO PLATFORM AXES	NO FIRST ORDER SENSITIVITY, BECAUSE ALL ACCELERATION VECTORS PRESENT DO NOT EXCITE ANISOELASTIC ERRORS.
EFFECT OF ACCELERATION LOADS UPON GIMBAL SERVO TORQUE DUE TO GIMBAL ANISOELASTICITY	SIGNIFICANT UNDER HIGH ACCELERATION	NOT PRESENT

Figure 3. Strapdown System vs. gimbal system capabilities comparison.

2. GENERAL AIRCRAFT REQUIREMENTS FOR INERTIAL NAVIGATION SYSTEMS IN A HIGH-PERFORMANCE AIRCRAFT

The navigation accuracy finally obtained from any inertial system is strongly influenced by environmental constraints given to the aircraft. Many of them differ from aircraft to aircraft or can be modified through cooling, shock mounts, or other protective measures. However, some of them can not and some significant values are given in Table 1 for orientation purposes.

Table 1. Typical Aircraft Dynamic Environments

Rates	Low	Typical	High
roll	± 100°/s	± 200°/s	± 500°/s
pitch	± 40°/s	± 80°/s	± 120°/s
yaw	± 40°/s	± 80°/s	± 120°/s
Angular accelerations			
roll, pitch, yaw	± 500°/s²	± 1000°/s²	± 1500°/s²
Linear accelerations			
all axes	± 5 g	± 10 g	± 15 g

Under these conditions, an unaided navigation accuracy of better than 1 nmi/h CEP can be obtained.

3. A STRAPDOWN SYSTEM IN AN EXPERIMENTAL INTEGRATED GUIDANCE AND CONTROL SYSTEM

3.1 The CCV F104 Test Bed

In 1974, the German MOD contracted MBB for the design, development, and flight test of a Control Configured Vehicle (CCV). The basic idea of improving aircraft performance by utilizing the reduction of drag in a statically unstable aircraft was combined with the approach for a modern guidance and control system.

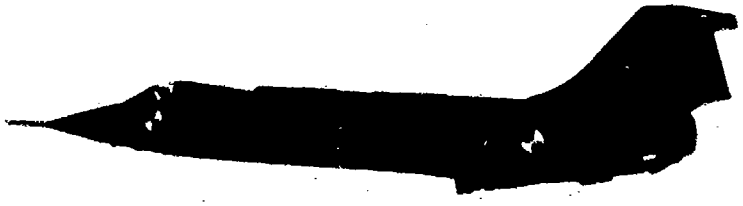

Figure 4. CCV-F104G in flight.

The CCV-F104G has been equipped with an integrated guidance and control system which provides, within a set of four redundant computers:

- Stabilization and Control
- Autopilot
- Air-Data Computation
- Strapdown Navigation
- Auto Navigation
- Redundancy Management
- Preflight Checkout

1.4

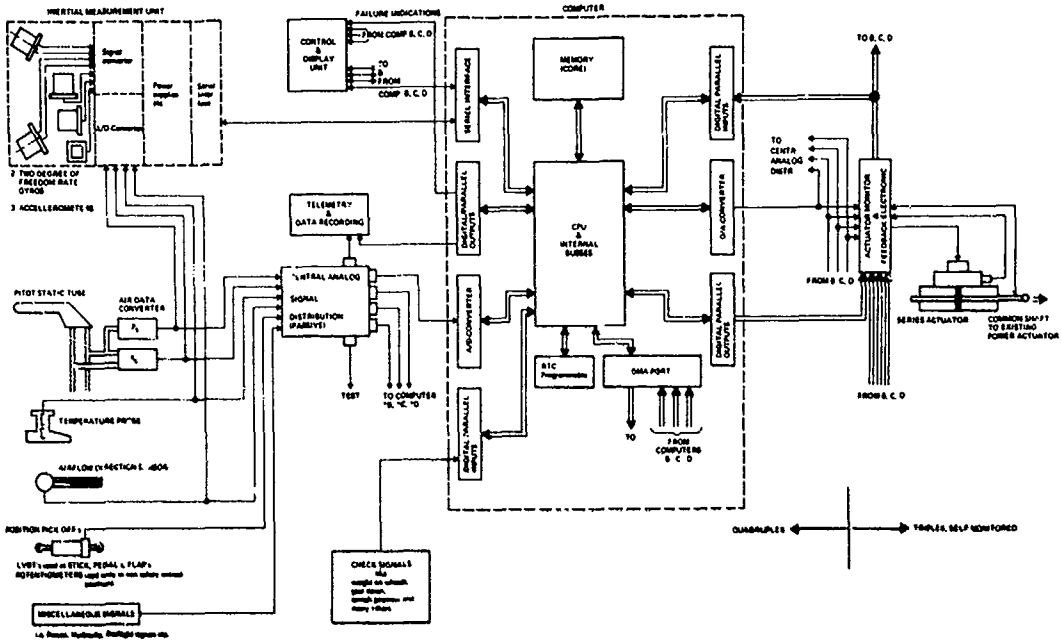

Figure 5. CCV-F104G guidance and control system (one channel).

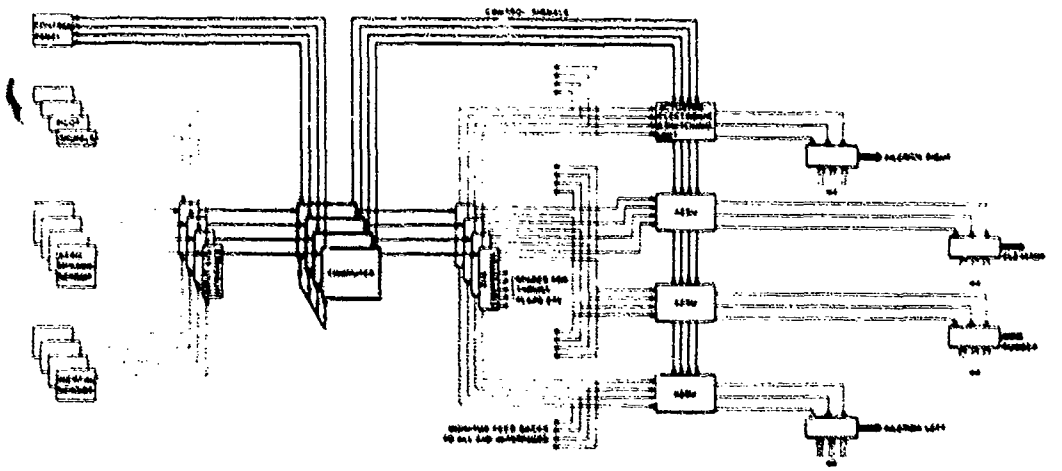

Figure 6. CCV-F104G guidance and control system.

3.2 The CCV-F104 Strapdown System

3.2.1 Design Considerations

In 1974, the risk in choosing strapdown sensors as the basic signal source for such an aircraft was quite high. No strapdown system had been used before for flightsafety determinations. On the other hand, the advantages offered by the strapdown system (in terms of simpler redundancy management and multiple signals derived from only one source) led to the selection of a quadrupally redundant strapdown system for the CCV-F104.

3.2.2 Strapdown Sensors

The basic signals in the CCV-F104 that are sensed are four non-orthogonal body-fixed rates, and three orthogonal body-fixed accelerations.

These are measured by

Dry Tuned Rate Gyros	Accelerometers
Teledyne Systems Co.	Systron Donner
Model SGD5	Model 4841

The open end shows semiskewed gyros and orthogonal accelerometers. The utilization of skewing technique allowed the IMU to sustain higher aircraft roll rates.

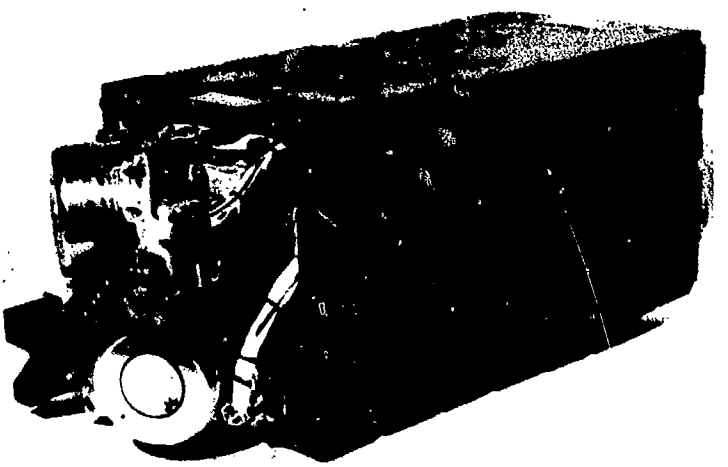

Figure 7. Strapdown inertial measurement unit TDS-3D.

3.2.3 The Inertial Measurement Unit (TDS-3D)

The CCV-F104 strapdown system concludes four TDS-30 Inertial Measurement Units (IMUs) (see Figure 7). Each IMU contains

(1) Instrument assembly
(2) Gyro caging electronics
(3) Digital conversion electronics
(4) IMU Power
(5) Serial interface to computer

Among others, three key elements can be identified for the successful solution of the strapdown problem

(1) Selection of excellent sensors.
(2) Accurate conversion of the analog gyro and accelerometer pickoff signals.
(3) Good sensor models for mathematical error compensation.

Since a description of sensors used is given elsewhere in this lecture series, only two remarkable features (from the user's point of view) shall be mentioned:
(1) Heating: No heaters are needed for the sensors.
(2) Run-up time: 30 seconds after turn on, the system is fully operational, normal alignment time is 8 minutes.

The conversion of the analog pickoff signals is done by voltage-to-frequency (V/F) converters. Figures 8 and 9 show a simplified 1-axis caging loop and a gyro-axis conversion diagram, respectively.

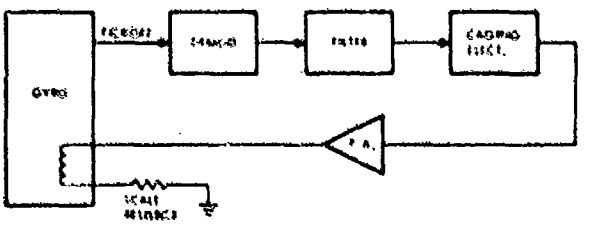

Figure 8. Simplified 1-axis caging loop

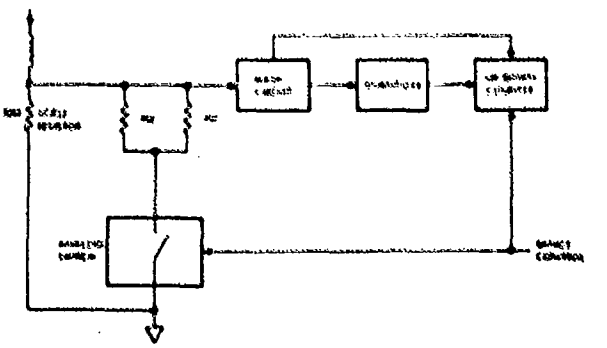

Figure 9. Gyro-axis conversion diagram.

1.6 It should be mentioned that although the V/F conversion represents the most accurate conversion technique, its disadvantage is that each signal needs a separate converter (i.e., more hardware). It also may be noticed that since V/F conversion is an integrating technique, the output is

$$s_i^* = \frac{1}{\Delta t} \int_0^t s_i dt$$

This short-term integration smooths the signals and essentially eliminates the effects of noise. On the other hand, a proper selection of the integration/sampling period Δt has to be made to avoid adverse phase-lag effects. In the CCV-F104 project, no adverse effect has been encountered.

3.2.4 The Computers

The computation of all jobs for the strapdown equations as well as for all other tasks in the integrated guidance and control system is done in a set of four redundant computers. For comparison purposes, some representative performance values of the Teledyne TDY 43 are given:

Cycle time	: 1,13 µs	
Add	: 1,49 µs	} Immediate
Multiply	: 3,87 µs	}
Double-word arithmetic	: Yes	
Memory	: 16k Core	
Programming language	: Assembler	

All computers run identical programs. They are start-up synchronized only; after start up, they are free-running, a point to be referred to later.

3.2.5 System mechanization

Figure 10 reviews the functional allocation of tasks to the IMU Computer and Control and Disply Unit (CDU).

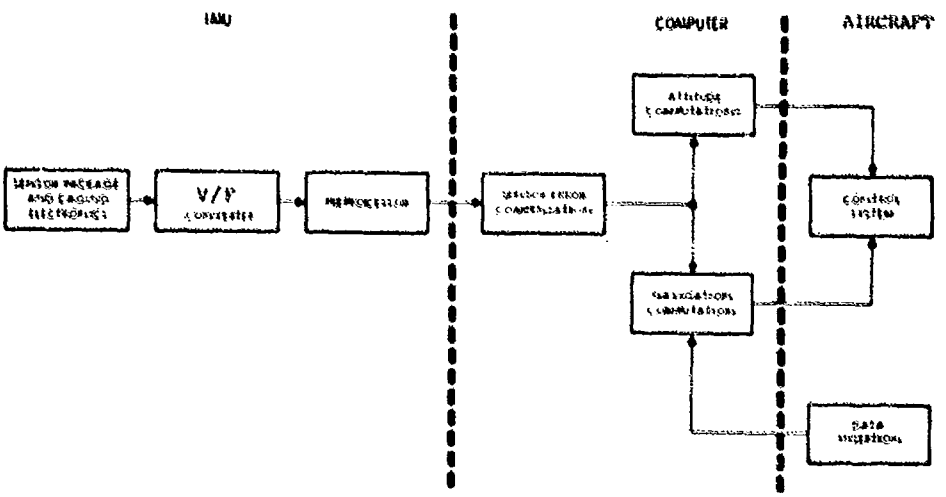

Figure 10. System functional block diagramm.

3.3 Strapdown Computation

As mentioned before, all strapdown computation is done within each of the redundant computers. There is no worksharing between computers.

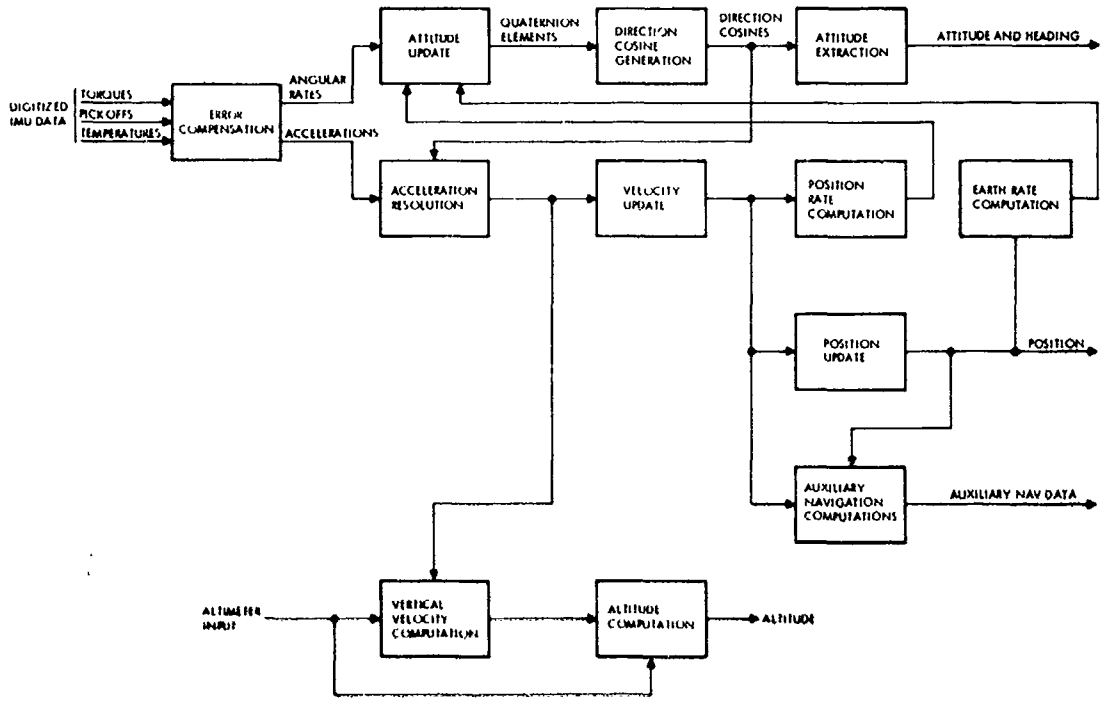

Figure 11. Computational flow diagram.

Figure 11 does not describe the whole program. Since other tasks must be solved quasi-simultaneously, a careful testing of program parts was undertaken. This is best illustrated by Figures 12, 13, and 14.

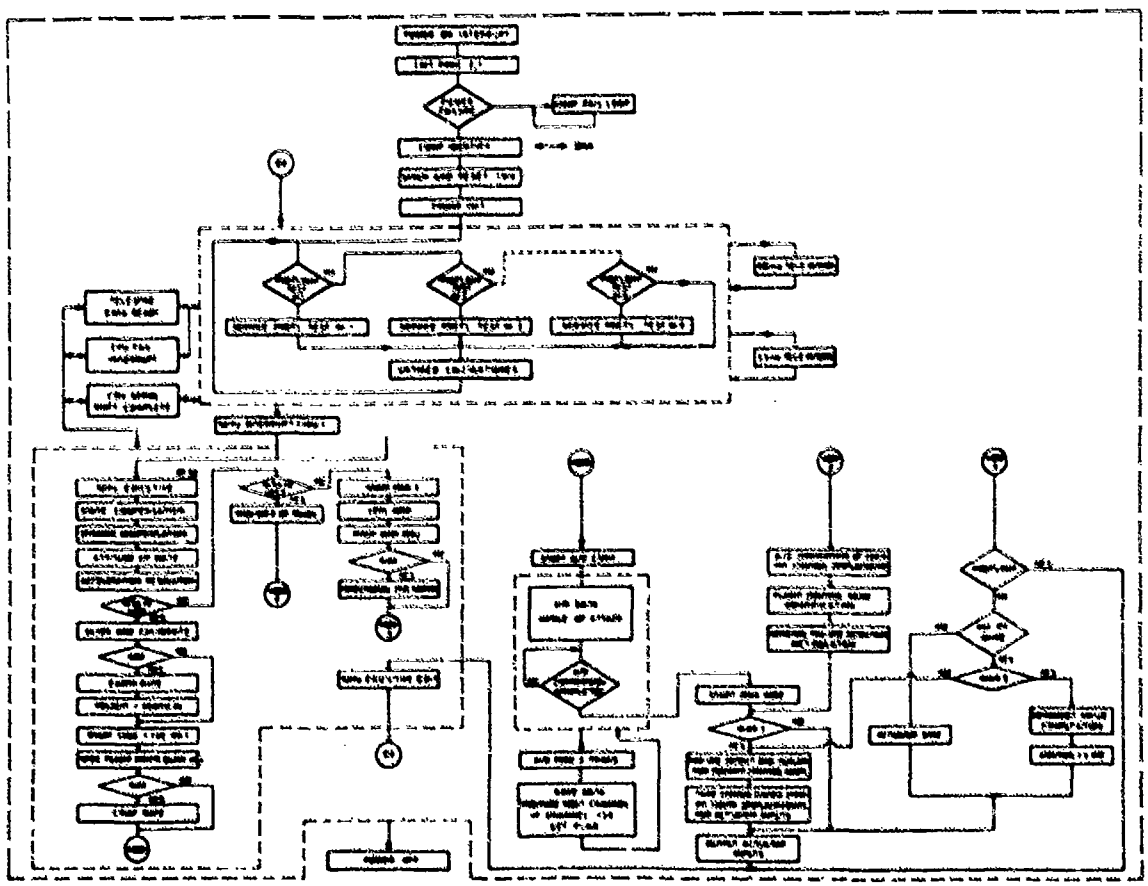

Figure 12. CCV program flow.

1.0

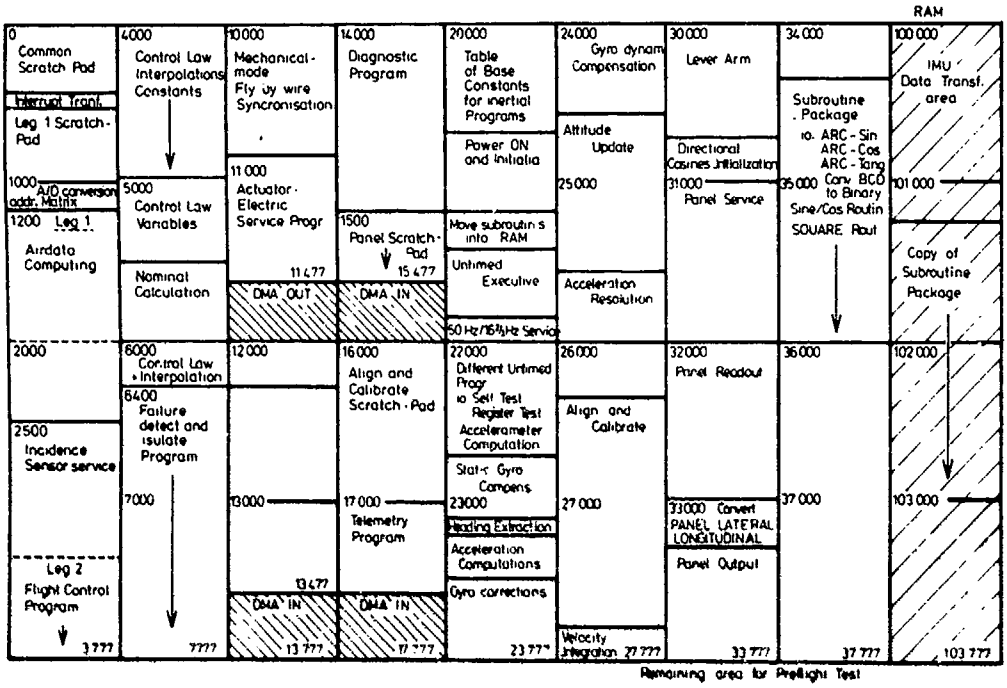

Figure 13. Computer memory occupation: 16k + 2k RAM.

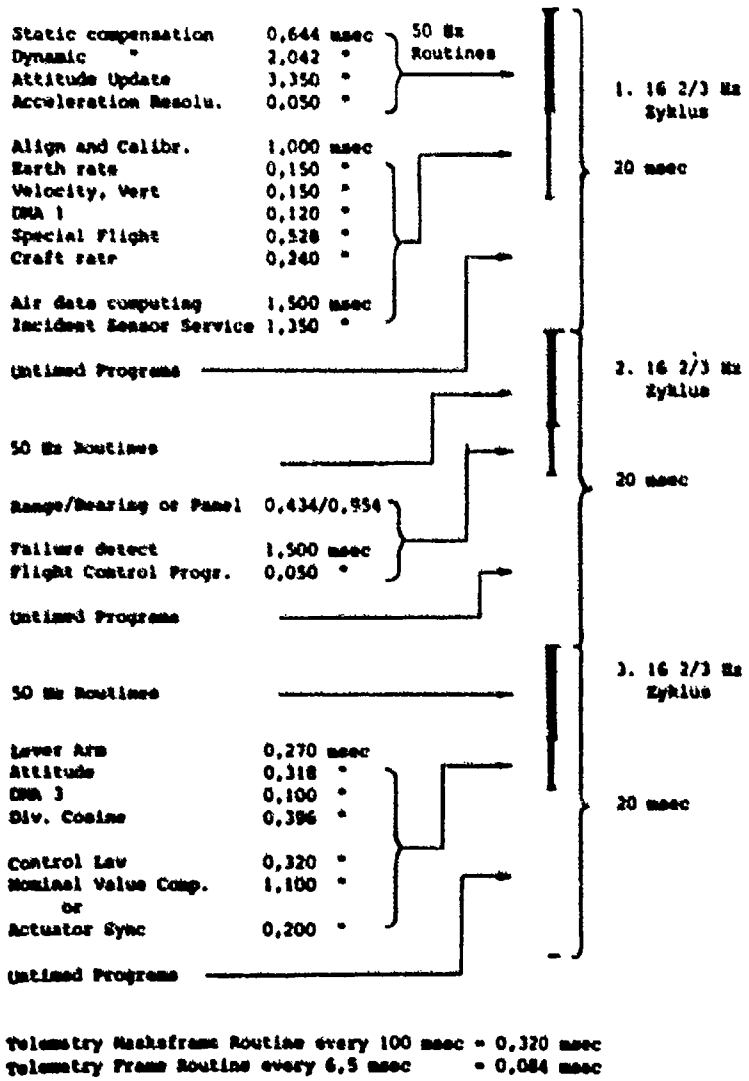

Telemetry Masksframe Routine every 100 msec = 0,320 msec
Telemetry Frame Routine every 6,5 msec = 0,084 msec

Together, the program flow diagram (Figure 12) and the timing diagram (Figure 14) illustrate the difficult job of satisfying different requirements within a restricted time frame and a given computer capability. An additional problem was that the software had been written by two different teams (Teledyne Systems provided the strapdown software, MBB all other parts).

The detailed core occupation may look different depending upon programmers' arrangements. In our case, it was also influenced by the four DMA areas for computer-computer communication which have fixed core locations. The total occupied core for the strapdown computation inclusively of the Auto Nav is 8k words. In addition, 2k of IC-RAM are utilized by the strapdown program. Standard subroutines are copied into the RAM during the power-on routine. This faster memory saves 2/3 µs per instruction and helps speeding up.

The software provides an automatic self-alignment and gyrocompassing. Within the self-alignment, the following functions are performed:

Fast level	High gain	gyrocompass
Fine level	Low gain	gyrocompass
Wide-angle gyrocompassing (or use stored heading)	North biasing	optional if time available
Fine-level gyrocompassing	Vertical biasing	optional if time available

3.4 Strapdown System Outputs

The raw data are received from the IMU and compensated. The subsequent integration utilizes a fourth-order Runge Kutta algorithm for the quaternion representation of attitude.

The following elements of the Inertial State Vector are available to the user within the computer, and most of them are also available for readout via a CDU.

a_x, a_y, a_z	body accelerations	p	roll rate
		q	pitch rate
		r	yaw rate
ϕ	roll attitude	u	velocity along x-body-axis
θ	pitch attitude	v	velocity along y-body-axis
ψ	heading	w	velocity along z-body axis
$\|V\|$	absolute velocity	$\dot{h}$	vertical geodetic velocity
V_{GND}	ground speed	h	altitude (supported by air data)
α	angle of attack	γ	ground-track angle
β^*	sideslip angle	ϕ	latitude
γ	flightpath angle	λ	longitude
RNG	range to destination	XTR	crosstrack error
BRG	bearing to destination	TTG	time to go to destination

It should be noted that:

(1) Since the attitude is also internally available as quaternions and the CCV-F104G control system uses attitude as feedback (among other variables), the control system engineers confronted with the old attitude/singularity problem became accustomed to quaternions. Now they have converted their control laws such that quaternions are directly fed into the control laws.

(2) The state vector contains the angle of attack (α) and sideslip angle (β^*). It should be noticed, that α does not contain the gust term α_g and β^* contains also the drift angle σ.

The direct use of α_{IN} for stabilization (feedback) will be tested in the CCV-F104. No final assertion can be made about an appropriate filter etc. for the elimination of σ in the β_{IN} signal. Investigations and tests are under way.

3.4 Use of a Strapdown System for Guidance and Control

3.4.1 Flight Safety Considerations

Any equipment used in a flight-safety critical position has to satisfy two requirements. The first is the reliability figure, which is hard to get and harder to believe in case one is working with prototypes. The second, which we are concentrating on, is the operational requirement. In case of the CCV-F104 program, double fail-op requirement was assumed.

The solution is strictly a majority-decision software logic within the computers, which act as central voters and monitors.

Since the number of new technologies involved already have been enough, principles such as skewing or self-monitoring have not yet been incorporated.

In order to accomplish the failure detection and isolation for all data, the inertial and non-inertial data have to be exchanged between computers, done here by DMA data exchange (see Figure 15). This is a very fast and software-saving method.

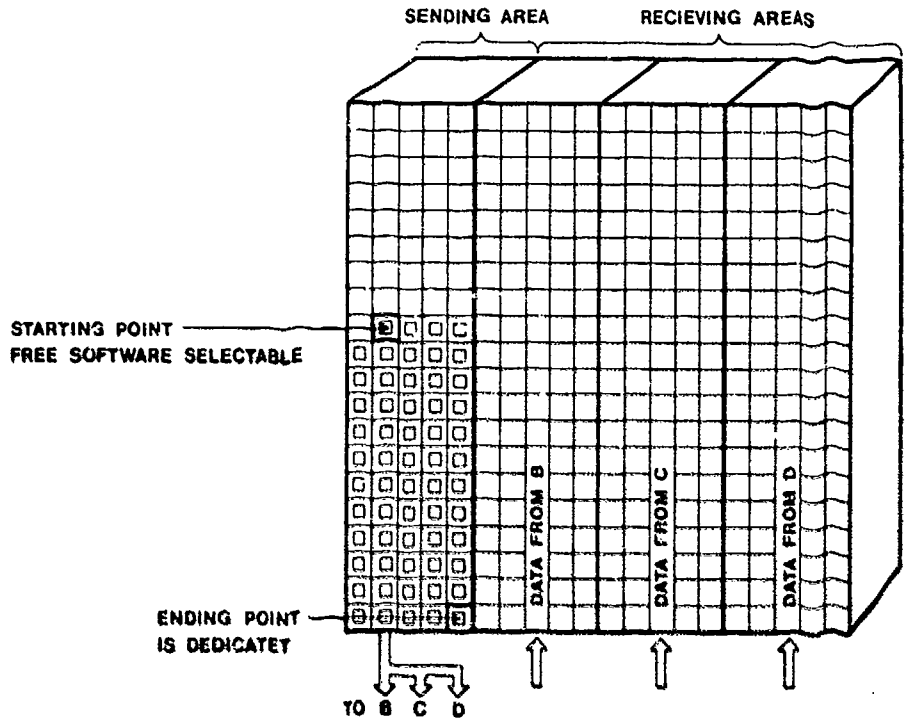

Figure 15. Principle of DMA data exchange.

Because of the DMA data-exchange feature, each computer possesses all variables stored in its own memory and in the memories of the other three computers. Thus it can vote (see Figure 16).

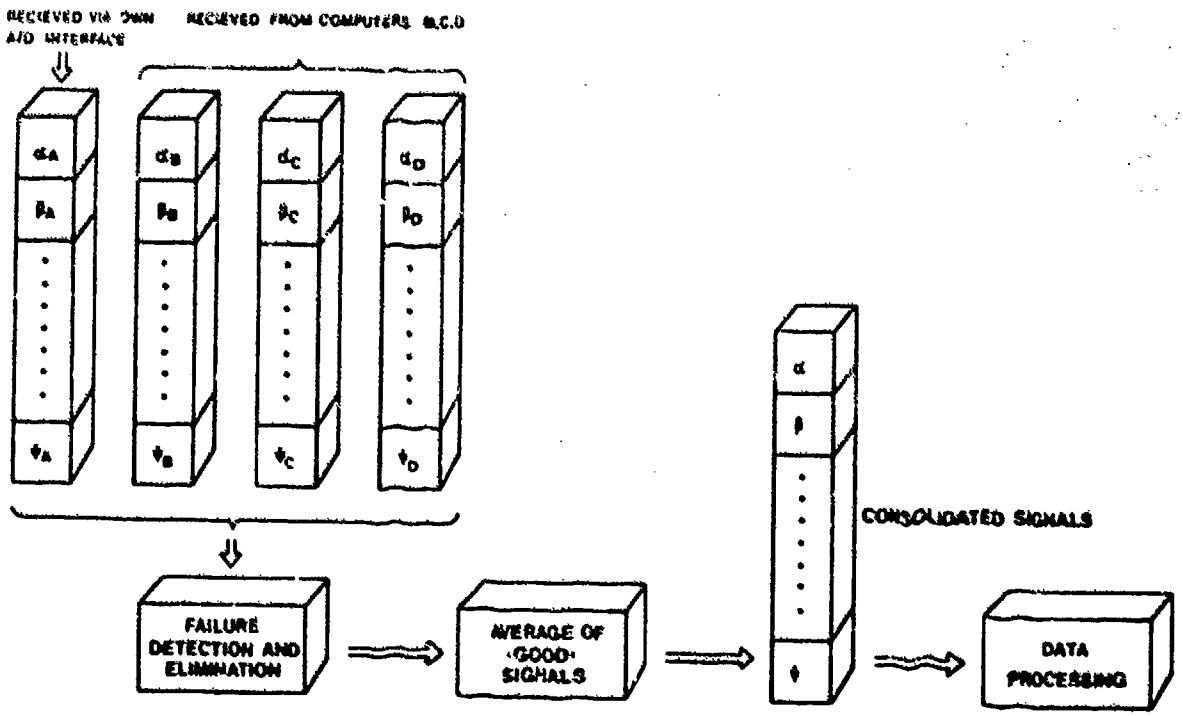

Figure 16. Principle of signal consolidation.

As mentioned before, the computers run identical but nonsynchronized software. This feature, which is imposed by computer hardware, has resulted in an undesired effect. In general, it forces one to use higher failure thresholds. In case of the strapdown signals it did not allow us to consolidate the error-compensated raw signals as initially intended. Since the asynchronism between computers may be as big as 60 ms with a maximum angular acceleration of 1000°/s², rate thresholds of 60°/s arising out of this asynchronism are not tolerable. In practice, failure detection, therefore, is done based upon attitude and velocities. The asynchronism problem is not considered to be a major problem; however, any future system should run soft-synchronized to ease the programmers' work.

3.4.2 Functional Integration

The integration of all functions of the CCV-F104 Guidance and Control System is done by software integration. All functions are executed by the four redundant computers.

Using clear software conventions and a modular technique no major problem was encountered even between teams writing software parts ten thousands of miles away from each other. The main problem occurring was a timing problem within the computer. Especially for the stabilization task, the time used between data sampling, computing, and output to the actuators needed to be minimized.

With a given computer performance the problem was solved by:

(1) Selection of a reasonable basic frame of 60 ms ≙ 16-2/3 Hz for the stabilization.

(2) Subframes of 20 ms for the fast strapdown update (50 Hz).

(3) Low rate update for noncritical variables.

(4) Utilizing "left-over" time for an untimed computation for the "nice to have" information.

The timing diagram (Figure 14) shows that, in addition, phase-lag-critical parts have been nested together in order to minimize the time between data input and output.

It should be noticed that the sampling period of 60 ms, although it appears to be long, is noncritical. This is taken into account during control law design. The real problem is to avoid unnecessary phase lag during computation.

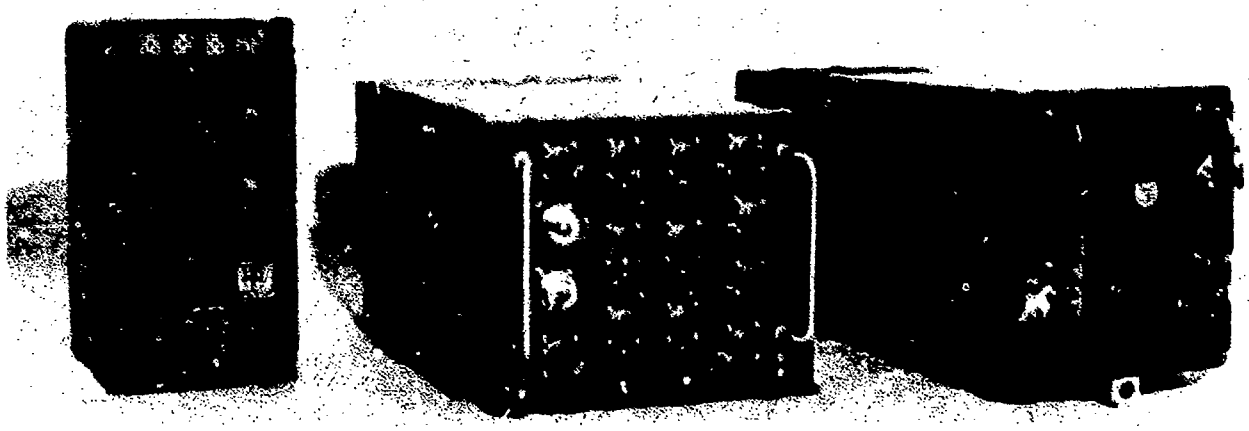

Figure 17. Control and display unit, computer TDY 43 and inertial measurement unit TDS-3-D.

3.5 Flight-Test Results

At the time when this paper was written, the CCV-F104 had completed a first test-phase, which was a pure calibration phase for the aerodynamic sensors. A total of 11 flights were performed. One IMU (part of the flights two IMUs) was installed, but was not subjected to detailed tests. However, the navigation accuracy observed was between 1 and 3 nmi/h CEP.

At the time of writing, phase II of the flight-tests with the fully equipped plane had just commenced. Four shakedown flights have been performed. These and a few follow-on flights are purely dedicated to aircraft open-loop performance evaluation since some external modifications may affect the aircraft aerodynamics.

Therefore, more detailed information is not included in this paper.

7.12

4. OUTLOOK/GROWTH POTENTIAL

From the point of view of the user (who also has accompanied a considerable part of the design and development of the described strapdown system), some remarks and predictions shall be given.

4.1 Performance

It goes without saying, that the basic sensor improvement will improve the ~~final~~ result. A considerable performance improvement is expected in the following areas:

(1) Error model improvements will result in better accuracy without hardware effort.

(2) Calibration and alignment improvements will have an additional effect.

(3) Faster computers will reduce phase lag and avoid stability problems. In addition, will allow one to use extended error models.

(4) Conversion technique improvents (for the pickoff signals of gyros and accelerometers) using improved V/F converters or digital caging loops will reduce noise effects and increase accuracy.

4.2 Safety of Flight/Redundancy

The IMUs used in the CCV-F104-program did not give any reason for complaints. To date the functions have been flawless. However, the amount of hardware needed in order to satisfy the $(fail\text{-}op)^3$ requirement is very large. Some possiblilities are given in the following subsections.

4.2.1 Failure Self-Monitoring

Failure self-monitoring, satisfying the same operational requirement $(fail\text{-}op)^3$, would reduce the necessary hardware by 25% if available with 100% confidence. Instead of four channels only three channels would be needed. However, this technique has not progressed above 90% confidence level depending on the particular hardware being used.

4.2.2 Semiskewing

The simiskewing technique monitors three orthogonal sensors by a fourth sensor arranged 2 x 45° as shown in Figure 18 and 19.

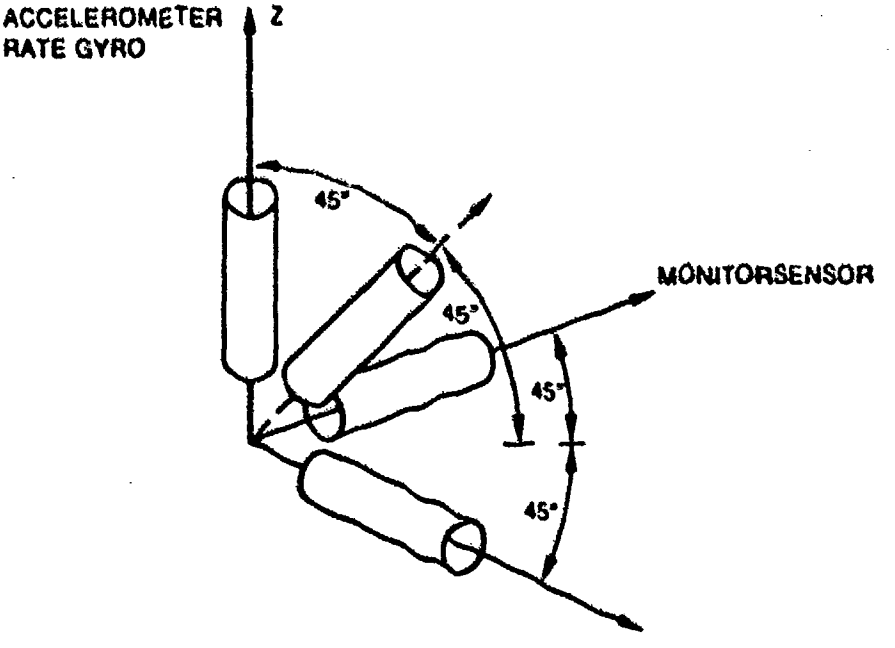

Figure 18. Sensor monitoring with skewed sensor.

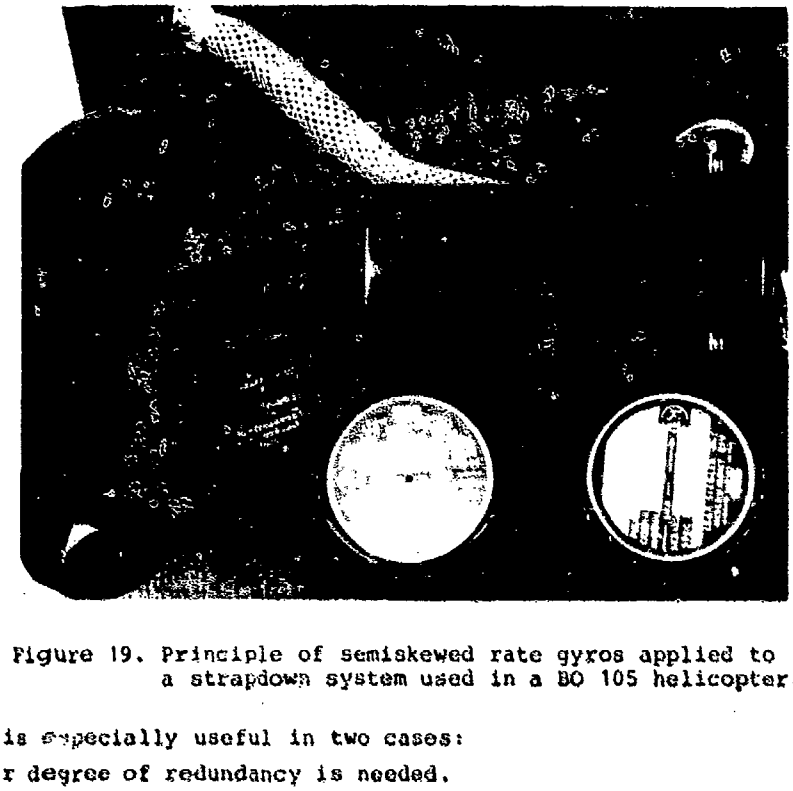

Figure 19. Principle of semiskewed rate gyros applied to a strapdown system used in a BO 105 helicopter.

This technique is especially useful in two cases:

(1) when a lower degree of redundancy is needed,

(2) when maintenance and easy replacement are important.

4.2.3 Full Skewing

Full skewing, here, means the three-dimensional orientation of a set of sensors such that the number of each set of sensors needed to fulfill the operational requirement is minimized.

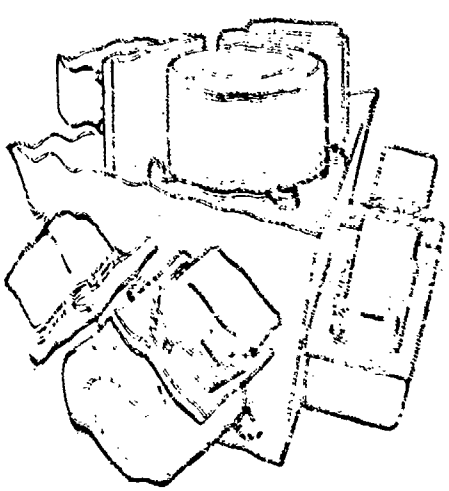

Figure 20. Fail-op' gyro and accelerometer full skewed arrangement using two-degree-of-freedom gyros.

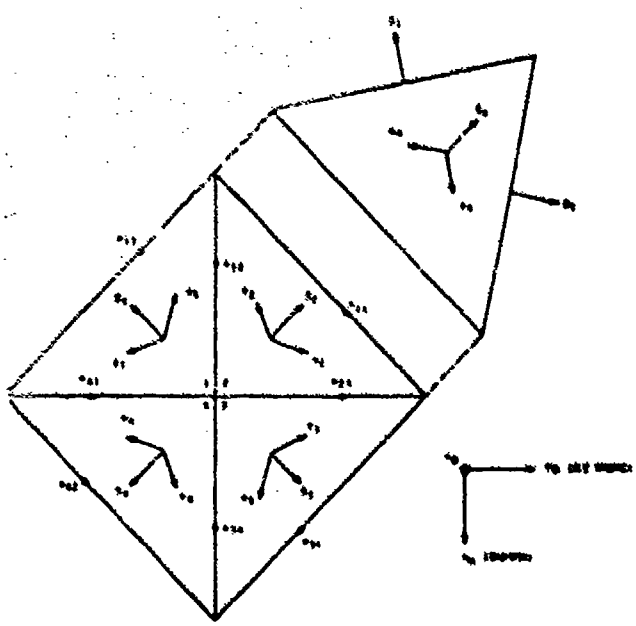

Figure 21. Semioctahedral gyro axis orientation as proposed by [4].

In comparison to parallel redundancy for a (fail-op)' requirement, the number of gyros is reduced from eight to only four as shown in Figure 21.

This method is especially useful in space applications, where no recovery/repair is possible.

For an aircraft application the following list of advantages/disadvantages has been gathered:

1.14

(1) Advantages

(a) Minimizes hardware.

(b) Saves space.

(c) Reduces power consumption.

(2) Disadvantages

(a) Power redundancy difficult/ not solved yet.

(b) Repair: in case of one sensor-failure, the whole sensor assembly has to be replaced and eventually recalibrated.

(c) In case of a sensor failure, a sensitivity reduction may occur because the sensor taking over the function may not be optimally oriented.

4.2.4 Timing and Cross-Strapping

In the case of redundant applications, a synchronious running of all units and computations is essential because it eases software implementation and improves early failure detection. Cross-strapping all sensor information to all computers is recommended, because it allows each computer to run its software with consolidated data without cross-communication prior to computation.

4.3 Sensor Distribution and Vulnerability

The distribution of redundant sensors due to vulnerability considerations often has been discussed but has not been implemented to date. The reason lies in the difficult handling of the redundancy management, since each sensor measures local information, which contains a considerable part of elastic body motion contribution. Since this complicates the redundancy management seriously, it has not been used yet. On the other hand, new requirements for measuring local inertial information arise (i.e., rates or accelerations for control of elastic aircraft motions). No new solution can be offered yet, but a new contribution can be made to the sensor-distribution discussion.

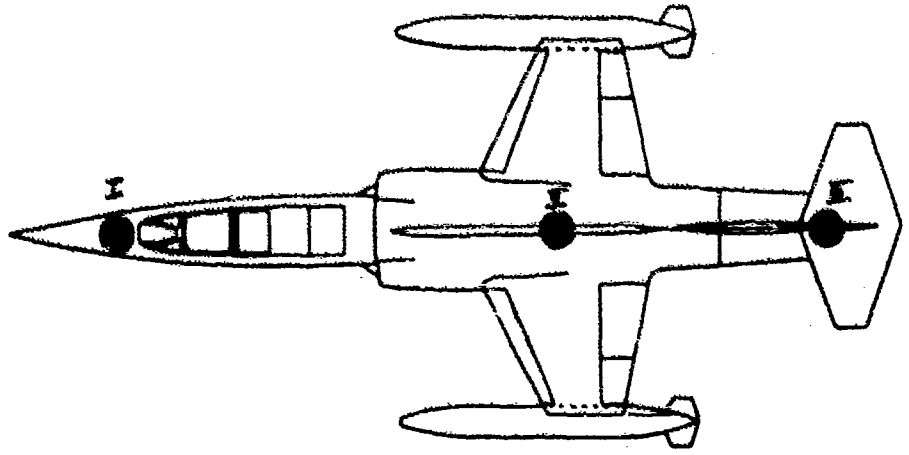

Figure 22. Sensor distribution in an aircraft.

In Figure 22, sensor set I is mounted to the forward-looking radar, II at the center of gravity, and III in the rear to an aft-looking radar. Assuming, all sets are self monitoring, the following requirements can be satisfied.

(1) (Fail op)^2 operational requirement.

(2) Reduction of vulnerability by sensor decentralization.

(3) Close alignment between forward-looking radar to inertial navigation systems.

(4) Close alignment between aft-looking radar to inertial navigation systems.

(5) Control of elastic fuselage bending mode is possible.

As stated before, this does not present a solution; it should be understood as a new input to a long-last[illegible] discussion.

4.4 Strapdown Sensors and the Data Bus

The introduction of a data-bus to new a/c is undoubtedly a must. The question concerning inertial information from this user point-of-view only is, WHEN? This means: Shall we put raw data on the bus? Shall we compensate first? Shall we have a complete IN-computation at the place of data gathering? etc.

The present data-bus standard (MIL-STD 1553 B) uses a 1-MHz bit rate, with 20 bits per word. This results in a maximum word rate of 50.000 words per second, which will additionally be reduced by communication overhead. An inertial state-vector information transmission (as described in section 3.3) needing 28 16-bit-words for 26 data takes 560 µs from the first to the last bit. This does not include any overhead!

Early measures have to be undertaken to avoid the dangers of

(1) Bus overload.

(2) Untolerable phase lag.

These two problems do not have a generally applicable solution. Therefore, two solutions shall be presented for discussion.

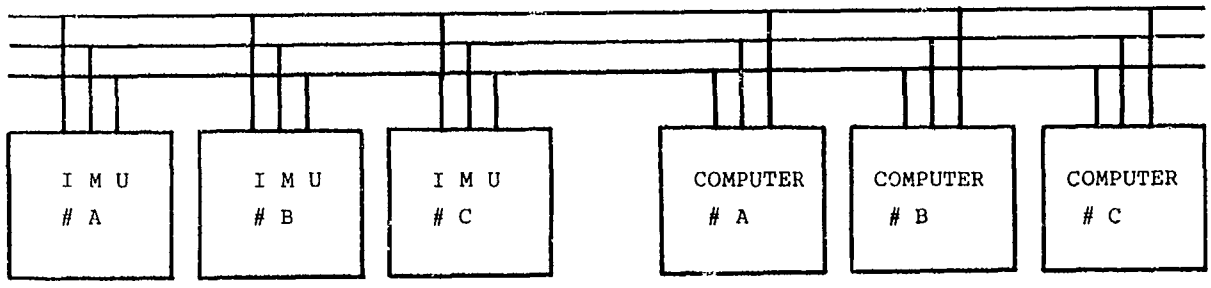

Figure 23. Strapdown sensor data-bus configuration for accommodating bus overload.

In the solution diagrammed in Figure 23, the IMUs deliver error-compensated rates and accelerations; the triplicated data-bus connection takes care that each computer gets all information.

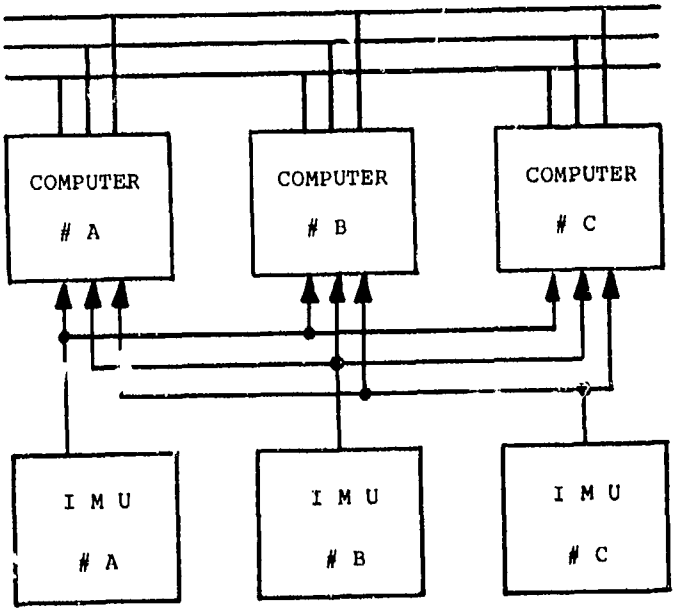

Figure 24. Strapdown sensor data-bus configuration for accommodating untolerable phase lag.

The second solution (Figure 24) does not put any unnecessary information on the bus, and can be made much faster than the first one. But it takes more interfaces and some more wiring.

In both cases, the inertial information will be made available to other users. This avoids the unnecessary multiple installations we experienced in the past.

5. CONCLUSIONS

Based upon our experience with a quadrupally redundant strapdown system, and on the growth potential observed here and on other occasions, we find strapdown inertial technology to be an excellent innovative technique. Especially in redundant and integrated guidance and control systems strapdown sensors are the prime candidates for new projects.

Strapdown offers a significant reduction of hardware and cost and considerably reduces the effort in those applications where not only redundant rates and accelerations but also redundant altitudes and other higher information are needed.

REFERENCES

[1] Dr. Donoghue, P. J., "System Description and Performance Characteristics of a Quad Redundant Strapdown Inertial Navigation and Flight Control System", presented at the National Aerospace and and Electronics Conference, May 18, 1977, Dayton, Ohio.

[2] Irvine, R. B., Ritter, J. W., "An Examination of Low Power Spectral Density (PSD) Noise Performance of a Dry Tuned Gimbal Two-Degree-Of-Freedom Gyroscope, and Methods for Further Noise Reduction", presented at the Eighth Biennial Guidance Test Symposium.

[3] Dr. Kubbat, W., "A Multifunctional Guidance and Control System", Proceedings of the IEEE 1977 National Aerospace and Electronics Conference NAECON '77, Dayton Convention Center, Dayton, Ohio, May 1977.

[4] Siouris, G. M., "A Survey of New Inertial Sensor Technology", Zeitschrift Flugwiss. Weltraumforschung 1 (1977), Heft 5, p. 345 - 353.

[5] Dr. Kubbat, W., "Evaluation of a Digital Helicopter Control System", paper No. 33, presented at the Third European Rotorcraft and Powered Lift Aircraft Forum, Association Aeronautique et Astronautique de France, Sept. 7-9, 1977, Aix-en-Provence, France.

[6] "CCV-F104 System Handbook", Vol. II, MBB internal report, Munich, 1977.

S I L 3
SYSTEME DE GUIDAGE INERTIEL STRAP-DOWN POUR ENGIN TACTIQUE

8-1

par
G. Cattan - J. Michelin
Société de Fabrication d'Instruments de Mesure
13, avenue Ramolfo Garnier
91301 Massy
FRANCE

RESUME

Parmi les systèmes strap-down développés par la Société de Fabrication d'Instruments de Mesure (SFIM) à partir des différents modèles de Gyroscopes Accordés Miniatures GAM 1 et GAM 3, le plus élaboré est le SIL 3 destiné au guidage précis des engins tactiques.

Le SIL 3 réunit dans un même boîtier les deux gyroscopes GAM 3, les trois accéléromètres, les circuits de bouclage et de calcul.

Le gyroscope GAM 3, spécialement développé par la SFIM, est un gyroscope deux axes à suspension souple, construit pour mesurer les vitesses angulaires jusqu'à 100°/s avec une précision de 100 ppm sur la linéarité et le facteur d'échelle. Un bouclage numérique permet l'entrée directe dans les circuits de calcul très élaborés. L'utilisation efficace d'une modélisation poussée contribue aux performances du système.

La SFIM a développé également les moyens de simulation et de test qui permettent de prévoir et de contrôler les performances du système pour les différentes ambiances prévues à l'utilisation.

1. HISTORIQUE

C'est en 1972 que la Société de Fabrication d'Instruments de Mesure (SFIM) dont l'activité principale est consacrée à l'étude et à la réalisation d'équipements gyroscopiques, a réellement débuté dans l'étude des systèmes strap-down avec le développement d'un premier gyroscope à suspension souple accordé de conception entièrement originale.

Le Gyroscope Accordé Miniature GAM 1 est actuellement réalisé en série pour un grand nombre d'applications. C'est un gyroscope robuste, de conception très simple et de réalisation très économique (Figure 1), dont les caractéristiques peuvent varier suivant les modèles :

(1) De 1 à 30°/h pour la dérive jour à jour.

(2) De 15 à 400°/s pour la vitesse de précession.

(3) De 0,2 à 0,5 % pour la linéarité du facteur d'échelle.

Il est principalement utilisé pour la stabilisation fine des systèmes de visée et conduites de tir (optique, télévision, infrarouge, radar) et la mesure des vitesses angulaires avec un bouclage à sortie numérique.

Ce gyroscope est incorporé dans des systèmes de guidage strap-down pour les applications où le prix de revient est plus important que les performances.

(1) Le SIL 1 (Figure 2) comprend trois gyroscopes dont deux balourdés associés à un calculateur.

(2) Le SIL 2 (Figure 3) comprend deux gyroscopes et trois accéléromètres associés à un calculateur.

En 1974 la SFIM commence le développement du système strap-down SIL 3 destiné au guidage des engins tactiques, dont la description fait l'objet du présent exposé.

2. PRESENTATION GENERALE DU SYSTEME SIL 3 (Figure 4)

2.1. Domaine d'Utilisation

L'étude du SIL 3 est axée dans un premier temps sur le guidage d'un missile tactique. Elle s'applique aussi au préguidage de missiles possédant un autodirecteur.

Le système assure :

(1) La mesure des vitesses angulaires et des accélérations.

(2) Le calcul du cap, de l'attitude.

(3) Le calcul des vitesses selon les trois axes et du point.

Il permet ainsi le pilotage et la navigation du missile, en guidage inertiel total, ou en préguidage inertiel.

Les objectifs retenus en matière de performances, de volume ou de poids sont relativement raisonnables. Mais il faut y inclure la recherche d'une grande robustesse, nécessaire dans les conditions d'environnement sévères propres aux missiles, d'un taux de fiabilité élevé, d'un coût réduit, tant à l'achat qu'à la maintenance.

Toutes les solutions retenues tiennent compte en premier lieu de ces critères.

L'étude du SIL 3 a été décomposée en trois phases :

(1) Dans un premier temps, la SFIM a développé le gyroscope GAM 3. Ce gyroscope, spécialement étudié pour répondre au problème posé, mais s'appuyant cependant sur l'expérience acquise avec le GAM 1 et le GAM 2, est un gyroscope accordé, deux axes. Il a un seul anneau de cardan, est dessiné pour avoir une grande robustesse. Il peut précessionner à plus de 100°/s.

(2) Dans une deuxième phase, la SFIM réalise un système strap-down dans lequel un boîtier unique groupe deux gyroscopes GAM 3, trois accéléromètres, ainsi que toute l'électronique nécessaire à la mise en oeuvre de ces capteurs et à l'acquisition des mesures. Le développement du logiciel est effectué sur un mini-ordinateur du commerce tandis que se développe parallèlement la réalisation des éléments de calcul embarquables SYCOMORE, répondant par leurs performances élevées et leur volume réduit aux spécifications strap-down.

(3) Enfin la réalisation du SIL 3 est l'aboutissement logique des phases précédentes, en ce sens que les capteurs, leur électronique, ainsi que les circuits de calcul et d'interface sont regroupés dans un boîtier unique, constituant ainsi un système de navigation strap-down totalement intégré.

2.2. Description Générale

Le SIL 3 se présente sous la forme d'un boîtier de 208 x 190 x 190 mm (Figure 6) dont la masse est d'environ 7 Kg.

L'avant du boîtier reçoit le bloc senseur sur lequel sont fixés les deux gyroscopes GAM 3 et les trois accéléromètres.

Le bloc senseur est suspendu par rapport au boîtier.

Le boîtier par lui-même renferme un bloc d'alimentation et un ensemble de cartes électroniques.

Cet ensemble comprend :

(1) Les boucles d'asservissement des gyroscopes.

(2) Le codage des informations d'accélération.

(3) Les circuits de conversion analogique/numérique.

(4) Les circuits numériques d'acquisition et d'échanges avec le calculateur.

(5) Les éléments de calcul SYCOMORE et leur mémoire.

(6) L'interface permettant le dialogue, par l'intermédiaire d'un BUS simple, avec le missile.

La Figure 7 donne le bloc diagramme fonctionnel de l'ensemble.

Le système reçoit du missile son alimentation sous forme d'un 28 V batterie.

Toutes les informations reçues ou échangées sont de type numérique et transitent par le bus.

Le SIL 3 ne comprend aucun réglage fin de biais, de dérive ou de facteur d'échelle.

Le calibrage est entièrement effectué au moyen de tests semi-automatiques, et les valeurs mesurées lors de ces tests mises en mémoire par le calculateur.

De même, la compensation des erreurs des capteurs en fonction des accélérations, de la température, etc... est entièrement effectuée par logiciel.

Un convertisseur statique assure la génération à partir de la tension 28 V batterie du missile, de toutes les tensions nécessaires à la mise en rotation des gyroscopes, à l'excitation de leurs détecteurs de position angulaire, à l'alimentation des accéléromètres et de l'ensemble des circuits électroniques.

Les signaux délivrés par les détecteurs de position angulaire des gyroscopes sont utilisés pour commander les moteurs de précession par l'intermédiaire de boucles binaires, fonctionnant en modulation de largeur.

Chaque boucle comprend des correcteurs, une source de courant très précise, un commutateur en H, ainsi que les circuits logiques associés.

Les accéléromètres sont des accéléromètres "secs" pendulaires bouclés en continu. Leurs informations de sortie sont converties en incréments de vitesse par des circuits de codage qui sont eux aussi binaires, et à modulation de largeur.

Afin de permettre la compensation, par logiciel, des erreurs des capteurs, un convertisseur analogique/numérique multiplexé prend en compte les informations d'écart résiduel des gyroscopes, ainsi que la température de chaque gyroscope et de chaque accéléromètre.

La mesure de la période de rotation de chaque toupie permettra de corriger les erreurs dues au phénomène de "wheel-hunting" des gyroscopes.

L'ensemble des mesures ainsi effectuées est acquis en multiplexé pour être transmis au SYCOMORE, associé à ses mémoires ROM, RAM, et EAROM.

Les circuits d'interface assurent le dialogue, par l'intermédiaire du BUS, entre SYCOMORE et le missile.

3. DESCRIPTION DU SYSTEME

3.1. Le gyroscope GAM 3

Le capteur gyroscopique est certainement l'élément le plus difficile à réaliser dans un système inertiel strap-down ; en effet, il doit posséder, en plus des qualités demandées à des gyroscopes classiques montés sur des supports asservis en rotation, une capacité de précession à des vitesses angulaires élevées de l'ordre de plusieurs dizaines de degrés par seconde, autrement dit, il doit être à la fois un bon gyroscope et un excellent gyromètre.

3.1.1. Performances

Le capteur gyroscopique utilisé dans la référence inertielle SIL 3 est un gyromètre asservi deux axes à joint souple accordé monocardan ; il est muni d'un moteur-couple de précession galvanométrique (voir Figure 8).

Ses principales caractéristiques, données par le tableau 1 ci-dessous, peuvent subir quelques variations, en fonction de l'application envisagée pour le système.

Tableau 1

Encombrement (avec préampli) :	
diamètre	52 mm
longueur	65 mm
Moment cinétique	1,6 à $3,2.10^5$ CGS
Vitesse de rotation	160 à 320 t/s
Temps de mise au synchronisme	10 à 20 s
Domaine de liberté du rotor	$\pm$ 30 mn.d'arc
Dérive aléatoire	0,03 à 1 °/h
Domaine des vitesses angulaires :	
permanentes	$\pm$ 20 à $\pm$ 50°/s
temporaires	$\pm$ 100 à $\pm$ 200°/s

3.1.2. Détails Technologiques (Figure 9)

Le GAM 3 est constitué essentiellement (voir Figure) d'une part d'un corps rigide sur lequel est fixé le moteur d'entraînement (spin motor) à hystérésis multipolaire, les 4 circuits des détecteurs angulaires de position à réluctance variable, les 4 bobinages des moteurs-couples galvanométriques X et Y ; d'autre part, d'un élément tournant comprenant un axe relié à la partie fixe par 2 roulements précontraints et au volant par un cardan souple compensé.

Le volant est constitué essentiellement de 4 couronnes monobloc d'aimants permanents au Samarium Cobalt et de 2 cylindres en acier doux pour refermer le circuit magnétique.

Le champ radial créé par ces aimants permanents mobiles agit sur les bobinages fixes situés dans les entrefers pour exercer les couples nécessaires à l'obtention des fortes vitesses angulaires de précession.

La principale caractéristique de ce gyromètre 2 axes est sa simplicité de réalisation et par conséquent son faible coût compte tenu de ses performances ; en effet, la partie la plus délicate qui est l'articulation du volant est réalisée à l'aide d'un joint souple monocardan constitué de quatre "bras" de section cruciforme dont 2 sont reliés à l'axe d'entrainement par une fourche , les 2 autres étant fixés sur le volant ; l'anneau intermédiaire qui relie les 2 axes du cardan a des dimensions très réduites qui lui confèrent une inertie très faible autour de l'axe du spin ; la compensation des couples de rappel élastique du cardan est obtenue par 2 petites masses vissées de part et d'autre de l'anneau intermédiaire.

Ce joint souple de disposition originale est réalisé très simplement d'une seule pièce par électro érosion ; il donne toute satisfaction pour les performances recherchées du gyroscope.

Le GAM 3 est équipé d'une résistance chauffante interne et d'une sonde pour permettre un préchauffage éventuel du gyroscope.

La butée qui a été disposée entre l'axe d'entrainement et le volant enlève toute fragilité au gyroscope.

Parmi les difficultés qu'il a fallu surmonter pour la mise au point du GAM 3, on peut citer l'influence de la température sur les aimants et la sensibilité magnétique du gyroscope.

La variation de l'induction des aimants permanents au Samarium Cobalt en fonction de la température est en effet de l'ordre de 5.10^{-4} par degré centigrade ; un shunt magnétique corrige la quasi totalité de cette variation. Le résidu est annulé par compensation dans le calculateur du facteur d'échelle des moteurs-couples en fonction de la température mesurée du volant.

Pour éliminer l'influence de l'environnement magnétique, le gyroscope est fermé par un boîtier servant de blindage magnétique.

3.2. L'accéléromètre MICAL (Figure 10)

3.2.1. Principe

L'accéléromètre utilisé dans le système SIL 3 est le "MICAL" développé par la Société Française d'Equipements pour la Navigation Aérienne (SFENA). C'est un accéléromètre miniature, de classe 100 ppm, d'un coût de production faible obtenu par une analyse minutieuse de la valeur, et par la réduction ou la suppression des opérations de réglage.

L'accéléromètre MICAL fonctionne selon le principe du pendule asservi, à un degré de liberté et à amortissement électronique (single axis, pendulous force balancing system).

Un pendule à rappel électromagnétique, suspendu par deux barres flexibles formant une charnière, constitue l'élément sensible.

Toute accélération appliquée suivant l'axe de mesure tend à écarter le pendule de sa position d'équilibre.

Un détecteur d'écart angulaire, de type capacitif, délivre un signal alternatif dont la phase et l'amplitude sont fonction de l'écart mesuré.

Après amplification, démodulation, filtrage et correction de phase, ce signal est intégré et appliqué sur un amplificateur de puissance à courant continu. Celui-ci engendre dans la bobine de rappel du moteur-couple à aimants permanents et dans la résistance de mesure le courant nécessaire pour équilibrer l'action de l'accélération et ramener le pendule dans sa position initiale.

3.2.2. Caractéristiques

L'accéléromètre MICAL, avec son électronique d'asservissement incorporée, se présente sous la forme d'un parallélépipède de 36 x 20 x 23,5 mm.

Sa masse est de 60 g.

L'alimentation nécessite une source de tension $\pm$ 15 V.

La mise en oeuvre est instantanée. Aucun préchauffage n'est nécessaire.

La gamme des températures de fonctionnement est de -30 à +95°C.

Le domaine de mesure est de $\pm$15 g, avec un facteur d'échelle de 0,5 V/g.

3.3. Support des Capteurs

Le support des capteurs (Figure 11) est constitué d'une structure sur laquelle sont fixés les deux gyroscopes et les trois accéléromètres.

Les gyroscopes ont leurs spins à 90° l'un de l'autre, et leurs axes de mesure sont placés à 45° par rapport aux axes engin.

Ainsi, les deux gyroscopes sont utilisés pour mesurer la vitesse angulaire de roulis, un seul pour mesurer la vitesse angulaire de tangage ou de lacet. Cette disposition présente de nombreux avantages, le principal étant d'augmenter le domaine de mesure en roulis.

Les accéléromètres sont placés sur trois axes rectangulaires.

Deux accéléromètres placés à + et - 45° de l'axe de roulis sont utilisés pour mesurer l'accélération longitudinale.

Le support des capteurs est lié à la structure du missile par une suspension élastique constituée de 4 plots en élastomère.

Les caractéristiques de la suspension sont adaptées en fonction de l'utilisation. D'une façon générale, elle doit permettre d'isoler les capteurs des chocs et des vibrations à fréquence élevée, tout en n'introduisant pas de déphasage ou de mouvement angulaire parasite à fréquence basse. Dans tous les cas, la suspension ne doit pas engendrer de mouvement conique.

Les dimensions du support, équipé de ses capteurs sont de 150 x 65 x 65 mm.

3.4. Electronique

3.4.1. Fonctions Générales (Figure 12)

(1) Un convertisseur statique reçoit la tension 28 V continu venant de la batterie du missile.
Il génère les différentes tensions continues nécessaires au fonctionnement du système. L'ensemble de ces tensions est isolé galvaniquement de la source 28 V.
La puissance délivrée est de l'ordre de 80 W en régime permanent et peut atteindre 200 W en crête.
Les circuits comprennent :

(a) une alimentation à découpage 28 V/ 20 V
(b) le convertisseur proprement dit, fonctionnant à 12 kHz
(c) un ensemble de régulateurs

(2) Les gyroscopes ont une vitesse de rotation de 320 Hz environ. Ils utilisent des moteurs d'entraînement triphasés, synchrones, à hystérésis, ayant 4 paires de poles.
L'alimentation de ces moteurs reçoit une fréquence d'entrée de 7.680 Hz obtenue par division, à partir de l'oscillateur principal. Un diviseur par 6, suivi d'un registre à décalage, produisent 6 signaux logiques à 1.280 Hz de rapport cyclique 1/3, décalés de 1/6 de période les uns par rapport aux autres.

Ces signaux logiques, associés deux à deux, commandent les trois amplificateurs de puissance fonctionnant en mode saturé bloqué.
Les deux gyroscopes utilisent des fréquences différentes, décalées de 3.10^{-3}.

(3) Les enroulements primaires des détecteurs de position des gyroscopes sont excités à une fréquence de 50 kHz, en tension sinusoïdale.
Un signal logique à 50 kHz, issu par division de l'oscillateur principal, est envoyé à un filtre sélectif dont la sortie fournit directement la puissance nécessaire. Une détection associée à une boucle de régulation assure la stabilité de la tension de sortie.

3.4.2. Bouclage des Gyroscopes

Le bouclage des gyroscopes est réalisé par une commande quantifiée, binaire, fonctionnant en modulation de largeur (Figure 13). Le choix de cette méthode, de préférence à celle du bouclage ternaire, ou du bouclage continu suivi d'un codage, a été fait en fonction des critères suivants :

(1) Régime thermique constant : cette méthode est celle qui permet le mieux de minimiser les erreurs dues aux variations de températures liées à la vitesse d'entrée.

(2) Relative simplicité. De plus, la sortie se fait directement en numérique, sous forme d'incréments angulaires. Il n'y a pas de circuits de conversion extérieurs à la boucle.

(3) Excellente résolution.

(4) Bonne linéarité et bonne symétrie, en particulier autour du zéro.

(5) Fonction de transfert proche de celle d'une commande analogique.

La réalisation pratique des circuits de bouclage répond par ailleurs à des critères fondamentaux :

(1) Respect des spécifications de précision définies lors de l'étude théorique.

(2) Maintien de la puissance dissipée à un niveau raisonnable. Ce point nous a d'ailleurs conduits à réaliser une commande à deux niveaux de courant avec commutation automatique.

(3) Respect des spécifications de gain et de bande passante nécessaires à l'ensemble du système.

L'étude théorique d'un bouclage binaire adapté et optimisé pour un gyroscope accordé deux axes a conduit la SFIM à réaliser un ensemble de simulations reproduisant le plus exactement possible le comportement d'un tel gyroscope.

Par ailleurs, une méthode d'analyse originale a été développée. Cette méthode, faisant appel à des fonctions de transfert complexes permet l'utilisation, sur des systèmes à deux axes, des lieux complexes de NYQUIST ou de BLACK.

Appliquée dans un premier temps à l'étude de stabilité et à l'optimisation d'un bouclage analogique, cette méthode a démontré une excellente corrélation avec les résultats expérimentaux. Cette même méthode, adaptée, a été ensuite utilisée pour la définition des correcteurs de la boucle binaire. Les résultats obtenus ont été confirmés tant en simulation, que, plus tard, expérimentalement.

La Figure 14 donne un exemple des résultats obtenus.

L'aspect général de la boucle est donné par la Figure 15.

(1) Les détecteurs de position du gyroscope délivrent deux tensions alternatives proportionnelles aux écarts en X et en Y.

(2) Ces tensions sont préamplifiées, démodulées, filtrées.

(3) Des circuits de compensation croisée réalisent une fonction de la forme :

$$V_{Sx} = a\ V_{ex} - b\ V_{ey}$$

$$V_{Sy} = a\ V_{ey} + b\ V_{ex}$$

Ils sont complétés par des correcteurs à action proportionnelle et intégrale.

(4) La tension de sortie du correcteur intégral est comparée à une rampe, puis synchronisée par une bascule pour générer un signal logique modulé en largeur.
Ce signal logique est traité pour limiter les valeurs extrêmes du taux de modulation, et déterminer les changements de niveaux de courant ; il est ensuite utilisé pour commander le passage en positif ou en négatif d'un courant de référence Io dans l'enroulement du moteur de précession.
La commutation du courant est réalisée par l'intermédiaire d'un ensemble de transistors montés en H.
Le courant de référence est généré par une source de courant utilisant une diode Zener à très haute stabilité suivie d'amplificateurs opérationnels et de transistors de puissance. La réponse dynamique de cette source de courant, intervenant principalement lors des commutations du H, est un paramètre important.

Le commutateur en H est dessiné de façon à minimiser les échanges de courant entre circuits de commande et circuits commandés. Il doit par ailleurs commuter rapidement et présenter des fuites aussi faibles que possible dans les branches verticales du H.

L'ensemble de la chaîne de bouclage a une bande passante de 50 Hz. La fréquence du cycle limite est de 800 Hz. Le poids de l'incrément angulaire est de 0,7 seconde d'arc en mode lent et 3,6 secondes d'arc en mode rapide.

3.4.3. *Conversions A/N. Interface Calculateur*

(1) Les accéléromètres du SIL 3 sont bouclés en continu. Les informations d'accélérations sont donc des tensions continues qui sont converties en incréments de vitesse par un codeur binaire utilisant la modulation de largeur (Figure 16).

La précision statique et les performances dynamiques du codeur ont été particulièrement étudiées en fonction de l'application strap-down. L'utilisation de circuits de codage comportant un bouclage du 2ème ordre assure l'élimination de l'erreur de traînage lorsque l'entrée est en forme de rampe.

Le poids de l'incrément de vitesse est de 2.10^{-3} m/s.

La fréquence de coupure des circuits de codage est de 100 Hz.

La fréquence du cycle limite est de 800 Hz.

(2) La compensation des informations fournies par les gyroscopes et les accéléromètres nécessite la prise en compte par le calcul :

(a) Des angles d'écart mesurés par les détecteurs inductifs des gyroscopes.
(b) Des températures de chaque gyroscope et de chaque accéléromètre, mesurées par des sondes résistives.

Cette prise en compte est réalisée par l'intermédiaire d'un convertisseur A/N fonctionnant en multiplexé (Figure 16). La cadence de conversion est de 10 ms le temps total de conversion de 200 µs. Pendant ces 200 µs le convertisseur code successivement les 4 tensions d'écart, 1 température, et 3 tensions de test. Un deuxième multiplexeur assure la répartition sur 8 cycles de 10 ms du codage de l'ensemble des températures.
Une logique de séquencement pilote à la fois les multiplexeurs et l'adressage de la mémoire de rangement recevant les informations codées et assurant leur transfert aux éléments de calcul par le bus interne.

(3) L'acquisition de l'ensemble des informations associées à des modulations de largeur, c'est à dire les 4 informations de vitesse angulaire des gyroscopes et les 4 informations d'accélération, est réalisée par un seul compteur reversible, associé à une mémoire de travail, et fonctionnant en multiplexé (Figure 17).
Un autre compteur, également associé à une mémoire et multiplexé, effectue la mesure de la période de rotation de chacun des deux gyroscopes. Cette information, prélevée avec une grande résolution, permettra la correction des erreurs de type "wheel-hunting".

Une mémoire de rangement reçoit l'ensemble des informations délivrées par les compteurs et assure leur transfert au calculateur par le bus interne.
Le dialogue entre le calculateur et les mémoires de rangement s'effectue par l'intermédiaire d'un sérialiseur.

3.5. Ensemble de traitement SYCOMORE

3.5.1. Principe

Les traitements à réaliser dans le système strap-down SIL 3 sont de deux natures :

(a) Calculs très rapides de nature mathématique :
- corrections gyromètres
- corrections accéléromètres
- détermination de l'attitude et des vitesses

(b) Calculs plus lents orientés vers les opérations logiques :
- séquencement du système
- entrées/sorties vers le panneau de commande et visualisation
- sortie des informations sur le bus système
- autotests du système

Une solution permettant de traiter l'ensemble du problème consiste à utiliser un calculateur universel rapide, mais cette solution n'a pas été retenue pour le matériel embarqué.

En effet, afin de minimiser les volumes et les coûts, il est nécessaire d'utiliser les composants standards les plus intégrés disponibles sur le marché.

La solution optimale retenue a consisté à associer un microprocesseur et un opérateur rapide travaillant uniquement sur des nombres flottants.

Ces deux unités de traitement peuvent travailler en simultanéité, formant ainsi une véritable configuration bi-processeur.

Cet ensemble de calcul se nomme SYCOMORE (Système de Calcul à Organisation Multi-Opérateur pour Réalisations Embarquées).

L'opérateur rapide effectue les tâches de type a et le microprocesseur les tâches de type b.

3.5.2. Organisation (Figure 18)

Le système est organisé autour de deux bus principaux :

(1) Le bus mémoire regroupant 15 lignes d'adresses, 16 lignes de données bidirectionnelles et un certain nombre de commandes de la mémoire.

(2) Le bus entrées/sorties.

Le bus mémoire est utilisé par les deux processeurs.
Une logique d'accès permet de résoudre les conflits.

Le bus entrées/sorties est géré par le microprocesseur.

La mémoire est organisée en mots de 16 bits. Elle est partagée en trois parties :

(1) Les programmes en mémoire morte.

(2) Les données volatiles en RAM.

(3) Un certain nombre de données particulières en mémoire protégée.

Les entrées/sorties du système sont constituées par :

(1) Les informations fournies par les gyromètres et accéléromètres.

(2) Le couplage du panneau de commande et visualisation.

(3) La génération du bus de sortie distribuant les paramètres d'attitude et de navigation vers les utilisateurs.

3.5.3. Fonctionnement (Figure 19)

Les tâches sont gérées par le microprocesseur qui effectue lui-même les tâches les moins prioritaires et sous-traite à l'opérateur flottant les tâches de calcul rapide. Ces tâches une fois lancées sont entièrement réalisées par l'opérateur flottant qui accède directement aux programmes de traitement en mémoire.

Les interruptions sont gérées par le microprocesseur qui a la faculté d'interrompre l'opérateur flottant pour lui faire exécuter des tâches plus prioritaires. Le changement de contexte est alors géré par l'opérateur flottant lui-même.

L'opérateur flottant signale qu'il a terminé sa tâche par l'intermédiaire d'une interruption générée vers le microprocesseur.

8-8

3.5.4. Caractéristiques et Performances

(1) Microprocesseur

Le microprocesseur utilisé possède :

(a) Une unité de traitement sur 16 bits.
(b) Un système de 16 interruptions hiérarchisées avec changement de contexte automatique.
(c) 69 instructions permettant les traitements sur mots, sur octets ou sur bits.
(d) Une vitesse moyenne d'instruction de l'ordre de 6 µs.
(e) Un bus entrées/sorties série.

(2) Opérateur flottant (voir Figure 19)

L'opérateur flottant est une unité de calcul microprogrammée, manipulant des nombres flottants de 32 bits dont 8 bits d'exposant (2^{-128} à 2^{127}) et 24 bits de mantisse (dont 1 bit de signe).

(a) Programmation
Les tâches de calcul sont exprimées sous forme de programmes situés dans la mémoire. L'opérateur dispose donc d'un jeu d'instructions qui lui est propre et de moyens logiciels adaptés à la génération des programmes de calcul (compilateur)

(b) Microprogrammation
A chaque instruction, correspond un microprogramme réalisé à l'aide de micro-instructions. L'enchainement des micro-instructions est géré par un microséquenceur pouvant adresser 512 mots de mémoire de microprogramme. Afin d'obtenir la meilleure rapidité d'exécution possible, il n'existe pas à proprement parler de jeu de micro-instructions. Une micro-instruction est décrite par un mot de 72 bits répartis en plusieurs champs indépendants, exprimant des codes composés ou des microcommandes discrètes.

Cet arrangement permet de décrire plusieurs actions simultanées, et, par conséquent, entraine un accroissement sensible de la vitesse d'exécution des microprogrammes optimisés au mieux. Des dispositions particulières ont été prises pour que la microprogrammation puisse disposer de constantes, ce qui est particulièrement intéressant pour l'exécution d'instruction complexe. A l'aide des moyens particuliers on peut réaliser des microprogrammes à la demande.

(c) Unité de traitement
Dans un but de simplification des matériels, l'opérateur de base est à 32 bits, dont 8 bits réservés à l'exposant et 24 bits réservés à la mantisse. Il utilise les éléments LSI AMD 2900. Fondamentalement, l'unité de traitement est organisée comme une machine à pile. Elle comprend une unité arithmétique et logique, une pile d'opérandes flottants à 8 crans, utilisée dans la plupart des instructions, et une mémoire registre de 8 registres banalisés dont certains sont spécialisés (compteur ordinal, base d'adressage, index) et les autres utilisés comme mémoire rapide de travail.

(d) Temps d'exécution
Les opérations s'effectuent essentiellement sur pile. Les temps d'exécution maximaux sont les suivants (avec mémoire rapide bipolaire) :

Addition flottante	6 µs
Multiplication flottante	7 µs
Push ou pull de la pile	2,4 µs
Sinus, arc tangente	80 µs

3.5.5. Génération du Logiciel (Figure 20)

Afin de faciliter l'écriture des programmes, on a défini un sous-ensemble du FORTRAN susceptible d'être compilé pour une exécution sur l'opérateur flottant.

L'intérêt du FORTRAN réside dans le fait qu'il permet une écriture aisée des programmes de calcul et donne la possibilité d'effectuer une mise au point sur la plupart des calculateurs.

Les programmes testés sont ensuite compilés afin de générer un programme objet susceptible d'être exécuté sur SYCONORE.

Ces programmes sont associés aux programmes écrits en assembleur pour le microprocesseur et après édition de liens, ils sont chargés dans la mémoire de SYCONORE.

Un système d'aide à la mise au point permet ensuite de faire fonctionner le système en temps réel tout en l'associant à des moyens informatiques de contrôle.

3.6. Logiciel d'Application

3.6.1. Principes

Le logiciel d'application a été défini pour répondre aux applications très générales citées plus haut.

On a tenu compte, bien sûr, de caractéristiques de la mission (durée de vol, ambiances dynamiques linéaires et angulaires). L'objectif est le suivant : le logiciel ne doit pas apporter d'erreur propre supérieure à 10% de l'erreur totale du système.

Une étude préalable très complète du fonctionnement d'un gyroscope sec, et d'un accéléromètre pendulaire, en ambiance dynamique sévère, nous a conduit à définir des algorithmes de corrections d'erreurs très complets. Par ailleurs, la bande passante cherchée (> 30 Hz) nous imposait une cadence minimale pour les principaux algorithmes de calcul.

8-9

L'optimisation du logiciel a porté essentiellement sur :

(1) La minimisation du volume et du temps de calcul.

(2) La modularisation du programme : de cette façon, les mêmes modules principaux peuvent être réutilisés pour les diverses séquences de vol (alignement, calage, tir, ...).

Les divers modules (séquences de calculs, algorithmes) sont déclenchés, suivant les cas :

(1) Par interruption externe provenant du bloc senseur.

(2) Par interruption interne programmée.

(3) Par flag, à l'intérieur d'un même programme.

On peut décrire rapidement les principaux modules, et leurs cadences associées, dans deux cas :

(1) Vol (tir) de l'engin.

(2) Alignement du système lors d'essais en vol sur avion de transport civil.

3.6.2. Vol de l'Engin

Un train d'interruptions venant du bloc capteur, synchronise le calcul "temps réel" :

(1) Acquisition des informations gyrométriques incrémentales ; compensation des erreurs de facteur d'échelle suivant un modèle d'erreur mémorisé. On acquiert en même temps quelques informations annexes (décalages des toupies gyro....)
Cadence 100 Hz

(2) Acquisition des informations incrémentales accélérométriques (et des températures) ; compensation (à l'aide d'un modèle mémorisé) des erreurs de facteur d'échelle.
Cadence 50 Hz

(3) Compensation des erreurs dynamiques des gyromètres et accéléromètres (on utilise des modèles de fonctionnement bien connus, pour un gyro sec et un accéléromètre pendulaire).
Cadence 50 Hz

(4) Calcul de l'attitude. On utilise la représentation mathématique par les quaternions (4 paramètres) ; la variation du quaternion en fonction de la vitesse angulaire mesurée dans les axes engin (ω) est bien connue :

$$\dot{Q} = \frac{1}{2} Q \cdot \omega$$

$$Q = (q_1, q_2, q_3, q_4)^T$$

Une intégration numérique du troisième ordre, compensée pour les accélérations angulaires, suffit pour les performances cherchées.
Cadence 50 Hz

(5) Le quaternion calculé par intégration numérique, est corrigé à intervalles réguliers pour tenir compte des dérives lentes (dérives des gyroscopes en accélérations, calculées suivant un modèle mémorisé ; précession du trièdre de navigation, et rotation terre). On calcule ensuite la matrice d'attitude (fonction des composantes du quaternion), N étant le trièdre de navigation :

$$C_B^N = \begin{matrix} q_1^2 + q_2^2 - q_3^2 - q_4^2 & 2(q_2q_3 - q_1q_4) & 2(q_3q_4 + q_1q_3) \\ 2(q_2q_3 + q_1q_4) & q_1^2 - q_2^2 + q_3^2 - q_4^2 & 2(q_3q_4 - q_1q_2) \\ 2(q_2q_4 - q_1q_3) & 2(q_3q_4 + q_1q_2) & q_1^2 - q_2^2 - q_3^2 + q_4^2 \end{matrix}$$

Cadence 25 Hz

(6) Avant d'effectuer le changement d'axes B → N sur les incréments de vitesse fournis par les accéléromètres, on compense l'erreur de commutabilité, due à l'intégration dans un trièdre mobile.
Cadence 25 Hz

(7) On effectue ensuite les calculs de navigation classiques (vitesse, point, ...) à une cadence de 12,5 Hz, ou moins.

(8) D'autres tâches pourront être effectuées à quelques Hz.

(a) Traitement des températures (les senseurs sont modélisés en température).
(b) Test de validité sur certaines mesures, qui permettent de se brancher sur des procédures de compensation spéciales.

(c) Sortie sur bus engin.

La Figure 21 résume l'organisation du logiciel pour la phase VOL ; la Figure 22 en donne le séquencement "temps réel".

Le volume de calcul peut se résumer ainsi :

(a) 100 additions + 100 multiplications en flottant 24 + 8 bits à effectuer par pas de 10 ms.
(b) Occupance du calculateur SYCOMORE de l'ordre de 50%.

3.6.3. Alignement

Le mode d'alignement du SIL 3 dépend essentiellement du type de mission attribué au missile, et ne peut donc être défini a priori.

Toutefois, dans le cadre des essais en vol effectués sur un avion de transport civil, un alignement en vol par comparaison avec les informations délivrées par la centrale inertielle de référence a été prévu.

Cette procédure est décrite au Paragraphe 4.2.3.3..

4. DEVELOPPEMENT ET MISE EN OEUVRE DU SYSTEME SIL 3

Le développement du système SIL 3 a nécessité la mise en oeuvre d'outils divers, parmi lesquels :

(1) Un ensemble de simulations du système.

(2) La définition des méthodes d'essais et des moyens associés.

4.1. Simulations

Une simulation des diverses parties du système SIL 3 a été développée. Le but de cette simulation est triple :

(1) Il s'agit avant tout de bien comprendre le rôle des divers éléments comme source d'erreur, afin d'en donner une définition optimale (bouclage numérique des gyromètres, logiciel, ...).

(2) Cette simulation fournit une évaluation des performances du système, pour toutes conditions de fonctionnement.

(3) Les résultats de ces simulations sont comparés aux mesures obtenues au cours des essais. Cela a conduit à une identification d'un modèle de SIL 3, pour diverses ambiances dynamiques.

On peut citer comme simulations partielles effectuées :

(1) Simulation du gyroscope avec son bouclage numérique. Cela a conduit à une optimisation de la boucle complète (bande passante, transitoires, comportement dynamique du gyroscope). Un exemple de réponse du gyromètre GAM 3, à un échelon de vitesse angulaire, est montré Figure 23.

(2) Simulation du logiciel spécifique (intégration de l'attitude, changement d'axes sur les incréments de vitesse ...) ; le traitement mathématique des informations a ainsi été vérifié.

(3) Simulation des procédures d'alignement en vol utilisées lors des essais (filtre de Kalman, défini suivant la théorie exposée au Paragraphe 4.2.3.3.). La Figure 29 donne un exemple d'alignement ainsi réalisé.

(4) Quelques simulations annexes (suspension, modèle thermique du gyroscope ...).

Une simulation du système complet a été effectuée ; la Figure 24 donne une portion de vol-type (vitesses angulaires et accélérations) ; la Figure 25 donne les valeurs à 1σ des erreurs d'attitude et de point de système complet SIL 3.

Une méthode de Monte Carlo a été utilisée pour qualifier le système en simulation.

Une même portion de vol-type est utilisée plusieurs fois comme entrée à la simulation du système (senseurs + logiciel). Les divers paramètres d'erreurs aléatoires sont tirés au hasard suivant une loi gaussienne ; les valeurs calculées des attitudes, vitesses, et point ... sont comparées aux valeurs de référence, ce qui fournit les erreurs du système, pour le tirage aléatoire effectué. La procédure est répétée, et fournit par une statistique, les écarts-type des erreurs du système SIL 3, pour un profil de vol donné. La Figure 26 schématise la procédure employée.

L'ensemble de la simulation est développé en FORTRAN à l'aide d'une configuration informatique comprenant

(1) Un CPU avec flottant câblé.

(2) Une console de dialogue.

(3) 2 unités de disque ; 1 unité de bande magnétique ; 1 imprimante ; 1 traceur XY ; 1 lecteur de ruban.

4.2. Méthodes et Moyens de Test

4.2.1. Gyroscope

Les essais classiques des gyroscopes utilisés en plateforme portent principalement sur leur comportement en accélération :

(1) Essais statiques donnant les termes d'un modèle en accélération.

(2) Essais en vibrations linéaires.

L'utilisation prévue nécessite d'étudier en plus le comportement :

(1) Des moteurs-couples (facteur d'échelle, stabilité, ligne d'action).

(2) Du gyroscope et de la boucle en vibrations angulaires.

La SFIM a dû se doter de méthodes et de moyens nouveaux satisfaisant à ces exigences, en tenant compte des principes suivants :

(1) Moyens d'essais statiques distincts des équipements pour les tests dynamiques.

(2) Association étroite avec des moyens de traitement de données.

(3) Ces équipements doivent être utilisables pour les essais syatèmes.

4.2.1.1. Moyens d'essais statiques

Le "banc de test automatique CAM 3" (Figure 27) permet :

(1) La mise en oeuvre du gyroscope avec bouclage analogique ou numérique des axes.

(2) La régulation thermique du gyro.

(3) Le conditionnement de certains paramètres tels que températures, écarts d'asservissement, couples de précession.

(4) La surveillance du bon fonctionnement et la gestion des sécurités.

(5) L'acquisition des paramètres sur bande perforée et sur imprimante suivant deux modes de fonctionnement:

Mode accélération utilisé pour déterminer les termes du modèle en accélération. Le banc mesure les couples de dérive intégrés pendant un temps donné, pour différentes positions du gyro par rapport au champ de pesanteur.

Mode table le banc de test est associé à une table tournante à axe sur laquelle est positionné le gyro dont les axes sont bouclés en gyromètre. Il enregistre les couples de précession sur chaque axe, intégrés sur un angle donné, ainsi que la vitesse de rotation moyenne de la table pour le parcours de cet angle.

4.2.1.2. Dépouillement des Essais Statiques

Les résultats de mesures, transférés par bandes perforées sur ordinateur sont dépouillés par des méthodes statistiques classiques capables de prendre en compte les redondances présentes dans une série complète de mesures. On évalue les coefficients les plus probables des modèles décrivant le gyroscope en accélération et ses moteurs-couples, ainsi que les incertitudes associées à ces coefficients.

Deux bancs de test automatiques ont été construits et fonctionnent actuellement, associés à une table (Goerz ou MFW). Le traitement des informations est effectué sur PDP 11/45.

4.2.1.3. Moyens d'Essais Dynamiques (Figure 28)

On pourrait se limiter à l'étude du comportement global du gyromètre au cours d'essais dynamiques. Le moyen décrit précédemment serait alors suffisant. Il est plus instructif de connaître à chaque instant le comportement du gyromètre, en fonction des paramètres des contraintes d'entrée. Dans ce but, une *baie d'acquisition rapide* a été conçue et réalisée. Elle est pilotée par le processeur rapide SFIM MARINA S, travaillant avec une mémoire vive à tores de 8k mots de 16 bits. Cette baie permet l'acquisition des informations définies par le Tableau 2.

8.12

Tableau 2

PARAMETRES	NOMBRE	NATURE	PRECISION	FREQUENCE D'ACQUISITION (max en Hz)
Couples de précession gyro	4	numérique	12 bits + signe	500
Position table	1	numérique	20 bits	500
Position angulaire	3	synchro	15 bits	500
Ecarts angulaires gyro	4	analogique	12 bits	500
Angle de phase toupie/moteur	2	numérique	12 bits	200
Températures	4	analogique	12 bits	80
Divers	6			120

Les informations sont stockées sur un enregistreur à bande magnétique, la mise en oeuvre est effectuée par une console de dialogue équipée d'une imprimante et de lecteur de cassettes.

Ce moyen d'essai est prévu pour être associé à :

(1) Une table oscillante 1 axe, 2 axes, ou 3 axes.

(2) Un pot vibrant.

4.2.1.4. Dépouillement des Essais Dynamiques

A la suite d'un essai, on dispose de toutes les données pour reconstituer en temps différé le comportement du gyromètre. On peut alors :

(1) Etudier le comportement global de l'ensemble.

(2) Déterminer les termes d'un modèle du gyromètre en rotation angulaire en fonction de certaines entrées simples (sinusoïdales).

(3) Comparer les résultats expérimentaux à ceux obtenus par simulation avec procédure de correction du modèle simulé.

Une baie d'acquisition rapide a été construite et fonctionne actuellement, associée à une table 1 axe (Goerz, MPW), 3 axes (Carco) ou à un pot vibrant ; le traitement des données est assuré par un PDP 11/45.

4.2.2. Accéléromètres

De même que pour les gyromètres, il est nécessaire d'étudier le comportement des accéléromètres en ambiance statique et dynamique (vibrations linéaires et angulaires).
Les coefficients du modèle en rotation sont mesurés sur table oscillante, en enregistrant les grandeurs d'entrée et de sortie grâce à la baie d'acquisition rapide décrite ci-dessus.

4.2.3. Système

4.2.3.1. Essais Statiques

Ils ont pour but de mesurer les performances des senseurs placés dans le système :

(1) Influence mutuelle des senseurs.

(2) Positionnement des senseurs sur le bloc.

(3) Comportement thermique.

Comme pour l'étude du gyroscope, ces mesures sont réalisées pour différentes positions du bloc dans le champ de pesanteur, ou sur table tournante 1 axe. La saisie de données utilise la baie d'acquisition rapide décrite ci-dessus.

4.2.3.2. Essais Dynamiques

Ils ont pour but de définir les performances globales du système pour une mission et des conditions d'ambiance déterminées :

(1) Essais en oscillation axiale 1 axe.

(2) Essais en ambiance dynamique (rotation) quelconque : table 3 axes.

(3) Essais en vibrations linéaires sur pot vibrant.

Le système, couplé à son calculateur fournit un résultat lié à ses performances globales.

4.2.3.3. Essais en Vol - Initialisation du Système

Les essais en vol du SIL 3 seront effectués sur un avion de transport civil de type CARAVELLE. Pour chaque vol de l'avion, d'une durée de 1 heure à 1 heure 30, plusieurs vols engins durant chacun quelques minutes pourront être simulés. Les résultats seront enregistrés sur système d'acquisition et d'enregistrement magnétique, et exploités au sol, en différé.

Le principal problème posé par cette procédure est celui de l'initialisation en vol du système strap-down. La méthode d'initialisation en vol a donc fait l'objet d'une étude particulière résumée ci-après :

(1) *Généralités*

Le temps de fonctionnement du SIL 3 en inertie pure est du fait des performances des instruments beaucoup plus faible que le temps moyen de vol de l'avion de transport grâce auquel les essais seront effectués.

Comme il n'est pas envisageable de poser l'avion toutes les cinq minutes ou de n'exploiter que cinq minutes d'un vol d'au moins une heure, il est nécessaire de prévoir des initialisations en vol. On peut ainsi au cours d'un vol effectuer une dizaine d'essais durant cinq minutes chacun.

Cette initialisation est effectuée grâce à l'utilisation en référence de la centrale inertielle classique de l'avion.

Elle comprend trois phases distinctes :

(a) Calcul du quaternion initial grâce aux angles d'Euler fournis par la centrale puis démarrage du calcul de l'attitude.

(b) Comparaison de l'attitude calculée et de l'attitude fournie par la centrale inertielle de référence.
Le résultat de cette comparaison est utilisé pour recaler à travers un filtrage le quaternion représentant l'attitude.

(c) Initialisation des composantes de la vitesse aux valeurs fournies par la centrale inertielle. Démarrage du calcul de la vitesse à partir des informations accélérométriques. Comparaison de la vitesse calculée et de la vitesse de la centrale inertielle de référence. Le résultat de cette comparaison est utilisé pour recaler à travers un filtrage sous-optimal le quaternion d'attitude.

(2) *Description des différents modes*

(a) Le premier mode ne demande pas d'explication fonctionnelle. On peut dire simplement que cette initialisation très rapide peut laisser subsister des erreurs d'attitude importantes dues à différentes causes :
- Erreurs des recopies angulaires de la référence inertielle.
- Défauts d'harmonisation des deux centrales :
  . bruit électrique (codage d'une crête)
  . erreur de codage de la recopie (non-linéarité, quantification)
  . vieillissement de l'information entrainant des erreurs si l'initialisation a lieu pendant des évolutions

(b) Le second mode qui ne dure que quelques secondes permet l'élimination d'une partie de l'erreur laissée par le calage précédent, et effectue le filtrage des trois derniers types d'erreurs qui sont à fréquence relativement élevée.
Le schéma du système est le suivant :

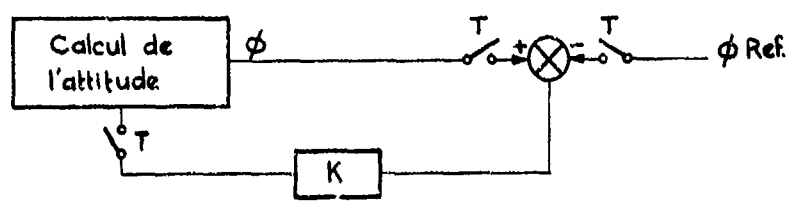

L'utilisation d'un coefficient K nettement inférieur à 1 donne au système les caractéristiques d'un filtre du premier ordre.

(c) Le troisième mode qui effectue le calage fin de l'attitude n'utilise plus les sorties angulaires de la centrale inertielle de référence.

8.14

Ce calage fin s'effectue par comparaison de l'accélération ou plus exactement des variations de vitesses calculées par les deux systèmes de navigation. En effet l'erreur d'attitude $\underline{\delta\phi}$ provoque une erreur d'accélération $\underline{\delta A}$ qui est fonction de l'accélération $\underline{A}$:

$$\underline{\delta A} = \underline{\delta\phi} \times \underline{A}$$

On voit donc qu'une accélération permet l'évaluation des erreurs d'attitude situées dans un plan perpendiculaire à cette accélération. La présence permanente de l'accélération de la pesanteur donne donc - chose classique - l'erreur de verticale. Cependant si l'avion évolue, une composante horizontale de l'accélération permettra l'évaluation de l'erreur de cap.

On est donc amené à effectuer une correction d'attitude qui dépend de l'accélération qui règne au moment de la comparaison ; cette correction doit être aussi pondérée par la connaissance de l'erreur sur chacun des axes. Une manière simple de réaliser ces deux actions simultanément est l'utilisation d'un filtre de Kalman.

Cependant ces erreurs d'attitude évoluent et ne sont pas les seules à agir sur le système. Une étude complète montre qu'il est nécessaire d'utiliser un vecteur d'état de dimension 39 dont les composantes sont pour la plupart faiblement observables. Comme il n'est pas concevable d'embarquer le filtre optimal associé, on élimine les variables faiblement observables, ce qui ramène la dimension du vecteur d'état à 5, dont on remplace l'action sur l'attitude et la vitesse par un cheminement aléatoire.

Il convient donc d'ajuster ces deux grandeurs pour que le fonctionnement du filtre sous-optimal soit correct. Pour cela, on va comparer la covariance d'estimation optimale P_1, la covariance estimée P_2, et la covariance réelle P_3. Plaçons-nous dans le cas d'observations discrètes. Les algorithmes définissant P_1, P_2 et P_3 en fonction du temps sont définis dans le Tableau 3 ci-dessous. La première ligne est justifiée car la correction calculée grâce au gain K est réellement appliquée au système par recalage du quaternion. L'optimisation du filtre sous-optimal est réalisée par réglage de R_2 et Q_2 pour obtenir, pour un certain nombre de trajectoires, les conditions $P_2 \approx P_3$ et P_3 légèrement supérieure à P_1.

Tableau 3 (1)

COVARIANCE D'ESTIMATION	OPTIMALE P_1	SOUS-OPTIMALE P_2	REELLE P_3
Calcul de la covariance d'estimation avant observation $P_{K/K-1}$	$P_{1K/K-1} = \Phi_1 P_{1K/K-1} \Phi_1^T + Q_1$	$P_{2K/K-1} = \Phi_2 P_{2K/K-1} \Phi_2^T + Q_2$	$P_{3K/K-1} = \Phi_1 P_{3K/K-1} \Phi_1^T + Q_1$
Calcul du gain K	$K_{1K/K-1} = P_{1K/K-1} H_{1K}^T (H_{1K} P_{1K/K-1} H_{1K}^T + R_{1K})^{-1}$	$K_{2K/K-1} = P_{2K/K-1} H_{2K}^T (H_{2K} P_{2K/K-1} H_{2K}^T + R_{2K})^{-1}$	
Calcul de la covariance d'estimation après observation	$P_{1K} = (I - K_{1K} H_{1K}) P_{1K/K-1}$	$P_{2K} = (I - K_{2K} H_{2K}) P_{2K/K-1}$	$P_{3K} = (I - K_{2K} H_{1K}) P_{3K/K-1} (I - K_{2K} H_{1K})^T + K_{2K} R_{1K} K_{2K}^T$

Φ matrice de transition H matrice d'observation Q covariance du bruit agissant sur le système R covariance du bruit d'observation

5. CONCLUSIONS

Le SIL 3 tel qu'il vient d'être présenté, correspond à une solution rapidement utilisable pour le guidage des missiles tactiques.

Ce système est actuellement en essais au sol, et subira ses essais en vol au début de l'année prochaine.

L'application envisagée aux missiles tactiques ne constitue pas une limitation.

Le système est, par la puissance de calcul disponible, extensible à bien d'autres applications, par exemple : navigation hybride, avec Doppler, oméga ..., des hélicoptères ou des avions de transport, ou encore guidage de torpilles ....

Ses dimensions peuvent également être fortement réduites, car cette première application ne fait pas appel à de l'électronique hybride. Enfin les capteurs eux-mêmes peuvent voir leur domaine de performances étendu dans un proche avenir.

(1) Référence AGARD lecture séries 82

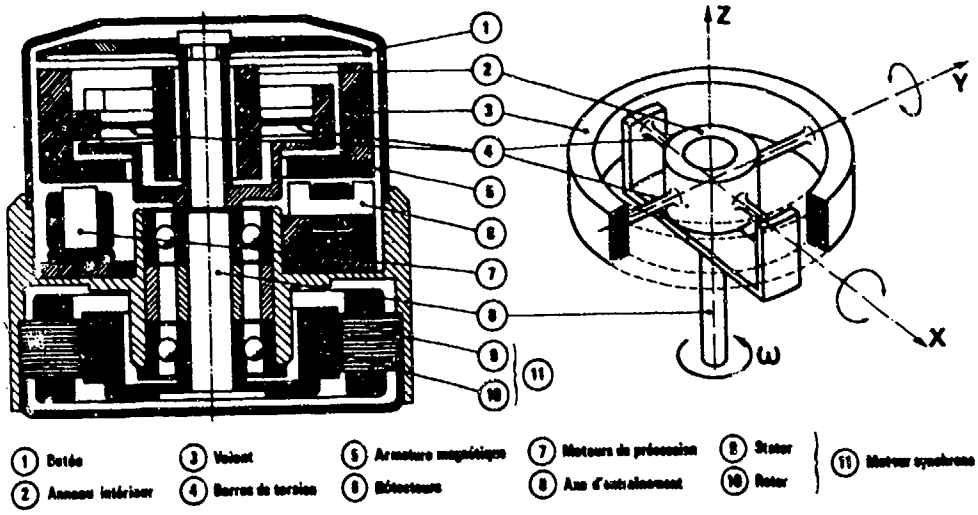

Figure 1 - Gyroscope GAM1

- 3 gyromètres GAM1 [dont 2 balourdés]
- Etendue de mesure
  - 400°/s
  - 15g

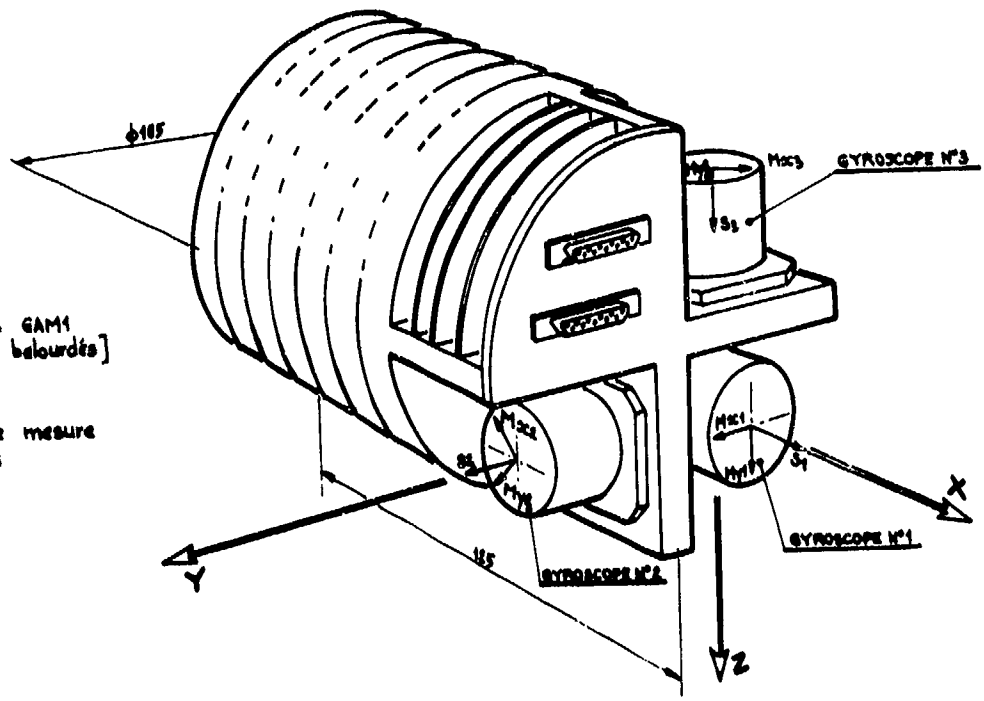

Figure 2 - SIL1

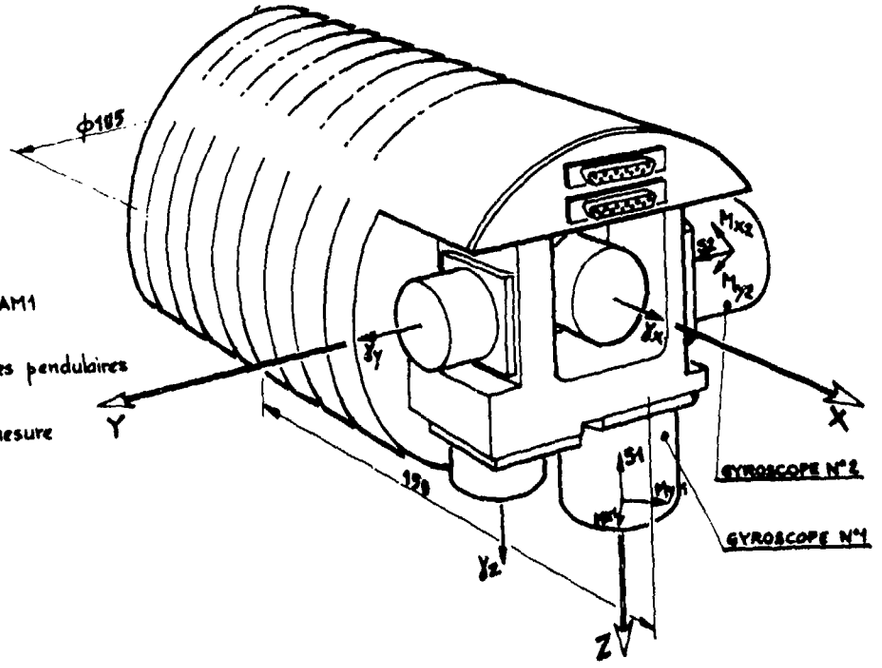

Figure 3 _ SIL2

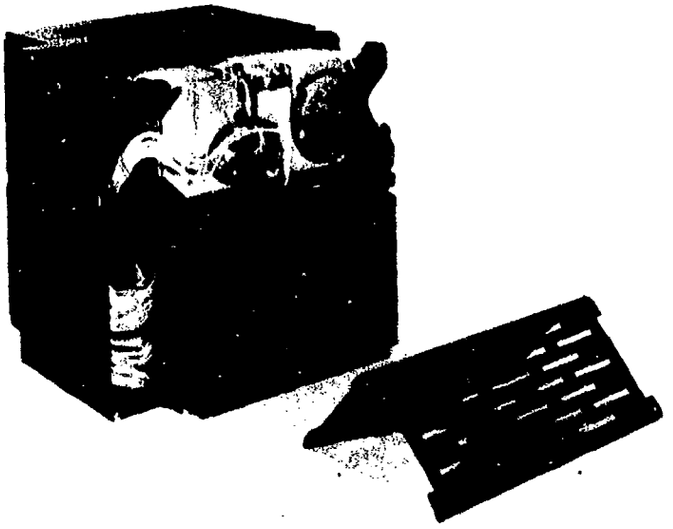

Figure 4

SIL3

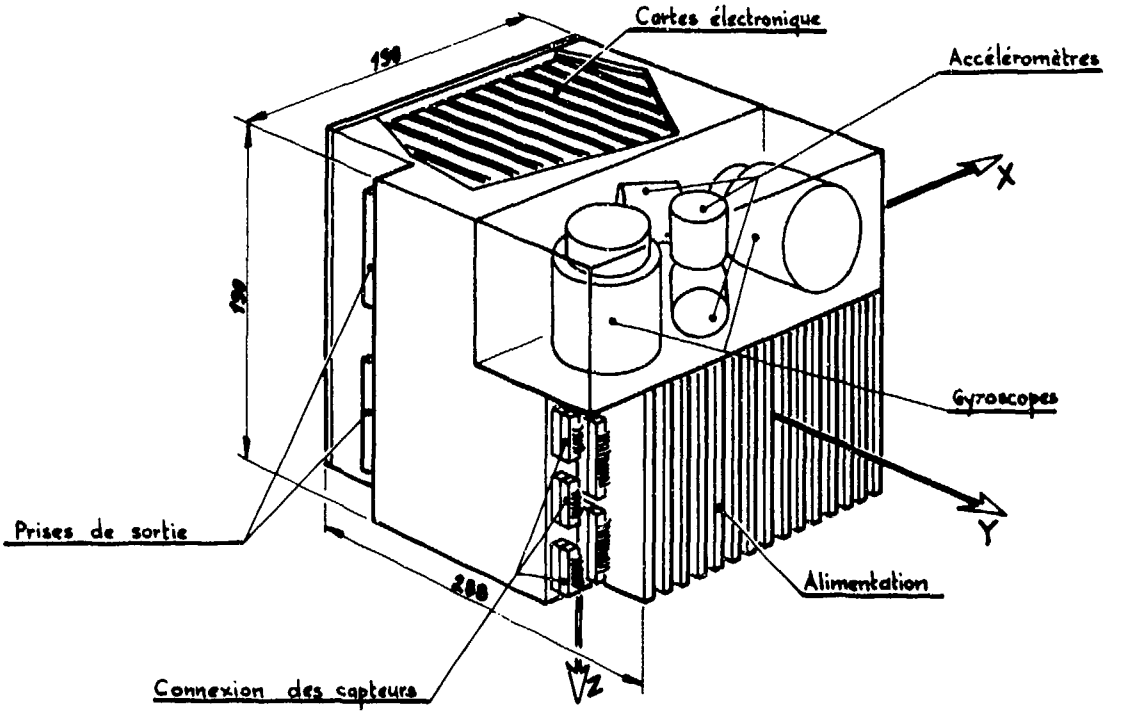

Figure 6 _ SIL3

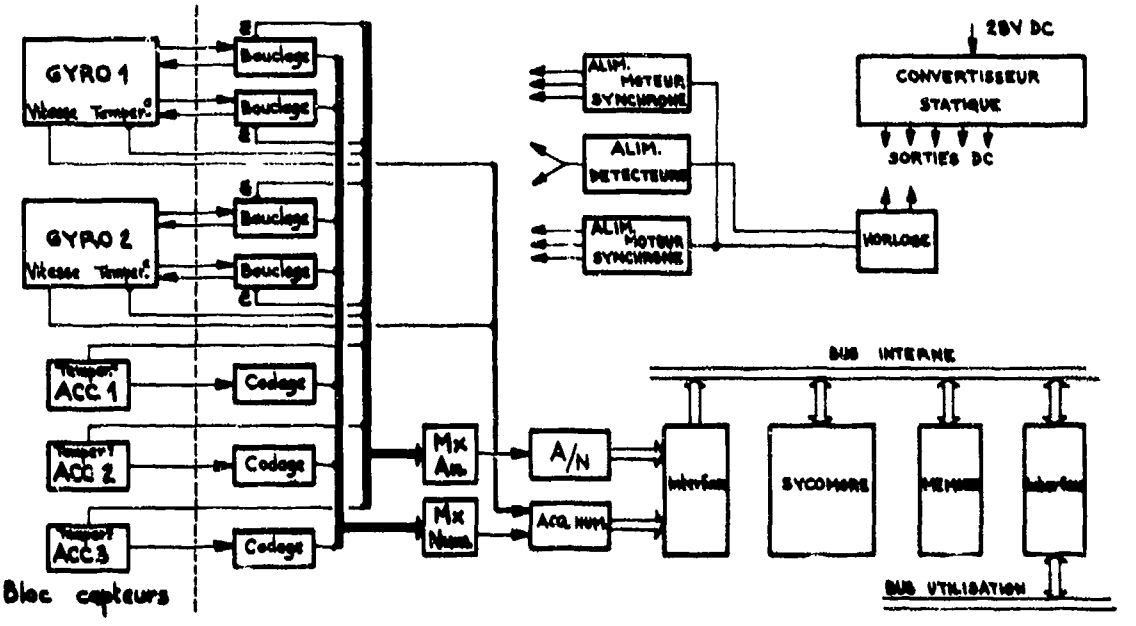

Figure 7 : Diagramme fonctionnel SIL3

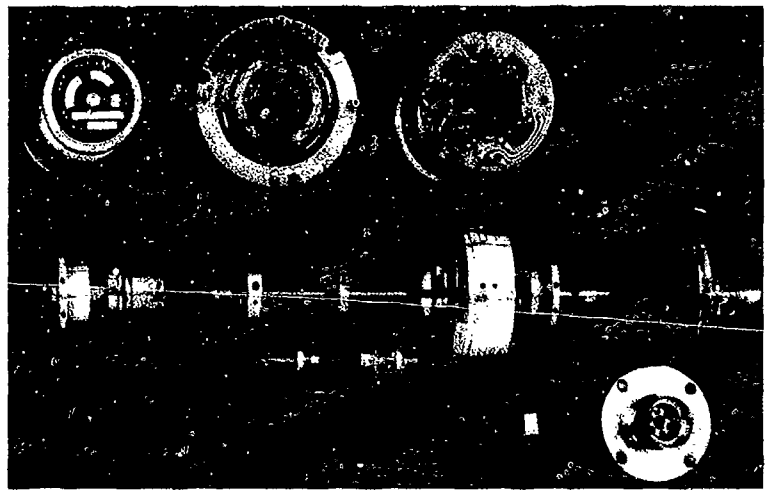

Figure 8

Gyroscope GAM3

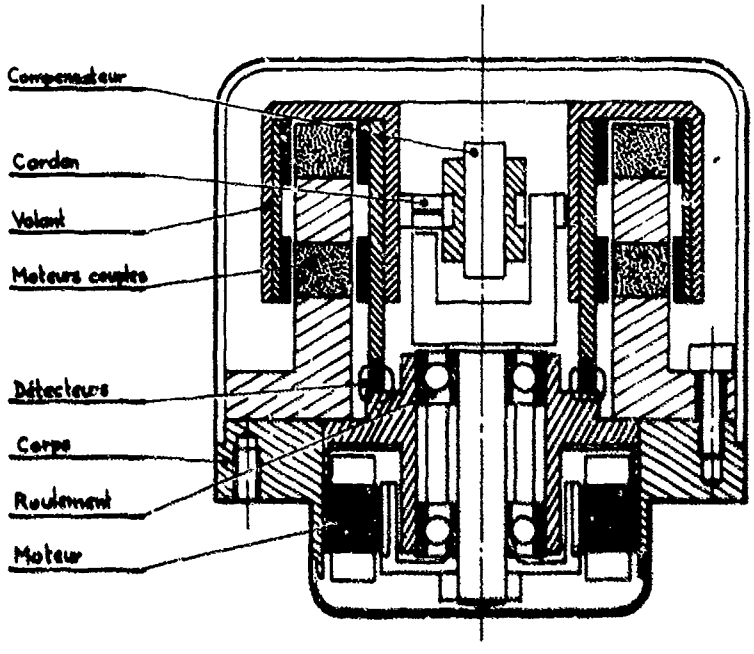

Figure 9

Gyroscope GAM3

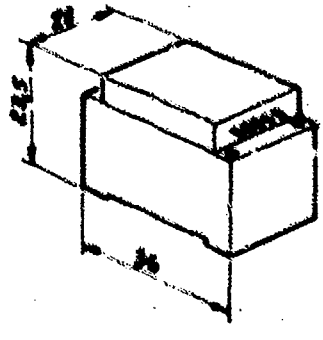

Figure 18

Accéléromètre MICAL

Figure 11

Bloc capteurs

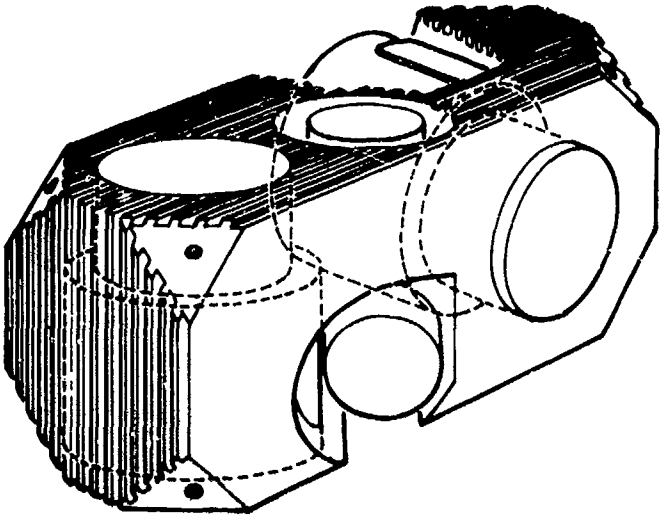

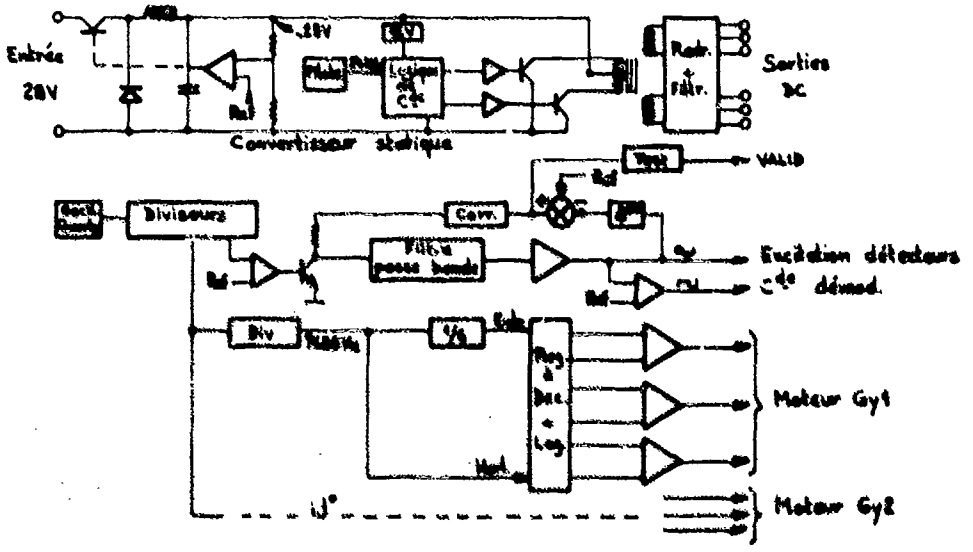

Figure 12 – Fonctions générales

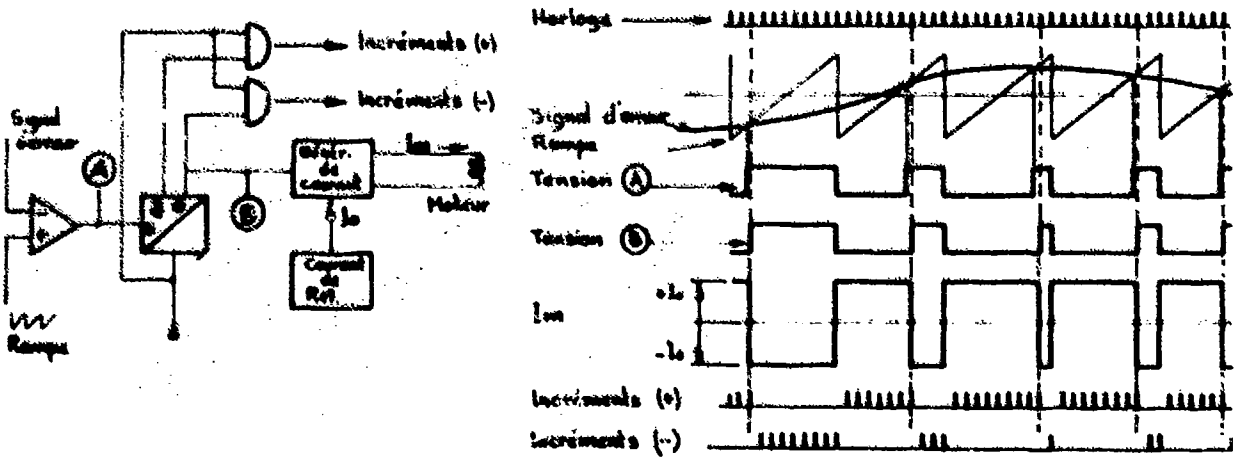

Figure 13 – Principe de bouclage en modulation de largeur

8.20

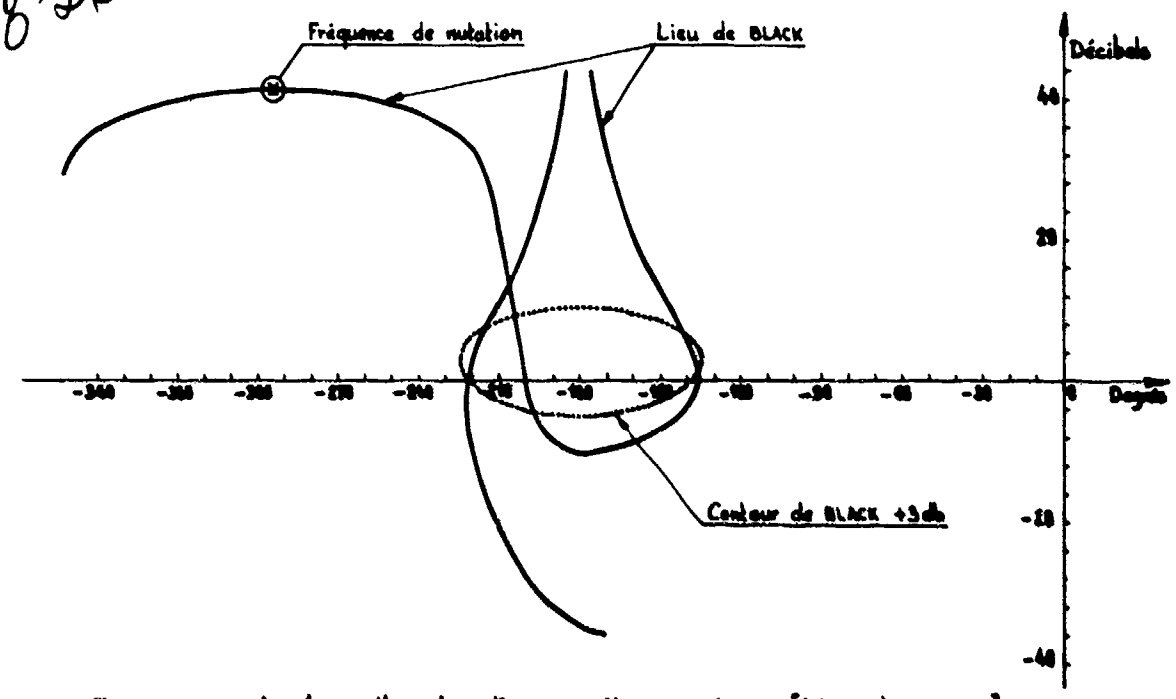

Figure 14 _ Analyse d'une boucle gyromètre numérique [Lieu de BLACK]

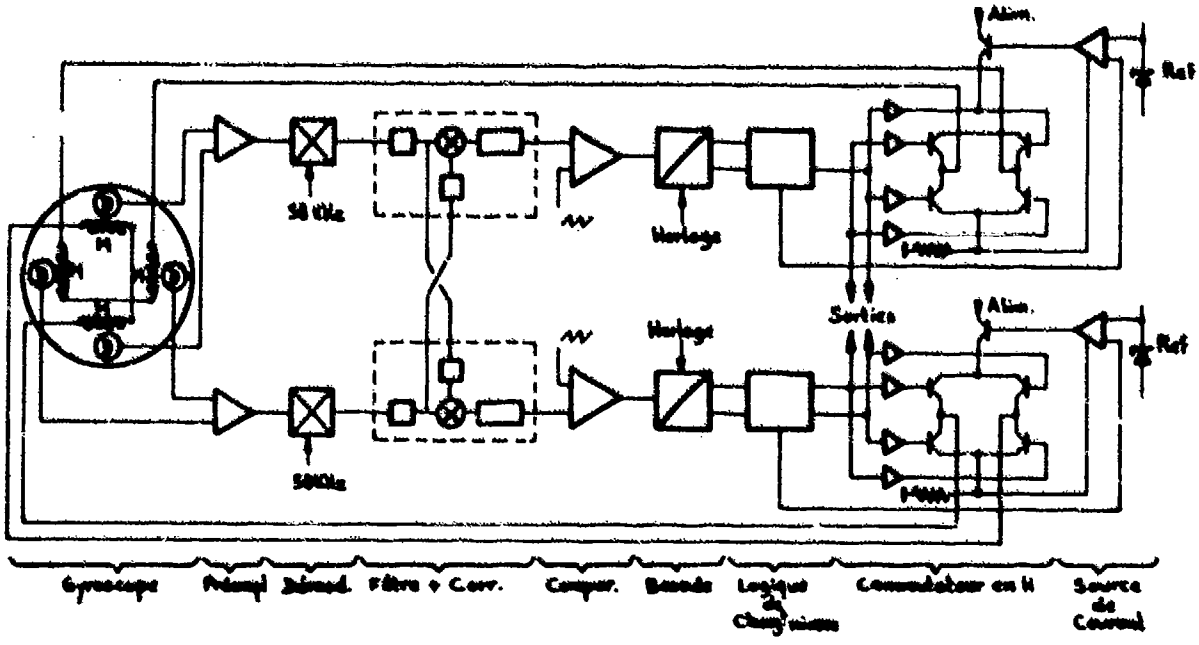

Figure 15 _ Boucle gyromètre . Schéma de principe

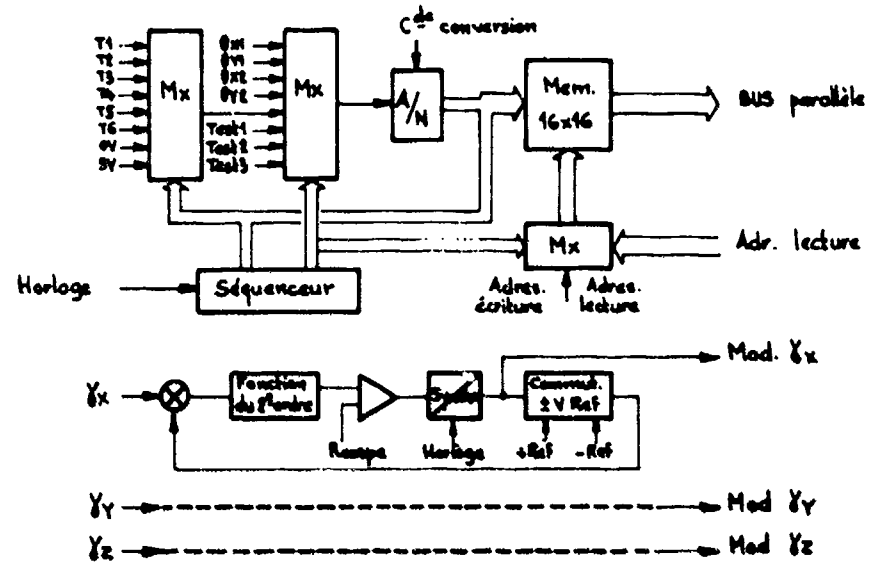

Figure 16

Codage A/N

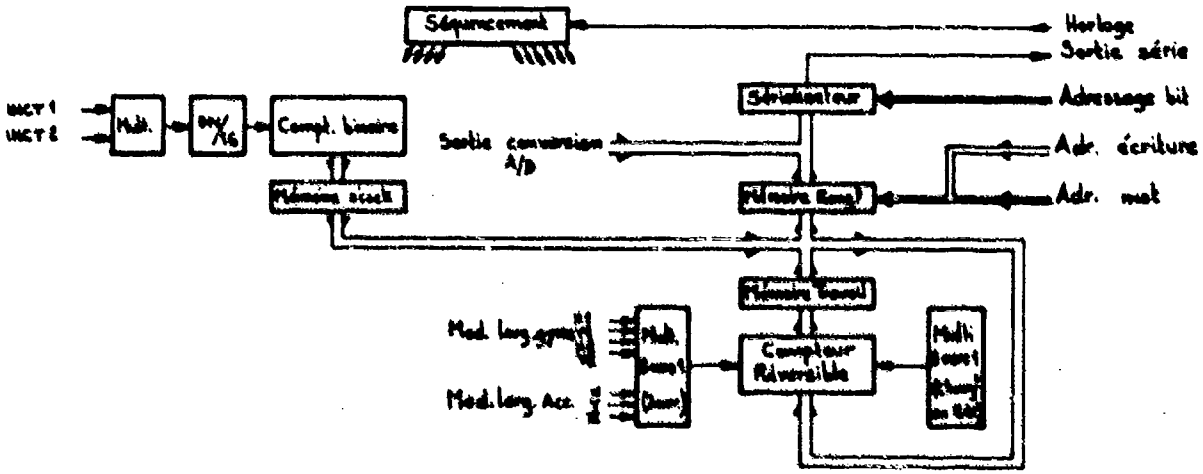

Figure 17 - Logique de comptage et transmission série

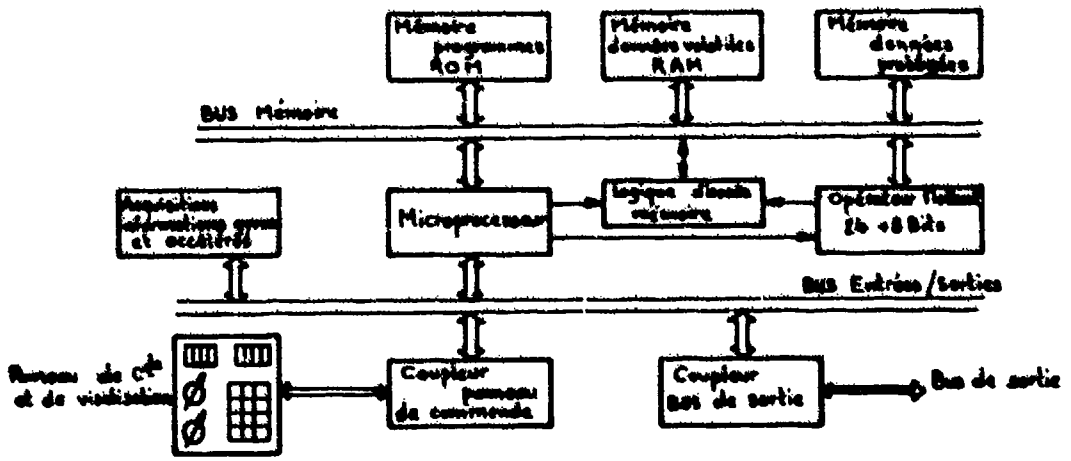

Figure 18 - SYCOMORE. Organisation

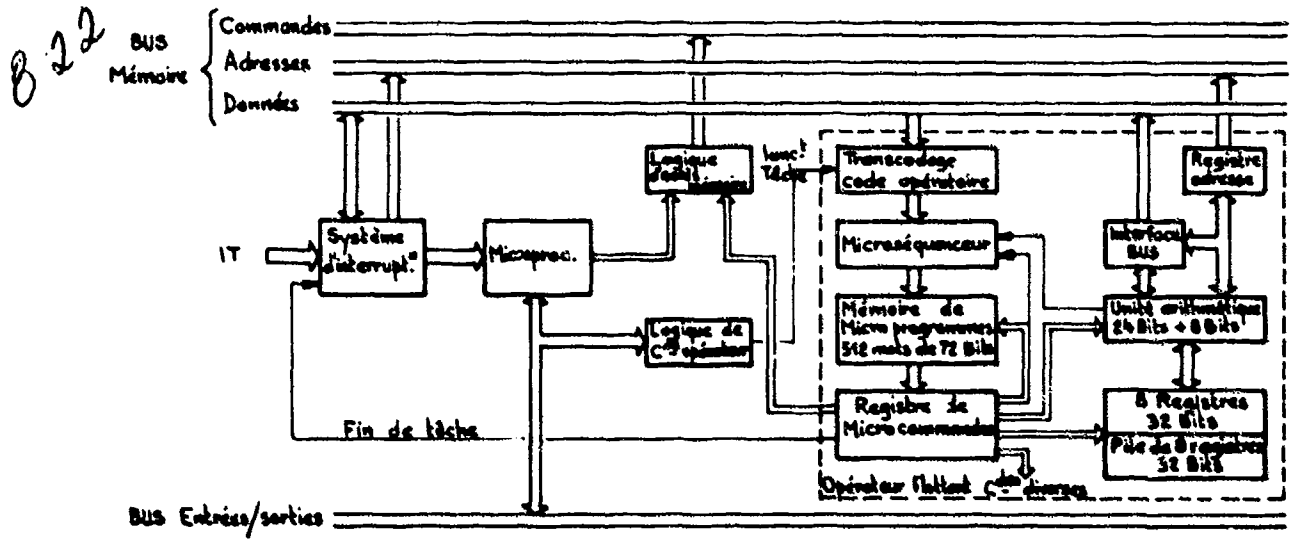

Figure 19 _ SYCOMORE . Fonctionnement

Figure 20

SYCOMORE

Génération du logiciel

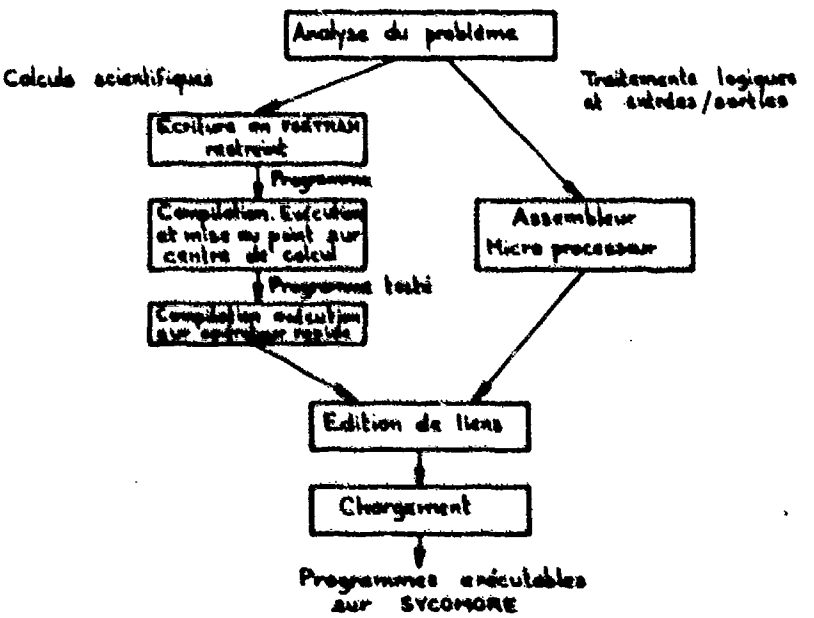

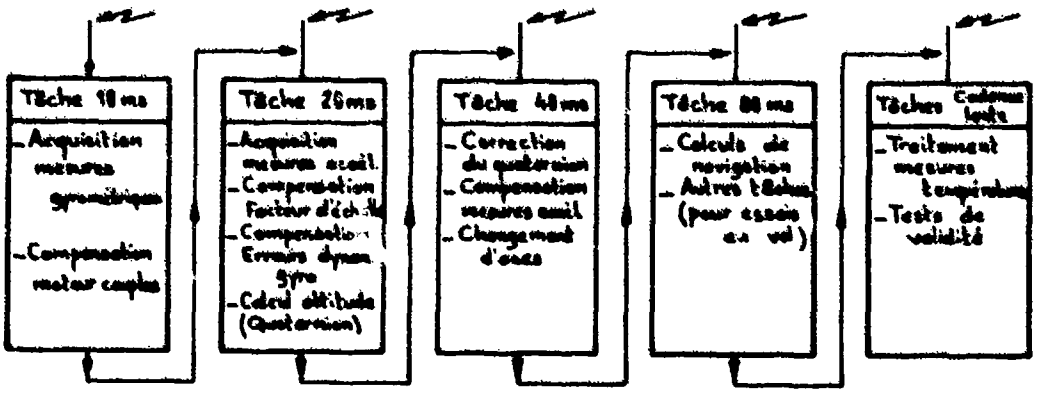

Figure 21 _ Description du logiciel d'application

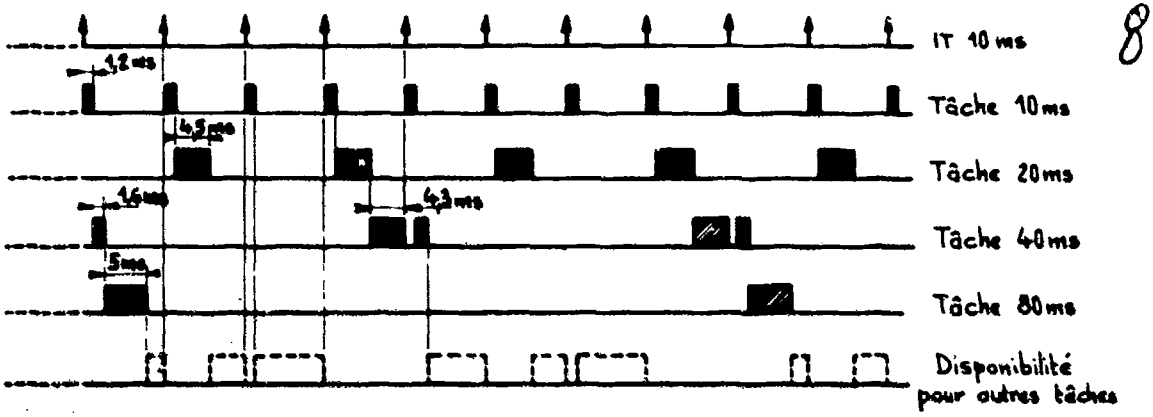

Figure 22 _ Séquencement des taches temps réel

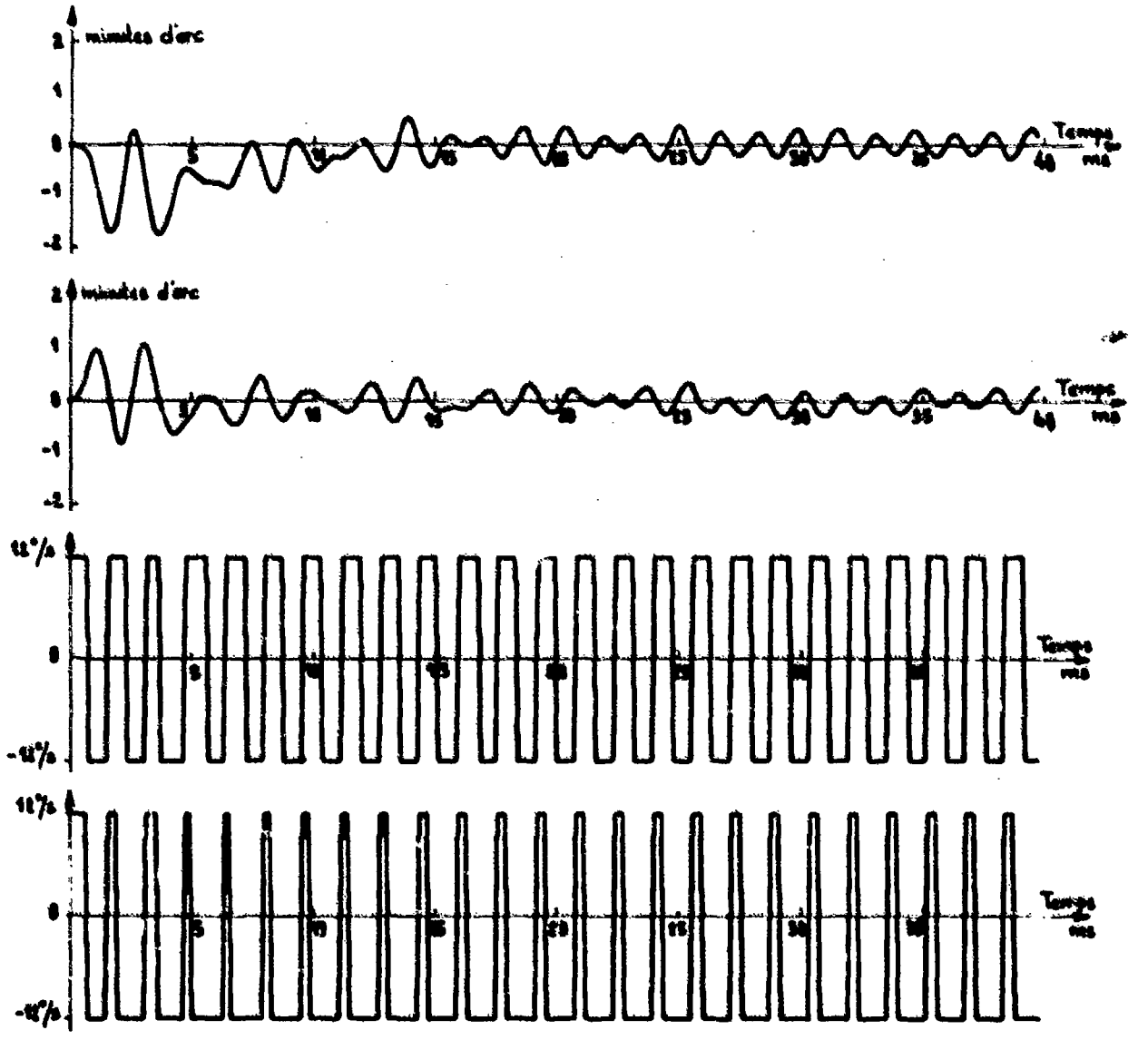

Figure 23 _ Simulation de la réponse d'un gyro GAMS à un échelon de vitesse angulaire

8·24

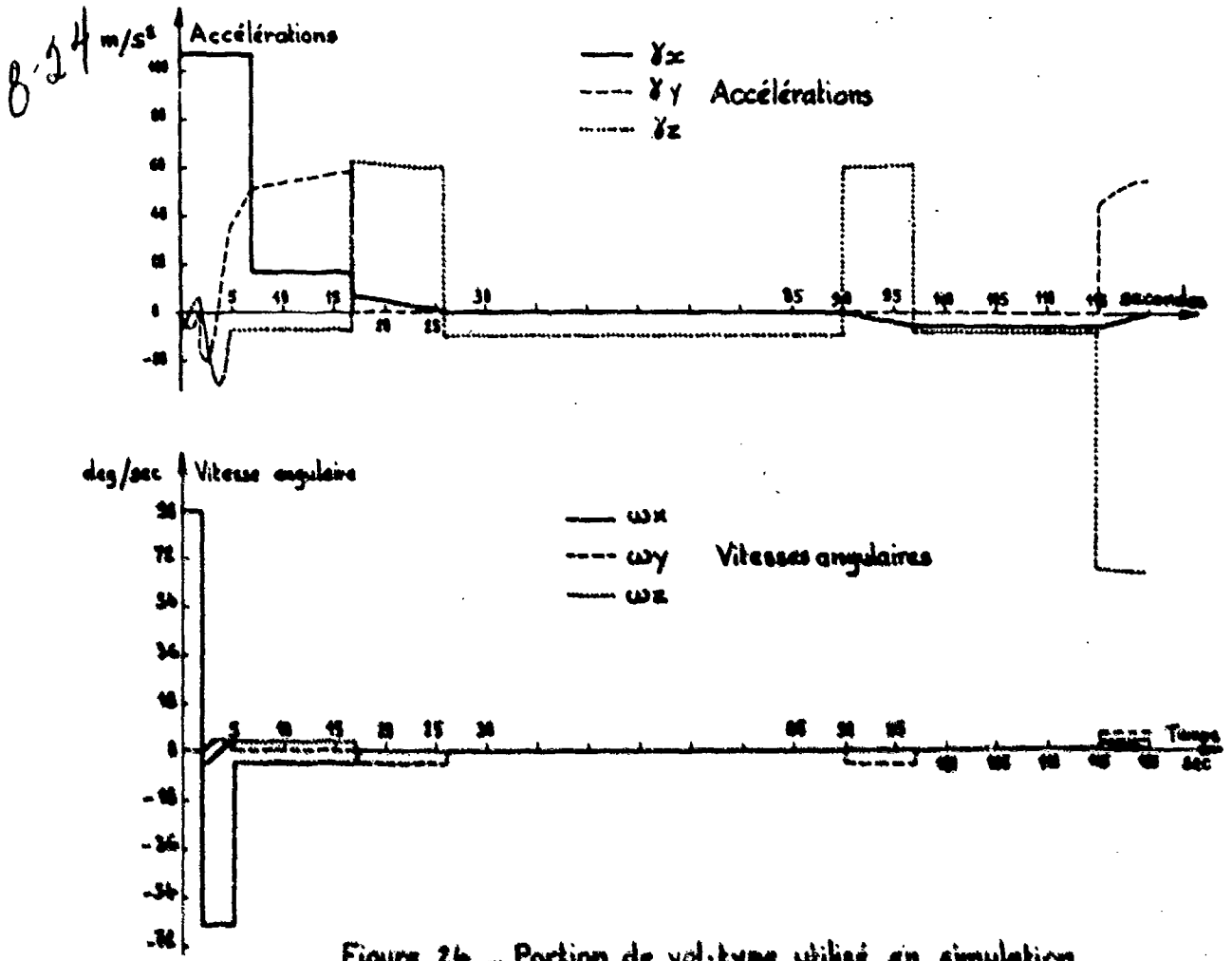

Figure 24 – Portion de vol-type utilisé en simulation

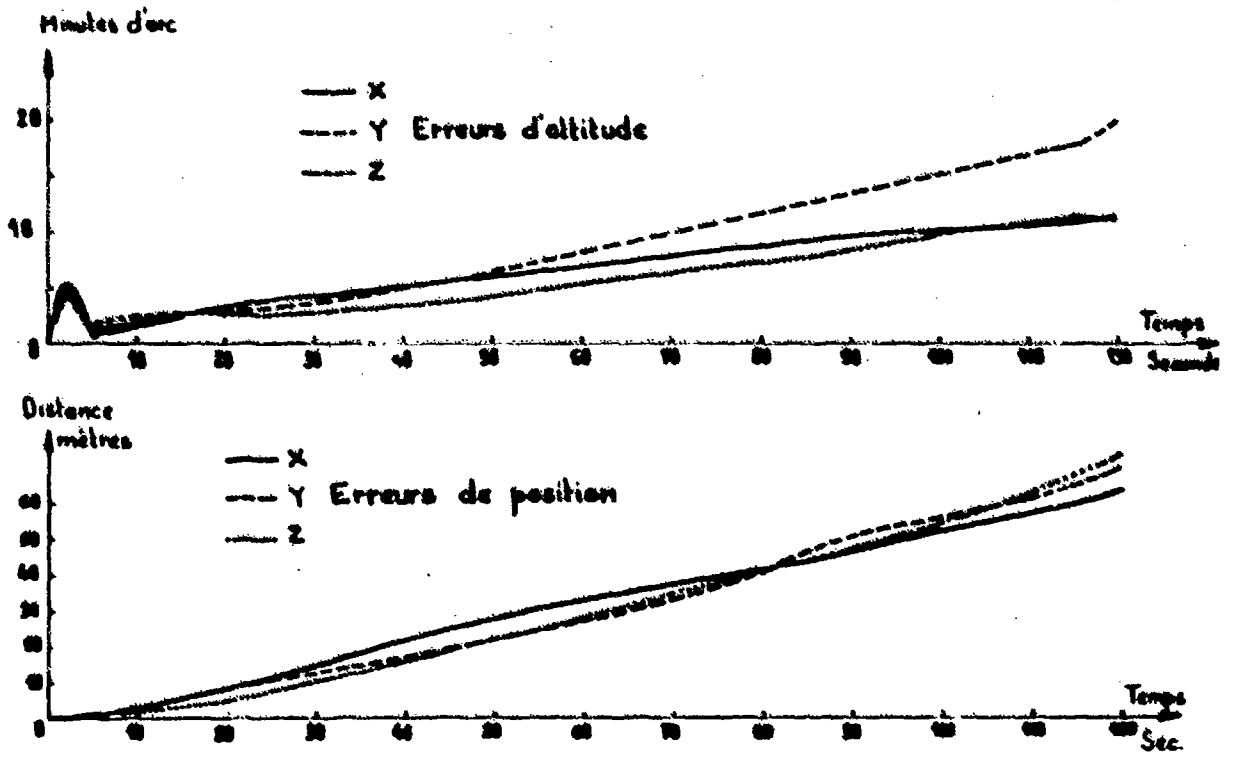

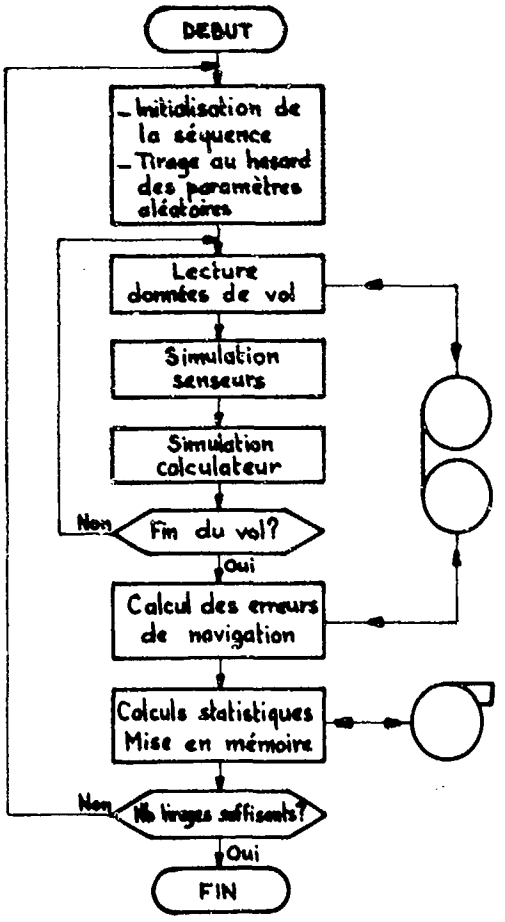

Figure 26

Méthode d'étude statistique des erreurs

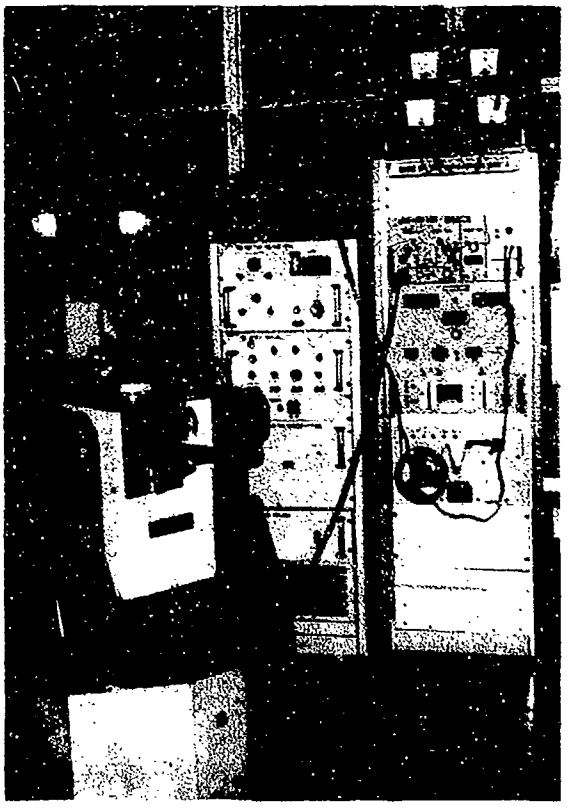

Figure 27

Banc de mesures statiques

Figure 28

Configuration d'essais dynamiques

8.26

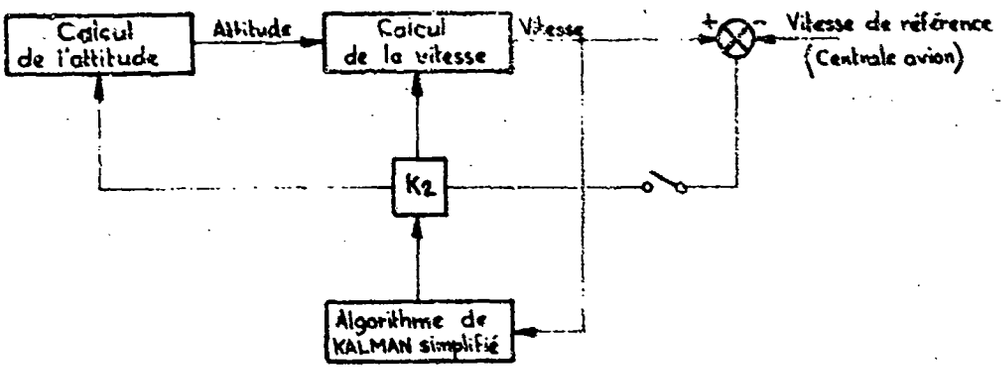

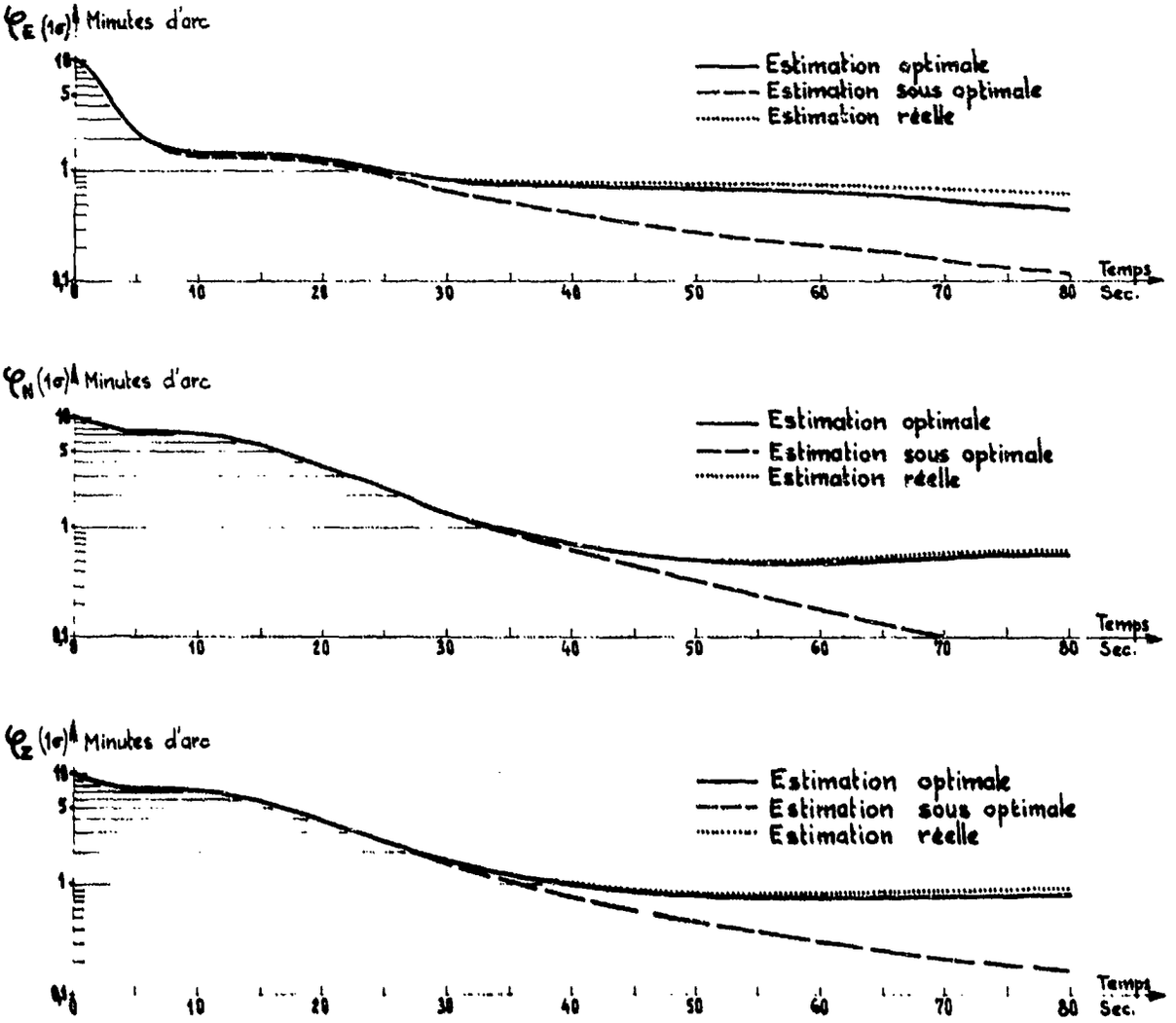

_ Figure 29 _
Simulation d'alignement

8-17

SIL 3
STRAP-DOWN INERTIAL, GUIDANCE SYSTEM FOR TACTICAL MISSILES

by
G. Cattan - J. Michelin
Société de Fabrication d'Instruments de Mesure
13, avenue Ramolfo Garnier
91301 Massy
FRANCE

SUMMARY

Among the strap-down systems developed by SFIM from the various models of the Miniature Tuned Gyroscopes GAM-1 and GAM-3, the most advanced is the SIL 3, intended for exact guidance of tactical missiles.

The SIL 3 combines in the one case two gyroscopes GAM-3, three accelerometers, the associated loops and computing circuits.

The GAM-3 gyroscope, specially developed by SFIM, is a dry, tuned, two-axis gyroscope, built to measure angular rates up to 100 degrees per second with 100ppm accuracy on scale factor and linearity. Direct entry into extremely elaborate computing circuits is allowed by digital loop closing. The efficient use of advanced modelling contributes to the performance of the system.

SFIM has also developed test and simulation means which enable the prediction and checking of the system performance for the various environments specified in its use.

1. BACKGROUND

It was in 1972 that the Company SFIM (Société de Fabrication d'Instruments de Mesure), whose main activities were devoted to the design and manufacture of gyroscopic equipments, really began the design of strap-down systems, with the development of a first dry tuned gyroscope of an entirely new concept.

The GAM 1 Gyroscope (Gyroscope Accordé Miniature = Miniature Tuned Gyroscope) is to day produced for a large number of applications. It is a rugged gyroscope, very simply designed and of very economic manufacture (Fig.1); its characteristics can be settled according to the models :

(1) From 1 to 30°/h for the day to day drift

(2) From 15 to 400°/s for the precession rate

(3) From .2 to .5% for the scale factor linearity.

It is mainly used for fine stabilisation of aiming and fire control systems (optical, television, infrared, radar) and angular rates measurement, with a digital rebalance loop.

This gyroscope is incorporated in strap-down guidance systems for applications where the price is more important than performance.

(1) The SIL 1 (Fig.2) includes three gyroscopes, two of them with mass unbalance, associated with a computer.

(2) The SIL 2 (Fig.3) includes two gyroscopes and three accelerometers associated with a computer.

In 1974 SFIM began the development of the SIL 3 strap-down system for tactical missiles guidance. This is the subject of the present paper.

2. GENERAL PRESENTATION OF THE SIL 3 SYSTEM (Fig.4)

2.1. Range of application

SIL 3 is primarily designed for the guidance of a tactical missile. It can also be used for preguidance of missiles having a homing head.

The system provides :

(1) Angular rates and accelerations measurement.

(2) Heading and attitude computation.

(3) Computation of velocities along the three axes and of position.

It thus allows flight control and navigation of the missile in total inertial guidance or in inertial preguidance.

The aims adopted for performance, volume or weight are relatively reasonable. But they are associated with the search for great ruggedness - necessary in the severe environmental conditions found in missiles -, for a high degree of reliability, for a low cost, both for purchase and for maintenance.

All the solutions adopted take these criteria into account as a prime need.

The design of SIL 3 has been broken down into three phases:

(1) As a first step SFIM developed the GAM 3 gyroscope. This gyro, specially designed to solve the problem raised, but nevertheless based on experience acquired with GAM 1 and GAM 2, is a two axis dry tuned gyroscope. It has a single gimbal ring and is built to have great ruggedness. It can precess at more than 100°/s.

(2) As a second step, SFIM develops a strap-down system in which a single case contains two GAM 3 gyroscopes, three accelerometers and also all the electronics necessary for operating the sensors and the data acquisition. The soffware development is performed on a commercial general purpose mini-computer while in parallel the airborne SYCOMORE computing elements are being developed, meeting the strap-down specification in their high performance and small volume.

(3) Finally, the realization of SIL 3 is the logical outcome of the previous phases, in the sense that the sensors, their electronics and also the computing and interface circuits are combined in a single case, so forming a fully integrated strap-down navigation system.

2.2. General description

The SIL 3 is in the form of a box, 208 x 190 x 190 mm (Fig.6). Its mass is about 7 kg.

The front of the box takes the sensor unit to which are fixed the two GAM 3 gyroscopes, and the three accelerometers.

The sensor unit is suspended in relation to the box.

The box itself encloses a power supply unit and a collection of circuit boards.

This collection comprises :

(1) Gyros rebalance loops.

(2) Acceleration data quantizers.

(3) Analog/digital conversion circuits.

(4) Digital circuits for data acquisition and exchange with the computer .

(5) SYCOMORE computing elements and memory.

(6) Interface circuits providing the dialogue, through a simple BUS, with the missile.

Fig.7 gives the functional circuit diagram of the whole. The system is powered from the 28 volts DC missile battery.

All the data received or exchanged are digital and pass through the bus.

The SIL 3 has no fine bias, drift or scale factor adjustment.

Calibration is entirely made by semi-automatic tests and the values measured during these tests are stored by the computer.

Similarly, sensors error compensation, (i.e. accelerations , temperature, etc..coefficients) is performed entirely by software.

A static inverter provides generation from the missile battery 28 V of all the voltages necessary to start up the gyroscopes, for excitation of their angular position pick-offs, for supplying the accelerometers and all the electronic circuits.

The signals from the angular position pick-offs are used to control torquers through binary rebalance loops, working in pulse width modulation.

Each loop comprises correctors, a very accurate current source, an H switch, and also the associated logic circuits.

The accelerometers are pendulous, dry type with analog loops. Their output data are converted into velocity increments by the coding circuits, which are also binary and Pulse Width Modulated.

To allow compensation by software of sensor errors, a multiplexed analog/digital converter takes into account the residual deviation of the gyroscopes and also the temperature of each gyroscope and of each accelerometer.

The measurement of the rotation period of each rotor will enable gyroscopes "wheel hunting" errors to be corrected.

All the measurements so made are acquired in multiplex form to be transmitted to SYCOMORE, together with its ROM, RAM and EAROM memories.

The interface circuits provide the dialogue , through the bus, between SYCOMORE and the missile.

3. DESCRIPTION OF THE SYSTEM

3.1. The gyroscope GAM 3

The gyroscope sensor is certainly the most difficult element to realize in an inertial strap-down system. In fact, it has to have, in addition to the qualities required of conventional gyros, fitted on supports slaved in rotation, a precession capability at high angular rates of the order of several tens of degrees per second. In other words, it has to be both a good gyroscope and an excellent rate gyro.

3.1.1. Performances

The gyroscopic sensor used in the SIL 3 inertial reference is a two axis slaved rate gyro with a mono-gimbal flexible joint. It is provided with a galvanometric torquer (Fig.8).

Its main characteristics, given in table 1 below , can be adjusted according to the application sought for the system.

Table 1

Dimensions	diameter length	52 mm 65 mm
Angular momentum		1,6 to 3,2 10^5 CGS
Wheel speed		160 to 320 rev/s
Run up time		10 to 20 s.
Limit stops		$\pm$ 30 arc min.
Random drift		0.03 to 1°/h
Angular rates range : Permanent		$\pm$ 20 to $\pm$ 50°/s
	Transient	$\pm$ 100 to $\pm$ 200°/s

3.1.2. Technological details (Figure 9)

GAM 3 is constituted essentially (see fig.) on the one hand of a rigid housing to which is fixed the multipolar hysteresis spin motor , the 4 cores of angular position sensors (variable reluctance), the 4 windings of the galvanometric torquers , for X and Y axes, and, on the other hand, of a rotating element comprising a shaft connected to the fixed part by two preloaded ball bearings and to the rotor by a compensated flexible universal joint.

The rotor is formed essentially of 4 samarium cobalt permanent magnet monobloc rings and two mild steel cylinders to close the magnetic circuit.

The radial field created by the moving permanent magnets acts on the fixed windings placed in the gaps to exert the torques necessary to obtain high angular precession rates.

The main characteristic of this 2-axes rate gyro is the simplicity of construction and so its low cost compared to its performance. In fact, the most difficult part, which is the rotor suspension, is achieved by means of a mono-gimbal flexible joint, formed of four " arms " of cruciform section, two of which are linked to the drive shaft by a fork, the other two being fixed to the rotor. The intermediate ring of the gimbal has very small dimensions, which gives it a very low inertia about the spin axis. The compensation of the torsional stiffness of the flexure is by means of 2 small tuning masses screwed either side of the intermediate ring.

This original arrangement for the flexible joint is made very simply from a single piece of material by electro-erosion. It is really satisfactory for the performances sought for the gyroscope.

The GAM 3 is fitted with an internal heating resistor and a sensor to enable any necessary preheating of the gyroscope.

The stop which has been arranged between the drive shaft and the rotor eliminates any source of damage to the gyroscope.

Among the difficulties which had to be overcome for developing the GAM 3 can be quoted the effect of temperature on the magnets and the magnetic sensitivity of the gyroscope.

The variation of induction of samarium cobalt permanent magnets with temperature is about 5×10^{-4} per degree celsius. A magnetic shunt corrects almost the whole of this variation. The residue is cancelled out by a calculated compensation of the torquers scale factor in relation with the measured temperature of the rotor.

To eliminate the effect of the magnetic environment the gyroscope is enclosed by a case which is used as a magnetic screen.

3.2. The MICAL accelerometer (Fig.10)

3.2.1. Principle

The accelerometer used in the SIL 3 is the " MICAL ", developed by SFENA (Société Française d'Equipements pour la Navigation Aérienne). This is a miniature accelerometer, of 100 ppm class, of low production cost, obtained by careful value analysis and by reduction or elimination of the adjustment operations.

The " MICAL " accelerometer works on the principle of a single axis, pendulous force balancing system.

A pendulum with electromagnetic return, suspended by two flexible strips forming a hinge, constitutes the sensitive element.

Any acceleration applied along the sensitive axis tends to move the pendulum from its equilibrium position.

An angular capacitive pick-off, provides an a.c. signal of phase and amplitude in relation with the measured deviation.

After amplification, demodulation, filtering and phase correction, the signal is integrated and applied to a d.c. power amplifier. The latter produces in the return coil of the permanent magnet torquer and in the measuring resistor the current necessary to balance the action of the acceleration and bring the pendulum to its original position.

3.2.2. Characteristics

The MICAL accelerometer, with its incorporated rebalance electronic is in the form of a parallelepiped, 36 x 20 x 24.5 mm.

Its mass is 60 g.

The supply requires a $\pm$ 15 V voltage source.

Operation is instantaneous. No preheating is necessary.

The operating temperature range is from - 30° to + 95°C.

The input range is $\pm$ 15 g, with a scale factor of 0.5 V/g.

3.3. Sensors mounting block

The sensors mounting block (Fig.11) is formed of a rigid structure on which are fixed the two gyroscopes and the three accelerometers.

The gyroscopes spins are at 90° to each other and their measuring axes are placed at 45° to the missile axes.

So the two gyroscopes are used to measure the roll angular rate and only one to measure the pitch or yaw angular rate. This arrangement has many advantages, the main one being to increase the roll measuring range.

The three accelerometers are placed on the three rectangular coordinate axes. Two accelerometers placed at + and - 45° of the roll axis are used to measure the fore and aft acceleration.

The sensors mounting block is linked to the missile structure by an elastic suspension formed of four elastomer studs.

The suspension characteristics are adapted to the use. Generally it has to enable the sensors to be isolated from high frequency shocks and vibrations, while introducing no phase shift or parasitic low-frequency angular motion. Any way, the suspension must not cause conical motion.

The dimensions of the block, fitted with the sensors, are 150 x 65 x 65 mm.

3.4. Electronics

3.4.1. General functions (Figure 12)

(1) A static inverter receives the 28 V d.c. voltage from the missile battery.
It generates the various voltages necessary for the working of the system. The whole of these voltages are galvanically insulated from the 28 V source.
The power supplied is of the order of 80 W in steady state and can peak to 200 W.
The circuits comprise :

a) a 28 V/20 V switching supply
b) the inverter itself, operating at 12 kHz
c) an assembly of regulators.

(2) The gyroscopes have a wheel speed of about 320 Hz. They use synchronous three-phase hysteresis drive motors, having four pole pairs.
The supply of these motors receives an input frequency of 7,680 Hz, obtained by division, from the main oscillator. A 1/6-divider, followed by a shift register produce 6 logic signals at 1,280 Hz, of 1/3 dutycycle stepped 1/6 th period from each other.

These logic signals, combined by two, control three power switching amplifiers.
The two gyroscopes use different frequencies, having an offset of . 3%.

(3) The primary windings of the position pick-offs are excited by a 50 kHz frequency, sine voltage.
A 50 kHz logic signal, from division of the main oscillator, is applied to a selective filter whose output provides the necessary power. A detection network associated with a feed back loop provides the output voltage stability.

3.4.2. Gyros rebalance loops

The gyros rebalance is achieved by a binary, quantified pulse width modulated loop (fig.13). The choice of this method over that of ternary rebalance, or analog rebalance with follow-up digitizer was made on the following criteria :

(1) Constant heat state : this method best enables errors due to temperature variations connected with the input rate to be minimised.

(2) Relative simplicity. Moreover, the input is then directly digital, in the form of angular increments. There are no conversion circuits external to the loop.

(3) Excellent resolution.

(4) Good linearity and good symmetry, particularly near zero.

(5) Transfer function near to that of an analog loop.

The practical execution of the looping circuits moreover meets fundamental criteria :

(1) Conformity to accuracy specifications defined in the theoretical design.

(2) Maintaining the dissipated power at a reasonable level. This point also led us to make a rebalance loop with two current levels and automatic switching.

(3) Conformity to the gain and bandpass specifications necessary for the whole system.

The theoretical study of a binary rebalance loop adapted and optimised for a two-axes tuned gyroscope led SFIM to make a simulation set reproducing as exactly as possible the behaviour of such a gyroscope.

Moreover, an original method of analysis has been developed. This method, making use of complex transfer functions, allows the use on two-axes systems of complex NYQUIST or BLACK locus.

Applied as a first step to the study of stability and the optimisation of an analog loop, this method has shown excellent correlation with the experimental results. This same method, adapted, has been then used for the definition of the binary loop correctors. The results obtained have been confirmed both by simulation and, later, experimentally.

Figure 14 gives an example of the results obtained.

The general appearance of the loop is given in fig. 15.

(1) The gyro pick-offs provide two a.c. voltages proportional to the X and Y deviations.

(2) These voltages are preamplified, demodulated, filtered.

(3) The cross compensation circuits make a function of the form :

$$V_{Sx} = a\,V_{ex} - b\,V_{ey}$$

$$V_{Sy} = a\,V_{ey} + b\,V_{ex}$$

They are supplemented by integral and proportional correctors.

(4) The output voltage of the integral corrector is compared to a ramp and then synchronised by a flip-flop to generate a pulse width modulated logic signal. This logic signal is processed to limit the extreme values of the modulation depth and to determine the current level changes. It is then used to control the passing to positive or to negative of a reference current Io in the torquers windings. Switching of the current is through an H-mounted assembly of transistors.

The reference current is generated by a current source using a very high stability Zener diode followed by operational amplifiers and power transistors. The dynamic response of this current source, acting mainly during the H switchings, is an important parameter.

The H-switch is designed to minimise the current exchanges between circuits controlled and those controlling. It has also to switch rapidly and have as little leakage as possible in the vertical branches of the H.

The whole of the rebalance loop has a bandpass of 50 Hz. The limit cycle frequency is 800 Hz. The weight of the angular increment is.7 arc sec. in low rate mode and 3.6 arc sec. in high rate mode.

3.4.3. A/D conversions and Computer interface

(1) The accelerometers of SIL 3 are d.c. rebalanced. The acceleration data are therefore d.c. voltages which are converted into velocity increments by a binary quantizer using pulse width modulation. (fig. 16) .

The static accuracy and the dynamic performance of the quantizer have been especially studied for the strap-down application. The use in the quantizer of a second order loop prevents for the drag error when the input is in a ramp shape.

The weight of the velocity increment is 2×10^{-3} m/s. The quantizer has a bandpass of 100 Hz.

The limit cycle frequency is 800 Hz.

(2) The compensation of the gyros and accelerometers data requires to be taken into account in the computing :

a) deviation angles measured by the gyros inductive pick-offs
b) temperatures of each gyro and of each accelerometer, measured by the resistive detectors.

These are taken into account by an A/D converter working in multiplex (Fig.16) . The rate of conversion is 10 ms; the total conversion time 200 µs. During these 200 µs the converter codes in succession the four deviation voltages, 1 temperature and 3 test voltages. A second multiplexer provides for the distribution over 8 x 10 ms cycles of the coding of all the temperatures.
A sequencing logic at the same time drives the multiplexers and the addressing of the storage memory receiving the coded data and providing their transfer to computing elements through the internal bus.

(3) The acquisition of all the datas associated with the width modulations, i.e. the 4 angular rate signals from the gyros and the 4 acceleration signals, is performed by a single reversible counter together with a memory and working in multiplex mode (Fig.17).
Another counter, also with a memory and multiplexed, measures the rotation period of each of the two gyroscopes. This information, taken with high resolution, will enable the correction of " wheel-hunting " type errors.

A storing memory receives all the data supplied by the counters and provides for their transfer to the computer through the internal bus.
The dialogue between the computer and the memories is accomplished through a serialiser.

3.5. SYCOMORE processing network

3.5.1. Principle

The processing to be carried out in the SIL 3 strap-down system is of two kinds :

(a) Very rapid computations of a mathematical nature :
- rate-gyro corrections
- accelerometer corrections
- determination of attitudes and velocities.

(b) Slower computations for the logic operations :
- sequencing of the system
- inputs/outputs to the Control and Display Unit
- output of data on the system bus
- self-tests of the system.

A solution enabling the whole of the problem to be processed consists in using a fast universal computer, but this has not been adopted for the airborne equipment.

In fact, in order to minimise volumes and costs it is necessary to use the most integrated standard components on the market.

The optimum solution adopted consisted in combining a microprocessor and a fast operator working only on floating numbers.

These two processing units can work simultaneously, so forming a true bi-processor configuration.

This computing network is called SYCOMORE (Système de Calcul à Organisation Multi-Operateur pour Realisations Embarquées = Computing System with Multi-Operator Organisation for Airborne Use).

The fast operator carries out the type (a) tasks and the microprocessor the type (b) tasks.

3.5.2. Organization (Figure 18)

The system is arranged around two main busss :

(1) The memory bus combines 15 addess lines, 16 bidirectional data lines and a number of memory controls.

(2) The inputs/outputs bus.

The former is used by the two processors. An access logic enables conflicts to be resolved.
The inputs/outputs bus is managed by the microprocessor.
The memory is arranged in 16 bit words. It is divided into three parts :

(1) the programs in the static memory (ROM)

(2) the transient data in RAM

(3) a number of special data in a protected memory.

The inputs/outputs of the system are constituted by :

(1) datas provided by the rate gyros and accelerometers

(2) coupling of the Control and Display Unit

(3) generation of the output bus distributing the attitude and navigation parameters to the users.

3.5.3. Functioning (Figure 19)

The tasks are managed by the microprocessor which process the tasks of low priority and let to the floating operator the fast computing tasks. When these tasks are started, they are completely processed by the floating operator, which has a direct access to the programs in memory . The interrupts are managed by the microprocessor which can interrupt the floating operator to cause it to execute tasks of greater priority.

The context change is then managed by the floating operator itself.

The floating operator indicates that it has completed its task by means of a generated interruption to the microprocessor.

3.5.4. Characteristics and performances

(1) Microprocessor

The microprocessor used has :

a) a 16 bits central processing unit.
b) a system of 16 prioritized interrupts with automatic context change,
c) 69 instructions enabling processing on words, octets or bits,
d) a mean instruction execution time of the order of about 6 µs.
e) an input/output serial bus.

(2) Floating operator (see Fig.19)

The floating operator is a microprogrammed computing unit, manipulating floating numbers of 32 bits, including 8 exponent bits (2-128 to 2-127) and 24 mantissa bits (including 1 sign bit).

a) Programming
The computing tasks are expressed in the form of programs placed in the memory. The operator thus has a set of instructions of his own and software means adapted to the generation of computing programs (compiler).

b) Micro-programming
To each instruction corresponds a micro-program made with micro-instructions. The linking up of micro-instructions is managed by a micro-sequencer which can address 512 micro-program memory words. In order to obtain the best possible speed of execution, there is, strictly speaking, no set of micro-instructions. A micro-instruction is described by a 72 bit word, spread over several independent fields, expressing composed codes or discrete micro-controls.

This arrangement enables several actions to be described simultaneously and, consequently, entails an appreciable increase in execution speed of optimised microprograms.
Special arrangements have been made for the microprogramming to have constants available, which is of particular interest for executing complex instructions.
With the use of special facilities microprograms can be made on demand.

c) Processing Unit
With the aim of simplifying equipment, the basic operator is of 32 bits, with 8 bits reserved for the exponent and 24 for the mantissa. It uses LSI AMD 2900 elements.
Basically, the processing unit is arranged like a stack machine. It comprises an Arithmetic and Logic Unit, a floating operands stack with eight steps, used in most of the instructions, and a memory work space of 8 registers, some of which are specialized(program counter, addressing base, index) and the others used as a fast memory work space.

d) Execution time :
The operations are carried out essentially on the stack. The maximum execution times are the following (with fast bipolar memory) :

Floating addition 6 µs
Floating multiplication 7 µs
Push or pull on stack 2.4 µs
Sine, arc tan 80 µs

3.5.5. Software Generation (Figure 20)

To facilitate the writing of programs, a sub-assembly of FORTRAN is specified, which can be compiled for execution on the floating operator.

The interest of FORTRAN is that it enables an easier writing of computing programs and gives the possibility of carrying out debugging on most computers.

The programs tested are then compiled in order to generate an object program which can be executed on SYCOMORE.

These programs are associated with programs written in an assembler for the microprocessor and after link edition they are fed into the SYCOMORE memory.

A system used to aid final development then enables the real time operating of the system while it is combined with data processing checking facilities.

3.6. Application software

3.6.1. Principles

The application software has been specified to meet the very general applications mentioned above.

Of course, the characteristics of the mission have been taken into account (flight duration , linear and angular dynamic environments). The aim is as follows : the software must not bring any inherent error greater than 10% of the total error of the system.

A very exhaustive prior study of the working of a dry gyroscope and of a pendulous accelerometer in very severe dynamic conditions led us to define very complete error correction algorithms. Moreover, the band pass sought (> 30 Hz) set a minimum rate for the main computations algorithms.

The software optimisation related mainly to :

(1) Minimisation of the volume and of the computing time

(2) Modularisation of the program. In this way the same main modules can be re-used for various flight sequences (alignment, calibration, flight).

The various modules (computing sequences, algorithms) are triggered according to the case :

(1) By external interrupt coming from the sensor block.

(2) By internally programmed interrupt.

(3) By flag inside a given program.

The main modules and associated rates can be described rapidly in two cases :

(1) Missile flight

(2) Alignment of the system in flight tests on a civil transport aircraft.

3.6.2. Flight of the Missile

A series of interrupts coming from the sensor unit synchronises the " real time " computation :

(1) Acquisition of incremental rate gyro data; scale factor errors compensation according to a stored error model. At the same time some associated data are acquired(the gyros rotors offset...) rate 100 Hz.

(2) Accelerometer incremental data (and temperatures)acquisition scale factor errors compensation (with a stored model), rate 50 Hz .

(3) Compensation of rate gyros and accelerometers dynamic errors (well known working models are used, for a dry gyro and a pendulous accelerometer); rate 50 Hz.

(4) Attitude computation. The mathematical representation by four quaternions (four parameters) is used. The variation of the quaternion with the angular rate measured in the missile axes (ω) is well known:

$$\dot{Q} = \frac{1}{2} Q \cdot \omega \qquad\qquad Q = (q_1, q_2, q_3, q_4)^T$$

A third order numerical integration, compensated for angular accelerations, suffices for the performances sought.
Rate 50 Hz

(5) The quaternion calculated by numerical integration is corrected at regular intervals for slow drifts (drifts of the gyroscopes in accelerations, calculated according to a stored model; precession of the navigation coordinate system, and earth rotation). Then the attitude matrix is computed (function of the quaternion components). N being the navigation coordinate system :

$$C_B^N = \begin{matrix} q_1^2 + q_2^2 - q_3^2 - q_4^2 & 2(q_2q_3 - q_1q_4) & 2(q_2q_4 + q_1q_3) \\ 2(q_2q_3 + q_1q_4) & q_1^2 - q_2^2 + q_3^2 - q_4^2 & 2(q_3q_4 - q_1q_2) \\ 2(q_2q_4 - q_1q_3) & 2(q_3q_4 + q_1q_2) & q_1^2 - q_2^2 - q_3^2 + q_4^2 \end{matrix}$$

Rate 25 Hz

(6) Before the B←N coordinates transformation on the rate increments provided by the accelerometers, the commutability error, due to integration in a moving coordinate system, is compensated.
Rate 25 Hz

(7) The conventional navigation calculations are then made (velocity, position, ...) at a rate of 12,5 Hz or less.

(8) Other tasks can be carried out at a few Hz.

a) Processing of temperature (the sensors are temperature modelled)
b) Validity test on some measurements, which enables special compensation procedures to be connected up.
c) output on missile bus.

Figure 21 summarises the software arrangement for the FLIGHT phase : the figure 22 gives the " real time " sequencing.

The computing volume can be summarised thus :

a) 100 additions + 100 multiplications in floating 24 + 8 bits to be made in 10 msec steps.

b) Occupancy of the SYCOMORE computer of about 50%.

A.P.S. Alignment

The mode of alignment of the SIL 3 depends essentially on the type of mission given to the missile and so cannot be defined a priori.

However, within the scope of the flight tests made on a civil transport aircraft, an alignment in flight by comparison with the data supplied by the inertial reference unit has been provided for.

This procedure is described in paragraph 4.2.3.3.

4. DEVELOPMENT AND CHECKING OF THE SIL 3 SYSTEM

The development of the SIL 3 system required the use of various tools, among which are :

(1) A set of system simulations

(2) The definition of test methods and the associated means.

4.1. Simulations

A simulation of the various parts of the SIL 3 system has been developed. This simulation has a triple purpose :

(1) First of all an understanding of the part of the various elements as an error source, in order to give them an optimum definition (digital rebalance of gyros, software...).

(2) This simulation provides an evaluation of the system performance for all working conditions.

(3) The results of these simulations are compared with measurements obtained during tests. This led to an identification of SIL 3 model for various dynamic environments.

As partial simulations can be mentioned :

(1) Simulation of the gyroscope with its digital rebalance loop. This led to optimisation of the whole loop (bandpass, transients, dynamic behaviour of the gyroscope). An example of the response of the GAM 3 gyro to an angular rate step is shown in fig. 23.

(2) Simulation of the specific software (integration of the attitude, coordinate transformation on rate increments...); the processing of the mathematical data has thus been checked.

(3) Simulation of the in flight alignment procedures used during the tests (Kalman filter, specified according to the theory stated in 4.2.3.3.). Fig. 29 gives an alignment example.

(4) Some related simulations (suspension, gyro thermal model ..).

A simulation of the whole system has been made. Fig.24 gives a portion of the standard flight (angular rates and accelerations); Fig. 25 gives the 1σ values of attitude and position errors of the whole SIL 3 system.

A Monte Carlo method was used to qualify the system in simulation.

A given portion of flight is used several times as input to the system simulation (sensors + software). The various random error parameters are drawn at random to a Gaussian law. The calculated values of attitudes, rates, and position... are compared to the reference values, thus providing the system errors for the random drawing made. The procedure is repeated and by a statistical analysis provides the standard deviations of the SIL 3 system errors, for a given flight profile. Fig.26 outlines the procedure used.

All of the simulation is developed in FORTRAN by means of a data processing system comprising :

(1) A CPU with wired float.

(2) A dialogue console.

(3) 2 disc units; 1 magnetic tape unit; 1 printer; 1 XY plotter; 1 tape reader.

4.2 Test methods and means

4.2.1. Gyroscope

The standard tests for gyroscopes used in platforms relate mainly to their behaviour in acceleration :

(1) Static tests giving the terms of a model in acceleration.

(2) Tests in linear vibration.

The use anticipated requires, rather, study of the behaviour :

(1) of torquers (scale factor, stability, misalignment)

(2) of the gyroscope and its rebalance loop in angular vibration.

SFIM had to provide new means and methods to take these needs into account and also the following principles :

(1) Static test means different from those for dynamic tests.

(2) Test equipments associated with data processing means.

(3) These test means must can be used for system tests.

4.2.1.1. Static Tests Means

The GAM 3 automatic test set allows :

(1) The gyro operation with analog or digital rebalance loops.

(2) The thermal control of the gyroscope.

(3) The conditioning of some parameters such as temperatures, loop deviations errors, precession torques.

(4) The monitoring of the correct operation and safety management .

(5) The data acquisition on punched tape and on a printer according to two working modes :

Acceleration Mode used to determine the terms of the model in acceleration. The test set records the integrated drift torques for a given time for different positions of the gyro in relation to the gravity field.

Table mode . The test set is combined with a one-axis rotating table on which is positioned the gyro slaved on its two axis as a rate gyro. It records the precession torques on each axis, integrated over a given angle, and also the mean angular rate of the table through this angle.

4.2.1.2. Analysis of the Static Tests

The results of measurements, transfered by punched tape to the computer are analysed by standard statistical methods which can take into account the redundancies present in a complete series of measurements. The most probable coefficients of models describing the gyro in acceleration and its torquers are evaluated, and also the uncertainties associated with these coefficients.

Two automatic test sets have been built and are to day working , together with a table (Goerz or MPW). The data are processed on PDP 11/45.

4.2.1.3. Dynamic Test Means (Figure 28)

During dynamic tests the study could be limited to the overall behaviour of the rate gyro. The means described above would then suffice. It is more instructive to know at each moment the behaviour of the rate gyro, with respect to the parameters of input conditions. With this aim, a fast data acquisition set has been designed and built. It is controlled by the SFIM MARINA S fast processor, working with a 8K x 16 bits core memory. This test set enables the acquisition of the data defined on table 2 below.

Table 2

Parameters	No.	Nature	Accuracy	Acquisition Frequency (max .Hz)
Gyro precession torques	4	digital	12 bit+sign	500
Table position	1	digital	20 bit	500
Angular position	3	synchro	15 bit	500
Gyro angular deviations	4	analog	12 bit	500
Wheel/motor phase angle	2	digital	12 bit	200
Temperatures	4	analog	12 bit	80
Misc.	6			120

The data are stored on a magnetic tape recorder; operation is by a dialogue console fitted with a printer and cassette reader.

This test set is planned to be associated with :

(1) An oscillating table, mono-axis, two-axes or three-axes.

(2) A vibrator.

4.2.1.4. Dynamic Tests Analysis

After a test there are available all the data to reconstitute offline the behaviour of the rate gyro. One can then :

(1) Examine the overall behaviour of the unit.

(2) Determine the terms of a model of the rate gyro in angular rotation for some simple inputs (sine).

(3) Compare the experimental results with those obtained by simulation with correction procedure of the simulated model.

A fast acquisition set has been constructed and is now working, together with a 1 axis table (Goerz, MPW), 3 axes (Carco) or with a vibrator. Data processing is on a PDP 11/45.

4.2.2. Accelerometers

As for the rate gyros, it is necessary to study the behaviour of the accelerometers in static and dynamic conditions (angular and linear vibrations).
The coefficients of the model in rotation are measured on the oscillating table, by recording the input and output data by means of the fast acquisition set described above.

4.2.3. System

4.2.3.1. Static Tests

Their purpose is to measure the performance of the sensors placed in the system :

(1) Mutual influence of the sensors.

(2) Positioning of the sensors on the block.

(3) Thermal behaviour.

As in the gyro study, these measurements are made for different positions of the unit in the gravity field, or on a 1 axis rotating table. The data are recorded with the fast acquisition set, previously described.

4.2.3.2. Dynamic Tests

These are for defining the overall performance of the system for a given mission and environmental conditions :

(1) 1 axis axial oscillation tests,

(2) Tests in any dynamic ambience (rotation) ; 3 axes table,

(3) Linear vibration tests, on the vibrator.

The system, coupled to its computer, provides a result connected with its overall performances.

4.2.3.3. Flight Tests - System initialising

The SIL 3 flight tests will be made on a Caravelle type civil transport aircraft. For each aircraft flight of 1 to 1.30 hour duration, several missileflights,each of a few minutes, can be simulated. The results will be recorded on a magnetic acquisition and recording system and exploited off-line on the ground.

The main problem set by this procedure is that of the initialising in flight the strap-down system. The method has therefore been the subject of a special study, summarised below :

(1) General

The operation time of the SIL 3 in inertial mode is, because of the performance of the instruments, much less than the mean flight time of the transport aircraft in which the tests will be made.

As it is not feasible to land the aircraft every five minutes or to make use of a flight of at least an hour for only five minutes, it is necessary to provide for initialisation in flight. Then a dozen five-minute tests can be made during a flight. This initialisation iscarried out by using as reference the aircraft standard inertial unit.

It comprises three separate phases :

(a) Calculation of the initial quaternion from the Euler angles supplied by the inertial unit, then starting up the attitude computation.

(b) Comparison of the computed attitude and the attitude supplied by the reference inertial unit.
The result of this comparison is used to readjust, through filtering, the quaternion representing the attitude.

(c) Initialisation of the velocity components at values provided by the inertial unit. Starting up the computation of velocity from accelerometer data. Comparison of the computed velocity and the velocity from the reference unit. The result of this comparison is used to readjust, through a sub-optimum filtering, the attitude quaternion.

(2) Description of the different modes

(a) The first mode needs no functional explanation. It can simply be said that this very rapid initialisation can leave considerable attitude errors due to different causes :

- errors in angular repeat of the inertial reference,
- harmonisation defects in the two units
  - . electrical noise (coding a peak)
  - . coding error of the repeat (nonlinearity , quantification)
  - . ageing of the data , entailing errors if the initialisation takesplace during evolutions.

(b) The second mode, which lasts only a few seconds, enables a part of the error from the previous setting to be eliminated and carries out the filtering of the last three types of errors, which are at relatively high frequency.
The diagram of the system is :

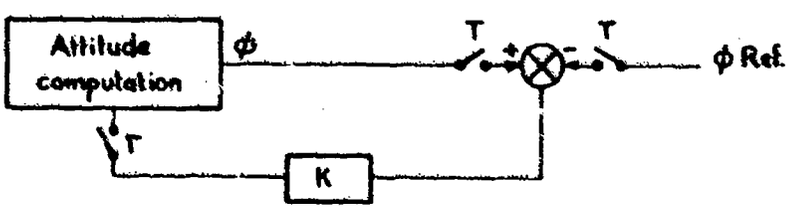

The use of a K coefficient lower than 1 gives the system the characteristics of a first order filter.

(c) The third mode, which performs the fine setting of the attitude, does not use the angular outputs from the reference inertial unit.

The fine setting is achieved by comparison of the acceleration, or, more precisely, of the velocity variations calculated by the two navigation systems. In fact, the attitude error $\underline{\delta\phi}$ causes an acceleration error $\underline{\delta A}$, which is a function of the acceleration $\underline{A}$:

$$\underline{\delta A} = \underline{\delta\phi} \times \underline{A}$$

It can be seen that an acceleration enables the evaluation of the attitude errors in a plane perpendicular to this acceleration. The permanent presence of the gravity acceleration therefore gives - a standar case - the vertical error. However, if the aircraft manoeuvres a horizontal component of the acceleration will allow the heading error to be evaluated.

We are therefore led to make an attitude correction based on the acceleration which prevails at the time of comparison. This correction must be also weighted by knowledge of the error on each of the axes. A simple way of carrying out these two actions simultaneously is by using a Kalman filter.

However, these attitude errors change and are not the only ones to act on the system. A full study shows it is necessary to use a state vector of dimension 39 whose components are generally not easily observed. As it is not conceivable to carry the associated optimum filter, the variables which are not easily observed are eliminated (thus reducing the state vector dimension to 5) and their action on the attitude and velocity is replaced by a random processing.

It is therefore necessary to adjust these two magnitudes so that the functioning of the sub-optimum filter is correct. For this, the optimum estimation covariance P_1, the estimated covariance P_2 and the real covariance P_3 are going to be compared. Now take the case of discrete observations. The algorithms defining P_1, P_2, and P_3 with respect to the time are defined in Table 3 below. The first line is justified since the correction calculated from gain K is actually applied to the system by the readjusting of the quaternion. The optimisation of the suboptimum filter is achieved by setting of R_2 and Q_2 to obtain, for a number of trajectories, the conditions $P_2 \quad P_3$ and P_3 slightly above P_1

Table 3 (1)

Estimation covariance	Optimum P_1	Sub-optimum P_2	Real P_3
calculation of the estimation covariance of the $P_{K/K-1}$ observation	$P_{1K/K-1}$ $= \Phi_1 P_{1K/K-1} \Phi_1^T + Q_1$	$P_{2K/K-1}$ $= \Phi_2 P_{2K/K-1} \Phi_2^T + Q_2$	$P_{3K/K-1} = \Phi_1 P_{3K/K-1} \Phi_1^T + Q_1$
Calculation of the gain K	$K_{1K/K-1} = P_{1K/K-1} H_{1K}^T$ $(H_{1K} P_{1K/K-1} H_{1K}^T + R_{1K})^{-1}$	$K_{2K/K-1} = P_{2K/K-1} H_{2K}^T$ $(H_{2K} P_{2K/K-1} H_{2K}^T + R_{2K})^{-1}$	
Calculation of the estimation covariance after observation	$P_{1K} = (I - K_{1K} H_{1K})$ $P_{1K/K-1}$	$P_{2K} = (I - K_{2K} H_{2K})$ $P_{2K/K-1}$	$P_{3K} = (I - K_{2K} H_{1K} - P_{3K/K-1}$ $(I - K_{2K} H_{1K})^T + K_{2K} R_{1K} K_{2K}^T$

Φ transition matrix H observation matrix Q covariance of the noise acting on the system R covariance of the observation noise.

5. CONCLUSIONS

The SIL 3, as just presented, represents a solution quickly usable for the guidance of tactical missiles.

This system is at present being ground tested and will undergo its flight tests at the beginning of next year.

The application considered for tactical missiles is not a limitation.

The system is, by the computing power available, capable of extension to other applications, for example : hybrid navigation, with Doppler, Omega,..of helicopters or transport aircrafts, or, again, guidance of torpedoes....

Its dimensions can also be greatly reduced, for this application does no make use of hybrid electronics. Finally, the sensors themselves can have an extended range of performance in the near future.

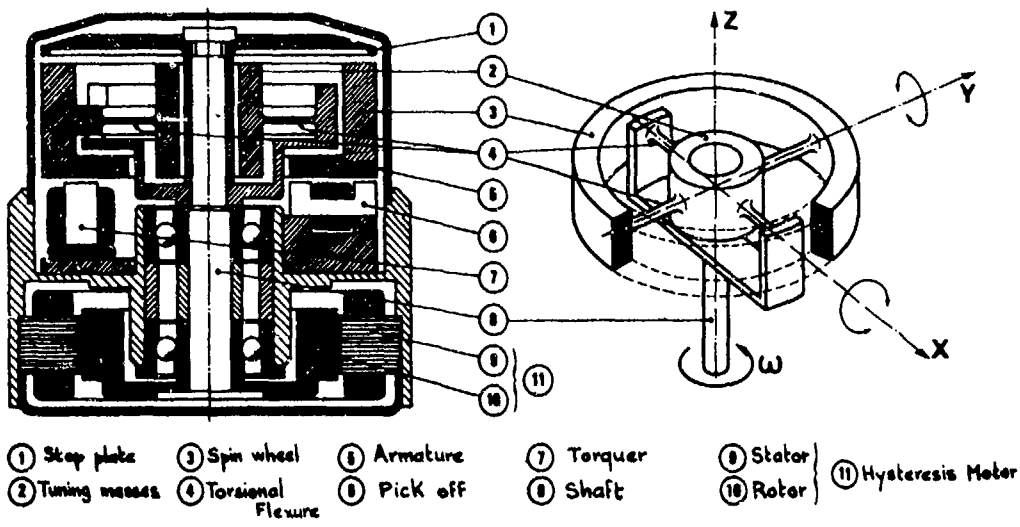

Figure 1 – GAM1 GYRO.

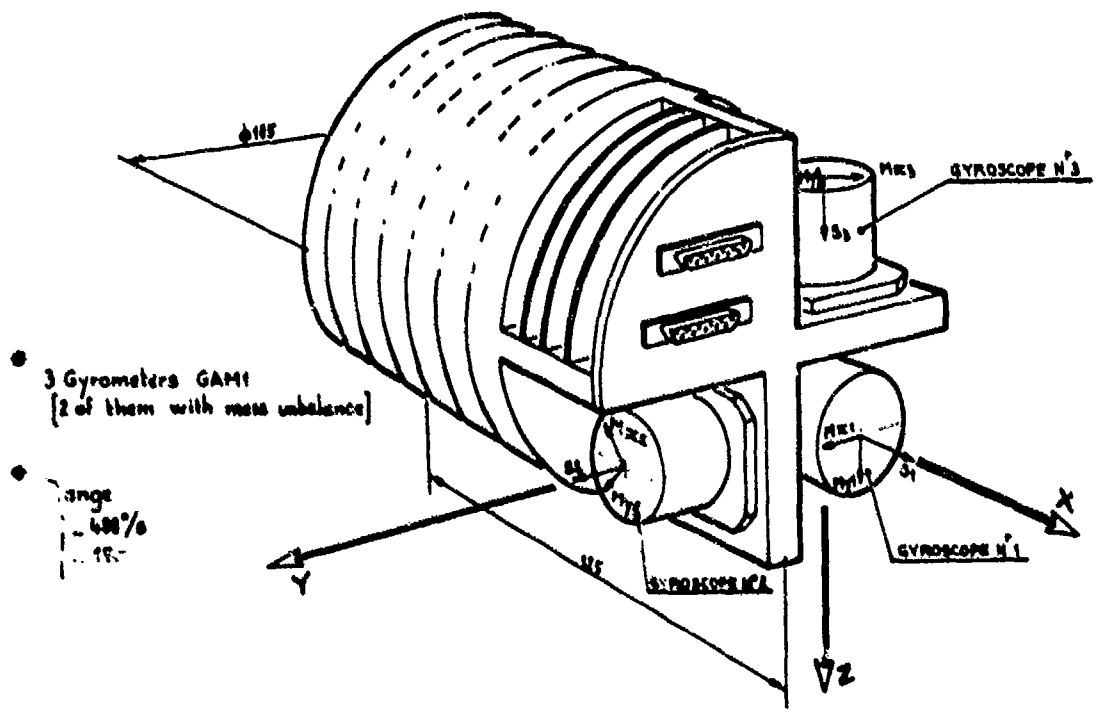

Figure 2 – SIL1

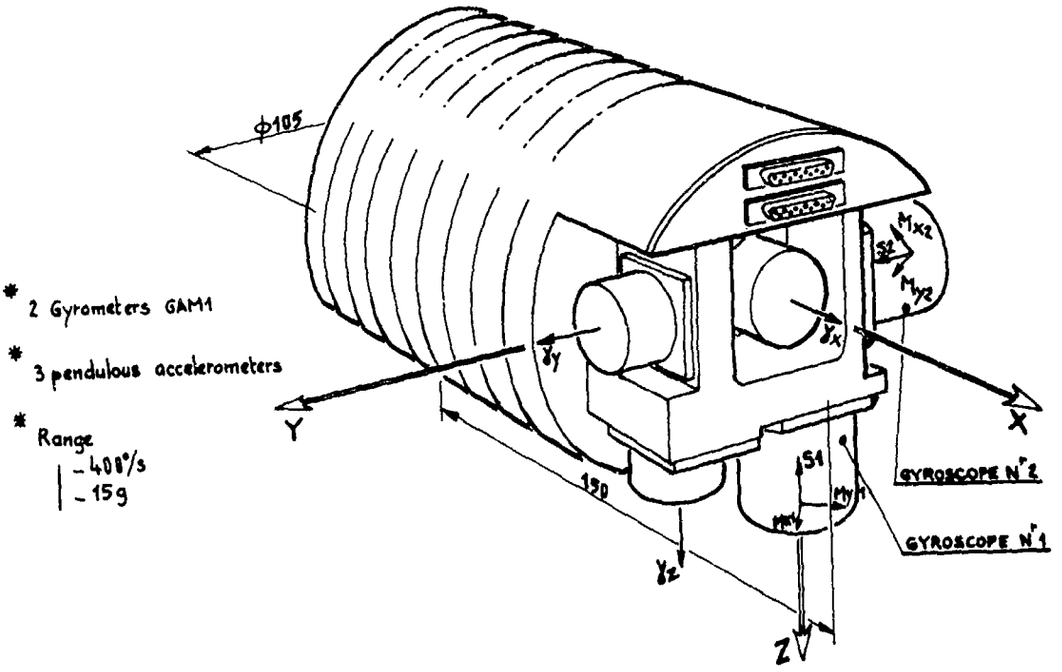

Figure 3 - SIL2

Figure 4

SIL3

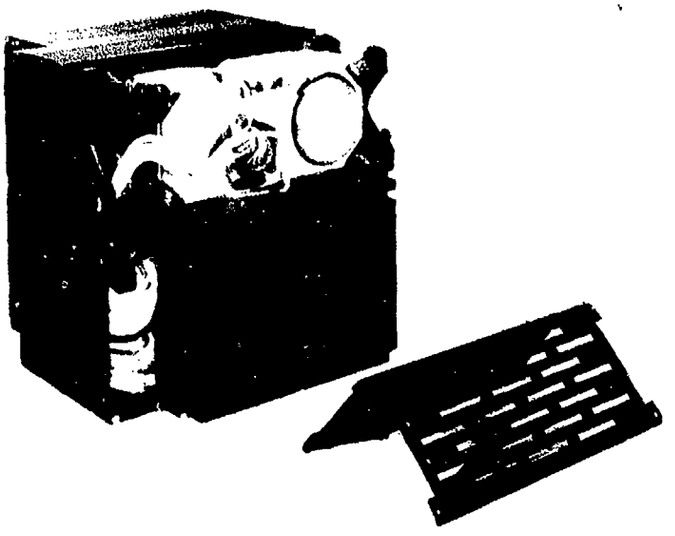

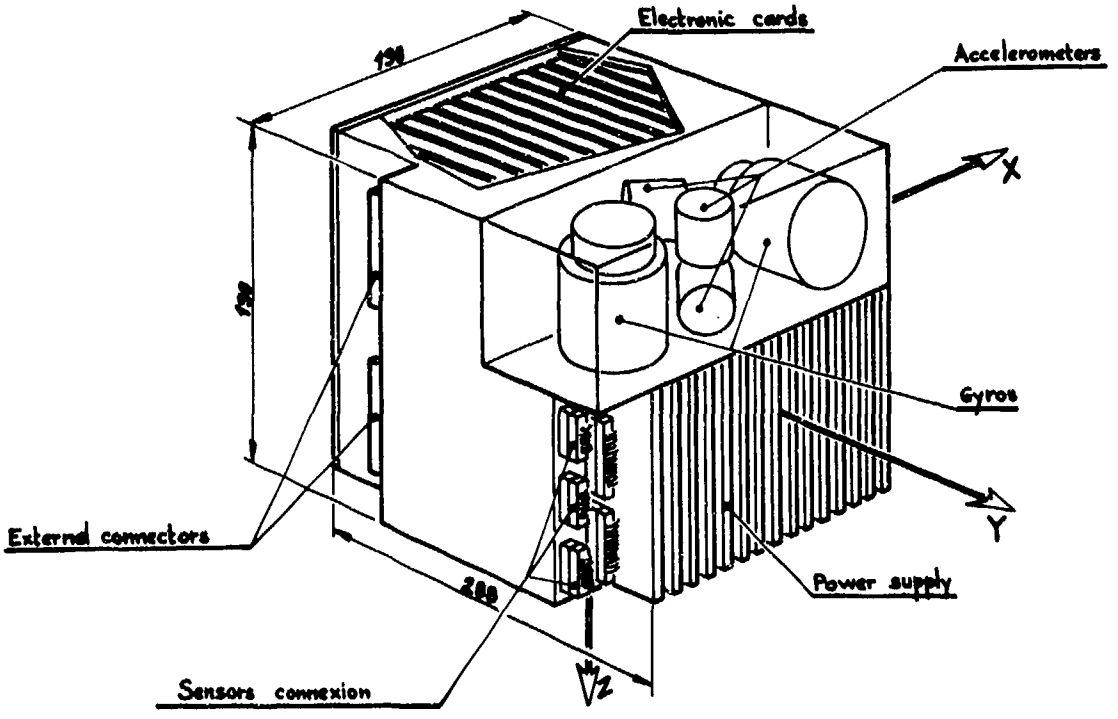

Figure 6 – SIL3

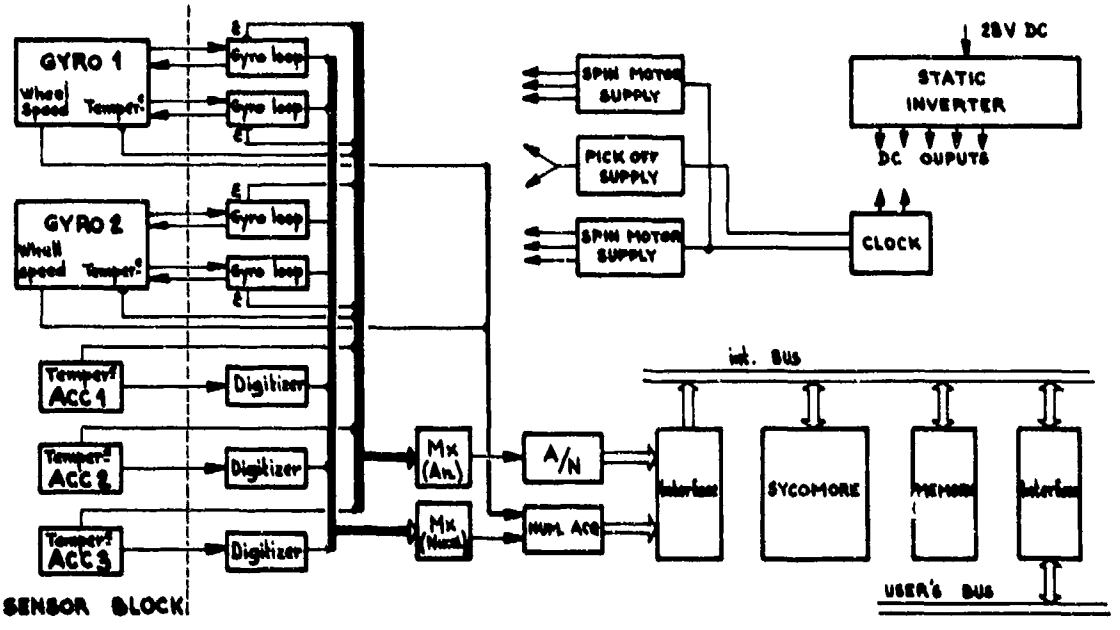

Figure 7 – SIL3 Functional diagram

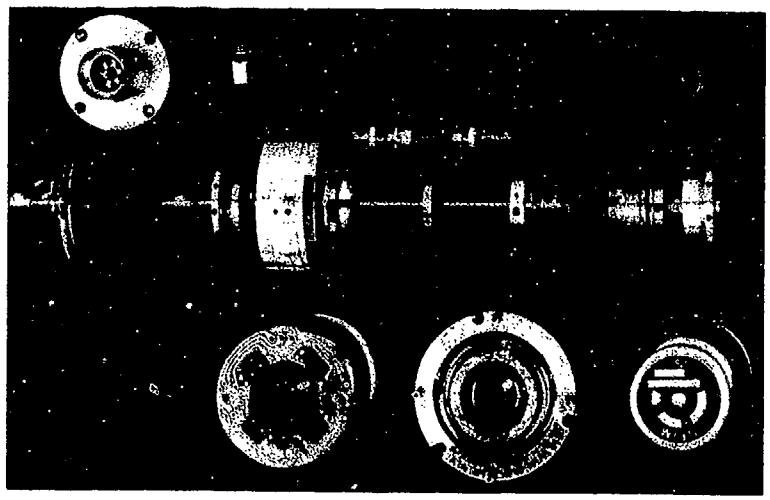

Figure 8

GAM3 Gyroscope

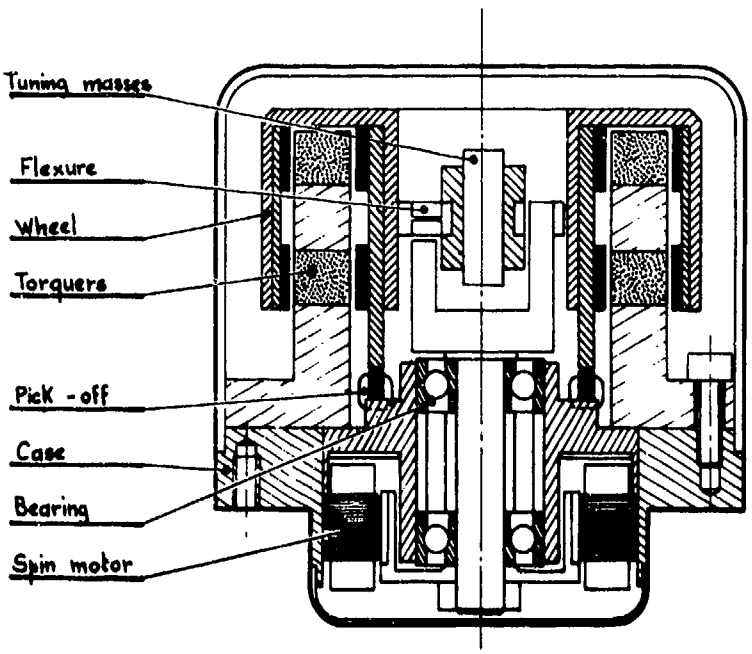

Figure 9

GAM3 Gyro

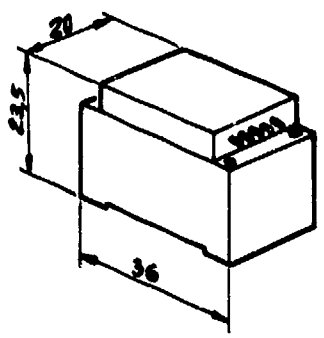

Fig 10

MICAL accelerometer

Figure 11

Sensor block

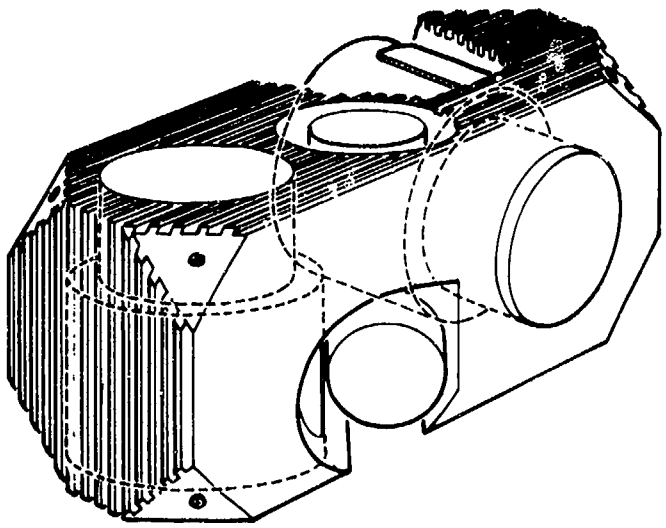

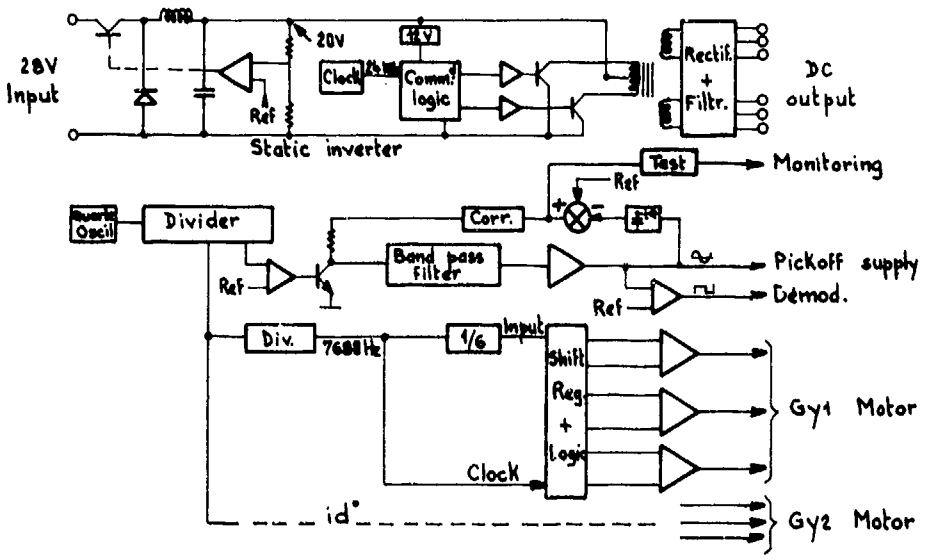

Figure 12 _ General functions

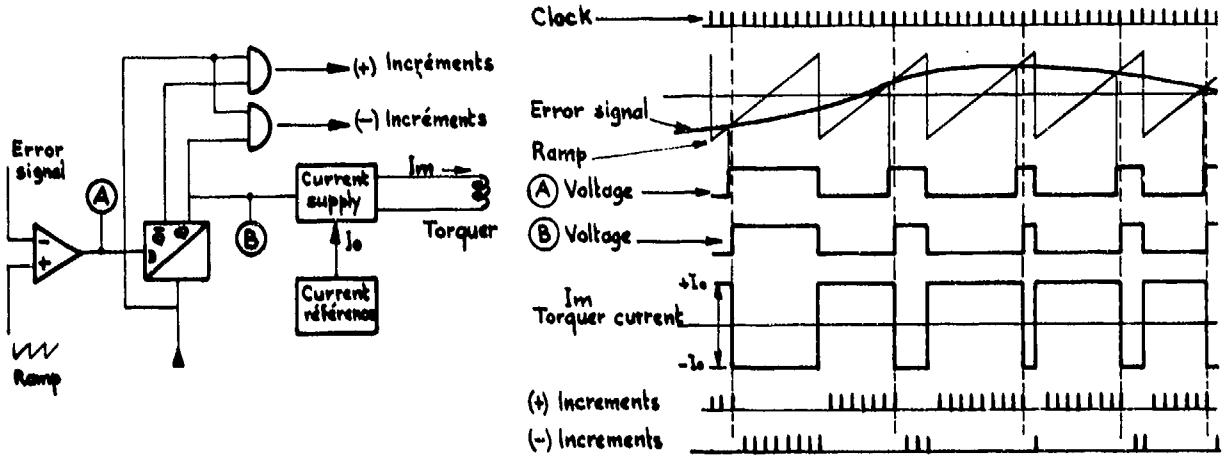

Figure 13 _ PWM Rebalance loop

8.46

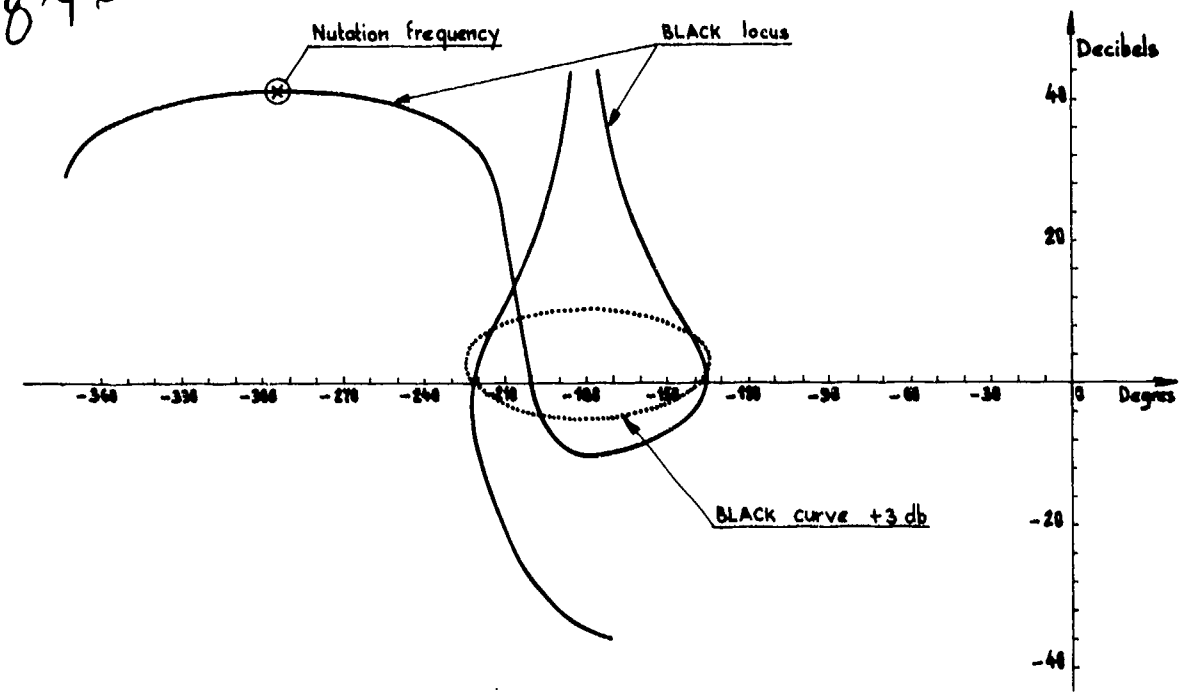

Figure 14 _ Sampled gyrometric loop analysis [BLACK locus]

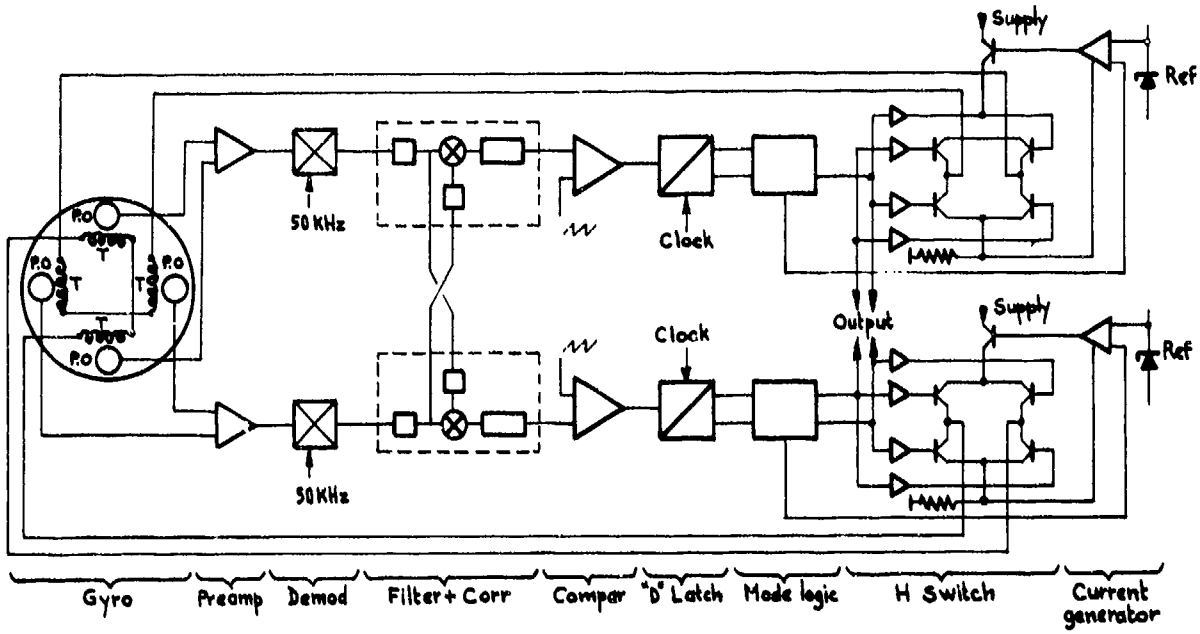

Figure 15 _ Gyro rebalance loop

Figure 16

A/D Conversions

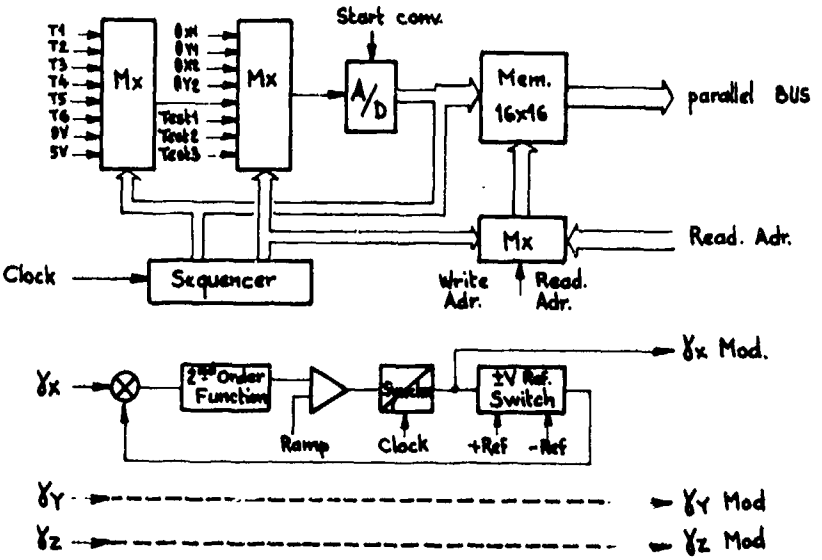

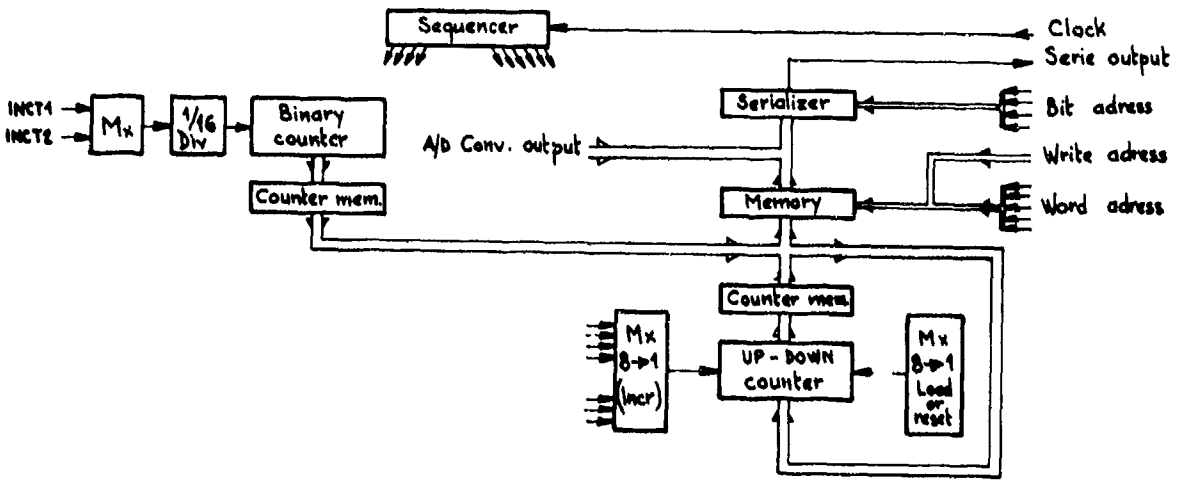

Figure 17 – Counting and serializing logic

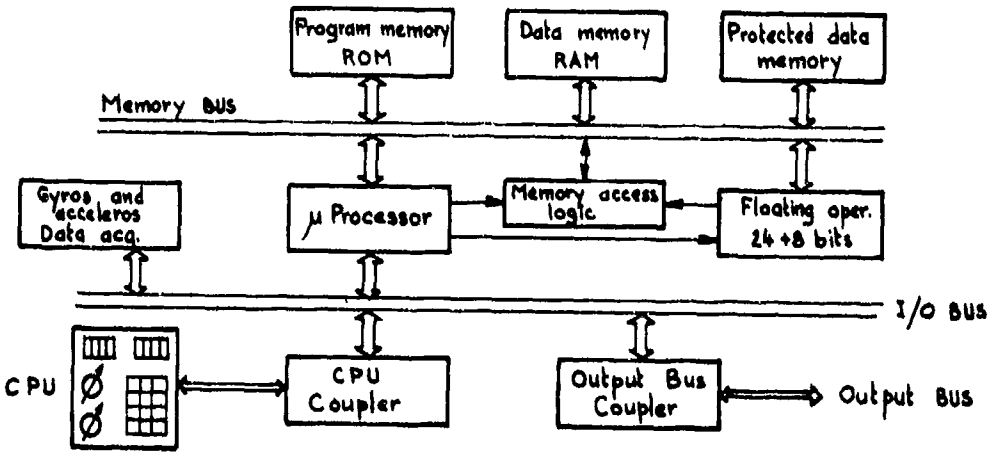

Figure 18 – SYCOMORE Organization

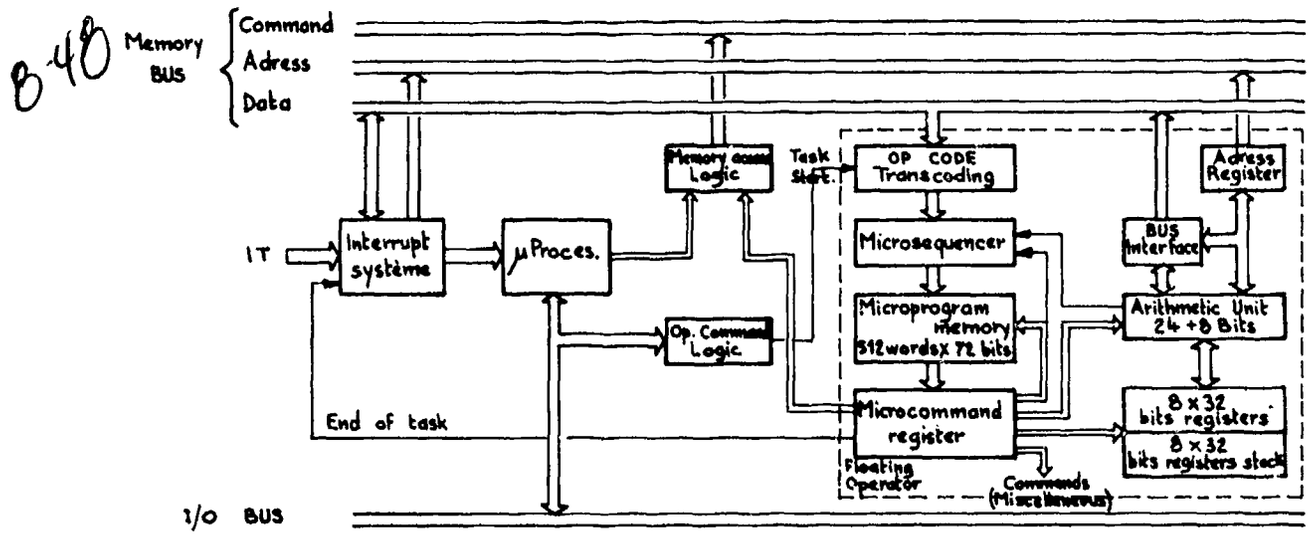

Figure 19 – SYCOMORE Functional diagram

Figure 20

SYCOMORE

Software generation

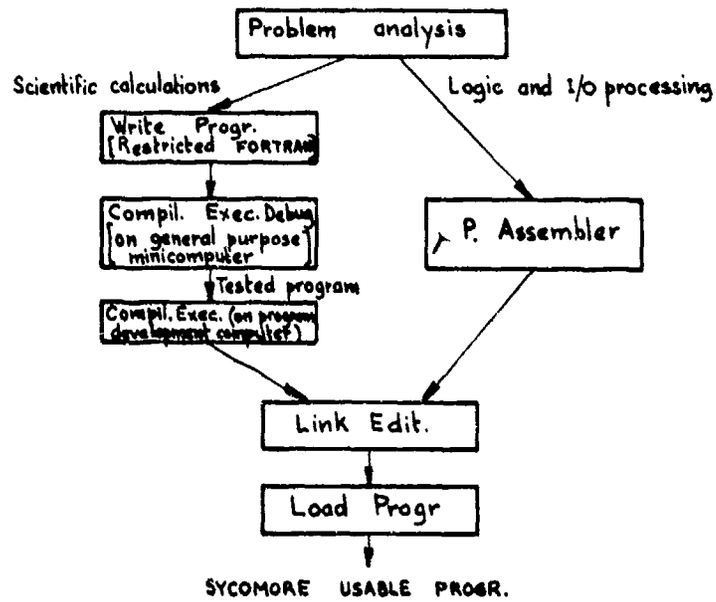

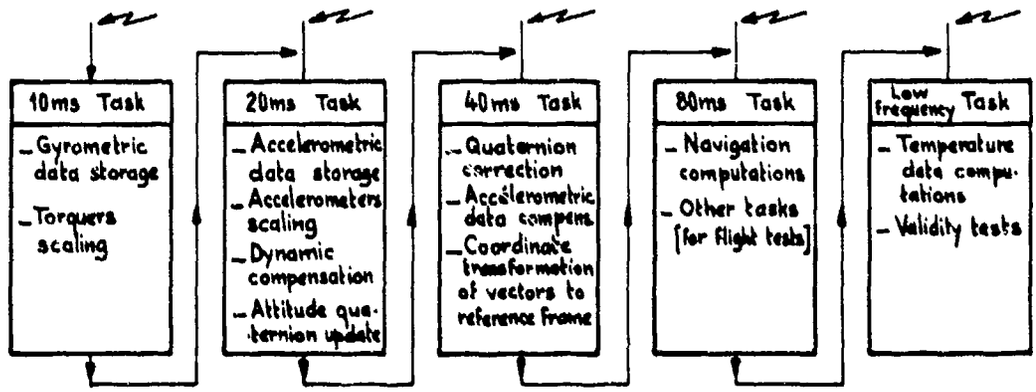

Figure 21 – Real time software organization

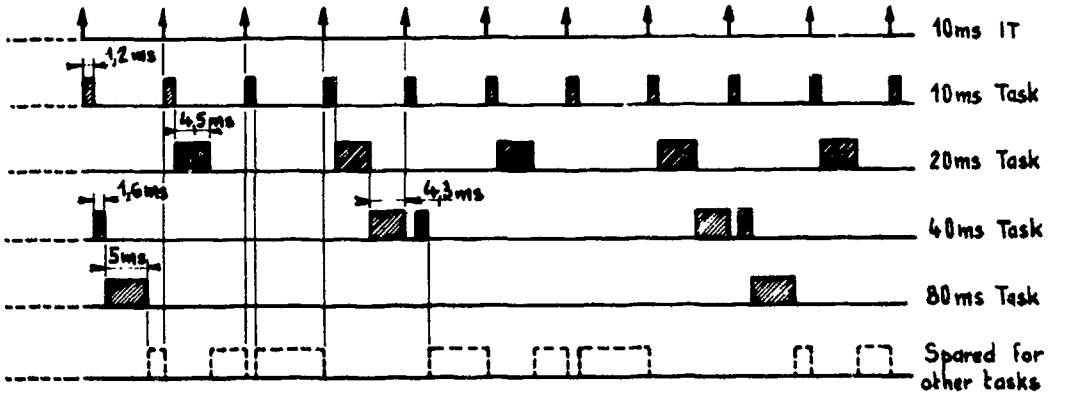

Figure 22 _ 'Real time' Tasks timing

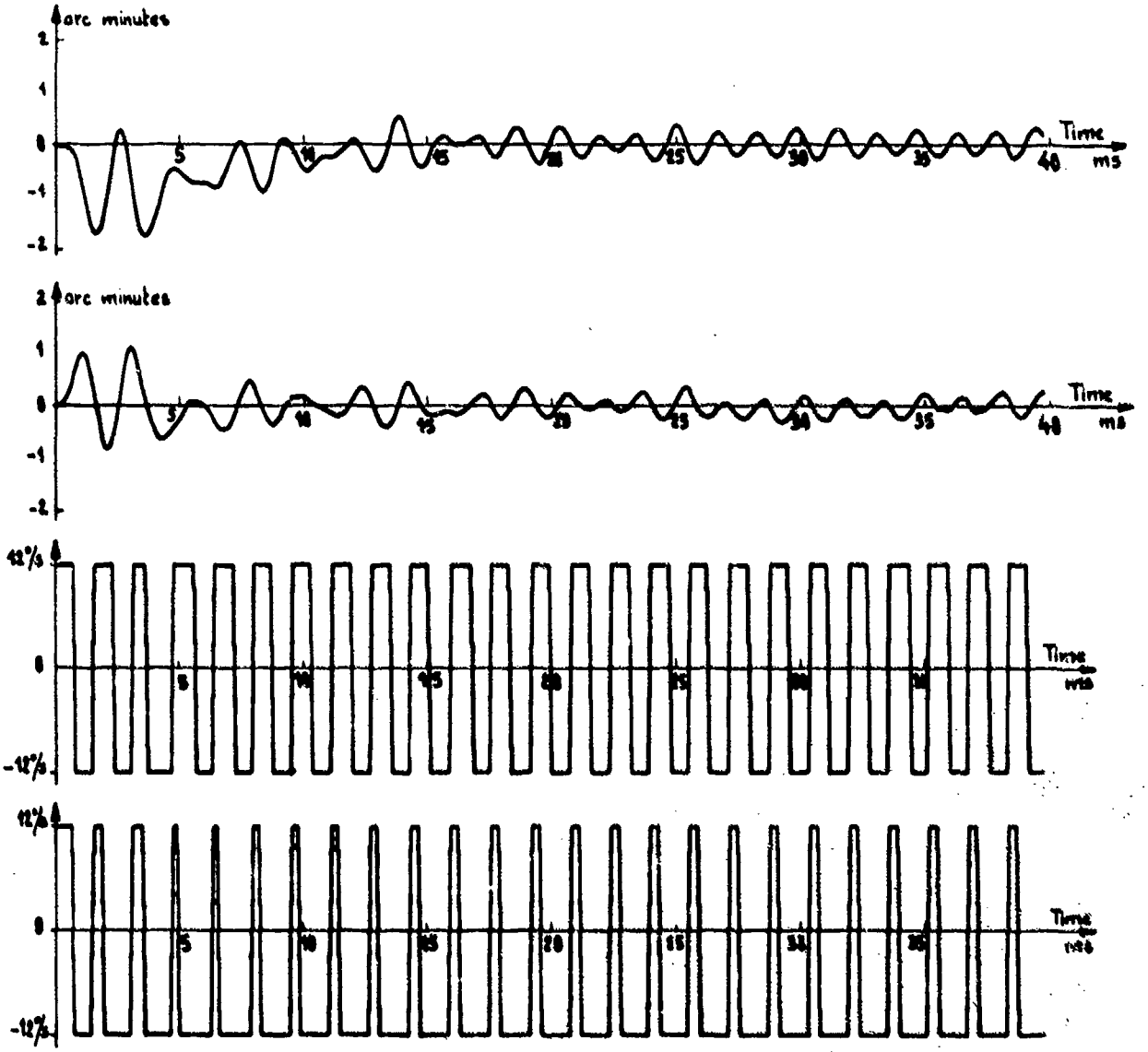

Figure 23 _ GAM3 gyrometer simulation . Response to an angular rate step input

B-50

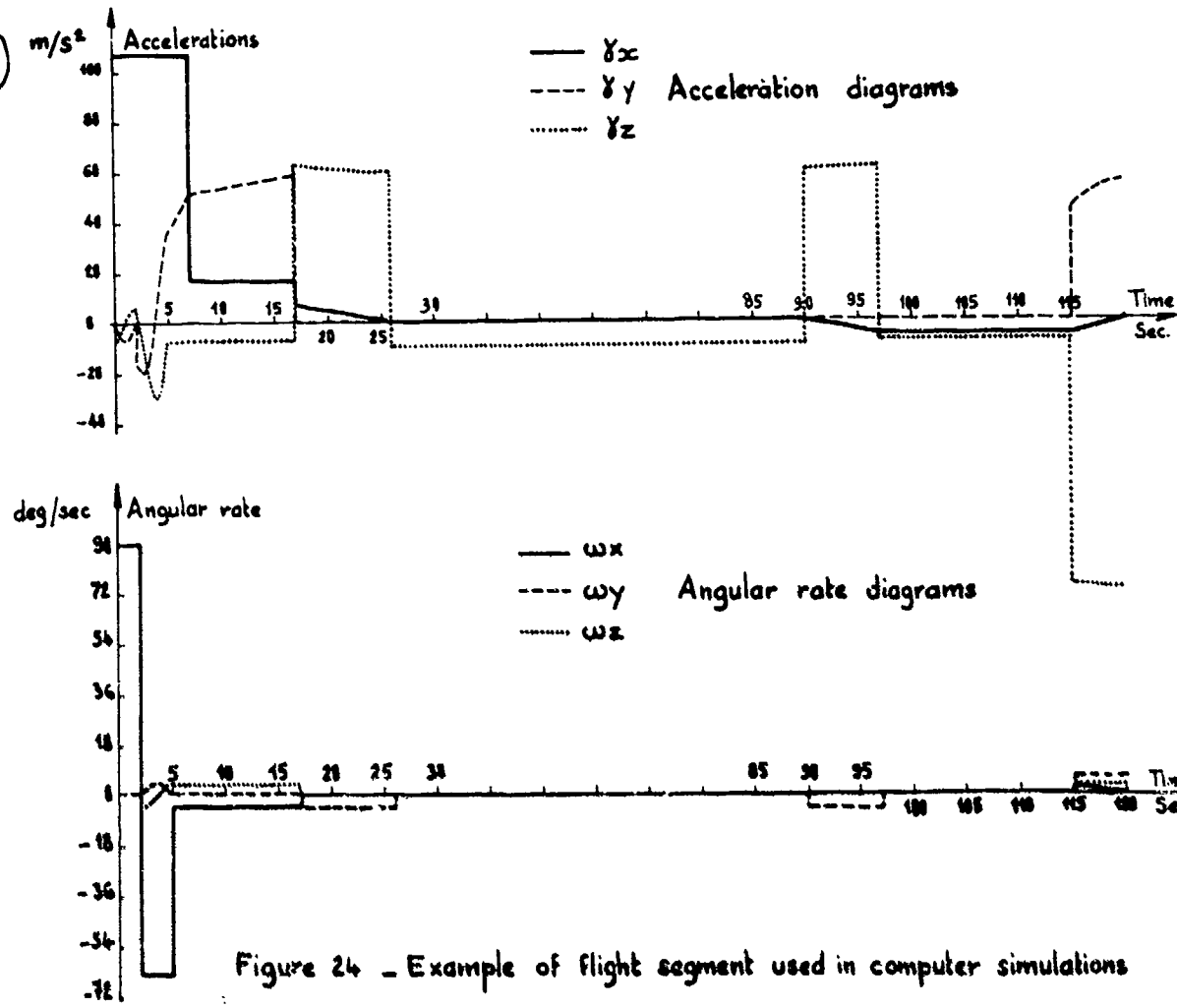

Figure 24 _ Example of flight segment used in computer simulations

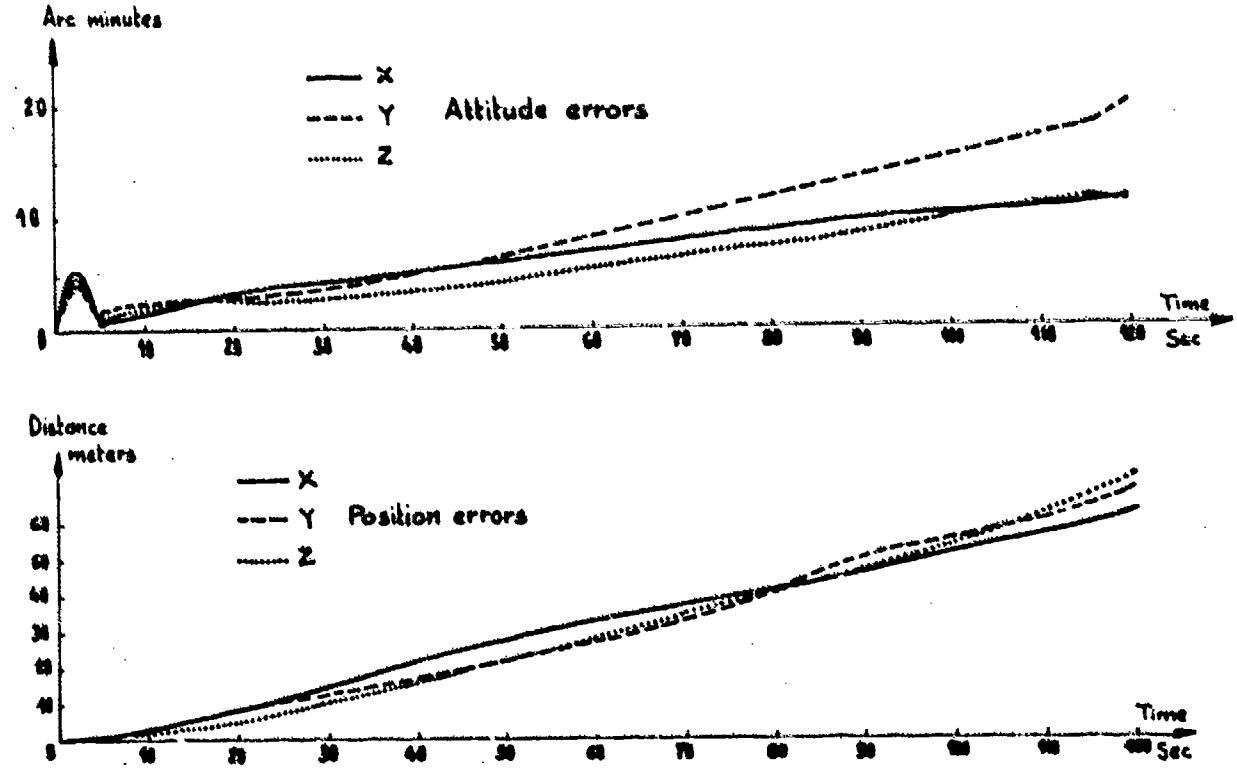

Figure 25 _ System simulation

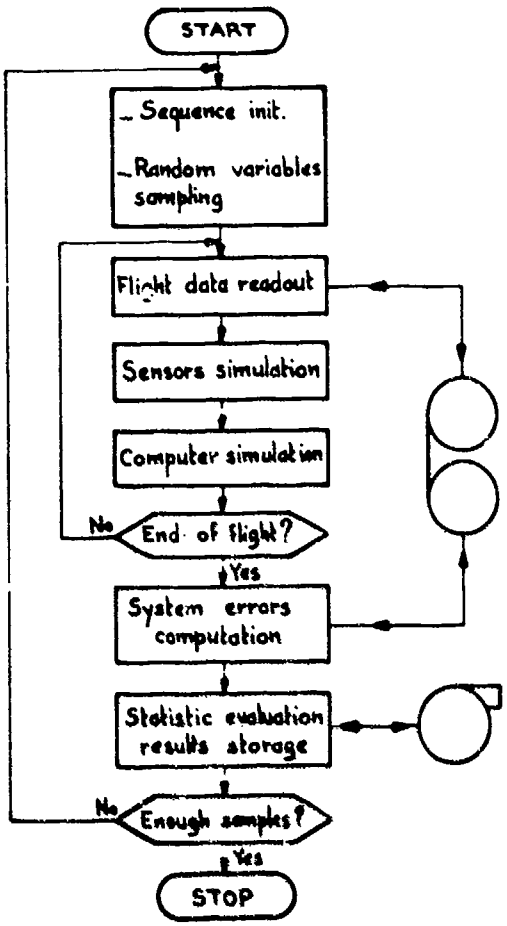

Figure 26

Statistical analysis of system errors

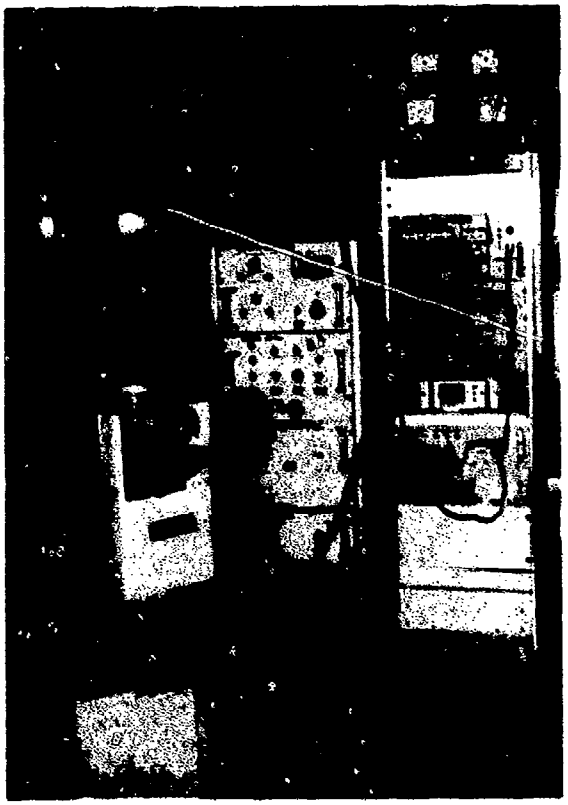

Figure 27

Static tests configuration

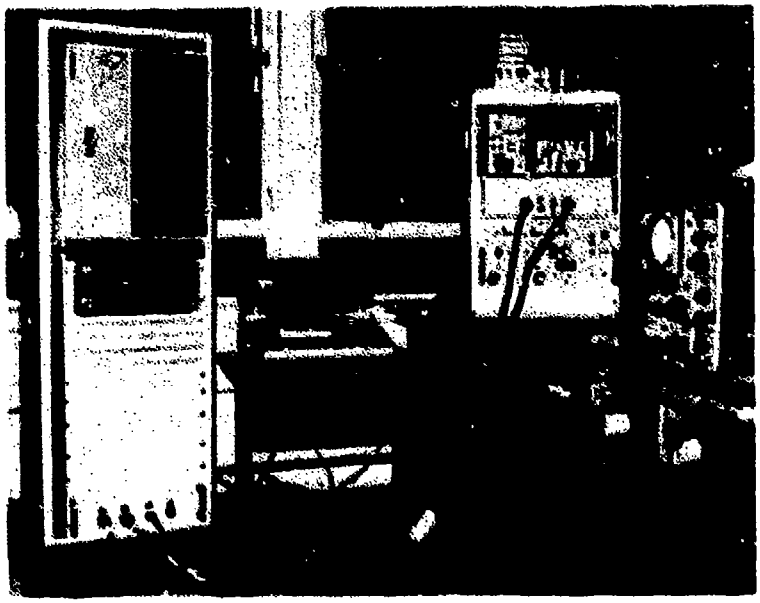

Figure 28

Dynamic tests configuration

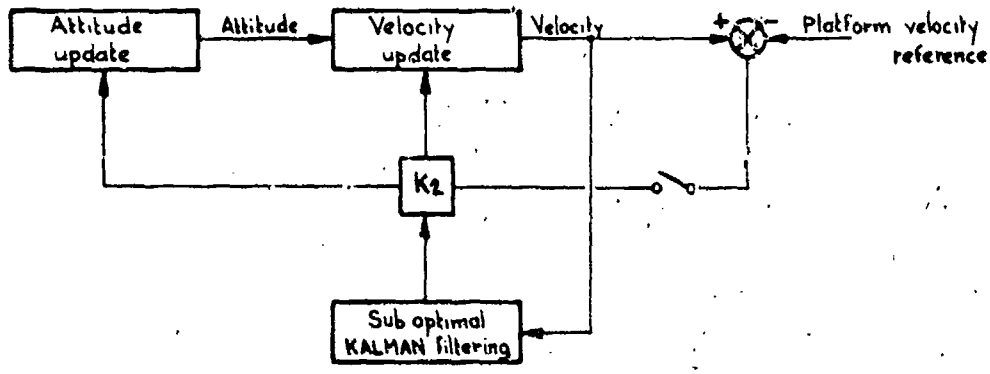

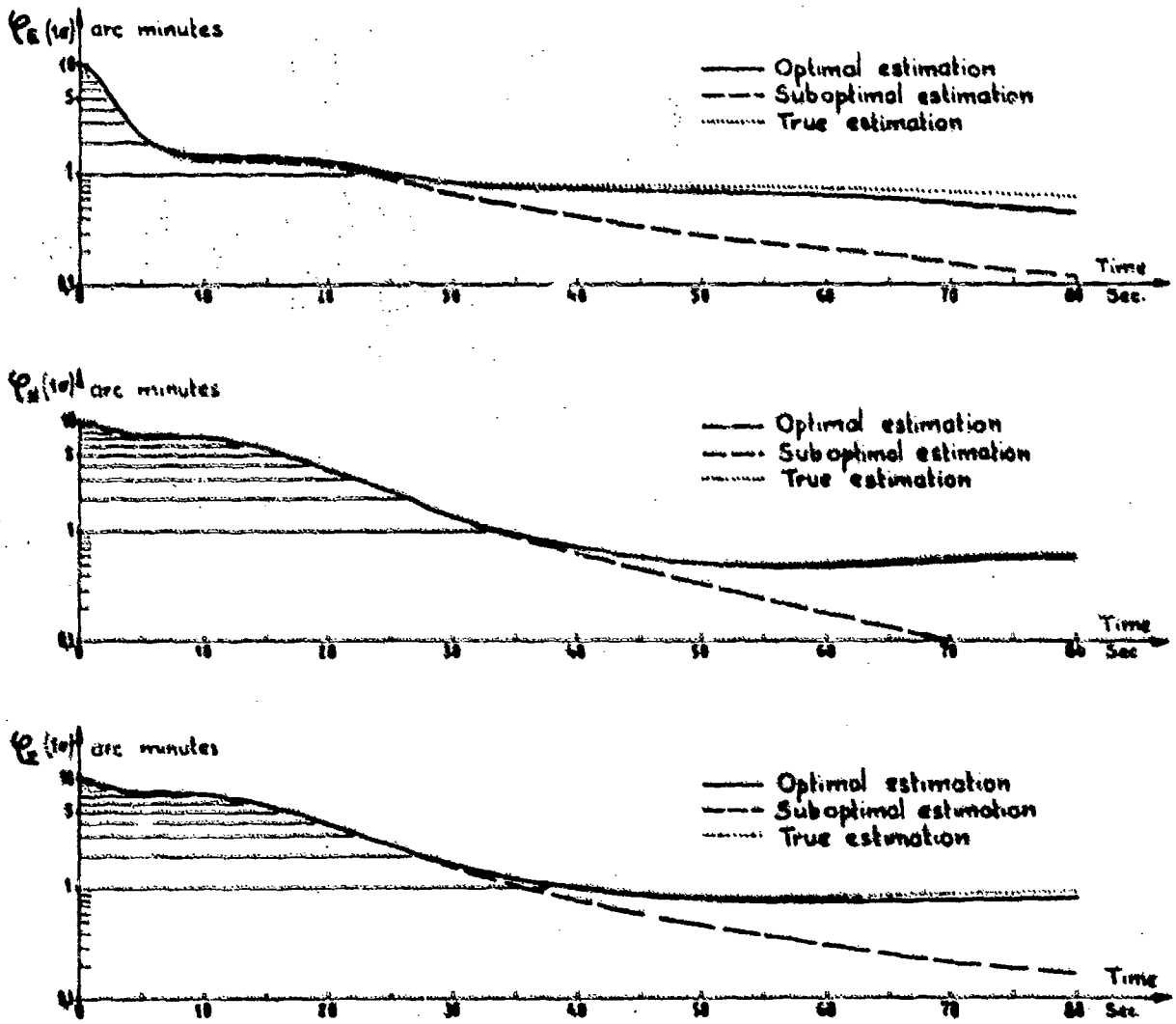

_ Figure 29 _

Alignment simulation

SELECTIVE BIBLIOGRAPHY

The bibliography which follows has been prepared by the AGARD Technical Information Panel and is a compilation of references selected specially to suit this particular Lecture Series: it is not intended to be comprehensive. It is regretted that AGARD cannot undertake to provide copies of the documents listed. These should be sought from the organizations which published them.

PART 1

NASA-CR-151013 DN-D0410-007 76/03/24 76N33276
A DETAILED DESCRIPTION OF THE SEQUENTIAL PROBABILITY RATIO TEST FOR 2-IMU FDI
Rich, T.M.
McDonnell Douglas Technical Services Co., Inc., Houston, Tex. (Astronautics Div.)

The sequential probability ratio test (SPRT) for 2-IMU FDI (Inertial Measuring Unit Failure Detection/Isolation) is described. The SPRT is a statistical technique for detecting and isolating soft IMU failures originally developed for the strapdown inertial reference unit. The flowchart of a subroutine incorporating the 2-IMU SPRT is included. ABA author.

RAE-TR-71241 BR28129 71/12/00 73N27571
A STAR-POINTING ATTITUDE CONTROL SYSTEM FOR SKYLARK
Abbott, J.K.
Royal Aircraft Establishment, Farnborough (England).

A three-axis star-pointing attitude control system was developed for the Skylark sounding rocket. The system uses a simple strap-down inertial system to carry out precision maneuvers to locate the target star, starting from an initial moon-pointing orientation. The star sensor is capable of providing adequate error information for stars down to visual magnitude 5. ABA author.

NASA-CR-67459 REPT-1726-FR2 64/12/30 76N70963
A STUDY PROGRAM ON A STRAPDOWN MINIATURE ELECTROSTATIC GYRO
Honeywell, Inc., Minneapolis, Minn.

AD-A039338 76/12/00 77N30156
A KALMAN FILTER APPLICATION TO THE ADVANCED TACTICAL INERTIAL GUIDANCE SYSTEM OF THE AIR-LAUNCHED LOW VOLUME RAMJET CRUISE MISSILE
Vandevender, J.A.
Naval Postgraduate School, Monterey, Calif.

A Montecarlo simulation is conducted to ascertain performance of the ATIGS system which is a proposed air-launched cruise missile configuration. The simulation is conducted within a local-level inertial frame consisting of down-range, cross-range, and up as primary reference vectors. Efforts are made to measure the relative effects associated with the intended pure position reset provided by a Micrad sensor as compared with those effects which could be expected from a linear suboptimal Kalman filtering scheme used in conjunction with the Micrad sensor. ABA author (GRA).

NASA-CR-144998 TRW-22817-6002-RU-00-VOL-1 76/03/31 76N28263
ADVANCED APPLICATION FLIGHT EXPERIMENTS PRECISION ATTITUDE DETERMINATION SYSTEM. VOLUME 1 - STRAPDOWN STAR TRACKER DEVELOPMENT
TRW Systems Group, Redondo Beach, Calif.

A strapdown star tracker is described which utilizes an image dissector tube in the photon counting mode. Stars as dim as +10 M_v can be tracked with the 60 sq cm aperture of this device. This makes the 1 deg by 1 deg field of view practical without a decrease in star availability. A unique pulse processing circuitry is utilized which, combined with the photon counting technique, allows star magnitudes from +10 M_v to 0 M_v to be acquired and tracked without changing electronic circuitry or scaling. Position variation with star intensity is less than 2 arc seconds from +10 M_v to 2.5 M_v. The electronic design consists mostly of digital circuits; the search and track electronics are completely digital. The optical-mechanical structure is fabricated from graphite/epoxy composite material, and the optics were fabricated from cervit. Both of these materials improve the thermal stability of the electro-optical boresight. Testing of the tracker was completely automated and used a collimated star source. ABA author.

NASA-CR-144999 TRW-22817-6002-RU-00-VOL-2 76/03/31 76N28264
ADVANCED APPLICATION FLIGHT EXPERIMENTS PRECISION ATTITUDE DETERMINATION SYSTEM. VOLUME 2 SYSTEM TESTS
TRW Systems Group, Redondo Beach, Calif.

The performance capability of each of two precision attitude determination systems (PADS), one using a strapdown star tracker, and the other using a single-axis gimbal star tracker was measured in the laboratory under simulated orbit conditions. The primary focus of the evaluation was on the contribution to the total system accuracy by the star trackers, and the effectiveness of the software algorithms in functioning with actual sensor signals. A brief description of PADS, the laboratory test configuration and the test facility, is given along with a discussion of the data handling and display, laboratory computer programs, PADS performance evaluation programs, and the strapdown and gimbal system tests. Results are presented and discussed. ABA author.

NASA-Case-ARC-10716-1 US-Patent-4,012,018; US-Patent-Appl-SN-403695; US-Patent-Class-244-165; US-Patent-Class-235-150.2; US-Patent-Class-235-150.25; US-Patent-Class-244-3.21; US-Patent-Class-244-171
77/03/15 77N20399
ALL SKY POINTING ATTITUDE CONTROL SYSTEM
Lorell, K.R.; Murphy, J.P.
National Aeronautics and Space Administration. Ames Research Center, Moffett Field, Calif.

In a strapped-down gyroscope space vehicle attitude control system, a method and appartus are provided for gyro drift and input axis misalignment error compensation employing a sun and a star tracker and preselected vehicle calibration maneuvers. The outputs of two-axis strapped-down gyroscopes nominally aligned with the optical axis of the sun and star trackers are measured to provide gyro drift calibration, roll, pitch and yaw axis scale factors and values corresponding to the degree of nonorthogonality between the roll axis and the pitch and yaw gyro input axes and the nonorthogonality of the roll and pitch axes relative to the yaw axis. The vehicle is then rolled and yawed through precomputed angles as modified by the calibrated data stored in a digital computer, and acquires a target without recourse to external references. ABA Offical Gazette of the US Patent Office.

NASA-CR-140313 T-569 72/02/00 75N10042
AN ADAPTIVE TECHNIQUE FOR A REDUNDANT-SENSOR NAVIGATION SYSTEM
Chien, T.T.
Draper (Charles Stark) Lab., Inc., Cambridge, Mass.

An on-line adaptive technique is developed to provide a self-contained redundant-sensor navigation system with a capability to utilize its full potentiality in reliability and performance. The gyro navigation system is modeled as a Gauss-Markov process, with degradation modes defined as changes in characteristics specified by parameters associated with the model. The adaptive system is formulated as a multistage stochastic process -- (1) a detection system, (2) an identification system and (3) a compensation system. It is shown that the sufficient statistics for the partially observable process in the detection and identification system is the posterior measure of the state of degradation, conditioned on the measurement history. ABA author.

76/08/00 76N32176
AN OPTIMALLY INTEGRATED PROJECTED MAP NAVIGATION SYSTEM
Reid, D.B.; Harman, R.K.; Frame, D.J.
Computing Devices of Canada, Ltd., Ottawa (Ontario). In AGARD Medium Accuracy Low Cost Navigation 31 P (see N76-32148 23-04)

A unique integrated tactical navigation system (ITNS) concept for helicopter applications is described. This concept, which could be extended for application in high performance tactical aircraft, is based on the projected map system, PMS 5-6, currently in production. The primary navigation unit of the ITNS is the Doppler dead reckoning (DR) subsystem which uses simple directional and vertical gyros as heading and attitude sensors. Auxiliary navigation data are supplied by a projected map display (PMD) and a triad of magnetometers strapped to the airframe. The PMD displays aircraft position, track and bearing to destination pictorially, providing excellent pilot orientation and position fixing capability. The magnetic sensor measures three components of the earth's field, from which additional heading and attitude information are derived. A digital Kalman filtering algorithm is implemented to estimate system errors from DR, PMD and strapdown magnetic data. The error estimates are fed back to correct DR position and null sensor errors, resulting in a fully integrated system which provides excellent performance at low cost. Simulation results indicate that system accuracy without position fixes will be better than 2 per cent of distance travelled (95 per cent confidence). ABA author.

NASA-CR-124126 TR-147-2 70/06/30 73N19641
ANALYSIS OF STRAPDOWN SENSOR TESTING
Crawford, B.S.
Analytic Sciences Corp., Reading, Mass.

Some topics related to dynamic testing of strapdown sensors are analyzed, with emphasis on measuring parameters which give rise to motion-induced error torques in single-degree-of-freedom inertial sensors. The objective is to determine the dynamic inputs, test equipment characteristics and data processing procedures best suited for measuring these parameters. Single axis, low frequency vibration tests and constant rate tests are studied in detail. Methods for analyzing the effects of test motion errors and measurement errors are developed and illustrated by examples. Candidate test data processing methods are compared and recommendations concerning test equipment and data processing are made. ABA author.

NASA-CR144219 IBM-76-227-002 76/03/02 76N20181
ANALYSIS OF TEST DATA ON THE SIMPLEX STRAPDOWN NAVIGATION SYSTEM
International Business Machines Corp., Huntsville, Ala. (Federal Systems Div.)

The results of a study of test data taken on the simplex strapdown navigation system were presented. That system consisted of the following components: strapdown platform, altimeter, digital computer, tape recorder, typewriter, and power source. The objective of these tests was to isolate error sources which may cause degradation of the system's

accuracy and to recommend appropriate changes to the system test procedures or computer software. The following recommendations were made: (1) addition of a gyro compassing alignment program into the navigation program, (2) addition of line drivers at the signal processor end of the transmission line, (3) need for extensive laboratory testing to determine sensor misalignements, biases, and scale factors, (4) need to stabilize the power source to prevent transients during power transfer, (5) need to isolate and eliminate the source of the large noise inputs. ABA Y.J.A.

AD-A008649 REPT-3811-FR1 SAMSO-TR-74-221 75/03/01 75N30143
AUTONOMOUS NAVIGATION TECHNOLOGY. PHASE 1A – STUDY
Paulson, D.C.
Honeywell, Inc., St Petersburg, Fla. (Aerospace Div.)

The program objective has been to provide the design of a space navigation system for unmanned earth satellites. The system is required to provide accurate determination of the ephemeris state and to be autonomous. The equations of motion of the satellite are integrated using a detailed model of the earth's gravitational field. The effects of residual errors in the gravity field, unmodeled forces, and uncertainties in initial conditions are reduced by measurements. The selected approach employs two down sensors to track unidentified earth landmarks surface; this unknown tracking method obtains to line of sight angular velocity (V/H). The phase I objective was to design and test an engineering model down sensor, a strapdown telescope. The measurement is obtained by digital correlation of signals from photodetector arrays in its image plane. ABA GRA.

NASA-CR-124234 TRW-18313-6004-RU-00 73/04/00 73N22608
COMPETITIVE EVALUATION OF FAILURE DETECTION ALGORITHMS FOR STRAPDOWN REDUNDANT INERTIAL INSTRUMENTS
Wilcox, J.C.
TRW Systems Group, Redondo Beach, Calif.

Algorithms for failure detection, isolation, and correction of redundant inertial instruments in the strapdown dodecahedron configuration are competitively evaluated in a digital computer simulation that subjects them to identical environments. Their performance is compared in terms of orientation and inertial velocity errors and in terms of missed and false alarms. The algorithms appear in the simulation program in modular form, so that they may be readily extracted for use elsewhere. The simulation program and its inputs and outputs are described. The algorithms, along with an eight algorithm that was not simulated, also compared analytically to show the relationships along them. ABA author.

AD-A034278 GE/EE/76D-23 76/12/00 77N24095
COVARIANCE ANALYSIS OF KALMAN FILTERS PROPOSED FOR A RADIOMETRIC AREA CORRELATOR/ INERTIAL NAVIGATION GUIDANCE SYSTEM
Fitschen, C.K.
Air Force Inst. of Tech., Wright-Patterson AFB, Ohio. (School of Engineering.)

In this report, a covariance analysis is performed on two Kalman filters proposed for use in a weapon system utilizing a strapdown inertial navigation system (INS), updated by position data from a radiometric area correlator (RAC), for guidance. Filter performance is analyzed when primary navigation information is provided by Sperry INS, which uses laser gyroscopes, and when an INS employing conventional dry-tuned gyroscopes, manufactured by Hamilton-Standard, is incorporated into the weapon system. For the covariance analysis, truth models in the form of linear state equations are presented which reflect the best description of the weapon system when either the Sperry or Hamilton-Standard INS is used. The Sperry system model is composed of 46 states and the Hamilton-Standard system model 61 states. Primary emphasis in this investigation is placed on minimizing system terminal navigation error. ABA GRA.

NASA-CR-144085 TR-EE/EL-1 74/08/01 76N13197
DESIGN OF A TORQUE CURRENT GENERATOR FOR STRAPDOWN GYROSCOPES
McKnight, R.D.; Blalock, T.V.; Kennedy, E.J.
Tennessee Univ., Knoxville. (Dept. of Electrical Engineering.)

The design, analysis, and experimental evaluation of an optimum performance torque current generator for use with strapdown gyroscopes, is presented. Among the criteria used to evaluate the design were the following: (1) steady-state accuracy; (2) margins of stability against self-oscillation; (3) temperature variations; (4) aging; (5) static errors drift errors, and transient errors, (6) classical frequency and time domain characteristics; and (7) the equivalent noise at the input of the comparater operational amplifier. The dc feedback loop of the torque current generator was approximated as a second-order system. Stability calculations for gain margins are discussed. Circuit diagrams are shown and block diagrams showing the implementation of the torque current generator are discussed. ABA author.

74/00/00 75N21583
DESIGN OF A TORQUE CURRENT GENERATOR FOR STRAPDOWN GYROSCOPES
McKnight, R.D.
Tennessee Technological Univ., Cookeville.

The design, analysis, and evaluation is discussed of an optimum performance torque current generator for use with strapdown gyroscopes. The criteria used to evaluate the design were: steady-state accuracy; margins of stability against self-oscillation, temperature variations, aging, etc.; static and drift errors; PVR errors; transient errors; classical

frequency and time domain characteristics; and the equivalent noise at the input of the comparator operational amplifier. ABA dissert. abstr.

B-H

NASA-CR-123513 TRW-18313-6003-RO-00 71/12/29 73N17711
DETAILED TEST PLAN REDUNDANT SENSOR STRAPDOWN IMU EVALUATION PROGRAM
Hartwell, T.; Miyatake, Y.; Wedekind, D.E.
TRW Systems Group, Redondo Beach, Calif.

The test plan for a redundant sensor strapdown inertial measuring unit evaluation program is presented. The subjects discussed are: (1) test philosophy and limitations, (2) test sequence, (3) equipment specifications, (4) general operating procedures, (5) calibration procedures, (6) alignment test phase, and (7) navigation test phase. The data and analysis requirements are analyzed. ABA author.

NASA-CR-124333 S-25 73/07/13 73N28649
DEVELOPMENT OF A WIDTH-MODULATED PULSE REBALANCE ELECTRONICS LOOP FOR STRAPDOWN GYROSCOPES
Blalock, T.V.; Kennedy, E.J.; McKnight, R.D.
Tennessee Univ., Knoxville. (Dept. of Electrical Engineering.)

A new width modulated pulse rebalance electronics loop was developed for use with strapdown gyroscopes. Advantages of the width modulated binary over the ternary loop are the following: (1) the H-switch is easier to implement; (2) torque is applied in finely quantized increments; (3) the analog-to-digital conversion for data generation is inside the loop and is directly determined by the torque pulse; (4) on part of the loop compensation network bypasses the gyroscope; and (5) the torquer is fed constant power. ABA author.

AD-A014505 GRR-005-0675 75/04/00 76N15869
DEVELOPMENT OF AN OPTICAL RATE SENSOR
Skripka, J.L.; Fredricks, R.J.
Lear Siegler, Inc., Grand Rapids, Mich. (Instrument Div.)

This report documents the results of a feasibility investigation program of optical rate sensing by a unique technique of differential phase shift measurement between counter-traveling light beams forming a closed path. The program involved the design, build, and test of a discrete component research test model of the sensor, and an investigation of the applicability of integrated optics technology to such a sensor. Such a sensor possesses many of the attributes of the ring laser gyro without the problem of frequency lock-in which is characteristic of that device. It also offers the potential advantage of size reduction without performance degradation through the use of multiple turns of fiber optics for an effective area increase and replacement of the gas laser with a solid state source. The purpose of the program was to evaluate a complete sensor using the research test model and to determine how well integrated optics can be applied to the optical rate sensor. The results indicate that fiber optics and the solid state laser can be used to overcome problems encountered in the discrete component model and to achieve performance in the one-half to ten degree per hour bias stability range in a sensor configured for a maximum rate of 400 degrees/second. An optical rate sensor using only integrated optics components, although promising, requires further research developments in the field of integrated optics. ABA author (GRA).

75/05/00 75N30076
DEVELOPMENTAL MICRON LABORATORY TEST RESULTS
Warzynski, R.R.; Radic, G.C.
Air Force Avionics Lab., Wright-Patterson AFB, Ohio. In AGARD – The Guidance and Control of V/STOL Aircraft and Helicopter at Night and in Poor Visibility 3 P (see N75-30052 21-01)

A moderately accurate, low cost of ownership inertial navigator system, called micro-navigator (micron) was developed which will satisfy a wide range of applications including V/STOL aircraft and helicopters. The gyroscope for micron is an electrostatic gyro (ESG) operated in a strapdown mechanization. The gyro's performance in a developmental micron system, designated the N57A-1, was verified. The N57A-1 was subjected to heading sensitivity, repeatability, Scorsby, shock, vibration, angular rates, cold soak, and mobile tests; over 70 navigation runs were conducted. The N57A-1 demonstrated performance better than the goals of 1 nm/hr and 5 ft/sec for all tests. ABA author.

NASA-CR-124161 TR-147-5 72/09/00 73N20682
DYNAMIC ERRORS IN A TUNED FLEXURE-MOUNTED STRAPDOWN GYRO
Bortz, J.E., Sr
Analytic Sciences Corp., Reading, Mass.

Motion induced errors in a tuned, flexure-mounted strapdown gyro are investigated. Analytic expressions are developed for errors induced by linear vibrations, angular motion, and detuning. Sensor-level errors (gyro drift rate) and system-level errors (navigation errors) that are stimulated by an actual dynamic motion environment are computed. ABA author.

NASA-CR-140296 E-2525 70/08/00 74N78010
DYNAMIC TESTING OF SINGLE DEGREE-OF-FREEDOM STRAPDOWN GYROSCOPE
Feldman, J.
Massachusetts Inst. of Tech., Cambridge. (Charles Stark Draper Lab.) Presented at the 5th Biennial Guidance Test Symp., Holloman AFB, N. Mex., 14–16 October 1970.

73/02/00 73N20697
DYNAMICALLY TUNED GYROS IN STRAPDOWN SYSTEMS
Craig, R.J.G.
Teledyne Systems Co., Northridge, Calif. In AGARD Inertial Navigation Components and Systems 26 P (see N73-20684 11-21)

A review is presented of the basic principles of operation of the dynamically tuned instrument and shows a gyro configuration designed for the strapdown use. Characteristic errors in a multigimbal design are discussed and the basic error models for the gyro, together with its dynamic characteristics, are presented. ABA author.

NAL-TR-302 72/00/00 73N24652
ESTIMATION OF GUIDANCE ERRORS BY KALMAN-BUCY FILTERING TECHNIQUE
Murata, M.
National Aerospace Lab., Tokyo (Japan).

The application is described of Kalman-Bucy filter theory to postflight guidance error analysis. Trajectory reconstruction and the estimation of guidance hardware errors and radar system errors are emphasized, such as accelerometer bias, gyro drift rate, radar location uncertainty and the like, by processing both guidance telemetered and radar tracking data. The filtering technique is developed in full detail for a launch vehicle with a strapdown inertial navigation system. Digital simulations are also presented. The results demonstrate that the approach is very promising for postflight guidance-trajectory analysis. ABA author.

NASA-CR120427 R-826-VOL-1 74/07/00 74N32099
EVALUATION OF SELECTED STRAPDOWN INERTIAL INSTRUMENTS AND PULSE TORQUE LOOPS, VOLUME I
Sinkiewicz, J.S.; Feldman, J.; Lory, C.B.
Draper (Charles Stark) Lab., Inc., Cambridge, Mass.

Design, operational and performance variations between ternary, binary and forced-binary pulse torque loops are presented. A fill-in binary loop which combines the constant power advantage of binary with the low sampling error of ternary is also discussed. The effects of different output-axis supports on the performance of a single-degree-of-freedom, floated gyroscope under a strapdown environment are illustrated. Three types of output-axis supports are discussed: pivot-dithered jewel, ball bearing and electromagnetic. A test evaluation on a Kearfott 2544 single-degree-of-freedom, strapdown gyroscope operating with a pulse torque loop, under constant rates and angular oscillatory inputs is described and the results presented. Contributions of the gyroscope's torque generator and the torque-to-balance electronics on scale factor variation with rate are illustrated for a SDF 18 IRIG Mod-B strapdown gyroscope operating with various pulse rebalance loops. Also discussed are methods of reducing this scale factor variation with rate by adjusting the tuning network which shunts the torque coil. A simplified analysis illustrating the principles of operation of the teledyne two-degree-of-freedom, elastically-supported, tuned gyroscope and the results of a static and constant rate test evaluation of that instrument are presented. ABA author.

NASA-CR-137730 76/00/00 76N16061
FAILURE DETECTION AND ISOLATION INVESTIGATION FOR STRAPDOWN SKEW REDUNDANT TETRAD LASER GYRO INERTIAL SENSOR ARRAYS
Eberlein, A.J.; Lahm, T.G.
Honeywell, Inc., Minneapolis, Minn. (Government and Aeronautical Products Div.)

The degree to which flight-critical failures in a strapdown laser gyro tetrad sensor assembly can be isolated in short-haul aircraft after a failure occurrence has been detected by the skewed sensor failure-detection voting logic is investigated along with the degree to which a failure in the tetrad computer can be detected and isolated at the computer level, assuming a dual-redundant computer configuration. The tetrad system was mechanized with two two-axis inertial navigation channels (INCS), each containing two gyro/accelerometer axes, computer, control circuitry, and input/output circuitry. Gyro/accelerometer data is crossfed between the two INCS to enable each computer to independently perform the navigation task. Computer calculations are synchronized between the computers so that calculated quantitites are identical and may be compared. Fail-safe performance (identification of the first failure) is accomplished with a probability approaching 100 percent of the time, while fail-operational performance (identification and isolation of the first failure) is achieved 93 to 96 percent of the time. ABA author.

B-6

NASA-CR-144089 SR-S-28 74/05/31 76N13374
FEASIBILITY STUDY OF A DIGITAL REBALANCE LOOP FOR A DRY TUNED TDF GYRO
Coffman, D.E.
Tennessee Univ., Knoxville. (Dept. of Electrical Engineering.)

A two degrees-of-freedom (TDF) rate integrating gyro in the strapdown mode is a candidate for attitude sensing in a spacecraft navigation system, since it provides an additional axis of information for a relatively small increase in hardware complexity. A type of gyro which has not been fully exploited is of the dry, tuned, TDF design, in which the spring constant of the suspension system is effectively cancelled by the dynamic antispring of a swiveling, rotating, gimbal. The use of this unconventional gyro in a digital rebalance loop was investigated. ABA author.

NASA-TM-73163 A-6924 77/06/00 77N26111
FLIGHT TEST RESULTS OF THE STRAPDOWN HEXAD INERTIAL REFERENCE UNIT (SIRU). VOLUME 1 – FLIGHT TEST SUMMARY
Hruby, R.J.; Bjorkman, W.S.
(Analytical Mechanics Assoc., Inc., Mountain View, Calif.) National Aeronautics and Space Administration. Ames Research Center, Moffett Field, Calif.

Flight test results of the strapdown inertial reference unit (SIRU) navigation system are presented. The fault-tolerant SIRU navigation system features a redundant inertial sensor unit and dual computers. System software provides for detection and isolation of inertial sensor failures and continued operation in the event of failures. Flight test results include assessments of the system's navigational performance and fault tolerance. ABA author.

NASA-CR-130722 TRW-18313-6002-RO-00 71/11/08 73N17712
GENERAL TEST PLAN REDUNDANT SENSORS STRAPDOWN IMU EVALUATION PROGRAM
Hartwell, T.; Irwin, H.A.; Miyatake, Y.; Wedekind, D.E.
TRW Systems Group, Redondo Beach, Calif.

The general test plan for a redundant sensor strapdown inertial measuring unit evaluation program is presented. The inertial unit contains six gyros and three orthogonal accelerometers. The software incorporates failure detection and correction logic and a land vehicle navigation program. The principal objective of the test is a demonstration of the practicability, reliability, and performance of the inertial measuring unit with failure detection and correction in operational enviroments. ABA author.

NASA-TM-X-2848 H-735 73/08/00 73N29713
GROUND AND FLIGHT EXPERIENCE WITH A STRAPDOWN INERTIAL MEASURING UNIT AND A GENERAL PURPOSE AIRBORNE DIGITAL COMPUTER
Wolf, T.D.; McCracken, R.C.
National Aeronautics and Space Administration. Flight Research Center, Edwards, Calif.

Ground and flight tests were conducted to investigate the problems associated with using a strapdown inertial flight data system. The objectives of this investigation were to develop a three axis inertial attitude reference system, to evaluate a self-alignment technique, and to examine the problem of time-sharing a general purpose computer for the several tasks required of it. The performance of the strapdown platform/computer system that was developed was sufficiently accurate for the tasks attempted. For flight on the order of 45 minutes duration, attitude angle errors of + or −.035 radian (+ or −2 deg) in all axes were observed. Laboratory tests of the self-alignment technique gave accuracies of + or −.00075 radian in pitch and roll axes and + or −0.0045 radian in the yaw axis. Self-alignment flight results were inconsistent, since a stable solution was not obtained on windy days because of aircraft rocking motions. ABA author.

AD-A022324 Honeywell-17512865 SAMSO-TR-43 74/12/00 77N73657
HIGH ALTITUDE ATTITUDE REFERENCE STUDY
Kert, M.; Boutelle, J.O.
Honeywell, Inc., St Petersburg, Fla. (Aerosapce Div.)

NASA-CR-144086 TR-EE/EL-2 74/09/23 76N13375
HIGH-RESOLUTION WIDTH-MODULATED PULSE REBALANCE ELECTRONICS FOR STRAPDOWN GYROSCOPES AND ACCELEROMETERS
Kennedy, E.J.; Blalock, T.V.; Bryan, W.L.; Rush, K.
Tennessee Univ., Knoxville. (Dept. of Electrical Engineering.)

Three different rebalance electronic loops were designed, implemented, and evaluated. The loops were width-modulated binary types using a 614.4 kHz keying signal; they were developed to accommodate the following three inertial sensors with the indicated resolution values: (1) Kearfott 2412 accelerometer – resolution = 260 micro-G/data pulse, (2) Honeywell GG334 gyroscope – resolution = 3.9 milli-ARC-sec/data pulse, (3) Kearfott 2401-009 accelerometer – resolution = 144 milli-G/data pulse. Design theory, details of the design implementation, and experimental results for each loop are presented. ABA author.

CNES-NT-32 76/02/00 76N27324
INERTIAL NAVIGATION
Vanderlinden, C.
Centre National d'Etudes Spatiales, Toulouse (France).

Guidance, control, and navigation are discussed, using the launching of a satellite as a typical case. The principal possibilities for the realization of an inertial navigation (strapped down or gimballed platform) are explained. The functioning of the inertial platform system in particular is described by considering the method of platform stabilization, the principle of operation of the integrating rate gyroscope, the measurement of acceleration, and the alignment process of the instrument cluster with particular reference to the method of gyro compassing. ABA author (ESA).

AGARD-CP-116 73/02/00 73N20684
INERTIAL NAVIGATION COMPONENTS AND SYSTEM
Advisory Group for Aerospace Research and Development, Paris (France).
Presented at the 15th Meeting of the Guidance and Control Panel of AGARD, Florence, 2–5 October 1972.

76/00/00 77N14160
INERTIAL UNITS FOR ATTITUDE CONTROL OF PROBE ROCKETS
Monier, M.G.
Societe d'Application Generales d'Electricite et de Mechanique, Paris (France).
In ESA European programmes on sounding-rocket and balloqn res. in the auroral zone P 513-524 (see N77-14120 05-12)

A Cassiopee attitude control system used for the payload of Faust astronomical rockets is described. It is a typical example of inertial system utilization on probe rockets. The Cassiopee system includes a gimballed type, inertial attitude reference unit and a strapped down type fine inertial sensor used to provide stabilization around a fixed direction. In both these units, the inertial sensor is a SAGEM F type ingrating gyro. The flight tests carried out in 1974 and 1975 were successful. The equipment which, from 1977 onwards, will replace the Cassiopee inertial elements, will be highly miniaturized. ABA author (ESA).

NLR-TR-76039-U 76/01/14 77N21411
INVESTIGATION OF A CROSS-COUPLING DRIFT COMPENSATION METHOD ON A SINGLE AXIS GYRO STABILIZED PLATFORM
Bosgra, J.A.; Mooy, A.J.; Smilde, H.
National Aerospace Lab., Amsterdam (Netherlands). (Space Flight Div.)

The rectification drift phenomenon in a semi-strapdown system mechanized as a single axis platform (SAP), and a method to compensate for it, were investigated both theoretically and experimentally. In a hardware test setup, using an experimental SAP composed of surplus parts from the former Eldo-A program, the theoretical result as well as a proposed method of compensation was verified. ABA author (ESA).

NASA-CR-132419 74/04/00 74N21289
INVESTIGATION OF APPLICATION OF TWO-DEGREE-OF-FREEDOM DRY TUNED-GIMBAL GYROSCOPES TO STRAPDOWN NAVIGATION SYSTEMS
Teledyne Systems Co., Northridge, Calif.

The work is described which was accomplished during the investigation of the application of dry-tuned gimbal gyroscopes to strapdown navigation systems. A conventional strapdown configuration, employing analog electronics in conjunction with digital attitude and navigation computation, was examined using various levels of redundancy and both orthogonal and nonorthogonal sensor orientations. It is concluded that the cost and reliability performance constraints which had been established could not be met simultaneously with such a system. This conclusion led to the examination of an alternative system configuration which utilizes an essentially new strapdown system concept. This system employs all-digital signal processing in conjunction with the newly-developed large scale integration (LSI) electronic packaging techniques and a new two-degree-of-freedom dry tuned-gimbal instrument which is capable of providing both angular rate and acceleration information. Such a system is capable of exceeding the established performance goals. ABA author.

AD-784907 AFOSR-74-136TR 74/06/30 75N77920
INVESTIGATION OF STRAPDOWN REFERENCE SYSTEMS
Bowles, W.M.
Oklahoma State Univ., Stillwater. (School of Mechanical and Aerospace Engineering.)

AD-A009231 NADC-75030-60 75/04/04 75N76484
LABORATORY INVESTIGATION OF THE SUNDSTRAND Q-FLEX ACCELEROMETER
Sapp, W.F.
Naval Air Development Center, Warminster, Pa. (Naval Navigation Lab.)

FOA-C-20055-E4 75/08/00 77N81671
MEASUREMENTS ON THE EXPERIMENTAL SYSTEM IN THE PROJECT: BODY-FIXED (STRAPPED-DOWN) NAVIGATION
Lekzen, L.; Olseon, K.E.
Research Inst. of National Defence, Stockholm (Sweden).

AD-A021526 C74-455/201-VOL-1 AFAL-TR-75-210-Vol-1 76/02/00 77N12033
MICRO NAVIGATOR (MICRON) PHASE 2A. VOLUME 2 – TECHNICAL REPORT
Miller, J.M.
Rockwell International Corp., Anaheim, Calif. (Autonetics Group)

The micro navigator (Micron) is a low-cost highly reliable, and moderately accurate strapdown inertial navigator. The heart of the Micron system is the microelectrostatic gyro (MESG) an instrument which incorporates an all-attitude, whole-angle readout from an electrostatically suspended rotor. Under previous Air Force contracts two developmental navigation systems (N57A-1 and N57A-2) were developed. The objective of the Micron phase 2A contract was to test N57A-1 and N57A-2; to design, fabricate and integrate two gyro subassemblies and one gyro test station; to test gyros and gyro sub-assemblies; and to perform analyses, studies and trade-offs for use in defining the Micron system. Both N57A systems were flight tested and the capability of the system to meet the position accuracy requirement was demonstrated. N57A-1 was used to demonstrate in-motion Polhode damping. System reliability screen, Scorsby and heading sensitivity tests were successfully conducted on N57A-2. ABA GRA.

76/08/00 76N32154
MICRO-NAVIGATOR (MICRON)
Schwarz, J.A.
Rockwell International Corp., Anaheim, Calif.
In AGARD Medium Accuracy Low Cost Navigation 14 P (see N76-32148 23-04)

The Micron strapdown inertial navigation system, developed to be a low cost medium accuracy (one nautical mile per hour radial position error CEP rate) navigation system for future aircraft/missiles requiring medium accuracy, was described. The heart of the Micron system is the micro-electrostatic gyro, which consists of a one centimeter diameter spherical rotor suspended electrostatically by eight capacitor plates. The rotor is untorqued, thus avoiding the accuracy degradation and reliability degradation from gyro torquing electronics. The gyro is used in a strapdown mechanization and utilizes a unique mass-unbalance modulation technique for obtaining whole angle readout over all attitude angles. Two brassboard Micron systems have been fabricated and tested. The test results indicate better performance than the one nautical mile/hr performance goal under all environments tested (laboratory, vibration, shock, cold soak, Scorsby, van and flight test). The prototype Micron system is currently being designed, and a full evaluation test program is planned. ABA author.

74/00/00 74N28096
ON-LINE ESTIMATION OF PARAMETERS USING EXPERIMENTALLY DEVELOPED GYRO MODELS, AND OTHER APPLICATIONS
Coffman, V.D.
Stanford Univ., Calif.

Strapdown attitude reference systems with body fixed attitude sensors rely on gyros to maintain the reference between attitude measurements. In the past, gyro drift rate was compensated in inertial navigators but scaling errors were of only minor importance. However, for maneuvering vehicles, both the gyro scale factor and drift must be compensated. This research is an investigation of performance that could reasonably be expected from gyro hardware after compensating both multiplicative (gyro scale factor) and additive (gyro drift) error sources. A major part of the effort was devoted to acquiring test data on six gyros and developing models to fit these data. An estimator was developed that will determine the gyro model parameters on-line. This formulation for the filter equations employs direct utilization of measurements. ABA dissert. abstr.

AD-751654 72/06/00 73N16633
OPTIMIZATION OF THE SHORT RANGE WEAPONS CONTROL SYSTEM
Allen, J.W.
Naval Postgraduate School, Monterey, Calif.

The report deals with the evaluation of the performance of a strapped down air-to-air tracker for the short range weapons control system. The system was designed, built, and evaluated at the Naval Weapons Center. The subsystems of the tracker which contributed to the problem areas discovered by flight tests are described. An evaluation of the short-comings of the tracking scan mode and the automatic gain control circuit is discussed and circuit modifications are proposed which include a collapsing square scan for target tracking and a variable width window discriminator.

AD-759561 TOR-1001(9990)-5 SAMSO-TR-73-183 66/09/20 73N73226
OPTIMUM REDUNDANT CONFIGURATIONS OF INERTIAL SENSORS
Ephgrave, J.T.
Aerospace Corp., El Segundo, Calif. (Technical Operations.)

NASA-CR-112206 73/03/00 73N20721
PERFORMANCE EVALUATION OF A STRAPDOWN ELECTRICALLY SUSPENDED GYRO FOR SPACE
Elwell, D.F.; Wacker, J.C.; Miletich, J.M.
Honeywell, Inc., St Petersburg, Fla. (Aerospace Div.)

B-9

The engineering development directed to improvement in strapdown electrically suspended gyro (SD/ESG) readout accuracy are described. The results of this development effort were represented by new and modified parts which were assembled into a strapdown ESG which was evaluated in terms of its readout system accuracy. The program performance goal was the demonstration of gyro readout to an accuracy of 15 arc-seconds or better. The results of calibrating over two sets of data were error amounts of 11.4 and 12.7 arc-seconds rms. The rms values of readout error were 12.7 and 13.8 arc-seconds for two sets of data not included in the calibration. The techniques for rotor preparation which were investigated under this contract included the application of a thin metal coating to the rotor surface in addition to the use of bare, polished beryllium rotors. Patterning application means which were utilized included a laser for pattern exposure of a photoresist coating and a grit-blast patterning machine which applied the pattern directly onto the metal surface of the rotor. ABA author.

NASA-CR-144220 IBM-76-227-003 76/03/02 76N20182
POSITION ERROR PROPAGATION IN THE SIMPLEX STRAPDOWN NAVIGATION SYSTEM
International Business Machines Corp., Huntsville, Ala. (Federal Systems Div.)

The results of an analysis of the effects of deterministic error sources on position error in the simplex strapdown navigation system were documented. Improving the long term accuracy of the system was addressed in two phases, understanding and controlling the error within the system, and defining methods of damping the net system error through the use of an external reference velocity or position. Review of the flight and ground data revealed error containing the Schuler frequency as well as non-repeatable trends. The only unbounded terms are those involving gyro bias and azimuth error coupled with velocity. All forms of Schuler-periodic position error were found to be sufficiently large to require update or damping capability unless the source coefficients can be limited to values less than those used in this analysis for misalignment and gyro and accelerometer bias. The first-order effects of the deteministic error sources were determined with a simple error propagator which provided plots of error time functions in response to various source error values. ABA author.

NASA-CR-145305 DOC-403314 76/10/00 77N21074
PRELIMINARY DESIGN OF A REDUNDANT STRAPPED DOWN INERTIAL NAVIGATION UNIT USING TWO-DEGREE-OF-FREEDOM TUNED-GIMBAL GYROSCOPES
Litton Systems, Inc., Woodland Hills, Calif.

This redundant strapdown INS preliminary design study demonstrates the practicality of a skewed sensor system configuration by means of: (1) devising a practical system mechanization utilizing proven strapdown instruments, (2) thoroughly analyzing the skewed sensor redundancy management concept to determine optimum geometry, data processing requirements, and realistic reliability estimates, and (3) implementing the redundant computers into a low-cost, maintainable configuration. ABA author.

73/02/00 73N20699
PROGRESS IN STRAPDOWN TECHNOLOGY
Hung, J.C.; Doane, G.B., III
(Tenn. Univ., Knoxville) National Aeronautics and Space Administration. Marshall Space Flight Center, Huntsville, Ala.
In AGARD Inertial Navigation Components and Systems 9 P (see N73-20684 11-21)

An overview is presented of typical inertial grade instrumentation available to mechanize precision strapdown attitude reference systems as well as a novel scheme of redundancy management, if two degree of freedom instruments are used. The instrumentation is divided between conventional and unconventional sensors with some assessment of their readiness included. ABA author.

NASA-CR-86198-(DEL) TRW-07398-6027-RO-00-(DEL) 68/11/00 74N70335
RADIO/OPTICAL/STRAPDOWN INERTIAL GUIDANCE STUDY FOR ADVANCED KICK STAGE APPLICATIONS. VOLUME 2 – DETAILED STUDY RESULTS (TASKS 3 AND 4). PART 2 – PRELIMINARY MODULAR DESIGN (DEL.)
TRW Systems Group, Redondo Beach, Calif.

NASA-CR-140328 E-2398 69/06/00 75N70026
REAL-TIME STRAPDOWN-ATTITUDE PACKAGE EVALUATIONS
Gilmore, J.P.; McKern, R.A.; Swanson, D.W.
Massachusetts Inst. of Tech., Cambridge. (Instrumentation Lab.)
Presented at AIAA Guidance, Control and Flight Mech. Conf., Princeton, N.J., August 1969.

B-12

NASA-CR-138838 HSER-6197 73/00/00 74N29116
RI 1170 ADVANCED STRAPDOWN GYRO
Hamilton Standard, Windsor Locks, Conn.

The major components of the RI 1170 gyroscope are described. A detailed functional description of the electronics including block diagrams and photographs of output waveshapes within the loop electronics are presented. An electronic data flow diagram is included. Those gyro subassemblies that were originally planned and subsequently changed or modified for one reason or another are discussed in detail. Variations to the original design included the capacitive pickoffs, torquer flexleads, magnetic suspension, gas bearings, electronic design, and packaging. The selection of components and changes from the original design and components selected are discussed. Device failures experienced throughout the program are reported and design corrections to eliminate the failure modes are noted. Major design deficiencies such as those of the MSE electronics are described in detail. Modifications made to the gas bearing parts and design improvements to the wheel are noted. Changes to the gas bearing prints are included as well as a mathematical analysis of the 1170 gas bearing wheel by computer analysis. The mean free-path effects on gas bearing performance is summarized. ABA author.

AD-A024977 RG-76-41 76/01/00 77N12102
SIMULATION MODELS AND BASELINE GUIDANCE AND CONTROL FOR INDIRECT-FIRE MISSILES WITH STRAPDOWN-INERTIAL GUIDANCE
Jordan, W.E.
Army Missile Research, Development and Engineering Lab., Redstone Arsenal, Ala.
(Guidance and Control Directorate.)

The simulation models and baseline guidance and control described in this report were developed to define performance requirements for the airframe, propulsion, guidance, autopilot, and control systems for strapdown-inertially guided indirect-fire missiles. A type of proportional navigation guidance using missile to target relative velocity and position is derived and has the property of being able to shape the missile trajectory for range extension and instrument error minimization. Typical inputs for inertial instruments and control system performance and sizing are obtained. ABA author (GRA).

SAND-76-0620 77/01/00 77N30104
SIMULATION OF INERTIAL INPUTS TO A STRAPDOWN PLATFORM FOR INERTIAL GREAT CIRCLE TRAJECTORIES
Perdreauville, F.J.
Sandia Labs., Albuquerque, N. Mex.

Equations are developed for computing inertial accelerations and angular rates that would be measured by the accelerometers and gyroscopes in a strapdown inertial platform. The accelerations and angular rates are computed for a body that is moving in an inertial great circle trajectory. A Fortran computer code which implements the calculations is listed. ABA ERA.

NASA-CR-147679 REPT-0872-11055-VOL-1 72/10/06 76N75141
SPACE SHUTTLE STRAPDOWN INERTIAL MEASURING UNIT PROGRAM ANALYSIS. VOLUME I - MANAGEMENT SUMMARY
Honeywell, Inc., St Petersburg, Fla. (Aerospace Div.)

NASA-CR-147680 REPT-0872-11055-VOL-2 72/10/06 76N75142
SPACE SHUTTLE STRAPDOWN INERTIAL MEASURING UNIT PROGRAM ANALYSIS. VOLUME 2 - TECHNICAL
Honeywell, Inc., St Petersburg, Fla.

75/00/00 76N19221
SPACEFLIGHT TECHNOLOGY AT NLR
National Aerospace Lab., Amsterdam (Netherlands).

The inertial guidance system testing facilities built for the Eldo Europa 2 launch vehicle are described. Strapdown inertial systems and double gimballed momentum wheels for attitude control of spacecraft were developed. Mission analysis studies for ESRO satellites were performed. The astronomical Netherlands satellite is controlled by an NLR operations team. Studies for ESRO Helos (EXOSAT) satellite experiments and ESRO spacelab user requirements were also performed. ABA ESA.

NASA-CR-120428 R-826-VOL-2 74/07/00 74N32100
STANDARDIZED STRAPDOWN INERTIAL COMPONENT MODULARITY STUDY, VOLUME 2
Feldman, J.
Draper (Charles Stark) Lab., Inc., Cambridge, Mass.

To obtain cost effective strapdown navigation, guidance and stabilization systems to meet anticipated future needs a standardized modularized strapdown system concept is proposed. Three performance classes, high, medium and low,

are suggested to meet the range of applications. Candidate inertial instruments are selected and analyzed for interface compatibility. Electronic packaging and processing, materials and thermal considerations applying to the three classes are discussed and recommendations advanced. Opportunities from automatic fault detection and redundancy are presented. The smallest gyro and accelerometer modules are projected as requiring a volume of 26 cubic inches and 23.6 cubic inches, respectively. Corresponding power dissipation is projected as 5 watts, and 2.6 watts respectively. ABA author.

B-11

NASA-CR-137585 75/00/00 75/N17328
STRAPDOWN COST TREND STUDY AND FORECAST
Eberlein, A.J.; Savage, P.G.
Honeywell, Inc., Minneapolis, Minn. (Government and Aeronautical Products Div.)

The potential cost advantages offered by advanced strapdown inertial technology in future commercial short-haul aircraft are summarized. The initial procurement cost and six year cost-of-ownership, which includes spares and direct maintenance cost were calculated for kinematic and inertial navigation systems such that traditional and strapdown mechanization costs could be compared. Cost results for the inertial navigation systems showed that initial costs and the cost of ownership for traditional triple redundant gimbaled inertial navigators are three times the cost of the equivalent skewed redundant strapdown inertial navigator. The net cost advantage for the strapdown kinematic system is directly attributable to the reduction in sensor count for strapdown. The strapdown kinematic system has the added advantage of providing a fail-operational inertial navigation capability for no additional cost due to the use of inertial grade sensors and attitude reference computers. ABA author.

NASA-CR-150458 77/10/00 78N11368
STRAPDOWN GYRO TEST PROGRAM
Irvine, R.B.; Vanalstine, R.
Teledyne Systems Co., Northridge, Calif.

The power spectral noise characteristic performance of the teledyne two-degree-of-freedom dry tuned gimbal gyroscope was determined. Tests were conducted using a current configuration SDG-5 gyro in conjunction with test equipment with minor modification. Long term bias stability tests were conducted as well as some first difference performance tests. The gyro, test equipment, and the tests performed are described. Results are presented. ABA author.

73/02/00 73N20688
STRAPDOWN INERTIAL GYROSCOPE
Sapuppo, M.S.
Massachusetts Inst. of Tech., Cambridge. (Charles Stark Draper Lab.)
In AGARD Inertial Navigation Components and Systems 10 P (see N73-20684 11-21)

A miniature single-degree-of-freedom gyroscope has been developed for the application to a strapdown inertial guidance system. This development is based on many years of experience with the design and development of high-performance pendulous integrating gyroscopic accelerometers (PIGA). By utilizing basic design principles of the gyroscopic element contained in the PIGA, which by nature of the PIGA operation presents a slew environment to the gyroscopic element, a strapdown gyroscope evolves which operates and performs exceptionally well under high linear accelerations and high slew rates. This paper describes a strapdown gyroscope that is less than 1 1/2 inches in diameter by 2 inches in length and weighing under 1/2 pound. The angular momentum is only 8.5 x 1,000 dyne-cm-sec, which gives it several natural benefits of small size, low power consumption, high reliability, and reasonable cost. To achieve high performance with low angular momentum, low uncertainty torques are required about the output axis of the gyroscope. The design of this strapdown gyroscope involved the systematic identification of each error source coupled with the introduction of subcomponent design principles to reduce these error magnitudes and therefore minimize the consequential source of uncertainty torque. ABA author.

NASA-CR-133055 TR-147-1 70/01/31 73N72958
STRAPDOWN SENSOR TESTS AND TEST DATA ANALYSIS
Crawford, B.S. AV026075

NASA-CR-135484 R-743-VOL-1 73/02/00 73N31609
STRAPDOWN SYSTEM PERFORMANCE OPTIMIZATION TEST EVALUATIONS (SPOT), VOLUME I
Blaha, R.J.; Gilmore, J.P.
Massachusetts Inst. of Tech., Cambridge. (Charles Stark Draper Lab.)

A three axis inertial system was packaged in an Apollo gimbal fixture for fine grain evaluation of strapdown system performance in dynamic environments. These evaluations have provided information to assess the effectiveness of real-time compensation techniques and to study system performance tradeoffs to factors such as quantization and iteration rate. The strapdown performance and tradeoff studies conducted include (1) compensation models and techniques for the inertial instrument first-order error terms were developed and compensation effectivity was demonstrated in four basic environments; single and multi-axis slew, and single and multi-axis oscillatory. (2) the theoretical coning bandwidth for the first-order quaternion algorithm expansion was verified. (3) gyro loop quantization was identified to affect proportionally the system attitude uncertainty. (4) land navigation evaluations identified the requirement for accurate initialization alignment in order to pursue fine grain navigation evaluations. ABA author.

B-12

NASA-CR-136083 R-743-VOL-2 73/02/00 74N12355
STRAPDOWN SYSTEM PERFORMANCE OPTIMIZATION TEST EVALUATIONS (SPOT), VOLUME 2
Blaha, R.J.; Gilmore, J.P.
Massachusetts Inst. of Tech., Cambridge. (Charles Stark Draper Lab.)

A three axis inertial system is packaged in an Apollo gimbal fixture for fine grain evaluation of strapdown system performance in dynamic environments. These evaluations have provided information to assess the effectiveness of real-time compensation techniques and to study system performance tradeoffs to factors such as quantization iteration rate. The strapdown performance and tradeoff studies conducted in this program are discussed. ABA author.

73/02/00 73N20685
STRAPPED DOWN INERTIAL GUIDANCE SYSTEM STUDY
Fontana, R.B.
Officine Galileo SpA, Florence (Italy).
In AGARD Inertial Navigation Components and Systems 42 P (see N73-20684 11-21)

The sources and magnitudes of errors occurring in a strapped down environment are discussed. The functions of the accelerometers and gyroscopes in a strapped down system are described. The parameters which must be investigated and defined to evaluate the performance of a stabilized platform are tabulated. The requirements of inertial sensors for maintaining vehicle attitude, velocity, and position are examined. Mathematical models for determining the errors produced by various parameters which affect the inertial system are developed. Diagrams of typical strapdown systems are included. ABA P.N.F.

ESS/SS-738-VOL-1 ESA-CR(P)-920-VOL-1 77/01/00 77N23179
STUDY OF STRAPDOWN INERTIAL OPTICAL ATTITUDE MEASUREMENT SYSTEMS, VOLUME 1
Todman, D.; Eardley, D.; Hutcheson, J.; Callard, L.
British Aircraft Corp. (Operating) Ltd., Bristol (England). (Electronics and Space Systems Group.)

A study is reported on attitude measurement systems using outputs of optical and inertial sensors combined to provide a high quality attitude reference of spacecraft or inertial platforms, undergoing both small attitude precision motion (pointing mode), and large angle slewing motion. The systems considered use a star tracker capable of tracking two stars, and inertial quality rate integrating gyros. Processing is carried out digitally using a processor based on the adaptive control electronics (ACE) computer. Two types of sensor mathematical models are discussed. Methods are evaluated of determining the satellite's attitude during a large angle slew maneuver. ABA ESA.

ESS/SS-738-VOL-2 ESA-CR(P)-920-VOL-2 77/01/00 77N23180
STUDY OF STRAPDOWN INERTIAL OPTICAL ATTITUDE MEASUREMENT SYSTEMS, VOLUME 2
Todman, D.; Eardley, D.; Hutcheson, J.; Callard, L.
British Aircraft Corp. (Operating) Ltd., Bristol (England). (Electronics and Space Systems Group.)

A study is reported on attitude measurement systems using outputs of optical and inertial sensors combined to provide a high quality attitude reference of spacecraft or inertial platforms, undergoing both small attitude precision motion (pointing mode), and a large angle slewing motion. The systems considered use a star tracker capable of tracking two stars, and inertial quality rate integrating gyros. Processing is carried out digitally using a processor based on the adaptive control electronics (ACE) computer. The determination of the attitude, expressed in times of modified Euler angles, using filtering techniques is described. These factors are derived using Wiener theory, and they optimally mix the star tracker and gyro outputs. Application of the preferred form of attitude measurement is considered for a specific satellite mission. ABA ESA.

ESS/SS-772-VOL-3 ESA-CR(P)-920-VOL-3 77/02/00 77N23181
STUDY OF STRAPDOWN INERTIAL OPTICAL ATTITUDE MEASUREMENT SYSTEMS, VOLUME 3
Todman, D.
British Aircraft Corp. (Operating) Ltd., Bristol (England). (Electronics and Space Systems Group.)

A study is reported on attitude measurement systems using outputs of optical and inertial sensors combined to provide a high quality attitude reference of spacecraft or inertial platforms, undergoing both small attitude precision motion (pointing mode), and a large angle slewing motion. The systems considered use a star tracker capable of tracking two star stars, and inertial quality rate integrating gyros. Processing is carried out digitally by a microprocessor. Major results and problem areas are summarized. ABA ESA.

NAL-TR-349 75/11/00 76N7635
STUDY ON A WIDE ANGLE MINIATURE INTEGRATING GYRO FOR STRAPDOWN SYSTEM
Otsuki, M.; Shingu, H., Suzuki, T.; Enkyo, S.; Tabata, J.
National Aerospace Lab., Tokyo (Japan).

B-13

76/08/00 76N32174
SYSTEM APPROACH TO PRACTICAL NAVIGATION
Chin, J.W.; Weaver, R.E., Jr
(Northrop Electronics Div.) Air Force Avionics Lab., Wright-Patterson AFB, Ohio.
In AGARD Medium Accuracy Low Cost Navigation 14 P (see N76-32148 23-04)

A background introduction is presented of various navigation sensors discussing their characteristics and limitations. The forthcoming satellite navigation system, Navstar Global Positioning System (GPS), will be exploited as an ultimate capability of providing L band signals from which position, velocity, and time can be determined. This dual capability will simplify the implementation of integrated systems. A typical medium accuracy system is described. The widely accepted inclusion of an inertial subsystem will be emphasized on the merit of a multifunctional capability beyond that for navigation. Roles in flight control, instrumentation, and augmentation of mission avionics are recognized. The strapdown mechanization and associated instruments are introduced to discuss a potential alternative to the conventional all attitude, gimballed platform. These advances provide the attributes to accomplish low cost designs of medium accuracy navigation systems. Integration of available sensor data to provide the required navigation performance is considered the most effective method of attaining low cost equipment. Modularity expressed in the design will provide flexibility and adaptability to a broad class of users. A total performance, costs of ownership, approach is used to verify system design and selection. ABA author.

NASA-CR-136033 R-746-VOL-1 73/07/00 74N10616
SIRU DEVELOPMENT. VOLUME 1 - SYSTEM DEVELOPMENT
Gilmore, J.P.; Cooper, R.J.
Massachusetts Inst. of Tech., Cambridge. (Charles Stark Draper Lab.)

A complete description of the development and initial evaluation of the strapdown inertial reference unit (SIRU) system is reported. System development documents the system mechanization with the analytic formulation for fault detection and isolation processing structure; the hardware redundancy design and the individual modularity features; the computational structure and facilities; and the initial subsystem evaluation results. ABA author.

NASA-CR-135509 R-746-VOL-2 73/06/00 73N31608
SIRU DEVELOPMENT. VOLUME 2 - GYRO MODULE
Cooper, R.; Shuck, T.
Massachusetts Inst. of Tech., Cambridge. (Charles Stark Draper Lab.)

The design, operation, performance and test of the gyro module and its circuit components are described for the strapdown inertial reference unit system. ABA author.

NASA-CR-128965 R-746-VOL-3 73/03/00 73N27567
SIRU DEVELOPMENT. VOLUME 3 - SOFTWARE DESCRIPTION AND PROGRAM DOCUMENTATION
Oehrle, J.
Massachusetts Inst. of Tech., Cambridge. (Charles Stark Draper Lab.)

The development and initial evaluation of a strapdown inertial reference unit (SIRU) system are discussed. The SIRU configuration is a modular inertial subsystem with hardware and software features that achieve fault tolerant operational capabilities. The SIRU redundant hardware design is formulated about a six gyro and six accelerometer instrument module package. The six axes array provides redundant independent sensing and this symmetry enables the formulation of an optimal software redundant data processing structure with self-contained fault detection and isolation (FDI) capabilities. The basic SIRU software coding system used in the DDP-516 computer is documented. ABA author.

NASA-CR-138574 R-747-VOL-1 74/03/00 74N28098
SIRU UTILIZATION. VOLUME 1 - THEORY, DEVELOPMENT AND TEST EVALUATION
Musoff, H.
Draper (Charles Stark) Lab., Inc., Cambridge Mass.

The theory, development, and test evaluations of the strapdown inertial reference unit (SIRU) are discussed. The statistical failure detection and isolation, single position calibration, and self alignment techniques are emphasized. Circuit diagrams of the system components are provided. Mathematical models are developed to show the performance characteristics of the subsystems. Specific areas of the utilization program are identified as: (1) error source propagation characteristics and (2) local level navigation performance demonstrations. ABA author.

NASA-CR-136022 R-747-VOL-2 73/06/00 74N10617
SIRU UTILIZATION. VOLUME 2 - SOFTWARE DESCRIPTION AND PROGRAM DOCUMENTATION
Oehrle, J.; Whittredge, R.
Massachusetts Inst. of Tech., Cambridge (Charles Stark Draper Lab.)

A complete description of the additional analysis, development and evaluation provided for the SIRU system as identified in the requirements for the SIRU utilization program is presented. The SIRU configuration is a modular subsystem with hardware and software features that achieve fault tolerant operational capabilities. The SIRU redundant hardware design is formulated about a six gyro and six accelerometer instrument module package. The modules are mounted in

B-14

this package so that their measurement input axes form a unique symmetrical pattern that corresponds to the array of perpendiculars to the faces of a regular dodecahedron. This six axes array provides redundant independent sensing and the symmetry enables the formulation of an optimal software redundant data processing structure with self-contained fault detection and isolation (FDI) capabilities. Documentation of the additional software and software modifications required to implement the utilization capabilities includes assembly listings and flow charts. ABA author.

/6/08/00 76/N32162
THE APPLICATION OF RING LASER GYRO TECHNOLOGY TO LOW-COST INERTIAL NAVIGATION
Ball, W.F.
Naval Weapons Center, China Lake, Calif.
In AGARD Medium Accuracy Low Cost Navigation 16 P (see N76-32148 23-04)

The advanced tactical inertial guidance system (ATIGS), a strapdown system using ring laser gyros (RLGS), low-cost accelerometers, and large-scale integrated circuitry computer technology, was described. Although primarily developed for a long-range tactical missile application, the system mechanization that has evolved is directly applicable to aircraft inertial navigation. The first ATIGS unit entered captive flight evaluations in a pod on a A-7E aircraft on 20 June 1974. Results achieved during this first series of tests showed approximately 4 nmi/hr radial error. In March 1975, ATIGS was flight-tested as an aircraft navigator, with ground self-alignment and with flight times of 3 to 4 hours. In these tests an average circular error probable radial error of 2.16 nmi/hr was obtained. The ring laser gyro RLG appears to offer a truly low-cost alternative for future aircraft inertial navigation based on the results of the ATIGS program. Further ATIGS results have indicated that excellent long-term stability can be expected from these unconventional instruments. These factors indicate that, if properly integrated with low-cost accelerometers and appropriate low-cost digital computers, a medium-accuracy, low cost inertial navigator is possible. ABA author.

73/02/00 73N20698
THE EVOLUTION OF ESG TECHNOLOGY
Warzynski, R.R.; Ringo, R.L.
Air Force Avionics Lab., Wright-Patterson AFB, Ohio.
In AGARD Inertial Navigation Components and Systems 8 P (see N73 20684 11-21)

Two electrostatic gyro (ESG) navigation systems are described, the gimbaled ESG aircraft navigation system (GEANS) and the strapdown ESG micro-navigator (Micron). The ESG, its drift error sources, the exploratory program that preceded the development of the GEANS and Micron, and the status of the GEANS and Micron development are reported. ABA author.

NASA-CR-140327 E-2392 69/06/00 75N74041
THE GYROSCOPE IN TORQUE-TO-BALANCE STRAPDOWN APPLICATION
Gilmore, J.P.; Feldman, J.
Massachusetts Inst. of Tech., Cambridge. (Instrumentation Lab.)
Presented at AIAA Guidance, Control and Flight Mech. Conf., Princeton, N.J., August 1969.

NASA-CR-150048 SGD-4284-0742 74/03/00 77N71120
THREE AXIS STRAPDOWN RING LASER GYRO INERTIAL MEASUREMENT UNIT MODEL 8300
Sperry Gyroscope Co., Great Neck, N.Y.

AD-784752 AFFDL-TR-73-80 73/10/00 75N10908
WANDER AZIMUTH IMPLEMENTATION ALGORITHM FOR A STRAPDOWN INERTIAL SYSTEM
Maybeck, P.S.
Air Force Flight Dynamics Lab., Wright-Patterson AFB, Ohio.

The report develops the algorithm for deriving attitude, heading, and navigation information from a strapdown inertial system. Beginning with the fundamental physical relationships, it develops all required equations and progresses to the onboard implementation of the algorithm. Significant features of the algorithm include: (1) computations performed in the wander azimuth coordinate frame to provide a system capable of operating in the polar regions; (2) separation into four loops of different interaction rates. This maintains rapid, accurate updating of the direction cosine matrix involving vehicle attitude, while processing other information and extracting display data at appropriately slower rates; (3) fourth order Runge-Kutta integration of quaternions, using second order rate extraction, to update the attitude direction cosine matrix; (4) specification of the computations that require double precision for adequate performance; (5) third order damping of the vertical channel by means of barometric altimeter data. The applicability of this algorithm to a range of vehicle and mission environments is indicated, the required adaptations being easily performed for each particular implementation. ABA author (GRA).

B-15

77/00/00 77A32962
'STRAPDOWN SYSTEMS' – A NEW GENERATION OF INERTIAL NAVIGATION SYSTEMS
Stieler, B.
(Deutsche Forschungs- und Versuchsanstalt fuer Luft-und Raumfahrt, Institut fuer Flugfuehrung, Braunschweig, West Germany)
Ortung und Navigation, No.1, 1977, p.65-100. In German.

A description is presented on the principles of operation of strapdown systems. Advantages and technological problems of strapdown systems in comparison to conventional platform systems are discussed. The technological problems are mainly related to the employed gyroscope. Attention is given to difficulties encountered in connection with the use of various gyroscope types. Problems related to the self-alignment of the system and the more exacting requirements in the case of the navigational computer are also considered. ABA G.R.

75/00/00 76A10117
A COMPUTER COMMUNICATION SYSTEM FOR CALIBRATION OF A PRECISION STRAPDOWN INERTIAL NAVIGATION SYSTEM
Kourilsky, G.N.; Donoghue, P.J.
(Teledyne Systems Co., Northridge, Calif.)
In Appli d Communication Technology; Proceedings of the Region Six/Western USA/Conference, Salt Lake City, Utah, May 7–9, 1975. (A76-10115 01-32) New York, Institute of Electrical and Electronics Engineering, Inc., 1975, p.96, 97.

The paper describes a computer communication system designed to automate the acquisition, annotation, transfer, and processing of data for the system calibration of a strapdown inertial system. Four calibration procedures are identified: (1) static calibration, which produces torquer bias error, mass balance, and quadrature calibration constants, (2) ANISO calibration, yielding ANISO elasticity constants, (3) rate calibration, producing torquer scale factor and misalignment constants, and (4) temperature sensitivity procedure, giving temperature sensitivity constants for torquer bias error and mass unbalance. The basic calibration procedure consists of three steps: (1) creation of data tape files, (2) creation of calibration constant tape files, and (3) entering the calibration constants. ABA P.T.H.

AIAA Paper 75-583 75/04/00 75A26736
A DISTRIBUTED COMPUTER SYSTEM USING UNIVERSAL MICROPROCESSOR ELEMENTS
Banes, A.V.
(Teledyne Systems Co., Northridge, Calif.)
American Institute of Aeronautics and Astronautics, Digital Avionics System Conference, Boston, Mass., April 2–4, 1975, 6 p.

Modern avionics systems, while configured around large centralized computers, have often distributed many of the computational tasks to varied specialized processors creating an organization with serious logistical problems. The introduction of microprocessors causes one to reconsider the total problem. A properly configured microprocessor can be used alone for modest processing tasks such as air data calculations, or several can be used together to provide parallel processing capability for more complex tasks such as strapdown inertial navigation. A distribution of individual or clustered microprocessors may be made amongst the various computer functions each using common microprocessor elements. Communicating together, these may provide modern avionics with total processing capability and greatly reduced logistical problems. ABA author.

76/00/00 77A20693
A LASER IMU PERFORMANCE EVALUATION SYSTEM
Pugh, R.E., Hung, J.C.
(US Army, Missile Command, Redstone Arsenal, Ala.); (Tennessee, University, Knoxville, Tenn.)
In Annual Southeastern Symposium on System Theory, 8th, Knoxville, Tenn., April 26, 27, 1976, Proceedings. (A77-20679 07-63) New York, Institute of Electrical and Electronics Engineers, Inc., 1976, p.333-337.

Ring laser gyros are particularly suitable for use as attitude sensors in a strapdown inertial measurement unit (IMU). The performance of a ring laser gyro strapdown IMU is known to be dictated both by the performance of ring laser gyros and accelerometers and by the performance of the analytical platform which depends on the software and hardware of the computer involved. The paper describes a recently developed computerized laser IMU performance evaluation system, which allows an evaluation computer to receive signals from the IMU computer at various computation points and to analyze these signals by using appropriate deterministic and statistical analysis procedures. Topics discussed include the test facility, performance data desired, and analysis procedures. Only static tests are examined ABA S.D.

76/00/00 77A20645
A LOW COST PRECISION INERTIAL-GRADE ACCELEROMETER
Morris, H.D.
(Systron-Donner Corp., Concord, Calif.)
In Symposium on Gyroscope Technology, Braunschweig, West Germany, March 31–April 1, 1976, Reports.

p.16

(A77-20643 07-35) Dusseldorf, Deutsche Gesellschaft fuer Ortung und Navigation, 1976, p.25-59.

A description is presented of an inertial-grade accelerometer which has been developed specifically for use in strapped-down tactical missile guidance and in aircraft inertial navigation systems. The instrument is designed for high performance without temperature control. Attention is given to aspects of design configuration, mechanical design, range capability, and electronic desgin. The instrument performance characteristics are discussed, taking into account linearity, bias, scale factor, alignment, thermal coefficients, the bias temperature coefficient, the scale factor temperature coefficient, the alignment temperature coefficient, stability with time, and repeatability at turn-on. Applications of the accelerometer include a use in the Pioneer-Venus planetary probes. ABA G.R.

AIAA 76-1967 76/00/00 76A41496
A MISSILE LASER GYRO RATE SENSOR
Morrison, R.F; Strang, C.B.
(Sperry Rand Corp., Sperry Gyroscope, Great Neck, N.Y.); (Martin Marietta Aerospace, Orlando, Fla.)
In Guidance and Control Conference, San Diego, Calif., August 16–18, 1976, Proceedings. Conference sponsored by the American Institute of Aeronautics and Astronautics. New York, American Institute of Aeronautics and Astronautics, Inc., 1976. 6 p. Research supported by Martin Marietta Aerospace.

The paper describes the Sperry Slic-7 laser gyro, designed to satisfy severe dynamic and environmental requirements of an advanced interceptor missile. The laser gyro has the following design features: (1) a low expansion CER-VIT material for perimeter stability; (2) all-mirror, multilayer dielectric corner reflectors; (3) a helium-neon gas discharge tube; (4) a lock-in avoidance mechanism; and (5) a configuration which provides a unique arrangement of three axes of laser gyros integrated into a common structure. The laser gyro electronics assembly – signal processor, laser gyro control, and power supply – is described, and preliminary test results are presented. ABA B.J.

76/00/00 77A20665
A MODULAR FAIL OP FAIL SAFE STRAPPED-DOWN NAVIGATOR
Giardina, C.R.
(Singer Co., Kearfott Div., Wayne, N.J.)
In New Frontiers in Aerospace Navigation; Proceedings of the Bicentennial National Aerospace Symposium, Warminster, Pa., April 27, 28, 1976. (A77-20655 07-04) Washington, D.C., Institute of Navigation, 1976, p.69-74.

A redundant modular ring laser strapdown navigation system is presented with a full fail op fail safe capability. Fail op fail safe is a term used to denote a system which will fully operate even after any two hard component failures have occurred or after any one soft and one hard (in that order) component failures have occurred. The complete modular building block approach is used along with the application of a sequential multiple classification technique for sensor failure detection and isolation. Reliability is found as a function of component reliabilities, probability of false alarm errors and probability of undetected failure errors. ABA author.

77/00/00 78A15640
A MULTIFUNCTIONAL GUIDANCE AND CONTROL SYSTEM
Kubbat, W.J.
(Messerschmitt-Boelkow-Blohm GmbH, Munich, West Germany)
In NAECON '77; Proceedings of the National Aerospace and Electronics Conference, Dayton, Ohio, May 17–19, 1977. (A78-15551 04-33) New York, Institute of Electrical and Electronics Engineers, Inc., 1977, p.758-766.

A quadruply redundant fully digital guidance and control system for a test A/C (CCV-F104G) has been developed and installed. First test results from a sensor/system open loop test phase have been obtained. The system features also functional integration of former control and stabilization-, autopilot-, air data computation- and navigation systems within redundancy management and preflight check out. Strap down inertial sensors are used as basic information sources together with skewed airflow direction sensors and air data (pressure) transducers. New selfmonitored FBW actuators have been developed for this project. A description of this guidance and control system is given together with the basic design rationale, first experience and an outlook for future projects. ABA author.

AIAA 77-1478 77/00/00 78A12235
A NUCLEAR MAGNETIC RESONANCE GYROSCOPE
Kanegsberg, E.
(Litton Systems, Inc., Woodland Hills, Calif.)
In Digital Avionics Systems Conference, 2nd, Los Angeles, Calif., November 2–4, 1977, Collection of Technical Papers. (A78-12226 02-04) New York, American Institute of Aeronautics and Astronautics, Inc., 1977, p.40-44.

A nuclear magnetic resonance (NMR) gyroscope is under development for use as a low cost angle sensor in strapdown inertial measurement systems. The gyro operates on the principle that the magnetic moments of certain atoms precess at a known frequency in a magnetic field and that changes in phase of this frequency can be sensed to determine the inertial angular displacement of the device about the direction of the field. Optically pumped magnetometer techniques are used for detection and for precise control of the magnetic field. A breadboard model of an NMR gyro has recently been built and is currently undergoing test and evaluation. Preliminary data of gyro bias drift rate characteristics includes a nine hour regment with a drift rate relative to the average bias of about 0.05 deg/hr. ABA author.

B-17

76/00/00 77A20667
A PROPOSITION FOR AN ADVANCED AIRCRAFT NAVIGATION SYSTEM FOR CIVIL AIR TRANSPORT
Collin, G.; Rigaudias, J.B.
(Compagnie Nationale Air France, Direction du Developpement Technique, Orly Aerogare, Val-de-Marne, France)
In New Frontiers in Aerospace Navigation; Proceedings of the Bicentennial National Aerospace Symposium, Warminster, Pa., April 27, 28, 1976. (A77-20655 07-04) Washington, D.C., Institute of Navigation, 1976, p.80-85.

The paper shows that an advanced integrated aircraft navigation system should take into account network extension, aircraft flexibility, productivity improvements, air traffic system constraints, cost effectiveness, safety, and frequency spectrum constraints. The main improvements in takeoff are discussed relative to bad weather conditions, aborted take-off decision, and rotation control. Navigation aspects in climb, cruise, and descent are examined in terms of accuracy capability and versatility. Approach and landing are considered for routine autoland, all-weather operations, and pitch control. The proposed cost-effective integrated navigation system is based on advanced distance measuring equipment (DME), advanced inertial navigation system (INS), and augmented instrument landing system (ILS). Advanced DME implies improved accuracy and capacity, repetitive coded message, channel listening; advanced INS comprises low cost through strapdown mechanization and improved gyros; and augmented ILS incorporates smoothing and independent landing monitor, both based on INS. Major advantages of such a system are noted. ABA S.D.

76/00/00 77A20688
A PSEUDO ROOT-LOCUS METHOD FOR THE DESIGN OF A CLASS OF TWO-INPUT-TWO-OUTPUT SYSTEMS
Kao, M.K.; Hung, J.C.; Berry, E.H.
(Tennessee, University, Knoxville, Tenn.); (NASA, Marshall Space Flight Center, Huntsville, Ala.). National Aeronautics and Space Administration. Marshal Space Flight Center, Huntsville, Ala.; Tennessee Univ., Knoxville.
In Annual Southeastern Symposium on System Theory, 8th, Knoxville, Tenn., April 26, 27, 1976, Proceedings. (A77-20679 07-63) New York, Institute of Electrical and Electronics Engineers, Inc., 1976, p.264-268.

This paper presents the design of digital rebalance loops for a tuned-rotor gyro which is intended to be an attitude sensor in a strapdown inertial measurement unit. A tuned-rotor gyro is a two-degree-of-freedom gyro which has two input axes, with cross-coupling between them. The rebalance loop of the gyro serves for two purposes. First, it restores the position of the rotor to its null position after experiencing an attitude input. Second, the rebalancing signal, which is proportional to the attitude change, is calibrated to give the desired attitude information. Since the gyro has more than one input and one output, a multivariable control technique is needed for designing the rebalance loop. The analytic model for the gyro is described and the available design methods are examined. A new root-locus design technique specially developed for the present problem is outlined. The design of the rebalance loop using the new technique is given. The computer simulation result of the designed system is presented and discussed. ABA author.

AIAA Paper 73-876 73/08/00 73A38813
A REAL-TIME SIX-DEGREE-OF-FREEDOM HYBRID SIMULATION FACILITY FOR GUIDANCE SYSTEM TESTING
Hogan, J.J.; Welch, J.T.
(Goodyear Aerospace Corp., Akron, Ohio).
American Institute of Aeronautics and Astronautics, Guidance and Control Conference, Key Biscayne, Fla., August 20–22, 1973, 8 p. USAF-supported research.

A real-time six-degree-of-freedom (6 DOF) simulation capability has been developed for the purpose of evaluating electro-optically-guided missiles with hardware tie-in. The simulation facility includes digital and analog computers, a three-axis gimballed platform, and a three-degree-of-freedom target area image projection system. The basic structure of the 6-DOF program is presented and functional tie-in of the various hardware components is explained. Typical results of 6-DOF tests with hardware are presented, using an air-to-surface glide vehicle guided by a strapdown electro-optical area correlation guidance system. ABA author.

AIAA Paper 75-1095 75/08/00 75A41660
A RING LASER GYRO STRAPDOWN INERTIAL NAVIGATION SYSTEM – PERFORMANCE ANALYSIS AND TEST RESULTS
Paskik, D.J.; Gneses, M.I.; Taylor, G.R.
(Raytheon Co., Sudbury, Mass.).
American Institute of Aeronautics and Astronautics, Guidance and Control Conference, Boston, Mass., August 20–22, 1975, 12 p.

A ring laser gyro (RLG) inertial navigation system has been extensively tested. An unusual characteristic of the RLG – random walk in its angular output – is described and analyzed. Four classes of test data are presented calibration/alignment, static navigation, dynamic free navigation, and dynamic filtered navigation. Free navigation performance is about five miles per hour; filtered navigation, using self-damping without external sensors, is more than an order of magnitude better. The data confirm the performance analysis, and it is shown that future RLG systems, in which the random walk is better controlled, may show high accuracy performance. ABA author.

B-10

AIAA Paper 75-1054 75/08/00 75A42382
A STRAPDOWN GYRO SYSTEM TECHNOLOGY APPLIED TO A CREW ESCAPE SYSTEM
Eckles, G.A.; Slater, F.W.
(Northrop Corp., Norwood, Mass.)
American Institute of Aeronautics and Astronautics, Guidance and Control Conference, Boston, Mass., August 20–22, 1975, 16 p.

This paper describes the attitude control problems of a crew escape module and deals with the studies relating to the design of a maneuvering rocket control system. Discussed are the means of measurement of roll and pitch angles and the implementation of proper control laws which will allow safe ejection of a separable crew module from an aircraft under all flight conditions, including low-altitude, inverted ejection. The evolution of the design which includes a pyrotechnically-initiated abort system, a strapdown gyro attitude measuring system including analog strapdown computer, and the logic network implemented to provide proper control laws for the vehicle is presented. The ball screw actuator subsystem, which provides the force ouput to position two gimballed solid rocket boosters, is also described. The strapdown gyro system mechanization, permitting the use of low-cost, spring-restrained rate gyros while maintaining required accuracy for long flight periods, is discussed in detail. The system test program (including simulation testing and rocket sled tests) is summarized briefly. ABA author.

74/00/00 74A38588
A STRAPDOWN LASER GYRO NAVIGATOR
Garret, H.; Walls, B.; Morrison, R.
(NASA, Marshall Space Flight Center, Huntsville, Ala.); (Sperry Rand Corp., Sperry Gyroscope Div., Great Neck, N.Y.)
In NAECON '74; Proceedings of the National Aerospace and Electronics Conference, Dayton, Ohio, May 13–15, 1974. (A74-38517 19-09) New York, Institute of Electrical and Electronics Engineers, Inc., 1974, p.572-583. NASA-sponsored research.

A broad spectrum of commercial and military vehicles employ some form of inertial measurement equipment. In general this equipment has a special purpose in that it was tailored for each specific application thereby resulting in high installation and maintenance costs. Recently the emphasis has been directed toward developing low cost building blocks from which the desired inertial functions can be derived. This paper describes a National Aeronautics and Space Administration (NASA) program that combines inertial system sensor and computational advances into a flight demonstration configuration. Specifically, an inertial navigation system employing strapdown laser gyro angular rate sensors and a miniature, modular digital flight computer is described. The objective of this program is to demonstrate, via flight test evaluation, the capabilities of the advanced sensor and computer as they apply to future low cost, high reliability inertial system applications. ABA author.

75/00/00 76A32401
A STUDY OF ATTITUDE REFERENCE COMPUTATIONS FOR STRAPDOWN INERTIAL SYSTEMS
Naka, M.; Yamamoto, H.; Homma, K.
(National Aerospace Laboratory, Chofu, Tokyo, Japan)
In International Symposium on Space Technology and Science, 11th, Tokyo, Japan, June30 – July 4, 1975, Proceedings. (A76-32301 15-12) Tokyo, AGNE Publishing, Inc., 1975, p.731-736.

This paper presents a modification method of Gibbs vector scheme for calculating the transformation matrix of strapdown inertial systems. This method is compared with other schemes such as Euler angles, direction cosines, and Euler parameters. Especially, for the commutativity error compensation, higher order terms are derived and evaluated for some special cases. Simulation results on an on-board computer model indicates the superiority of modified Gibbs vector and Euler parameters methods over the other schemes. ABA author.

NACA-CR-67459 REPT-1726-FR2 64/12/30 76N70963
A STUDY PROGRAM ON A STRAPDOWN MINIATURE ELECTROSTATIC GYRO
Honeywell, Inc., Minneapolis, Minn.

77/00/00 77A21610
A UNIDIMENSIONAL CONVERGENCE TEST FOR MATRIX ITERATIVE PROCESSES APPLIED TO STRAPDOWN NAVIGATION
Bar-Itzhack, I.Y.
(Technion – Israel Institute of Technology, Haifa, Israel)
International Journal for Numerical Methods in Engineering, Vol.11, No.1, 1977, p.115-130.

The investigation of the convergence properties of matrix iterative processes usually involves test matrices of high order. This fact may prohibit an analytic approach to the problem. In this paper a method is presented which converts the multidimensional test procedure into a scalar one. The method is presented in conjunction with the problem of matrix orthogonalization which exists in strapdown inertial navigation. Three examples are presented in which the convergence of matrix orthogonalization techniques is investigated. The examples demonstrate the use of the unidimensional convergence test in determining the order of the processes and in finding sufficient conditions for convergence. Numerical results are presented. ABA author.

B-19

AIAA Paper 74-268 74/01/00 74A18673
A VARIATIONAL INTEGRAL APPROACH TO DIRECTION COSINE MATRIX PROPAGATION
Bowles, W.M.; Ebbesen, L.R.
(Oklahoma State University, Stillwater, Okla.)
American Institute of Aeronautics and Astronautics, Annual Meeting and Technical Display, 10th, Washington, D.C., January 28–30, 1974, 4 p.

The study is concerned with the application of a new procedure for propagating direction cosine matrices. The technique is based on the use of the 'variational integral' approach developed by Ebbesen (1972) for numerical solution of differential equations. Preliminary research indicates that the proposed method offers advantages of increased accuracy and reduced noise sensitivity in comparison to convential procedures. ABA F.R.L.

76/00/00 77A20663
ADVANCED DEVELOPMENT PROGRAM FOR THE RING LASER GYRO NAVIGATOR
Bachman, K.L.; Carson, E.W.
(US Naval Material Command, Naval Air Development Center, Warminster, Pa.); (Honeywell, Inc., St Louis Park, Minn.)
In New Frontiers in Aerospace Navigation; Proceedings of the Bicentennial National Aerospace Symposium, Warminster, Pa., April 27, 28, 1976. (A77-20655 07-04) Washington, D.C., Institute of Navigation, 1976, p.52-58.

Results are presented for an advanced development program designed to provide base line data from which ring laser gyro strapdown production systems can be developed to achieve the maximum cost-of-ownership benefits possible with this new technology. It is shown that the ring laser gyro, with an inherent digital output and essentially unlimited input capability, provides an ideal solution for the strapdown gyro dynamic range problem. The paper gives the functional description of an advanced development model for the ring laser gyro navigator consisting of an internal navigation unit (INU), control display unit (CDU), mode select unit, and battery. The INU provides position, velocity, and attitude information to the CDU and other aircraft systems. The INU consists of three orthogonal body-mounted laser gyros and accelerometers, a digital computer, I/O electronics, sensor electronics, and a power supply. Particular attention is given to the inertial sensors, electrical design, packaging configurations, software, and reliability and maintainability. ABA S.D.

74/00/00 74A38586
ADVANCEMENTS IN STRAPDOWN NAVIGATION
Roantree, J.P.
(United Aircraft Corp., Hamilton Standard Div., Windsor Locks, Conn.)
In NAECON '74; Proceedings of the National Aerospace and Electronics Conference, Dayton, Ohio, May 13–15, 1974 (A74-38517 19-09) New York, Institute of Electrical and Electronics Engineers, Inc., 1974, p.548-555.

This paper discusses the evolution of strapdown inertial navigation systems for space vehicles, boost vehicles, aircraft and missile applications. The performance capabilities and reliability of several present-day systems are shown and performance capabilities and reliability of future systems under development are projected. Brief discussion of strapdown inertial sensors and their electronics are also discussed. Specific areas of concern include performance under low and high vehicle angular rates. Techniques for complete self-contained inertial measurement unit calibration and alignment are presented along with test results. Such techniques require no external equipment such as autocollimators or mirrors. ABA author.

75/10/00 76A10690
ADVANCES IN INERTIAL NAVIGATION - SENSOR TECHNOLOGY
McKinlay, W.H.
(Ferranti, Ltd., Hollinwood, Lancs., England)
(Royal Institute of Navigation and Institution of Electronics and Radio Engineers, Meeting, London, England, January 15, 1975.) Journal of Navigation, Vol.28, October 1975, p.407-415.

Development of inertial navigation and of increasingly sophisticated navigation displays has been rapid in the area of electronic technology and relatively slow in the case of basic sensors. General cost trends are down due to implementation of digital data processing and improved reliability. Strapped down systems substituting low-cost digital software for mechanical gimbals, place stringent requirements on instruments. The 'dry', or tuned rotor, gyroscope is coming into increasing use in place of the floated gyroscope, and the latest systems have significant size and weight advantages. Spherical rotor and 'laser gyros' are under development. Advances in electronic technology for generation of navigation displays are used primarily in numerical displays, with continued use of projection technique and film storage for required topographical information. ABA C.K.D.

76/00/00 77A37419
ADVANTAGES OF GIMBALLED INERTIAL NAVIGATION SYSTEMS
Peterson, R.
(Litton Industries, Inc., Guidance and Control Systems Div., Woodland Hills, Calif.)
In NAECON '76; Proceedings of the National Aerospace and Electronics Conference, Dayton, Ohio, May 18–20, 1976. (A77-37352 17-33) New York, Institute of Electrical and Electronics Engineers, Inc., 1976, p.508-514.

Strapdown and gimballed inertial navigators are compared with respect to a number of important characteristics. Factors

affecting accuracy are reviewed and simulation results are provided which show that gimballed systems are far less sensitive to a number of error sources common to all inertial navigators. Special constraints imposed on inertial instruments to enable strapdown operation are discussed along with computer requirements for gimballed and strapdown navigators. Data showing the effect of gimbals on overall inertial navigation system reliability is presented. The application of strapdown and gimballed navigators in quadruple redundant installations is discussed and strapdown systems are found to have some hardware advantages. Conclusions are reached relative to the near term advantage of gimballed inertial navigation systems. ABA author.

73/00/00 73A38048
AIRBORNE IRP ALIGNMENT USING ACCELERATION AND ANGULAR RATE MATCHING
Schultz, R.L.; Keyes, C.L.
(Honeywell, Inc., Systems and Research Div., Minneapolis, Minn.)
In Joint Automatic Control Conference, 14th, Columbus, Ohio, June 20–22, 1973, Preprints of Technical Papers. (A73-38028 19-10) New York, Institute of Electrical and Electronics Engineers, Inc., 1973, p.427-436.

The combined acceleration angular rate matching Kalman filter described is specifically design to overcome the limitations of earlier approaches for in-flight alignment of two inertial reference packages. The mathematical equations describing the problems are considered together with problems regarding the choice of covariance matrices, aspects of filter performance, and questions of error analysis. It is found that the angular rate matching approach greatly reduces the alignment time and the maneuver requirements on the pilot prior to missile launch. ABA G.R.

73/06/00 73A40026
AN ATTITUDE REFERENCE SYSTEM WITH ELECTRICALLY SUSPENDED GYROS
Elwell, D.F.
(Honeywell, Inc., Aerospace Div., St Petersburg, Fla.)
Institute of Navigation, Annual Meeting, 29th, St Louis, Mo., June 19–21, 1973, Paper. 25 p.

The electrically suspended gyro consists of a spinning metal sphere suspended by an electric force so that friction is virtually eliminated. This type of gyro has demonstrated performance which qualifies it for use in a system for attitude determination. A significant advantage of this system, on board a maneuvering spacecraft, would be the long periods of attitude performance between stellar updates. A readout accuracy improvement in the gyro and the attitude reference system in which it may be used are discussed. ABA author.

72/00/00 73A15274
AN AUTONOMOUS NAVIGATION TECHNOLOGY SYSTEM
Toda, N.F.
(IBM Corp., Owego, N.Y.)
In Symposium on Nonlinear Estimation Theory and its Applications, 3rd, San Diego, Calif., September 11-13, 1972, Proceedings. (A73-15251 04-10) North Hollywood, Calif., Western Periodicals Co., 1972, p.254-259.

The IBM autonomous navigation technology (ANT) system is a strapdown orbital navigation system which has four major subsystems: a known landmark tracker, an attitude determination system, a horizon sensor, altimeter, and a digital computer. Accurate navigation requires a landmark tracker while rapid convergence from large initial conditions is facilitated by employing a horizon sensor. To provide realistic gravitational and drag uncertainties the Air Force provided two different real world ephemeris tapes which were used to drive the simulation and to determine the error in the estimated ephemeris. ABA author.

77/00/00 77A47349
AN EVALUATION OF FUTURE RPV AUTOMATIC NAVIGATION SYSTEMS
McKeel, G.J.
(Rockwell International Corp., Missile Systems Div., Columbus, Ohio)
In the RPV - Complement to Manned Systems; Proceedings of the Fourth Annual Symposium, Washington, D.C., June 5-9, 1977. (A77-47333 22-05) Dayton, Ohio, National Association for Remotely Piloted Vehicles, 1977, p.102-108.

A combination of dead reckoning and position fixing systems is recommended as best suited to future navigation system requirements for remote-piloted vehicles (RPV) designed for electronic warfare, reconnaissance, or selective strike sorties. Strapdown inertial dead reckoning is given preference over the gimballed inertial variant, and position fixes can be obtained from line-of-sight, over-horizon, or correlator type (Terrain contour, radiometric) systems. ABA R.D.V.

75/07/00 75A40678
AN OPTIMAL NORMALIZATION SCHEME
Giardina, C.R.; Bronson, R.; Wallen, L.
(Singer Co., Little Falls, N.J.); (Fairleigh Dickenson University, Teaneck, N.J.); (Hawaii, University, Honolulu, Hawaii)
IEEE Transactions on Aerospace and Electronic Systems, Vol. AES-11, July 1975, p.443-446.

An attitude normalization scheme, based on quaternion updates of the attitude matrix in a strapdown system, is presented which is optimal in the two-norm sense. Furthermore, the algorithm requires minimal computer time and memory load. ABA author.

74/04/00 74A28623
ANALYSIS AND TEST OF A PRECISION PULSE-REBALANCE GYROSCOPE
Clark, R.N.; Fosth, D.C.
(Washington, University, Seattle, Wash.); (Boeing Co., Seattle, Wash.)
Journal of Spacecraft and Rockets, Vol.11, April 1974, p.264-266.

B-21

A method for deriving the rebalance signal which uses a triangular wave modulation of the gyro signal is described. This method is intended for use in strapdown attitude reference systems of advanced spacecraft and missiles, and discussed by Fehr et al. (1972). A compensation network which assured a high static gain of the control loop and stability was required. Without this compensation the control loop exhibited a prominent limit cycle oscillation which had to be eliminated by the compensation. The steady-state accuracy of the entire system was determined to assess the suitability of this instrument for strap-down application. Both attitude and attitude rate can be determined from the signal provided by this instrument. ABA F.R.L.

77/00/00 78A15639
ANALYSIS OF A KALMAN FILTER FOR A STRAPDOWN INERTIAL/RADIOMETRIC AREA CORRELATOR GUIDANCE SYSTEM
Maybeck, P.S.
(USAF, Institute of Technology, Wright-Patterson AFB, Ohio)
In NAECON '77; Proceedings of the National Aerospace and Electronics Conference, Dayton, Ohio, May 17–19, 1977. (A78-15551 04-33) New York, Institute of Electrical and Electronics Engineers, Inc., 1977, p.751-757.

Position measurements can be generated for navigation purposes by correlating a radiometric 'picture' of the terrain immediately below an aerospace vehicle with a prestored reference map of the desired region. Because of stringent storage restrictions, a very simple Kalman filter has been proposed for optimally aiding a strapdown inertial system with data from a radiometric area correlator (RAC) onboard a weapon system currently under development. However, the adequacy of two decoupled 3-state filters to meet performance specifications was subject to significant question, and a covariance analysis has been conducted to determine estimation capabilities in a realistic environment. ABA author.

76/00/00 77A31369
ANALYSIS OF QUANTIZATION ERRORS IN COMPUTING ORIENTATION PARAMETERS
Panov, A.P.
(Akademiia nauk Ukrainskoi SSR, Institut Kibernetiki, Kiev, Ukranian SSR)
Kibernetika i Vychislitel'naia Tekhnika, No.34, 1976, p.92-96. In Russian.

An analysis of the errors in computing orientation parameters due to the quantization of the pulsed signals of the integrating gyroscopes in platformless inertial systems is performed. Some results of digital computer modeling of quantization errors for conical motion of an object are discussed. The requirements on the level of quantization of gyroscope signals for achieving a given computational accuracy are determined. ABA P.T.H.

77/00/00 77A40776
APPLICATIONS OF MODERN GYRO TECHNOLOGY; PROCEEDINGS OF THE SYMPOSIUM, LONDON, ENGLAND, JANUARY 12, 1977
Symposium sponsored by the Royal Aeronautical Society, London, Royal Aeronautical Society, 1977, 175 p.
(For individual items see A77-40777 to A77-40783)

Papers dealing with innovations in gyroscope technology since 1964 are presented, with attention given to the impact of major technical developments, such as the introduction of digital computing, as well as to specific innovations, such as ring laser gyros. Topics included are: alternatives in sub-inertial and inertial navigation systems; development of a subminiature rate sensor for use in missile seeker heads; miniaturization of flex gyros for shipborne navigation systems; improvements in low cost dynamically tuned gyros; problems in manufacture of floated gyroscope systems; comparison of strapdown and gimballed gyros; and the performance characteristics of laser gyroscopes. In particular, problems encountered in miniaturization of rate sensors and navigation systems, and in developing strapdown gyro systems are discussed. Relative cost and effectiveness of floated gyros and dynamically tuned gyros are analyzed, and mention is made of the special advantages of highly accurate systems, such as the ring laser gyro. ABA J.M.B

75/03/00 75A25884
ATTITUDE AND ORBIT ESTIMATION USING STARS AND LANDMARKS
White, R.L.; Adams, M.B.; Grant, F.D.; Geisler, E.G.
(Charles Stark Draper Laboratory, Inc., Cambridge, Mass.)
IEEE Transaction on Aerospace and Electronic Systems, Vol. AES-11, March 1975, p.195-203.

An extended Kalman filter is used to process line-of-sight measurements to stars and known landmarks providing a statistical indication of performance in estimating spacecraft attitude, orbital ephemeris, and the bias drift of a set of three strapdown gyros. The landmark measurements were assumed to have been taken from the imagery of an earth-observing multispectral scanner. It is shown that filtering of these noisy measurements results in highly accurate estimates of the above parameters. Results are given showing the sensitivity of performance to various system parameters such as star tracker accuracy, errors in the knowledge of landmark position, and number of stars and landmarks processed. ABA author.

B-22

75/00/00 76A28896
ATTITUDE CONTROL SUBSYSTEM FOR THE AUTOMATIC INTERPLANETARY SPACECRAFT MARS-2-MARS-7
Demekhin, A.S.; Grubrin, V.E.; Panteleev, V.P.
(Akademiia nauk SSSR, Institut Kosmicheskikh Issledovanii, Moscow, USSR)
In International Federation of Automatic Control, Triennial World Congress, 6th, Boston and Cambridge, Mass., August 24–30, 1975, Proceedings. Part 4. (A76-28778 13-63) Pittsburgh, Pa., Instrument Society of America, 1975, p.14.6-14.6 8.

The major tasks of the attitude control systems of Mars-2 and Mars-7 probes included initial spacecraft rate reduction after its separation from the launch vehicle, acquisition of the reference bodies (the Sun, Canopus and the Earth) within the specified time period. Single axis spacecraft cruise mode relative to the Sun, three-axis spacecraft cruise mode, precise determination of the strapdown reference system during maneuvers and onboard measurements of center of mass motion. Attitude control system equipment including Sun sensors, star and Earth trackers are discussed along with the functional logic. The nature of the feedback loops in the attitude control system is discussed and the control of transient processes is examined. Some specific examples of Mars-2 and Mars-7 attitude control system flight performance are presented including correction in antenna Earth orientation performed aboard Mars-4 and the insertion of Mars-7 into Mars orbit. ABA B.J.

76/00/00 77A24812
ATTITUDE DETERMINATION ALGORITHM FOR A STRAPDOWN IMU
O'Connor, B.J.; Zomick, D.A.
(Bendix Corp., Guidance Systems Div., Teterboro, N.J.)
In Symposium on Automatic Control in Space, 7th, Rottach-Egern, West Germany, May 17–21, 1976, Preprints. Volume 2. (A77-24777 10-12) Dusseldorf, VDI/VDE-Gesellschaft Mess- und Regelungstechnik, 1976, p.397-411.

Concentrating on the quanternion approach to attitude determination for a strapdown inertial measurement unit, a technique is developed to facilitate selection of algorithmic order without resort to digital simulation. The procedure is demonstrated for algorithms through fourth order and for three specific types of vehicle motion, indicating a third-order solution to be adequate for most applications. A final section addresses the computational burden imposed by the candidate quaternion solutions. ABA author.

AIAA Paper 73-900 73/08/00 73A38834
ATTITUDE DETERMINATION FOR A STRAPDOWN INERTIAL SYSTEM USING THE EULER AXIS/ANGLE AND QUATERNION PARAMETERS
Grubin, C.
(Hughes Aircraft Co., Culver City, Calif.)
American Institute of Aeronautics and Astronautics, Guidance and Control Conference, Key Biscayne, Fla., August 20–22, 1973, 10 p.

AIAA Paper 75-1096 75/08/00 75A41661
AUTONOMOUS SATELLITE ORBITAL NAVIGATION USING KNOWN AND UNKNOWN EARTH LANDMARKS
Kau, S.P.
(Honeywell, Inc., St Petersburg, Fla.)
American Institute of Aeronautics and Astronautics, Guidance and Control Conference, Boston, Mass., August 20–22, 1975, 13 p.

Two concepts of satellite autonomous navigation using strapdown landmark sensors are considered. In the unknown landmark concept, the sensor measures the rate at which the image of unidentified earth features travels across sensor field of view. Correlation interpolation techniques are used for processing of random images. In the known landmark concept, sightings to known linear earth features are obtained. Edge enhancement and detection techniques are used for the somewhat deterministic landmark signature. The known landmark approach is shown to be superior due to its lower sensitivity to pointing errors. ABA author.

72/00/00 73A15266
AUTONOMOUS SATELLITE NAVIGATION FROM STRAPDOWN LANDMARK MEASUREMENTS
Paulson, D.C.
(Honeywell, Inc., St Petersburg, Fla.)
In Symposium on Nonlinear Estimation Theory and its Applications, 3rd, San Diego, Calif., September 11–13, 1972, Proceedings. (A73-15251 04-10) North Hollywood, Calif., Western Periodicals Co., 1972, p.167-183.

A new concept for accurate autonomous determination of position and velocity of an orbiting spacecraft is presented. This concept makes use of strapdown landmark sensors which measure relative motion of imaged ground terrain through the sensor field of view as the satellite moves over the terrain. Data from two such sensors, when combined with attitude from an inertial reference and the time from a long term clock, is sufficient to bound navigation errors. The general concept of what is termed line-of-sight-rate navigation is described. Navigation algorithms and simulation results are presented. Results show performance comparable to the gimbaled unknown landmark tracking mechanization and better than the much-analyzed horizon sensor/inertial reference approach. ABA author.

B-23

74/00/00 74A38541
AVIONICS APPLICATION ON AN ADVANCED LSI MICROPROGRAMMED PROCESSOR
Thoennes, W.P.
(Rockwell International Corp., Anaheim, Calif.)
In NAECON '74; Proceedings of the National Aerospace and Electronics Conference, Dayton, Ohio, May 13–15, 1974. (A74-38517 19-09) New York, Institute of Electrical and Electronics Engineers, Inc., 1974, p.229-236.

Description of an advanced MOS/LSI microprogrammed processor being developed for application as the digital processor in the advanced micro-navigator (Micron) system. Micron, being a 'strapdown' navigation system, has unique processing requirements. Additional requirements are defined to meet system objectives in the areas of size, weight, power, reliability, radiation hardness and cost of ownership. A processor configured to meet these requirements is described. ABA author.

75/00/00 76A44968
BODY FIXED OPTICS IN SEEKERS – THEIR REWARDS AND PITFALLS
Baker, M.L.
(Martin Marietta Aerospace, Orlando, Fla.)
In Electro-Optical Systems Design Conference and International Laser Exposition, Anaheim, Calif., November 11–13, 1975, Proceedings of the Technical Program. (A76-44926 23-35) Chicago, Industrial and Scientific Conference Management, Inc., 1975, p.618-674.

Rewards and pitfalls are examined for a strapdown optics seeker that permits one-shot kill of evasively moving targets which have been designated by lasers. This seeker combines the fixed optics of the early pursuit system with the inertially stabilized line of sight of the gimballed optics seeker. The basic operation of the present system is outlined in terms of the theory of nodal points from geometrical optics. Among the rewards of the system, it is noted that the fixed lens system is easy to install, the inertially stabilized mirror is easily torqued for guidance, and the detector is fixed, requiring no slip rings or exacting wiring to bring the leads out from a gimbal. Pitfalls discussed include lens aberrations, vignetting, and mirror pivot-arm length. Ways to deal with and correct for these pitfalls are considered. ABA F.G.M.

73/00/00 73A35210
CALIBRATING THE DRIFT RATES OF STRAPDOWN ELECTROSTATIC GYROSCOPES
Andrews, A.
(Rockwell International Corp., Autonetics Div., Anaheim, Calif.)
In NAECON 73; Proceedings of the National Aerospace Electronics Conference, Dayton, Ohio, May 14–16, 1973. (A73-35201 17-09) New York, Institute of Electrical and Electronics Engineers, Inc., 1973, p.76-81.

A technical approach to the problem of calibrating the precession rates of the spin axis of a strapdown electrostatic gyroscope (ESG) is presented. The problem is complicated by the fact that the spin axis is not constrained in direction with respect to its support bearing, and the precession rates depend upon this direction. The virtual work technique is used for modeling the bearing torques on the rotor. This has the advantages that the model equations are applicable to any ESG design, and that the functional form of the model is more transparent than that obtained by the force/lever-arm technique for defining torques. This approach also leads to an appropriate functional analysis for unmodeled torques. The resulting calibration problem is linearized and lends itself to conventional statistical methods. ABA author.

76/00/00 77A28300
COMPARATIVE STUDY OF PULSE-REBALANCED INERTIAL SENSORS WITH DIFFERENT DYNAMICS
Rahlfs, D.
(Deutsche Forschungs- und Versuchsanstalt fuer Luft- und Raumfahrt, Braunschweig, West Germany)
In International Navigational Congress, Boston, Mass., August 3 6, 1976, Proceedings. (A77-28285 11-04) Washington, D.C., Institute of Navigation, 1976, p.280-285.

Pulse rebalance loops are applied when high precision is required for the digital readout of inertial sensors. The arrangement of high precision readout electronics developed by DFVLR is described and discussed. Test results for pendulous accelerometers of different dynamics and construction are presented. Criteria for the optimal layout of pulse rebalancing loops of inertial sensors are provided. ABA author.

76/00/00 76A44794
COMPARATIVE STUDY OF PULSE-REBALANCED INERTIAL SENSORS WITH DIFFERENT DYNAMICS
Rahlfs, D.
(Deutsche Forschungs- und Versuchsanstalt fuer Luft- und Raumfahrt, Braunschweig, West Germany)
Ortung und Navigation, No.2–3, 1976 p.177-194.

Basic principles of pulse torque readout electronics are examined and approaches for the generation of high precision current time increments are considered, taking into account an H-switch with a highly stable switch delay and current control loops. The application of pulse rebalance loops for the readout of pendulous accelerometers is discussed and a description is presented of the criteria for the layout of pulse-rebalanced sensors. Attention is given to the mechanical part of a sensor, the torque generator, aspects of angular readout, and the regulator and quantizer. ABA G.R.

p24

AIAA Paper 73-835 73/08/00 73A38791
COMPETITIVE EVALUATION OF FAILURE DETECTION ALGORITHMS FOR STRAPDOWN REDUNDANT INERTIAL INSTRUMENTS
Wilcox, J.C.
(TRW Systems Group, Redondo Beach, Calif.)
American Institute of Aeronautics and Astronautics, Guidance and Control Conference, Key Biscayne, Fla., August 20–22, 1973, 11 p.

Seven algorithms for failure detection, isolation, and correction of strapdown inertial instruments in the dodecahedron configuration are competitively evaluated by means of a digital computer simulation that provides them with identical inputs. Their performance is compared in terms of orientation errors and computer burden. The analytical foundations of the algorithms are presented. The features that are found to contribute to superior performance are use of a definite logical structure, elimination of interaction between features, different thresholds for first and second failures, use of the 'parity' test signals, and avoidance of iteration loops. ABA author.

AD-763579 ESD-TR-73-89 72/11/00 73A26635
CONSTANT-Q PULSED FEEDBACK ELECTRONICS FOR STRAPPED-DOWN GYRO SYSTEMS
Millner, A.R.
(MIT, Lexington, Mass.)
IEEE Transactions on Aerospace and Electronic Systems, Vol. AES-8, November 1972, p.762, 763. USAF-sponsored research.

For rate-integrating strapped-down gyros, such as those used in space platform orientation systems, a new feedback design is described that employs a precision, temperature-compensated metallized teflon capacitor charged to a precise voltage as a source of constant charge which discharges through a torquer to provide the feedback current pulse. The system provides a constant time-average power dissipation in the torquer, which simplifies temperature control. Thus, system simplicity is retained and very low power consumption can be achieved in the electronics, with predicted accuracy of 40 ppm per year, limited mainly by the capacitor. ABA M.V.E.

75/00/00 76A11843
COST CONSIDERATIONS IN A STRAPDOWN NAVIGATION SYSTEM USING DRY TUNED INSTRUMENTS
Craig, R.J.G.; Russel, J.G.
(Litton Industries, Inc., Woodland Hills, Calif.)
In Intercon 75; International Convention and Exposition, New York, N.Y., April 8–10, 1975, Conference Record. (A76-11826 02-33) New York, Institute of Electrical and Electronics Engineers, Inc., 197 i, p.1 35/4-6 35/4.

Design guidelines are stated for a low cost strapdown navigation system using mature technology of tuned-gimbal gyros. Components of the system designed in accordance with these guidelines are described. Mature technology is defined as one which is characterized by complete and thorough understanding and production experience. It is asserted that near future large volume procurements for strapdown navigation systems will favor those systems that are based on mature technologies because these technologies are more amenable to accurate cost predictions and analyses. Discussions of system costs such as life cycle cost, acquisition costs, initial logistics cost and recurring costs is presented and comparison between gimballed systems and strapdown system using similar technologies is made. ABA author.

76/00/00 77A20666
DIFFERENTIAL LASER GYRO DEVELOPMENT
Bresman, J.; Cook, H.; Lysobey, D.
(United Technologies Corp., Hamilton Standard Div., Windsor Locks, Conn.)
In New Frontiers in Aerospace Navigation; Proceedings of the Bicentennial National Aerospace Symposium, Warminster, Pa., April 27, 28, 1976. (A77-20655 07-04) Washington, D.C., Institute of Navigation, 1976, p.75-79.

The paper outlines the design concept, construction, operation, and tested capabilities of the differential laser gyro (DILAG) provided with four simultaneously operating modes, resulting in a significant advancement in strapdown inertial guidance. The DILAG concept eliminates bias stability and dithering problems by simultaneously operating two complete laser gyros in the same laser cavity. In one gyro, both the clockwise traveling wave and the counterclockwise traveling wave are right circularly polarized, while in the other gyro both waves are left circularly polarized. Both gyros are biased out of their respective deadband regions by the same Faraday cell. The DILAG cavity is constructed from a block of ultra-low-expansion quartz. The detector electronics and the servo controls for cavity length and discharge current are constructed on a printed circuit board and mounted on top of the block. Test results showed examples of noise suppression and error cancellation, excellent pulse moding characteristics, and scale factor linearity at low rates. A self-check technique leading to a wide-ranging error compensation and calibration capability is discussed. ABA S.D.

76/00/00 76A47229
DIFFERENTIAL LASER GYRO
Stowell, W.K.; McAdory, R.W.; Roantree, J.P.
(USAF, Avionics Laboratory, Wright-Patterson AFB, Ohio); (United Technologies Corp., Hamilton Standard Div., Farmington, Conn.)
In Engineering in a Changing Economy; Proceedings of the Southeast Region, 3 Conference, Clemson, S.C., April 5–7,

1976. (A76-47201 24-99) New York, Institute of Electrical and Electronics Engineers, Inc., 1976, p.227-229.

B-25

The differential laser gy[illegible]ILAG) is being developed as a solution to the instabilities and error sources inherent in conventional techniques of overcoming the low angular rate lock-in threshold (the rotation rate below which the laser gyro has no response). The DILAG concept consists of operating two ring lasers in the same optical cavity and biasing them with the same optical element. This makes it possible to obtain rate sensing with the same scale factor and bias terms in each of the laser gyros. Results of performance testing of the DILAG are discussed. ABA B.J.

76/00/00 77A20649
DIGITAL READOUT IN THE CASE OF INERTIAL SENSORS
Rahlfs, D.
(Deutsche Forschungs- und Versuchsanstalt fuer Luft- und Raumfahrt, Institut fuer Flugfuehrung, Braunschweig, West Germany)
In Symposium on Gyroscope Technology, Braunschweig, West Germany, March 31 - April 1, 1976, Reports. (A77-20643 07-35) Dusseldorf, Deutsche Gesellschaft fuer Ortung und Navigation, 1976, p.127-177. In Ger[illegible]an.

The output signals of inertial measurement systems, particularly in the case of strapped-down systems, are further processed with the aid of a digital procedure. The approaches used in the assignment of digital values to the measured quantitites are discussed, taking into account the derivation of the transfer function for pendulum acceleration measurement devices, a general analysis of suitable methods, and nonintegrating and integrating digitizing procedures. A description is presented of the electronic methods developed in West Germany for the implementation of incremental readout processes. ABA G.R.

NASA-CR-140296 E-2525 76/08/00 74N78010
DYNAMIC TESTING OF A SINGLE DEGREE-OF-FREEDOM STRAPDOWN GYROSCOPE
Feldman, J.
Massachusetts Inst. of Tech., Cambridge. (Charles Stark Draper Lab.)
Presented at the 5th Biennial Guidance Test Symp., Holloman AFB, N. Mex., 14 16 October 1970.

75/07/00 75A40689
ESTIMATING ANGULAR VELOCITY FROM OUTPUT OF RATE-INTEGRATING GYRO
Friedland, B.
(Singer Co., Little Falls, N.J.)
IEEE Transactions on Aerospace and Electronic Systems, Vol. AES-11, July 1975, p.551-555.

It is shown that the Kalman filtering technique can be used to improve estimates of angular velocity in a strapped-down navigation system on the basis of angular increment (rate integral) data. A model for the evolution of the angular velocity is developed, and estimation equations are obtained by applying the general equations of Kalman filtering to the model. It is found that a simple second-order constant-coefficient digital filter can yield significant improvement for very high or very low values of a defined noise-to-signal ratio and that improvement is negligible for ratios of the order of unity. ABA F.G.M.

AIAA Paper 75-1071 75/08/00 75A41637
ESTIMATION OF GYRO PARAMETERS FOR EXPERIMENTALLY DEVELOPED GYRO MODELS
Coffman, V.D.; Debra, D.B.
(Lockheed Missiles and Space Co., Inc., Sunnyvale, Calif.); Stanford University, Stanford, Calif.)
American Institute of Aeronautics and Astronautics, Guidance and Control Conference, Boston Mass., August 20 22, 1975, 13 p.

Strapdown attitude reference systems with body fixed attitude sensors rely on gyros to maintain the reference between attitude measurements. For maneuvering vehicles both gyro scale factor and drift are observable for adequate amplitude and frequency of motion. Performance is investigated using compensation for both multiplicative (scale factor) and additive (drift) error sources. Six gyros were tested to develop models that provide improvement in the accuracy of the references. On-line estimation of model parameters is obtained by appending additional states and using measured vehicle rate directly in the state matrix, leading to a linear, recursive Kalman filter formulation with time varying coefficients. ABA author.

77/00/00 78A15711
EVALUATION TECHNIQUES FOR INS ALGORITHMS
Nurse, R.; Schmidt, G.; Kaiser, D.
(Charles Stark Draper Laboratory, Inc., Cambridge, Mass.); (USAF, Avionics Laboratory, Wright-Patterson AFB, Ohio)
In NAECON '77; Proceedings of the National Aerospace and Electronics Conference, Dayton, Ohio, May 17 - 19, 1977. (A78-15551 04-33) New York, Institute of Electrical and Electronics Engineers, Inc., 1977, p.1268-1281.

The paper considers the design of the numerical simulator program (NUMSIM) developed to determine INS navigation errors in position, velocity and attitude resulting from mechanization of the navigation equations on a digital computer for an error-free IMU. The program provides a simulation of the navigation computation for three different IMU mechanizations, namely a local-level wander-azimuth platform stabilization, a space-stabilized platform, and a strapdown

B-26

configuration. A functional and structural overview of the simulator is presented and a short parametric study using the simulator is described. ABA B.J.

AIAA Paper 73-902 73/08/00 73A38836
EXPERIMENTAL TRAJECTORIES VIA KALMAN FILTERING
Barton, R.; Gurwell, N.
(KMS Technology Center, El Segundo, Calif.)
American Institute of Aeronautics and Astronautics, Guidance and Control Conference, Key Biscayne, Fla., August 20–22, 1973, 9p.

A computerized method for estimating the trajectory of a maneuvering reentry vehicle and systematic sensor error sources has been developed. The program utilizes measurements from radars, optical sensors, and an inertial reference system composed of strapdown and stable platform instrumentation. These measurements are combined, utilizing the extended Kalman filter theory, to yield minimum-variance estimates of nearly all trajectory parameters and systematic errors in the instrumentation. The analytical formulation of the trajectory estimation problem and the characteristics of the associated computer program are described. ABA author.

75/05/00 75A31980
FAILURE ISOLATION FOR A MINIMALLY REDUNDANT INERTIAL SENSOR SYSTEM
Harrison, J.V.; Chien, T.-T.
(Charles Stark Draper Laboratory, Inc., Cambridge, Mass.)
IEEE Transactions on Aerospace and Electronic Systems, Vol. AES-11, May 1975, p.349-357.

The application of two-degree-of-freedom inertial sensors in a minimally redundant strapdown configuration is considered. The potential improvement in reliability which can be achieved by exploiting the failure isolation capability unique to this configuration is evaluated. A unified, statistical approach to the detection and isolation of both hard and soft sensor failures is presented. The effectiveness of this unified approach to FDI in terms of the mean time to detection, the mean time between false alarms, and the accumulated attitude error prior to detection is indicated by simulation results. ABA author.

77/00/00 78A15641
SYSTEM DESCRIPTION AND PERFORMANCE CHARACTERISTICS OF A QUAD REDUNDANT STRAPDOWN INERTIAL NAVIGATION AND FLIGHT CONTROL SYSTEM
Donoghue, P.J.
(Teledyne Systems Co., Northridge, Calif.)
In NAECON '77; Proceedings of the National Aerospace and Electronics Conference, Dayton, Ohio, May 17 - 19, 1977. (A78-15551 04-33) New York, Institute of Electrical and Electronics Engineers, Inc., 1977, p.767-774.

This paper describes the system design and development of a quadruply redundant strapdown inertial information and computation system. This system was developed for application to a digital fly-by-wire controlled configuration vehicle. Design rationale and implementation of the system are described in four major areas: (1) sensors, (2) digital conversion techniques, (3) digital computer and (4) systems implementation. ABA author.

77/00/00 78A15642
FLIGHT-CONTROL/NAVIGATION INERTIAL REFERENCE SYSTEM
Ebner, R.E.
(Litton Systems, Inc., Woodland Hills, Calif.).
In NAECON '77; Proceedings of the National Aerospace and Electronics Conference, Dayton, Ohio, May 17 - 19, 1977. (A78-15551 04-33) New York, Institute of Electrical and Electronics Engineers, Inc., 1977, p.775-782.

The preliminary design of a redundant strapdown navigation system for integrated flight-control/navigation use has been completed. Based on application of tuned-gimbal gyros, a compact configuration (13 in x 13 in x 14 in) has been achieved for fail-operational/fail-operational redundancy. Test data are presented for strapdown system test programs including flight testing of the LN-50 tuned-gimbal gyro system. Testing of a redundant sensor configuration is currently in process. Strapdown gyro development also includes ring laser and nuclear magnetic resonance techniques. ABA author.

77/00/00 78A15938
FLIGHT-VEHICLE STABILIZATION WITH A PLATFORMLESS INERTIAL SYSTEM
Lebedev, R.K.
Moscow, Izdatel 'Stvo Mashinostroenie, 1977. 142 p. In Russian.

This book outlines the theoretical principles of a platformless flight-vehicle stabilization system in which results of calculations performed by an on-board computer in real time [illegible] flight are used as the inertial coordinate baseline. Principles of attitude control without a gyrostabilized platform are considered, and a mathematical description of the flight vehicle as an object to be stabilized in a platformless system is given. Techniques for determining instantaneous attitude of a flight vehicle relative to inertial space are described along with methodological errors associated with the algorithms used in constructing the inertial coordinate baseline. Attention is also given to the formulation of control commands, the control channel, and techniques for preventing control errors. It is noted that the formalisms of control theory may be employed in computing the dynamical properties of the platformless inertial system. ABA P.C.M.

B-27

76/00/00 77A37356
FLOATED MULTISENSOR FOR LOW-COST NAVIGATION
Weinberg, M.
(Charles Stark Draper Laboratory, Inc., Cambridge, Mass.)
In NAECON '76; Proceedings of the National Aerospace and Electronics Conference, Dayton, Ohio, May 18- 20, 1976. (A77-37352 17-33) New York, Institute of Electrical and Electronics Engineers, Inc., 1976, p.20-27.

The Charles Stark Draper Laboratory (CSDL) multisensor is a single-degree-of-freedom floated integrating gyroscope with the output axis purposely unbalanced to obtain pendulosity; thus, specific force in addition to angular rate can be measured. Analytical and design studies are being performed, and further testing of a previously constructed feasibility instrument is planned. Performance objectives are 1-meru (0.015 deg/h) bias and gyro scale-factor stability, and 100-microgram bias and 50-ppm scale-factor stability for the accelerometer function. The feasibility instrument has demonstrated the basic potential of the multisensor concept as a viable multisensor instrument for avionics and tactical guidance and navigation application. This paper deals with the description of the basic concept, reviews the test data from the feasibility multisensor, and discusses the dynamics of the instrument and associated error torque mechanism. ABA author.

76/00/00 77A17633
FREQUENCY CHARACTERISTICS OF RECURRENT ALGORITHMS FOR CALCULATING DIRECTION COSINES IN PLATFORMLESS SYSTEMS
Lebedev, R.K.
Priborostroenie, Vol.19, No.10, 1976, p.79-82. In Russian.

Two algorithms the interpolation and the extrapolation algorithms used for calculating direction cosines of strapdown navigation systems are examined and compared. It is found that the interpolation algorithm has a relatively small amplitudinal error but can create a stability problem in closed systems due to significant phase distortion. The extrapolation algorithm has an almost ideal phase characteristic but its maximum amplitudinal error is about four times greater than that of the reference algorithm. ABA B.J.

73/03/00 73A29214
HIGH-RELIABILITY STRAPDOWN PLATFORMS USING TWO-DEGREE-OF-FREEDOM GYROS
Hung, J.C.; Doran, B.J.
(Tennessee, University, Knoxville, Tenn.); (NASA, Marshall Space Flight Center, Huntsville, Ala.)
IEEE Transactions on Aerospace and Electronic Systems, Vol. AES-9, March 1973, p.253-259.

This paper presents a new concept of high-reliability strapdown attitude sensing systems for space vehicles. Each system utilizes a set of redundant two-degree-of-freedom gyros. An optimum system configuration is obtained for maximum system reliability and the best measurement accuracy. Improved accuracy of the final data is obtained by using the least-square data reduction technique. Each system possesses a 'sensor performance management' feature which is capable of failure detection, faulty gyro identification, system reconfiguration, and, possibly, sensor recalibration. Improvement in reliability, as compared to other types of strapdown systems, is demonstrated. Details of the development are described in terms of a system containing four gyros. ABA author.

AIAA Paper 74-867 74/08/00 74A37854
INERTIAL NAVIGATION SYSTEM TESTS HAVING IMPROVED OBSERVABILITY OF ERROR SOURCES
Widnall, W.S.; Grundy, P.A.; Murch, W.G.
(Intermetrics, Inc., Cambridge, Mass.); (USAF, Holloman AFB, N. Mex.)
American Institute of Aeronautics and Astronautics, Mechanics and Control of Flight Conference, Anaheim, Calif., August 5 9, 1974, 14p. USAF-supported research.

Optimal filtering of simulated inertial navigation system (INS) test data is used to evaluate alternate laboratory and flight test techniques, which are intended to determine the value of each significant source of navigation error. Tests of both gimbaled and strapdown systems are evaluated. The major problem preventing more accurate determination of the dozens of sources of error in an INS is the high correlation between the contributions of many of the sources of error. Laboratory test sequences and flight test trajectories are presented that reduce these correlations and improve the observability of the individual sources of error. ABA author.

76/00/00 76A45796
INTEGRATED AIRCRAFT NAVIGATION
Farrell, J.L.
(Westinghouse Electric Corp., Systems Development Div., Baltimore, Md.)
New York, Academic Press, Inc., 1976, 365p.

An integrated textbook drawing upon elements required from various science and engineering disciplines contributing to aircraft navigation systems. Material is drawn upon from theoretical dynamics, inertial measurements, radar, radio navaids, celestial observations, statistical estimation techniques, avionics, gravity measurements, error analysis, Kalman filters, computer tracking techniques. Problem exercises are appended to each chapter. Strapdown coordinates, air-to-air tracking, gyrodynamics, rotational transforms, point nav mode, and suboptimal damping are among the topics treated. The underlying functional similarity of aircraft navigation and tracking, spheroidal earth navigation, gimballed platform

B-20

and strapdown inertial navigation, space stable, geographic, and wander azimuth coordinate references, damped and undamped inertial navigation systems, radio/radar/optical updating, and block or recursive estimation algorithms for updating, is pointed out. ABA R.D.V.

75/00/00 76A32400
INVESTIGATION OF A ROLL STABILIZED ANALYTIC PLATFORM/RSAP/TYPE INERTIAL NAVIGATION SYSTEM
Vepa, N.M.; Higashiguchi, M.
(Indian Space Research Organization, Control Guidance and Instrumentation Div., Trivandrum, India); (Tokyo, University, Tokyo, Japan)
In International Symposium on Space Technology and Science, 11th, Tokyo, Japan, June 30–July 4, 1975. Proceedings. (A76-32301 15-12) Tokyo, Agnes Publishing, Inc., 1975, p.721-729.

The paper describes the so-called roll stabilized analytic platform type inertial navigation system, in which the sensors (three rate integrating gyros and three accelerometers) are mounted on a table that is electromechanically stabilized about the roll axis and for which the coordinate orientation with respect to the inertial frame is established analytically. The system preserves the advantages of a strapdown system in addition to isolating the sensors from the roll motions of the vehicle, which results in a great reduction in sensor errors. Simple coordinate transformation algorithms – two Euler angle algorithms and the DCM algorithms – are proposed for platform stabilization. A new non-iterative orthogonalization technique based on the DCM algorithm is proposed for analytical coordinate orientation and the performance of the inertial system studied here is compared with the performance of a strapdown system by simulating both systems and comparing their typical motions. ABA B.J.

AD-784907 AFOSR-74-1367TR 74/06/30 75N77920
INVESTIGATION OF STRAPDOWN REFERENCE SYSTEMS
Bowles, W.M.
Oklahoma State Univ., Stillwater. (School of Mechanical and Aerospace Engineering)

75/00/00 76A22634
INVESTIGATION OF TIME-SHARING OF REBALANCE ELECTRONICS FOR SENSORS IN STRAPDOWN NAVIGATION PLATFORMS
Coffman, D.E.; Hung, J.C.
(Tennessee, University, Knoxville, Tenn.) Tennessee Univ., Knoxville.
In Electricity an Expanding Technology; Proceedings of the Southeast Region 3 Conference, Charlotte, N.C., April 6–9, 1975. Volume 1. (A76-22626 09-31) New York, Institute of Electrical and Electronics Engineers, Inc., 1975, p.3E-2-1 to 3E-2-10.

This article reports the results of an investigation on time-sharing of a rebalance electronics among several sensors used in a strapdown navigation platform. Various concepts are given. The merits and dements of the time-sharing for a typical situation are discussed in detail. A possible hardware realization is proposed. In addition, this study develops a general approach, applicable to other systems, for evaluating the use of time-sharing concept. ABA author.

75/01/00 75A20803
ITERATIVE OPTIMAL ORTHOGONALIZATION OF THE STRAPDOWN MATRIX
Bar-Itzhack, I.Y.
(Technion – Israel Institute of Technology, Haifa, Israel)
IEEE Transactions on Aerospace and Electronic Systems, Vol. AES-11, January 1975, p.30-37.

This paper treats the problem of finding an orthogonal matrix which is the closest, in the Forbenius norm, to a given nonorthogonal matrix. This nonorthogonal matrix is the result of a fast but rather inaccurate computation of the well-known direction cosine matrix (DCM) of a strapdown inertial navigation system. The known closed-form solution to this problem is rederived using the directional derivative method, and the conditions for minimum distance are derived and discussed. A new iterative technique for solving this problem is derived as a result of the application of the gradient projection technique and the directional derivative method. The practical computational problems involved in this technique are discussed. The new technique is demonstrated by three examples. Although particular attention is given to the 3 x 3 direction cosine matrix, the conclusions are nonetheless valid higher order matrices. ABA author.

75/00/00 76A11826
INTERCON 75; INTERNATIONAL CONVENTION AND EXPOSITION, New York, N.Y., April 8–10, 1975, Conference Record: Convention sponsored by the Institute of Electrical and Electronics Engineers. New York, Institute of Electrical and Electronics Engineers, Inc., 1975. 621p.

Papers are presented describing recent advances in computer hardware, electronic instrumentation, automatic test equipment, and communications systems. Some of the topics covered include sampling measurements for simplifying automatic test equipment design, emerging technologies in local exchange communication networks, design of microprocessor based terminals, testability enhancement in digital system design, random file processing in a storage hierarchy, satellite system considerations for computer data transfer, and techniques for achieving low cost strapdown navigation. Individual items are announced in this issue. ABA P.T.H.

76/00/00 76A47227
LASER INERTIAL PLATFORM FOR ARMY MISSILES
Johnston, J.V.; Pugh, R.E.
(US Army, Missile Command, Redstone Arsenal, Ala.)
In Engineering in a Changing Economy; Proceedings of the Southeast Region 3 Conference, Clemson, S.C., April 5–7, 1976. (A76-47201 24-99) New York, Institute of Electrical and Electronics Engineers, Inc., 1976, p.221-223.

The system aspect of a laser gyro strapdown inertial measurement unit applicable to US Army missiles is examined. The sensor assembly contains a single triad that mounts the three ring laser gyros and three accelerometers. Attention is given to the unique conditions for application of laser gyro IMUs to army missiles, the general parameters of strapdown IMUS, strapdown navigation software, operating modes, and the performance evaluation system. ABA B.J.

76/00/00 77A37432
LOW COST INERTIAL GUIDANCE WITH GPS UPDATE FOR TACTICAL WEAPONS
Cox, J.W.
(USAF, Armament Laboratory, Eglin AFB, Fla.)
In NAECON '76; Proceedings of the National Aerospace and Electronics Conference, Dayton, Ohio, May 18–20, 1976. (A77-37352 17-33) New York, Institute of Electrical and Electronics Engineers, Inc., 1976, p.623-626.

The Air Force Armament Laboratory has recently initiated new efforts to develop a low cost inertial guidance subsystem (LCIGS) for tactical guided weapons. The efforts are to: (1) define the inertial strapdown subsystem requirements, (2) design, develop and test an engineering model LCIGS, and (3) develop new low cost inertial instruments for long range improvement of performance and reduction cost. The result will be a design data package suitable for a competitive, non-proprietary procurement of inertial strapdown subsystems. LCIGS will be optimally designed to receive position and/or velocity updates from alternative navigation schemes such as Navstar global positioning system. A digital processor will be designed to handle system integration for a modular family of tactical missile configurations. ABA author.

77/00/00 78A14944
MICROPROCESSOR APPLICATIONS IN STRAPDOWN INERTIAL NAVIGATION
Napjus, G.A.
(Teledyne Systems, Northridge, Calif.)
In Military Electronics Defence Expo '76; Proceedings of the Conference, Wiesbaden, West Germany, October 6–8, 1976. (A78-14926 03-33) Geneva, Interavia, S.A., 1977, p.514-526.

Attention is given to strapdown inertial navigation systems and their advantages over gimbal systems. The system uses three limited-capacity microcomputers in place of a minicomputer, and microprocessor techniques in place of analog electronics in the gyroscope control loops for inertial sensor control. Microprocessor flexibility may be applied to redundant strapdown navigation systems and associated digital flight control systems, such as for the navigation, guidance, and control of commercial aircraft, fighter aircraft, space vehicles, and sounding rockets. ABA S.C.S.

73/00/00 73A27168
MICROPROGRAMMED DIGITAL FILTERS FOR STRAPDOWN GUIDANCE APPLICATION
Kapadia, K.; Dunn, W.R.
(Santa Clara, University, Santa Clara, Calif.)
In Asilomar Conference on Circuits and Systems, 6th, Pacific Grove, Calif. November 15–17, 1972, Conference Record. (A73-27151 12-10) North Hollywood, Calif., Western Periodicals Co., 1973, p.419-423.

Discussion of an approach for implementing digital filters using microprogrammed control logic with read only memory (ROM) for strapdown guidance applications, and description of a second-order multiplexed system using multiprogrammed control instruction. The microprogramming technique for control using ROM is shown to enhance higher order digital filter realization. The high speed of digital circuits reduces propagation time and facilitates multiplexing. Programmed ROM's can be altered easily for different algorithms. ABA M.V.E.

73/00/00 73A40037
MICRON A STRAPDOWN INERTIAL NAVIGATOR USING MINIATURE ELECTROSTATIC GYROS
Duncan, R.R.
(Rockwell International Corp., Autonetics Div., Anaheim, Calif.)
In National Aerospace Meeting, Washington, D.C., March 13, 14, 1973, Proceedings. (A73-40035 21-21) Washington, D.C., Institute of Navigation, 1973, p.13-23. USAF-supported research.

An overview is presented of a small, low cost, strapdown, inertial navigator (Micron) which uses two miniature electrostatically suspended gyros (MESG's) to establish the required inertial frame. The system performance goals are a position error of 1 nm/h CEP rate, a velocity error of 5 ft/sec rms per axis and an attitude error of 4 min of arc rms per axis. The physical characteristics of the MESG instrument are defined with particular reference to the unique whole angle attitude readout scheme. The latter is achieved by electrically sensing a deliberate radial mass unbalance of the rotor within the MESG. The analytic modeling fundamentals of the calibration techniques for gyro drift rate and whole angle readout are presented. Functional block diagrams of the Micron experimental demonstration system are illustrated with detailed

B-30

discussion of the gyrocompass alignment and navigation mechanization applicable to the Micron strapdown system. ABA.

76/00/00 77A37438
MICRON LIFE CYCLE COST PREDICTION MODEL
Gibson, K.J.
(Rockwell International Corp., Autonetics Group, Anaheim, Calif.)
In NAECON '76; Proceedings of the National Aerospace and Electronics Conference, Dayton, Ohio, May 18–20, 1976. (A77-37352 17-33) New York, Institute of Electrical and Electronics Engineers, Inc., 1976, p.674-681.

Micron is a strapdown inertial navigator which uses the microelectrostatically supported gyro. The Micron model is analytical, employing cost estimating algorithms based on average maintenance rates, repair times, test characteristics, etc. Spares requirements are calculated using a Poisson cost minimization routine. Some parametric relationships are provided for estimating data page counts and training requirements. ABA B.J.

77/00/00 78A15643
MIRA – THE MULTIFUNCTION INERTIAL REFERENCE ASSEMBLY
Harrington, E.V., Jr; Bell, J.W; Raroha, G.H.
(USAF, Avionics Laboratory, Wright-Patterson AFB, Ohio)
In NAECON '77; Proceedings of the National Aerospace and Electronics Conference, Dayton, Ohio, May 17–19, 1977. (A78-15551 04-33) New York, Institute of Electrical and Electronics Engineers, Inc., 1977, p.783-787.

The MIRA is being developed to satisfy the combined kinematic data requirements of flight control, navigation, weapon delivery and terminal area control, the key to practical implementation of these sensor functions being the digitilazation of avionic and flight control functions. This paper describes basic MIRA concepts with attention given to sensor commonality and data utilization, location considerations and redundancy. ABA B.J.

74/00/00 74A35242
NEW DEVELOPMENT IN HIGH RELIABILITY STRAPDOWN PLATFORMS USING TDF SENSORS
Tsuei, Y.D.; Hung, J.C.
(Tennessee, University, Knoxville, Tenn.)
In Joint Automatic Control Conference, 15th, Austin, Tex., June 18–21, 1974, Proceedings. (A74-35232 17-10) New York, American Institute of Chemical Engineers, 1974, p.83-91.

New development in high reliability strapdown navigation platform using two-degree-of-freedom sensors and redundancy concept is presented in this paper. The development is based on the assumption that each axis of the sensor can fail without affecting the remaining axis. The systems reliability is investigated, the optimum redundancy configurations are proposed, a technique of sensor performance management is developed for the proposed systems. ABA author.

76/00/00 77A20655
New Frontiers in Aerospace Navigation; Proceedings of the Bicentennial National Aerospace Symposium, Warminister, Pa., April 27, 28, 1976. Symposium sponsored by the Institute of Navigation and US Navy. Washington, D.C., Institute of Navigation, 1976, 162p.

The present collection of papers is concerned with advances in aerospace navigation, from the latest aerospace applications of celestial, radio, inertial and satellite navigation to the development of sophisticated navigation systems such as laser gyros. Featured topics include improved navigation using adaptive Kalman filtering, navigation for sea-based remotely piloted vehicles, ring laser gyro strapdown systems, and microwave holographic imaging of aircraft with space-borne illuminating source. Additional developments in software will further improve navigation accuracy in terms of prediction, correction and more complete control of the navigation process. Individual items are announced in this issue. ABA S.D.

75/00/00 75A37623
NAECON '75; Proceedings of the National Aerospace and Electronics Conference, Dayton, Ohio, June 10–12, 1975. Conference sponsored by the Institute of Electrical and Electronics Engineers. New York, Institute of Electrical and Electronics Engineers, Inc., 1975, 768 p.

Papers are presented dealing with advances in electronic components, hardware, software, and systems for a wide variety of applications, including communications, radar, weapon systems, avionics, electrooptical imaging, satellite and radio navigation, cybernetic systems, and environmental measurements and data processing. Some of the topics covered include a wideband data link computer simulation model, optimal linear tracking of vehicles with uncertain system models, a multimegawatt fuel cell power system, design of a modular avionic processor, the blue-spot electrooptical sensor/laser, and 4-D navigation using integrated strapdown inertial/differential Loran. Individual items are announced in this issue. ABA P.T.H.

FOA-2-C-2674-E4 74/06/00 76N71450
ON ALGORITHMS FOR ATTITUDE EVALUATION IN NAVIGATION SYSTEMS WITH STRAPDOWN COMPONENTS
Wolff, P.
Research Inst. of National Defence, Stockholm (Sweden)

B-31

76/03/00 76A26389
ON THE CONVERGENCE OF ITERATIVE ORTHOGONALIZATION PROCESSES
Bar-Itzhack, I.Y.; Meyer, J.
(Technion – Israel Institute of Technology, Haifa, Israel)
IEEE Transactions on Aerospace and Electronic Systems, Vol. AES-12, March 1976, p.146-151

It is necessary in many aerospace systems (e.g., strapdown inertial guidance) to periodically transform vectors from a rotating Cartesian coordinate system to a reference Cartesian system. But since the corresponding computational algorithm is not perfect the resultant transformation matrix is often not orthogonal. An orthogonalization process is used to obtain an estimate of the correct orthogonal transformation matrix in order to correct the nonorthogonality error of the matrix. Polar decomposition of matrices is used to study the convergence properties of this iterative orthogonalization process. In applying this decomposition, the investigation of a general iterative process of a certain form can be reduced to the investigation of a scalar iterative process. ABA B.J.

74/00/00 74A38589
OPTIMAL GYRO MOUNTING CONFIGURATIONS FOR A STRAPDOWN SYSTEM
Giardina, C.R.
(Singer Co., Kearfott Div., Little Falls; Fairleigh Dickinson University, Rutherford, N.J.)
In NAECON '74; Proceedings of the National Aerospace and Electronics Conference, Dayton, Ohio, May 13–15, 1974. (A74-38517 19-09) New York, Institute of Electrical and Electronics Engineers, Inc., 1974, p.584-591.

New gyro mounting procedures, failure detection, isolation and data reduction techniques have been determined for high reliable redundant strapdown systems utilizing two degree of freedom (TDF) gyros. ABA author.

76/00/00 77A51193
OPTIMAL ORTHONORMALIZATION OF STRAPDOWN GUIDANCE SYSTEMS
Bar-Itzhack, I.Y.
(Technion – Israel Institute of Technology, Haifa, Israel)
In Position Location and Navigation Symposium, San Diego, Calif., November 1–3, 1976, Proceedings. (A77-51178 24-04) New York, Institute of Electrical and Electronics Engineers, Inc., 1976, p.122-127.

The requirement for orthonormalization of the direction cosine matrix (DCM) in strapdown guidance systems is explained. The orthonormalization problem is formulated in mathematical terms and a closed form solution is given in two equivalent forms. Three iterative processes to compute this matrix are introduced in order to alleviate the problem of computing square roots of matrices needed for the closed form solution. Using polar decomposition of matrices the convergence rate and range of the iterative processes are investigated. Finally, the computational effort required for the implementation of the iterative processes is examined theoretically and empirically. It is concluded that the 'dual process' is superior and should be used whenever the DCM is computed directly. ABA author.

77/04/00 77A32943
PERFORMANCE OF A FRENCH AIRBORNE OMEGA RECEIVER AND OUTLOOK FOR ITS USE
Kergoat, H.
(Secretariat General à l'Aviation Civile, Service Technique de la Navigation Aerienne, Paris, France)
Navigation (Paris), Vol.25, April 1977, p.167-174. In French.

Results of flight tests and ground tests on a French airborne automatic Omega receiver are described. A novel phase correction technique offers the user improved protection against propagation anomalies (including SID and polar cap absorption fadeout problems), and more compact memory space. A possible future for the Crouzet-Sercel Omega receiver described in civil aviation applications is envisaged, in view of the attitude (vertical, heading) information it can furnish, and its strapdown inertial performance. ABA R.D.V.

AIAA 77-1039 77/00/00 77A42755
PERFORMANCE TESTS OF TWO PRECISION ATTITUDE DETERMINATION SYSTEMS
McAloon, K.J.; Farrenkopf, R.L.; Belsky, F.J.; Mann, R.J.
(TRW Defense and Space Systems Group, Redondo Beach, Calif.)
TRW Defense and Space Systems Group, Redondo Beach, Calif. In Guidance and Control Conference, Hollywood, Fla., August 8–10, 1977, Technical Papers. (A77-42751 20-35) New York, American Institute of Aeronautics and Astronautics, Inc., 1977, p.24-32.

Results of laboratory performance tests of two satellite attitude determination systems are given. One system employed a strapdown star tracker and gyro assembly, the other a single axis, gimballed star tracker and a gyro assembly. The laboratory tests simulated those orbit conditions which would be experienced on a three axis stabilized, earth pointed satellite in geosynchronous orbit. A ground-fixed laboratory test was performed in which system axes remained stationary in the laboratory coordinates while revolving star beams stimulated the star trackers. The laboratory instrumentation techniques used to meet the stringent accuracy requirements are described. Results are presented which show both systems met the performance goal of 3.6 arc seconds. Comparative analyses of both systems are also discussed. ABA author.

B-32

75/05/00 75A36239
PLATFORM ALIGNMENT USING A STRAPDOWN STELLAR SENSOR
Nash, J.M.; Wells, G.R.
(Logicon, Inc., San Pedro, Calif.)
AIAA Journal, Vol.13, May 1975, p.659-664.

This paper examines the use of a body-mounted stellar-sighting device to align an aerospace vehicle's gimballed inertial measurement unit. The fundamental observability of not only platform misalignments but also time-invariant sensor-mounting errors is demonstrated. The performance of an inflight estimation algorithm is shown to be a function of several environmental and navigation hardware parameters as well as the characteristics of the sighting device itself. Parametric case studies are presented for a sample system. ABA author.

77/05/00 77A35839
PRACTICAL COMPARISON OF ITERATIVE MATRIX ORTHOGONALIZATION ALGORITHMS
Meyer, J.; Bar-Itzhack, I.Y.
(Technion – Israel Institute of Technology, Haifa, Israel)
IEEE Transactions on Aerospace and Electronic Systems, Vol. AES-13, May 1977, p.230-235.

Three promising algorithms for orthogonalizing the direction cosine matrix employed in strapdown inertial navigation and similar arrangements to describe the rotation of a coordinate system relative to a reference coordinate system are introduced; convergence rate and range of the algorithms were investigated. The variant dubbed dual algorithm is found far superior to the other two in speed, computer memory, accuracy, and convergence rate. ABA R.D.V.

75/00/00 75A37204
PRECISION ON-BOARD ATTITUDE REFERENCE USING THE GENERALIZED INVERSE
McElroy, T.T.; Iwens, R.P.
(TRW Systems Group, Redondo Beach, Calif.)
In Annual Allerton Conference on Circuit and System Theory, 12th, Monticello, Ill., October 2–4, 1974, Proceedings. (A75-37201 17-63) Urbana, Ill., University of Illinois, 1975, p.180-184.

A sequential estimation algorithm is presented for spacecraft attitude determination using the generalized inverse (pseudo-inverse). Relative to the Kalman filter, computational requirements are significantly reduced. The sensors used are a three-axis strapdown gyro package and strapdown star trackers. Digital simulation in conjunction with a truth model is employed to evaluate performance, indicating three-axis accuracy better than 30 arc seconds. ABA author.

67/00/00 77A37415
PRECISION POINTING USING STRAPDOWN GYRO TECHNIQUES
Gilmore, J.; Bukow, G.
(Charles Stark Draper Laboratory, Inc., Cambridge, Mass.)
In NAECON '76; Proceedings of the National Aerospace and Electronics Conference, Dayton, Ohio, May 18–20, 1976. (A77-37352 17-33) New York, Institute of Electrical and Electronics Engineers, Inc., 1976, p.479-488.

This paper presents a mechanization for the maintenance of an inertially referenced pointing system line-of-sight. The approach presented utilizes a wide bandwidth strapdown gyro package mounted to the line-of-sight control member. The strapdown package is uniquely suited for pointing applications requiring high resolution angle measurement over a wide dynamic range. The gyro also can provide inertial rate sensing and control for the pointing system. Illustrative data is presented showing arcsecond measurement accuracy over large angle rotations at high rates. Field site test results on a 48-in optical telescope are also presented indicating wide band low-noise gyro sensing capability and its applicability for pointing, stabilization, and tracking control. ABA author.

77/00/00 77A39519
PROJECT WORK ON A STRIKE RPV
Spintzyk, J.
Dornier-Post (English Edition), No.2, 1977, p.26-29.

A proposal for a highly cost-effective strike RPV with high deterrent value is outlined. The RPV is intended for launch from rear fields for sorties against previously reconnoitred mobile or fixed targets. Both outward and return flight are pre-programmed and take place near the ground at high speeds. Low-level bombing is carried out without terminal guidance. Landing is automatic. A hybrid navigation system, with a strapdown inertial system for air-derived navigation, is under consideration. A configuration with fuselage-stored weapons and external engines appears suitable. ABA C.K.D.

75/00/00 76A23145
PROPAGATING RESPONSES OF LINEAR SYSTEMS INVOLVING NOISY, TIME-DEPENDENT DYNAMICS
Bowles, W.M.; Sebesta, H.R.
(Oklahoma State University, Stillwater, Okla.)
In Modeling and Simulation. Volume 6 – Proceedings of the Sixth Annual Pittsburgh Conference, Pittsburgh, Pa., April 24, 25, 1975. Part 1. (A76-23110 09-59) Pittsburgh, Pa., Instrument Society of America, 1975, p.511-515.

The employment of two approaches in the study of the responses of time-varying, linear, vector-matrix differential

equations of a given form is considered, taking into account Galerkin's technique and a commutative algorithm. It is found that Galerkin's method may be used to develop accurate propagation algorithms with low sensitivity to high frequency noise. The commutative methods provide generally more computationally efficient algorithms. ABA G.R.

B-33

73/11/00 74A19402
PROPAGATION AND SYSTEM ACCURACY IMPACT OF MAJOR SENSOR ERRORS ON A STRAPDOWN AIRCRAFT NAVIGATOR
Stambaugh, J.S.
(Singer Kearfott Research Center, Little Falls, N.J.)
IEEE Transactions on Aerospace and Electronic Systems, Vol. AES-9, November 1973, p.838-846.

A strapdown system is considered as an unaided inertial navigator aboard an aircraft. Presented here are simulation results detailing the propagation of navigation errors (in nautical miles) due to strapdown sensor errors for four trajectories. They indicate the type of performance that can be expected from a strapdown system utilizing good off the shelf gyros and accelerometers, and dramatically illustrate the improvements necessary in these components to obtain navigation performance comparable to that available from a good gimballed inertial system. The total navigation error for each trajectory is broken down to show the contribution from each of the various error sources. This breakdown quickly reveals which are the critical error sources for a given trajectory class, and also points up the relationship that exists between each individual error source, aircraft maneuvers, and the resulting navigation error. ABA author.

NASA-CR-86198-(DEL) TRW-07398-6027-RO-00-(DEL) 68/11/00 74N70335
RADIO/OPTICAL/STRAPDOWN INERTIAL GUIDANCE STUDY FOR ADVANCED KICK STAGE APPLICATIONS. VOLUME 2: DETAILED STUDY RESULTS (TASKS 3 AND 4). PART 2: PRELIMINARY MODULAR DESIGN (DEL.)
TRW Systems Group, Redondo Beach, Calif.

NASA-CR-140328 E-2398 69/06/00 75N70026
REAL-TIME STRAPDOWN-ATTITUDE PACKAGE EVALUATIONS
Gilmore, J.P.; McKern, R.A.; Swanson, D.W.
Massachusetts Inst. of Tech., Cambridge. (Instrumentation Lab.)
Presented at AIAA Guidance, Control and Flight Mech. Conf., Princeton, N.J., August 1969.

75/00/00 76A11840
RECENT ADVANCES IN STRAPDOWN INERTIAL NAVIGATION
Napjus, G.A.
(Teledyne Systems Co., Northridge, Calif.)
Teledyne Systems Co., Northridge, Calif. In Intercon 75; International Convention and Exposition, New York, N.Y., April 8-10, 1975, Conference Record. (A76-11826 02-33) New York, Institute of Electrical and Electronics Engineers, Inc., 1975, p. 1 35/1-5 35/1.

The computational requirements and basic features of strapdown gyroscopes for inertial navigation are discussed. Strapdown navigators currently require 20 to 50% of the available time of a minicomputer with a capability of several hundred thousand operations per second; memory requirements are 2000 to 3000 16-bit words. A system in which these computational demands are met by three limited capability microcomputers is described. A technique using dedicated microprocessors in the place of analog electronics in the gyroscope control loops is discussed, and attention is given to applications of microprocessor technology in redundant strapdown navigation systems and associated flight control systems. ABA C.K.D.

AIAA Paper 73-898 73/08/00 73A38833
RECENT TEST RESULTS - A STRAPDOWN IMU UTILIZING HYDRODYNAMIC SPIN BEARING RATE SENSORS AND PULSE REBLANCE LOOPS
Dieselman, J.; McNeil, J.; Callahan, J.
(Northrop Corp., Precision Products Dept., Norwood, Mass.)
American Institute of Aeronautics and Astronautics, Guidance and Control Conference, Key Biscayne, Fla., August 20-22, 1973, 10p.

AIAA Paper 73-852 73/08/00 73A41969
REDUNDANCY MANAGEMENT OF INERTIAL SYSTEMS
McKern, R.A.; Musoff, H.
(MIT, Cambridge, Mass.)
American Institute of Aeronautics and Astronautics, Guidance and Control Conference, Key Biscayne, Fla., August 20-22, 1973, 11p.

The paper reviews developments in failure detection and isolation techniques applicable to gimballed and strapdown systems. It examines basic redundancy management goals of improved reliability, performance and logistic costs, and explores mechanizations available for both input and output data handling. The meaning of redundant system reliability in terms of available coverage, system MTBF, and mission time is presented and the practical hardware performance

B24

limitations of failure detection and isolation techniques are explored. Simulation results are presented illustrating implementation coverages attainable considering IMU performance models and mission detection threshold requirements. The implications of a complete GN & C redundancy management method on inertial techniques are also explored. ABA author.

AIAA 77-1109 77/00/00 77A42808
REDUNDANT INTEGRATED FLIGHT CONTROL/NAVIGATION INERTIAL SENSOR COMPLEX
Ebner, R.E.; Mark, J.G.
(Litton Systems, Inc., Woodland Hills, Calif.)
Litton Systems, Inc., Woodland Hills, Calif. In Guidance and Control Conference, Hollywood, Fla., August 8–10, 1977, Technical Papers. (A77-42751 20-35) New York, American Institute of Aeronautics and Astronautics, Inc., 1977, p.503-511.

A redundant strapdown inertial navigation system for integrated flight control/navigation use is described. Design of the system, which consists of four tuned-gimbal gyros, eight accelerometers, and four processors, is discussed, with emphasis on its compact configuration (13 by 13 by 14 in), based on symmetry properties of an octahedron. A matrix operator for least-squares combination of data from an arbitrary number of two-degree-of-freedom gyros is derived, and general parity equations for error analysis are given. Self-contained detection and isolation of a two-axis gyro failure is considered; system failure probability, which depends on component failure rates and self-correction capacities, is analyzed. Test data, including typical parity equation responses during motion and simulated gyro and accelerometer failures, are also presented. ABA J.M.B.

76/00/00 77A51191
REDUNDANT CAROUSEL STRAPDOWN GUIDANCE SYSTEM
Oshika, E.M.; Parziale, A.J.
(General Motors Corp., Goleta, Calif.)
In Position Location and Navigation Symposium, San Diego, Calif., November 1–3, 1976, Proceedings. (A77-51178 24-04) New York, Institute of Electrical and Electronics Engineers, Inc., 1976, p.106-115.

This paper describes the design principles applied to obtain a highly reliable, low cost navigation system with unique performance features. The redundant Carousel strapdown system uses proven components in a novel configuration to obtain significant performance increases. The benefits of low cost and high component reliability are obtained by using components derived from parts in volume production for the Carousel IV aircraft navigator, Carousle V (USGS) space navigator and the F-16 fire control computer. On the system level, improved reliability and navigation accuracy are obtained by using a redundant configuration that allows the advantages of the Carousel technique to be applied to all of the navigation sensors. The configuration results in the practical elemination of attitude drift during free fall space flight, while maintaining the accurate self-alignment features of the USGS space navigator. The combination of redundant sensors with the Carousel technique also results in a simple and unique failure detection procedure to isolate subsystem failures. ABA author.

76/00/00 76A47228
REDUNDANT STRAPDOWN LASER GYRO NAVIGATION SYSTEM
McPherson, B.W.; Walls, B.F.; White, J.B.
(IBM Corp., Huntsville, Ala.); (NASA, Marshall Space Flight Center, Huntsville, Ala.)
International Business Machines Corp., Huntsville, Ala.; National Aeronautics and Space Adminstration. Marshall Space Flight Center, Huntsville, Ala. In Engineering in a Changing Economy; Proceedings of the Southeast Region 3 Conference, Clemson, S.C., April 5–7, 1976. (A76-47201 24-99) New York, Institute of Electrical and Electronics Engineers, Inc., 1976, p.224-226.

For the last several years, NASA has pursued the development of low-cost high-reliability inertial navigation systems that would satisfy a broad spectrum of future space and avionics missions. Two specific programs have culminated in the construction of a redundant strapdown laser gyro navigation system. These two programs were for development of a space ultrareliable modular computer (SUMC) and a redundant laser gyro inertial measurement unit (IMU). The SUMC is a digital computer that employs state-of-the-art large-scale integrated circuits configured in a functional modular breakdown. The redundant laser gyro IMU is a six-pack strapdown sensor package in a dodecahedron configuration which uses six laser gyros to provide incremental angular positions and six accelerometers for linear velocity outputs. The sensor arrangement allows automatic accommodation of two failures; a third failure can be tolerated provided it can be determined. The navigation system also includes redundant power supplies, built-in test-equipment (BITE) circuits for failure detection, and software which provides for navigation, redundancy management, and automatic calibration and alignment. ABA author.

AIAA Paper 74-893 77/08/00 74A37874
RETROACTIVE FAILURE CORRECTION FOR STRAPDOWN REDUNDANT INERTIAL INSTRUMENTS
Wilcox, J.C.
(TRW Systems Group, Redondo Beach, Calif.)
American Institute of Aeronautics and Astronautics, Mechanics and Control of Flight Conference, Anchelm, Calif., August 5–9, 1974, 7 p.

An algorithm is derived that eliminates the errors that build up in a redundant strapdown inertial navigator between the time that a soft failure occurs and the time that it is isolated and the failed instrument taken off-line. (Hard failures are isolated before any erroneous data is used, by definition.) Although the algorithm is presented for the dodecahedron configuration as an example, it is applicable to any redundant system which uses least squares to combine the outputs of the unfailed instruments. Since only soft failures need be retroactively corrected, the errors involved are small and linearization can be used to reduce the data storage and computational requirements. ABA author.

B-3

73/00/00 73A38057
SENSOR CONCEPT AND ALGORITHMS FOR A COMPLETELY STRAPDOWN AUTONOMOUS NAVIGATION APPROACH
Kau, S.P.; Paulson, D.C.
(Honeywell, Inc., Aerospace Div., St Petersburg, Fla.)
In Joint Automatic Control Conference, 14th, Columbus, Ohio, June 20–22, 1973, Preprints of Technical Papers. (A73-38028 19-10) New York, Institute of Electrical and Electronics Engineers, Inc., 1973, p.643, 644.

NASA-CR-147679 REPT-0872-11055-VOL-1 72/10/06 76N75141
SPACE SHUTTLE STRAPDOWN INERTIAL MEASURING UNIT PROGRAM ANALYSIS. VOLUME 1: MANAGEMENT SUMMARY
Honeywell, Inc., St Petersburg, Fla. (Aerospace Div.)

NASA-CR-147680 REPT-0872-11055-VOL-2 72/10/06 76N75142
SPACE SHUTTLE STRAPDOWN INERTIAL MEASURING UNIT PROGRAM ANALYSIS. VOLUME 2: TECHNICAL
Honeywell, Inc., St Petersburg, Fla.

AAS Paper 75-144 75/08/00 76A12790
SPACE TUG LASER GYRO IMU
Morrison, R.; Walls, B.
(Sperry Rand Corp., Sperry Gyroscope, Great Neck, N.Y.); (NASA, Marshall Space Flight Center, Huntsville, Ala.)
National Aeronautics and Space Administration. Marshall Space Flight Center, Huntsville, Ala.; Sperry Rand Corp., Great Neck, N.Y. AAS, AIAA, IEEE, ORSA, and IMS, Meeting on Space Shuttle Missions of the 80's, Denver, Colo., August 26–28, 1975, AAS 20 p.

A redundant inertial measuring unit (IMU) incorporating six strapdown laser gyros and six accelerometers, arranged so that sensitive axes are normal to the faces of a dodecahedron, provides enhanced reliability with reduced hardware weight. Software monitoring of sensor outputs senses failure of sensors and the system is designed for triple redundancy, with built-in test equipment. Attention is centered on redundancy and fail-safe features, and on the closed-path ring laser gyro arrangement. ABA R.D.V.

73/03/00 73A36955
STRAP-DOWN INERTIAL GUIDANCE SYSTEMS STUDY
Fontana, R.B.
(Officine Galileo S.P.A., Florence, Italy)
(NATO, AGARD, Symposium on Inertial Navigation Components and Systems, Florence, Italy, October 2–5, 1972.)
Revue Scientifique et Technique Ceeles/Cers, Vol.5, January–March 1973, p.35-37.

Possible instrumentation for use in a strap-down system is considered, and a pendulum accelerometer and rate integrating gyro are found to be suitable. The environmental factors are determined, and the resulting instrumentation errors are estimated. These, together with the estimates of digital computation errors, are used to find the resulting injection errors for a typical Europa vehicle mission. ABA author.

74/00/00 74A38587
STRAPDOWN ATTITUDE AND HEADING REFERENCE SYSTEM
Donoghue, P.J.
(Lear Siegler, Inc., Grand Rapids, Mich.)
In NAECON '74; Proceedings of the National Aerospace and Electronics Conference, Dayton, Ohio, May 13–15, 1974. (A74-38517 19-09) New York, Institute of Electrical and Electronics Engineers, Inc., 1974, p.556-563.

This paper presents the problem formulation, system models, analysis and simulation results obtained for an aided strapdown attitude and heading reference system utilizing a Kalman filter. The results presented provide a baseline of achievable performance for an airspeed and compass aided reference system, as well as the basis for predicting corresponding strapdown navigator performance. ABA author.

74/07/00 74A37289
STRAPDOWN GUIDANCE ERROR ANALYSIS
Mortensen, R.E.
(California, University, Los Angeles, Calif.)
IEEE Transactions on Aerospace and Electronic Systems, Vol. AES-10, July 1974, p.451-457.

B-36

A crucial part of so-called 'strapdown' techniques for inertial guidance systems is the generation of the matrix of direction cosines relating the body axes to the reference axes. This is generally done by direct integration of a set of differential equations having the body angular velocities as inputs. This paper is devoted to an error analysis of two commonly used integration schemes, namely, direction cosines and quaternions. Scale, skew, and drift errors are defined, and the susceptibility of the integration schemes to these types of error is examined. It is concluded that the quaternion scheme offers an advantage because it intrinsically yields zero skew error. The paper is presented in two parts, for convenience. ABA author.

77/00/00 77A40782
STRAPDOWN INERTIAL NAVIGATION – THE GYROSCOPE CHALLENGE
Harris, D.G.
(Marconi-Elliott Avionic Systems, Ltd., Rochester, England)
In Applications of Modern Gyro Technology; Proceedings of the Symposium, London, England, January 12, 1977. (A77-40776 19-17) London. Royal Aeronautical Society, 1977, 15 p.

The development of inertial navigation technology is surveyed, with comparison made between the two alternative systems, gimballed and strapdown. Aside from the three sensors, the three gyro stable platform used in gimballed systems includes electronic equipment, the failure of which is frequently an error source in the system.. In contrast, strapdown devices require only the triad of sensors, thus reducing failures and maintenance problems. To implement the strapdown gyro concept, a high-performance angular sensor is needed, providing drift stability of .01 degree per hour, high dynamic range, and ability to rapidly stabilize in a wide range of temperatures. Four candidates for strapdown design are described single degree of freedom rate integrating gyros; two degree of freedom 'dry' gyros; electrostatically suspended gyros; and ring laser gyros. Advantages of the ring laser system are emphasized, including economy, simpler manufacture, easier handling, and much improved reliability; design programs for the system are summarized, among them development of interface circuits between sensors and computers, and development of computer programs. ABA J.M.B.

73/00/00 73A40036
STRAPDOWN INERTIAL NAVIGATION PRACTICAL CONSIDERATIONS
Halamandaris, H.
(Teledyne Systems, Co., Northridge, Calif.)
In National Aerospace Meeting, Washington, D.C., March 13, 14, 1973, Proceedings. (A73-40035 21-21) Washington, D.C., Institute of Navigation, 1973, p.1-12.

This paper delineates a concept of strapdown navigation using dry inertial instruments and a high speed, general purpose digital computer. Distinct life cycle cost advantages are shown for both support-to-acquisition cost and cost-per-flying hour for the strapdown system. Further, the strapdown system is compared to gimbaled systems using dry instruments characteristic of the present technology and floated instruments employed in current systems. Several redundant instrument configurations are presented with their attendant relative merits. The strapdown system imposes additional computer constraints since the attitude matrix must be propagated in real time. Primary constraints are duty cycle and storage requirements. Two basic attitude propagation algorithms are presented. These two mechanizations are direction cosines and quaternions. Implementation considerations reflecting service rates and drift errors as a function of integration algorithm are presented. ABA author.

73/00/00 73A35211
STRAPDOWN INERTIAL NAVIGATION PRACTICAL CONSIDERATIONS
Halamandaris, H.
(Teledyne Systems Co., Northridge, Calif.)
In NAECON 73; Proceedings of the National Aerospace Electronics Conference, Dayton, Ohio, May 14–16, 1973. (A73-35201 17-09) New York, Institute of Electrical and Electronics Engineers, Inc., 1973, p.82-91.

This paper delineates a concept of strapdown navigation using dry inertial instruments and high speed, general purpose digital computer. Distinct life cycle cost advantages are shown for both support-to-acquisition cost and cost-per-flying hour for the strapdown system. Further, the strapdown system is compared to gimbaled systems using dry instruments characteristic of the present technology and floated instruments employed in current systems. Several redundant instrument configurations are presented with their attendant relative merits. The strapdown system imposes additional computer constraints since the attitude matrix must be propagated in real time. Primary constraints are duty cycle and storage requirements. Two basic attitude propagation algorithms are presented. These two mechanizations are direction cosines and quaternions. ABA author.

73/04/00 73A26377
STRAPDOWN INERTIAL SYSTEM ALIGNMENT USING STATISTICAL FILTERS – A SIMPLIFIED FORMULATION
Deyst, J.J., Jr; Sutherland, A.A., Jr
(MIT, Cambridge, Mass.); (Analytic Sciences, Corp., Reading Mass.)
AIAA Journal, Vol.11, April 1973, p.452-456.

76/01/00 76A20779
STRAPDOWN MATRIX ORTHOGONALIZATION – THE DUAL ITERATIVE ALGORITHM
Bar-Itzhack, I.Y.; Meyer, J.; Fuhrmann, P.A.
(Technion – Israel Institute of Technology, Haifa, Israel); (Negev, University, Beersheba, Israel)
IEEE Transactions on Aerospace and Electronic Systems, Vol. AES-12, January 1976, p.32-38.

There exist several algorithms for the optimal orthogonalization of the direction cosine matrix used in navigation, control and simulation. One of these recursive algorithms is shown to be derived form a dual solution to the optimal orthogonalization problem. The duality of the algorithm is demonstrated and its convergence properties are investigated. Quadratic convergence is proven and the condition for convergence is determined and illustrated with numerical examples. ABA author.

AIAA Paper 77-1105 77/08/00 77A51619
STRAPDOWN NAVIGATION TECHNOLOGY – A LITERATURE SURVEY
Garg, S.C.; Morrow, L.D.; Mamen, R.
(Toronto, University, Toronto, Canada); (SPAR Aerospace Products, Ltd., Toronto, Canada); (Department of Communications, Ottawa, Canada)
American Institute of Aeronautics and Astronautics, Guidance and Control Conference, Hollywood, Fla., August 8–10, 1977, 18 p.

This paper presents the results of a comprehensive literature survey of approximately 300 technical papers and reports on strapdown navigation technology. It provides a general survey for those seeking a source of references and an overview of the entire field. The paper does not dwell on comparisons between strapdown and gimballed systems. Rather, it aims at an organized and coherent summary of existing work on strapdown technology by reviewing the following topics basic terms and concepts, strapdown components, analytical aspects, error generation and propagation, system data processing, reliability enhancement and current trends. An extensive bibliography is included. ABA author.

NASA-CR133055 TR-147-1 70/01/31 73N72958
STRAPDOWN SENSOR TESTS AND TEST DATA ANALYSIS
Crawford, B.S. AV026075

73/07/00 73A37876
STRAPPED DOWN INERTIAL NAVIGATION SYSTEMS
Collinson, R.P.G.
(Marconi-Elliott Avionics Systems, Ltd., Rochester, England)
Journal of Navigation, Vol.26, July 1973, p.341-351.

The basic ingredients of these navigation systems are discussed, covering vehicle orientation measurement techniques, the Euler angle computer, gyro systems and latitude and longitude computation procedures. The advantages of these systems are summarized as reliability, simpler temperature control, lower power consumption, simplified build and commission phase, reduced investment, lower grade servicing skills, largely solid state electronics, lower development costs, size and weight reduction through the elimination of gimballing system, flight control with body-referenced data, and economical redundancy for failure absorption. Strapped down systems are characterized as a major step in inertial navigation technology, eliminating the complexity of gimballing systems and providing the major advantages of greater reliability, lower costs, lower power consumption, and excellent failure absorption characteristics. ABA V.Z.

NAL-TR-349 75/11/00 76N6235
STUDY ON A WIDE ANGLE MINIATURE INTEGRATING GYRO FOR STRAPDOWN SYSTEM
Otsuki, M.; Shingu, H.; Suzuki, T.; Enkyo, S.; Tabata, J.
National Aerospace Lab., Tokyo (Japan)

77/00/00 78A15641
SYSTEM DESCRIPTION AND PERFORMANCE CHARACTERISTICS OF A QUAD REDUNDANT STRAPDOWN INERTIAL NAVIGATION AND FLIGHT CONTROL SYSTEM
Donoghue, P.J.
(Teledyne Systems Co., Northridge, Calif.)
In NAECON '77; Proceedings of the National Aerospace and Electronics Conference, Dayton, Ohio, May 17-19, 1977. (A78-15551 04-33) New York, Institute of Electrical and Electronics Engineers, Inc., 1977, p.767-774.

This paper describes the system design and development of a quadruply redundant strapdown inertial information and computation system. This system was developed for application to a digital fly-by-wire controlled configuration vehicle. Design rationale and implementation of the sytem are described in four major areas: (1) sensors, (2) digital conversion techniques (3) digital computer and (4) systems implementation. ABA author.

B30

73/00/00 73A38058
SYSTEM ERROR ANALYSIS AND ALGORITHMS FOR A STRAPDOWN NAVIGATION SYSTEM
Nelson, J.B.; Lochrie, W.D.
(McDonnel Douglas Astronautics Co., St Louis, Mo.)
In Joint Automatic Control Conference, 14th, Columbus, Ohio, June 20–22, 1973, Preprints of Technical Papers. (A73-38028 19-10) New York, Institute of Electrical and Electronics Engineers, Inc., 1973, p.645, 646.

77/00/00 78A15604
TACTICAL GUIDANCE REQUIREMENTS FOR STRAPDOWN INERTIAL
Mueller, C.E.; Phelps, R.K.; Scheidenhelm, R.
(Honeywell Systems and Research Center, Minneapolis, Minn.); (Honeywell, Inc., Defense Systems Div., Minneapolis, Minn.); (Honeywell, Inc., Avionics Div., St Petersburg, Fla.)
In NAECON '77; Proceedings of the National Aerospace and Electronics Conference, Dayton, Ohio, May 17–19, 1977. (A78-15551 04-33) New York, Institute of Electrical and Electronics Engineers, Inc., 1977, p.433-440. USAF-supported research.

An analysis of tactical inertial performance requirements for three strapdown inertial guidance system mechanizations – pure inertial, RAC aided inertial, and GPS aided inertial – is described. Cost-optimal performance requirements are determined for a family of powered and unpowered guided conventional weapons. Stochastic sensor error modeling. Velocity-matching transfer alignment, and optimal and suboptimal Kalman filtering are also discussed. ABA author.

75/00/00 76A11842
TECHNIQUES FOR ACHIEVING LOW COST STRAPDOWN NAVIGATION
Gilmore, J.P.; McKern, R.A.; Musoff, H.
(Charles Stark Draper Laboratory, Inc., Cambridge Mass.)
In Intercon 75; International Convention and Exposition, New York, N.Y., April 8–10, 1975, Conference Record. (A76-11826 02-33) New York, Institute of Electrical and Electronics Engineers, Inc., 1975, p. 1 35/3-4 35/3.

Accurate, reliable and less vulnerable radio navigation systems (GPS, Omega, DME and Loran) have been forecast for the early 1980's. This radio navigation capability permits a reformation of the INS implementation requirements from those of stand-alone navigation to that of high-bandwidth aiding of the radio navigator. Use of low cost strapdown technology in this application area becomes very attractive. Modularity concepts in both hardware and software are presented as a basis for achieving such a low cost goal. This paper presents a detailed system concept showing how to implement a strapdown system in the high-bandwidth aiding problem and how to integrate all of the conventional inertial-avionics subsystems into a unified strapdown system. ABA author.

75/00/00 76A10607
TEST EVALUATION OF A HIGH PERFORMANCE PULSE REBALANCED GYRO FOR STRAPDOWN IMU APPLICATIONS
Bendett, R.M.; Kleine, H.D.; Weinstein, S.P.; Zomick, D.A.
(Bendix Corp., Guidance Systems Div., Teterboro, N.J.)
In National Aerospace Meeting, Alamogordo, N. Mex., May 12, 13, 1975, Proceedings. (A76-10601 01-04) Washington, D.C., Institute of Navigation, 1975, p.32-42.

The paper describes the results of tests and analytical evaluation of the 64 permanent magnet rate integrating gyroscope (64 PM RIG) – an inertial grade single-degree-of-freedom sensor containing an advanced ceramic hydrodynamic gas bearing wheel assembly driven by a synchronous motor. The sensor is operated with binary pulse rebalance servo electronics using quantized pulse width modulation of the gyro torquing signal. Drift rate stability tests of the 64 PM RIG showed a bias variability over a 15-hour period of less than 0.001 deg/hr. Results are also given for rate sensor scale factor linearity and stability and on output axis slew compensation. ABA P.T.H.

76/00/00 77A26942
TESTING OF THE LUNAR EXCURSION MODULE ABORT SENSOR ASSEMBLY AT THE CENTRAL INERTIAL GUIDANCE TEST FACILITY/CIGTF/
Jaenke, M.G.; Ingold, N.L.
(USAF, Central Inertial Guidance Test Facility, Holloman AFB, N. Mex.)
In The Eagle has Returned; Proceedings of the Dedication Conference of the International Space Hall of Fame, Alamogordo, N. Mex., October 5–9, 1976. (A77-26926 11-12) San Diego, Calif., American Astronautical Society; Univelt, Inc., 1976, p.317-330.

A strapped-down system, the abort sensor assembly to be used in the Apollo program's lunar excursion module, was tested in terms of its suitability for two areas of application: missile space guidance in general, and guidance of a launch vehicle during the boost phase. The following characteristics were to be determined: the system's error coefficients, the operational suitability of the system, and system reliability. Two types of tests were performed: laboratory tests under strictly controlled conditions, and operational tests simulating essential features of missile launches such as accelerations and jerks combined with realistic vibration levels. ABA B.J.

74/00/00 76A16724
THE APPLICATION OF MICROPROCESSORS TO STRAPDOWN INERTIAL NAVIGATION
Napjus, G.A.
(Teledyne Systems Co., Northridge, Calif.)
Teledyne Systems Co., Northridge, Calif. In Microprocessors; Workshop on Electronics, Ecole Polytechnique Federale de Lausanne, Lausanne, Switzerland, October 14–17, 1974, Proceedings (Microprocesseurs; Journees d'Electronique, Ecole Polytechnique Federale de Lausanne, Switzerland, October 14–17, 1974, Comptes Rendus). Workshop sponsored by the Association Suisse des Electriciens, Ecole Polytechnique Federale de Lausanne, and IEEE. Lausanne, Ecole Polytechnique Federale de Lausanne, 1974, p.381-391.

The paper describes the nature of strapdown navigators and the computational requirements associated with them. A current system design is then described in which three limited-capability microcomputers perform the tasks previously assigned to a powerful minicomputer. In addition, a technique employing dedicated microprocessors in place of conventional analog electronics in the gyroscope control loops is discussed. ABT P.T.H.

74/10/00 75A26665
THE APPLICATION OF MICROPROCESSORS TO STRAPDOWN INERTIAL NAVIGATION
Napjus, G.A.
(Teledyne Systems Co., Northridge, Calif.)
International Conference on Microprocessors, Lausanne, Switzerland, October 14 - 17, 1974, Paper. 12 p.

The fundamental concepts of inertial navigation are briefly examined. In a strapdown inertial navigator the accelerometers and gyros are mounted directly on the vehicle frame. The development of strapdown systems, which have important advantages over gimbal systems, has been mainly retarded by the computational requirements involved. However, the current availability of suitable minicomputers combined with other technological advances has now opened the way for a more widespread use of strapdown inertial navigators. ABA G.R.

73/00/00 74A28129
THE DEVELOPMENT OF A STAR POINTING SYSTEM FOR THE SKYLARK ROCKET
Stinchcombe, P.F.
(Marconi Space and Defense Systems, Ltd., Frimley, England)
In Conference on Space Optics, 4th, Marseille, France, November 6–8, 1973, Proceedings. (A74-28101 12-14) Paris, Centre National d'Etudes Spatiales, 1973, p.233-239.

A three-axis star-pointing attitude control system has been developed for the Skylark sounding rocket. The system carries out precision inertial maneuvers using strapdown gyros from an initial attitude determined by the moon and magnetic vectors. The area of sky which contains the target star is scanned by a star sensor which locates the brightest star and subsequently provides error signals for locking the vehicle onto the target which may be +5 magnitude. Where extreme accuracy is required, within plus or minus 1 arc second, the sensor forms part of the scientific experiment. ABA author.

77/00/00 77A40780
THE DYNAMICALLY TUNED GYROSCOPE - A SENSOR FOR LOW COST ATTITUDE REFERENCE AND NAVIGATION SYSTEM
Bonfield, D.G.
(British Aircraft Corp., Ltd., Stevenage, Herts., England)
In Applications of Modern Gyro Technology; Proceedings of the Symposium, London, England, January 12, 1977. (A77-40776 19-17) London, Royal Aeronautical Society, 1977. 40 p.

The dynamically tuned gyroscope (DTG), a true two axis rotation sensor comparable in accuracy to floated gyroscopes but smaller and cheaper, is described. The history of the Hookes joint gyroscope is summarized, and the advantages of the present generation of devices are listed, including low cost of acquisition and maintenance; simplified assembly; and high shock resistance. Sources and control of errors in the DTG are considered, among them angular vibration ('twice spin speed sensitivity'), linear vibration, elastic restraint, and sensitivity to the compliance of the mounting and the support structure. Stability tests for a prototype DTG suggest ready attainment of .02 degree drift per hour in laboratory conditions. Problems in developing strapdown DTG systems are also discussed, including handling of power dissipation without adverse effects on gyro performance. In conclusion, DTGs are feasible alternatives in civil and military aircraft, missiles and other applications requiring low cost equipment and low drift characteristics. ABA J.M.B.

77/00/00 77A40777
THE EFFECT OF MODERN TECHNOLOGY ON GYROS
Smith, S.G.
(Royal Aircraft Establishment, Farnborough, Hants., England)
In Applications of Modern Gyro Technology; Proceedings of the Symposium, London, England, January 12, 1977. (A77-40776 19-17) London, Royal Aeronautical Society, 1977, 14 p.

Innovations in gyroscope technology from 1964 to the present are summarized. In particular, the introduction of digital computing to supplant analog systems allowed for automatic gyro testing, and, within the systems themselves, permitted

B-40

less stringent gyro parameters, since mass unbalance, rotation effects, and temperature coefficients to the scale factor could be corrected by airborne digital computers. The development of strapdown gyros (i.e., those mounted directly on the airframe) entailed achievement of accuracy in high dynamic ranges. In the sub-inertial field alternatives to the rotating wheel rate sensor have been produced, including the dual axis rate transducer (DART), the gas jet sensor, the vibrating wire sensor, and the magnetohydrodynamic sensor. For inertial navigation, the US has relied increasingly on dynamically tuned gyros, while in the UK improvements (e.g., substitution of gas spin bearings for ball bearings) and cost reductions have kept the single degree of freedom, floated gyro dominant. Also mentioned are dynamically tuned free-rotor gyros, electrostatically-supported gyros, ring laser gyros, and nuclear magnetic resonance gyros. ABA J.M.B.

NASA-CR-140327 E-2392 69/06/00 75N74041
THE GYROSCOPE IN TORQUE-TO-BALANCE STRAPDOWN APPLICATION
Gilmore, J.P.; Feldman, J.
Massachusetts Inst. of Tech., Cambridge. (Instrumentation Lab.)
Presented at AIAA Guidance, Control and Flight Mech Conf., Princeton, N.J., August 1969.

73/06/00 73A40025
THE IMPACT OF SPACE NAVIGATION ON THE SPHERICAL GAS BEARING GYRO
Drew, T.A.
(Rockwell International Corp., Autonetics Div., Anaheim, Calif.)
Institute of Navigation, Annual Meeting, 29th, St Louis, Mo., June 19–21, 1973, Paper. 11 p.

Results of a detailed program to evaluate the spherical gas bearing gyro with respect to the demanding requirements of satellite navigation. The goal of the research activity was to take the current platform type spherical gas bearing gyro and, by modifying the rotor and torquer only slightly to minimize the possible loss of demonstrated reliability, achieve the higher torquing rate required for strapdown implementation. The resulting strapdown gyro was evaluated for its performance capability relative to space application. The investigation was directed in two areas one was the gyro's compatibility with space applicable environments and the second was the evaluation of the gyro's performance in a strapdown mode. Highly satisfactory results were achieved for three space applicable environments i.e., long-term vacuum exposure (362 days), sterilization exposure (135 C for 96 hr), and zero-G power characteristics. ABA author.

AIAA Paper 74-926 74/08/00 74A37901
THE DELTA LAUNCH VEHICLE GUIDANCE AND NAVIGATION SYSTEM
Dhuyvetter, H.J.
(McDonnel Douglas Astronautics Co., Huntington Beach, Calif.)
American Institute of Aeronautics and Astronautics, Mechanics and Control of Flight Conference, Anaheim, Calif., August 5–9, 1974, 11 p.

The delta inertial guidance system (DIGS), which is an operationally proven versatile system, is described. The different vehicle configurations and mission definitions flown with DIGS over a period of approximately two years are indicated. From a simplicity standpoint, the DIGS provides for all first-stage and second-stage guidance, control, and vehicle sequencing functions using a minimal set of hardware. This hardware consists of a strapdown inertial measuring unit (IMU) and a 4096-word digital computer located in the second stage, two electronics packages for providing an analog servo loop for both first-stage and second-stage gimballed engines, and sequencing distribution boxes in each stage for housing various relays used to sequence vehicle functions. The development of a simple but effective set of guidance and steering equations is presented and demonstrated through flight data. ABA F.R.L.

75/00/00 75A37702
THE HONEYWELL LASER INERTIAL NAVIGATION SYSTEM/LINS/
Savage, P.G.
(Honeywell, Inc., Minneapolis, Minn.)
In NAECON '75; Proceedings of the National Aerospace and Electronics Conference, Dayton, Ohio, June 10–12, 1975. (A75-37623 18-01) New York, Institute of Electrical and Electronics Engineers, Inc., 1975, p.609-616.

The Honeywell strapdown LINS (laser inertial navigation system) is described including hardware elements, software elements, and sensor performance. The system utilizes Honeywell GG1300 laser gyros as the basic sensing elements which have a demonstrated capability for achieving 1–3 mile per hour system level performance. The LINS hardware is modular in construction to meet individual user interface requirements and system redundancy levels when needed using skewed sensor geometries. Advantages of LINS compared to conventional inertial navigation equipment are faster reaction time and a factor of two lower procurement cost and maintenance costs. A LINS engineering system is currently being road tested at Honeywell in preparation for flight test evaluation at Holloman Air Force base during April–June 1975. ABA author.

76/00/00 77A20664
THE SLIC-15 LASER GYRO IMU FOR MIDCOURSE MISSILE GUIDANCE
Morrison, R.F.; Levinson, E.; McAdory, R.W.
(Sperry Rand Corp., Sperry Gyroscope Div., Great Neck, N.Y.); (USAF, Avionics Laboratory, Wright-Patterson AFB, Ohio)
In New Frontiers in Aerospace Navigation; Proceedings of the Bicentennial National Aerospace Symposium, Warminster,

Pa., April 27, 28, 1976. (A77-20655 07-04) Washington, D.C., Institute of Navigation, 1976, p.59-68.

B41

The paper outlines the design and capabilities of the SLIC-15 strapdown laser gyro inertial measurement unit (IMU) of compact sensor configuration. The IMU consists of a laser gyro triad machined into a single ceramic-vitreous structure with three orthogonal linear accelerometers. It is shown that the unique design features of this unit offer advantages in low cost, small size, high reliability and long storage life. An error analysis for a typical glide bomb mission revealed that the SLIC-15 strapdown laser gyro IMU is suitable for midcourse guidance of tactical missiles. The capabilities of the IMU promote its use in a broad spectrum of applications in addition to tactical missile guidance. ABA S.D.

77/00/00 78A15681
THE SLIC-7 LASER GYRO INERTIAL GUIDANCE SYSTEM
Morrison, R.F.; Levinson, E.; Bryant, B.L., Jr
(Sperry Rand Corp., Sperry Gyroscope, Great Neck, N.Y.)
In NAECON '77; Proceedings of the National Aerospace and Electronics Conference, Dayton, Ohio, May 17 19, 1977. (A78-15551 04-33) New York, Institute of Electrical and Electronics Engineers, Inc., 1977, p.1045-1061. Army-sponsored research.

Sperry is developing a unique low-cost miniature ring-laser gyro strapdown inertial guidance system that is suitable for a broad spectrum of aerospace applications. The key features of this system are described and the latest laboratory performance test data are presented. Mission application capabilities, including tactical missile guidance, torpedo guidance and mixed navigation system are defined. Life cycle cost advantages are delineated. ABA author.

75/02/00 75A21528
THERMOELECTRIC TEMPERATURE CONTROL OF INSTRUMENTATION A SAMPLE DESIGN
Martorana, R.T.
(Charles Stark Draper Laboratory, Inc., Cambridge, Mass.)
IEEE Transactions on Industrial Electronics and Control Instrumentation, Vol. IECI-22, February 1975, p.69-75.

Current technology has produced high-performance semiconductor thermoelectric modules that can be a design option for temperature control of electronics and instrumentation. It seems reasonable that their advantages would be helpful to electronics and process control designers who may not be aware of the tremendous advances in the state-of-the-art of thermoelectrics. When dc current is available, thermoelectrics can be used for active bimodal control. This paper describes their fundamental operation, derives some performance relationships, and presents computation techniques for their integration into a system. An example is given where thermoelectrics were used to temperature control the SIMS II strapdown inertial navigator. Test results showed that temperature control of the gyros and accelerometers was achieved to within 0.1 degree F in ambients between 20 and 120 F. ABA author.

NASA-CR-150048 SGD-4284-0742 74/03/00 77N71120
THREE AXIS STRAPDOWN RING LASER GYRO INERTIAL MEASUREMENT UNIT MODEL 8300
Sperry Gyroscope Co., Great Neck, N.Y.

75/00/00 75A37641
TRANSFER ALIGNMENT FOR MOTION STABILIZATION OF COHERENT RADARS
Ryles, J.C.; Reeves, R.M.
(USAF, Avionics Laboratory, Wright-Patterson AFB, Ohio)
In NAECON '75, Proceedings of the National Aerospace and Electronics Conference, Dayton, Ohio, June 10 12, 1975. (A75-37623 18-01) New York, Institute of Electrical and Electronics Engineers, Inc., 1975, p.171-177.

Some of the design tradeoffs involved in a special-purpose antenna-mounted motion compensation system for use with a forward-looking multimode radar capable of producing high-resolution, real-time, synthetic-aperture radar (SAR) maps. The application considered is for a strapdown inertial measurement unit (IMU) mounted on a phased-array antenna and slaved to the aircraft inertial navigation system (INS) using transfer alignment techniques. The limit on constant acceleration error is defined as a function of radar wavelength, range to the center of the map, map resolution, aircraft velocity, and viewing angle. ABA S.J.M.

76/00/00 77A28809
UPDATE STRATEGY FOR A STRAPDOWN STELLAR-INERTIAL NAVIGATION SYSTEM
Kau, S.P.; Steadman, S.S.
(Honeywell, Inc., Aerospace Div., St Petersburg, Fla.)
In Conference on Decision and Control and Symposium on Adaptive Processes, 15th, Clearwater, Fla., December 1 3, 1976, Proceedings. (A77-28801 13-63) New York, Institute of Electrical and Electronics Engineers, Inc., 1976, p.58-64.

The paper describes the update strategy for a [illegible] stellar inertial system for orbital navigation, with space-shuttle-related applications. A six state Kalman filter was selected for update processing of star sensor data based upon algorithm tradeoff studies performed on a [illegible] state simulation. A covariance analysis simulation tool developed for attitude determination problems is used to generate the system analysis data for the stellar inertial update strategy. ABA B.J.

B.42

76/01/00 76A26566
USE OF CALIBRATION MANEUVERS FOR IMPROVED PERFORMANCE OF STRAPDOWN ATTITUDE REFERENCE SYSTEMS
Lorell, K.R.
(NASA, Ames Research Center, Moffett Field, Calif.)
National Aeronautics and Space Administration. Ames Research Center, Moffett Field, Calif. Journal of Spacecraft and Rockets, Vol.13, January 1976, p.31-36. Research supported by the National Research Council.

Conventional strapdown configurations require precise knowledge of the orientation of the gyro input axes as well as a moderately large, fast computer to provide inertial attitude. This paper presents the mechanization and discusses the operation and performance of an omnidirectional, strapdown pointing control system called all sky pointer which does not require precise gyro alignment or a sophisticated computer. Errors caused by gyro-optical sensor misalignment, gyro-integrator bias, and scale factor error are compensated for by the use of calibration maneuvers. Control and computation are provided by an electronics package utilizing technology similar to that found in hand-held calculators. Simulation results indicate that sub arc-minute pointing performance is possible and pointing errors are reduced by as much as an order of magnitude compared with uncompensated systems. ABA author.

SAE Paper 751103 75/11/00 76A22317
VERTICAL ATTITUDE TAKEOFF AND LANDING REMOTELY PILOTED DEMONSTRATION VEHICLE
Eilertson, W.H.
(US Naval Material Command, David W.Taylor Naval Ship Research and Development Center, Carderock, Md.)
Society of Automotive Engineers, National Aerospace Engineering and Manufacturing Meeting, Culver City, Calif., November 17–20, 1975, 19 p.

The VATOL remotely piloted vehicle for demonstration purposes incorporates a delta wing, has its power plant located at the rear of the aircraft, and uses a close coupled canard to extend maximum lift. A single vertical tail is used for horizontal flight directional stability, and elevons on the wing and a rudder on the vertical tail are used for horizontal flight control. The Harpoon midcourse guidance unit serves as both an autopilot and an inertial navigator by means of an attitude reference assembly in a strapdown inertial sensor configuration, a digital computer autopilot and a self-contained power supply. Experimental data on aerodynamic performance (trim lift vs trim drag, longitudinal stability, lateral stability), jet vane performance, velocity distribution, and exhaust flow conditions at lift-off are discussed. The results of engine installation tests are presented, together with the planning of future flight tests, tethered hover tests, horizontal flight tests, and ship interface tests. ABA B.J.

SAE Paper 750601 74/05/00 75A40510
WHITHER ALL WEATHER -- AN AIRPLANE MANUFACTURER'S POINT OF VIEW
Tobie, H.N.
(Boeing Commercial Airplane Co., Renton, Wash.)
Society of Automotive Engineers, Air Transportation Meeting, Hartford, Conn., May 6 -8, 1975, 6 p.

Automatic landing has been developed to the point where all the wide-bodies jets have it as basic equipment. The techniques presently employed are generally founded upon the technology of the last two decades - especially with respect to analog computation and gyroscope references. Several new techniques are now available which can substantially improve the autoland systems for the next generation of transport aircraft. These include airborne digital computers, the use of integrated air-data and strapdown airplane motion reference systems, expanded use of automatic system test, and the development and employment of the microwave landing system (MLS). These new technology developments promise to provide expanded operational benefits, reduced maintenance, and increased availability over that of contemporary autoland systems. ABA author.

75/00/00 75A3' 701
4-D NAVIGATION USING INTEGRATED STRAPDOWN INERTIAL/DIFFERENTIAL LORAN
Wierenga, R.D.
(Lear Siegler, Inc., Instrument Div., Grand Rapids, Mich.)
In NAECON '75; Proceedings of the National Aerospace and Electronics Conference, Dayton, Ohio, June 10 12, 1975. (A75-37623 18-01) New York, Institute of Electrical and Electronics Engineers, Inc., 1975, p.602-608.

This paper describes a four-dimensional terminal area navigation, control, and display system that uses strapdown inertial sensors combined with differential Loran to accurately determine aircraft position, velocity, attitude and heading. The functional and hardware requirements of the system are given. A unique integration filter is defined which combines the strapdown inertial and differential Loran data. The four-dimensional path generation technique that is used is briefly described as is the hybrid computer and cockpit simulator being used to evaluate the system. ABA author.

B350
4

AGARD
NATO OTAN
7 RUE ANCELLE · 92200 NEUILLY-SUR-SEINE
FRANCE
Telephone 745.08.10 · Telex 610176

DISTRIBUTION OF UNCLASSIFIED AGARD PUBLICATIONS

AGARD does NOT hold stocks of AGARD publications at the above address for general distribution. Initial distribution of AGARD publications is made to AGARD Member Nations through the following National Distribution Centres. Further copies are sometimes available from these Centres, but if not may be purchased in Microfiche or Photocopy form from the Purchase Agencies listed below.

NATIONAL DISTRIBUTION CENTRES

BELGIUM
Coordonnateur AGARD – VSL
Etat-Major de la Force Aérienne
Quartier Reine Elisabeth
Rue d'Evere, 1140 Bruxelles

CANADA
Defence Scientific Information Service
Department of National Defence
Ottawa, Ontario K1A 0Z2

DENMARK
Danish Defence Research Board
Østerbrogades Kaserne
Copenhagen Ø

FRANCE
O.N.E.R.A. (Direction)
29 Avenue de la Division Leclerc
92 Châtillon sous Bagneux

GERMANY
Zentralstelle für Luft- und Raumfahrtdokumentation und -information
c/o Fachinformationszentrum Energie, Physik, Mathematik GmbH
Kernforschungszentrum
7514 Eggenstein-Leopoldshafen 2

GREECE
Hellenic Armed Forces Command
D Branch, Athens

ICELAND
Director of Aviation
c/o Flugrad
Reykjavik

ITALY
Aeronautica Militare
Ufficio del Delegato Nazionale all'AGARD
3, Piazzale Adenauer
Roma/EUR

LUXEMBOURG
See Belgium

NETHERLANDS
Netherlands Delegation to AGARD
National Aerospace Laboratory, NLR
P.O. Box 126
Delft

NORWAY
Norwegian Defence Research Establishment
Main Library
P.O. Box 25
N-2007 Kjeller

PORTUGAL
Direcção do Serviço de Material
da Força Aerea
Rua da Escola Politecnica 42
Lisboa
Attn: AGARD National Delegate

TURKEY
Department of Research and Development (ARGE)
Ministry of National Defence, Ankara

UNITED KINGDOM
Defence Research Information Centre
Station Square House
St. Mary Cray
Orpington, Kent BR5 3RE

UNITED STATES
National Aeronautics and Space Administration (NASA)
Langley Field, Virginia 23365
Attn: Report Distribution and Storage Unit

THE UNITED STATES NATIONAL DISTRIBUTION CENTRE (NASA) DOES NOT HOLD STOCKS OF AGARD PUBLICATIONS, AND APPLICATIONS FOR COPIES SHOULD BE MADE DIRECT TO THE NATIONAL TECHNICAL INFORMATION SERVICE (NTIS) AT THE ADDRESS BELOW.

PURCHASE AGENCIES

Microfiche or Photocopy
National Technical
Information Service (NTIS)
5285 Port Royal Road
Springfield
Virginia 22151, USA

Microfiche
Space Documentation Service
European Space Agency
10, rue Mario Nikis
75015 Paris, France

Microfiche
Technology Reports
Centre (DTI)
Station Square House
St. Mary Cray
Orpington, Kent BR5 3RF
England

Requests for microfiche or photocopies of AGARD documents should include the AGARD serial number, title, author or editor, and publication date. Requests to NTIS should include the NASA accession report number. Full bibliographical references and abstracts of AGARD publications are given in the following journals:

Scientific and Technical Aerospace Reports (STAR)
published by NASA Scientific and Technical
Information Facility
Post Office Box 8757
Baltimore/Washington International Airport
Maryland 21240, USA

Government Reports Announcements (GRA)
published by the National Technical
Information Services, Springfield
Virginia 22151, USA

Printed by Technical Editing and Reproduction Ltd